Development of novel nAChR modulators

Inaugural-Dissertation

zur Erlangung des Doktorgrades
der Mathematisch-Naturwissenschaftlichen Fakultät
der Heinrich-Heine-Universität Düsseldorf

vorgelegt von

Jesko Fabian Kaiser

aus Aschaffenburg

Düsseldorf, den 26.06.2024

aus dem Institut für Pharmazeutische und Medizinische Chemie

der Heinrich-Heine-Universität Düsseldorf

Gedruckt mit der Genehmigung der
Mathematisch-Naturwissenschaftlichen Fakultät der
Heinrich-Heine-Universität Düsseldorf

Berichterstatter:

1. Prof. Dr. Holger Gohlke

2. Prof. Dr. Matthias Kassack

Tag der mündlichen Prüfung: 08.01.2025

EIDESSTATTLICHE ERKLÄRUNG

Ich, Jesko Fabian Kaiser, versichere an Eides Statt, dass die Dissertation von mir selbständig und ohne unzulässige fremde Hilfe unter Beachtung der „Grundsätze zur Sicherung guter wissenschaftlicher Praxis an der Heinrich-Heine-Universität Düsseldorf“ erstellt worden ist.

Diese Dissertation wurde in der vorgelegten oder einer ähnlichen Form bei noch keiner anderen Institution eingereicht, und es wurden bisher keine erfolglosen Promotionsversuche von mir unternommen.

Düsseldorf, 26.06.2024

TO MY FAMILY

TABLE OF CONTENTS

LIST OF PUBLICATIONS

This thesis is based on the following publications:

J. Kaiser (Contribution: 40%), C.G.W. Gertzen, T: Bernauer, G: Höfner, K.V. Niessen, T: Seeger, F.F: Paintner, K.T. Wanner, F. Worek, H. Thiermann, H. Gohlke; *A novel binding site in the nicotinic acetylcholine receptor for MB327 can explain its allosteric modulation relevant for organophosphorus-poisoning treatment,* Toxicol Lett, 2023. **373**: p. 160-171.

2024 Impact Factor: 3.5

V. Nitsche, G. Höfner, J. Kaiser (Contribution: 15%), C.G.W. Gertzen, T. Seeger, K. V. Niessen, D. Steinritz, H. Thiermann, F. Worek, H. Gohlke, F.F. Paintner, K.T. Wanner; *MS Binding Assays with UNC0642 as reporter ligand for the MB327 binding site of the nicotinic acetylcholine receptor;* Toxicol Lett, 2024. **392**: p. 94-106.

2024 Impact Factor: 3.5

J. Kaiser (Contribution: 35%), C.G.W. Gertzen, T. Bernauer, V. Nitsche, G. Höfner, K.V. Niessen, T. Seeger, F.F. Paintner, K.T. Wanner, D. Steinritz, F. Worek, H. Gohlke; *Identification of ligands binding to MB327-PAM-1, a binding pocket relevant for resensitization of nAChRs;* Toxicol Lett, 2024. *in press*.

2024 Impact Factor: 3.5

T. Bernauer, V. Nitsche, J. Kaiser (Contribution: 15%), C.G.W. Gertzen, G. Höfner, K.V. Niessen, T. Seeger, D. Steinritz, F. Worek, H. Gohlke, K.T. Wanner, F.F. Paintner, *Synthesis and Biological Evaluation of Novel MB327 Analogs as Resensitizers for Desensitized Nicotinic Acetylcholine Receptors after Intoxication with Nerve Agents,* Toxicol Lett, 2024. **397**: p. 151-162.

2024 Impact Factor: 3.5

During the work on this thesis, the following publications were additionally authored:

T. Pauly*, N. Bolakhrif*, J. Kaiser, L. Nagel-Steger, L. Gremer, H. Gohlke, D. Willbold, *Met/Val129 polymorphism of the full-length human prion protein dictates distinct pathways of amyloid formation,* J Biol Chem, 2022. **298**(10): 102430.

C. Lin, E.O. Kuffour, N.V. Fuchs, C.G.W. Gertzen, J. Kaiser, M. Hirschenberger, X. Tang, H.C. Xu, O. Michel, R. Tao, A. Haase, U. Martin, T. Kurz, I. Drexler, B. Görg, P.A. Lang, T. Luedde, K.M.J. Sparrer, H. Gohlke, R. König, C. Münk, *Regulation of STING activity in DNA sensing by ISG15 modification,* Cell Rep, 2023. **42**: 113277.

C. Lin*, E.O. Kuffour*, T. Li, C.G.W. Gertzen, J. Kaiser, T. Luedde, R. König, H. Gohlke, C. Münk, *The IS15-Protease USP18 Is a Pleiotropic Enhancer of HIV-1 Replication*, Viruses, 2024. **16**(4): 485.

Pacholewska, M. Lienhard, M. Brüggemann, H. Hänel, L. Bilalli, A. Königs, B. Timmermann, K. Becker, K. Köhrer, J. Kaiser, H. Gohlke, N. Gattermann, M. Hallek, C. Herling, J. König, C. Grimm, R. Herwig, K. Zarnack, M.R. Schweiger, *Long-read transcriptome sequencing of CLL and MDS patients uncovers molecular effects of SF3B1 mutations*, submitted manuscript, bioRxiv: 10.1101/2024.01.26.576051.

Y. Gao, M. Frank, N. Teusch, D. Woschko, C. Janiak, A. Mandi, T. Kurtán, R. Hartmann, K. Schiedlauske, L. van Geelen, R. Kalscheuer, J. Kaiser, C.G.W. Gertzen, H. Gohlke, B.-G. Wang, P. Proksch, Z. Liu, *Aplospojaveedins A–C, sulfur-containing novel alkaloids produced by the endophytic fungus Aplosporella javeedii using OSMAC strategy,* submitted manuscript.

* Authors contributed equally to this work.

T. Bernauer*, V. Nitsche*, G. Höfner, J. Kaiser, C.G.W. Gertzen, K.V. Niessen, T. Seeger, D. Steinritz, F. Worek, H. Gohlke, K.T. Wanner, F.F. Paintner, *Structure-Affinity Relationship of Quinazoline Derivatives as Potential Resensitizers of Desensitized nAChRs After Nerve Agent Intoxication,* manuscript in preparation.

* Authors contributed equally to this work.

ABBREVIATIONS

ACh	Acetylcholine
AChE	Acetylcholinesterase
CNA	Constraint Network Analysis
cryoEM	Cryogenic Electron Microscopy
ECD	Extracellular Domain
GIST	Grid Inhomogeneous Solvation Theory
ICD	Intracellular Domain
LBDD	Ligand-Based Drug Design
mAChR	Muscarinic Acetylcholine Receptor
MD	Molecular Dynamics
nAChR	Nicotinic Acetylcholine Receptor
OPC	Organophosphorus Compounds
PAM	Positive Allosteric Modulator
PDB	Protein Data Bank
RMSD	Root Mean Square Deviation
SBDD	Structure-Based Drug Design
TMD	Transmembrane Domain

ABSTRACT

Despite being banned by international treaties, several chemical attacks using organophosphorus compounds (OPCs) have been recorded over the last decades. By inhibiting the acetylcholinesterase, OPCs cause an increase of ACh concentrations in the synaptic gap, resulting in muscle weakness and respiratory paralysis after desensitization of nicotinic acetylcholine receptors (nAChRs). The current treatment of OPC poisonings is insufficient, with no treatment option targeting nAChRs directly. Recent progress in this area was made by the identification of MB327, a positive allosteric modulator (PAM) of nAChRs, able to resensitize the receptor. However, MB327 also acts as inhibitor of nAChRs at slightly higher concentrations, counteracting its therapeutic effect. Experimental data indicates that the therapeutically relevant effect is being transmitted via an allosteric binding site, but the precise binding site remained unknown, making structure- and ligand-based optimization of the compounds demanding. Within this thesis, I focused on proposing a binding site for these compounds as well as identifying more potent analogs of known binders and compounds featuring novel chemotypes acting as PAMs in nAChRs.

More precisely, in **PUBLICATION I**, I predicted a novel allosteric binding site for MB327, MB327-PAM-1, by using blind docking experiments in combination with molecular dynamics (MD) simulations and rigidity analysis. By performing free ligand diffusion MD simulations, I disentangled that MB327 may also bind to the orthosteric binding site, probably explaining the inhibitory effect of the ligand at higher concentrations. Based on this knowledge, more potent analogs of MB327 could be designed. Furthermore, in **PUBLICATION II**, I unraveled the potential binding mode of UNC0646, a recently described binder in MB327-PAM-1 with increased affinity compared to MB327.

Based on the knowledge gathered in the first two publications, structure- and ligand-based drug design approaches became feasible. In **PUBLICATION III**, I performed a variety of virtual screening approaches to identify more affine substituents of the UNC0646 quinazoline moiety and to identify novel chemotypes acting as PAMs with a higher affinity compared to MB327, enriching the pool of lead structures. In **PUBLICATION IV**, Grid Inhomogeneous Solvation Theory computations helped revealing entropically unfavored water molecules within MB327-PAM-1. Substituting these water molecules with novel substituents at the MB327 bispyridinium core resulted in an MB327 analog with higher potency compared to MB327.

ZUSAMMENFASSUNG

Obwohl die Verwendung von Organophosphorverbindungen (OPCs) als chemische Waffen durch internationale Verträge verboten ist, wurden sie in den letzten Jahrzehnten wiederholt eingesetzt. Durch irreversible Hemmung der Acetylcholinesterase führen sie zu einer erhöhten Konzentration von Acetylcholin im synaptischen Spalt. Dies führt zur Desensitisierung von nikotinischen Acetylcholinrezeptoren (nAChR), einhergehend mit Muskelschwäche und Atemstillstand. Behandlungsoptionen von OPC-Vergiftungen sind unzureichend, und keine Medikamente adressieren den nAChR direkt. Mit der Identifikation von MB327, einem positiv allosterischen Modulator (PAM) von nAChRs, der die Muskelkraft in somanvergiftetem Gewebe wieder herstellen kann, wurde ein entscheidender Fortschritt gemacht. Allerdings weist MB327 bei unwesentlich höheren Konzentrationen einen inhibitorischen Effekt auf, was den therapeutisch relevanten Effekt antagonisiert. Die genaue Lokalisation der therapierelevanten allosteren Bindetasche ist unbekannt, was struktur- und ligandenbasierte Optimierungen der Moleküle anspruchsvoll macht. In dieser Forschungsarbeit habe ich mich darauf konzentriert, die Bindetasche dieser Moleküle zu identifizieren und neue, potentere Analoga bekannter PAMs und PAMs mit neuem chemischen Grundgerüst zu entwickeln.

Genauer gesagter habe ich in **Publikation I** eine neue Bindestelle von MB327, MB327-PAM-1, basierend auf *blind docking* Experimenten in Kombination mit Molekulardynamik (MD) Simulationen und Rigiditätsanalyse vorhergesagt. Die Durchführung von *free ligand diffusion* MD-Simulationen hat nahegelegt, dass MB327 auch Affinität zur orthosteren Bindetasche aufweist, was vermutlich den inhibitorischen Effekt erklärt. Darauf basierende strukturbasierte Optimisierungsansätze führten zu MB327-Analoga mit erhöhter Aktivität. In **Publikation II** habe ich einen plausiblen Bindemodus von UNC0646 in MB327-PAM-1, einem kürzlich beschriebenen Liganden mit erhöhter Affinität im Vergleich zu MB327, präsentiert. In **Publikation III** habe ich basierend auf den Erkenntnissen der ersten beiden Publikationen verschiedene virtuelle Screeningansätze verwendet, um neue Substituenten des Chinazolinbausteins von UNC0646 mit erhöhter Affinität zu identifizieren. Außerdem konnte ich PAMs mit neuem chemischen Grundgerüsten identifizieren, die eine erhöhte Affinität im Vergleich zu MB327 aufweisen, was die Anzahl an Leitstrukturen erhöht. In **Publikation IV** konnte ich, basierend auf *Grid Inhomogeneous Solvation Theory* Berechnungen, entropisch ungünstige Wassercluster in MB327-PAM-1 identifizieren. Die Verdrängung dieser Wassercluster durch variierende Substituenten am MB327-Grundgerüst führte zu einem im Vergleich zu MB327 potenteren Analogon.

1. INTRODUCTION

Handling with organophosphorus compounds (OPCs) is highly restricted, and their use as chemical warfare agents is prohibited by international treaties [1]. Nevertheless, the occurrence of OPC poisonings is far from over. The most serious cases of OPC poisoning happened in the Syrian civilian war in 2013 and 2017, resulting in the death of thousands of people [2, 3]. Besides that, OPCs are also attractive for terrorist groups. In 1995, a terroristic sarin attack on the Tokyo subway killed thirteen and sickened thousands of people [4-6]. Thus, OPCs persist as a significant threat to the civilian and military population. Furthermore, the use of organophosphorus insecticides repeatedly led to intoxications around the globe [7-11]. OPCs act by covalently inhibiting the acetylcholinesterase (AChE), an enzyme crucial for degrading the neurotransmitter acetylcholine (ACh) in the synaptic gap (**chapter 2.1.2**) [1, 12-20]. The resulting overstimulation of postsynaptic muscarinic (mAChRs) and nicotinic acetylcholine receptors (nAChRs) leads to receptor-specific symptoms, such as miosis and bradycardia (mAChR) and muscle weakness and respiratory paralysis (nAChR), leading to life-threatening situations [1, 5, 6, 21-23]. Noteworthy, overstimulation of nAChRs does not lead to an overactivation of the receptor but results in receptor desensitization associated with a non-functional, non-activatable configuration (**chapter 2.1.4**) [24, 25].

Current treatment options for OPC poisoning focus on inhibiting the overstimulation of mAChRs by application of the inhibitor atropine and reactivating the AChE with oximes, targeting both receptors indirectly [1]. Even though oximes are widely considered to have beneficial effects, certain OPCs are insensitive to a variety of oximes, and oximes are generally ineffective after an aging process of the OPC-AChE complex (**chapter 2.1.2**) [1, 26-43]. No treatment options currently target nAChRs directly, resulting in a substantial therapeutic gap after OPC poisoning. Recent progress was made by the identification of MB327, acting as a positive allosteric modulator (PAM) of nAChRs, able to reestablish the muscle force in soman-poisoned rat diaphragms and to potentiate the cholinergic effect (**chapter 2.1.3**) [44-47]. At slightly higher concentrations, the ligand itself acts as an inhibitor of the receptor, resulting in a tight therapeutic index [46]. Thus, MB327 cannot be used in the treatment of OPC poisonings directly but can be considered as a promising lead structure. Since the identification of MB327, a variety of analogs have been synthesized and tested regarding their affinity, but no groundbreaking increase in binding affinity has been observed in any analog [48, 49]. A small number of selected MB327 analogs also showed no beneficial effects compared to MB327 regarding their potency in reestablishing muscle force in soman-poisoned tissue [46]. Recently,

by *in vitro* screening of a database using an MB327 MS Binding Assay, UNC0646 has been identified with increased affinity to the MB327 binding site compared to MB327 [pK_i (UNC0646)= 6.23 ± 0.02; pK_i (MB327) = 4.73 ± 0.03] [48, 50]. Despite the increased affinity, activity measurements performed by our collaboration partners at the Bundeswehr Institute of Pharmacology and Toxicology in Munich (Figure 1) revealed a reduced potency of UNC0646 compared to MB327, making the use of UNC0646 as a treatment option unattainable (**PUBLICATION II**) [51]. Thus, further studies are required to understand the mechanism of action of PAMs and identifying novel PAMs of nAChRs with increased potency and with a lack of inhibitory effects on the receptor to ultimately close the therapeutic gap in OPC poisoning treatment. For the design of or search for such ligands, knowledge of the binding mode of MB327 and UNC0646 in the nAChR would be beneficial. These, however, remained elusive prior to my thesis.

Within this thesis, I utilized computational methods to predict the binding mode of known ligands and to suggest novel analogs of known binders and compounds featuring novel chemical scaffolds as potential PAMs. To verify my predictions and to strengthen the assumptions made within my predictions, I worked in close collaboration with experimentalists from the Ludwig Maximilians University in Munich – performing synthesis of novel suggested analogs and *in vitro* affinity testing using UNC0642 MS Binding Assays – and from the Bundeswehr Institute of Pharmacology and Toxicology – performing *ex vivo* activity testing of suggested compounds in soman-poisoned rat diaphragm assays (Figure 1). Gathered experimental data was then used to strengthen our computational models.

One way to identify optimized analogs of known binders or novel chemotypes acting as PAMs are structure- (SBDD) and ligand-based (LBDD) drug design approaches (**chapters 2.2.3.2** and **2.2.3.1**, respectively). Therefore, knowledge of the binding mode of ligands is crucial. At the beginning of my work, experimental data suggested that MB327 binds to an allosteric binding site, responsible for the therapeutically relevant effect [46, 52]. However, the location of this binding site within the protein remained elusive. Also, the pocketome of nAChRs remains incompletely understood with several Protein Data Bank (PDB) structures featuring a variety of potential allosteric binding sites - for PAMs, these are preferably localized at the transition from the extracellular domain (ECD) to the transmembrane domain (TMD) of the receptor, or in the upper part of the TMD (**chapter 2.1.5**), yet differ between different PAMs [53-68]. Uncertainty about the binding site and the binding mode of the positive allosteric modulators make structure- and ligand-based approaches to generate novel binders challenging.

To identify the binding site of MB327, blind docking experiments in combination with molecular dynamics (MD) simulations may be performed (**chapters 2.2.2.1** and **2.2.2.2**), accompanied by rigidity analysis (**chapter 2.2.2.3**) to predict allosteric impacts transmitted via this binding site. Applying these techniques to identify a potential binding site revealed that MB327 may bind at the transition from the ECD to the TMD in a binding site called MB327-PAM-1 (**PUBLICATION I**). MB327-PAM-1 can also be occupied by calcium ions acting as positive allosteric modulators of nAChRs [65, 69]. Allosteric impacts transmitted via this binding site are in line with experimental results [45-47] (**PUBLICATION I**). Furthermore, free ligand binding MD simulations (**chapter 2.2.2.2**) revealed that MB327 may also bind to the orthosteric binding site (**PUBLICATION I**), probably acting as an inhibitor, in line with recent experimental results [70]. Furthermore, a plausible binding mode of UNC0646 in MB327-PAM-1 was suggested using a combination of docking experiments and MD simulations (**PUBLICATION II**).

In addition to ligand-based screenings based on the two-dimensional structure of UNC0646, the novel proposed binding mode enabled performing ligand-based screenings based on the three-dimensional bound conformation of a UNC0646 analog, resulting in the identification of substituents of the quinazoline moiety within UNC0646 that increase its affinity. Furthermore a virtual high-throughput structure-based screening in MB327-PAM-1 resulted in four new chemotypes binding to MB327-PAM-1 with increased affinity compared to MB327, including cycloguanil, the active metabolite of the approved antimalaria drug proguanil [71, 72] (**PUBLICATION III**). Cycloguanil was also tested regarding its ability to reestablish muscle force after soman poisoning and showed increased potency compared to MB327.

Lastly, novel MB327 analogs were designed based on adjusting substituents of the bispyridinium core to replace entropically unfavored water clusters within MB327-PAM-1, as observed during MD simulations of MB327 bound to the binding site (**chapter 2.2.3.3**) resulting in the identification of PTMD90-0012, an analog with increased affinity compared to MB327 (**PUBLICATION IV**).

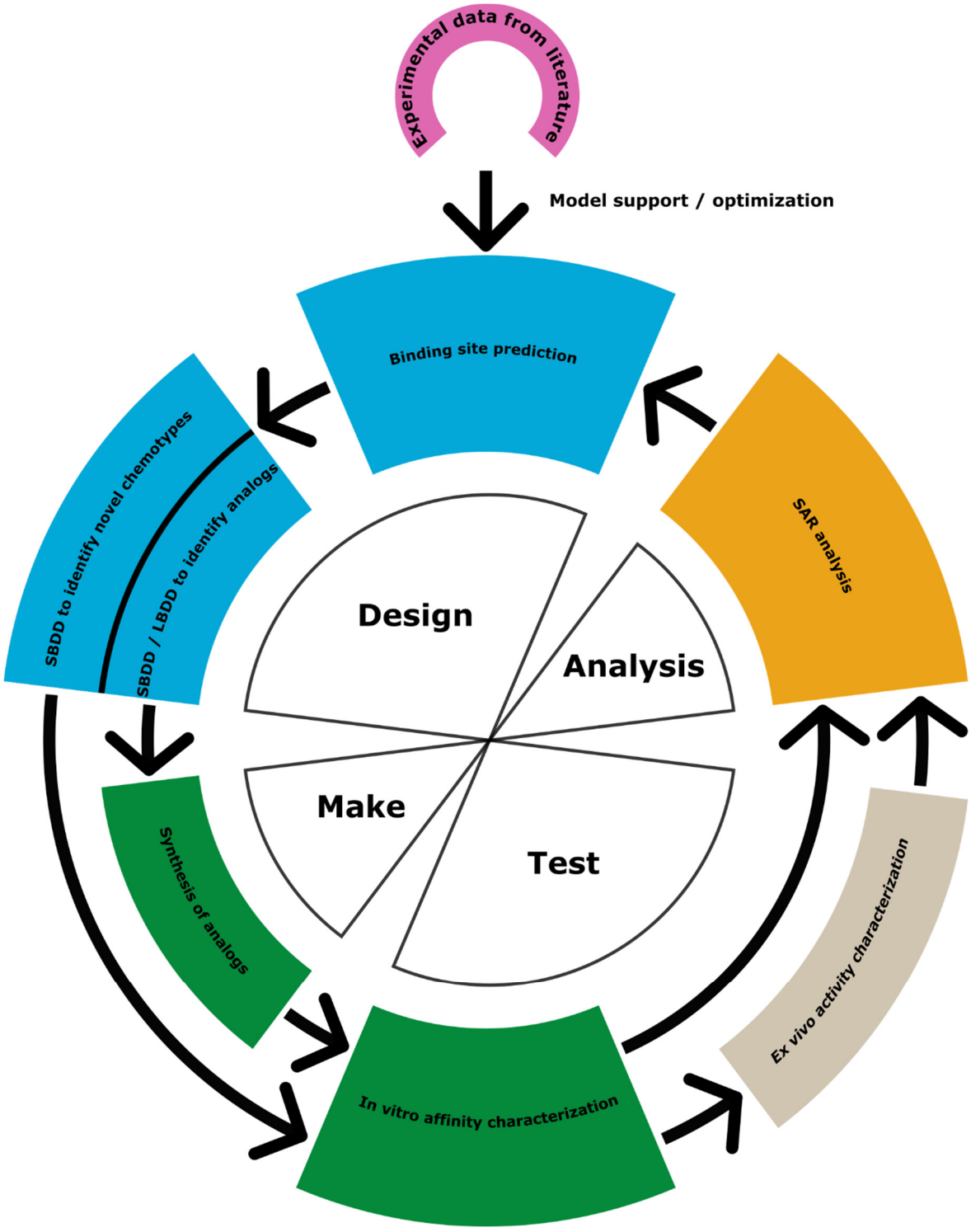

Figure 1: Design-Make-Test-Analysis workflow to identify novel chemical scaffolds acting as PAMs respectively to optimize the structure of known PAMs. Blue colors indicate computational studies performed at the Heinrich Heine University in Düsseldorf, green colors indicate experiments performed by our collaboration partners at the Ludwig Maximilians University in Munich, beige colors indicate experiments performed by our collaboration partners at the Bundeswehr Institute of Pharmacology and Toxicology, and yellow colors indicate analysis conducted in collaboration among all working groups. I utilized computational approaches to predict the binding site and performed SBDD to identify commercially available novel chemical scaffolds binding to the MB327 binding site. Furthermore, I performed SBDD and LBDD to identify analogs with potentially increased potency compared to MB327 and UNC06464, respectively. Analogs were then synthesized and compounds with novel chemical scaffolds were purchased commercially. All compounds were tested in *in vitro* MS Binding Assays to characterize the affinity towards the MB327 binding site. Selected compounds were tested in an *ex vivo* activity assay to discover their potential in reestablishing muscle force in soman-poisoned rat diaphragm. Structure-affinity/activity relationships (SAR) derived from experimental results obtained within this workflow and experimental results gathered from literature are continuously used to support and optimize our model.

2. BACKGROUND

In the following section, I will first give a brief overview of the physiological role of ACh, particularly its role as a neurotransmitter, followed by an outline of how OPCs disturb the ACh pathway. Then, I will give insights into the currently unsatisfactory treatment of OPC poisoning and will highlight current research attempting novel promising approaches to close the therapeutic gap with a focus on MB327, a PAM of the nAChR. Since the binding site of MB327 remained elusive, I will also focus on the three-dimensional structure of nAChRs and the current knowledge about its pocketome.

In the second subchapter, I will introduce the methods we used to identify the binding site of MB327 first, followed by the identification of novel, more potent PAMs of the nAChR.

2.1. Organophosphorus poisoning

2.1.1. Physiological and pathophysiological role of acetylcholine

The neurotransmitter ACh plays a crucial role in physiological processes within animals and humans [24, 73-86]. ACh is synthesized in the synaptic cell by acetylation of choline and stored in intracellular vesicles containing thousands of molecules per vesicle [87-93]. After an occurring action potential, ACh is released into the synaptic gap [83, 84, 86]. There, ACh can bind to two classes of receptors, the mAChR and nAChR, eliciting action potentials in the postsynaptic cell [16, 94-103] (Figure 2A). The mAChR is a G-protein coupled receptor, transmitting signals via secondary messengers after ACh binding and thereby indirectly influencing the ion concentrations within the cell [104-114]. In contrast, the nAChR is a pentameric ligand-gated ion channel, directly influencing the ionic concentrations within the cell by letting ions pass through the receptor after ACh binding [115-120]. Following its release, thereby activating the aforementioned postsynaptic receptors, ACh is rapidly hydrolyzed to choline and acetate by the AChE [12-17].

Disruption of the ACh transmission is associated with several diseases and intoxications. Myasthenia gravis, a neuromuscular junction disease, is an autoimmune disease associated with the formation of antibodies against nAChRs [121-126]. In Alzheimer's disease, inhibitors of AChE are used in treatment since the neurodegenerative disease is associated with a disruption of ACh signaling [127-137]. However, covalently inhibiting the AChE is also the mechanism of action of many OPCs, such as insecticides (e.g., parathion) and chemical warfare nerve agents (e.g., sarin, soman, tabun, and Novichok compounds) [1, 138-144]. Despite being forbidden by international treaties, such as the Chemical Weapons Convention and the 1990

Chemical Weapons Accord, OPCs are still being used as chemical weapons and thus remain a serious threat to the civilian and military population [1, 145], especially because current treatment options are unsatisfactory. Thus, as much knowledge as possible about OPCs is required to ultimately close the therapeutic gap.

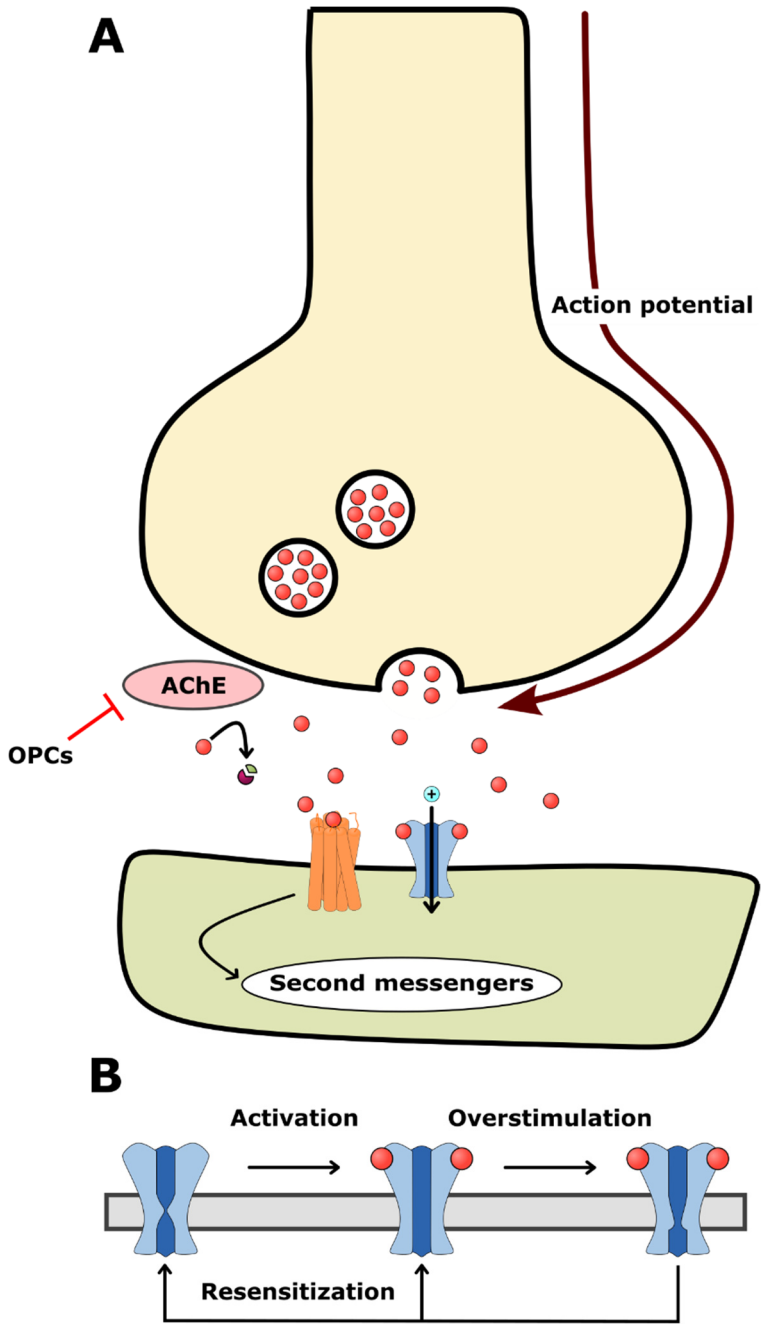

Figure 2: Transmission of an action potential via the synaptic cleft by the neurotransmitter ACh. **A)** ACh (red) is stored in vesicles in the presynaptic cell (sand). After being released in the synaptic gap as a result of an occurring action potential, ACh can bind to mAChRs (orange) and nAChRs (blue) located in the membrane of the postsynaptic cell (olive green). mAChRs can influence the ion concentration within the cell via second messengers, whereas activation of nAChRs leads to transmission of cations through the receptor pore. ACh is subsequently hydrolyzed to choline (purple) and acetate (green) via the AChE. OPCs act by inhibiting AChEs. **B)** Activation cycle of nAChRs according to Corradi and Bouzat [146]. Activation of nAChRs leads to the pore opening, resulting in a ligand-bound active state, whereas overstimulation of the receptor results in a ligand-bound overstimulated state of the receptor with a pore closed differently than the inactive state Overstimulation may occur after prolonged exposure to ACh, a result of the inhibition of the AChE. After a recovery time or by application of allosteric resensitizers, the receptor can be resensitized, resulting in a functional state. The grey box indicates the location of the membrane.

2.1.2. Mechanism of action and current treatment of OPC poisoning

The first OPC [tabun (GA)] was identified in Germany by Gerhard Schrader in the 1930s while developing organophosphorus-based insecticides [1]. During the Second World War and the following Cold War, further OPCs were developed, including members of the G-series [G for Germany, e.g., soman (GD)] and members of the more potent V-series (V for "Venomous") developed in Great Britain (e.g., VX) [1]. Despite, as mentioned above (**chapter 2.1.1**), the use of OPCs being internationally despised, they were used in various occurrences. In 1995, 13 people were killed by a terroristic act using sarin, causing long-term health effects on hundreds of people [4-6]. During the Syrian civil war, hundreds of people were killed in chemical attacks in 2013 and 2017 [2, 3]. Additionally, the former Russian military intelligence officer and later double agent for the United Kingdom, Sergei Skripal, and the Russian oppositionist Alexei Navalny were both victims of chemical attacks using Novichok in 2018 and 2020, respectively [147-149]. These cases clearly demonstrate the ongoing threat of OPC poisoning and stretch the importance of a successful treatment after poisoning.

In order to understand the current state and novel attempts to treat OPC poisoning, it is necessary to first describe the mechanism of action. OPCs can block the AChE covalently by binding to S203 which is part of the catalytic triad of AChE (Figure 2A, Figure 3), resulting in increased concentrations of ACh in the synaptic gap [1, 18-20, 150]. This leads to an overstimulation of both mAChRs and nAChRs, associated with the typical toxicological symptoms after OPC poisoning. Symptoms associated with the overstimulation of mAChRs include nausea, bradycardia, miosis, arrhythmia, and bronchoconstriction [1, 6, 21-23]. Overstimulation of nAChRs results in a closed, functionally inactivated conformation of the ion channel (Figure 2B) [24, 25, 151]. However, in contrast to the resting state of the receptor, this overstimulated, desensitized state is not activatable anymore and is being associated with toxicological symptoms, such as muscle weakness and respiratory paralysis [1, 5, 6, 21, 24, 25, 152].

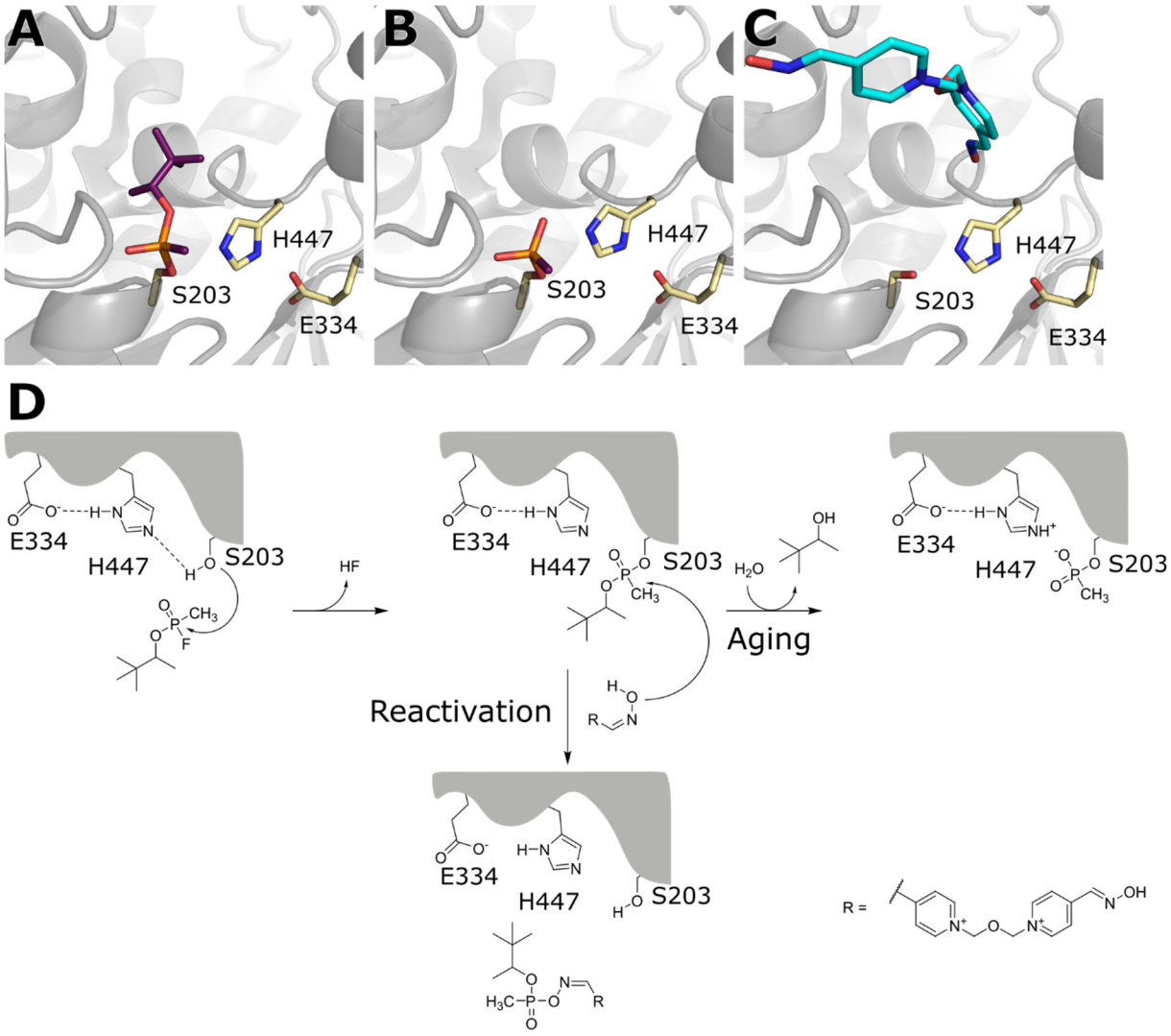

Figure 3: Mechanism of inactivation of AChE by OPCs and reactivation by oximes. Crystal structure of the *Torpedo californica* AChE with soman (purple) covalently bound to S203, part of the catalytic triad, **A)** before and **B)** after aging (PDB IDs: 2WFZ, 2WG0 [153]). For the sake of clarity, the amino acid numbering of the catalytic triad of *Torpedo californica* was adjusted to the amino acid numbering of the human AChE. Amino acids that are part of the catalytic triad are shown as sticks. **C)** Crystal structure of obidoxime bound to the catalytic region of mouse AChE (PDB ID: 2GYW [154]). **D)** Schematic reaction of the OPC soman with the catalytic triad of AChE. After soman phosphorylates S203, the ester bond may be hydrolyzed, resulting in an aged adduct that cannot be reactivated by oximes anymore. If AChE has not undergone an aging process yet, obidoxime may act as a reactivator of inhibited AChEs.

Although the function of both mAChRs and nAChRs is highly disturbed after OPC poisoning, current treatment options mainly focus on inhibiting the overstimulation of mAChRs and targeting both receptors indirectly by reestablishing the function of AChE. Atropine can be used to counteract the toxicological symptoms transmitted via mAChRs and shows beneficial effects after OPC poisoning *in vivo* [1, 6, 34, 36-38, 155, 156]. Yet, symptoms transmitted via overstimulation of nAChRs, such as respiratory paralysis leading to death, cannot be treated by atropine. In terms of AChE restoration, oximes are widely considered to have a beneficial effect on patient recovery [1, 26-38]. These compounds can displace the covalently bound OPC from AChE by hydrolyzing the serine-OPC bond [1, 29, 35, 157, 158] (Figure 3). However, certain oximes are ineffective against several OPCs and cannot be used after the OPC-bound AChE

undergoes an aging process [1, 26, 28, 39-43] (Figure 3D). Furthermore, two meta-analyses concluded no beneficial effect of oxime-treatment [159, 160]. Taken together, whereas specific drugs are available to alleviate the effects of overstimulated mAChRs, overstimulation of nAChRs can only be treated indirectly by reactivating the AChE. Nevertheless, the efficacy of these oximes is unsatisfactory. Thus, there is still a substantial therapeutic gap in the treatment of OPC poisonings, which might be closed by the development of resensitizing modulators that target nAChRs directly. However, in comparison to targeting the less complex mAChRs, where an antagonist binding in the orthosteric binding site can be beneficial to treat overstimulation, such ligands would have no beneficial effects on nAChRs. The desensitized state of nAChRs resulting from overstimulation represents a closed state, functionally comparable to the inactive state regarding its ability to transmit action potentials onto postsynaptic cells. Thus, orthosteric inhibitors would result in an inactivated conformation of the receptor, contradicting the goal of reactivating nAChR. Consequently, a PAM needs to be identified that is able to resensitize nAChRs and ultimately close the gap in OPC poisoning treatment.

2.1.3. Novel therapeutics in the treatment of OPC poisoning interacting directly with nAChRs

In previous work, a novel PAM of nAChRs, MB327 (Figure 4), was identified. Even though first results indicated that the ligand acts as an inhibitor of nAChRs [44], later studies revealed that MB327 can act as a PAM, and the small molecule drug has been shown to reestablish muscle force in soman-intoxicated rat diaphragms by interacting directly with nAChRs with a maximum effect at concentrations of 300 µM [45, 46]. The ligand is neither subtype- nor species-selective, indicating that MB327 can bind to a binding site highly conserved among several nAChR subtypes and species [45, 47, 52, 161]. Furthermore, *in vivo* experiments revealed that MB327, in combination with hyoscine and physostigmine, protects guinea pigs against OPC poisoning [44]. While these results indicate that MB327 can resensitize overstimulated nAChRs, solid-supported membrane-based electrophysiology experiments showed that MB327 can additionally enhance the cholinergic effect and increase binding of the orthosteric ligand [46, 47]. Nevertheless, the therapeutic index of MB327 and analogs is quite narrow, as they can cat as inhibitors of nAChRs at slightly higher concentrations - after a maximum muscle force restoration at MB327 concentrations of 300 µM, the restoration decreases at concentrations of 1000 µM [46]. Thus, MB327 is currently not usable in the treatment of OPC poisoning, and further work is needed to understand the underlying mechanisms leading to the positive allosteric and inhibitory effects (**PUBLICATION I**).

Noteworthy, a new paper, published after the work within this thesis was completed, states that MB327 has no positive allosteric modulation impact on nAChRs expressed in *Xenopus laevis* oocytes but, starting at high nanomolar concentrations, acts as an open channel blocker instead [162]. In this study, Haufe *et al.* suggested a binding site for the bispyridinium compounds at the transition region from the TMD to the ECD within the pore of the receptor, in line with the region we predicted for binding (**PUBLICATION I**). They excluded an impact of the expression system on the inhibitory effects of the bispyridinium compounds observed in their studies. However, while they confirmed the inhibitory effects of the bispyridinium compounds in an expression system used earlier to characterize the positive allosteric effect of MB327 (chinese hamster ovary cells), Haufe *et al.* co-applied 30 µM MB327 with the orthosteric agonist acetylcholine (100 µM) [47, 162]. In comparison, experiments performed by Scheffel *et al.* indicated a positive allosteric effect of 30 µM MB327 when co-applied with the orthosteric agonist nicotine (100 µM) [47]. As mentioned above, MB327 shows a very narrow therapeutic index resulting in an inhibitory effect of MB327 at concentrations > 70 µM when co-applied with 100 µM nicotine, as observed by Scheffel *et al.* [47]. Thus, the exchange of the orthosteric ligand from nicotine to acetylcholine might have an impact on the concentrations needed to observe the positive allosteric effect, which might explain why Haufe *et al.* only observed an inhibitory effect of MB327 on nAChRs in this expression system. However, this cannot explain why Haufe *et al.* could only observe a dose-dependent inhibition of nAChRs and no positive allosteric modulation in their initially used expression system (*Xenopus laevis* oocytes), despite starting at high nanomolar MB327 concentrations. Nevertheless, it has been shown that varying experimental setups can lead to contrary ligand binding properties [163, 164] and that nAChRs are prone to be modulated by their lipid environment [165]. Thus, although these findings require further investigations in the future, the fact that MB327 shows beneficial effects in reestablishing muscle force in rat diaphragm assays after OPC poisoning and that MB327 shows beneficial effects in *in vivo studies*, qualifies MB327 to be considered as lead structure to further develop antidotes targeting OPC poisoning.

In recent studies, several symmetrical and non-symmetrical analogs of MB327 with varying chemical properties in their substituents were synthesized and tested for their affinity towards the MB327 binding site [48, 49]. However, out of 56 analogs, only one analog, PTM0022 (Figure 4), bearing an additional phenyl substituent in the 3-position of the pyridinium ring ($pK_i = 5.16 \pm 0.07$ compared to 4.73 ± 0.03 for MB327), showed a substantial increase in binding affinity. Overall, only slight differences regarding affinity could be observed, and selected analogs showed a tight therapeutic index in *ex vivo* activity testing comparable to

MB327 [46, 48, 49]. Additionally, in a recent study, various MB327 analogs were tested for their muscle force restoration properties after OPC poisoning revealing that the linker length correlates with the capability to restore muscle function. A linker length of 2-5 carbon atoms between the *tert*-butyl substituted bispyridinium rings resulted in recovery of OPC poisoned rat diaphragm whereas longer linker lengths failed to recover muscle force [166]. Because MB327, featuring a trimethylene linker, showed the biggest effects on muscle recovery, a series of bispyridinium compounds with a trimethylene linker, analogous to MB327, was synthesized and tested for their capabilities to restore muscle force after soman poisoning [166, 167]. However, none of these compounds showed better muscle force restoration properties compared to MB327 [167]. Thus, it is crucial to identify novel ligands binding to the MB327 binding site that can be used as new lead structures to close the therapeutic gap in OPC poisoning. Recently, progress in this area has been made by our collaboration partners by identifying UNC0646 (Figure 4) displaying increased affinity to the MB327 binding site compared to MB327 [pK_i (UNC0646)= 6.23 ± 0.02; pK_i (MB327) = 4.73 ± 0.03] [48, 50]. However, because of its properties, UNC0646 already violates two rules of Lipinski's rule of five [168] and overall displays unsatisfactory pharmacokinetic and toxicological properties (**PUBLICATION III**). Thus, the identification of structures with novel chemical scaffolds binding to the MB327 binding site and reestablishing muscle force after OPC poisoning to ultimately close the therapeutic gap in the treatment of nerve agent poisoning is of utmost importance (**PUBLICATION III**).

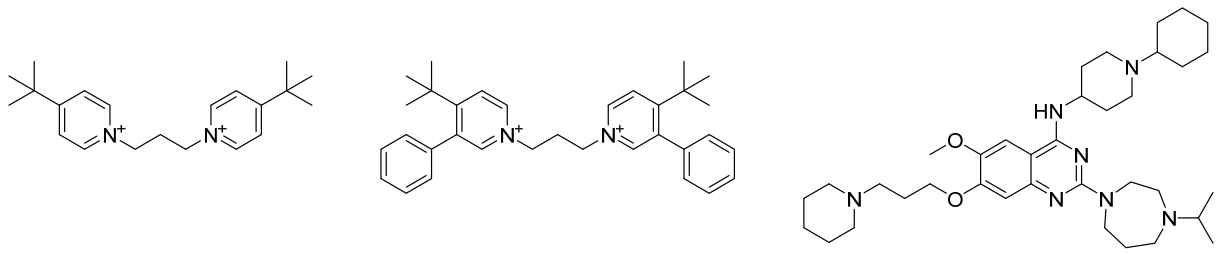

Figure 4: MB327 as a lead structure for PAMs of nAChRs in the treatment of OPC poisoning and later identified more potent binders in the MB327 binding site, PTM022 and UNC0646. Displayed affinity values are reported in ref. [48, 50].

One approach to identify novel binders is rational SBDD (**chapter 2.2.3.1**, **PUBLICATION III**). However, this requires knowledge of the structure, and particularly the binding site of the ligand of interest. For MB327, the binding site remained unknown. Experiments unraveled that MB327 acts as an allosteric modulator of nAChRs and that the affinity to the orthosteric binding site does not correlate with the concentrations needed for the

positive allosteric effects, thus ruling out the orthosteric binding site as the therapeutically relevant binding pocket [46, 52]. However, to further perform rational SBDD, knowledge of the binding site is crucial (**PUBLICATION I**). Therefore, adequate knowledge of the structure of nAChRs is needed.

2.1.4. The nicotinic acetylcholine receptor

The nAChRs belong to the family of the pentameric ligand-gated ion channels and consist of five subunits, each spanning an ECD, four transmembrane helices, and an intracellular domain [64-68, 151, 169-179] (Figure 5A). They can consist of different combinations of various subunits and can be divided into two subtypes, the neuronal-type and the muscle-type [118, 119, 180-190]. The human muscle-type nAChR, which is associated with life-threatening toxicological effects after OPC poisoning, is assembled by two α_1-, one β_1-, one δ-, and one ε- (respectively γ- in the embryonic form) subunit building a heteropentamer [191]. To the best of our knowledge, no PDB structure of the human muscle-type nAChR was available during the preparation of this thesis. Nevertheless, progress in structure resolution has helped further understanding the three-dimensional composition of various nAChRs subtypes, including structural differences in the different states of the receptor. Starting in 2001, several structures of the ACh-binding protein, respectively ACh-binding protein chimeras, a homologue of the ECD of nAChRs, have been published [53-63, 192-216]. Although these structures provided important insights into the structure of the ECD, including the orthosteric binding site, sole structural knowledge of the ECD cannot explain structural differences between the distinct states of the receptor, especially between the active and the desensitized state (Figure 5B). Structural data of nAChRs, including the TMD, was missing until 2005 [217]. However, these first structures only provided a rough insight into the overall architecture of the TMD. Because of a low resolution, residues within the TMD were incorrectly fitted, as verified by later structures and experimental results [64-68, 151, 169-176, 217-220]. The first structure featuring the correct location of transmembrane residues was published in 2015 [151]. Since then, several structures - including the TMD - containing different subtypes of nAChRs from several species were published [64-68, 151, 169-176]. Currently, to the best of my knowledge, PDB structures featuring all three states of the receptor (inactive, active, and desensitized) are available only for one nAChR subtype, the homopentameric neuronal-type α7-nAChR [65].

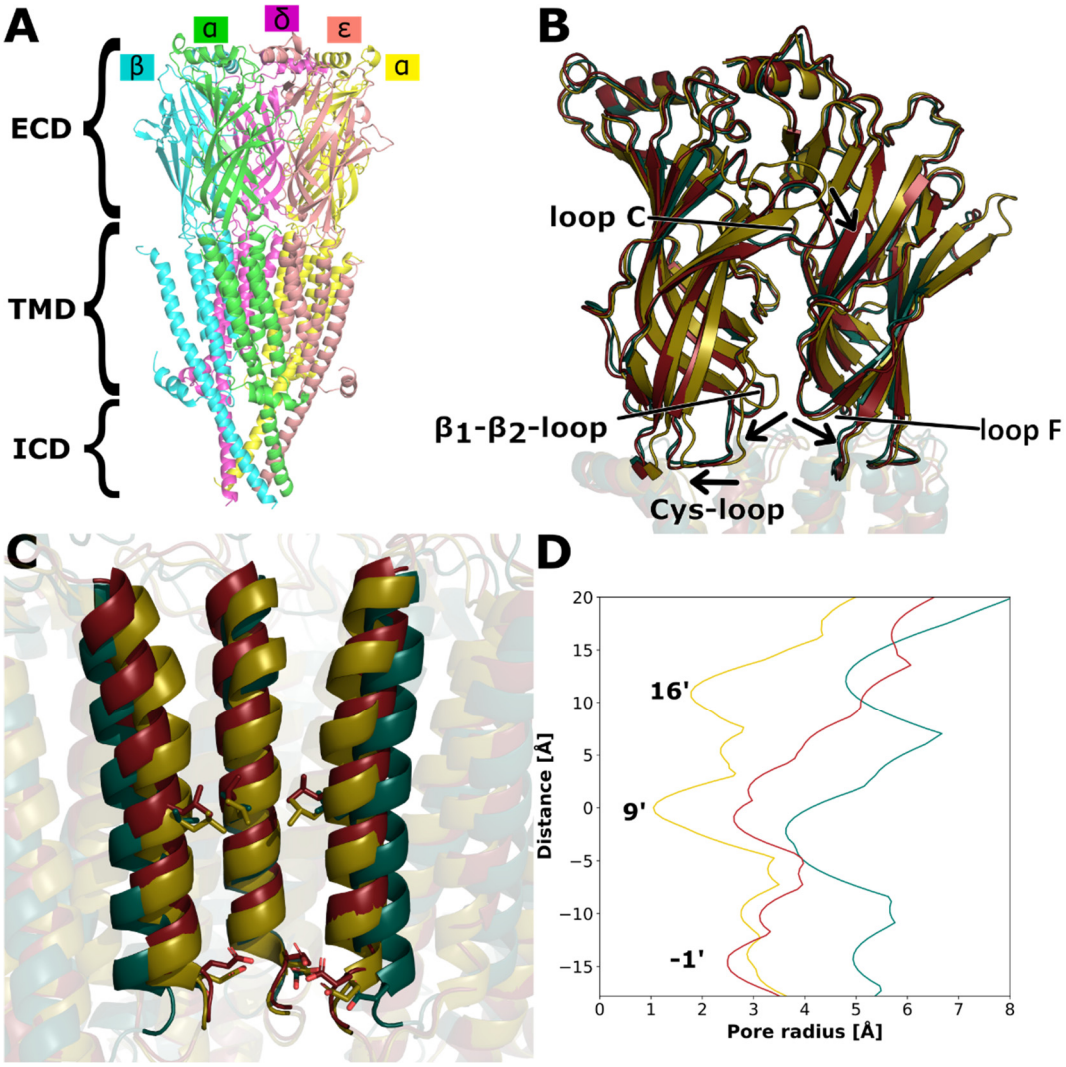

Figure 5: Structural rearrangements during the activation and desensitization cycle of nAChRs. **A)** Side view of the homology model of the human muscle-type nAChR (**PUBLICATION I**, ref. [221]) in the desensitized conformation featuring two α- (green and yellow), one β- (cyan), one δ- (purple) and one ε-subunit (salmon). Curly brackets indicate the location of the ECD, TMD and intracellular domain (ICD), respectively. **B)** Close-up of the ECD of all three states (active state shown in green, inactive state in yellow, and desensitized state in red) of the neuronal α-7 nAChR, the only subtype for which all three states were resolved during preparation of this thesis (PDB IDs: 7KOX, 7KOQ, 7KOO [65]). Arrows indicate differences between the inactive and active / desensitized state. The ECD of the inactive and desensitized state was aligned to the ECD of the active conformation. For clarity, only two subunits are shown. **C)** Close-up of helix 2 of the TMD of the α7-nAChR (PDB IDs: 7KOX, 7KOQ, 7KOO [65]), spanning the transmembrane pore. Amino acids at the inactive constriction site (9', LEU) and the desensitized constriction site (-1', GLU) are shown as sticks. The TMD of the inactive and desensitized state was aligned with the TMD of the active conformation. For clarity, only three subunits are depicted. **D)** Pore radius along the membrane normal of the transmembrane pore for the active (green), inactive (yellow), and desensitized (red) conformation computed with CAVER [222]. The inactive constriction side (9') has been set to 0 Å along the z-axis.

Unraveling the three-dimensional structure of the TMD also shed further light on the differences between the different states of the receptor, even though the mechanisms leading to structural rearrangements resulting in the different states of nAChRs are not fully understood [64-68, 151, 169-176]. The main difference between the states is located within the transmembrane pore region (Figure 5C, D). In the inactive structure, the pore gate is located at positions 9' and 16', inhibiting an ion passing through the receptor [64, 65, 67, 68, 169-172, 174]. In contrast, in the desensitized state, the transmembrane pore region adapts a funnel-shaped conformation with a constriction gate at the position -1' [64-68, 151, 173, 175, 176].

Surprisingly, the amino acid side chains of the glutamates at position -1' are all facing towards the pore, resulting in spatial proximity of the carboxy groups, which might be explained by the fact that some PDB structures of the desensitized state feature a sodium ion present at this position, potentially interacting with the negatively charged side chains [151, 175, 176]. In the active conformation, the pore region remains open so that ions can pass through the receptor [65]. Taken together, the conformation of the TMD varies between all three states. In contrast, as mentioned above, the ECD only undergoes notable structural rearrangements during the transition from the inactive to the active conformation, including the closing of loop C, surrounding the orthosteric binding site, and a movement of the Cys-loop, the β_1-β_2-loop, and the loop F (Figure 5B), as seen in the PDB structure of the α7-nAChR (PDB IDs: 7KOX, 7KOQ, 7KOO), the only PDB entry featuring all three states [65].

Thus, an allosteric ligand needs to bind in a binding site that can convey allosteric impacts on I) the TMD to transfer the receptor from a desensitized to an active conformation and II) the orthosteric binding site to enhance the cholinergic effect of competitive ligands, as described above (**chapter 2.1.3**, **PUBLICATION I**). Identifying the correct binding site and understanding the binding mode of PAMs is of utmost importance to perform LBDD and SBDD. Currently, the pocketome of nAChRs and, thereby, the binding site of PAMs remains incompletely understood. However, advances in structure resolution have not only helped to distinguish between the different states of nAChRs but have also helped to identify allosteric binding pockets [53-68].

2.1.5. Binding sites of allosteric modulators of nAChRs

PDB structures of nAChRs helped identifying a series of potential allosteric binding sites in nAChRs. First, analyzing the three-dimensional structures of the ACh-binding protein revealed several binding sites of co-crystallized small molecules, such as solvent molecules and buffer ingredients [53-63]. However, while binding of these compounds can occur basically all over the ECD of nAChRs, those compounds do not exhibit drug-like properties and are, in general, way smaller. Thus, not all pockets may be available for bulkier drug-like compounds, such as MB327. However, in the multitude of published nAChR structures, also binding sites for lead- and drug-like compounds were unraveled.

Small molecule compounds, showing properties of lead-like structures, were described to bind to four distinct pockets within the ACh-binding protein: the top pocket, located at the N-terminal helix of nAChRs; the agonist subpocket, located slightly underneath (towards the membrane) the orthosteric binding site; the vestibule pocket, located at the same height as the orthosteric binding site but facing towards the pore region; and the β8-β9 loop site, located in close proximity to the β-sheets 8 and 9 (Figure 6A) [61, 62]. However, all these identified compounds act as inhibitors of the human α7-nAChR [61, 62]. Notably, the agonist subpocket overlaps with the binding site of the inhibitor ketamine in the closely related GLIC pentameric ligand-gated ion channel [223, 224]. Furthermore, the β8-β9-binding site overlaps with the binding site of the inhibitor bromoform in pentameric ligand-gated ion channels from *Erwinia chrysanthemi* [225], further supporting the importance of those binding sites. Although these binding sites give first insights into the pocketome of nAChRs, only inhibitors of the receptor have been described in these pockets, and the lack of the TMD in the structures of the ACh-binding protein might also impact possible binding conformations. To unravel the binding site of the PAM MB327, required to rationally design more potent PAMs, binding sites able to transmit positive allosteric effects within the receptor are required.

Several binding sites for PAMs were described in the literature. The binding site of PNU-120596, an α7-nAChR specific PAM, is located at the upper part (towards the ECD) of the TMD (Figure 6B, C) [64, 226]. This binding site is identical to a recently identified binding site for PAMs, such as benzodiazepines and etomidate, in the closely related $GABA_A$ receptor [227-229], indicating the importance of this binding site for allosteric modulation in pentameric ligand-gated ion channels. However, investigating surrounding amino acids within the PNU-120596-binding site in the α7- and human muscle-type nAChR reveals that sterically demanding amino acids in the human muscle-type nAChR may inhibit binding of PAMs in this

binding site, explaining why PNU-120596 is α7-specific (Figure 6C). Nevertheless, browsing PDB structures of nAChRs in complex with PAMs suggests that these compounds favor binding to the transition of the ECD to TMD (Figure 6B).

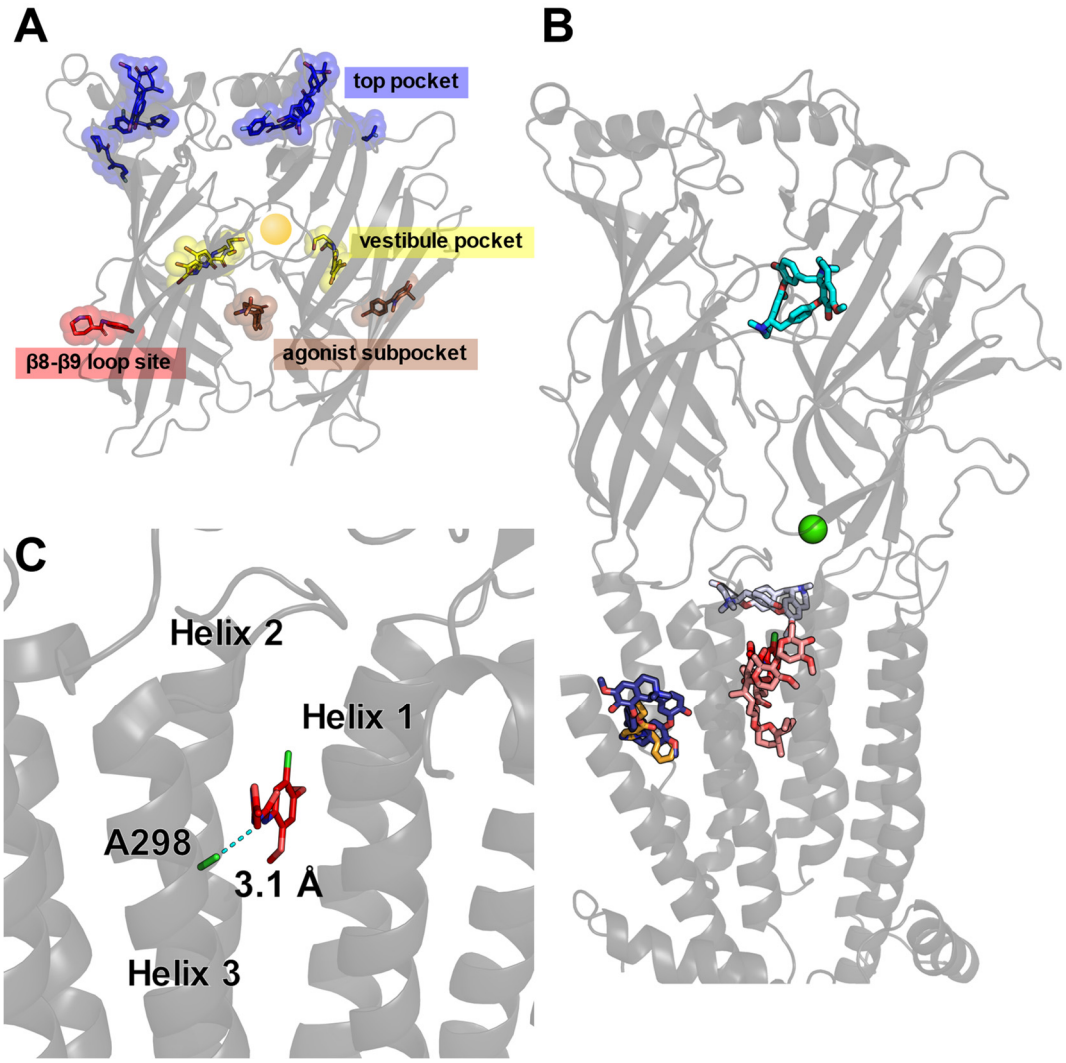

Figure 6: Allosteric binding sites of nAChRs. **A)** Binding sites of negative allosteric modulators in the top pocket (blue), the agonist subpocket (brown), the vestibule pocket (yellow), and the β8-β9 loop site (red) [61, 62]. Structures are aligned to the ACh-binding protein with negative allosteric modulators bound to the top and the agonist subpocket (PDB ID: 5AFJ [61]). The orthosteric binding site is indicated by a sphere colored in eggnog. **B)** Overview of allosteric modulators bound to the transition region from ECD to TMD of nAChRs. Displayed are the positive allosteric modulator calcium (green) [65], ivermectin (salmon) [66], PNU-120596 (red) [64], and the negative allosteric modulator etomidate (orange) [68], as well as the inhibitor *d*-tubocurarin bound to the orthosteric binding site (cyan), the pore region (blue-white), and the TMD (dark blue) [67]. Structures are aligned to the *Torpedo* nAChR in complex with etomidate (PDB ID: 8F6Y [68]). **C)** Close-up of the binding mode of PNU-120596 (red) in the human α7-nAChR (PDB ID: 7EKT [64]). A298 (green) within TMD helix 3 is mutated to leucine or methionine/isoleucine in the human muscle-type nAChR. Thus, the sterically more hindered amino acids would clash with the ligand.

Calcium has been shown to act as a PAM by interacting with E44 and E172 of the human α7-nAChR, located slightly above the TMD – this binding site has been recently verified by PDB structures [65, 69]. Furthermore, ivermectin, a PAM of full length nAChRs, was shown to bind to the upper part of the TMD in a desensitized state of an α7-nAChR construct lacking the ECD, a construct ivermectin can activate in the absence of an orthosteric ligand – this binding pocket

partially overlaps with the PNU-120596 binding site [66, 170, 230] further underlining the importance of the transition of the ECD to the TMD for positive allosteric modulation in nAChRs.

Besides PAMs, negative allosteric modulators also bind in a close region (Figure 6B). In comparison to $GABA_A$ receptors, where etomidate acts as a PAM, the compound transmits negative allosteric effects in nAChRs, binding to a binding site located within the TMD, stabilizing a desensitized state of the receptor [68]. *d*-Tubocurarine, an inhibitor of human muscle-type nAChRs, binds to the orthosteric binding site, inhibiting nAChRs at low concentrations, as observed in a cryo-EM structure of the muscle-type nAChR from the *Torpedo* ray [67, 231]. At higher concentrations, *d*-tubocurarine also binds to two allosteric binding sites – one located within the transmembrane pore region and one located at the upper part of the TMD [67]. It is noteworthy that all structures of nAChR in complex with *d*-tubocurarine, whether an agonist is present or not, represent a desensitized-like conformation [67]. This complex binding behavior is not unique for *d*-tubocurarine. Benzodiazepines such as diazepam can also bind into a second allosteric site located within the extracellular domain in $GABA_A$ receptors [227, 228]. Despite the overlap of the ivermectin and PNU-120596 binding site, the activation of the α7-nAChR construct lacking the ECD can be enhanced by coapplying PNU-120596 to ivermectin [170]. Thus, further binding pockets might have an impact on the positive allosteric impact of either compound, emphasizing the complexity of binding of allosteric modulators in nAChRs and related receptors.

Taken together, these results indicate that the pocketome of nAChRs is highly complex, and a variety of binding sites can transmit allosteric effects on the receptor. Nevertheless, the results also indicate that PAMs especially favor binding to the transition between the ECD and the TMD, giving insights in which region MB327 might bind. PAMs often interact with a binding pocket located at the upper part of the TMD in between helix 1, 2, and 3 in nAChRs and $GABA_A$ receptors. Nevertheless, to the best of my knowledge, all compounds binding to this binding site are not charged under physiological conditions. In comparison, calcium, a charged PAM, such as MB327, binds in a nearby binding pocket located slightly above the TMD. However, no single binding site for all PAMs can be identified, and thus, the potential binding site for MB327 needs to be identified. Computational methods can be a useful tool to identify binding sites of known binders (**PUBLICATION I**, **chapter 2.2.2**).

Using *in silico* methods, three binding sites for MB327 and analogous bispyridinium compounds were already suggested in the literature [70, 232]. First, Wein *et al.* [232] proposed

that MB327 may bind in two binding sites located in the human muscle-type nAChR. However, because a PDB structure of nAChR (PDB ID: 2BG9 [217]) with a low resolution and an improper fitting of the transmembrane residues, as revealed by later experiments and newer PDB structures of nAChRs, was used, one of these two binding sites is nonexistent [64-68, 151, 169-176, 217, 218, 232]. The second proposed binding site is located in the extracellular domain (ECD), an area that was correctly resolved in the used PDB structure [232]. However, as described above, allosteric modulators impacting the desensitized state of nAChRs, such as MB327, often bind to the transition of the ECD to the TMD.

Additionally, Epstein *et al.* [70] performed docking experiments, MD simulations (**chapter 2.2.2**), and mutagenesis experiments to show that related bispyridinium compounds can bind to the orthosteric binding site, inhibiting nAChRs [70]. While these results are in line with our findings (**PUBLICATION I**), this binding site may only explain the inhibitory effect of MB327. However, as mentioned above (**chapter 2.1.3**), the therapeutically relevant effect is a positive allosteric modulation of nAChRs [46].

Thus, the correct binding site of MB327, responsible for the therapeutically relevant effect, remained elusive prior to my thesis and needed to be identified. This binding site can then be used to perform SBDD to identify more potent MB327 and UNC0646 analogs as well as novel lead structures with higher efficacy in the treatment of OPC poisoning (**PUBLICATION I**, **PUBLICATION III**, and **PUBLICATION IV**). This may help to finally close the gap in OPC poisoning treatment in the future. To achieve this goal, we focused on using *in silico* methods. The following chapter will give insights into those techniques.

2.2. In silico methods used in the development of novel ligands

Nowadays, SBDD is widely used to rationally develop novel ligands for proteins of interest and has been proven successful in the development of various clinically approved drugs, starting with the angiotensin-converting enzyme inhibitor captopril in 1977 [233-243]. A quick PubMed (https://pubmed.ncbi.nlm.nih.gov/) search for the term "structure-based drug design" reveals more than 9,000 publications until 2023 with more than half of it published between 2017 and 2023, demonstrating the increasing importance of such techniques. Within this thesis, this approach shall be used to develop novel binders in the MB327 binding site. The following chapters will provide insights into the workflow used to perform computer-aided rational drug design (Figure 7), starting with homology modeling of proteins (**chapter 2.2.1**), including a discussion of newly available machine learning based tools to predict protein structures, such as AlphaFold [244, 245], followed by methods to identify novel binding sites in proteins (**chapter 2.2.2**) and an overview of how known ligands can be optimized, and how to identify ligands with novel chemotypes (**chapter 2.2.3**).

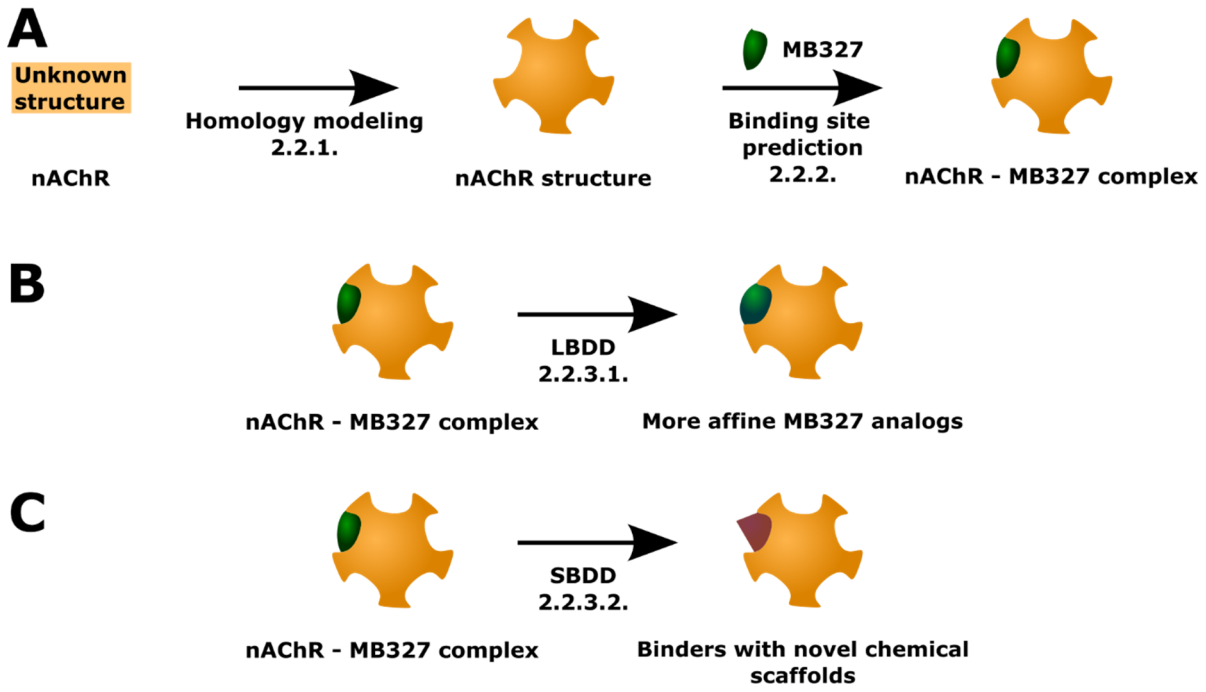

Figure 7: Schematic overview of methods used to identify novel binders in the MB327 binding site. **A)** At the beginning of this thesis, no structure of the human muscle-type nAChR was published. Thus, first, a high-quality homology model needed to be generated to predict the binding site of known binders, such as MB327. Knowledge of the binding site is of utmost importance to **B)** perform LBDD based on the three-dimensional conformation of the ligand within the binding site to identify analogs of known binders with increased affinity and **C)** to perform SBDD to identify binders with novel chemical scaffolds. Numbers under each method refer to the respective chapter describing the method.

To verify my predictions, I worked in close collaboration with experimentalists at the Ludwig Maximilians University in Munich and the Bundeswehr Institute of Pharmacology and Toxicology. There, synthesis and *in vitro* affinity measurements of the new compounds towards

the MB327 binding site and *ex vivo* activity measurements in soman-poisoned rat diaphragm were conducted (Figure 1).

2.2.1. Homology modeling

One way to retrieve high-quality protein structures, important to understand the binding mode of known ligands and identify more potent binders, is by retrieving their three-dimensional structural data from the PDB [88] (https://www.rcsb.org/). However, this presupposes that the structure of the protein of interest has been experimentally resolved and publicly deposited in the PDB. Nevertheless, for a huge number of proteins, including the human muscle-type nAChR, no three-dimensional structure is available yet. As an illustration, in 2021, less than half of the proteins encoded by the human genome were resolved and deposited in the PDB [246], illustrating the need for structure prediction approaches to generate high-quality models. One way to do so is by performing homology modeling, where the three-dimensional structure of proteins is predicted based on homologues with known structures. Therefore, first, a template structure needs to be identified based on the protein sequence. In general, it is considered that a sequence identity of ~30% is sufficient to generate high-quality models [247-249]. For instance, several PDB structures of different nAChR subtypes from various species in the desensitized state have been deposited in the PDB, all sharing a similar three-dimensional structure, despite sharing minimum sequence similarity of partially slightly less than 30% [64-68, 151, 173, 175, 176]. To identify potential target structures, several sequence comparison software packages are available, such as NCBI BLAST [250, 251], FASTA [252], and the HH-suite [253], or are directly implemented in homology modeling software packages, such as MODELLER [254], MOE [255], or TopModel [256]. Received sequence alignments can be further verified using alignment softwares considering the three-dimensional structure of template proteins, such as PROMALS3D [257]. Naturally, searching the PDB for highly related protein structures, such as structures of the same protein from different species, or with alternative subunits, can also lead to the desired outcome. In the case of the human muscle-type nAChR, no structure of the receptor itself is available in the PDB, but as aforementioned (**chapter 2.1.4**), several PDB structures, including different states of human nAChRs featuring alternative subunits and nAChRs of different species were deposited in the PDB making homology modeling approaches for the human muscle-type nAChR feasible [64-68, 151, 169-176]. After alignment of the sequences, homology modeling can be performed using a variety of software packages [254, 255, 258-265]. One regularly used software is MODELLER [254, 265]. This method applies the approach of satisfying spatial restraints to generate protein models. Therefore, first, the template structure distance and dihedral angle restraints are derived

from the alignment and then combined with CHARM22 force field terms into an objective function, which is then optimized in Cartesian space [254, 265-268]. However, side-chain and loop modeling can often lead to problems in model generation, especially if the sequence identity in the loop regions is low. Loops can consist of only a few amino acids, and fold prediction based on these short sequences can be challenging. For instance, identical amino acid sequences with up to seven positions can be found in both α-helices and β-sheets [269, 270]. To avoid wrong predictions based on databases, MODELLER uses conjugate gradient minimization in combination with MD simulations with simulated annealing for model optimization [265-267]. However, especially predicting loops consisting of longer sequences is often challenging since these are often not resolved in PDB structures and therefore templates for these loops are missing. Furthermore, side-chain conformations can often vary in the generated model, even if the amino acid is identical in the template. Thus, a thorough inspection of the amino acid side-chain conformation in the active site is of utmost importance. Amino acids can then be altered by choosing rotamers based on rotamer libraries, such as backbone-dependent libraries [271], MD-simulation-based libraries [272], or by energetical optimization using programs such as MOE [255]. However, the need to optimize side-chain conformations highly depends on the intended use of the model. If the model is used for MD simulations (**chapter 2.2.2.2**), receptor plasticity will be considered, and thus, orientations of the side chains will adapt energetically favored conformations based on force field parameters. However, if the protein will be used for molecular docking (**chapter 2.2.2.1**), side-chain optimization is of utmost importance to improve the likelihood of identifying potent hits interacting with the sidechains in the binding pocket.

Noteworthy is the recent progress in machine learning, which has provided new powerful methods to predict protein structures, such as TopModel [256] and AlphaFold [244, 245]. However, while TopModel was available during model generation of the nAChRs described in this thesis and AlphaFold became available shortly afterwards, two main limitations discouraged using these software packages. Although knowing the exact conformation of all amino acids within the binding site associated with a particular state of the receptor is crucial in drug design workflows, AlphaFold predicts the three-dimensional structure of a protein based solely on the amino acid sequence without considering the different states of a protein. In TopModel, certain models can be excluded or specifically included in template selection, and thereby, a certain state of the receptor can be targeted directly. However, the main limitation was that both approaches only predict single-chain models of the receptor that needed to be aligned in a specific order subsequently. Because only individual chains were predicted, side-

chain conformations often overlapped after aligning the subtypes. This shortage could be overcome by using MODELLER [265], where multimeric modeling is possible. Nowadays, after the modeling of nAChRs within this thesis was finished, new tools, such as ColabFold [273] and AlphaFold-Multimer [274], are available to predict models of complexes. However, because of the high sequence identity to several nAChR PDB structures, all sharing a similar three-dimensional structure, homology modeling can be considered as a trustworthy tool to predict models of high quality. Noteworthy, the release of the recently published Alphafold3 [275] even allows modeling of protein structures in complex with small molecules. Nevertheless, this is currently limited to very few biologically common ligands and thus cannot be used to predict the binding modes for PAMs of nAChRs. After models of the protein of interest are generated successfully, these structures can be used to identify the binding site of known binders, such as MB327.

2.2.2. Identification of novel binding sites

Several methods may be used to identify binding sites in proteins. One straightforward way is to analyze protein structures based on cavities and the properties of the amino acids enclosing this cavity, such as SiteFinder, as implemented in MOE [255], SiteMap, as implemented in Maestro [276-279], or the DoGSiteScorer, as implemented in the Proteins*Plus* server [280-282]. Furthermore, small molecule fragments with differing chemical properties can be used to dock over the full protein to unravel the pocketome [283]. These approaches are a good first step to identify allosteric binding sites, but a clear shortage is that they identify potential binding sites without considering the chemical properties of known ligands. For instance, known binders in the MB327 binding site always feature a least one positive charge [45, 46, 48-50], and therefore, negatively charged amino acids are most likely to occur in the binding site while a oppositely charged environment would be favored to bind negatively charged ligands. Thus, if a binding site is searched for a specific ligand, these techniques can only be used as a first indicator to identify potential allosteric sites. Crystal structures have also already revealed that a large number of allosteric binding sites can be targeted in nAChRs (**chapter 2.1.5**) [53-68]. To account for the chemical properties of MB327, such as charge, ligand size, and hydrogen bond donor / acceptor atoms, other approaches, such as blind docking experiments and free ligand diffusion MDs, may be used.

2.2.2.1. Molecular docking

Molecular docking is a widely used technique to predict the binding mode of a ligand and has been applied to a variety of target proteins [284-293]. A huge variety of methods is available

for this purpose [294-303]. One main feature of all these methods is that the ligand first needs to be placed in the binding site, followed by a scoring of the pose based on scoring functions. However, both the pose generation and scoring of the pose can vary largely between docking approaches. For instance, FRED uses an exhaustive search approach exploiting all possible translations and rotations of rigid conformers of the ligand of interest within the specified binding site. Poses clashing with the receptor are then discarded, and all leftover poses are subsequently scored and optimized [300]. In comparison, AutoDock relies on Lamarckian genetic algorithms where the conformers of the ligand of interest are being produced during the docking process to generate potential binding poses within the binding site [295]. For scoring poses, three main approaches are available. Physics-based scoring functions rank the poses according to an energy value derived from mathematical equations, generally featuring enthalpic terms, such as van der Waals and electrostatic energy terms [255, 301, 304]. Empirical scoring functions use weighting factors based on available experimental data [296, 305-311]. Knowledge-based scoring functions make use of the large number of protein-ligand structures that are available in the PDB and are based on a statistical assessment of frequently observed interactions [310, 312-316]. However, despite these differences, no single docking-scoring combination can be considered to be universally superior to other approaches, depending *inter alia* on the target system and ligand properties [316-327].

While docking is generally mainly used to gather information on the orientation of a ligand in a known binding pocket, blind docking studies can be used to dock the ligand of interest to the whole receptor and thereby identify its potential binding site [328-339]. In fact, this method was used to identify allosteric binding sites of negative allosteric modulators in nAChRs, and the proposed binding site was verified by mutational studies [339]. Currently, only a few methods have been developed specifically for blind docking [340-348]. These approaches often focus on, first, identifying potential binding sites within the protein without considering known ligand properties, followed by docking the ligand inside these binding sites [340-342, 344, 348]. This approach entails the risk of missing out on the correct binding site during initial binding site identification and thereby predicting a wrong binding site. To avoid overlooking the correct binding site, docking can also be performed on the whole protein using classical docking software packages and has been proven to be a successful tool for several known protein-ligand complexes using AutoDock as a docking engine [329]. For nAChRs, it has been shown that blind docking experiments can correctly predict the orthosteric binding site, and the predicted allosteric binding sites of galanthamine and negative allosteric modulators are in line with experimental results [338, 339]. Thus, blind docking can be a powerful tool to predict allosteric

pockets of known allosteric binders in nAChRs, such as MB327 (**PUBLICATION I**). Nevertheless, one shortcoming of molecular docking is that only a rigid structure is being considered, while proteins consist of amino acids with highly flexible side chains. Approaches to account for this flexibility are I) flexible docking approaches, such as those implemented in MOE [255], which allow the amino acid side chains to adapt several conformations during docking; II) to perform docking to several models featuring different side-chain conformations, this way considering protein flexibility implicitly; and III) MD simulations, often used to further solidify docking results [284, 285, 289, 290, 292, 293].

2.2.2.2. Molecular dynamics simulations

To account for the plasticity of the receptor during ligand binding, MD simulations can be performed. In MD simulations, equations of motion are solved numerically, resolving protein and ligand movements over short periods of time. Thus, MD simulations overcome the shortage of molecular docking with respect to only considering rigid receptors. However, while this method is more accurate compared to molecular docking, it also requires far more computational resources. MD simulations are, therefore, often used to validate the assumptions drawn from docking studies further by simulating the protein-ligand complex [284, 285, 289, 290, 292, 293]. Nevertheless, MD simulations can also be used to predict novel binding sites of known binders within a protein. In these free ligand diffusion MD simulations, the ligand is placed at random positions outside the receptor, and the movement of the ligand during the simulations is observed [289, 349-361] (**PUBLICATION I**). However, these free ligand diffusion MD simulations are generally limited by computational resources, with simulation times typically in the low µs range. Thus, ligands stuck in low-affinity binding sites can generate false positive results. For instance, as previously discussed, it is known that PAMs of pentameric ligand-gated ion channels, such as diazepam in $GABA_A$ receptors, may target multiple binding sites [227, 228]. Also, rocuronium and *d*-tubocurarin, inhibitors of nAChRs, can bind to multiple binding sites, indicating that nAChR ligands can feature complex binding properties [67, 68]. Thus, free ligand diffusion MD simulations might miss one of these binding sites for either compound. Furthermore, considering the maximum diffusion-limited association rate constant (k_{on}) of 10^9 M^{-1} s^{-1} [362] and ligand ([L]) and protein concentrations ([P]) of 1 mM – which is approximately in line with our free ligand diffusion MD simulations where concentrations of the receptor and ligand are slightly lower than 1 mM (**PUBLICATION I**) – the association rate would be 10^3 mol l^{-1} s^{-1} according to equation 1 [363]:

$$\boldsymbol{Association\ rate = k_{on} * [L] * [P]} \quad \textbf{(1)}$$

Thus, only when considering the diffusion-limited association rate constant and ligand and protein concentrations slightly higher than in our simulations, all ligands should be bound to the protein after 1 µs long simulations. However, as mentioned, the concentrations in the simulations of MB327 binding to nAChR performed within this thesis are even lower, which would lead to an incomplete binding, and the association rate constants measured in experiments can differ widely from 10^3 to 10^9 M^{-1} s^{-1} [364-386]. Thus, simulating 1 µs will, dependent on the k_{on}, not be sufficient to use free ligand diffusion MD simulations to predict the correct binding site for the ligand of interest. Although a low k_{on} value might result in binding in one replica, this funding would not be considered as reliable since observations in single replicas can often indicate false positives [387]. Nevertheless, it could be shown that free ligand diffusion MD simulations are a valuable, widely used tool in predicting binding sites [289, 349-361], including reproducing the binding site from PDB structures [350, 352, 361]. Once a potential binding site of MB327 is identified, further postprocessing of trajectories generated during MD simulations, such as rigidity analysis, can be performed to predict whether the identified binding site can account for the experimentally measured allosteric effects on the receptor.

2.2.2.3. Investigating allosteric ligand impacts through rigidity analysis

The rigidity of proteins can be investigated using our in-house software Constraint Network Analysis (CNA) to analyze the allosteric impacts of ligands on the protein [388]. CNA computes a network of bonds indicating covalent and non-covalent interactions between each residue (Figure 8) and groups the network into rigid and flexible regions. These networks are then subject to a constraint dilution simulation of the protein. Based on these simulations, the neighbor stability maps, indicating the local stability of the network, may be generated. This map features the rigid contacts between each residue (*i*) to all other residues within the protein (*j*), respectively, indicating the energy cutoff E_{cut} at which both residues do not belong to the same rigid cluster anymore. Based on this result, a chemical potential energy $E_{i,CNA}$ can be computed by summation over all contacts of residue *i* (Eq. 2) [388, 389]:

$$\boldsymbol{E_{i,CNA} = \frac{1}{2}\sum_{i \neq j}^{n} rc_{ij,neighbor}} \quad \textbf{(2)}$$

Based on these assumptions, the allosteric impact of a ligand on the protein may be computed as follows: Two dilution runs need to be performed, one in the presence of the ligand and one in the absence of the ligand (perturbed system). Thereby, we can compute $\Delta G_{i,CNA}$ (Eq. 3) by subtracting the chemical potential energy for each residue in the presence of the ligand from the chemical potential energy in the absence of the ligand, an approximation according to the linear interaction energy approach [388-391].

$$\boldsymbol{\Delta G_{i,CNA} = \frac{1}{2}(\langle E_{i,CNA}^{perturbed}\rangle - \langle E_{i,CNA}^{ground}\rangle)} \quad \textbf{(3)}$$

This value gives insights into which parts of the protein may be stabilized upon ligand binding. In the case of MB327, we would, therefore, expect to see two impacts on the receptor. First, the properties of MB327 that lead to reestablishing muscle force after soman poisoning indicate a resensitizing effect [45, 46]. Because structural differences between the active and desensitized conformation mainly occur in the TMD, we expect that MB327 allosterically impacts this region [64-68, 151, 173, 175, 176]. Second, MB327 has been shown to allosterically enhance the cholinergic response in nAChRs [46, 47]. Thus, MB327 most likely also exhibits allosteric effects on the orthosteric binding site. This approach can help to further support the newly identified binding site using *in silico* methods (**PUBLICATION I**). Once the potential binding site of MB327 is identified, rational computer-aided drug design approaches can be applied to subsequently optimize known chemotypes and identify novel chemotypes resensitizing nAChRs.

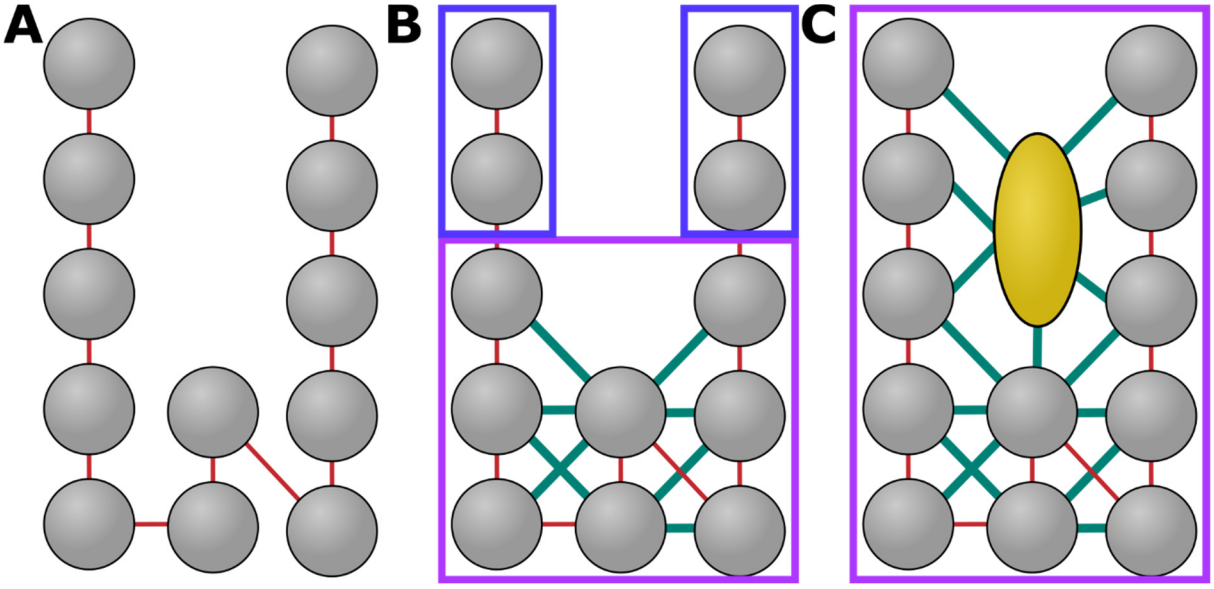

Figure 8: Schematic overview of the network generated with CNA. **A)** The amino acids within one protein (grey spheres) are connected via covalent bonds (red). **B)** Besides covalent bonds, amino acids may interact via non-covalent interactions (green), such as hydrogen bonds, leading to rigid clusters (purple) and flexible regions (blue). **C)** The addition of a ligand (yellow) introduces further non-covalent bonds, rigidifying the network.

2.2.3. Identification of novel analogs and chemotypes binding to MB327-PAM-1

Computational drug development approaches can be mainly divided into two classes. On the one hand, new ligands can be developed based on the structure of known ligands (LBDD), ideally resulting in compounds with an analogous structure but improved activity. On the other hand, ligands can be designed based on the three-dimensional structure of the residues spanning the ligand binding site (SBDD). This approach can help optimize known ligands but can also be used to identify novel chemotypes to act as new starting points in ligand optimization.

2.2.3.1. Ligand-based drug design

In LBDD, novel ligands are being designed based on the structure of known binders. For this purpose, the two- or three-dimensional structure can be considered. Usage of the three-dimensional structure may generally result in a more precise prediction because it is being considered whether analogs can adopt three-dimensional conformations analog to the bound ligand. To compare structures, several approaches were developed [255, 392-409]. One widespread method to identify analogs based on the two-dimensional structure is to compute fingerprints, such as the path-based Daylight fingerprints [403] that create a fingerprint for every compound based on fragments of the respective compound, followed by calculating a similarity coefficient, such as the Tanimoto score [406] (Eq. 4),

$$T = \frac{C}{A + B - C} \quad (4)$$

where T is the Tanimoto score, A and B are the number of features in the two compared compounds, respectively, and C is the number of features present in both compounds. Thereby, a similarity index is computed where values can range from 0 to 1, and higher values correspond to a higher similarity. This approach has been adopted for three-dimensional similarity searches using ROCS, where a Tanimoto score based on the shape of the ligand is combined with a color-based score which considers the overlap of points of defined molecular recognition properties within a ligand compared to the screened compounds [407], resulting in a method successfully used in drug discovery projects [289, 408, 410-421], including discovering allosteric modulators of nAChRs [422, 423]. However, while this approach is promising (**PUBLICATION III**), the fact that only compounds with similar structural features as already known compounds will be identified, restricts the identification of novel chemical scaffolds. To identify PAMs with novel chemical scaffolds, structure-based screening approaches may be conducted.

2.2.3.2. Structure-based drug design

To utilize SBDD approaches, knowledge of the binding site (**chapter 2.2.2**, **PUBLICATION I**) is fundamental. SBDD can then be performed by inspecting the binding mode and creating analogs of the known binders to optimize interactions with the receptor or by screening databases of chemicals to identify novel binders. Therefore, all compounds within a database containing up to millions of compounds are being docked in the binding site, and the resulting poses are being ranked using scoring functions to identify the best binders (**chapter 2.2.2.1**). Structure-based approaches have been successfully applied to identify novel nAChR binders [200, 203, 424]. However, as mentioned above, one shortcoming of docking approaches is that the receptor is generally rigid. Also, solvent atoms are commonly not included in the binding site despite often forming hydrogen bond bridges between ligand and receptor atoms [425-440]. Thus, similar to blind docking pipelines, binding poses can be further refined and affirmed using all-atom MD simulations. During this, entropically unfavored water molecules may be identified. Substitution of those water molecules may lead to analogues with increased binding affinities.

2.2.3.3. Adjusting ligand substituents to displace entropically unfavored water molecules

In many ligand binding events, water bridges the ligand to residues in the active site via hydrogen bonds [425-440]. In drug discovery efforts, substituting unfavorable water molecules with substituents of the ligand repeatedly led to potent binders [441-448]. MD simulations can be performed and post-processed to identify regions of unfavorable water molecules using the Grid Inhomogeneous Solvation Theory (GIST) tool [449]. In contrast to a variety of commercial softwares, such as WaterMap [450, 451], which only examines high-occupancy water sites, GIST operates by first spanning a three-dimensional grid over the binding region, and then computing density-weighted thermodynamic quantities of each voxel, and thereby also covering regions of low-density water [449]. As for the MB327 binding site, sterically more demanding ligands, such as UNC0646, bind with a higher affinity compared to MB327 [50]. Thus, it is likely that the binding site is still partly water filled when MB327 is bound. Therefore, GIST may be used to identify entropically unfavored water molecules and identify more potent MB327 analogs substituting these water molecules (**PUBLICATION IV**).

Taken together, computational methods are crucial and widely used in drug discovery projects. Both the identification of the binding site and the identification of novel binders have been successfully conducted using *in silico* techniques for several targets, including nAChRs. Thus, applying these techniques to nAChRs to close the therapeutic gap in treatment after nerve agent poisoning can be promising. In fact, applying blind docking, I first identified a novel potential binding site of MB327, MB327-PAM-1, within the human muscle-type nAChR, located at the transition of the ECD to the TMD, in line with the binding site location of other PAMs in nAChRs. I then performed MD simulations to support our assumption and used free ligand diffusion MD simulations to identify a second binding site of MB327 located within the orthosteric pocket. This finding is in line with recent results for related bispyridinium compounds and probably responsible for the inhibitory effect of MB327 [70] (**PUBLICATION I**). Further studies using molecular docking in combination with MD simulations revealed that the novel more affine ligand UNC0646 might also bind in MB327-PAM-1 (**PUBLICATION II**). Based on these results, ligand- and structure-based screenings were performed to identify MB327 analogs with higher activity in reestablishing rat diaphragm muscle force after nerve agent poisoning (**PUBLICATION I** and **PUBLICATION IV**), alternative substituents at the quinazoline moiety of UNC0646 with a higher affinity compared to the UNC0646 substituents were described, and most interesting I identified four new chemical scaffolds binding to MB327-PAM-1, including cycloguanil, an active metabolite of

the antimalaria drug proguanil [71, 72], demonstrating a higher potency in reestablishing muscle force after nerve agent poisoning than MB327 and UNC0646 (**PUBLICATION III**).

3. SCOPE OF THE THESIS

Despite being internationally banned, OPCs remain a serious threat to civilian and military populations. The toxicity of OPCs is based on their inhibition of the AChE, an enzyme involved in the decomposition of ACh in the synaptic gap, resulting in enhanced concentrations of ACh. This triggers overstimulation of mAChRs, associated with symptoms such as nausea and miosis, and nAChRs, associated with muscle weakness and respiratory paralysis. Currently, the treatment of OPC poisoning remains unsatisfactory, with no treatment option targeting the nAChR directly (**chapter 2.1.2**).

Recently, progress has been made by identifying MB327, a PAM of nAChRs, able to reestablish the muscle force of soman-poisoned rat diaphragm. However, MB327 has a narrow therapeutic index. At higher concentrations, it acts as an inhibitor of the receptor, making it impossible to use MB327 for treatment. Analogs of MB327 have, so far, shown only slightly increased affinity compared to the lead structure. Recently, UNC0646, binding to the MB327 binding site with a higher affinity compared to MB327, has been identified (**chapter 2.1.3**). However, experiments performed at the Bundeswehr Institute of Pharmacology and Toxicology in Munich showed that UNC0646 is less potent with respect to reestablishing muscle force after soman poisoning compared to MB327 (**PUBLICATION II**). Thus, to close the therapeutic gap in OPC poisoning treatment, further positive allosteric modulators need to be identified, and known binders need to be optimized. At the beginning of this thesis, little knowledge about the binding site of MB327 made computer-aided drug design approaches challenging.

Based on these observations, several questions arose:

- Where can MB327 bind, and how can this binding site explain the positive allosteric effect as well as the inhibitory effect of MB327 on nAChRs (**PUBLICATION I**)?
- How does UNC0646 bind to the novel identified binding pocket (**PUBLICATION II**)?
- How can MB327 and UNC0646 be optimized to generate more potent PAMs (**PUBLICATION I**, **III** and **IV**)?
- Are there other chemical scaffolds binding to the MB327 binding site, reestablishing the muscle force after soman poisoning, that can be considered as novel lead structures to ultimately close the therapeutic gap in OPC poisoning (**PUBLICATION III**)?

Within this thesis, those questions were addressed, resulting in the following publications.

4. PUBLICATION I

A novel binding site in the nicotinic acetylcholine receptor for MB327 can explain its allosteric modulation relevant for organophosphorus-poisoning treatment

J. Kaiser, C.G.W. Gertzen, T. Bernauer, G. Höfner, K.V. Niessen, T. Seeger, F.F. Paintner, K.T. Wanner, F. Worek, H. Thiermann, Gohlke, H

Toxicol Lett**,** 2023. **373**: p. 160-171.

Original publication, see pages 69 - 105.

The content covered in this chapter is taken from “A novel binding site in the nicotinic acetylcholine receptor for MB327 can explain its allosteric modulation relevant for organophosphorus-poisoning treatment” [221]. Sentences containing word-by-word citations are not highlighted explicitly.

4.1. Author contributions

J.K. performed modeling, screening, rigidity analysis, docking, and MD simulation experiments. C.G. supported the computational experiments. T.B. synthesized analogs of MB327 and T.S. performed rat diaphragm assays. H.G. conceived the study and supervised the project. G.H., K.N., F.P., K.W., F.W. and H.T. supervised respective study parts. All authors contributed to writing the manuscript.

4.2. Background

OPC poisoning remains a serious hazard to civilian and military populations [1]. Covalent inhibition of AChE by OPCs leads to an increase of ACh in the synaptic gap, resulting in several toxicological symptoms, such as nausea and miosis, triggered by mAChR overstimulation, and muscle weakness and respiratory paralysis, provoked by overstimulation and subsequent desensitization of nAChRs [1, 5, 6, 18-23]. Current treatment options focus on targeting mAChRs directly using the inhibitor atropine and both receptors indirectly by reactivating AChEs using oximes [1]. However, many OPCs are insensitive to certain oximes, and oximes are mostly ineffective after an aging process of the inhibited AChE [1, 26, 28, 39-43]. No treatment option is available targeting the desensitized nAChR directly.

Recently, MB327 has been identified, able to reestablish muscle force in OPC-poisoned tissue and to enhance the cholinergic effect, acting as an allosteric modulator [44-47]. Thus, this compound is promising as a lead structure to close the therapeutic gap in OPC poisoning

treatment. Nevertheless, MB327 also inhibits nAChRs at slightly higher concentrations, counteracting its positive effects [46]. At the start of this project, the binding site of MB327 remained elusive, making structure- and ligand-based compound optimization demanding.

Here, I used *in silico* methods to predict a novel allosteric binding site of MB327, responsible for the therapeutically relevant effect. I also performed free ligand diffusion MD simulations, unraveling that MB327 may bind in the orthosteric binding site, in line with a recent publication revealing that this binding site is responsible for the inhibitory effect of related bispyridinium compounds [70]. Finally, based on the novel knowledge about the binding mode, new MB327 analogs with increased potency compared to MB327 were designed.

4.3. Results

4.3.1. Utilizing blind docking to identify a potential new allosteric binding site

To identify a potential allosteric binding site of MB327, I first generated homology models of the human muscle-type and the α7-nAChR, two receptors in which MB327 binds using templates of desensitized nAChRs containing different subunits deposited in the PDB [151, 173, 175, 176, 201]. Blind docking experiments were subsequently performed using AutoDock3 [295] as a docking engine in combination with the knowledge-based scoring function DrugScore^{2018} [452], developed in-house. 100 docking runs were performed for each ligand – receptor combination. Because MB327 is permanently double positively charged, it is unlikely that the ligand crosses the membrane in a notable quantity. Therefore, I allowed MB327 to bind to the whole ECD, including the upper part of the TMD, during blind docking experiments. To verify the quality of the models and to ensure that blind docking experiments may lead to the prognosis of the correct binding site, I first performed dockings using the known orthosteric ligand ACh in the human-muscle type nAChR. In line with previous publications [338, 339], ACh was correctly placed in the orthosteric binding site in 58 out of 100 docking runs. This includes 30 poses in the highest-ranked cluster. By comparison, MB327 was favorably placed in a novel identified binding site, MB327-PAM-1, at the transition region of the ECD to the TMD in both the human muscle-type and α7-nAChR (Figure 9). Binding to this binding site was observed in 8 out of the 10 highest-ranked clusters for the human muscle-type nAChR and in 7 out of the 10 highest-ranked clusters in the α7-nAChR, including the biggest cluster in both cases. Since the α7-nAChR features a homopentameric structure, five potential binding sites for MB327, one between each subunit interface, are available. Notably, in the human muscle-type receptor, MB327 was also placed in MB327-PAM-1 of different subunits, indicating a multiplicity of binding sites.

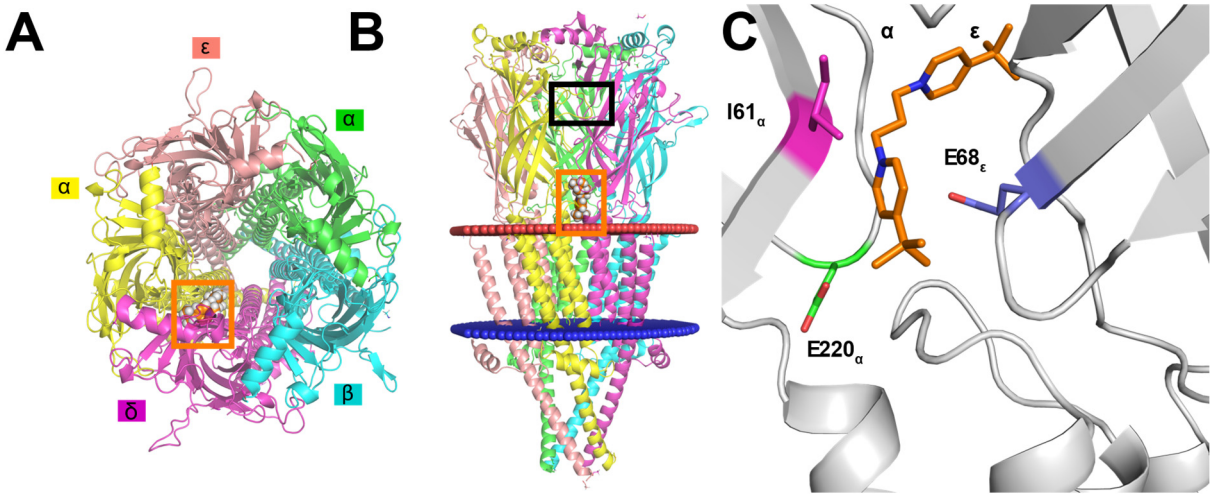

Figure 9: Localization of MB327-PAM-1 within the human nAChR. **A)** Extracellular and **B)** side view of nAChR with MB327 (orange spheres) exemplarily bound in MB327-PAM-1 in between the α- and δ-subunit. The orange and black boxes indicate the location of MB327-PAM-1 and the orthosteric binding site, respectively. **C)** Close-up view of MB327 bound to MB327-PAM-1 in between the ε- and α-subunit. The figure was taken and adjusted from **PUBLICATION I** [221] (see **REPRINT PERMISSION**).

4.3.2. Strengthening the suggestion of the new binding site using MD simulations

To study the impact of receptor plasticity on the binding of MB327 in the novel binding site, I performed 32 replicas of 100 ns long MD simulations of MB327 bound to MB327-PAM-1 in all five subunits of the human muscle-type nAChR. In 122 out of 160 cases (32 replicas à 5 binding sites), MB327 remained bound during MD simulations, as characterized by a distance < 5 Å to the highly conserved isoleucine of β1 [e.g., $I61_{\alpha}$ (Figure 9C)]. This unbinding occurred mainly in between the β- and α- (in 19 out of 32 replicas) and in between the α- and ε-subunit (in 16 out of 32 replicas). I identified two important glutamate side chains ($E220_{\alpha}$ and $E68_{\varepsilon}$, Figure 9C) interacting with the positively charged compound while MB327 remains bound. These two amino acids are highly conserved among different subunits and species of nAChR (Table 1), in line with experimental results that MB327 may bind to different nAChRs [45, 47, 52, 161] and in line with the assumption of MB327 binding to multiple binding sites in the human muscle-type nAChR. To scrutinize why, despite the high amino acid conservation, unbinding occurs in two binding sites, I looked at the docked binding mode of MB327, revealing that in these two binding sites, the distance to the positively charged atoms of MB327 to these two amino acids is > 5 Å, whereas the distance in the remaining three binding pockets to at least one side-chain oxygen is 4.5 Å or less. Thus, an incorrect placement of MB327 during the initial docking may be responsible for the ligand instability in these two binding sites.

Interestingly, $E220_{\alpha}$ of the human muscle-type receptor is located at the same position as E172 of the human α7-nAChR, a crucial amino acid in the stabilization of the positive allosteric

modulator calcium [65, 69], suggesting that positive allosteric modulation can be transmitted via this binding site.

Table 1: Sequence similarity of nAChR subunits at specific positions in various species.[a] Table taken from **PUBLICATION I** [214] (see **REPRINT PERMISSION**).

Human muscle-type				**α7**	**Torpedo marmorata**				**Rat**			
α	β	δ	ε	α7	α	β	δ	γ	α	β	δ	ε
Q	E	E	E68	*Q*	*Q*	E	E	E	*Q*	E	E	E
E220	*Q*	E	E	E	E	*Q*	E	E	E	*Q*	E	E
I61	I	I	I	M	I	L	I	I	I	I	I	I

[a] Amino acids shown in Figure 9C are highlighted with green shadings. Amino acids with deviating chemical properties are written in italics.

4.3.3. Investigation of allosteric impacts transmitted via MB327-PAM-1

To further test the assumption that this binding site can transmit the experimentally measured positive allosteric effects on the receptor, I performed CNA [388] computations of MB327 bound to nAChR. Thereby, I have shown that MB327 bound to MB327-PAM-1 is able to transmit allosteric effects on the orthosteric binding site, in line with experimental results that MB327 enhances the cholinergic effect [46, 47] (Figure 10A). The largest impact in the orthosteric binding side is shown on $W169_{\alpha}$, the only amino acid able interacting with the orthosteric ligand nicotine via a hydrogen bond in the PDB structure of the α3β4-nAChR (PDB ID: 6PV7 [175]). Allosteric effects are being transmitted via the β-sheets in both adjacent subunits with the highest impact on β1, β2, and β6 (Figure 10B). $W78_{\delta}$ of β2 belongs to the highly conserved aromatic residues encompassing the orthosteric ligand nicotine according to the PDB structure of the human α3δ4 nAChR (PDB ID: 6PV7 [175]). Furthermore, β7, β9, and β10 are being allosterically impacted. The orthosteric binding site is being formed by the loops of these sheets. Thus, MB327 binding to each of the five potential MB327-PAM-1 binding sites can have an impact on the orthosteric ligand because, in each case, at least one neighboring subunit is encompassing the orthosteric binding site. Furthermore, MB327 can transmit allosteric effects on the TMD, including the desensitization gate located at the intracellular site of the TMD (Figure 10C, D). This might indicate how MB327 can impact the desensitized state of nAChRs and act as a resensitizer, in line with experimental results [45, 46].

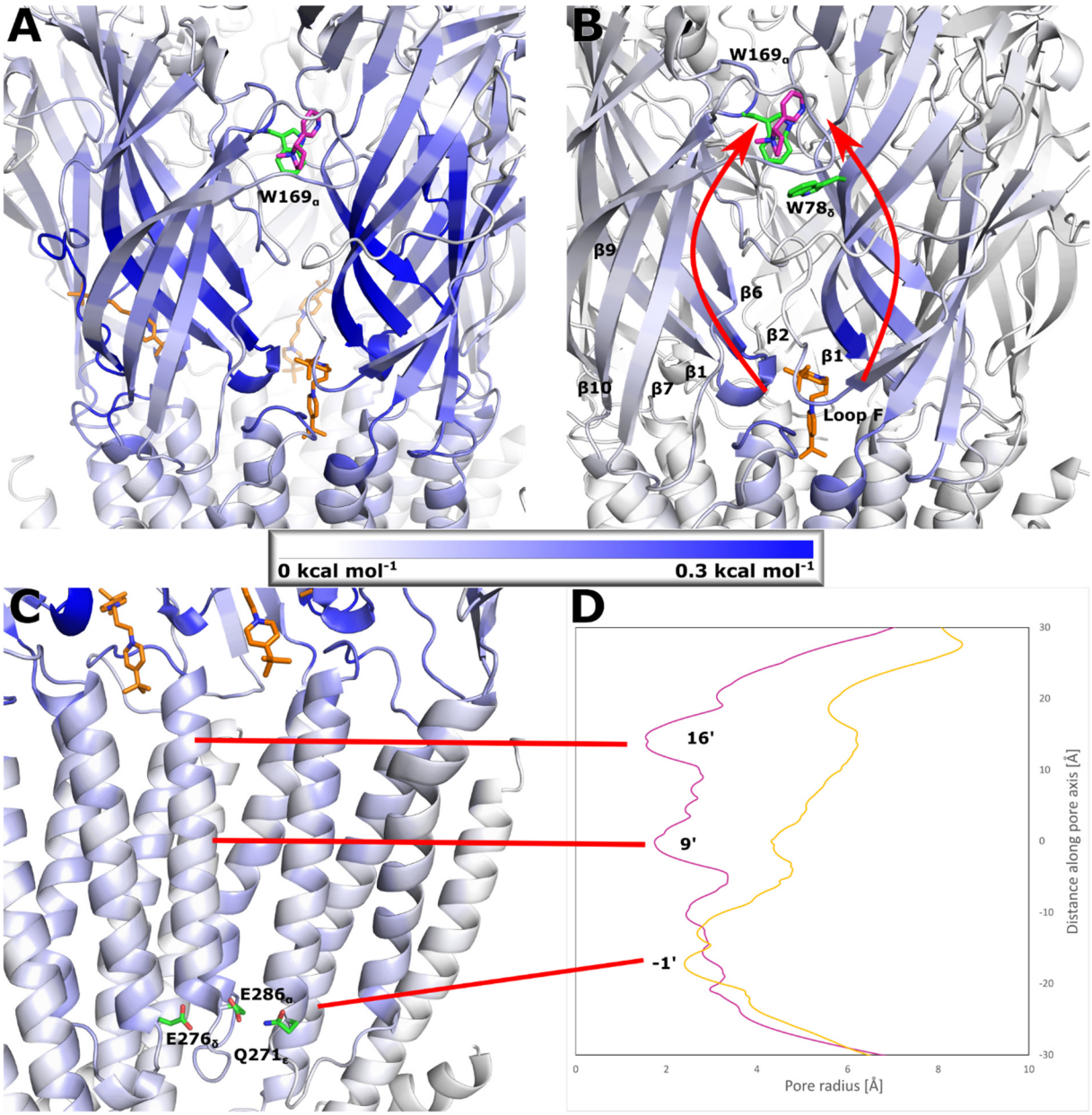

Figure 10: Allosteric impact of MB327 on nAChR transmitted via MB327-PAM-1. **A)** Allosteric impact of MB327 (orange) in the three subunits where the ligand remained stable during MD simulations on the ECD. Blue colors indicate the stabilizing impact of MB327 on the receptor; darker colors demonstrate a higher impact. The orthosteric ligand (purple) and the amino acids W169$_\alpha$ and W78$_\delta$ (green) are shown as sticks. **B)** Impact of MB327 located between the α- and ε-subunit on nAChR. Red arrows indicate the pathway of allosteric stabilization of the orthosteric ligand. **C)** The impact of MB327 bound to the three binding sites in which the ligand remained stable during MD simulations on the TMD. Amino acids located at the desensitization gate are shown as green sticks. **D)** Pore radius of the inactive (purple) and desensitized (yellow) nAChR along the pore axis. The distance along the pore axis is set to 0 Å at the gate of the inactive receptor at position 9'. The position of the gates is projected on the structure by red bars, respectively. Figure taken and adapted from **PUBLICATION I** [221] (see **REPRINT PERMISSION**).

4.3.4. MB327 may also bind to the orthosteric binding site

To further investigate the binding of MB327 to nAChRs, I also performed free ligand diffusion MD simulations (10 replicas à 900 ns) with the ligand placed at a random position within the simulation box outside of the receptor. Thereby, I could determine that MB327 may additionally bind to the orthosteric binding site of nAChRs, interacting with Y131$_\varepsilon$ (Figure 11A, B). Investigating the electrostatics surrounding the receptor revealed that the orthosteric

binding site is surrounded by a strong electric field attractive to positively charged ligands such as MB327 (Figure 11C, D). This binding site, including the interaction with the tyrosine crucial for ligand binding, was recently described as a binding site for related bispyridinium compounds, and experimental validation revealed that this binding site is responsible for an inhibitory effect [70]. Thus, this binding site may explain how MB327 acts as an inhibitor of the receptor at higher concentrations. Binding to MB327-PAM-1 could not be observed during the short simulations. However, as mentioned above (**chapter 2.2.2.2**), only binding sites with high k_{on} values can be identified in this experimental setup.

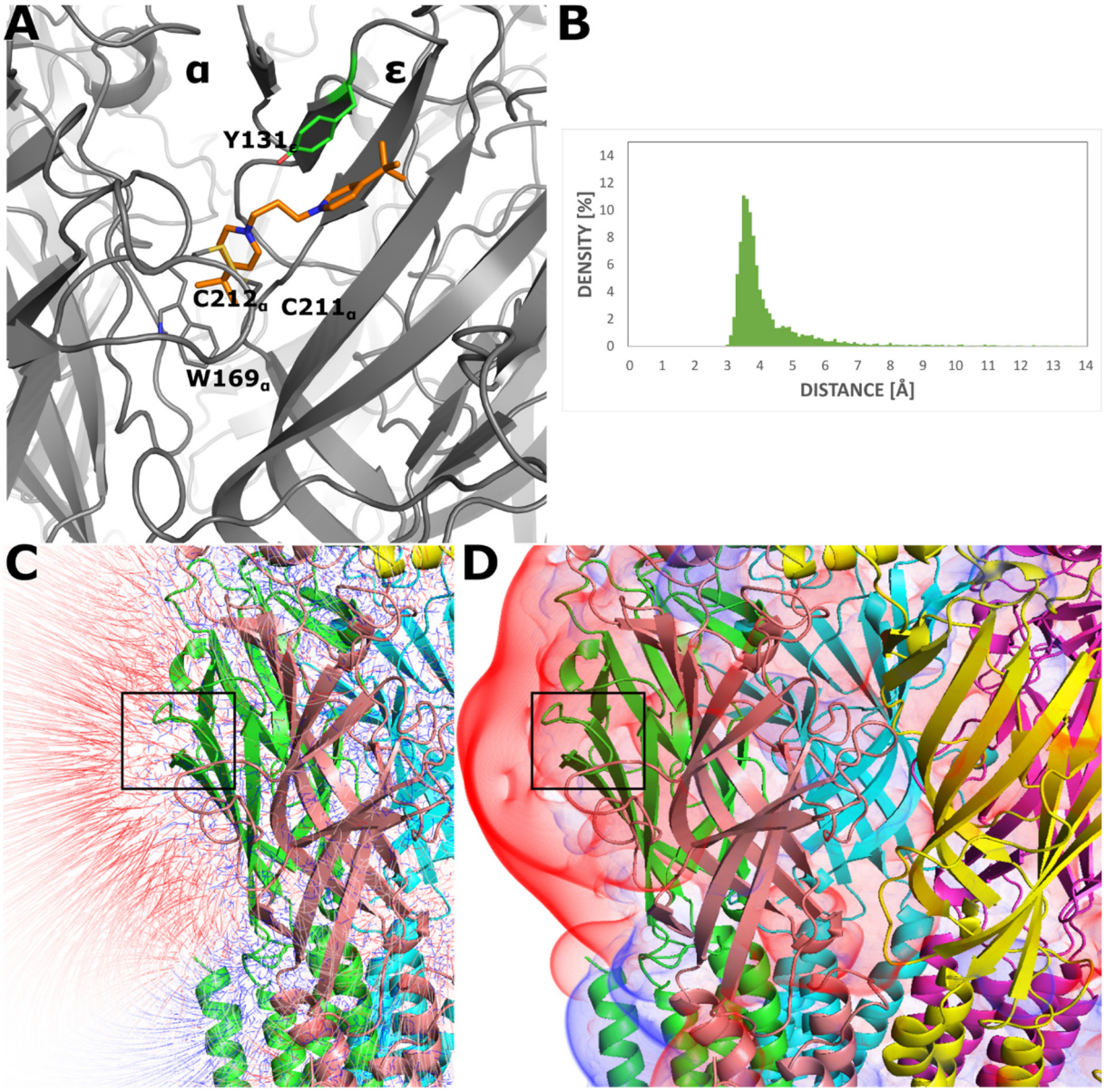

Figure 11: Affinity of MB327 to the orthosteric binding site of nAChRs based on free ligand diffusion MD simulations. **A)** Representative binding mode of MB327 (orange) in the orthosteric binding site in between the α- and ε-subunit. Highly conserved amino acids $C211_{\alpha}$, $C212_{\alpha}$, and $W169_{\alpha}$ are shown as sticks, as well as $Y131_{\varepsilon}$ (green) interacting with MB327. **B)** Minimum distance of aromatic heavy atoms of MB327 to aromatic heavy atoms of $Y131_{\varepsilon}$ while MB327 is bound to the orthosteric binding site. **C)** Electric flux lines and **D)** isocontour surface of the electrostatics surrounding the orthosteric binding site. Red colors indicate an electric field attractive to positively charged compounds. The black box indicates the location of the orthosteric binding site. Figure taken from **PUBLICATION I** [221] (see **REPRINT PERMISSION**).

4.3.5. Rational design of more potent MB327 analogs

Taken together, my results reveal that MB327 potentially binds in an allosteric binding site, MB327-PAM-1, responsible for the therapeutically relevant effect on MB327, located at the transition of ECD to TMD. Furthermore, the inhibitory effect of the ligand may be explained via binding to the orthosteric binding site. This novel knowledge facilitates structure-based optimization of the compound. In fact, one of the *tert*-butyl groups of MB327 is located in a polar part of MB327-PAM-1 (Figure 12A). Substituting the apolar moiety with a polar group, such as amines, should result in a higher potency of the ligands. Thus, I docked PTM0062 and PTM0063, bearing polar amino groups instead of the *tert*-butyl substituent (Figure 12B, C), into the binding site. In all but one subunit the docking score of the two ligands was better than MB327, and both compounds show an about two-fold higher reestablishment of muscle force in OPC-poisoned rat diaphragm compared to MB327 at concentrations of 100 and 300 µM[‡1] (Figure 12D - F).

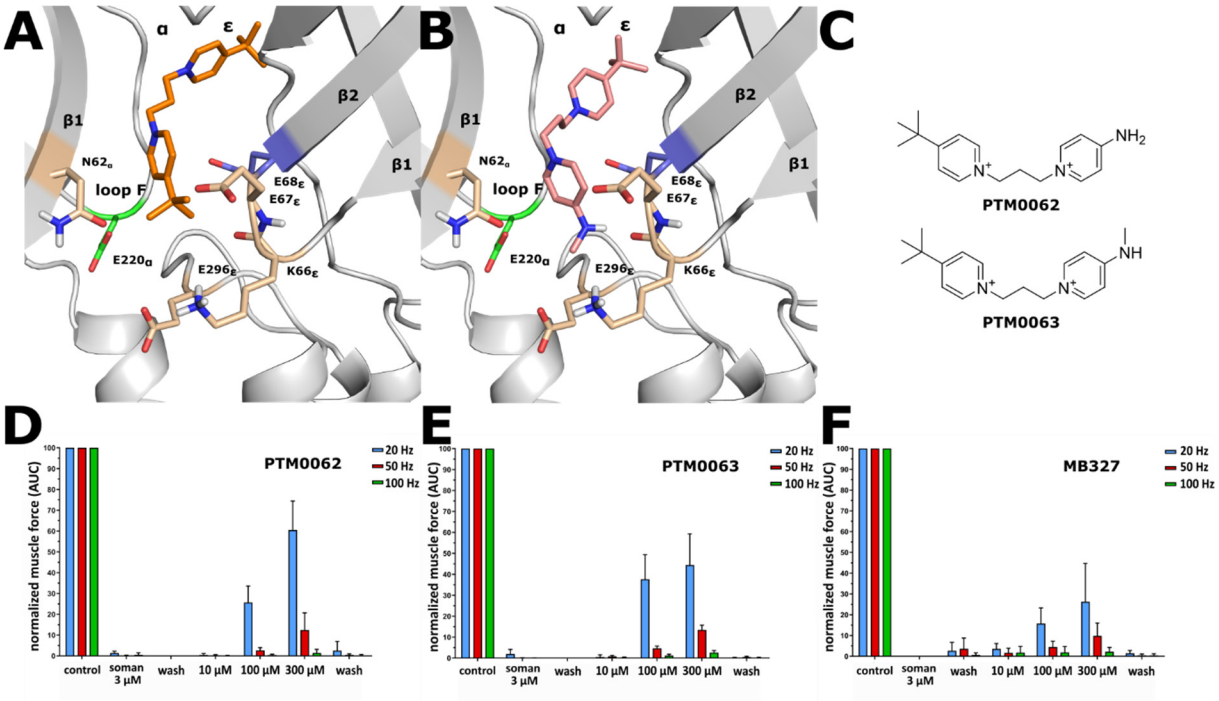

Figure 12: Structure-based ligand design based on the novel knowledge about MB327-PAM-1 results in analogs with increased potency compared to MB327. **A)** MB327 bound in MB327-PAM-1 in between the α- and ε-subunit. The *tert*-butyl substituent orientated towards the TMD is located in a polar part of MB327-PAM-1. **B)** Binding mode of PTM0063 based on docking results. The amino group can form additional interactions compared to MB327. **C)** Structure of PTM0062 and PTM0063. Muscle force restoration in soman-poisoned rat diaphragm after treatment with **D)** PTM0062, **E)** PTM0063, and **F)** MB327 (mean ± standard deviation is shown). Figure taken and adjusted from **PUBLICATION I** [221] (see **REPRINT PERMISSION**).

[‡1] Synthesis of the compounds was performed by Tamara Bernauer under supervision of Prof. Dr. Klaus T. Wanner and Prof. Dr. Franz F. Paintner at the Department of Pharmacy – Center for Drug Research, Ludwig Maximilians University, and *ex vivo* experiments were performed by Dr. Thomas Seeger at the Bundeswehr Institute of Pharmacology and Toxicology.

4.4. Conclusion and significance

With this study, I made a substantial contribution to understanding the mode of action of the PAM MB327 in a multidisciplinary, collaborative study. Prediction of a potential binding site facilitates SBDD, which may ultimately help to close the gap in OPC poisoning treatment. A recent publication demonstrated that the region of MB327-PAM-1 is crucial for exerting the positive allosteric modulation of nAChRs mediated by calcium ions, supporting the predictions made in our study that binding of MB327 to MB327-PAM-1 can mediate a positive allosteric modulation of nAChRs. Furthermore, MB327 analogs predicted to be more potent based on the novel knowledge about the MB327 binding mode showed a higher potency in *ex vivo* measurements.

The key results and findings of this study are:

- Blind docking experiments, followed by blind docking experiments and MD simulations, revealed a novel potential allosteric binding site of the PAM MB327, located at the transition from ECD and TMD. Amino acids that are important for ligand stabilization are also important for stabilizing calcium ions, acting as PAMs in nAChRs [65, 69].
- Rigidity analysis of MB327 bound to nAChR exposed an allosteric impact of MB327 on both the orthosteric binding site and the TMD, including the desensitization gate, in line with experimental findings that MB327 can enhance the cholinergic effect and act as a resensitizer [45-47].
- Affinity of MB327 to the orthosteric binding site could be observed using free ligand diffusion MD simulations. A recent publication revealed that related bispyridinium compounds act as inhibitors of the receptor after binding to the orthosteric binding pocket [70]. This may explain the inhibitory effect of MB327 at higher concentrations.
- The novel knowledge about the potential MB327 binding site can be used for structure-based compound optimization. In this study, PTM0062 and PTM0063 were designed because one *tert*-butyl group is facing in a polar part of the binding site. Both compounds show increased potency compared to MB327.

The results gathered in this first study allowed us to predict the binding mode of the recently identified more affine UNC0646 in MB327-PAM-1 (**PUBLICATION II**) and also enabled performing SBDD to identify MB327 analogs (**PUBLICATION IV**) and novel chemotypes reestablishing muscle force after OPC poisoning (**PUBLICATION III**).

5. PUBLICATION II

MS Binding Assays with UNC0642 as reporter ligand for the MB327 binding site of the nicotinic acetylcholine receptor

V. Nitsche, G. Höfner, J. Kaiser, C.G.W. Gertzen, T. Seeger, K.V. Niessen, D. Steinritz, F. Worek, H. Gohlke, F.F. Paintner, K.T. Wanner

Toxicol Lett**,** 2024. **392**: p. 94-106.

Original publication, see pages 106 - 127.

The content covered in this chapter is taken from "MS Binding Assays with UNC0642 as reporter ligand for the MB327 binding site of the nicotinic acetylcholine receptor" [51]. Sentences containing word-by-word citations are not highlighted explicitly.

5.1. Author contributions

V.N. established the MS Binding Assays and performed affinity screenings, supported by G.H. J.K. performed docking and MD simulation experiments. C.G. supported the computational experiments. T.S. performed rat diaphragm assays. K.N., D.S., F.W., H.G., F.P., and K.W. supervised respective study parts. All authors contributed to writing the manuscript.

5.2. Background

Even though MB327 is a promising lead structure to close the gap in OPC poisoning treatment, the tight therapeutic index makes the use of the compound unfeasible [45-47]. Recently, a screening at our collaboration partners site at the Ludwig Maximilians University in Munich identified UNC0646, binding to the MB327 binding site with a higher affinity compared to MB327 [50]. Because of the highly flexible substituents of the quinazoline structure of UNC0646, optimization of the compound using ligand-based screening approaches is demanding without knowing the binding pose of the ligand. In **PUBLICATION I**, I proposed a novel binding site of MB327, MB327-PAM-1, in line with experimental results. Thus, the question arose as to how UNC0646 may bind to MB327-PAM-1.

In this publication, our collaboration partners established novel MS Binding Assays to characterize compounds regarding their affinity to the MB327 binding site using *in vitro* measurements, using UNC0642, a slightly less affine analog of UNC0646, as a reporter ligand. To predict the potential binding mode of UNC0646 in MB327-PAM-1, I used a flexible docking

approach in combination with MD simulations. Thereby, I could predict interactions with amino acids decisive for ligand stabilization.

5.3. Results

5.3.1. Prediction of the UNC0646 binding mode

To identify the binding mode of UNC0646 in MB327-PAM-1, I performed flexible docking experiments using the PDB structure of the *Torpedo* nAChR (PDB ID: 6UWZ [174]), in line with the receptor used in novel MS Binding Assays to screen ligands in nAChRs presented in this publication[‡2]. Therefore, I docked UNC0646 into all five potential binding sites located between adjacent subunits. In two binding sites, located at the negative site of the α-subunits [in between the γ- and α-subunit (binding site A, Figure 13A), and between the β- and α-subunit (binding site B), respectively], the ligand was placed in a similar conformation. In the remaining three binding sites, the ligand was either more solvent-exposed or was placed spanning two binding pockets. However, in binding site B, the ligand was placed so that the piperidine nitrogen in the 4-position of the quinazoline moiety interacts with $E199_{\alpha}$ while the ligand was placed deeper in binding site A, facilitating an interaction between this nitrogen and $E65_{\gamma}$.

Subsequently, I performed MD simulations with UNC0646 bound to both binding sites to investigate whether the ligand stays within the binding site and to characterize important interacting residues. During 12 replicas of 500 ns long simulations, UNC0646 shows a higher movement in binding site B, as indicated by the root mean square deviation (RMSD) of the ligand (3.02 ± 0.30 Å vs. 5.13 ± 0.58 Å, $p = 0.004$ according to a two-sided *t*-test). Furthermore, in binding site B, the ligand leaves the binding site in 6 replicas, whereas the ligand remains within binding site A in all 12 replicas. Thus, I used the later binding site to further predict important amino acid interactions.

Based on interaction frequency, I concluded that $E65_{\gamma}$ is most important for ligand stabilization (Figure 13B) (interactions with the piperidine nitrogen in 4-position of the quinazoline moiety of UNC0646 in 71.8 ± 7.4 %). This amino acid was suggested to be important for MB327 stabilization in **PUBLICATION I** ($E68_{\varepsilon}$ in Figure 9C). Secondly, the nitrogen of the piperidine ring in the 7-position of the quinazoline moiety located in an area surrounded by four glutamates ($E69_{\alpha}$, $E199_{\alpha}$, $E286_{\alpha}$, and $E292_{\gamma}$) may be stabilized by interacting with the negatively charged side chains of these residues (in 40.3 ± 9.7 % of all frames, Figure 13C).

[‡2] The MS Binding Assays were established by Valentin Nitsche under supervision of Prof. Dr. Klaus T. Wanner and Prof. Dr. Franz F. Paintner at the Department of Pharmacy – Center for Drug Research, Ludwig Maximilians University.

The least conserved interactions could be observed for the diazepane ring interacting with E75$_\alpha$ and E64$_\gamma$ (19.4 ± 5.0% of all frames, Figure 13D). These results are in line with structure-activity relationships deduced from UNC0646, UNC0638, and UNC0642, where eliminating the positive charge in the 2-position of the quinazoline ring only has a minor impact on binding affinity [50].

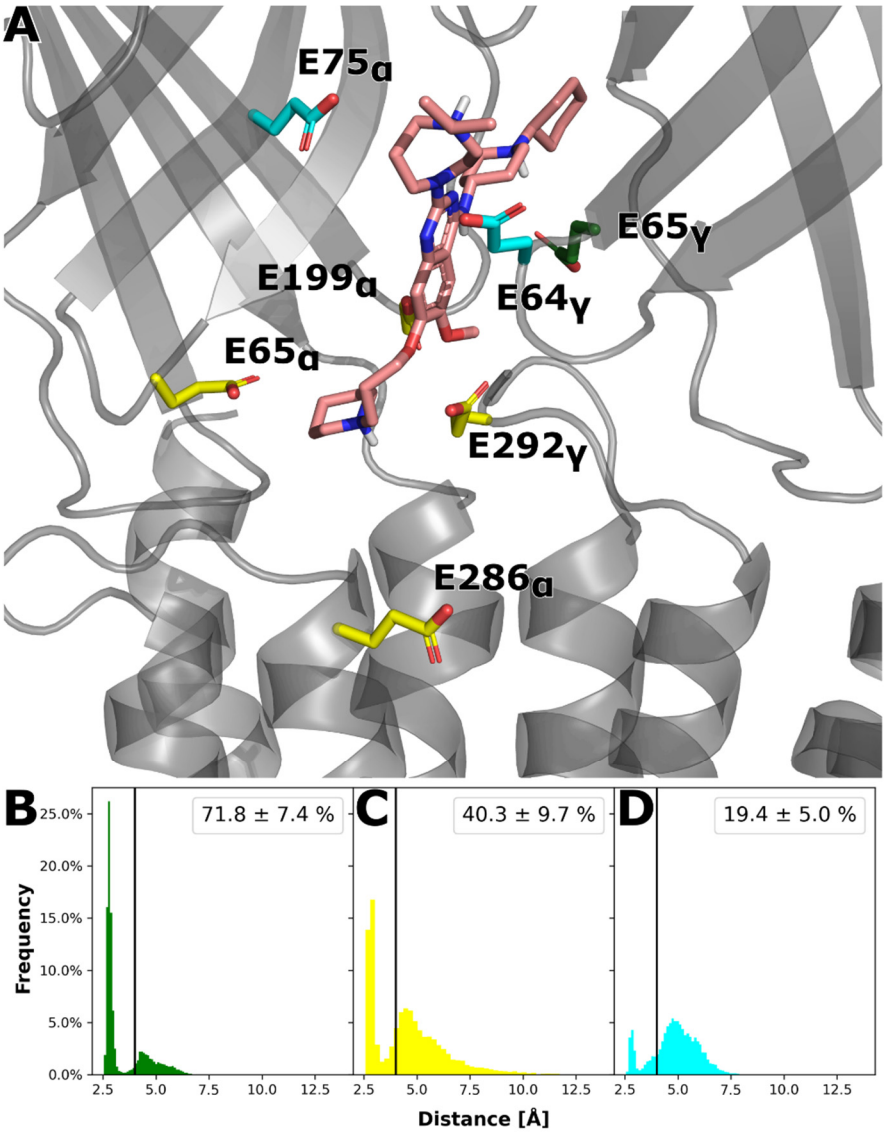

Figure 13: Proposed binding mode of UNC0646 within MB327-PAM-1. **A)** Docked binding mode of UNC0646 in between the γ- and α-subunit of the *Torpedo* nAChR. Acidic surrounding amino acids are shown as sticks. **B)** Minimal distance of the positively charged nitrogen of the quinazoline substituent in 4-position of UNC0646 to the side-chain oxygens of E65$_\gamma$. **C)** Minimal distance of the positively charged nitrogen of the quinazoline substituent in 7-position of UNC0646 to the side-chain oxygens of E199$_\alpha$, E65$_\alpha$, E286$_\alpha$, and E292$_\gamma$. **D)** Minimal distance of the positively charged nitrogen in the quinazoline substituent in 2-position of UNC0646 to the side-chain oxygens of E75$_\alpha$ and E65$_\gamma$. The colors in panels B-D correspond to the amino acid coloring in panel A. Values in the boxes indicate the frequency of interactions (minimal distance of nitrogen to oxygen < 4 Å; mean ± SEM are displayed, taken over 12 replicas each). The figure was taken and adapted from **PUBLICATION II** [51] (see **REPRINT PERMISSION**).

Despite the increased affinity of UNC0646 compared to MB327 towards MB327-PAM-1, experiments performed by our collaboration partners within this study revealed that UNC0646 and its analogs are less potent in reestablishing muscle force of soman-inhibited tissue[‡3]. Nevertheless, although the muscle force restoration is less pronounced compared to MB327, reestablishment of soman-inhibited rat diaphragm could be observed at lower concentrations compared to MB327, in line with the increased affinity.

5.4. Conclusion and significance

With the analysis described above, I made a significant contribution to a collaborative publication. I provided insights into the potential binding mode of UNC0646 within MB327-PAM-1, revealing that UNC0646 might bind to MB327-PAM-1, in line with experimental results that both ligands bind to the same binding pocket. Substituents in the 2-position of the quinazoline moiety show less conserved interactions with the receptor compared to substituents in the 4- and 7-position, in line with experimental results that removing the positively charged substituent in the 2-position only has minor impacts on ligand affinity [50].

The key results and findings of this study are:

- A plausible binding mode of UNC0646 in MB327-PAM-1 was provided using a combination of flexible docking experiments and MD simulations.
- Based on this binding mode, crucial amino acid interactions were proposed. E65$_\gamma$ shows the most highly conserved salt bridge interaction with the ligand, in line with interacting residues observed for MB327 in **PUBLICATION I**.

Understanding the binding mode of UNC0646 within MB327-PAM-1 enables LBDD approaches based on the three-dimensional structure of the ligand. These techniques were used in **PUBLICATION III** to identify novel UNC0646 analogs featuring substituents increasing the affinity towards nAChRs compared to the UNC0646 substituents.

[‡3] *Ex vivo* experiments were performed by Dr. Thomas Seeger at the Bundeswehr Institute of Pharmacology and Toxicology.

6. PUBLICATION III

Identification of ligands binding to MB327-PAM-1, a binding pocket relevant for resensitization of nAChRs

J. Kaiser, C.G.W. Gertzen, T. Bernauer, V. Nitsche, G. Höfner, K.V. Niessen, T. Seeger, F.F. Paintner, K.T. Wanner, D. Steinritz, F. Worek, H. Gohlke

Toxicol Lett, 2024. *in press*.

Original publication, see pages 128 – 184.

The content covered in this chapter is taken from "Identification of ligands binding to MB327-PAM-1, a binding pocket relevant for resensitization of nAChRs" [453]. Sentences containing word-by-word citations are not highlighted explicitly.

6.1. Author contributions

"J.K. performed modeling, screening, and MD simulation experiments. C.G. supported the computational experiments. T.B. synthesized analogs of UNC0646. V.N. performed MS Binding Assays, and T.S. performed rat diaphragm assays. H.G. conceived the study and supervised the project. G.H., K.N., F.P., K.W., D.S., and F.W. supervised respective study parts. All authors contributed to writing the manuscript." [453]

6.2. Background

In **PUBLICATION II**, I predicted a binding mode of UNC0646 within MB327-PAM-1. In this publication, our collaboration partners from the Ludwig Maximilians University Munich also provided novel MS Binding Assays based on UNC0642, a structural analog of UNC0646, as a reporter ligand. These two results enable LBDD to characterize optimized analogs of UNC0646 and to screen these compounds regarding their affinity using an *in vitro* assay. During this study, two compounds, MB327 and UNC0646, were already described in the literature as binders of the MB327 binding site [44-47, 50, 52, 161]. Despite showing a higher affinity for MB327-PAM-1, the potency of UNC0646 and analogs is reduced compared to MB327, showing only minor effects on muscle force reestablishment after OPC poisoning, as depicted in **PUBLICATION II** [50, 51]. However, in line with the increased affinity, the reestablishment of muscle force can be observed at lower concentrations compared to MB327 [51]. Nevertheless, identical to MB327, UNC0646 also acts as an inhibitor at higher concentrations [51]. Thus, the identification of novel chemotypes may help to ultimately close

the therapeutic gap after OPC poisoning. Knowledge about the binding site gained from **PUBLICATION I** is pivotal to performing structure-based virtual high-throughput screening.

In this publication, I performed both ligand- and structure-based screenings to identify UNC0646 analogs with substituents on the quinazoline moiety that may increase affinity towards MB327-PAM-1 compared to UNC0646 substituents. On the other hand, I identified four novel chemotypes that bind to MB327-PAM-1 with increased affinity compared to MB327. One of these compounds, cycloguanil, shows increased muscle force reestablishment of soman-poisoned tissue compared to MB327.

6.3. Results

In this publication, I performed screenings to identify novel binders of MB327-PAM-1 using three different methodical pathways (Figure 14), including ligand-based screening based on the two-dimensional structure of UNC0646 [Figure 14 (blue scheme)] and the three-dimensional structure of the UNC0646 analog PTMD01-0004 [Figure 14 (yellow scheme)], and two structure-based screenings [Figure 14 (green scheme)]. Selected compounds were subsequently tested in MS Binding Assays using, if not stated otherwise, triplicates with test compound concentrations of 10 µM and reporter ligand concentrations of 1 µM[‡4].

6.3.1. Two-dimensional ligand-based screening to identify UNC0646 analogs binding to MB327-PAM-1

First, we performed a ligand-based screening based on the two-dimensional structure of UNC0646 using the MolPort (https://molport.com) database [Figure 14 (blue scheme)]. Based on this screening, I selected a total of 12 compounds. Of these, 10 compounds displaced the reporter ligand from the binding site at concentrations of 1 µM and 10 µM for reporter and test compound, respectively (mean ± standard deviation < 100%)[‡4]. The strongest displacement was observed for PTMD01-0019C (**1a**, Table 2, compound numbering analog to the original publication, pages 128 - 184). Interestingly, in contrast to previously described analogs of UNC0646, no substituent of the quinazoline moiety features an aliphatic nitrogen. However, pK_a values of related compounds reveal that the two amino substituents present in PTMD-0019C can shift the pK_a value of the quinazoline moiety above 7. Furthermore, 4-aminopyridine has a pK_a value of 9.17, indicating that the compound may be protonated.

[‡4] Experiments were performed by Valentin Nitsche under supervision of Prof. Dr. Klaus T. Wanner and Prof. Dr. Franz F. Paintner at the Department of Pharmacy – Center for Drug Research, Ludwig Maximilians University.

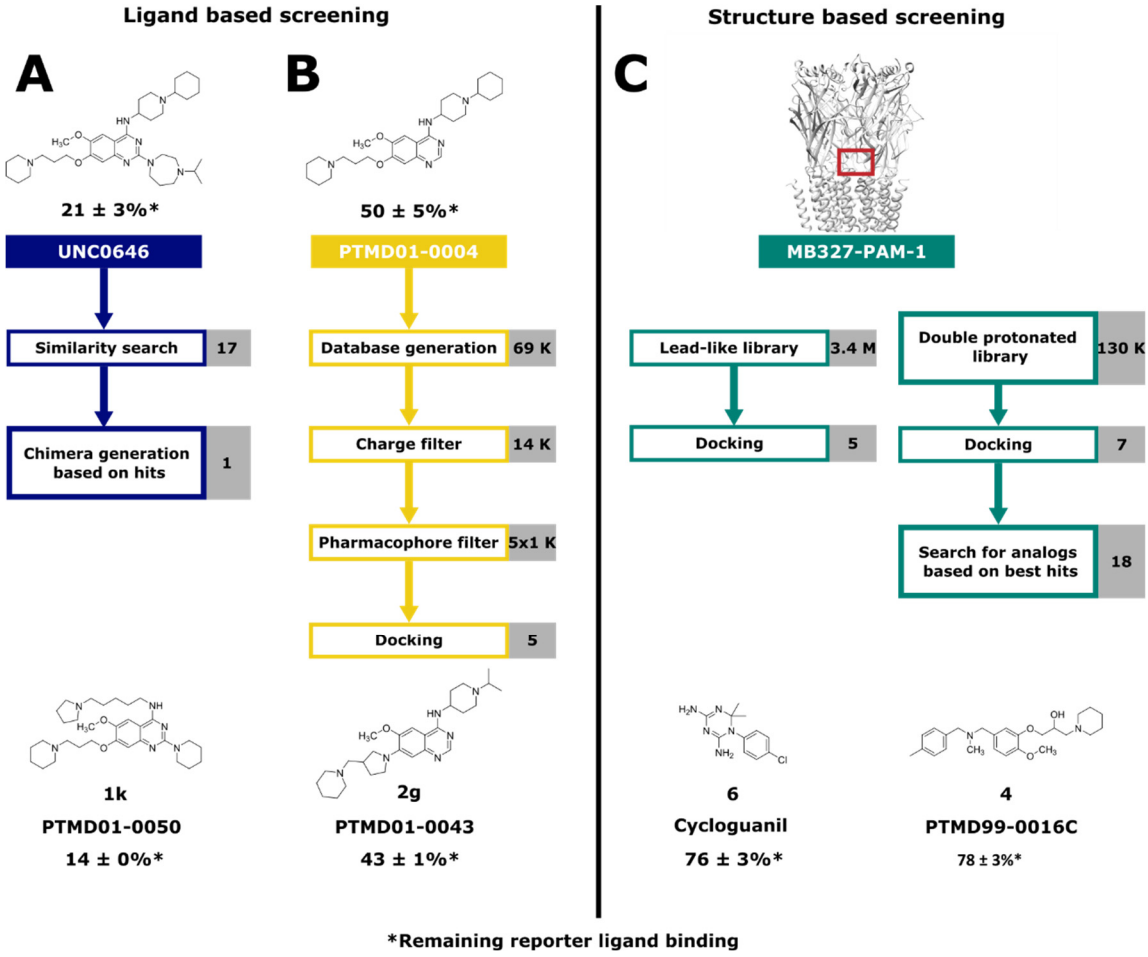

Figure 14: Screening scheme to identify novel analogs of UNC0646 and its analog PTMD01-0004 (**2a**), respectively, and novel chemotypes acting as PAMs of nAChRs. **A)** Based on the two-dimensional structure of UNC0646, a ligand-based screening was performed (blue scheme), resulting in the generation of a chimera PTMD01-0050 (**1k**) inspired by UNC0646, UNC0642, and the novel identified binder UNC0379 (1b), with increased reporter ligand displacement in MS Binding Assays compared to UNC0646. **B)** Based on the three-dimensional proposed binding mode of PTMD01-0004 (**2a**), an analog of UNC0646 lacking the substituent in 2-position of the quinazoline moiety, PTMD01-0043 (**2g**) was identified, featuring a substituent enhancing reporter ligand displacement in MS Binding Assays compared to the UNC0646 substituents (yellow scheme). **C)** Based on a structure-based screening, a total of four new chemotypes were identified, replacing the reporter ligand in MS Binding Assays, with the highest replacement observed for Cycloguanil (**6**) and PTMD99-0016C (**4**). The figure was taken and adjusted from **PUBLICATION III** [453] (see **REPRINT PERMISSION**).

However, these results indicate that the location of the positive charge within the UNC0646 analogs is less crucial, further emphasized by the results observed for UNC0379 (**1b**), ZT-12-037-01 (**1c**), C-021 (**1d**), MS012 (**1e**), PTMD01-0020C (**1f**), PTMD01-0021C (**1g**), PTMD01-0024C (**1h**), and PTMD01-0025C (**1i**), and bunazosin (**1j**). This may be explained by the multitude of acidic amino acids located within MB327-PAM-1, as observed in **PUBLICATION I** and **PUBLICATION II**. Furthermore, the mean displacement of the marker ligand was second strongest for UNC0379, a ligand featuring a more flexible substituent in 4-position compared to UNC0646. Based on this result, PTMD01-0050, a chimera inspired by UNC0379, UNC0642, and UNC0646, was designed, showing increased reporter ligand displacement compared to UNC0646[‡5]. Taken together, ligand-based screening based on the two-dimensional structure of UNC0646 only resulted in ligands with minor impacts on reporter ligand displacement. However, these results indicate that the location of the positive charge of UNC0646 plays a secondary role, giving insights into structure-affinity relationships.

[‡5] Experiments were performed by Valentin Nitsche under supervision of Prof. Dr. Klaus T. Wanner and Prof. Dr. Franz F. Paintner at the Department of Pharmacy – Center for Drug Research, Ludwig Maximilians University.

Table 2: Analogs of UNC0646 identified by a ligand-based screening based on the two-dimensional structure of UNC0646 displacing the reporter ligand in the MS Binding Assays. Table was taken and adjusted from **PUBLICATION III** [453] (see **REPRINT PERMISSION**).

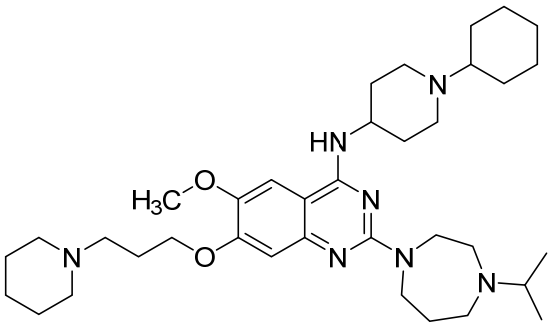

UNC0646

$pK_i = 5.83 \pm 0.05$[a]

Remaining reporter ligand binding: 21 ± 3 %[b]

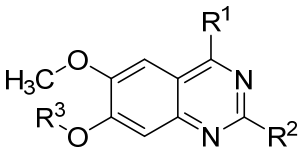

1a-k

Compound	Name / PTMD code	R^1	R^2	R^3	Remaining reporter ligand binding [%][b]
1a	PTMD01-0019C		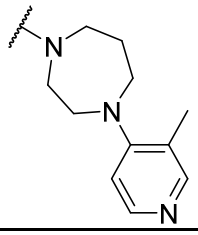		47 ± 3
1b	UNC0379	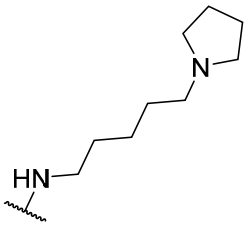	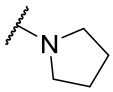		59 ± 4
1k	PTMD01-0050	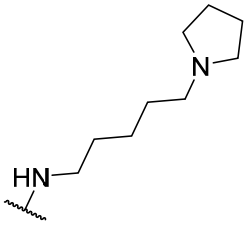	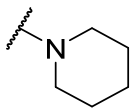	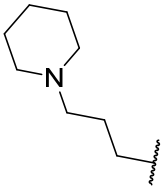	14 ± 0
1c	ZT-12-037-01	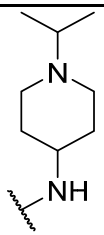	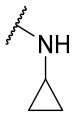		66 ± 5

1d	C-021	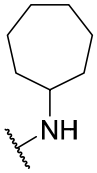	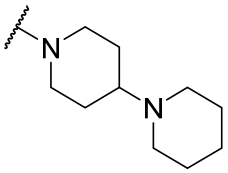		63 ± 2
1e	MS012	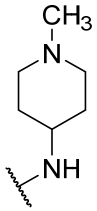	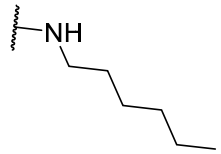		83 ± 6
1f	PTMD01-0020C		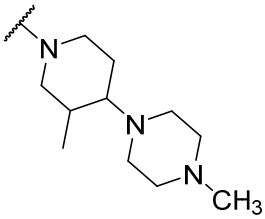		73 ± 7
1g	PTMD01-0021C		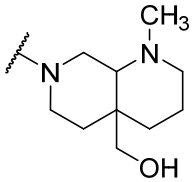		87 ± 2
1h	PTMD01-0024C		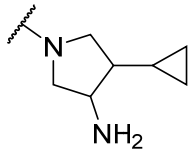		83 ± 4
1i	PTMD01-0025C		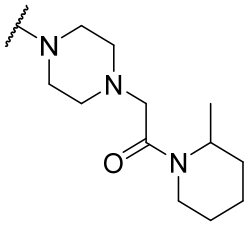		81 ± 5
1j	Bunazosin		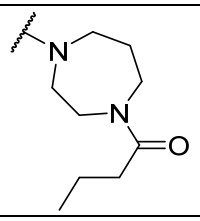		90 ± 7

[a] The pK_i value has been reported in ref. [51].

[b] Characterized by UNC0642 MS Binding Assays; Percentage of remaining reporter ligand binding in the presence of test compounds is hown. 100% reporter ligand binding indicates the absence of a competitor. Thirty measurements were performed for UNC0646 and three measurements for all other compounds at test compound concentrations of 10 μM and reporter ligand concentrations of 1 μM, respectively. Displayed are the mean and standard deviation.

6.3.2. Three-dimensional ligand-based screening based on an UNC0646 analog with a reduced molecular structure

To also consider the three-dimensional structure of UNC0646 bound to MB327-PAM-1, I performed ligand-based screenings based on the proposed binding mode of PTMD01-0004 (**2a**) [Table 3, Figure 14 (yellow scheme)], a UNC0646 analog lacking the quinazoline substituent in 2-position and thus, in contrast to UNC0646, not violating the molecular weight rule according to Lipinski's rule of five [168]. Therefore, I first created a virtual database of PTMD01-0004 (**2a**) analogs featuring varying substituents in the 4- and 7-position of the quinazoline moiety. This database was then subjected to a two-step screening with an initial ligand-based screening followed by docking of the 1000 best-rated compounds in each binding site in combination with an upstream pharmacophore filter based on the orientation of the quinazoline ring and the location of the positively charged nitrogens. The best hits were synthesized, and reporter ligand displacement was subsequently measured *in vitro*[‡6]. All five compounds showed remarkable reporter ligand displacement. However, varying the substituent in the 4-position of the quinazoline building block [PTMD01-0032 (**2b**), PTMD01-0053 (**2c**), PTMD01-0027 (**2d**), and PTMD01-0030 (**2e**)] only showed minor effects on binding affinity and no increased reporter ligand displacement could be observed compared to PTMD01-0004. In contrast, substitution in 7-position in PTMD01-0043 (**2g**) led to increased reporter ligand displacement in comparison to PTMD01-0005 (**2f**), an analog of UNC0646 bearing the same substituents in 2- and 4-position compared to PTMD01-0043 (**2g**), indicating that the substituent of PTMD01-0043 (**2g**) is favored in comparison to the UNC0646 substituent in 7-position. Taken together, the two ligand-based screening approaches led to the identification of novel substituents of the quinazoline moiety of UNC0646, displaying increased reporter ligand displacement in comparison to the UNC0646 substituents. However, only slight improvements could be made since all compounds feature a high similarity to UNC0646, a consequence of the techniques used.

[‡6] Synthesis of the compounds and MS Binding Assays experiments were performed by Tamara Bernauer respectively Valentin Nitsche under supervision of Prof. Dr. Klaus T. Wanner and Prof. Dr. Franz F. Paintner at the Department of Pharmacy – Center for Drug Research, Ludwig Maximilians University.

Table 3: Analogs of PTMD01-0004 (**2a**) identified in a ligand-based screening based on the three-dimensional structure of the proposed binding mode of PTMD01-0004 (**2a**). The table was taken and adjusted from **PUBLICATION III [453]** (see **REPRINT PERMISSION**).

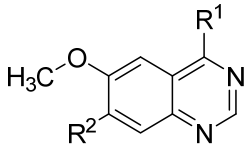

2a-g

Compound	PTMD code	R^1	R^2	Remaining reporter ligand binding [%][a]
2a	PTMD01-0004[b]	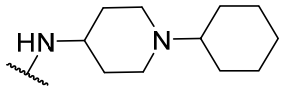	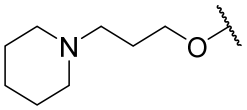	50 ± 5[c]
2b	PTMD01-0032	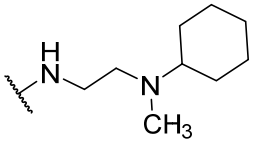	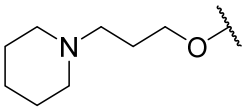	50 ± 7
2c	PTMD01-0053	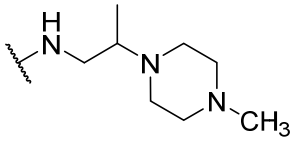	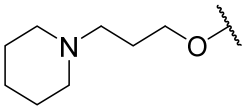	76 ± 7
2d	PTMD01-0027	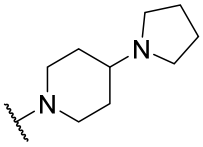	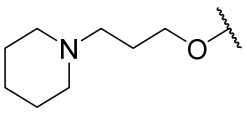	71 ± 3
2e	PTMD01-0030	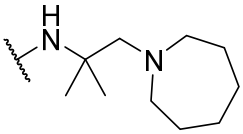	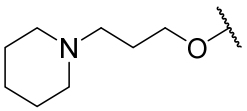	60 ± 3
2f	PTMD01-0005[b]	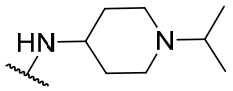	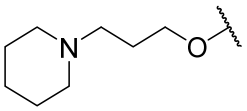	63 ± 4[d]
2g	PTMD01-0043	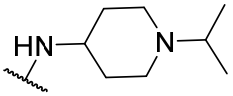	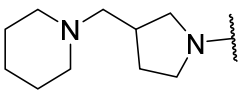	43 ± 1

[a] Characterized by UNC0642 MS Binding Assays; Percentage of remaining reporter ligand binding in the presence of test compounds is shown. 100% reporter ligand binding indicates the absence of a competitor. Results are based on three measurements at test compound concentrations of 10 µM and reporter ligand concentrations of 1 µM if not stated otherwise. The mean and standard deviation are shown.

[b] PTMD01-0004 (**2a**) and PTMD01-0005 (**2f**) [Bernauer *et al.,* unpublished] are shown as reference structures to compare to PTMD01-0043 (**2g**) and were not identified in this study

[c], [d] Results are derived from twelve and six measurements, respectively, at test compound concentrations of 10 µM and reporter ligand concentrations of 1 µM. The mean and standard deviation are shown.

6.3.3. Identification of novel chemotypes binding to MB327-PAM-1 based on structure-based screenings

To identify novel chemotypes binding to MB327-PAM-1, I performed high-throughput virtual screenings [Figure 14 (green scheme)]. Therefore, I docked a lead-like database featuring 3,434,621 compounds and a database with double positively charged compounds featuring 129,606 compounds to MB327-PAM-1 of all subunits in the human and *Torpedo* nAChR model, respectively. Thus, side-chain flexibility is being considered implicitly because of different side-chain orientations in each subunit resulting from homology modeling. Based on visual inspection of the best 1,000 hits per subunit and database (in total, 5 x 2 x 1,000 hits), I selected 12 compounds for testing. In a preliminary version of the MS Binding Assays, three compounds (PTMD99-0006C, PTMD99-0010C, and PTMD99-0014C) displaced the reporter ligand UNC0642[‡7]. Thus, after another round of visual inspection of the docking results, I selected three analogs of PTMD99-0006C [including PTMD99-0016C (**4**)], seven analogs of PTMD99-0010C [including PTMD01-0026C (**5**)], and eight analogs of PTMD99-0014C [including cycloguanil (**6)**]. Although all three compounds (PTMD99-0006C, PTMD99-0010C, and PTMD99-0014C) did not show marker ligand displacement in the final version of the MS Binding Assays, PTMD01-0001C (**3**, Figure 15A) and at least one of the ordered analogs for each chemotype were able to displace the reporter ligand (Figure 15B-D)[‡7]. Thus, I identified four new chemotypes binding to the MB327 binding site with a higher displacement of the reporter ligand compared to MB327 (102 ± 9%, n = 6 [454]). For two of those compounds, the displacement of the reporter ligand slightly fails to be significantly different from 100% {$p < 0.05$ according to a two-sided one-sample t-test; p [PTMD99-0001C (**3**)] = 0.064, p [PTMD99-0016C (**4**)] = 0.005, p [PTMD99-0026C (**5**)] = 0.079, p [cycloguanil (**6**)] = 0.006}.

[‡7] Experiments were performed by Valentin Nitsche under supervision of Prof. Dr. Klaus T. Wanner and Prof. Dr. Franz F. Paintner at the Department of Pharmacy – Center for Drug Research, Ludwig Maximilians University.

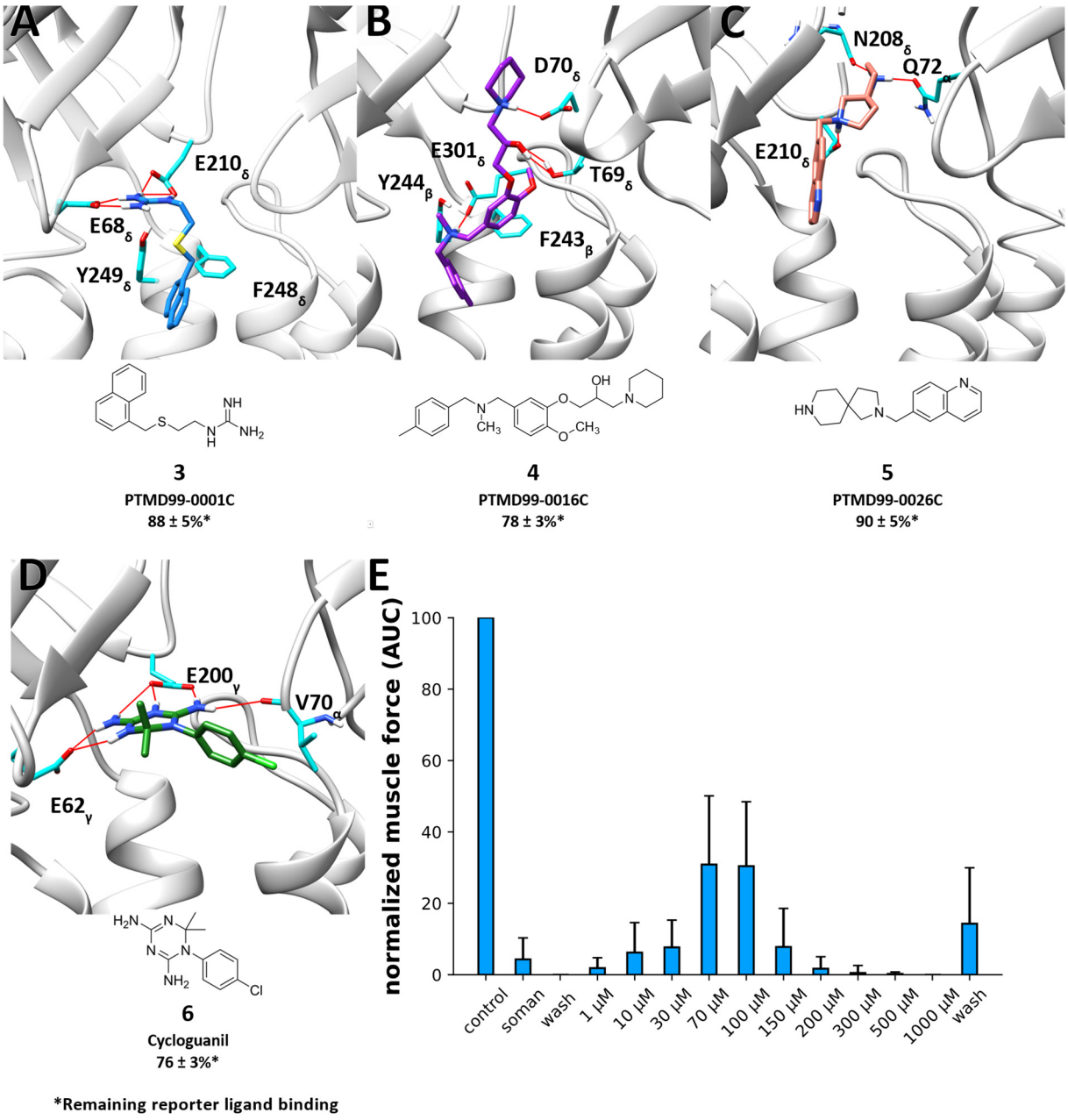

Figure 15: Docked binding modes of novel chemical scaffolds displacing the reporter ligand in MS Binding Assays identified based on structure-based screenings. For each chemical scaffold, the ligand with the highest reporter ligand displacement within this group is shown [**A)** PTMD99-0001C (**3**), **B)** PTMD99-0016C (**4**), **C)** PTMD99-0026C (**5**), **D)** Cycloguanil (**6**)]. Interacting amino acids are shown as sticks and the remaining reporter ligand binding derived from MS Binding Assays is displayed in percentage. **E)** Restoration of muscle force in soman-poisoned rat muscles after cycloguanil (**6**) treatment. The figure was taken from **PUBLICATION III** [453] (see **REPRINT PERMISSION**).

Of note, cycloguanil (**6**) is already well described as the active metabolite of proguanil, a compound used in the treatment of malaria [71, 72]. The ligand is forming salt bridges with $E62_{\gamma}$ and $E200_{\gamma}$ in the docked pose and in subsequent MD simulations (Figure 15D, Figure 16), located at analog positions as E44 and E172, important for stabilization of the PAM calcium in the α7-nAChR [65, 69]. Cycloguanil (**6**) is the only compound where enough substance was commercially available to conduct *ex vivo* experiments on the reestablishing capability in soman-poisoned rat diaphragm[‡8]. The compound showed a reestablishment of muscle force of 30.87 ± 19.23% (mean ± SD) at 70 μM (Figure 15E). In comparison, for a similar degree of muscle force reestablishment, concentrations of 300 μM MB327 are required, and none of the tested UNC0646 concentrations in **PUBLICATION II** show comparably high muscle force reestablishment [51, 221]. Like MB327, UNC0646, and their analogs, cycloguanil (**6**) shows an inhibitory effect at slightly higher concentrations, resulting in a tight therapeutic index. Nevertheless, cycloguanil (**6**) together with PTMD99-0001C (**3**), PTMD99-0016C (**4**), and PTMD99-0026C (**5**) can be considered as new lead structures and starting points to ultimately close the gap in OPC poisoning treatment.

6.3.4. Pharmacokinetic and toxicological properties of new hits

To focus on lead structures with satisfactory pharmacokinetic and toxicological properties, I predicted those properties for the most interesting hits and UNC0646. Especially UNC0646 was predicted to have unsatisfactory pharmacokinetic and toxicological properties, including a predicted inhibition of HERG K^+ channels and the violation of two rules of Lipinski's rule of five (Table 4, Table 5). In contrast, the four new chemotypes show reasonable properties except for PTMD01-0026C, which raises considerable toxicological concerns.

[‡8] *Ex vivo* experiments were performed by Dr. Thomas Seeger at the Bundeswehr Institute of Pharmacology and Toxicology.

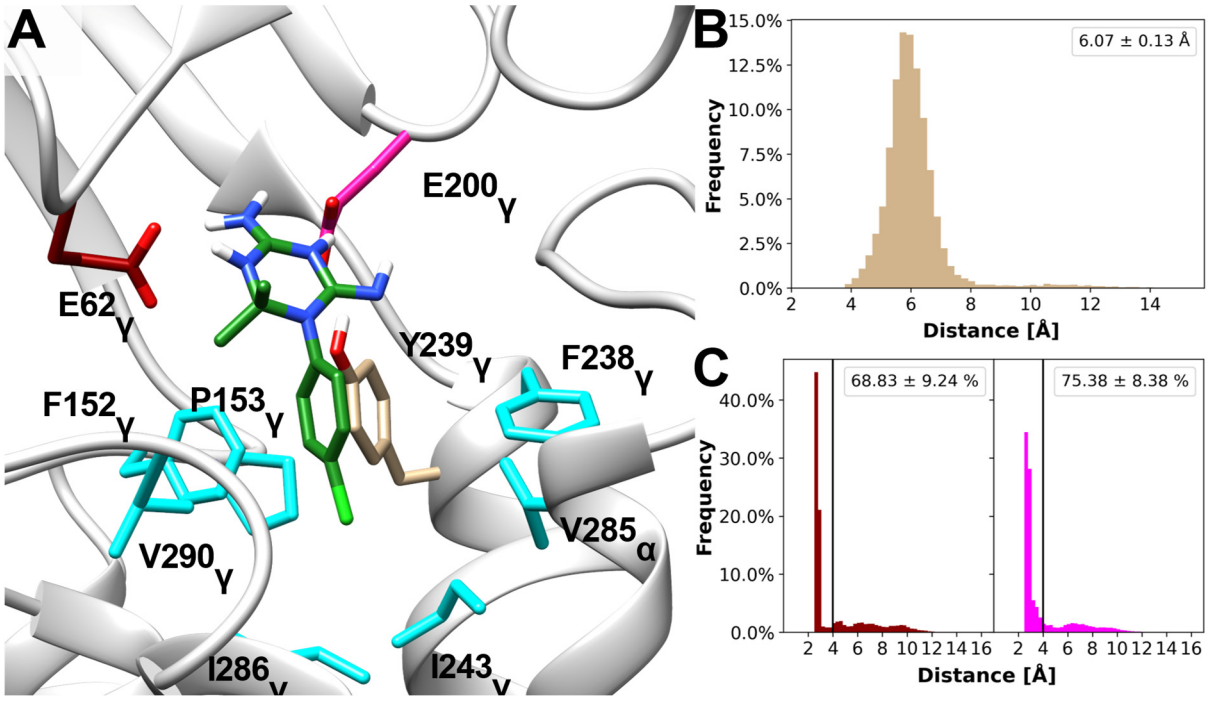

Figure 16: Binding mode of cycloguanil based on MD simulations. **A)** Representative [based on a k-means clustering including receptor and ligand atoms (10 replicas of 1 µs length each); the biggest cluster containing 48.2% of all frames] binding mode of cycloguanil (**6**, green) in MB327-PAM-1. Polar interacting amino acids [$E62_{\gamma}$ (dark red) and $E200_{\gamma}$ (purple)] and amino acids part of an apolar part of the pocket (sand and cyan, respectively) are shown as sticks. **B)** Distance distribution of the center of mass of the cycloguanil phenyl ring to the center of mass of the aromatic ring of $Y239_{\gamma}$. Values in the legend represent the mean ± SEM. **C)** Distance distribution of the nitrogens of cycloguanil acting as hydrogen bond donors to the side-chain oxygens of $E62_{\gamma}$ and $E200_{\gamma}$. Colors correspond to the amino acid coloring in panel A. Values in the legend represent the frequency ± SEM of interaction (distance between nitrogens and oxygens < 4 Å). The figure was taken and adjusted from **PUBLICATION III [453]** (see **REPRINT PERMISSION**).

Table 4: Predicted pharmacokinetic properties of UNC0646 and compounds identified in **PUBLICATION III** with the highest reporter ligand displacement. The table was taken and adjusted from **PUBLICATION III** [453] (see **REPRINT PERMISSION**).

Compound	#stars[a]	QPlogPo/w[b]	QPPCaco[c]	RuleOfFive[d]	RuleOfThree[e]
UNC0646	7	6.01	125.43	2	1
PTMD01-0050 (**1k**)	1	5.61	428.53	2	0
PTMD01-0043 (**2g**)	0	4.54	297.48	0	0
PTMD99-0001C (**3**)	0	2.57	615.24	0	0
PTMD99-0016C (**4**)	0	3.72	277.07	0	1
PTMD99-0026C (**5**)	0	2.45	201.63	0	0
Cycloguanil (**6**)	1	1.59	446.49	0	0

[a] Number of properties falling outside the 95% range of similar values for known drugs.
[b] Octanol/water partition coefficient (recommended values: -2.0 – 6.5).
[c] Caco-2 cell permeability [nm/s] as a model for gut-blood barrier permeation (values < 25 poor, > 500 great).
[d] Number of violations of Lipinski's rule of five.
[e] Number of violations of Jorgensen's rule of three.

Table 5: Predicted toxicological properties of UNC0646 and compounds identified in **PUBLICATION III** with the highest reporter ligand displacement. The table was taken and adjusted from **PUBLICATION III** [453] (see **REPRINT PERMISSION**).

Compound	QPlogHERG[a]	Toxicological alert count[b]	Bacterial mutagenicity[d]
UNC0646	-8.22	4	EQUIVOCAL
PTMD01-0050 (**1k**)	-6.11	2	EQUIVOCAL
PTMD01-0043 (**2g**)	-7.46	4	EQUIVOCAL
PTMD99-0001C (**3**)	-4.98	0	INACTIVE
PTMD99-0016C (**4**)	-6.13	2	INACTIVE
PTMD99-0026C (**5**)	-6.53	4	PLAUSIBLE
Cycloguanil (**6**)	-3.99	1	INACTIVE

[a] IC_{50} value for blockage of HERG K^+ channels (recommended values: above -5).
[b] Number of alerts for toxicological predictions.
[c] Bacterial mutagenicity *in vitro*.

6.4. Conclusion and significance

In this multidisciplinary, collaborative study, I predicted new compounds binding to MB327-PAM-1 using *in silico* studies. Binding to the MB327 binding site was verified by our collaboration partners using MS Binding Assays. Besides analogs of UNC0646, four new chemotypes binding to the MB327 binding site were described. For one of those compounds, the active metabolite of the approved antimalaria drug proguanil, cycloguanil, the predicted binding was further verified by our collaboration partners using *ex vivo* studies on soman-poisoned rat diaphragm.

The key results and findings of this study are:

- I performed a ligand-based screening based on the two-dimensional structure of UNC0646 to identify analogs binding to MB327-PAM-1. Thereby, new insights into structure-affinity relationships can be deduced, and based on the novel identified compounds, a chimera compound with a higher reporter ligand displacement compared to UNC0646 was identified.
- Based on the proposed binding mode of UNC0646 characterized in **PUBLICATION II**, I performed a two-step screening approach using ligand-based methods considering the three-dimensional structure of PTMD01-0004, an analog of UNC0646 lacking the substituent in 2-position of the quinazoline moiety, in combination with docking studies. Variation of the substituents in 7-position revealed a substituent leading to a higher reporter ligand displacement compared to the according substituent of UNC0646.

- The binding site prediction I performed in **PUBLICATION I** enables performing structure-based virtual screening. This led to four new chemotypes binding to the MB327 binding site, including cycloguanil. Cycloguanil has subsequently been proven to reestablish muscle force in soman-poisoned rat diaphragm. The novel chemotypes display improved predicted pharmacokinetic and toxicological properties compared to UNC0646.

Virtual screening approaches proved to be efficient in the identification of novel binders to the MB327 binding site and the identification of novel PAMs of nAChRs. These compounds can be considered as novel lead structures. Only for cycloguanil, enough substance was available to test the compound in the rat diaphragm assay. Despite the reestablishment of muscle force being promising, like MB327, cycloguanil acts as an inhibitor of the receptor at higher concentrations. Nevertheless, this compound can be considered a novel lead structure, and further structure optimization and reduction of the inhibitory potential might finally lead to closing the gap in OPC poisoning treatment. Furthermore, the three remaining compounds featuring novel chemotypes shown to bind to the MB327 binding site need to be tested regarding their potential to reestablish muscle force to decide on the most promising lead structure for further optimization.

7. PUBLICATION IV

Synthesis and biological evaluation of novel MB327 analogs as resensitizers for desensitized nicotinic acetylcholine receptors after intoxication with nerve agents

T. Bernauer, V. Nitsche, J. Kaiser, C.G.W. Gertzen, G. Höfner, K.V. Niessen, T. Seeger, D. Steinritz, F. Worek, H. Gohlke, K.T. Wanner, F.F. Paintner

Toxicol Lett**,** 2024. **397**: p. 151-162.

Original publication, see pages 185 – 214.

The content covered in this chapter is taken from "Synthesis and biological evaluation of novel MB327 analogs as resensitizers for desensitized nicotinic acetylcholine receptors after intoxication with nerve agents" [454]. Sentences containing word-by-word citations are not highlighted explicitly.

7.1. Author contributions

T.B. synthesized analogs of MB327. V.N. performed MS Binding Assays. J.K. performed MD simulation experiments including suggestions for analogs based on GIST computations. C.G. supported the computational experiments. T.S. performed rat diaphragm assays. G.H., D.S., F.W., H.G., K.W., and F.P. supervised respective study parts. All authors contributed to writing the manuscript.

7.2. Background

Although a series of MB327 analogs have been synthesized, only minor improvements in affinity towards MB327-PAM-1 have been observed [48, 49]. Furthermore, analogs of MB327 generally feature a similar tight therapeutic index, making the use of these compounds for OPC poisoning treatment currently impossible [46]. However, in the literature, only few analogs of MB327 were characterized regarding their potential to reestablish muscle force in soman-poisoned tissue [46]. This publication focuses on the identification of analogs of MB327, including *in vitro* characterization of their affinity towards the MB327 binding site and *ex vivo* measurements on soman-poisoned rat diaphragm.

The novel binding site of MB327 that I identified in **PUBLICATION I** enables performing SBDD. Despite water often playing an important role in ligand binding [425-440], its existence is often neglected in SBDD. Displacing energetically unfavored water molecules has repeatedly led to the identification of potent binders [441-448]. Thus, in this publication, I contributed by

predicting MB327 analogs based on their potential to displace entropically unfavored water clusters.

7.3. Results

7.3.1. Substitution of potential entropically unfavored water clusters within MB327-PAM-1

To identify entropically unfavored water molecules, I performed 12 replicas of 1 μs long MD simulations with MB327 bound to MB327-PAM-1 in all five subunits of the nAChR. These trajectories were then post-processed using GIST [449] computations. I then investigated entropically unfavored water clusters in proximity to MB327 bound to MB327-PAM-1. Initially, in preliminary results after finishing the first few replica (5 out of 12) of MD simulations, based on an entropically unfavored water cluster in between $E65_{\alpha}$, $V66_{\alpha}$, and $Q68_{\alpha}$, PTMD90-0015 was designed (Figure 17A, B). However, after completion of all 12 replicas, PTM90-0015 would not result in displacing entropically unfavored water molecules anymore. Based on the results of the full 1 μs long MD simulations, PTMD90-0012 was designed, potentially replacing an entropically unfavored water cluster in between $I63_{\varepsilon}$, $E65_{\varepsilon}$, and $E204_{\varepsilon}$ (Figure 17A, C, D). The two glutamates interacting with the PAM calcium in α7-nAChRs are analogous to $E65_{\varepsilon}$ and $E204_{\varepsilon}$ [65, 69].

After synthesis of the compounds, the ligands were characterized based on their ability to displace the reporter ligand in MS Binding Assays and to reestablish muscle force in soman-poisoned rat diaphragm[‡9]. PTMD90-0015, designed based on initial results from the MD simulations, showed decreased affinity towards MB327-PAM-1 compared to MB327 [pK_i (PTMD90-0015) = 3.29 ± 0.05, pK_i (MB327) = 3.40 ± 0.04] and no beneficial effects on muscle force reestablishment in rat diaphragm assays (Figure 17E). In contrast, PTMD90-0012, designed based on the complete MD simulations, showed increased affinity compared to MB327 (pK_i = 3.69 ± 0.03, $p < 0.01$ using a two-sided t-test). The restoration of muscle force in soman-poisoned rat muscles is higher when treating the muscle with 100 μM PTMD90-0012 (25.6 ± 17.5%, n = 11, Figure 17F) compared to MB327 (14.8 ± 9.2%, n = 29, data taken from ref. [46]), although not significant (p = 0.075, according to a two-sided Welch's t-test).

[‡9] Synthesis and i*n vitro* experiments were performed by Tamara Bernauer and Valentin Nitsche, respectively, under supervision of Prof. Dr. Klaus T. Wanner and Prof. Dr. Franz F. Paintner at the Department of Pharmacy – Center for Drug Research, Ludwig Maximilians University. *Ex vivo* experiments were performed by Dr. Thomas Seeger at the Bundeswehr Institute of Pharmacology and Toxicology.

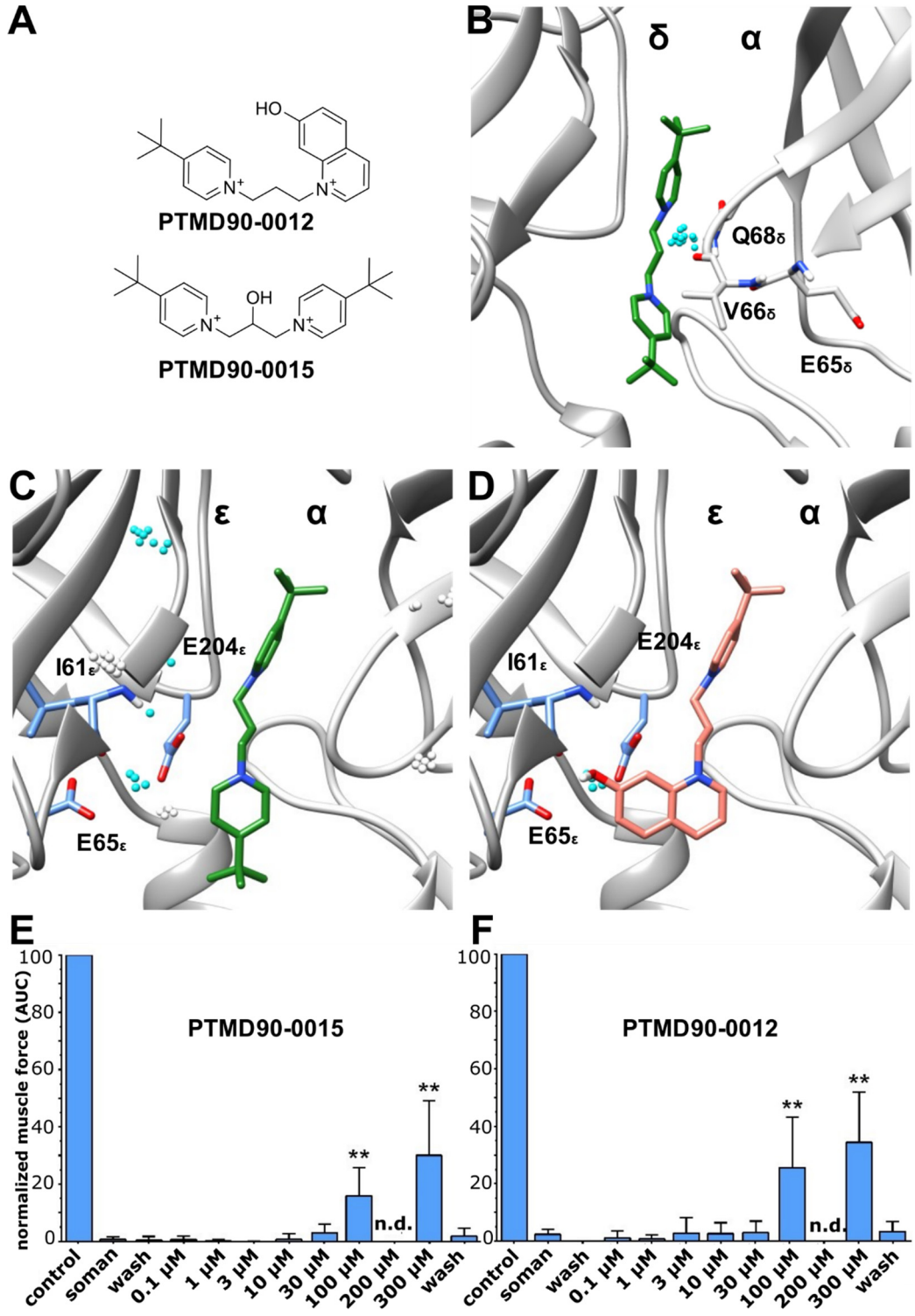

Figure 17: Design of MB327 analogs based on the identification of unfavored water clusters within MB327-PAM-1. **A)** Structure of the novel MB327 analogs PTMD90-0012 and PTMD90-0015. **B)** MB327 bound in between the α- and δ-subunits. During the first 5 out of 12 replicas, an entropically unfavored water cluster was observed between E65α, V66α, and Q68α, close to the *C3*-linker of MB327 leading to the design of PTMD90-0015. Water clusters are shown as spheres, and water clusters within 5 Å of MB327 are colored cyan. **C)**MB327 (green) bound in between the α- and ε-subunit. Water clusters are shown as spheres, and water clusters within 5 Å of MB327 are colored cyan. $E204_{\varepsilon}$, $E65_{\varepsilon}$, and $I61_{\varepsilon}$ interacting with a water cluster in proximity to the aromatic ring of MB327 facing towards the TMD (downwards in this projection) are shown as sticks. **D)** Variation of MB327 to PTMD90-0012 can result in displacement of the entropically unfavored water cluster in proximity. Concentration-dependent muscle force restoration of soman-poisoned rat muscles after treatment with **E)** PTMD90-0015 and **F)** PTMD90-0012. Bars indicate the standard deviation and asterisks indicate significant higher values compared to soman (** $p < 0.01$). n.d. means that no measurements at these concentrations were determined. The figure was taken and adjusted from **PUBLICATION IV** [454] (see **REPRINT PERMISSION**).

7.4. Conclusion and significance

I used MD simulations to identify entropically unfavored water molecules in MB327-PAM-1 to contribute to a multidisciplinary, collaborative study. Based on these observations, novel MB327 analogs were designed and subsequently tested regarding their affinity towards nAChR and their activity in reestablishing muscle force in soman-poisoned rat diaphragm.

The key results and findings of this study are:

- Based on 12 replicas of 1 μs long MD simulations, I designed PTMD90-0012 aiming at substituting an entropically unfavored water cluster within the binding site. Compared to MB327, the affinity towards MB327-PAM-1 is increased.

These findings give further insights into the structure-activity relationships of MB327 analogs and indicate that substituting entropically unfavored water molecules can contribute to increasing ligand affinity.

8. SUMMARY AND PERSPECTIVE

In the present work I have utilized computational methods to further understand the binding mode of PAMs in nAChRs and contributed to the development of novel, more potent PAMs. The key findings of my thesis include:

- Proposing an allosteric binding site for MB327, MB327-PAM-1, in line with experimental results (**PUBLICATION I**).
- Providing an approach to explaining why MB327 acts as an inhibitor of nAChRs at higher concentrations (**PUBLICATION I**).
- Developing a plausible binding mode of UNC0646 (**PUBLICATION II**).
- Based on the knowledge about the binding site, developing new analogs of MB327 (**PUBLICATION I** and **IV**) with increased potency / affinity compared to MB327.
- Suggesting varying substituents of the quinazoline moiety of UNC0646 resulting in analogs with a higher reporter ligand displacement compared to the native UNC0646 quinazoline substituents (**PUBLICATION III**).
- Identifying four new chemotypes binding to MB327-PAM-1, including cycloguanil showing a higher muscle force reestablishment after soman poisoning compared to UNC0646 and its analogs and a reestablishment comparable to MB327 starting at lower compound concentrations compared to MB327 (**PUBLICATION III**).

However, while these approaches deliver important progress in the development of novel PAMs of nAChRs, one current drawback is that all compounds feature a tight therapeutic index, resulting in the inhibition of nAChRs at slightly higher concentrations than the therapeutically needed concentrations. Nevertheless, within this thesis, I developed the ground to address this problem by predicting the orthosteric binding site as a responsible binding pocket for the inhibitory effect. Thus, future PAM design should focus on enhancing the affinity to MB327-PAM-1 while simultaneously decreasing the affinity to the orthosteric binding site to ultimately close the therapeutic gap in OPC poisoning treatment. Furthermore, the recent experimental observations by Haufe *et al*. that MB327 does not act as PAM [162] need to be further investigated and the reason for these contrary findings need to be unraveled. Therefore, it is important to further elucidate the binding properties of the ligands in all proposed binding sites. Hence, experiments that would further help to understand binding properties include a thoroughly experimental characterization of binding affinities to all binding sites and a comparison of this data to each compound's capability of reestablishing muscle force after OPC

poisoning. This data can subsequently be compared to computational free energy computations of the compounds in the binding sites and to CNA computations investigating the allosteric impact of each compound on the orthosteric binding site and the desensitization gate. If experimental results are in line with computational predictions, free energy computations and allostery predictions using CNA can be implemented in the design workflow of new PAMs to avoid experimentally testing compounds that show no beneficial effects. Furthermore, based on this extensive data, structure-affinity relationships and machine learning tools can be developed, comprising data from experimental results and computational predictions that can ultimately be used to predict novel PAMs.

As a first step, in a manuscript that is currently in preparation [Bernauer *et al.*, unpublished, see **LIST OF PUBLICATIONS**], I provided qualitative structure-affinity relationships for UNC0646 analogs in MB327-PAM-1 (Figure 18) and developed a linear regression QSAR model using all compounds tested for remaining marker binding in the UNC0642 binding assay at test compound concentrations of 10 μM and reporter ligand concentrations of 1 μM [453, 454] [Bernauer *et al.*, unpublished], using AutoQSAR, as implemented in Maestro [455, 456]. Compounds displaying a remaining reporter ligand binding not significantly different from 100% ($p > 0.05$, based on a two-sided one-sample *t*-test) were removed from the dataset because the actual affinity values might vary widely. The remaining compounds were randomly split into an external validation set (20% of all compounds, 16 compounds), and the remaining compounds were divided into a training and test set (80% / 20%, 49 and 12 compounds, respectively). The resulting model shows high predictivity with an RMSE about 2.5 times the mean standard deviation derived in experimental testing. (RMSE test set: 10%; RMSE validation set: 9%; mean experimental standard deviation: 4%) (Figure 19). This data, including the variables contributing to a higher affinity according to the QSAR model (Table 6), may help in the design of novel PAMs targeting nAChRs in the future. However, as mentioned above, to ultimately predict the potency of PAMs for resensitizing nAChRs, further data needs to be implemented in a predictive model, such as the inhibitory effect of each compound on nAChRs and the capability to restore muscle function after OPC poisoning.

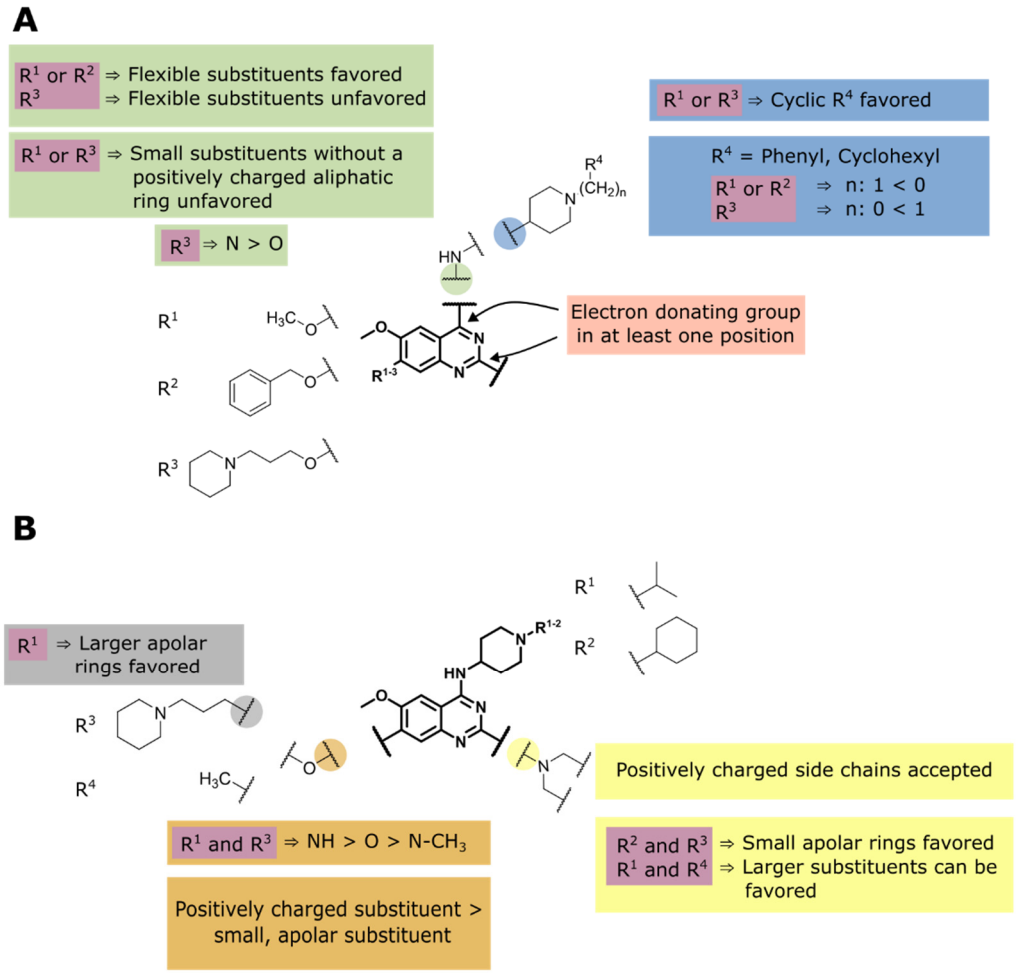

Figure 18: Summary of qualitative structure-affinity relationships of UNC0646 analogs described in [Bernauer *et al.,* unpublished]. Qualitative structure-affinity relationships in **A)** the 4-position of the quinazoline building block, contingent upon the substituent in the 7-position, **B)** in the 7-position of the quinazoline building block, depending on different substituents in the 4-position, and in the 2-position of the quinazoline building block, contingent upon different substituents in the 4- and 7-positions. Effects at different positions are depicted by varying colors. The quinazoline core structure is highlighted in bold. ">" refers to a higher reporter ligand substitution of the respective feature. Undefined substituents in 2-position in panels A) and B) indicate an interchangeability with various substituents. If certain trends are dependent on certain substituents in other positions, the substituents are indicated in purple boxes, respectively. Figure was taken from [Bernauer *et al.*, unpublished, see **LIST OF PUBLICATIONS**].

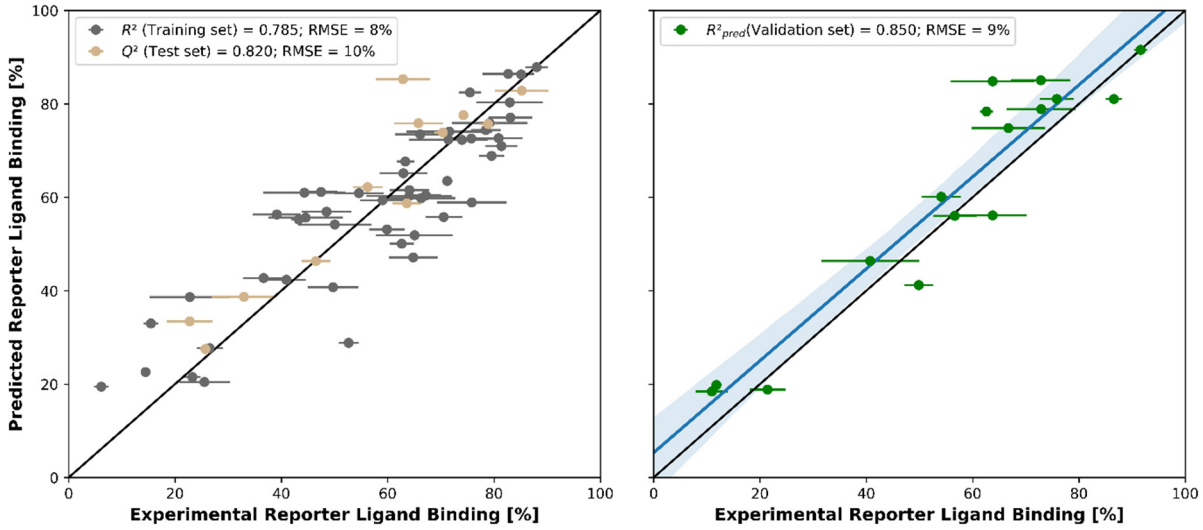

Figure 19: QSAR model based on compounds tested in the UNC0642 MS Binding Assay (test compound concentrations = 10 µM; reporter ligand concentrations = 1 µM). **A)** Results for the training (grey) and test set (sand color) are depicted. **B)** The results for the validation set are shown. The values for R^2, Q^2, R^2_{pred}, and RMSE are depicted in the legends, respectively. Black lines indicate a perfect prediction. For the validation set a regression line is shown in blue together with the 95% confidence interval as blue shade. Figure taken from [Bernauer *et al.*, unpublished, see **LIST OF PUBLICATIONS**].

Table 6: Variables[a] contributing to the QSAR model[b]. Table taken from [Bernauer et al., unpublished, see **LIST OF PUBLICATIONS**].

Variable	Coefficient
Intercept	3.34
CH_3 count	$3.16 * 10^{-1}$
Sum of topological distances between N N	$-2.39 * 10^{-3}$
Sum of topological distances between O O	$1.84 * 10^{-3}$
Neutral donor groups	$-4.49 * 10^{-2}$
ALOGP6[c]	$2.11 * 10^{-2}$
Randic connectivity	$-2.04 * 10^{-1}$
PEOE2[d]	$-6.51 * 10^{-3}$
PEOE7[d]	$-1.41 * 10^{-2}$

[a] For further information and explanations of the variables, we refer to ref. [457].

[b] Variables and Coefficients were extracted from the AutoQSAR output, as implemented in Maestro [455, 456].

[c] AlogP is an atomistic method to estimate the log *P* value of compounds [458]. AlogP6 refers to the surface area attributable to atoms with AlogP values in between 0.15 and 0.2.

[d] Surface area attributable to atoms with Gasteiger charges [459] within a certain bin. The number refers to the number of the bin where the binning scheme is [< -0.3, -0.3 to -0.25, …, 0.25 to 0.3, > 0.3]. Thus, PEOE2 and PEOE7 correspond to surface areas attributable to atoms with Gasteiger charges of -0.3 to -0.25 and -0.05 to 0, respectively.

While we predicted MB327-PAM-1 as binding site for MB327, further experimental evidence will be required to ultimately confirm these predictions. Therefore, mutational studies would give further insights into amino acids involved in stabilization of MB327 within its binding site. At best, a crystal or cryo-EM structure of a nAChR in complex with MB327 would be made available to unravel the exact binding mode of MB327. This would help to better understand crucial interactions on an atomistic level and thus to develop more potent PAMs.

Additionally, while MB327-PAM-1 is a promising binding site to identify novel PAMs, all currently known binders of MB327-PAM-1 feature a tight therapeutic index. Thus, in further studies it might be promising to target alternative binding sites, potentially transmitting positive allosteric effects. As mentioned above, several alternative binding sites for PAMs were already described in PDB structures. Furthermore, docking of fragments to the whole nAChR, as done by Hedderich *et al.* for G-protein coupled receptors [283], might help to further understand the pocketome of the receptor. Nevertheless, the later approach would not guarantee that newly identified pockets are sufficient to transmit positive allosteric effects on the receptor. Thus, it might be more promising to first focus on known allosteric pockets. There, it is crucial to also consider differences in the binding sites of the human muscle-type nAChR compared to the subtype in which the PAM binding site was originally described.

Furthermore, while I provided an explanation of how MB327 can transmit its allosteric effect on the receptor after binding to MB327-PAM-1, the exact mechanism of action facilitating changes in receptor configuration remains elusive. Thus, further studies need to be conducted to elucidate the mechanisms resulting in structural rearrangements associated with the different states of the receptor and the impact of MB327 on these pathways. Therefore, computational studies can be a helpful tool to sample the transition pathway between the states and thereby unravel mechanisms leading to desensitization of nAChRs. Based on these findings, novel PAMs can be designed to interact with amino acids crucial for preventing the receptor form desensitizing.

Taken together, my results provide insights into the binding sites of MB327, making SBDD and LBDD feasible, and demonstrate first successful examples identifying novel chemical scaffolds acting as PAMs. However, further studies are required to optimize these compounds and to finally close the therapeutic gap in OPC poisoning treatment.

9. ACKNOWLEDGMENTS

First and foremost, I would like to thank my supervisor **Prof. Dr. Holger Gohlke** for giving me the opportunity to work on this interesting topic within his group. I am deeply grateful for the precious guidance he provided throughout my work and his seemingly endless dedication to fostering academic excellence. I am also thankful for the countless hours Prof. Dr. Holger Gohlke spent on fruitful discussions, reviewing my results, and offering thoughtful suggestions to improve my work.

Thanks to all my colleagues in the CPC and CBC lab for all the suggestions and discussions during our group seminars, topic group meetings and whenever I had questions. Especially, I would like to thank **Dr. Christoph Gertzen** for his constant help in planning and conducting all the experiments. I would also like to thank **Dr. Christopher Pfleger** for providing a lot of insights into rigidity analysis and **Dr. Michele Bonus**, **Dr. Daniel Becker**, and **Dr. Stephan Schott-Verdugo** for offering their knowledge in all kinds of scientific questions. Additionally, I would like to thank **Dr. Michele Bonus**, **Dr. Christoph Gertzen**, and **Yu-Lin Ho** for proofreading my thesis. Also, I am deeply grateful to **Prof. Dr. Matthias Kassack** for being my second supervisor.

Furthermore, I would like to thank all my collaboration partners from the Ludwig Maximilians University and the Bundeswehr Institute of Pharmacology and Toxicology, **Dr. Karin Niessen**, **Dr. Thomas Seeger**, **Prof. Dr. Klaus T. Wanner**, **Prof. Dr. Franz F. Paintner**, **Tamara Bernauer**, **Valentin Nitsche**, **Prof. Dr. Dirk Steinritz**, **Prof. Dr. Franz Worek**, and **Prof. Dr. Horst Thiermann**, for a very joyful and great scientific collaboration, including a lot of fruitful discussions and suggestions during our meetings, and for conducting all the experiments suggested based on computational experiments.

Also, I would like to thank **Dr. David Bickel**, **Pegah Golchin**, **Dr. Daniel Becker**, **Yu Lin Ho**, **Rocco Gentile**, **Lisa Kersten**, **Gürbüz Önder**, and **Alena Endres** for making the lab work way more enjoyable.

Last, but not least, special thanks to my family, **Andreas**, **Britta**, and **Dr. Luca Kaiser** for always being there and supporting me throughout my life, to **Jelena Kaiser** for her unconditional love and support, and to **Taavi Kaiser** for always making me smile during the last part of my PhD.

10. REPRINT PERMISSION

Reprint permission was granted on the 20th of June 2024 for the following articles:

PUBLICATION I

This article was published in Toxicology Letters, Volume 373, Jesko Kaiser, Christoph G.W. Gertzen, Tamara Bernauer, Georg Höfner, Karin V. Niessen, Thomas Seeger, Franz F. Paintner, Klaus T. Wanner, Franz Worek, Horst Thiermann, Holger Gohlke, "A novel binding site in the nicotinic acetylcholine receptor for MB327 can explain its allosteric modulation relevant for organophosphorus-poisoning treatment", p. 160-171, Copyright Elsevier (2023).

PUBLICATION II

This article was published in Toxicology Letters, Volume 392, Valentin Nitsche, Georg Höfner, Jesko Kaiser, Christoph G.W. Gertzen, Thomas Seeger, Karin V. Niessen, Dirk Steinritz, Franz Worek, Holger Gohlke, Franz F. Paintner, Klaus T. Wanner, "MS Binding Assays with UNC0642 as reporter ligand for the MB327 binding site of the nicotinic acetylcholine receptor", p. 94-106, Copyright Elsevier (2024).

PUBLICATION III

This article was published in Toxicology Letters, Jesko Kaiser, Christoph G.W. Gertzen, Tamara Bernauer, Valentin Nitsche, Georg Höfner, Karin V. Niessen, Thomas Seeger, Franz F. Paintner, Klaus T. Wanner, Dirk Steinritz, Franz Worek, Holger Gohlke, "Identification of ligands binding to MB327-PAM-1, a binding pocket relevant for resensitization of nAChRs", *in press*, Copyright Elsevier (2024).

PUBLICATION IV

This article was published in Toxicology Letters, Volume 397, Tamara Bernauer, Valentin Nitsche, Jesko Kaiser, Christoph G.W. Gertzen, Georg Höfner, Karin V. Niessen, Thomas Seeger, Dirk Steinritz, Franz Worek, Holger Gohlke, Klaus T. Wanner, Franz F. Paintner , "Synthesis and biological evaluation of novel MB327 analogs as resensitizers for desensitized nicotinic acetylcholine receptors after intoxication with nerve agents", p. 151-162, Copyright Elsevier (2024).

11. PUBLICATIONS

11.1. Publication I

A novel binding site in the nicotinic acetylcholine receptor for MB327 can explain its allosteric modulation relevant for organophosphorus-poisoning treatment

Jesko Kaiser, Christoph G.W. Gertzen, Tamara Bernauer, Georg Höfner, Karin V. Niessen, Thomas Seeger, Franz F. Paintner, Klaus T. Wanner, Franz Worek, Horst Thiermann, Holger Gohlke

Toxicology Letters, 2023. **373**: p. 160-171. [§1]

[§1] See **REPRINT PERMISSION**

Toxicology Letters 373 (2023) 160–171

Contents lists available at ScienceDirect

Toxicology Letters

journal homepage: www.journals.elsevier.com/toxicology-letters

A novel binding site in the nicotinic acetylcholine receptor for MB327 can explain its allosteric modulation relevant for organophosphorus-poisoning treatment

Jesko Kaiser [a,1], Christoph G.W. Gertzen [a,2], Tamara Bernauer [b,3], Georg Höfner [b], Karin V. Niessen [c], Thomas Seeger [c], Franz F. Paintner [b,4], Klaus T. Wanner [b,5], Franz Worek [c], Horst Thiermann [c], Holger Gohlke [a,d,*,6]

[a] Institute for Pharmaceutical and Medicinal Chemistry, Heinrich Heine University Düsseldorf, Düsseldorf, Germany
[b] Department of Pharmacy – Center for Drug Research, Ludwig-Maximilians-Universität München, München, Germany
[c] Bundeswehr Institute of Pharmacology and Toxicology, München, Germany
[d] John von Neumann Institute for Computing (NIC), Jülich Supercomputing Centre (JSC), Institute of Biological Information Processing (IBI-7: Structural Biochemistry) & Institute of Bio, and Geosciences (IBG-4: Bioinformatics), Forschungszentrum Jülich, Jülich, Germany

ARTICLE INFO

Editor: Dr. Angela Mally

Keywords:
nAChR
Cooperativity
Bispyridinium compounds
Blind docking
Molecular dynamics simulations
Rigidity analysis

ABSTRACT

Organophosphorus compounds (OPCs) are highly toxic compounds that can block acetylcholine esterase (AChE) and thereby indirectly lead to an overstimulation of muscarinic and nicotinic acetylcholine receptors (nAChRs). The current treatment with atropine and AChE reactivators (oximes) is insufficient to prevent toxic effects, such as respiratory paralysis, after poisonings with various OPCs. Thus, alternative treatment options are required to increase treatment efficacy. Novel therapeutics, such as the bispyridinium non-oxime MB327, have been found to reestablish neuromuscular transmission by interacting directly with nAChR, probably via allosteric mechanisms. To rationally design new, more potent drugs addressing nAChR, knowledge of the binding mode of MB327 is fundamental. However, the binding pocket of MB327 has remained elusive. Here, we identify a new potential allosteric binding pocket (MB327-PAM-1) of MB327 located at the transition of the extracellular to the transmembrane region using blind docking experiments and molecular dynamics simulations. MB327 forms striking interactions with the receptor at this site. The interacting amino acids are highly conserved among different subunits and different species. Correspondingly, MB327 can interact with several nAChR subtypes from different species. We predict by rigidity analysis that MB327 exerts an allosteric effect on the orthosteric binding pocket and the transmembrane domain after binding to MB327-PAM-1. Furthermore, free ligand diffusion MD simulations reveal that MB327 also has an affinity to the orthosteric binding pocket, which agrees with recently published results that related bispyridinium compounds show inhibitory effects via the orthosteric binding site. The newly identified binding site allowed us to predict structural modifications of MB327, resulting in the more potent resensitizers PTM0062 and PTM0063.

1. Introduction

Despite the aim to ban chemical warfare agents, they remain a serious threat to the military and civilian population (Wiener and Hoffman, 2004). The highly toxic organophosphorus (OPCs) nerve agents block acetylcholinesterase (AChE) and lead to an increase of

* Correspondence to: Universitätsstr. 1, 40225 Düsseldorf, Germany.
E-mail address: gohlke@uni-duesseldorf.de (H. Gohlke).
[1] ORCID: 0000-0002-6429-0911
[2] ORCID: 0000-0002-9562-7708
[3] ORCID: 0000-0001-9570-1253
[4] ORCID: 0000-0002-6795-586X
[5] ORCID: 0000-0003-4399-1425
[6] ORCID: 0000-0001-8613-1447

https://doi.org/10.1016/j.toxlet.2022.11.018
Received 7 October 2022; Accepted 25 November 2022
Available online 26 November 2022

acetylcholine at cholinergic synapses, followed by overstimulation of muscarinic (mAChR) and nicotinic (nAChR) acetylcholine receptors. This is associated with several serious toxic effects, such as respiratory paralysis, which can lead to death (Wiener and Hoffman, 2004; Holmstedt, 1959).

So far, the treatment of OPC-poisonings mainly focuses on reestablishing the function of AChE with oximes and competitive antagonism at mAChR (Thiermann et al., 2013). Although oximes can have a remarkable positive indirect effect on nAChR function by restoring AChE functionality in poisonings with several OPCs, they lack efficacy with others, e.g., tabun- and soman-inhibited AChE, which results in a substantial therapeutic gap (Worek et al., 2004). Novel therapeutic approaches focus on ligands that interact directly with nAChR (Sheridan et al., 2005; Turner et al., 2011). As such, the bispyridinium compound MB327, which modulates several nAChR subtypes from different species, has been reported to reestablish neuromuscular transmission in vitro (Seeger et al., 2012; Niessen et al., 2016; Scheffel et al., 2018; Sichler et al., 2018). Furthermore, it leads to increased protection against soman-poisoning in guinea pigs in combination with hyoscine and physostigmine (Turner et al., 2011). However, to improve the efficacy of such compounds in a knowledge-driven molecular design workflow, detailed information of the binding mode is of utmost importance.

So far, three potential binding sites for bispyridinium compounds have been reported in nAChR. Based on blind docking experiments, Wein et al. suggested two potential binding sites of MB327, one in the extracellular domain and one in the upper part of the transmembrane domain (Wein et al., 2018). Recently, Epstein et al. proposed that bispyridinium compounds can bind in the orthosteric binding pocket and its neighboring region between the α- and ε-subunits, exerting an inhibitory effect, and confirmed their *in silico* findings using mutational studies (Epstein et al., 2021). Although this data explains the inhibitory effect of bispyridinium compounds, our previous studies indicated that MB327 probably acts as an allosteric modulator to reestablish muscular function (Niessen et al., 2018). Furthermore, the affinities of analogs of the bispyridinium compound SAD-128 to the orthosteric binding pocket do not correlate with the improvement of neuromuscular transmission, suggesting that this effect is not mediated via binding to the orthosteric binding site (Niessen et al., 2011). Additionally, the displacement of the orthosteric ligand [^{3}H]epibatidine by MB327 results in an $IC_{50} > 100$ μM, although the affinity of [^{3}H]epibatidine to nAChR was already increased at lower concentrations of MB327 (Niessen et al., 2013). Finally, pharmacological effects have been recorded at low μM concentrations of MB327 in the presence of carbamoylcholine. In the absence of carbamoylcholine, no effect has been detected. The latter findings further indicate an allosteric effect (Niessen et al., 2016).

In this study, we describe a novel potential binding site for M327 in nAChR, termed MB327-PAM-1, which was identified by a combination of molecular docking experiments, molecular simulations, and rigidity analyses. To explore the ligand-receptor dynamics, we performed molecular dynamics (MD) simulations and identified important interactions of MB327 with the receptor. The interacting amino acids are highly conserved among different subunits and different species, which can explain the promiscuity of MB327 towards several nAChR subtypes in different species. Furthermore, constraint network analysis (CNA) reveals that MB327 can allosterically impact both the orthosteric binding pocket and the transmembrane domain after binding to MB327-PAM-1. Free ligand diffusion MD simulations imply that MB327 is also affine to the orthosteric binding site, which might contribute to the inhibitory effect on nAChR at higher concentrations (Scheffel et al., 2018; Niessen et al., 2018). Finally, based on the newly identified binding mode of MB327, we predicted structural modifications of MB327, resulting in the more potent resensitizers PTM0062 and PTM0063.

2. Materials and methods

2.1. Homology modeling

The homology models of nAChR were created using MODELLER, version 9.19 (Webb and Sali, 2016). For modeling the desensitized state of nAChR, we only included receptor structures of nAChRs where the transmembrane domain is resolved and that are described to be in a desensitized state. All receptors that, to the best of our knowledge, were available in the PDB at the point of model generation were included. Receptors deposited by Unwin et al. (PDB-IDs 2BG9 (Unwin, 2005), 4AQ5, and 4AQ9 (Unwin and Fujiyoshi, 2012)) were not considered because later structures and experiments showed that, due to low resolution, the structures were wrongly fitted in the transmembrane domain (Mnatsakanyan and Jansen, 2013; Morales-Perez et al., 2016). Furthermore, to neglect a bias of similar protein backbone conformations from one publication, we only included one structure from each publication. However, because all of these receptors show a resolution above 3.5 Å and we expect MB327 to bind in the extracellular domain, we also included the crystal structure of the acetylcholine-binding protein in complex with the partial agonist 4-OH-DMXBA (PDB-ID: 2WN9 (Hibbs et al., 2009)). Concluding, for the human desensitized muscle-type nAChR, the PDB structures 6PV8 (Gharpure et al., 2019), 5KXI (Morales-Perez et al., 2016), 2WN9 (Hibbs et al., 2009), and 6CNK (Walsh et al., 2018) were used as templates.

For the human α7-nAChR, the PDB structures 6PV8 (Gharpure et al., 2019), 5KXI (Morales-Perez et al., 2016), 2WN9 (Hibbs et al., 2009), 6CNK (Walsh et al., 2018), and 6UR8 (Mukherjee et al., 2020) were used as templates. While not stated explicitly in that publication, the cryoEM structure of the α4β2 nAChR in complex with the partial agonist varenicline (PDB-ID: 6UR8 (Mukherjee et al., 2020)) shows a transmembrane domain typical for the desensitized state (SI Fig. 1). Thus, after analyzing the transmembrane pore of this receptor, we also included the receptor in the later created alpha7 nAChR models.

For the human inactive muscle-type nAChR, the PDB structure 6UWZ (Rahman et al., 2020) was used as a template. This was, to the best of our knowledge, the only PDB structure of the inactive nAChR available in the PDB at the time of model generation. To compare the binding site of PNU-120596 in the human muscle-type nAChR with α7-nAChR, the structure of the α7-nAChR in complex with PNU-120596 was used as a template (PDB-ID: 7EKT (Zhao et al., 2021)).

The alignments were created using BLAST (Altschul et al., 1990) and verified using PROMALS3D (Pei et al., 2008). Water molecules and crystallization artifacts were removed. Amino acids at the N- and C-termini and in the intracellular loop not resolved in the templates were not included in the models. 50 models were generated for the human muscle-type and α7-nAChR, respectively, and the final model was selected based on the DOPE potential (Shen and Sali, 2006), TopScore (Mulnaes and Gohlke, 2018), and visual inspection. The selected homology models were protonated using PROPKA (Olsson et al., 2011; Sondergaard et al., 2011) as implemented in Maestro (Schrödinger, 2020) at a pH of 7.4, and the termini were capped with NME and ACE using Maestro (Schrödinger, 2020).

2.2. Docking

For the docking, 3D structures of the ligands were generated using Maestro (Schrödinger, 2020). MB327 was placed in the middle of the extracellular part of the pore so that we could generate a docking box including the extracellular part of the receptor (SI Fig. S2). The ligands were subsequently docked into the receptor using AutoDock3 (Morris et al., 1998) in combination with DrugScore^{2018} (Dittrich et al., 2019) as the scoring function. During the docking, default parameters were used, with the exception that the margin of the box was set to 35 Å and the grid spacing to 1 Å.

MB327, PTM0062, and PTM0063 were also docked into the newly

identified binding pocket using FRED (OpenEye Scientific Software, 2020) with default parameters. Therefore, conformers of MB327 were generated using OMEGA (OpenEye Scientific Software, 2020) with default parameters. The receptor was prepared using MakeReceptor (OpenEye Scientific Software, 2020) with the highest-ranked pose of MB327 after the initial docking for each pocket, and the ligands were subsequently docked into the receptor. To avoid a bias of the placement of MB327 based on the initial dockings, no constraints for protein-ligand interactions were selected, resulting in an independent placement of the ligands in the newly identified pocket. The best poses were selected based on their docking scores and visual inspection. For MD simulations, nicotine was docked to the orthosteric binding pocket using the same two-step procedure. For the simulations with MB327 bound to all five subunits, nicotine was added to nAChR by aligning the PDB structure of the α3β4-nAChR (PDB ID 6PV7 (Gharpure et al., 2019)) to the models and subsequently minimized in the orthosteric binding site using SZYBKI (OpenEye Scientific Software, 2020).

2.3. Molecular dynamics simulations

The structures were embedded in a membrane consisting of 1-palmitoyl-2-oleoyl-*sn*-glycero-3-phosphocholine (POPC) lipids and solvated in a rectangular box of OPC water (Izadi et al., 2014) using Packmol-Memgen (Schott-Verdugo and Gohlke, 2019), with the edge of the box at least 12 Å away from the solute atoms. For the MD simulations with MB327 bound to all five subunits, sodium was placed in the pore by aligning the sodium ion from the human α3β4-nAChR (PDB ID 6PV7 (Gharpure et al., 2019)). For the free ligand diffusion MD simulations, ten independent simulation systems were generated by placing MB327 at random positions within the rectangular box.

The AMBER package of molecular simulation software (Case et al., 2005) and the *ff19SB* force field (Tian et al., 2020) in combination with the Lipid17 force field (Gould et al., unpublished) was used to perform MD simulations. Ligand charges were calculated using Gaussian16 (Frisch et al. 2016). The "Particle Mesh Ewald" method was used to consider long-range interactions; for all bonds involving hydrogens, the SHAKE algorithm was applied (Darden et al., 1993; Ryckaert et al., 1977). During the thermalization period, the time step was set to 2 fs with a direct-space, nonbonded cutoff of 9 Å. During the production runs, hydrogen mass repartitioning was used, and the time step was set to 4 fs with a direct-space, nonbonded cutoff of 8 Å (Hopkins et al., 2015).

Initially, a combination of steepest descent and conjugate gradient minimization was performed; positional harmonic restraints were applied to protein and bound ligand atoms and gradually reduced from 5 (25 for the simulation with MB327 bound to all subunits) to 0 kcal mol^{-1} $Å^{-2}$. Next, the system was heated to 100 K during 50 ps (5 ps for the simulations of the docked structure) of NVT-MD (constant number of particles, volume, and temperature). Subsequently, 50 ps (115 ps for the simulations of the docked structure) of NPT-MD (constant number of particles, pressure, and temperature) were conducted to heat the system to 300 K. During these steps, harmonic restraints with a force constant of 1 kcal mol^{-1} $Å^{-2}$ (25 kcal mol^{-1} $Å^{-2}$ for the simulations with MB327 bound to all subunits) were applied to receptor and ligand atoms. The harmonic restraints were then gradually reduced to 0 kcal mol^{-1} $Å^{-2}$ during NPT-MD simulations.

Thereafter, the production runs of 900 ns length for the free ligand diffusion MD simulations (100 ns for the simulations of the docked structure) were performed. Subsequently, the distances of the ligand to the receptor were analyzed using the *nativecontacts mindist* function as implemented in CPPTRAJ (Roe and Cheatham, 2013). Representative binding poses were created by clustering the frames using the k-means clustering algorithm as implemented in CPPPTRAJ (Roe and Cheatham, 2013). The RMSD of the heavy atoms of the protein and the ligands have been used as a cluster criterion. The backbone RMSD and electron density values of the system during MD simulations were computed using CPPTRAJ (Roe and Cheatham, 2013). We computed the effective binding energy of MB327 in each binding pocket using the MM-GBSA method in combination with the OBC implicit water model, as implemented in AMBER (Case et al., 2005; Onufriev et al., 2004; Miller et al., 2012). We calculated the mean over all replicas x in which MB327 stays stable in MB327-PAM-1 and the standard error of the mean (SEM) using the following equation as done previously (Twizerimana et al., 2020):

$$SEM_{all} = \frac{1}{x}\sqrt{\sum_{i=1}^{x} SEM_i^2}$$

2.4. Constraint network analysis (CNA)

Frames were extracted from the MD simulations of nAChR with MB327 bound to all five subunits and nicotine bound to both orthosteric binding sites every 1 ns using CPPTRAJ (Roe and Cheatham, 2013). To investigate a potential functional coupling between the ligand binding sites as well as with the transmembrane domain, we performed perturbation runs as implemented in CNA (Pfleger et al., 2013a). The perturbation approach performs two runs of constraint dilution simulations of the protein in the presence and absence of the ligands and, thereby, calculates a per-residue decomposition $\Delta G_{i,CNA}$ that indicates the ligands' effect on the structural stability of residue i. We performed three calculations, one where only MB327 was extracted from the system (s1), one where only nicotine was extracted (s2), and one where both ligands where extracted (s1/s2) to investigate the respective impact of the ligands. To investigate the statistical independence of the frames, we computed the autocorrelation function (ACF(τ)) of the first replica for $\Delta G_{CNA,s1}$ (Case et al., 2005). As ACF($\tau = 0.5$ ns) = 0.2 < 1/e, the frames are statistically independent. To predict cooperative effects in the system, $\Delta G_{CNA,\{s1/s2,\ s1,\ s2\}}$ was computed as the sum over all $\Delta G_{i,CNA}$ for the respective state. Then, the cooperative free energy $\Delta\Delta G_{CNA,n}$ was computed according to Eq. 1 as done previously (Pfleger et al., 2021),

$$\Delta\Delta G_{CNA,n} = \Delta G_{CNA,s1/s2} - (\Delta G_{CNA,s1} + \Delta G_{CNA,s2}) \quad (1)$$

where positive values indicate a negative cooperativity while negative values indicate a positive cooperativity.

To analyze the impact of calcium on the system, we removed the ligands from nAChR and performed two CNA runs, one where we manually added additional restraints in the form of covalent bonds between the two glutamates involved in calcium binding in three subunits, and one without additional restraints. The former mimics the local rigidifying effect of a bound calcium ion. Then, we calculated the difference in $\Delta G_{i,CNA}$ between the CNA analyses for the systems with and without additional restraints for each residue i to compute the impact of calcium on the structural stability of nAChR.

2.5. Similarity analysis of the binding pocket

For the similarity analysis of the binding pocket, the PDB structure 1UW6 (Celie et al., 2004) of the acetylcholine binding protein of *Lymnaea stagnalis* was aligned to the human muscle-type nAChR model using UCSF Chimera (Pettersen et al., 2004), and amino acids within 5 Å of nicotine were compared to the respective region in the δ-β-subunit using BLAST (Altschul et al., 1990).

2.6. Electrostatic analysis

The electrostatics was analyzed by solving the linear *Poisson-Boltzman* equation as implemented in APBS (Jurrus et al., 2018) using the APBS Pymol Plugin in the presence of positively (charge +1, ion radius 1.8 Å) and negatively (charge −1, ion radius 2.0 Å) charged counter ions in a concentration of 0.15 M. The dielectric constant of the solvent and the protein were set to 78.0 and 2.0, respectively.

2.7. Image generation

Images of nAChR were generated using PyMol (Schrödinger, 2015), version 2.3.0.

2.8. Analysis of the transmembrane pore radius

The transmembrane pore radius of proteins was analyzed using the CAVER PyMol Plugin (Pavelka et al., 2016).

2.9. Synthesis of PTM0062 (3a) and PTM0063 (3b)

Microwave reactions were carried out on a Discover SP microwave system by CEM GmbH. All chemicals were used as purchased from commercial sources. Solvents used for purification were distilled before use. ^{1}H and ^{13}C NMR spectra were recorded on a Bruker BioSpin Avance III HD 400. MestReNova (Version 14.1.0) from Mestrelab Research S.L. 2019 was used for data processing, and for calibration, the solvent signal was used. The purity of the test compounds was > 99 %, determined by means of quantitative NMR using TraceCERT® ethyl 4-(dimethylamino) benzoate from Sigma Aldrich as an internal calibrant (Cushman et al., 2014; Pauli et al., 2014). High-resolution mass spectrometry was performed on a Finnigan LTQ FT (ESI). Melting points were determined with a Büchi 510 melting point instrument and are uncorrected. For IR spectroscopy, an FT-IR Spectrometer 1600 from PerkinElmer was used.

2.9.1. 4-Amino-1-{3-[4-(tert-butyl)pyridin-1-ium-1-yl]propyl}pyridin-1-ium diiodide (3a)

A solution of 4-(*tert*-butyl)− 1-(3-iodopropyl)pyridin-1-ium iodide (**1**) (Rappenglück, 2018) (216 mg, 0.500 mmol, 1.0 eq.) and pyridin-4-amine (**2a**) (51.8 mg, 0.550 mmol, 1.1 eq.) in acetonitrile (1 mL) was stirred under microwave irradiation (150 W) for 1 h at 90 °C. The reaction mixture was concentrated in vacuo and the residue purified by recrystallization from EtOAc/EtOH (2:3) yielding **3a** (215 mg, 82 %) as yellow solid. mp.: 205 °C; IR (KBr): $\tilde{\nu}$= 3184, 1652, 1194, 839 cm^{-1}; ^{1}H NMR (400 MHz, CD_3OD): δ = 1.45 (s, 9 H, $C(CH_3)_3$), 2.58–2.70 (m, 2 H, NCH_2CH_2), 4.38 (t, *J* = 7.7 Hz, 2 H, $CH_2NCHCHCNH_2$), 4.75 (t, *J* = 7.8 Hz, 2 H, $CH_2NCHCHCC(CH_3)_3$), 6.82–6.90 (m, 2 H, $CHCNH_2$), 8.12–8.20 (m, 2 H, $CHCC(CH_3)_3$), 8.18–8.26 (m, 2 H, $CHCHCNH_2$), 8.93–9.00 (m, 2 H, $CHCHCC(CH_3)_3$); ^{13}C NMR (101 MHz, CD_3OD): δ = 30.22 [$C(CH_3)_3$], 33.11 (NCH_2CH_2), 37.66 ($C(CH_3)_3$), 55.54 ($CH_2NCHCHCNH_2$), 58.55 [$CH_2NCHCHCC(CH_3)_3$], 111.04 ($CHCNH_2$), 126.87 [$CHCC(CH_3)_3$], 144.08 ($CHCHCNH_2$), 145.39 [$CHCHCC(CH_3)_3$], 160.91 (CNH_2), 173.18 [$CC(CH_3)_3$]; HRMS-ESI *m/z* $[M\text{-}I]^+$ calcd for $C_{17}H_{25}N_3I$: 398.1093, found: 398.1082.

2.9.2. 4-(tert-Butyl)− 1-[3-(4-(methylamino)pyridin-1-ium-1-yl]propyl) pyridin-1-ium diiodide (3b)

Synthesis according to the procedure described above for the preparation of **3a** from 4-(*tert*-butyl)−1-(3-iodopropyl)pyridin-1-ium iodide (**1**) (Rappenglück, 2018) (216 mg, 0.500 mmol, 1.0 eq.) and *N*-methylpyridin-4-amine (**2b**) (56.8 mg, 0.525 mmol, 1.05 eq.). Recrystallization from EtOAc/EtOH (2:1). **3b** (210 mg, 78 %). Yellow solid. mp.: 180 °C; IR (KBr): $\tilde{\nu}$= 3013, 1654, 1194, 843 cm^{-1}; ^{1}H NMR (400 MHz, CD_3OD): δ = 1.45 [s, 9 H, $C(CH_3)_3$], 2.60–2.72 (m, 2 H, NCH_2CH_2), 2.99 (s, 3 H, NCH_3), 4.41 (t, *J* = 7.7 Hz, 2 H, $CH_2NCHCHCNHCH_3$), 4.78 [t, *J* = 7.8 Hz, 2 H, $CH_2NCHCHCC(CH_3)_3$)], 6.84–6.94 (m, 2 H, $CHCNHCH_3$), 8.13–8.22 [m, 3 H, $CHCHCNHCH_3$, $CHCC(CH_3)_3$], 8.33–8.40 (m, 1 H, $CHCHCNHCH_3$), 8.96–9.03 [m, 2 H, $CHCHCC(CH_3)_3$]; ^{13}C NMR (101 MHz, CD_3OD): δ = 29.80 (NCH_3), 30.23 [$C(CH_3)_3$], 33.19 (NCH_2CH_2), 37.65 [$C(CH_3)_3$], 55.39 ($CH_2NCHCHCNHCH_3$), 58.50 [$CH_2NCHCHCC(CH_3)_3$], 106.66 ($CHCNHCH_3$), 112.03 ($CHCNHCH_3$), 126.87 [$CHCC(CH_3)_3$], 142.39 ($CHCHCNHCH_3$), 144.92 ($CHCHCNHCH_3$), 145.40 [$CHCHCC(CH_3)_3$], 159.57 ($CNHCH_3$), 173.09 [$CC(CH_3)_3$]; HRMS-ESI *m/z* $[M\text{-}I]^+$ calcd for $C_{18}H_{27}N_3I$: 412.1250, found: 412.1230.

2.10. Rat diaphragm myography

All procedures using animals followed animal care regulations and were approved by the responsible ethics committee. Preparation of rat diaphragm hemispheres and experimental protocol of myography was performed as described before with slight modifications (Seeger et al., 2012, 2007). In short, for all procedures (including wash-out steps, preparation of soman and bispyridinium compound solutions) aerated Tyrode solution (125 mM NaCl, 24 mM $NaHCO_3$, 5.4 mM KCl, 1 mM $MgCl_2$, 1.8 mM $CaCl_2$, 10 mM glucose, 95 % O_2, 5 % CO_2; pH 7.4; 25 ± 0.5 °C) was used. After the recording of control muscle force, the muscle preparations were incubated in the Tyrode solution, containing 3 μM soman. Following a 20 min wash-out period, the test compounds PTM0062 or PTM0063 were added in ascending concentrations (1 μM, 10 μM, 100 μM, 300 μM). The incubation time was 20 min for each concentration. The electric field stimulation was performed with 10 μs pulse width and 0.2 A amplitudes. The titanic trains of 20 Hz, 50 Hz, 100 Hz were applied for 1 s and in 10 min intervals. Muscle force was calculated as a time-force integral (area under the curve, AUC) and constrained to values obtained for maximal force generation (muscle force in the presence of Tyrode solution without any additives; 100 %).

3. Results

3.1. Identifying a new potential binding site via blind docking

To identify a possible binding site of MB327 without bias towards any previously known binding site, we have used blind docking experiments. Here, binding to the complete extracellular domain and half of the transmembrane domain of the human adult muscle-type and the α7-nAChR was allowed (SI Fig. S2), as the permanently charged MB327 likely does not cross the plasma membrane in a notable quantity and, thus, likely does not interact with the intracellular parts of the receptor. Using AutoDock (Morris et al., 1998) and DrugScore^{2018} (Dittrich et al., 2019), we docked MB327 100 times to each subtype. This allows us to judge whether MB327 prefers the orthosteric binding site or alternative ones. The largest cluster, which was also the cluster with the best-ranked docking pose, placed MB327 in both receptors in a newly identified binding pocket, MB327-PAM-1, which is located in between two adjacent subunits at the transition from the extracellular to the transmembrane domain (Fig. 1, Fig. 2A, SI Table S1, SI Table S2). Since the α7-nAChR is a homopentamer, there are five potential, identical binding sites for MB327. The human muscle type nAChR is a heteropentamer containing 2 α_1, 1 β_1, 1 δ and 1 ε subunit. In 8 out of the 10 highest ranked clusters, MB327 binds to MB327-PAM-1 but in different subunits (SI Table S1) suggesting that MB327 can bind in the newly identified binding pocket between different subunits. By contrast, MB327 binds to the orthosteric binding site in the 28th and 34th highest ranked cluster only (SI Table S1). In comparison, in 58 out of 100 docking runs, including 30 poses in the highest ranked cluster, the orthosteric agonist acetylcholine was placed in the orthosteric binding pocket, confirming the quality of our predictions (SI Table S3).

3.2. MD simulations strengthen the suggestion of the new binding site

To consider receptor plasticity and assess the stability of the binding pose in the receptor, we performed 32 times 100 ns long MD simulations starting from the docked structure of MB327 in all five subunits of the human muscle-type nAChR embedded in an explicit bilayer membrane (SI Fig. S3). The initial blind docking procedure failed to place MB327 between the β- and α-subunit in the best 100 docked poses, however. Still, we expect that MB327 can bind in between all five subunits of the receptor because of the high sequence similarity of amino acids available for electrostatic interactions (Table 1). Hence, to enable simulations

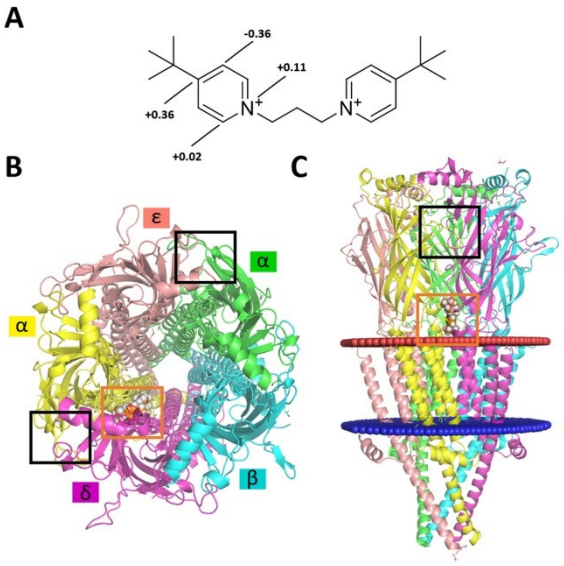

Fig. 1. Location of MB327-PAM-1 in the human adult muscle-type nAChR. (A) MB327 with restrained electrostatic potential (RESP) partial charges (Frisch et al., 2016; Bayly et al., 1993) of the nitrogen and carbons in the aromatic ring. nAChR is viewed from (B) the extracellular space and (C) the side. MB327 is displayed in orange spheres The orange box indicates the location of the newly identified allosteric binding site MB327-PAM-1. The orthosteric binding pocket is marked with a black box. The membrane is indicated with red (extracellular border) and blue (intracellular border) spheres. The membrane position was extracted from the α7-nAChR in a desensitized state (PDB ID 7KOQ (Noviello et al., 2021)) from the Orientations of Proteins in Membranes (OPM) database (Lomize et al., 2012).

with MB327 bound to all five subunits, we docked MB327 into MB327-PAM-1 between each subunit using FRED (OpenEye Scientific Software, 2020) (SI Fig. S4). Throughout the MD simulations, the receptor and the membrane remained structurally virtually invariant (SI Figs. S5, S6). To evaluate whether MB327 stays bound during the 100 ns long MD simulations, we evaluated the minimal distance of MB327 to the highly conserved isoleucine of β1 ($I61_{\alpha}$), located centrally in each respective subunit (Fig. 2A, SI Fig. S7). Since the largest distance among the docked structures in all five subunits of this isoleucine to MB327 is 4.2 Å (SI Table S4), we considered an unbinding of MB327 at distances above 5 Å. In 122 of 160 cases (32 replicas * 5 possible binding sites), MB327 stays bound in MB327-PAM-1. The unbinding events were mainly observed in between the β- and α-subunit (in 19/32 replicas) and in between the α- and ε-subunit (in 16/32 replicas), while we observed a rare unbinding in between the δ- and β-subunit (in 3/32 replicas) and no unbinding in between the α- and δ- as well as the ε- and α-subunit. This is in line with effective binding energy computations of MB327 in each subunit, revealing that MB327 binds most stably in between the α- and δ- (-23.01 ± 0.04 kcal mol^{-1}) and ε- and α-subunit (-24.43 ± 0.05 kcal mol^{-1}) and shows decreased free binding energies in between the δ- and β-subunit (-19.2 ± 0.05 kcal mol^{-1}), the α- and ε-subunit (-18.99 ± 0.07), and the β- and α-subunit (-14.30 ± 0.08 kcal mol^{-1}).

We next analyzed striking interactions with the receptor in the three binding pockets where MB327 remained predominantly bound. To do so, we computed the minimal distance of acidic side chains of the receptor to the partially positively charged atoms in MB327 when MB327 was bound. Because the nitrogen is part of an aromatic ring, its positive charge can be delocalized among the ring members. In fact, restrained electrostatic potential (RESP) partial charges (Frisch et al., 2016; Bayly et al., 1993) revealed that the positive charge is mainly located on the nitrogen and the carbon atom in *para* position (Fig. 1 A). Thus, we analyzed the minimal distance of these two atoms in each ring to the oxygen atoms of acidic side chains located in the binding pocket in each subunit where MB327 stays stable during the simulations (Fig. 2B, C, D). In between the α- and δ-subunit, MB327 mainly shows interactions with $E210_{\delta}$ located in loop F (Fig. 2B). This amino acid is highly conserved among different subunits of the heteropentamer. However, in between the δ- and β-subunit, this residue is mutated to glutamine (Table 1). There, MB327 shows almost no interactions with the side chain oxygen of this residue (SI Fig. S8C). However, in this subunit, MB327 forms good interactions with $E71_{\delta}$ located in the β1-β2-loop (Fig. 2C). In between the ε- and α-subunit, glutamates are present at both positions ($E220_{\alpha}$ and $E68_{\varepsilon}$, Fig. 2A). However, MB327 shows preferred interactions with $E68_{\varepsilon}$ located in the β1-β2-loop (Fig. 2D, SI Fig. S8D).

These results suggest the two acidic glutamates as major interaction partners for MB327. Both acidic amino acids are highly conserved among similar binding pockets in different subunits and different species (Table 1). In each subunit, at least one of the two acidic amino acids is present to stabilize MB327 in the binding pocket, strengthening the assumption that MB327 can bind in all subunits. This is in line with reports that MB327 can bind to nAChR of different species, e.g., *T. californica*, and to nAChRs containing different subunits, e.g., human α7-nAChR (Turner et al., 2011; Seeger et al., 2012; Niessen et al., 2016; Scheffel et al., 2018; Sichler et al., 2018). However, in our MD simulations, MB327 did not stay stable in the proposed binding pocket in two out of five subunits. There, MB327 might not have been placed correctly during the initial docking. In fact, in the two binding sites where MB327 unbound faster, the partially positively charged atoms of MB327 were more than 5 Å away from the carboxyl oxygens of the described amino acids, whereas in the other subunits, the distance to at least one oxygen is 4.5 Å or less (SI Table S4). Unsurprisingly, the effective binding energy is worst in between the β- and α-subunit where the ligand was placed farthest from the two glutamates in the binding site (SI Table S4). This further stresses the importance of these two amino acids. Thus, mutating one of these amino acids should lead to a significant decrease in binding affinity.

3.3. *Allosteric impacts originating from the newly proposed binding pocket*

To probe if the newly identified binding pocket MB327-PAM-1 couples functionally with other parts of nAChR, we applied a model of dynamic allostery introduced by us (Pfleger et al., 2013a, 2021) that describes allosteric effects due to ligand binding in terms of a free energy measure $\Delta G_{i,\mathrm{CNA}}$ computed from changes in biomolecular statics via CNA. To generate conformational ensembles for the analyses, we used the 32 times 100 ns long MD simulations with MB327 bound to all five subunits and nicotine bound to both orthosteric binding sites of the human muscle-type nAChR. However, due to the instability of MB327 in two subunits, we only considered the three subunits where MB327 remained stable in MB327-PAM-1. In 29 simulations, all three MB327 molecules were still bound after 100 ns; these replica were used to analyze the allosteric effect of MB327 binding on nAChR. For the perturbation run in CNA, all three MB327 molecules were removed to investigate the allosteric impact due to the ligand. Furthermore, to study the cooperative behavior of both ligands, two additional perturbation runs were performed: first, both nicotine molecules were removed; second, all stably bound ligands (three MB327 ligands and two nicotine molecules) were removed (SI Fig. S9).

CNA reveals that MB327 binding structurally stabilizes the extracellular domain, including amino acids in the orthosteric binding pocket (Fig. 3A, SI Fig. S10.). Interestingly, MB327 shows the largest impact in the orthosteric binding site on $W169_{\alpha}$, the only residue forming a hydrogen bond to the orthosteric ligand nicotine in the PDB structure of the human α3β4-nAChR (PDB-ID 6PV7) (Gharpure et al., 2019). MB327 transmits its allosteric information to the extracellular domain via both

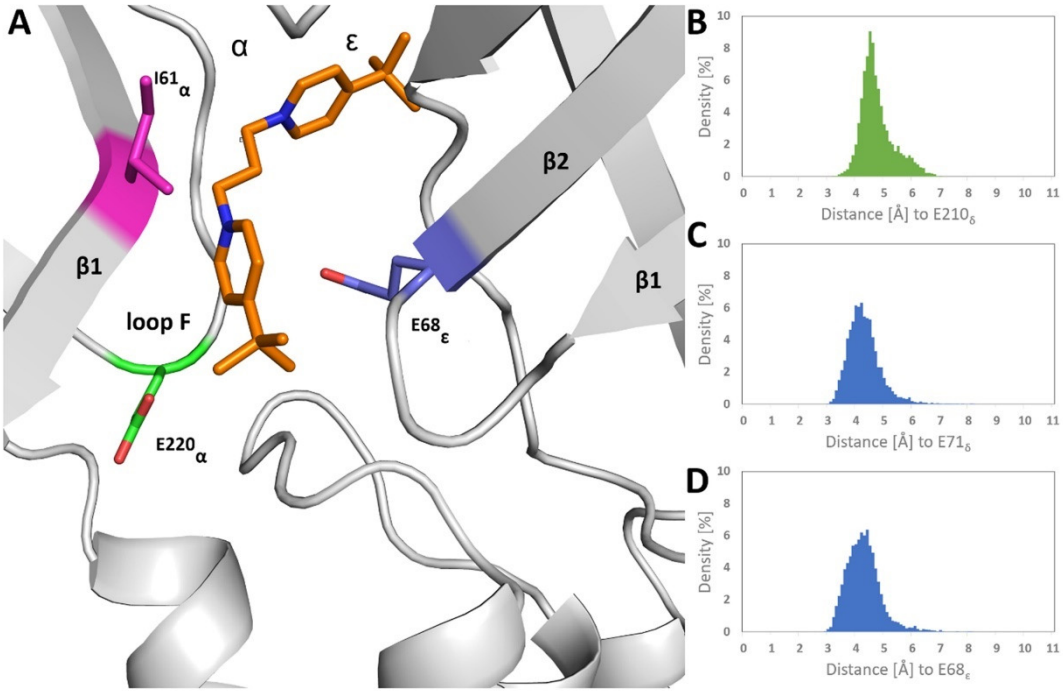

Fig. 2. Interactions of MB327 with nAChR in MB327-PAM-1. (A) Proposed binding mode of MB327 in MB327-PAM-1 between the ε- and α-subunits. The color of amino acids $E220_{\alpha}$ and $E68_{\varepsilon}$ relates to the figures in panels B-D. Minimum distance of the nitrogens and carbon atoms located in 4-position of MB327 to the carboxyl oxygens of (B) $E210_{\delta}$ of loop F in the α-δ-subunit (located at the same position as $E220_{\alpha}$, SI Fig. S4 B), (C) $E71_{\delta}$ of the β1-β2-loop in the δ-β-subunit (located at the same position as $E68_{\varepsilon}$, SI Fig. S4 C), and (D) $E68_{\varepsilon}$ of the β1-β2-loop in the α-ε-subunit.

Table 1
Sequence similarity of nAChR subunits in various species at specific positions in the MB327-PAM1 binding pockets.[a].

Human muscle type				α7	Torpedo marmorata				Rat			
α	β	δ	ε	α7	α	β	δ	γ	α	β	δ	ε
Q	E	E	E68	*Q*	*Q*	E	E	E	*Q*	E	E	E
E220	*Q*	E	E	E	E	*Q*	E	E	E	*Q*	E	E
I61	I	I	I	M	I	L	I	I	I	I	I	I

[a] Amino acids shown in Fig. 2A are represented with green shadings. Amino acids with deviating properties in other subunits are shown in italics.

adjacent subunits through the extracellular β-sheets (Fig. 3B). β-sheets have been demonstrated to be sensitive to changes in structural stability (Whiteley, 2005), and transition pathways along β-sheets have been reported previously (Pfleger et al., 2021, 2017). Especially, the stability of the three β-strands β1, β2, and β6 are affected by MB327 binding. β1 and the β1-β2-loop are both part of MB327-PAM-1. $W78_{\delta}$ in β2 is part of the highly conserved aromatic residues in which nicotine is enveloped according to the cryo-EM structure of the human α3β4-nAChR (PDB ID 6PV7 (Gharpure et al., 2019)). Additionally, via these three β-sheets, MB327 also impacts β7, β9, and β10. The loops of these three β-sheets form the orthosteric binding site. Because MB327 impacts both adjacent subunits, a binding of MB327 to each of the five possible binding pockets likely affects the binding of the orthosteric ligand since each binding site for MB327 features at least one subunit to which the orthosteric ligand binds. This qualitative observation suggests that MB327 addition can modulate cholinergic signals. Hence, we quantified cooperative effects between MB327 and nicotine binding according to Eq. 1 (Pfleger et al., 2021). Our results reveal a positive cooperative effect ($\Delta\Delta G_{CNA,n} = -3.97 \pm 0.71$ kcal mol^{-1}), in line with experimental findings that addition of MB327 leads to an enhancement of the cholinergic effect (Niessen et al., 2016). Therefore, binding of MB327 in MB327-PAM-1 is suggested to enhance cholinergic signals by increasing orthosteric ligand affinity.

Notably, a recently published PDB structure of the α7-nAChR (PDB ID 7KOX) shows calcium ions bound in the MB327-PAM-1 pocket (Noviello et al., 2021). Calcium binds in between E44 and E172. E172 is located in loop F, at the same position as $E220_{\alpha}$ (SI Fig. S11). A high concentration of calcium ions increases the cholinergic response in α7-nAChR, and our previous results suggest that the presence of divalent cations enhances the affinity of agonists in Torpedo nAChRs (Niessen et al., 2013; Galzi et al., 1996). Hence, we probed the effect of calcium binding in MB327-PAM-1 on the structural stability of the orthosteric site with CNA. To mimic the presence of the calcium ion which bridges two glutamates, we placed a constraint between the two carboxyl groups of E44 and E172. Similar to MB327, calcium leads to allosteric effects on the orthosteric binding site transmitted via the extracellular β-strands (SI Fig. S12). These findings strengthen the suggestion that positive allosteric modulation of the orthosteric ligand binding can originate

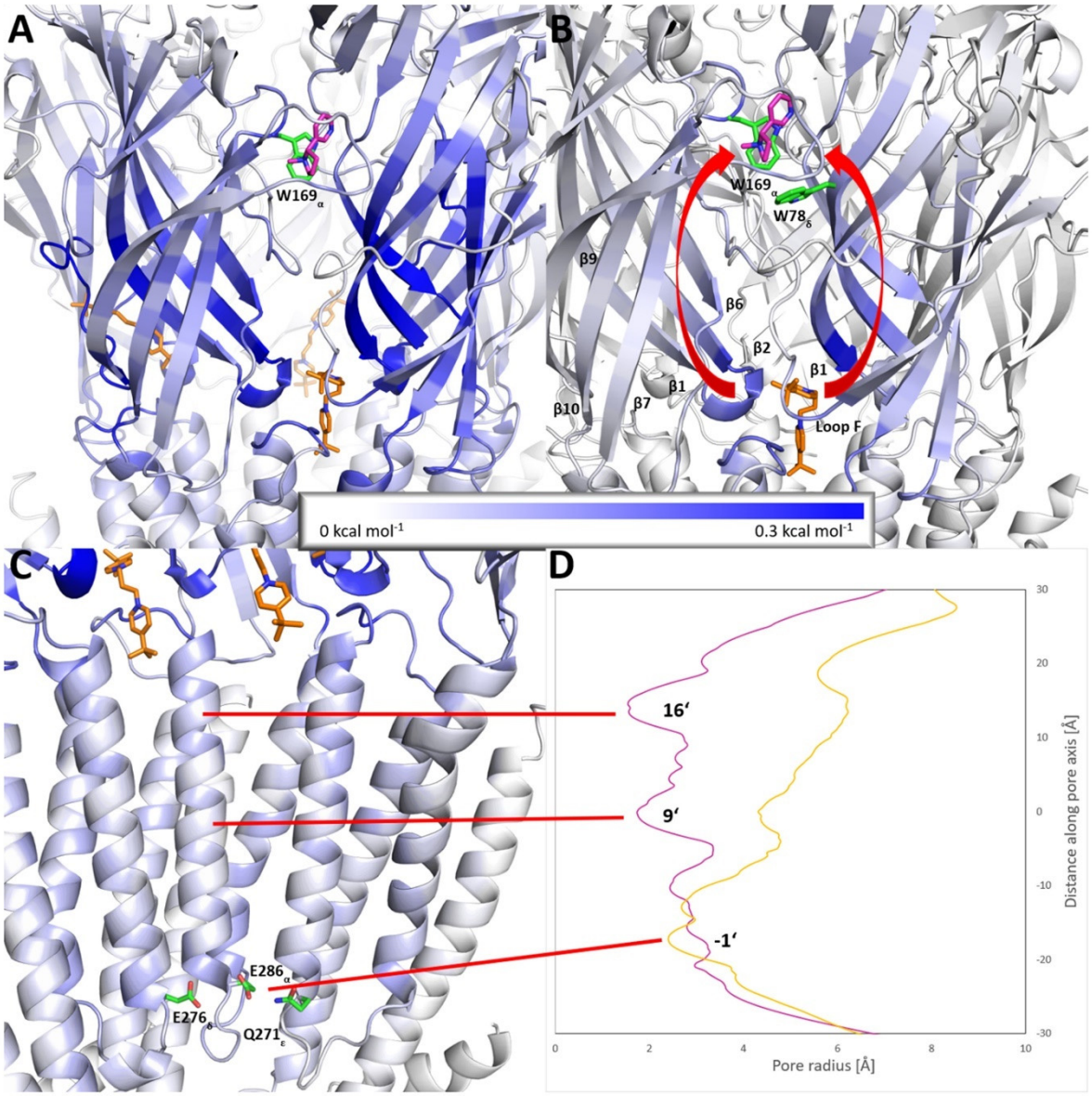

Fig. 3. Allosteric effect of MB327 (orange) on nAChR. Effect on the extracellular domain of (A) the three stable MB327 molecules and (B) MB327 located between the alpha- and ε-subunit. The receptor is colored according to the stabilizing impact of MB327 on the respective amino acid (bluish colors); darker colors indicate a higher impact. The pathway of the allosteric stabilization of the orthosteric binding pocket is indicated by red arrows. Nicotine (purple) is shown in the orthosteric binding pocket. $W169_{\alpha}$ and $W78_{\delta}$ are shown in green. (C) Allosteric effects of MB327 on the transmembrane domain of the human muscle type nAChR. For claritiy, only three subunits are shown. Amino acids at position − 1' are shown in green. (D) Pore radii of the desensitized (yellow) and inactive (purple) nAChR. The desensitization gate at position − 1′ and the inactive gates at positions 9′ and 16′ are projected on the structure by red bars. The distance along the pore axis has been set to 0 Å at position 9′.

from binding to MB327-PAM-1.

MB327 binding to MB327-PAM-1 also modulates the structural stability of the transmembrane region, including the amino acids at position − 1′ in helices 2 (Fig. 3C, D). X-ray and cryo-EM structures of nAChRs reveal that this position acts as a desensitization gate (Morales-Perez et al., 2016; Gharpure et al., 2019; Walsh et al., 2018; Noviello et al., 2021). The effects on the position − 1′ ($\Delta G_{E286\alpha,CNA} = 0.075 \pm 0.005$ kcal mol^{-1}, $\Delta G_{E276\delta,CNA} = 0.076 \pm 0.004$ kcal mol^{-1}, $\Delta G_{Q271\varepsilon,CNA} = 0.041 \pm 0.003$ kcal mol^{-1}) are significant. The effect on $W169_{\alpha}$, located at a central position in the orthosteric binding pocket, is even larger ($\Delta G_{W169\alpha,CNA} = 0.224 \pm 0.017$ kcal mol^{-1}), which may be due to helices being more stable, and, hence, less receptive to stability changes, in general (Whiteley, 2005). Furthermore, we used the rigidity index to compute ΔG_{CNA}; this index was described to show minor effects on helices (Pfleger et al., 2013b). Overall, the impact on the N-terminal region of helices 2 suggests a mechanism for how MB327 binding reestablishes the muscle function after desensitization, a second effect exerted by MB327 on nAChR (Seeger et al., 2012).

3.4. MB327 shows affinity to the orthosteric binding site

Previous results indicate that related bispyridinium compounds transmit their inhibitory effect on nAChR via the orthosteric binding site (Epstein et al., 2021). An inhibitory effect of MB327 has been reported at concentrations above 70 μM (Scheffel et al., 2018). To further investigate a possible binding of MB327 to the orthosteric binding site, we performed ten additional replicas of 900 ns long unbiased free ligand diffusion MD simulations with one MB327 molecule (0.57 mM) placed at a random position within the simulation box around the human muscle-type nAChR. The inhibitory effect of bispyridinium compounds was described to occur via the orthosteric binding site between the α- and ε-subunits (Epstein et al., 2021). Thus, in order to observe a potential binding to this binding site, the orthosteric ligand nicotine was only placed in the orthosteric binding site between the α- and δ-subunits. In three out of ten replicas, MB327 entered the orthosteric binding pocket. In two replicas, MB327 stayed within the binding pocket until the end of the simulation (after its entrance at 54 and 760 ns). In both replicas, MB327 can interact with $Y131_{\varepsilon}$ after binding (Fig. 4A, B), which is important for the stabilization of bispyridinium compounds (Epstein et al., 2021). In the third replica, MB327 bound to the binding pocket after 211 ns and left it after additional 130 ns. However, in this replica, MB327 showed a slightly different binding mode not interacting with $Y131_{\varepsilon}$ (SI Fig. S13).

We also analyzed the electrostatics surrounding the orthosteric binding pocket by solving the linear Poisson-Boltzmann equation for the human muscle-type nAChR. Since the minimum distance of $W169_{\alpha}$, a central amino acid in the orthosteric binding site, to the membrane is 27 Å, the membrane was neglected in calculating the electrostatic properties around the orthosteric binding site. A strong electric field

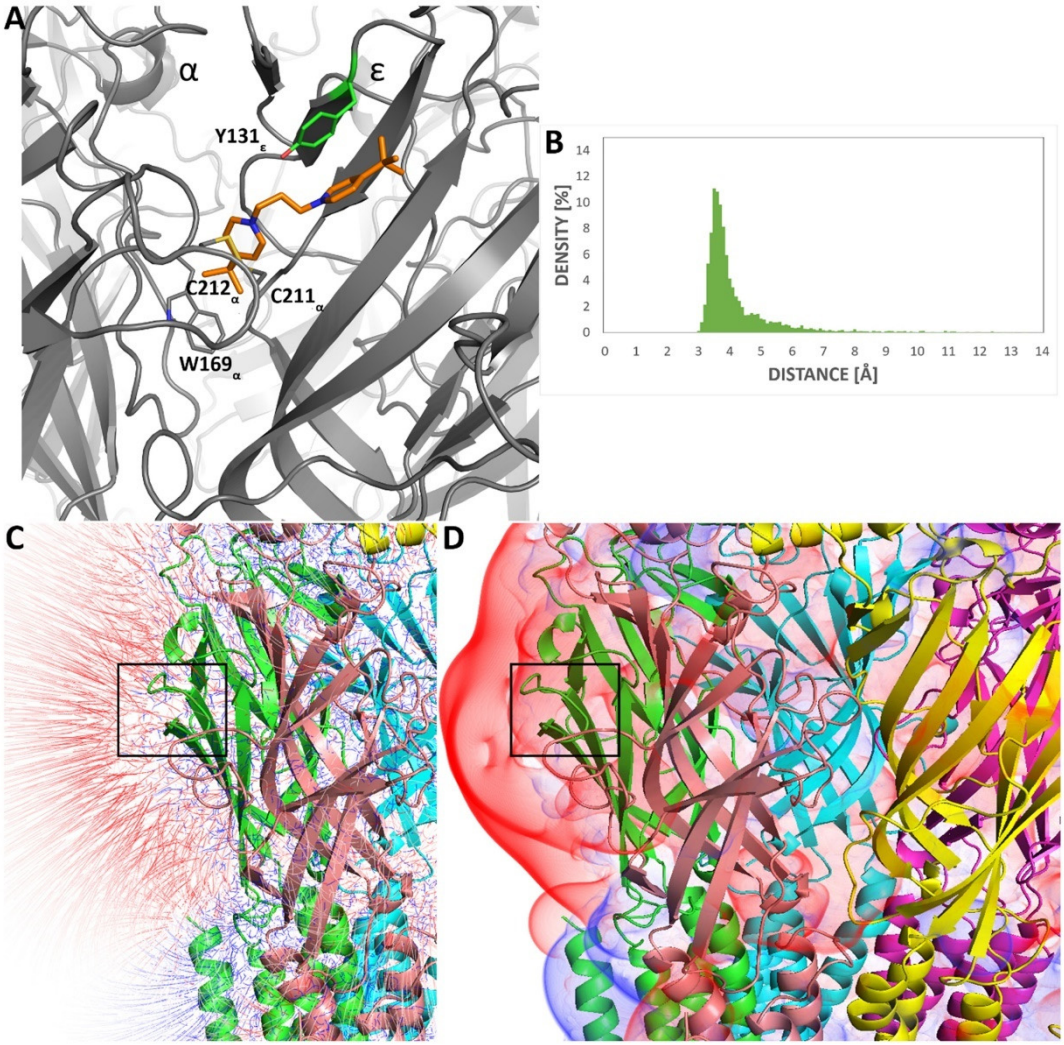

Fig. 4. Affinity of MB327 to the orthosteric binding site of nAChR. (A) Representative structure of MB327 (orange) bound to the orthosteric binding pocket and its adjacent region in between the α- and ε-subunit where no nicotine molecule was present during free ligand diffusion MD simulations. (B) Minimum distance of the heavy atoms of the aromatic ring of $Y131_{\varepsilon}$ as shown in (A) to the heavy atoms of the aromatic systems of MB327 while MB327 is bound. Electrostatics surrounding the orthosteric binding pocket between the α- (green) and ε- (salmon) subunits shown as (C) electric flux lines and (D) isocontour surfaces of the electrostatic potential. The location of the orthosteric binding pocket is marked with a black box. Notably, a strong electric field (red field lines) attractive to positively charged compounds such as MB327 surrounds the pocket entrance and leads towards the orthosteric binding pocket of the human nAChR.

attractive to positively charged compounds such as MB327 surrounds the pocket entrance and leads towards the orthosteric binding pocket. This may explain why bispyridinium compounds get dragged into this binding pocket (Fig. 4C,D).

3.5. Identification of MB327-PAM-1 allows rational design of more potent analogs

We used the knowledge gained from the binding mode of MB327 in MB327-PAM-1 to predict structural modifications of the ligand that should lead to more potent resensitizers. The *tert*-butyl group of MB327 facing toward the transmembrane domain is located in a polar part of the binding site (Fig. 5A). Thus, substituting the apolar with a polar substituent should increase the binding affinity (Fig. 5B). We, therefore, docked PTM0062 and PTM0063, which carry amino and methylamino groups, (Fig. 5C) in the binding site of all subunits. Both ligands were ranked better than MB327 in all but one subunit, respectively (Fig. 5B, SI Table S5). PTM0062 (**3a**) and PTM0063 (**3b**) were synthesized according to Rappenglück et al. by reacting **1** (Rappenglück, 2018) with pyridin-4-amine (**2a**) and *N*-methylpyridin-4-amine (**2b**), respectively, in acetonitrile under stirring and microwave irradiation for 1 h at 90 °C (Scheme 1) (Rappenglück, 2018). The bispyridinium salts were obtained

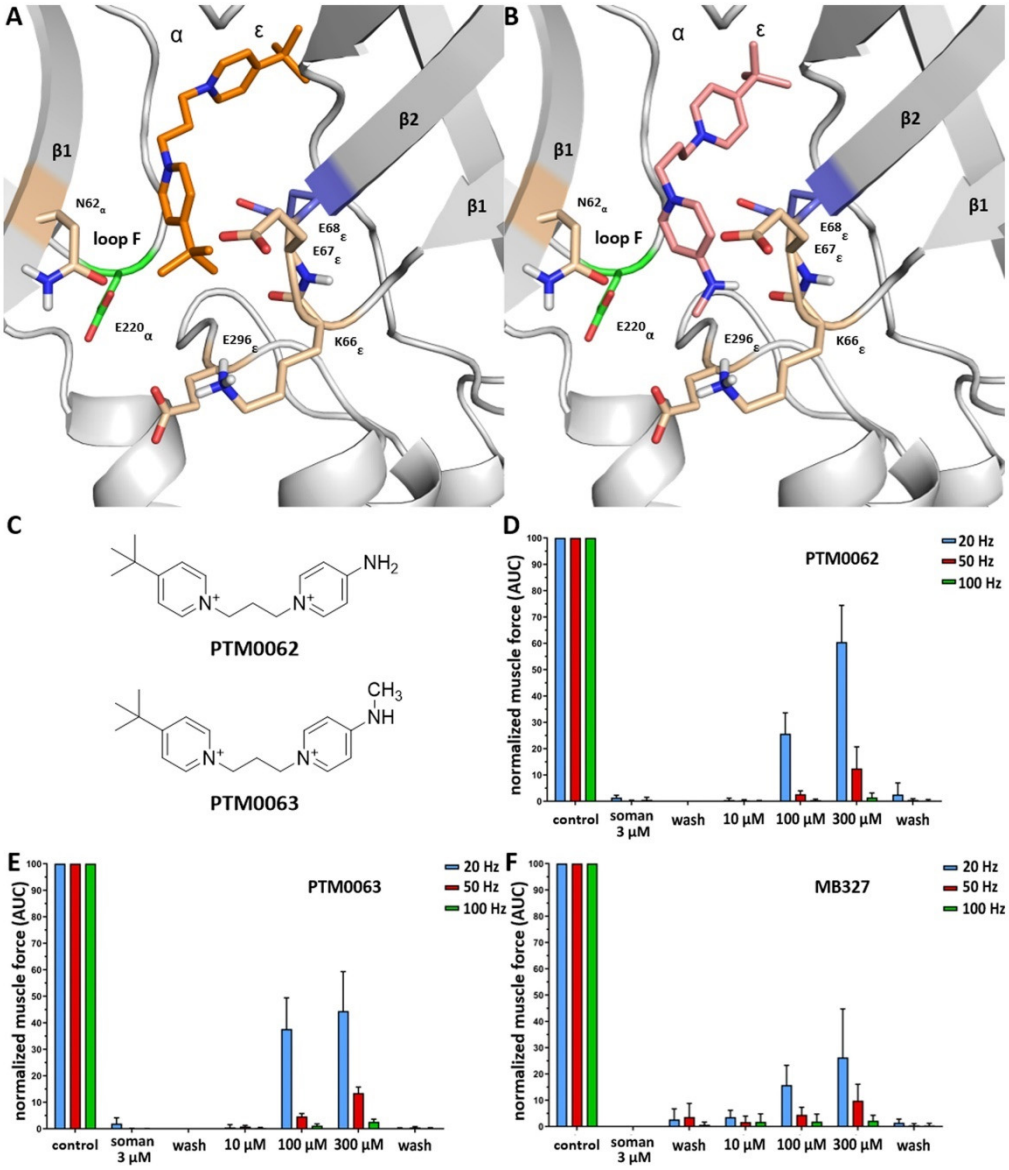

Fig. 5. Structure-based ligand design leads to novel compounds with increased resensitizing effects on nAChR. (A) Binding mode of MB327 in between the α- and ε-subunit. The *tert*-butyl substituent facing towards the transmembrane region is located in a polar part of the binding site. (B) Proposed binding mode of PTM0063. Polar substituents can enhance the interactions with the receptor. (C) Structure of the two newly identified positive allosteric modulators PTM0062 and PTM0063. Restoration of the muscle force of soman-poisoned muscles after treatment with (D) PTM0062, (E) PTM0063, and (F) MB327. The error bars indicate the standard deviation.

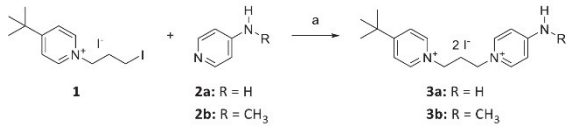

1 **2a:** R = H **2b:** R = CH_3 **3a:** R = H **3b:** R = CH_3

Scheme 1. Synthesis of PTM0062 (**3a**) and PTM0063 (**3b**): (a) **2a** (1.1 equiv.) or **2b** (1.05 equiv.), CH_3CN, microwave: 150 W, 90 °C, 1 h; **3a**: 82 %; **3b**: 78 %.

in good yields (3a: 82 %; 3b: 78 %) and high purities (> 99 %) by recrystallization of the residues resulting after the removal of the reaction solvent (Scheme 1). The compounds were subsequently evaluated in the rat diaphragm myography assay. PTM0062 (25.68 % ± 7.91 % (mean ± standard deviation) at 100 μM, 60.46 % ± 13.94 % at 300 μM) and PTM0063 (37.65 % ± 11.73 % at 100 μM, 44.43 % ± 14.88 % at 300 μM) both show increased resensitizing effects on muscles after OPC poisoning at a stimulation frequency of 20 Hz compared to MB327 (17.77% ± 7.5 % at 100 μM, 26.29 % ± 18.43 % at 300 μM) (Fig. 5D-F).

4. Discussion

We have identified a new potential binding site of MB327 in nAChR, MB327-PAM-1, using blind docking, MD simulations, and rigidity analyses. Previously, two allosteric and one orthosteric binding pocket were proposed for bispyridinium compounds using *in silico* methods (Wein et al., 2018; Epstein et al., 2021). MB327-PAM-1 is different from these three binding sites. Wein et al. suggested that MB327 might bind in between two adjacent subunits in the extracellular domain (MB327–1) or at the transition from the extracellular to the transmembrane domain (MB327–2) (Wein et al., 2018). In our blind dockings, we could also see a binding in the pocket MB327–1 but with worse docking scores compared to our newly identified binding pocket (SI Table S1). In the screening conducted to identify MB327–2, the structure of the *Torpedo marmorata* nAChR (PDB ID 2BG9 (Unwin, 2005)) was used (Wein et al., 2018). However, recently published structures and disulfide trapping experiments revealed that due to the structure's low resolution, the amino acids in the transmembrane domain were wrongly fitted, resulting in an amino acid shift (SI Fig. S14, SI Table S6) (Mnatsakanyan and Jansen, 2013; Morales-Perez et al., 2016). Without this shift, there is no MB327–2 pocket in nAChR (Wein et al., 2018).

During the MD simulations, MB327 is mainly stabilized via electrostatic interactions with glutamates located in the β1-β2 loop and loop F ($E220_\alpha$ and $E68_\varepsilon$ in Fig. 2A). These two amino acids are highly conserved among different subunits of the nAChR and different species. This corresponds to MB327 showing functional recovery of different types of nAChRs after overstimulation with agonists (Seeger et al., 2012; Niessen et al., 2016). Our newly identified binding pocket also occupies a region in which structural changes during desensitization occur (SI Fig. S15), which suggests that this binding site can be involved in allosteric modulation. Furthermore, CNA calculations show that MB327 might impact both the orthosteric binding site and the transmembrane domain after binding to MB327-PAM-1.

Several published structures of nAChRs and related Cys-loop receptors include allosteric modulators (Zhao et al., 2021; Noviello et al., 2021; Masiulis et al., 2019; Kim et al., 2020; Delbart et al., 2018; Spurny et al., 2013, 2015). A recent structure revealed that the binding site of a calcium ion overlaps with MB327-PAM-1 (Noviello et al., 2021). Calcium can act as a positive allosteric modulator of the α7-nAChR (Galzi et al., 1996). Additionally, mutating E172 of loop F to lysine in the α7-nAChR, which is located at the same position as $E220_\alpha$, leads to a loss of sensitivity to the orthosteric ligand acetylcholine (Zhang et al., 2015). A mutation of this amino acid in the α7-nAChR to glutamine also abolishes the enhancement of the physiological response to acetylcholine mediated through calcium ions (Galzi et al., 1996). These data underline the potential importance of this binding pocket in allosteric modulation. Mimicking the calcium ion in this binding pocket by including its interactions into the constraint network representation results in similar effects on the receptor as MB327 as shown with CNA computations. Notably, the calcium ion also exerts a similar effect on the transmembrane region, indicating that calcium might have a resensitizing effect on nAChR, too (SI Fig. S12).

Notably, the binding site of PNU-120596 has been revealed in an electron microscopy structure (PDB-ID: 7EKT (Zhao et al., 2021)) recently. This binding site overlaps with the newly identified allosteric binding site of diazepam in the $GABA_A$ receptor (PDB-IDs: 6X3X (Kim et al., 2020), 6HUP (Masiulis et al., 2019)). Because PNU-120596 also acts as a positive allosteric modulator (Hurst et al., 2005), we investigated whether MB327 may bind to this binding site. However, in the published PDB structure, no negatively charged amino acids are located within 5 Å of PNU-120596, which would lead to an insufficient stabilization of the double positively charged compound MB327 (SI Fig. S16A). Furthermore, PNU-120596 is a selective α7 modulator (Hurst et al., 2005). A reason for that may be that A298 is mutated to sterically larger amino acids in different subtypes of the receptor, which leads to a clash with PNU-120596. Thus, the binding site is critically smaller in other subtypes, including the human muscle-type nAChR (Fig. S16B). However, MB327 is known to bind to several subtypes of nAChR, including the muscle-type nAChR (Turner et al., 2011; Seeger et al., 2012; Niessen et al., 2016; Scheffel et al., 2018; Sichler et al., 2018). Therefore, binding of MB327 to the binding site of PNU-120596 is highly unlikely.

Furthermore, the multitude of binding sites and possible interactions within one binding site in the human muscle-type nAChR could lead to MB327 binding at lower concentrations to MB327-PAM-1 than to the orthosteric binding site. The binding of MB327 to the orthosteric binding pocket results in a binding pose where MB327 protrudes in part out of the pocket, but it completely fits into MB327-PAM-1. After poisoning with OPCs resulting in elevated levels of acetylcholine, MB327 would additionally need to displace acetylcholine in the orthosteric binding pocket because the binding pose of MB327 in the orthosteric pocket overlaps with the binding pose of the orthosteric ligand. Thus, binding to the orthosteric site would be expected at higher concentrations, where it can lead to an inhibitory effect. This inhibitory effect was shown by us in that an increase of MB327 concentration leads to a decrease of muscle force restoration after soman poisoning (Niessen et al., 2018). Furthermore, recent mutational studies showed that related bispyridinium compounds transfer their inhibitory effect via binding to the orthosteric pocket (Epstein et al., 2021).

Epstein et al. proposed that the therapeutic effect of bispyridinium compounds could be conducted via binding to the orthosteric binding site and its adjacent region (Epstein et al., 2021). We also see an affinity of MB327 to this binding site in our free ligand diffusion MD simulations. Epstein et al. performed docking experiments considering the orthosteric binding pocket and did not investigate binding to allosteric binding pockets. However, previous experimental results indicate that the bispyridinium compounds probably act as allosteric modulators of nAChR and, additionally, improvement of neuromuscular function is not correlated to their affinity to the orthosteric binding site (Niessen et al., 2016, 2018, 2011). Thus, although an inhibitory effect, detrimental to the therapeutic treatment, of the bispyridinium compounds might be conducted through binding to the orthosteric binding site at higher concentrations (Epstein et al., 2021; Niessen et al., 2018), our results suggest that for the allosteric modulation, relevant for treatment, MB327 binds to the newly identified binding pocket. This concentration-dependent binding to the allosteric and orthosteric binding site can also explain the therapeutic effect seen at lower concentrations of MB327 and the inhibition of the nAChR and loss of therapeutic effect at higher concentrations (Niessen et al., 2018). Thus, our results suggest that new drugs should show a high affinity to the newly identified binding pocket while showing a low affinity to the orthosteric binding site.

The knowledge of the binding mode is most important to predict

structure-based ligand modifications resulting in more potent resensitizers. Following this strategy, we predicted and validated PTM0062 and PTM0063, which are about two-fold more potent resensitizers than MB327. These findings further support that MB327 binds to MB327-PAM-1. Another way to enhance the affinity to the newly identified binding site might be to add chemical moieties that can form interactions via hydrogen bonds or salt bridges to the two glutamates $E220_{\alpha}$ and $E68_{\varepsilon}$, while maintaining the apolar part of the compounds.

Taken together, our newly identified binding pocket can explain the allosteric effect mediated by MB327 and, together with a binding to the orthosteric site, the concentration dependence of the observed therapeutic effect.

Declaration of Competing Interest

The authors declare that they have no known competing financial interests or personal relationships that could have appeared to influence the work reported in this paper.

Data availability

Data will be made available on request.

Acknowledgments

This work was supported by the German Ministry of Defense (E/U2AD/KA019/IF558). We are grateful for computational support and infrastructure provided by the "Zentrum für Informations- und Medientechnologie" (ZIM) at the Heinrich Heine University Düsseldorf and the computing time provided by the John von Neumann Institute for Computing (NIC) to HG on the supercomputer JUWELS at Jülich Supercomputing Center (JSC) (user IDs: HKF7, VSK33, nAChR). HG is grateful to OpenEye Scientific Software for granting a Free Public Domain Research License.

Appendix A. Supporting information

Supplementary data associated with this article can be found in the online version at doi:10.1016/j.toxlet.2022.11.018.

References

Altschul, S.F., et al., 1990. Basic local alignment search tool. J. Mol. Biol. 215 (3), 403–410.
Bayly, C.I., et al., 1993. A well-behaved electrostatic potential based method using charge restraints for deriving atomic charges: the RESP model. J. Phys. Chem. 97 (40), 10269–10280.
Case, D.A., et al., 2005. The Amber biomolecular simulation programs. J. Comput. Chem. 26 (16), 1668–1688.
Celie, P.H., et al., 2004. Nicotine and carbamylcholine binding to nicotinic acetylcholine receptors as studied in AChBP crystal structures. Neuron 41 (6), 907–914.
Cushman, M., et al., 2014. Absolute quantitative (1)h NMR spectroscopy for compound purity determination. J. Med Chem. 57 (22), 9219.
Darden, T., York, D., Pedersen, L., 1993. Particle mesh Ewald: an N·log(N) method for Ewald sums in large systems. J. Chem. Phys. 98 (12), 10089–10092.
OpenEye Scientific Software, I., *SZYBKI*. OpenEye Scientific Software: Santa Fe, NM.
Delbart, F., et al., 2018. An allosteric binding site of the alpha7 nicotinic acetylcholine receptor revealed in a humanized acetylcholine-binding protein. J. Biol. Chem. 293 (7), 2534–2545.
Dittrich, J., et al., 2019. Converging a knowledge-based scoring function: drugscore (2018). J. Chem. Inf. Model. 59 (1), 509–521.
Epstein, M., et al., 2021. Molecular determinants of binding of non-oxime bispyridinium nerve agent antidote compounds to the adult muscle nAChR. Toxicol. Lett. 340, 114–122.
M.J. Frisch, G.W.T, H.B. Schlegel, G.E. Scuseria, et al., Gaussian16. 2016, Gaussian Inc.: Wallingford CT.
Galzi, J.L., et al., 1996. Identification of calcium binding sites that regulate potentiation of a neuronal nicotinic acetylcholine receptor. EMBO J. 15 (21), 5824–5832.
Gharpure, A., et al., 2019. Agonist selectivity and ion permeation in the alpha3beta4 ganglionic nicotinic receptor. Neuron 104 (3), 501–511 e6.
Hibbs, R.E., et al., 2009. Structural determinants for interaction of partial agonists with acetylcholine binding protein and neuronal alpha7 nicotinic acetylcholine receptor. EMBO J. 28 (19), 3040–3051.
Holmstedt, B., 1959. Pharmacology of organophosphorus cholinesterase inhibitors. Pharm. Rev. 11, 567–688.
Hopkins, C.W., et al., 2015. Long-time-step molecular dynamics through hydrogen mass repartitioning. J. Chem. Theory Comput. 11 (4), 1864–1874.
Hurst, R.S., et al., 2005. A novel positive allosteric modulator of the alpha7 neuronal nicotinic acetylcholine receptor: in vitro and in vivo characterization. J. Neurosci. 25 (17), 4396–4405.
Izadi, S., Anandakrishnan, R., Onufriev, A.V., 2014. Building water models: a different approach. J. Phys. Chem. Lett. 5 (21), 3863–3871.
Jurrus, E., et al., 2018. Improvements to the APBS biomolecular solvation software suite. Protein Sci. 27 (1), 112–128.
Kim, J.J., et al., 2020. Shared structural mechanisms of general anaesthetics and benzodiazepines. Nature 585 (7824), 303–308.
Lomize, M.A., et al., 2012. OPM database and PPM web server: resources for positioning of proteins in membranes. Nucleic Acids Res. 40 (Database issue), D370–D376.
Masiulis, S., et al., 2019. GABAA receptor signalling mechanisms revealed by structural pharmacology. Nature 565 (7740), 454–459.
Miller 3rd, B.R., et al., 2012. MMPBSA.py: an efficient program for end-state free energy calculations. J. Chem. Theory Comput. 8 (9), 3314–3321.
Mnatsakanyan, N., Jansen, M., 2013. Experimental determination of the vertical alignment between the second and third transmembrane segments of muscle nicotinic acetylcholine receptors. J. Neurochem. 125 (6), 843–854.
Morales-Perez, C.L., Noviello, C.M., Hibbs, R.E., 2016. X-ray structure of the human alpha4beta2 nicotinic receptor. Nature 538 (7625), 411–415.
Morris, G.M., et al., 1998. Automated docking using a Lamarckian genetic algorithm and an empirical binding free energy function. J. Comput. Chem. 19 (14), 1639–1662.
Mukherjee, S., et al., 2020. Synthetic antibodies against BRIL as universal fiducial marks for single-particle cryoEM structure determination of membrane proteins. Nat. Commun. 11 (1), 1598.
Mulnaes, D., Gohlke, H., 2018. TopScore: using deep neural networks and large diverse data sets for accurate protein model quality assessment. J. Chem. Theory Comput. 14 (11), 6117–6126.
Niessen, K.V., et al., 2011. Interaction of bispyridinium compounds with the orthosteric binding site of human alpha7 and Torpedo californica nicotinic acetylcholine receptors (nAChRs). Toxicol. Lett. 206 (1), 100–104.
Niessen, K.V., et al., 2013. Affinities of bispyridinium non-oxime compounds to [(3)H] epibatidine binding sites of Torpedo californica nicotinic acetylcholine receptors depend on linker length. Chem. Biol. Interfaces 206 (3), 545–554.
Niessen, K.V., et al., 2016. Functional analysis of Torpedo californica nicotinic acetylcholine receptors in multiple activation states by SSM-based electrophysiology. Toxicol. Lett. 247, 1–10.
Niessen, K.V., et al., 2018. In vitro pharmacological characterization of the bispyridinium non-oxime compound MB327 and its 2- and 3-regioisomers. Toxicol. Lett. 293, 190–197.
Noviello, C.M., et al., 2021. Structure and gating mechanism of the alpha7 nicotinic acetylcholine receptor. Cell 184 (8), 2121–2134 e13.
OpenEye Scientific Software, I., OEDOCKING. 2020. Santa Fe, NM.
OpenEye Scientific Software, I., OMEGA. 2020. Santa Fe, NM.
Olsson, M.H., et al., 2011. PROPKA3: consistent treatment of internal and surface residues in empirical pKa predictions. J. Chem. Theory Comput. 7 (2), 525–537.
Onufriev, A., Bashford, D., Case, D.A., 2004. Exploring protein native states and large-scale conformational changes with a modified generalized born model. Proteins 55 (2), 383–394.
Pauli, G.F., et al., 2014. Importance of purity evaluation and the potential of quantitative (1)H NMR as a purity assay. J. Med. Chem. 57 (22), 9220–9231.
Pavelka, A., et al., 2016. CAVER: algorithms for analyzing dynamics of tunnels in macromolecules. IEEE/ACM Trans. Comput. Biol. Bioinform. 13 (3), 505–517.
Pei, J., Kim, B.H., Grishin, N.V., 2008. PROMALS3D: a tool for multiple protein sequence and structure alignments. Nucleic Acids Res. 36 (7), 2295–2300.
Pettersen, E.F., et al., 2004. UCSF Chimera – a visualization system for exploratory research and analysis. J. Comput. Chem. 25 (13), 1605–1612.
Pfleger, C., et al., 2013a. Constraint network analysis (CNA): a python software package for efficiently linking biomacromolecular structure, flexibility, (thermo-)stability, and function. J. Chem. Inf. Model. 53 (4), 1007–1015.
Pfleger, C., et al., 2013b. Global and local indices for characterizing biomolecular flexibility and rigidity. J. Comput. Chem. 34 (3), 220–233.
Pfleger, C., et al., 2017. Ensemble- and rigidity theory-based perturbation approach to analyze dynamic allostery. J. Chem. Theory Comput. 13 (12), 6343–6357.
Pfleger, C., et al., 2021. Allosteric signaling in C-linker and cyclic nucleotide-binding domain of HCN2 channels. Biophys. J. 120 (5), 950–963.
Rahman, M.M., et al., 2020. Structure of the native muscle-type nicotinic receptor and inhibition by snake venom toxins. Neuron 106 (6), 952–962 e5.
Rappenglück, S., et al., 2018. Synthesis of a series of non-symmetric bispyridinium and related compounds and their affinity characterization at the nicotinic acetylcholine receptor. ChemMedChem 13 (24), 2653–2663.
Roe, D.R., Cheatham 3rd, T.E., 2013. PTRAJ and CPPTRAJ: software for processing and analysis of molecular dynamics trajectory data. J. Chem. Theory Comput. 9 (7), 3084–3095.
Ryckaert, J.-P., Ciccotti, G., Berendsen, H.J.C., 1977. Numerical integration of the cartesian equations of motion of a system with constraints: molecular dynamics of n-alkanes. J. Comput. Phys. 23 (3), 327–341.
Scheffel, C., et al., 2018. Electrophysiological investigation of the effect of structurally different bispyridinium non-oxime compounds on human alpha7-nicotinic acetylcholine receptor activity – an in vitro structure-activity analysis. Toxicol. Lett. 293, 157–166.

Schott-Verdugo, S., Gohlke, H., 2019. PACKMOL-Memgen: a simple-to-use, generalized workflow for membrane-protein-lipid-bilayer system building. J. Chem. Inf. Model. 59 (6), 2522–2528.
Schrödinger, L.L.C., The PyMOL Molecular Graphics System, *Version 1.8.*, 2015.
Schrödinger, L.L.C., Maestro. 2020.
Seeger, T., et al., 2007. Reevaluation of indirect field stimulation technique to demonstrate oxime effectiveness in OP-poisoning in muscles in vitro. Toxicology 233 (1–3), 209–213.
Seeger, T., et al., 2012. Restoration of soman-blocked neuromuscular transmission in human and rat muscle by the bispyridinium non-oxime MB327 in vitro. Toxicology 294 (2–3), 80–84.
Shen, M.Y., Sali, A., 2006. Statistical potential for assessment and prediction of protein structures. Protein Sci. 15 (11), 2507–2524.
Sheridan, R.D., et al., 2005. Nicotinic antagonists in the treatment of nerve agent intoxication. J. R. Soc. Med. 98 (3), 114–115.
Sichler, S., et al., 2018. Development of MS Binding Assays targeting the binding site of MB327 at the nicotinic acetylcholine receptor. Toxicol. Lett. 293, 172–183.
Sondergaard, C.R., et al., 2011. Improved treatment of ligands and coupling effects in empirical calculation and rationalization of pKa values. J. Chem. Theory Comput. 7 (7), 2284–2295.
Spurny, R., et al., 2013. Multisite binding of a general anesthetic to the prokaryotic pentameric Erwinia chrysanthemi ligand-gated ion channel (ELIC). J. Biol. Chem. 288 (12), 8355–8364.
Spurny, R., et al., 2015. Molecular blueprint of allosteric binding sites in a homologue of the agonist-binding domain of the alpha7 nicotinic acetylcholine receptor. Proc. Natl. Acad. Sci. USA 112 (19), E2543–E2552.
Thiermann, H., Worek, F., Kehe, K., 2013. Limitations and challenges in treatment of acute chemical warfare agent poisoning. Chem. Biol. Interfaces 206 (3), 435–443.
Tian, C., et al., 2020. ff19SB: amino-acid-specific protein backbone parameters trained against quantum mechanics energy surfaces in solution. J. Chem. Theory Comput. 16 (1), 528–552.
Turner, S.R., et al., 2011. Protection against nerve agent poisoning by a noncompetitive nicotinic antagonist. Toxicol. Lett. 206 (1), 105–111.
Twizerimana, A.P., et al., 2020. Cell type-dependent escape of capsid inhibitors by simian immunodeficiency virus SIVcpz. J. Virol. 94 (23).
Unwin, N., 2005. Refined structure of the nicotinic acetylcholine receptor at 4A resolution. J. Mol. Biol. 346 (4), 967–989.
Unwin, N., Fujiyoshi, Y., 2012. Gating movement of acetylcholine receptor caught by plunge-freezing. J. Mol. Biol. 422 (5), 617–634.
Walsh Jr., R.M., et al., 2018. Structural principles of distinct assemblies of the human alpha4beta2 nicotinic receptor. Nature 557 (7704), 261–265.
Webb, B., Sali, A., 2016. Comparative protein structure modeling using MODELLER. Curr. Protoc. Bioinform. 54 (5 6 1-5 6 37).
Wein, T., et al., 2018. Searching for putative binding sites of the bispyridinium compound MB327 in the nicotinic acetylcholine receptor. Toxicol. Lett. 293, 184–189.
Whiteley, W., 2005. Counting out to the flexibility of molecules. Phys. Biol. 2 (4), S116–S126.
Wiener, S.W., Hoffman, R.S., 2004. Nerve agents: a comprehensive review. J. Intensive Care Med. 19 (1), 22–37.
Worek, F., Thiermann, H., Szinicz, L., 2004. Reactivation and aging kinetics of human acetylcholinesterase inhibited by organophosphonylcholines. Arch. Toxicol. 78 (4), 212–217.
Zhang, Q., et al., 2015. Functional impact of 14 single nucleotide polymorphisms causing missense mutations of human alpha7 nicotinic receptor. PLOS One 10 (9), e0137588.
Zhao, Y., et al., 2021. Structural basis of human α7 nicotinic acetylcholine receptor activation. Cell Res. 31 (6), 713–716.

Supporting information

A novel binding site in the nicotinic acetylcholine receptor for MB327 can explain its allosteric modulation relevant for organophosphorus-poisoning treatment

Jesko Kaiser[1], Christoph G.W. Gertzen[1], Tamara Bernauer[2], Georg Höfner[2], Karin V. Niessen[3], Thomas Seeger[3], Franz F. Paintner[2], Klaus T. Wanner[2], Franz Worek[3], Horst Thiermann[3], Holger Gohlke[1,4,*]

[1]Institute for Pharmaceutical and Medicinal Chemistry, Heinrich Heine University Düsseldorf, Düsseldorf, Germany

[2]Department of Pharmacy, Ludwig-Maximilians-Universität München, München, Germany

[3]Bundeswehr Institute of Pharmacology and Toxicology, München, Germany

[4]John von Neumann Institute for Computing (NIC), Jülich Supercomputing Centre (JSC), Institute of Biological Information Processing (IBI-7: Structural Biochemistry) & Institute of Bio- and Geosciences (IBG-4: Bioinformatics), Forschungszentrum Jülich, Jülich, Germany

Table of content

Supplemental Figures and Tables

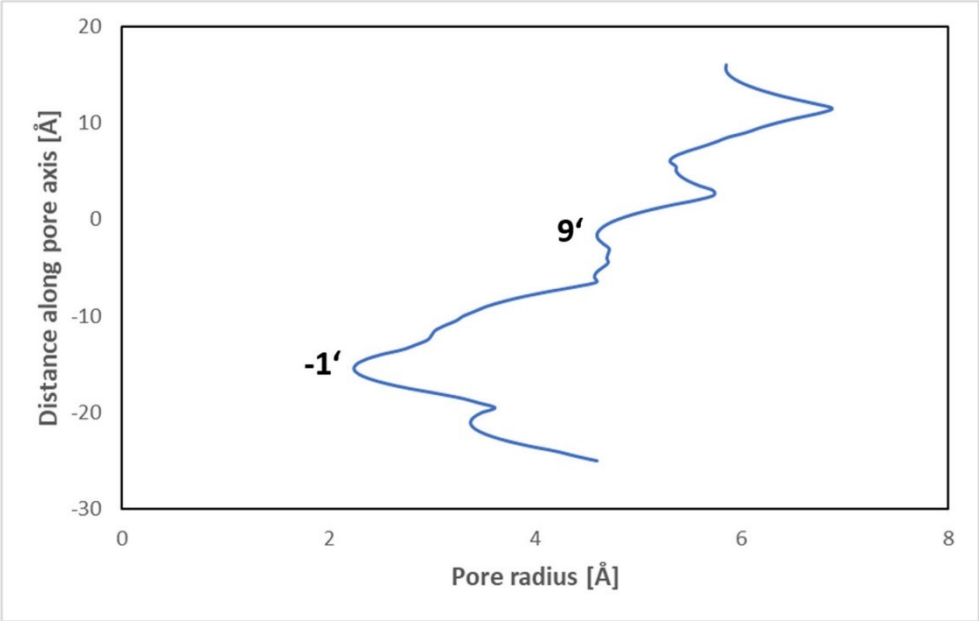

Figure S1: Pore radius of the α4β2 nAChR in complex with the partial agonist varenicline (PDB-ID: 6UR8[1]). The distance along the pore axis has been set to 0 Å at position 9'. The funnel-shaped structure with a gate at position -1' indicates a desensitized state.

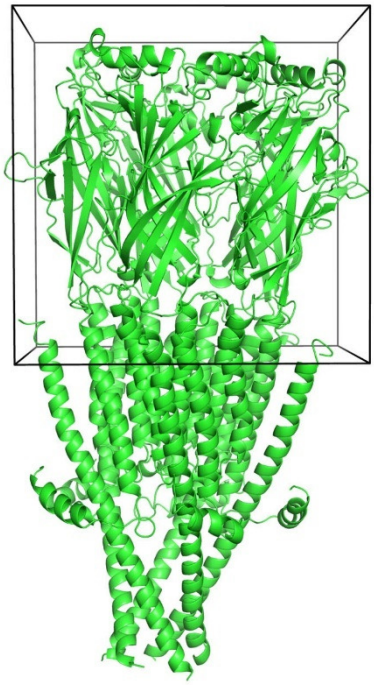

Figure S2: Model of the α7 nAChR. The displayed box indicates the part of the receptor that has been used to perform the blind docking experiments.

Table S1: Highest-ranked clusters of the blind docking experiments of MB327 in the human muscle-type nAChR.[a]

Cluster	Lowest docking energy [kcal/mol]	Number of poses in the cluster	Binding pocket	Subunits
1	-10.69	21	MB327-PAM-1	δ-β
2	-10.39	13	„orthosteric“[b]	δ-β
3	-9.83	5	MB327-PAM-1	ε-α
4	-9.70	1	MB327-PAM-1	α-ε
5	-9.56	10	MB327-PAM-1	α-δ
6	-9.48	2	MB327-PAM-1	δ-β
7	-9.39	8	MB327-PAM-1	α-δ
8	-8.8	1	MB327-PAM-1	α-ε
9	-8.73	1	MB327-PAM-1	α-δ
10	-8.60	1	„orthosteric“[b]	δ-β
11	-8.29	5	MB327-1	α-δ
28	-7.43	1	orthosteric	α-ε
34	-7.09	1	orthosteric	α-ε

[a] The ten highest-ranked clusters are shown. Additionally, the highest-ranked clusters where MB327 was placed in the orthosteric binding site (clusters 28 and 34) and MB327-1 as identified by Wein et al. [2] (cluster 11) are displayed.

[b] The orthosteric binding pocket is marked in quotes because the location of the binding pocket is identical between two neighboring subunits but acetylcholine only binds in between the α and its respective adjacent subunit. The sequence similarity of the “orthosteric” binding pocket between the δ- and β- subunits to the actual orthosteric binding pocket where nicotine binds (between the α- and δ-/ε- subunit)is 18%. MB327-PAM-1 refers to the newly identified pocket.

Table S2: Ten highest-ranked clusters of the blind docking of MB327 in the human α7-nAChR

Cluster	Lowest docking energy [kcal/mol]	Number of poses in the cluster	Binding pocket
1	-11.41	26	MB327-PAM-1
2	-10.91	1	MB327-PAM-1
3	-10.56	7	orthosteric
4	-9.69	11	MB327-PAM-1
5	-9.51	4	MB327-PAM-1
6	-9.32	5	orthosteric
7	-9.27	1	orthosteric
8	-9.27	15	MB327-1
9	-9.20	1	MB327-1
10	-9.11	1	MB327-1

Table S3: Four highest-ranked clusters of the blind docking experiments of acetylcholine in the human muscle-type nAChR.

Cluster	Lowest docking energy [kcal/mol]	Number of poses in the cluster	Binding pocket	Subunits
1	-6.51	30	orthosteric	α-ε
2	-6.44	10	„orthosteric“[a]	δ-β
3	-6.43	22	orthosteric	α-δ
4	-6.31	6	orthosteric	α-δ

[a] The orthosteric binding pocket is marked in quotes because the location of the binding pocket is identical between two neighboring subunits but acetylcholine only binds in between the α and its respective adjacent subunit. . The sequence similarity of the “orthosteric” binding pocket between the δ- and β- subunits to the actual orthosteric binding pocket where nicotine binds (between the α- and δ-/ε- subunit)is 18%. MB327-PAM-1 refers to the newly identified pocket.

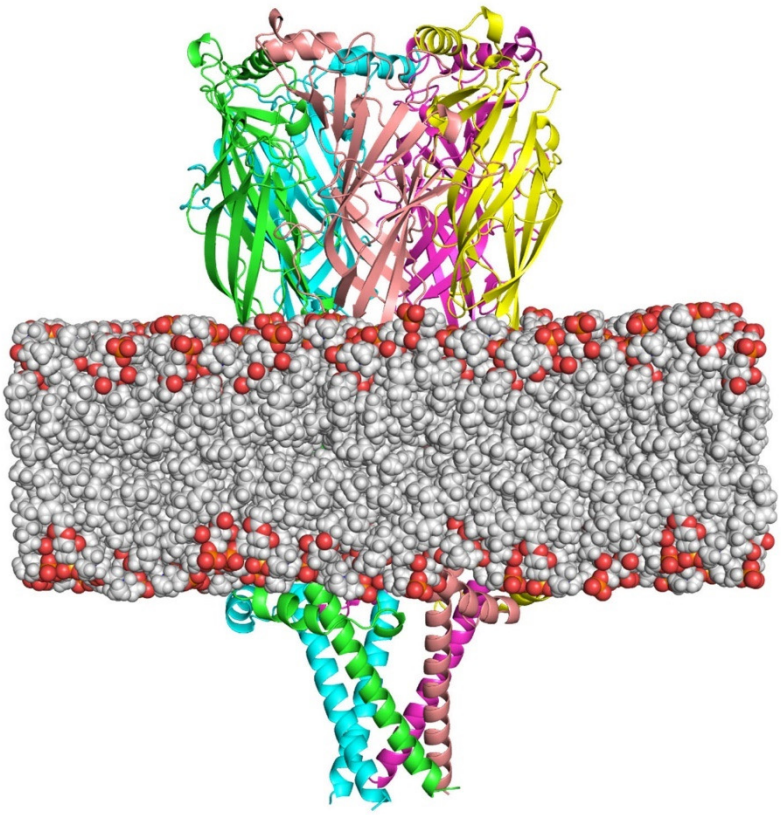

Figure S3: Starting structure for the MD simulations with MB327 bound to all five subunits. The membrane bilayer is shown as spheres. For clarity, water, potassium, and chloride molecules are not shown.

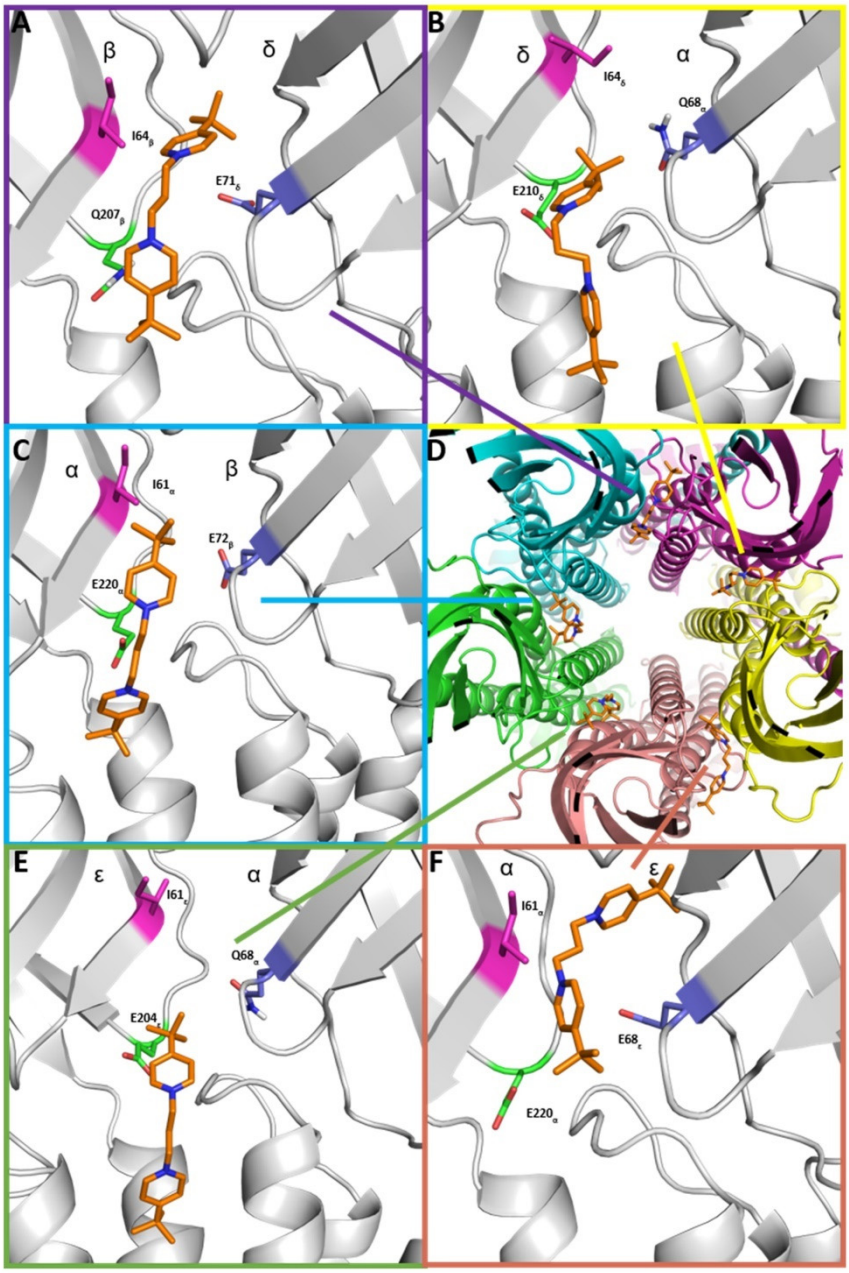

Figure S4: Docked binding mode of MB327 in MB327-PAM-1 in **A)** the β-δ-, **B)** δ-α-, **C)** α-β-, **E)** ε-α-, and **F)** α-ε-subunit. **D)** Extracellular view on MB327-PAM-1.

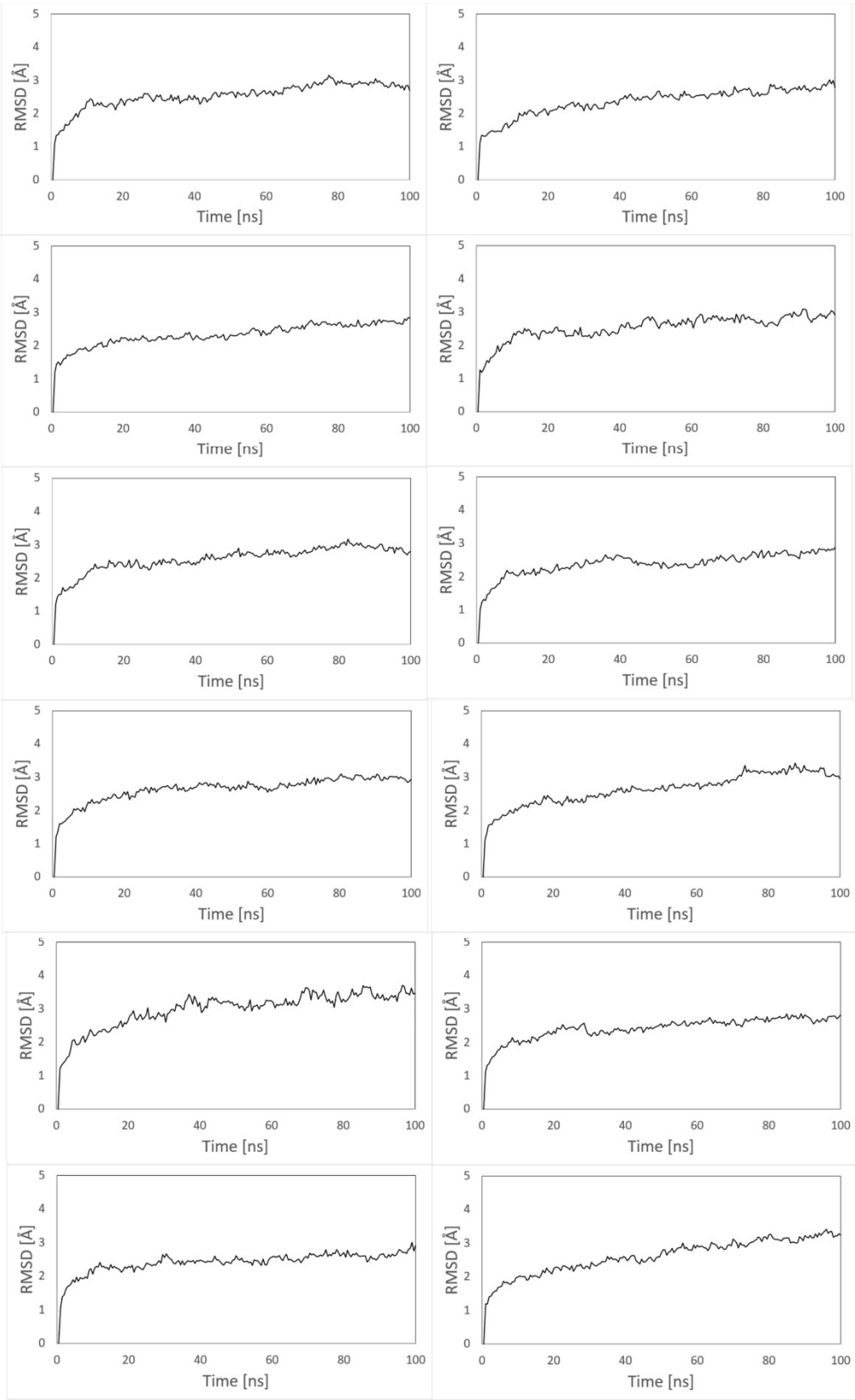
RMSD [Å]
Time [ns]
0
1
2
3
4
5
0
20
40
60
80
100

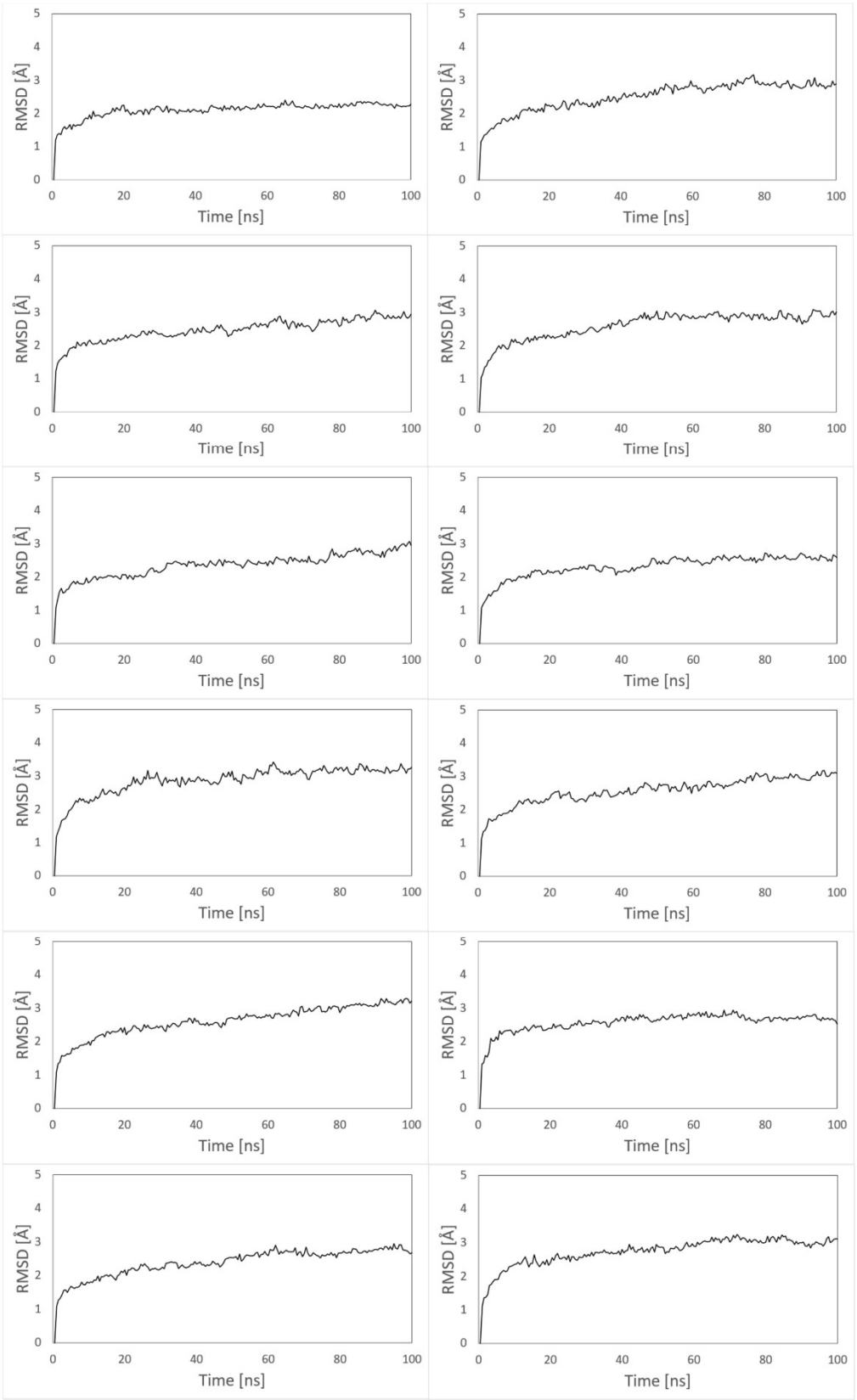
RMSD [Å]
Time [ns]
0
1
2
3
4
5
0
20
40
60
80
100

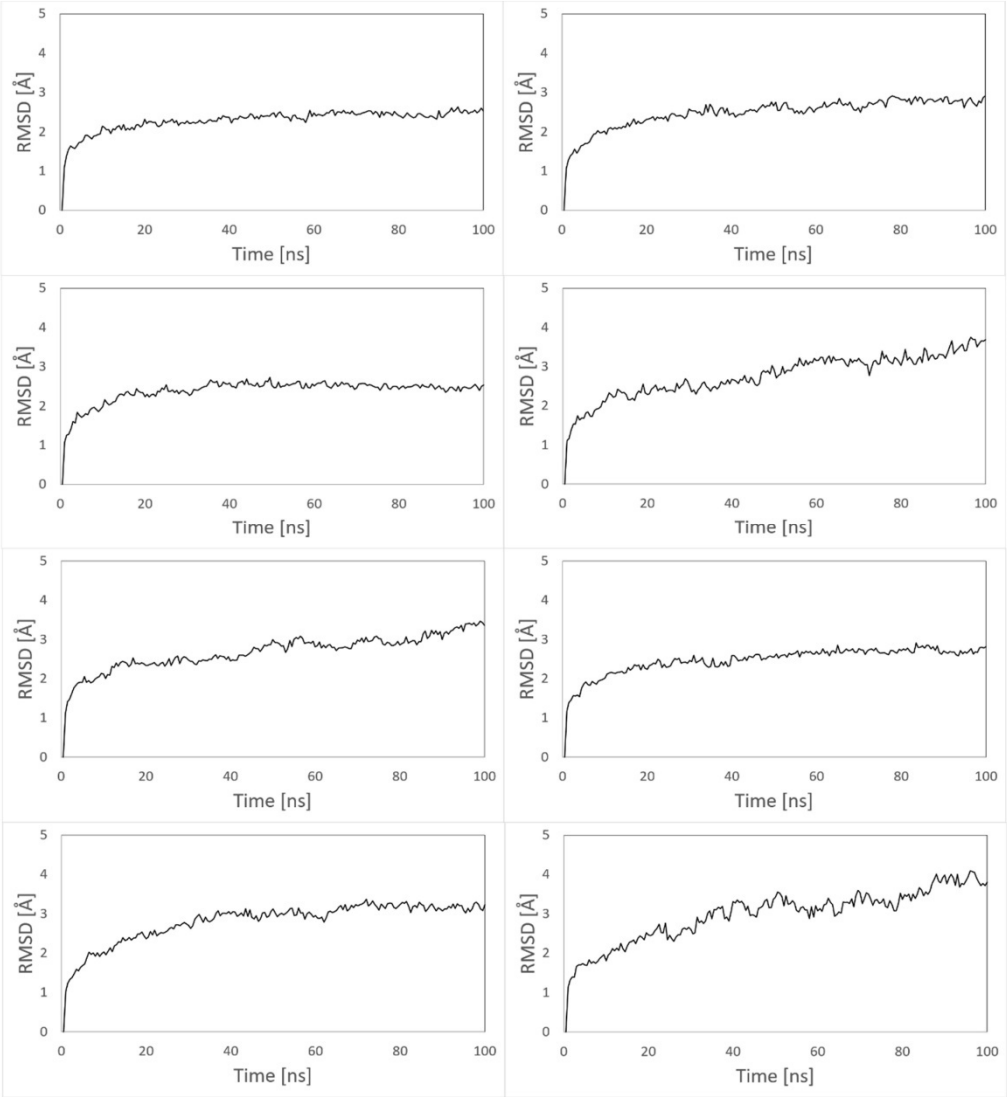

Figure S5: Backbone (C, CA, N) RMSD values of nAChR during 32 replicas of MD simulations with MB327 bound to all subunits.

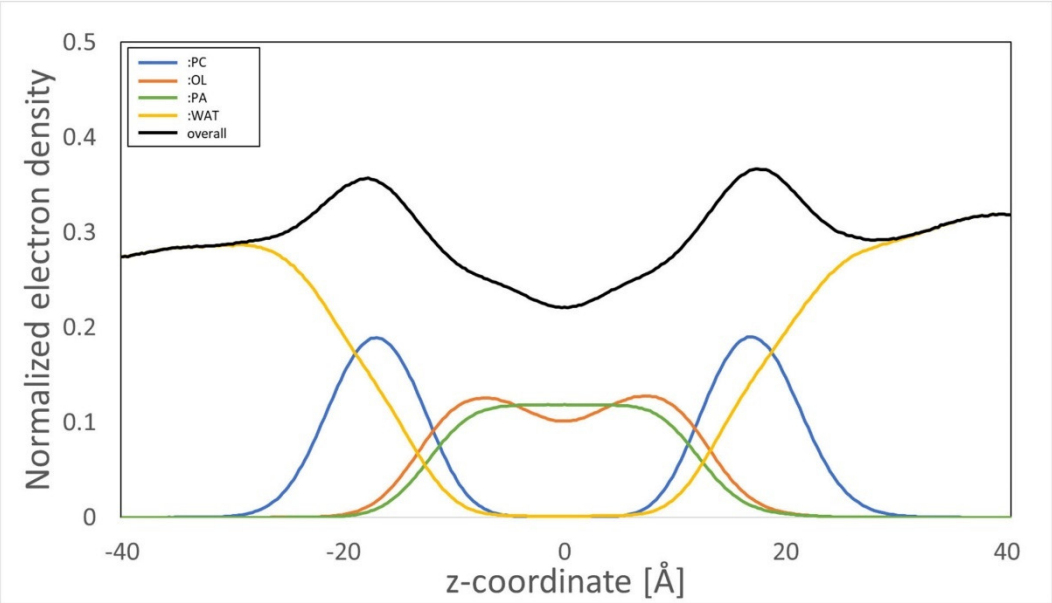

Figure S6: Electron density plot of membrane components and water based on all 32 replicas of the MD simulations with MB327 bound to nAChR. The electron density is plotted against the z-coordinate with the membrane centered at 0 Å for PC: phosphatidylcholine, OL: oleic acid, PA: palmitoylic acid, and WAT: water.

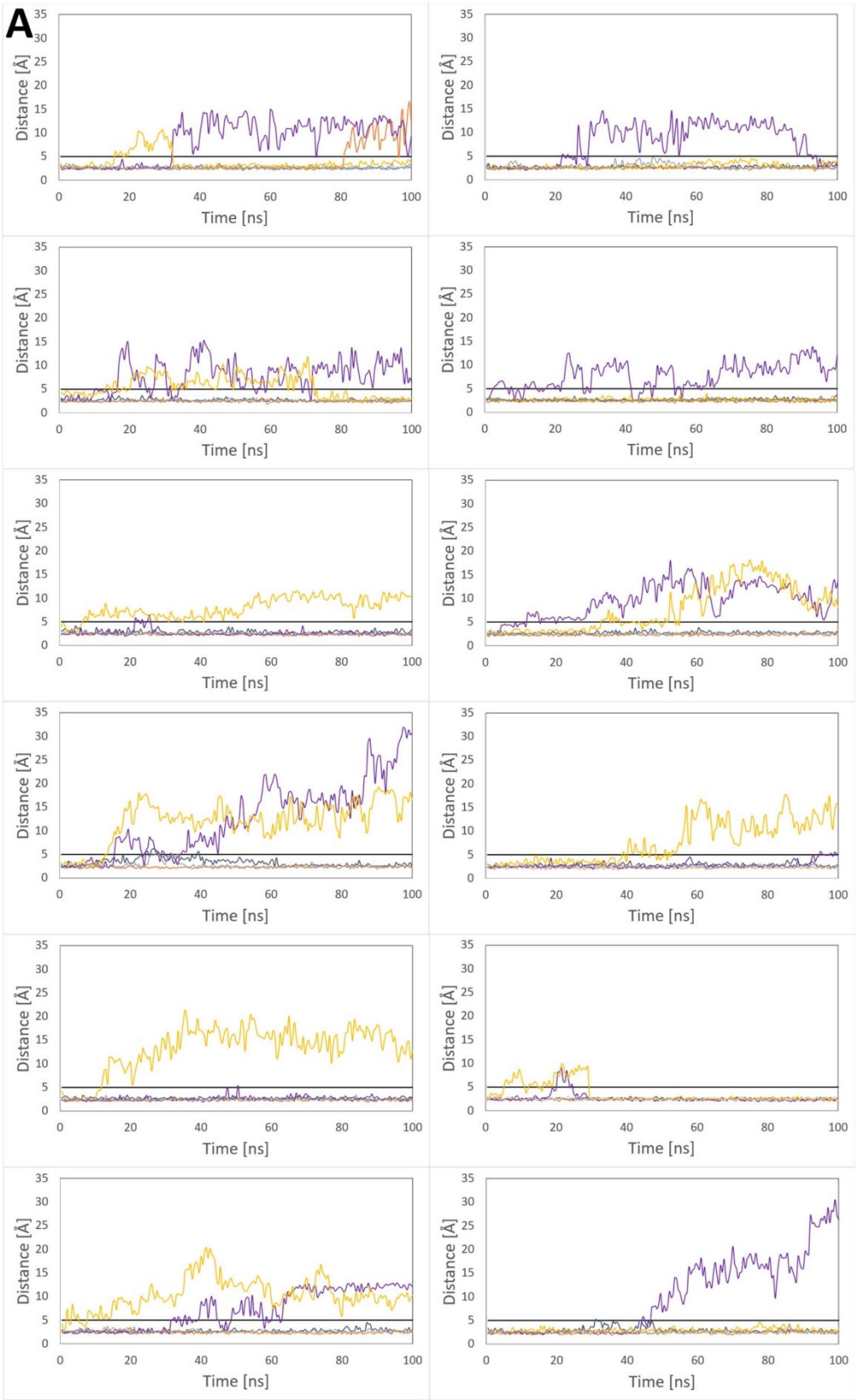
A
Distance [Å]
Time [ns]
0
5
10
15
20
25
30
35
0
20
40
60
80
100

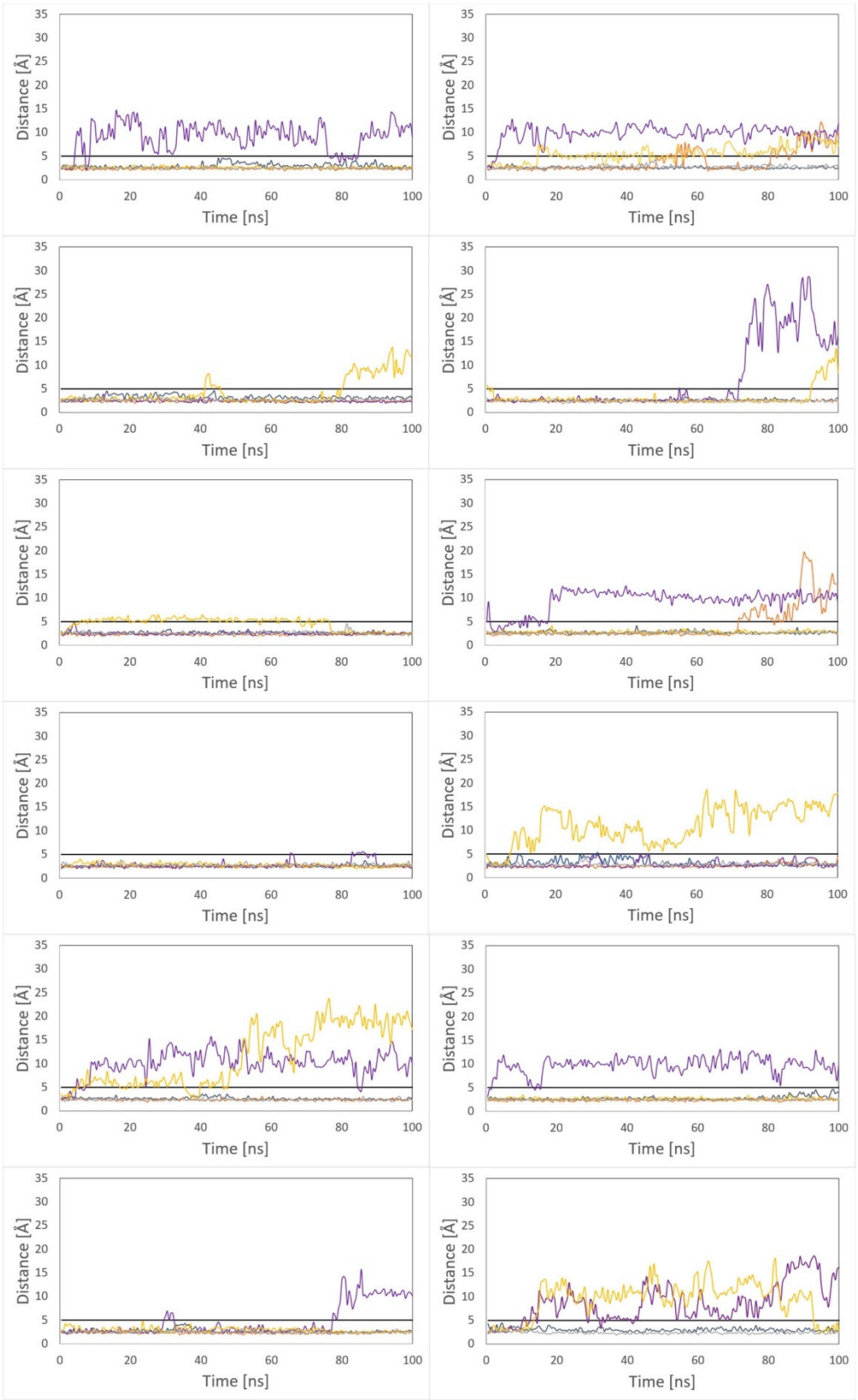
Distance [Å]
Time [ns]
0
5
10
15
20
25
30
35
0
20
40
60
80
100

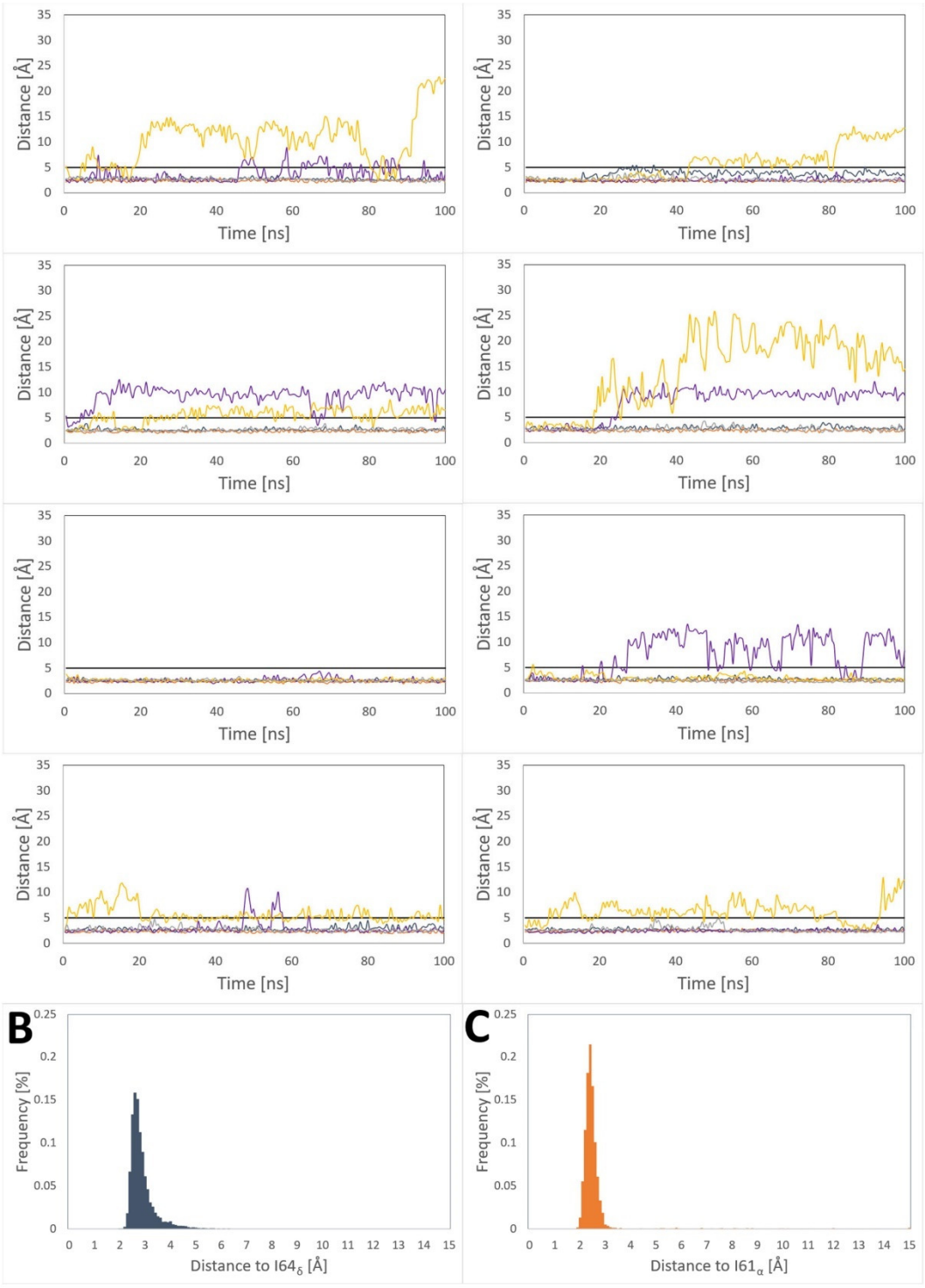
Distance [Å]
Time [ns]
B
Frequency [%]
Distance to I64δ [Å]
C
Frequency [%]
Distance to I61α [Å]

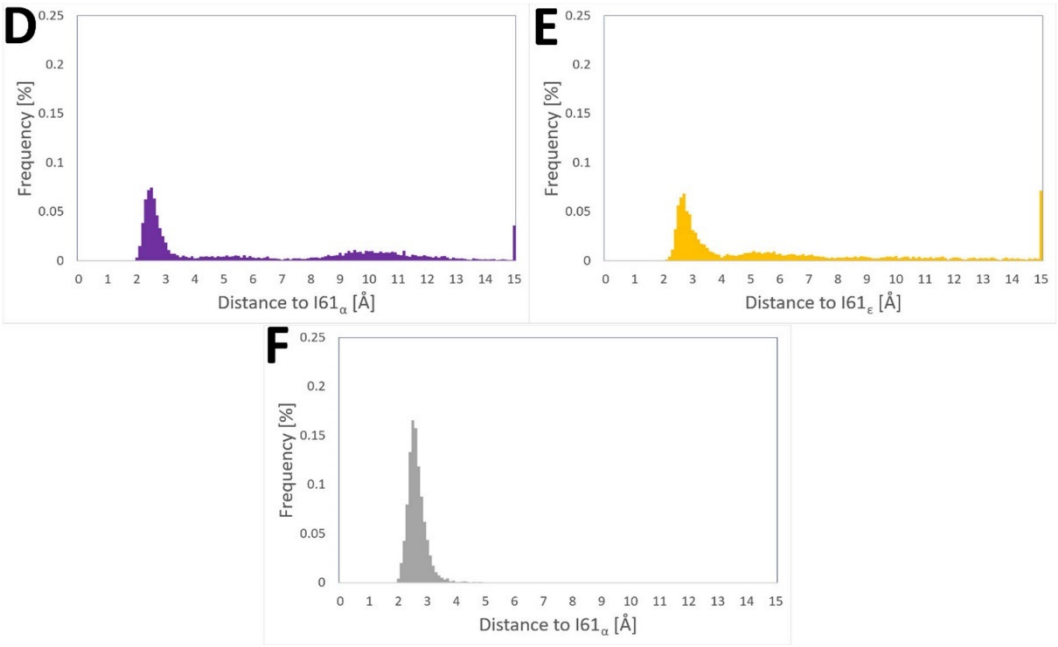

Figure S7: Distances of MB327 to the respective isoleucine in the binding site. **A)** The distance of MB327 of all 32 replicas during the simulations and the respective distance distributions **B)** in between the α- and δ-subunit to I64$_{\delta}$ is shown in dark blue, **C)** in between the δ- and β-subunit to I64$_{\beta}$ in orange, **D)** in between the β- and α-subunit to I61$_{\alpha}$ in purple, **E)** in between the α- and ε-subunit to I61$_{\varepsilon}$ in yellow, **F)** and in between the ε- and α-subunit to I61$_{\alpha}$ in grey. The distance cutoff of 5 Å is indicated by a black line in the distances plotted over the time during simulations. Values over 15 Å in the distance distributions are summarized in the last bin.

Table S4: Distances of docked MB327 to important amino acids in the binding site.[a]

Subunit	Distance to glutamate/glutamine in loop F[b]	Distance to glutamate/glutamine in β1-β2 loop[b]	Distance to isoleucine in β1[b]
α-δ	4.5	5.5	2.4
δ-β	6.1	3.9	1.1
β-α	7.4	10.6	1.5
α-ε	5.1	7.7	4.2
ε-α	4.9	3.2	3.0

[a] The distances to acidic sidechains represent the minimum distance of the partially positive charged atoms of the aromatic ring of MB327 (nitrogen and carbon in para position) to the oxygens of the respective sidechain. The distance to threonine represents the minimum distance to MB327.

[b] In Å.

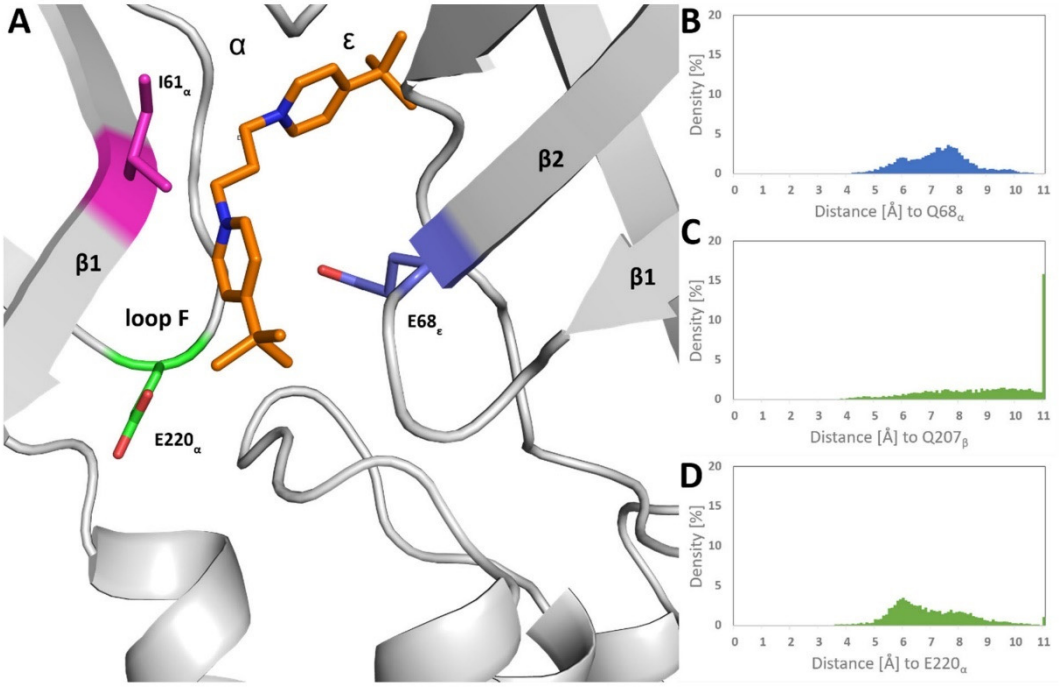

Figure S8: Distances of the nitrogens and carbon atoms in para position to the second acidic/polar residue in MB327-PAM-1. **A)** Proposed binding mode of MB327 in MB327-PAM-1 between the ε- and α-subunits. The color of amino acids E220 and E68 relates to the figures in panels B-D. Minimum distance of the nitrogens and carbon atoms located in the para position of MB327 to the side chain oxygens of **B)** $Q68_{\alpha}$, **C)** $Q207_{\beta}$, and **D)** $E220_{\alpha}$. Distances above 11 Å are summarized in the last bin.

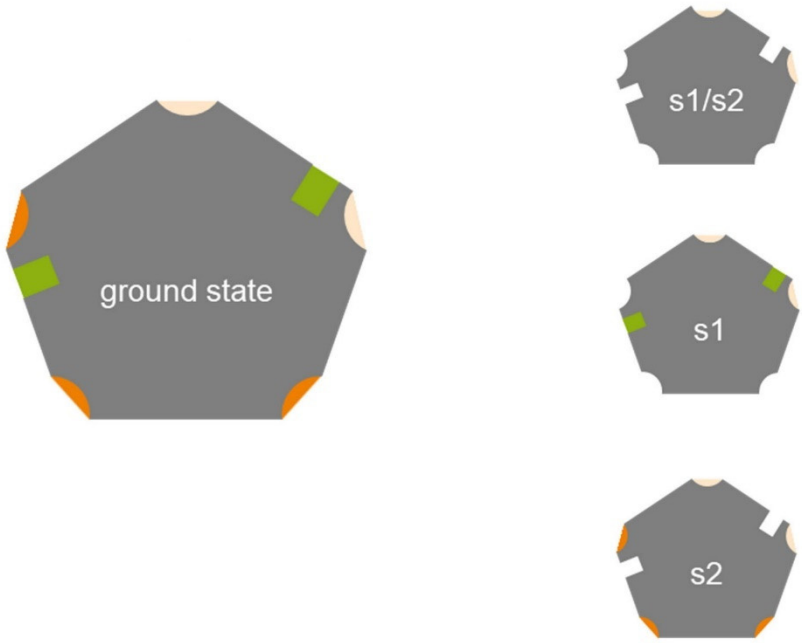

Figure S9: Performed perturbation runs in CNA to investigate the allosteric impact of MB327 and the cooperativity of binding of nicotine and MB327. The pentagon represents nAChR with its five subunits. During the MD simulations, MB327 is bound in all five possible binding sites, and nicotine is bound to both possible binding sites (left). The two MB327 molecules that did not stay stable in the binding site during MD simulations are shown in light orange. Three perturbation runs were performed: 1) s1/s2: all stable ligands were removed (top right); 2) s1: MB327 was removed in all stable binding sites (middle right); 3) s2: nicotine was removed in both binding sites (bottom right).

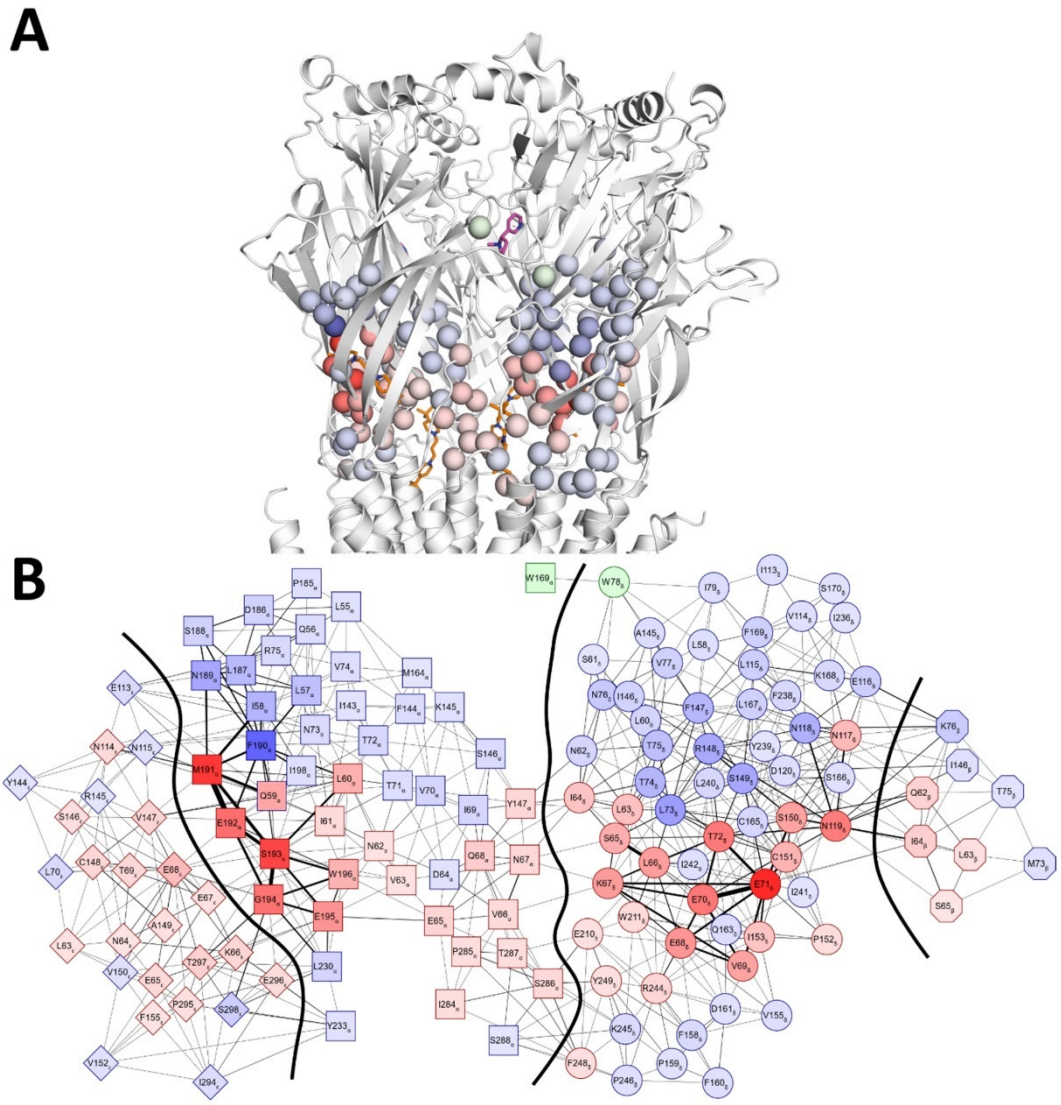

Figure S10: Allosteric effect of MB327 on the extracellular domain. **A)** Residues with significant changes of structural rigidity after removal of MB327 are shown as spheres. Residues located within 5 Å of MB327 are shown in red and those within 5 Å of the orthosteric ligand nicotine are shown in green. A cutoff of 0.15 kcal mol^{-1} was used to display residues. Thus, only an effect on the extracellular domain is shown. **B)** The information from **(A)** shown as a graph. The nodes represent residues, and edges the flow between these residues. Twisted squares represent residues from the ε-, squares residues from the α-, circles residues from the δ-, and octagons residues from the β-subunit.

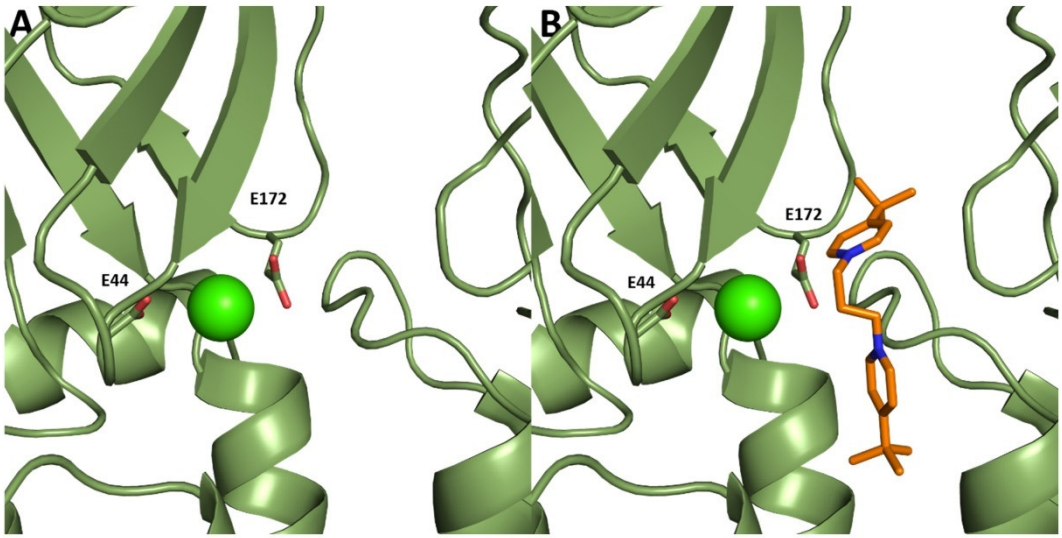

Figure S11: Location of calcium in MB327-PAM-1. **A)** Cryo-EM structure of α7-nAChR (PDB-ID: 7KOQ[3]) with calcium (green) located in between E44 and E172. **B)** Comparison of the calcium binding site to the docked binding mode of MB327 in the human muscle-type nAChR in MB327-PAM-1 between the α- and δ-subunit (orange) in α7-nAChR (PDB-ID: 7KOX [3]) after aligning the human muscle-type nAChR model to the cryo-EM structure of α7-nAChR.

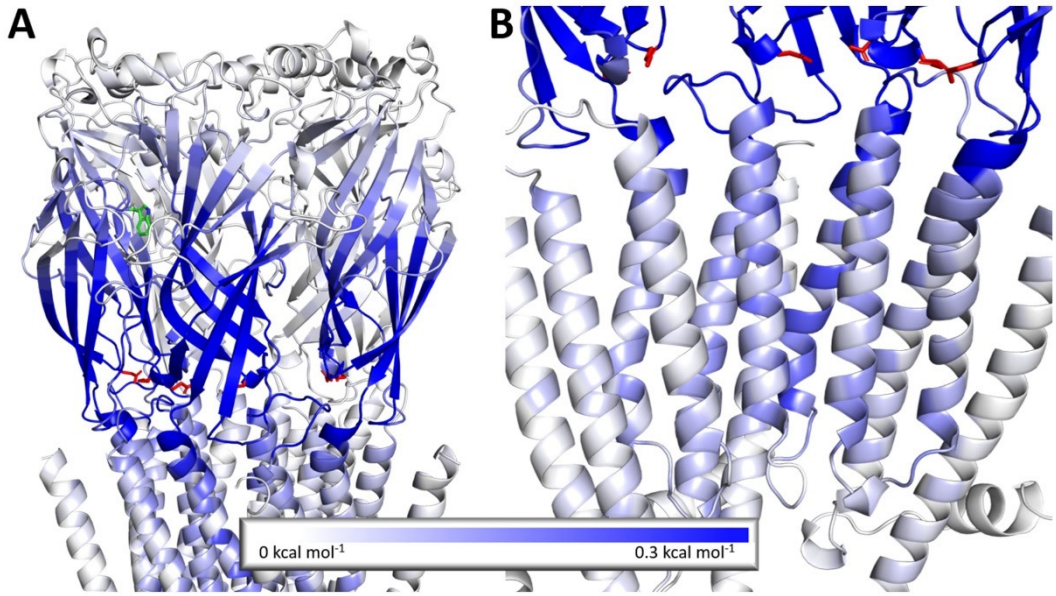

Figure S12: Allosteric effects of calcium on the **A)** the extracellular and **B)** the transmembrane domain of nAChR. The calcium ion was mimicked by setting constraints between the carboxy groups of the glutamates involved in calcium binding (shown in red). Blue colors indicate a stabilizing impact of calcium on the receptor. $W169_{\alpha}$, a central amino acid in the orthosteric binding site, is shown in green.

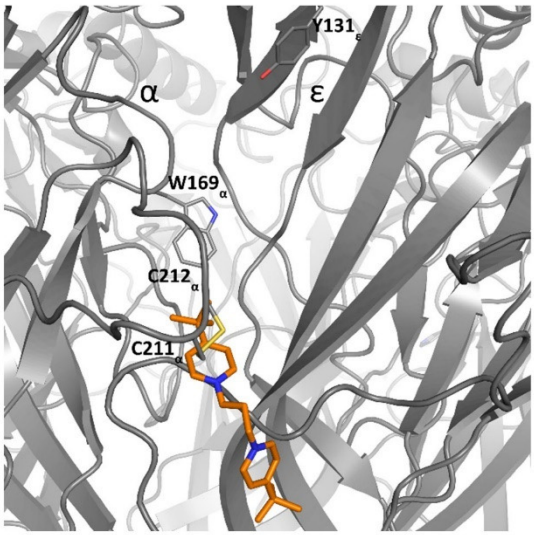

Figure S13: Representative binding mode of MB327 in the orthosteric binding pocket in the replica where MB327 stays only 130 ns within this pocket.

Table S5: Docking scores of MB327, PTM0062, and PTM0063 in all subunits of the muscle-type nAChR.

Subunit	Docking score of MB327	Docking score of PTM0062	Docking score of PTM0063
αδ	-8.62	-9.20	-8.51
δβ	-4.88	-5.76	-5.62
βα	-4.36	-6.17	-5.24
αε	-8.65	-8.13	-8.95
εα	-5.44	-6.01	-7.42

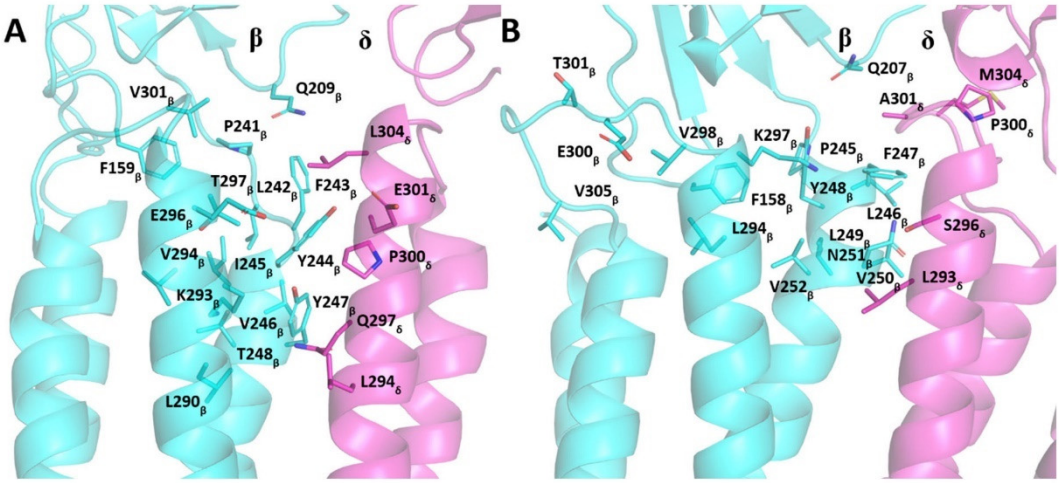

Figure S14: A) Amino acids that are part of the binding site MB327-2 in the PDB-structure 2BG9[4]. **B)** Amino acids that are part of M327-2 in our new models of the human muscle-type nAChR. The alignment of the amino acids is shown in Table S4.

Table S6: Alignment of the amino acids that are part of MB327-2 in the *Torpedo marmorata* and human muscle-type nAChR.

β		δ	
2BG9	human	2BG9	human
F159	F158	L294	L293
Q209	Q207	Q297	S296
P241	P245	P300	P300
L242	L246	E301	A301
F243	F247	L304	M304
Y244	Y248		
I245	L249		
V246	V250		
Y247	N251		
T248	V252		
L290	L294		
K293	K297		
V294	V298		
E296	E300		
T297	T301		
V301	V305		

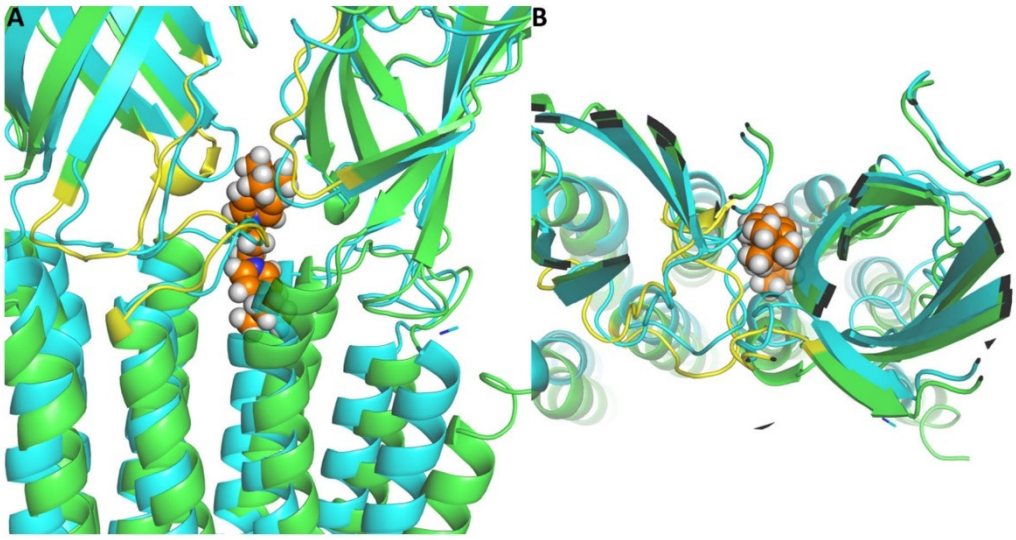

Figure S15: Aligned models of the human nAChR in the desensitized (green) and inactive (blue) state viewed from **A)** the side and **B)** the extracellular space. Structural changes that occur during desensitization in the region of the binding site of MB327 (orange spheres) are colored in yellow in the desensitized model. These regions are in line with the regions of structural changes in the glycine receptor, another pentameric ligand-gated ion channel, during desensitization[5]. For clarity, only two adjacent subunits (α and ε) are shown. Similar structural changes can be observed in all subunits of the receptor.

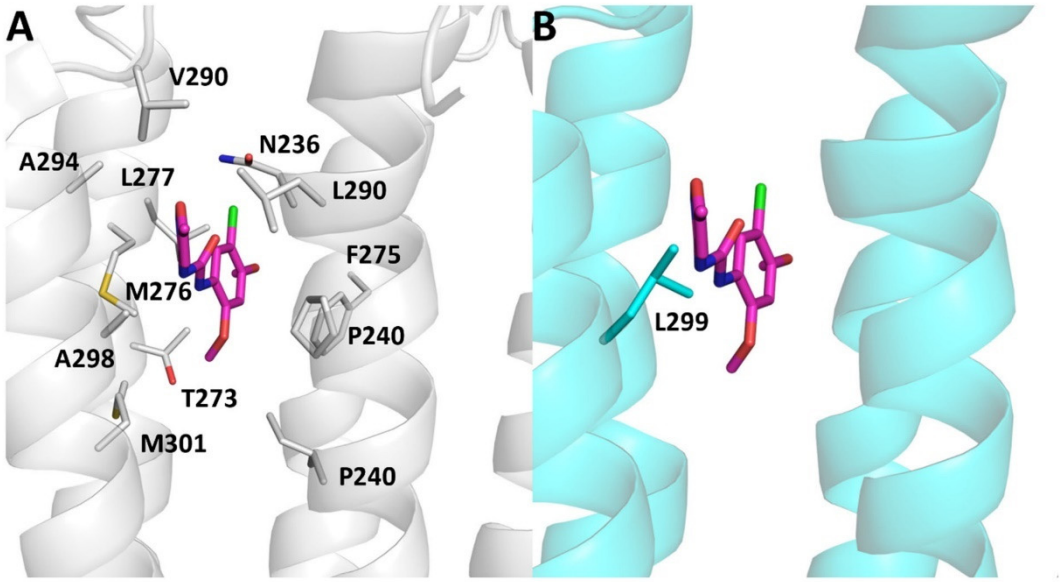

Figure S16: Comparison of the PNU-120596 binding site in the α7- and the human muscle-type nAChR. **A)** Amino acids located within 5 Å of PNU-120596 (purple) are shown as sticks. No charged amino acids are located in the binding site. **B)** A mutation of A298 in the α7-nAChR to L299 in the human muscle-type nAChR leads to a clash with the α7-selective modulator PNU-120596. The closest distance between heavy atoms of the ligand and heavy atoms of L299 is 0.9 Å.

Supplemental References

1. Mukherjee, S., et al., *Synthetic antibodies against BRIL as universal fiducial marks for single-particle cryoEM structure determination of membrane proteins.* Nat Commun, 2020. **11**(1): p. 1598.
2. Wein, T., et al., *Searching for putative binding sites of the bispyridinium compound MB327 in the nicotinic acetylcholine receptor.* Toxicol Lett, 2018. **293**: p. 184-189.
3. Noviello, C.M., et al., *Structure and gating mechanism of the alpha7 nicotinic acetylcholine receptor.* Cell, 2021. **184**(8): p. 2121-2134 e13.
4. Unwin, N., *Refined structure of the nicotinic acetylcholine receptor at 4A resolution.* J Mol Biol, 2005. **346**(4): p. 967-89.
5. Kumar, A., et al., *Mechanisms of activation and desensitization of full-length glycine receptor in lipid nanodiscs.* Nat Commun, 2020. **11**(1): p. 3752.

11.2. Publication II

MS Binding Assays with UNC0642 as reporter ligand for the MB327 binding site of the nicotinic acetylcholine receptor

Valentin Nitsche, Georg Höfner, **Jesko Kaiser**, Christoph G.W. Gertzen, Thomas Seeger, Karin V. Niessen, Dirk Steinritz, Franz Worek, Holger Gohlke, Franz F. Paintner, Klaus T. Wanner

Toxicology Letters, 2024. **392**: p. 94-106. [§2]

[§2] See **REPRINT PERMISSION**

Toxicology Letters 392 (2024) 94–106

Contents lists available at ScienceDirect

Toxicology Letters

journal homepage: www.journals.elsevier.com/toxicology-letters

MS Binding Assays with UNC0642 as reporter ligand for the MB327 binding site of the nicotinic acetylcholine receptor

Valentin Nitsche [a,1], Georg Höfner [a,2], Jesko Kaiser [b,3], Christoph G.W. Gertzen [b,4], Thomas Seeger [c,5], Karin V. Niessen [c,6], Dirk Steinritz [c,7], Franz Worek [c,8], Holger Gohlke [b,d,9], Franz F. Paintner [a,10], Klaus T. Wanner [a,*,11]

[a] Department of Pharmacy – Center for Drug Research, Ludwig-Maximilians-Universität München, Munich, Germany
[b] Institute for Pharmaceutical and Medicinal Chemistry, Heinrich Heine Universität Düsseldorf, Düsseldorf, Germany
[c] Bundeswehr Institute of Pharmacology and Toxicology, Munich, Germany
[d] Institute of Bio, and Geosciences (IBG-4: Bioinformatics), Forschungszentrum Jülich, Jülich, Germany

ARTICLE INFO

Editor : Dr. Angela Mally

Keywords:
Nicotinic acetylcholine receptor
UNC0642 MS Binding Assays
MB327-PAM-1 binding site
LC-MS
Resensitizer
In silico studies
Myographic studies

ABSTRACT

Intoxications with organophosphorus compounds (OPCs) based chemical warfare agents and insecticides may result in a detrimental overstimulation of muscarinic and nicotinic acetylcholine receptors evolving into a cholinergic crisis leading to death due to respiratory failure. In the case of the nicotinic acetylcholine receptor (nAChR), overstimulation leads to a desensitization of the receptor, which cannot be pharmacologically treated so far. Still, compounds interacting with the MB327 binding site of the nAChR like the bispyridinium salt MB327 have been found to re-establish the functional activity of the desensitized receptor. Only recently, a series of quinazoline derivatives with UNC0642 as one of the most prominent representatives has been identified to address the MB327 binding site of the nAChR, as well. In this study, UNC0642 has been utilized as a reporter ligand to establish new Binding Assays for this target. These assays follow the concept of MS Binding Assays for which by assessing the amount of bound reporter ligand by mass spectrometry no radiolabeled material is required. According to the results of the performed MS Binding Assays comprising saturation and competition experiments it can be concluded, that UNC0642 used as a reporter ligand addresses the MB327 binding site of the *Torpedo*-nAChR. This is further supported by the outcome of *ex vivo* studies carried out with poisoned rat diaphragm muscles as well as by *in silico* studies predicting the binding mode of UNC0646, an analog of UNC0642 with the highest binding affinity, in the recently proposed binding site of MB327 (MB327-PAM-1). With UNC0642 addressing the MB327 binding site of the *Torpedo*-nAChR, this and related quinazoline derivatives represent a promising starting point for the development of novel ligands of the nAChR as antidotes for the treatment of intoxications with organophosphorus compounds. Further, the new MS Binding Assays are a potent alternative to established assays and of particular value, as they do not require the use of radiolabeled material and are based on a commercially available compound as reporter ligand, UNC0642, exhibiting one of the highest binding affinities for the MB327 binding site known so far.

* Corresponding author.
E-mail address: klaus.wanner@cup.uni-muenchen.de (K.T. Wanner).
[1] 0009-0000-3351-1227
[2] 0000-0002-7957-4503
[3] 0000-0002-6429-0911
[4] 0000-0002-9562-7708
[5] 0009-0007-5713-4367
[6] 0009-0008-6810-5294
[7] 0000-0002-2073-5683
[8] 0000-0003-3531-3616
[9] 0000-0001-8613-1447
[10] 0000-0002-6795-586X
[11] 0000-0003-4399-1425

https://doi.org/10.1016/j.toxlet.2024.01.003
Received 19 November 2023; Received in revised form 28 December 2023; Accepted 6 January 2024
Available online 10 January 2024

1. Introduction

The poisoning with organophosphorus compounds (OPCs) as a result of exposure to respective insecticides or nerve agents represents a severe health problem (Buckley et al., 2004; Costanzi et al., 2018; Eddleston and Phillips, 2004; John et al., 2018). If not treated properly, an intoxication with OPCs can culminate in a cholinergic crisis, which can finally lead to death because of respiratory failure (Holmstedt, 1959; Newmark, 2004). As the principal mode of action, all OPCs have in common to inactivate acetylcholinesterase (AChE), an enzyme that is in charge of the breakdown of the neurotransmitter acetylcholine in the synaptic cleft of cholinergic neurons. This results in the accumulation of this neurotransmitter in the synaptic cleft whereupon the corresponding receptors, the muscarinic acetylcholine receptor (mAChR) and the nicotinic acetylcholine receptor (nAChR), become overstimulated. Being the main cause for the OPC-induced adverse health effects, medical measures aim, in general, at the elimination of this overstimulation. Thus, the standard treatment of OPC intoxication includes the application of the mAChR antagonist atropine to reduce neuronal signaling mediated by this receptor and the use of oximes, such as obidoxime, to reactivate the AChE and, thus, to lower the acetylcholine level by enzymatic breakdown (Shih et al., 2007; Thiermann and Worek, 2022; Worek et al., 2005). The use of oximes has, however, often been found to be insufficiently effective, which strongly depends on the type of OPC causing the intoxication (Thiermann et al., 2016). Hence, there is a strong need for pharmacological agents that may counteract overstimulation and resulting desensitization of the nAChRs receptors by direct intervention at this target.

Though antagonists for the acetylcholine binding site of the nAChR are known, their application to reduce nAChR overstimulation – in analogy to that of atropine for mAChR – is not feasible, as the therapeutic window of these compounds is too small (Sheridan, 2005). Yet, as an alternative, pharmacological agents that interact with nAChRs via an allosteric binding site and restore the functional activity of desensitized receptors may be applied. Among non-oxime bispyridinium salts, a series of compounds has been identified that act this way, of which MB327 (Fig. 1) can be considered the most prototypic representative. Interestingly, in electrophysiological measurements, MB327 has been demonstrated to restore the functional activity of nAChRs, which had been desensitized by overstimulation with orthosteric ligands (Niessen et al., 2016; Niessen et al., 2018). Furthermore, *in silico* studies led to the identification of a potential allosteric binding pocket for MB327 at nAChRs, termed MB327-PAM-1 binding site, where MB327 is thought to act as an allosteric modulator reestablishing receptor function (Kaiser et al., 2023). In addition, pharmacological effects for MB327 and some analogs have been recorded that demonstrate that these compounds can restore the muscle force of rat diaphragm muscles defunctionalized by soman treatment in *ex vivo* experiments (Niessen et al., 2018; Seeger et al., 2012). The ability of MB327 to reactivate soman-poisoned intercostal muscles has also been shown for tissue from humans (Seeger et al., 2012). Moreover, MB327 (respectively the corresponding methanesulfonate salt) was found to increase the survival rate of nerve agent-poisoned guinea pigs in *in vivo* studies when applied as a drug agent (Timperley et al., 2012; Turner et al., 2011). Unfortunately, with its low potency and small therapeutic window, MB327 is far from fulfilling the requirements for a drug candidate (Kassa et al., 2022). Hence, great efforts have been undertaken to identify more potent allosteric modulators of the MB327 binding site.

Sichler et al. have developed an MS Binding Assay addressing the MB327 binding site using [$^2H_6$]MB327 as a reporter ligand (Sichler et al., 2018). This has been extensively used for the characterization of the binding affinities of a plethora of bispyridinium salts related to MB327 that had been synthesized to gain insight into the structure-activity relationship of this compound class and to finally unveil representatives with distinctly higher affinities than MB327. Although binding affinities of most compounds were in the range of that of MB327 ($pK_i = 4.73 \pm 0.03$), one bispyridinium salt, PTM0022, delineated from MB327 by two additional phenyl residues, was found to surpass the binding affinity of MB327 to a small but statistically significant extent ($pK_i = 5.16 \pm 0.07$) (Rappenglück et al., 2018a, b). Significant progress was finally achieved when Sichler et al. used their [$^2H_6$]MB327-based MS Binding Assays addressing the MB327 binding site of the nAChR for the screening of a commercial compound library (Sichler et al., 2024). That way, a group of quinazoline derivatives with high affinities for the MB327 binding site was identified, with the highest affinities displayed by UNC0638 ($pK_i = 6.01 \pm 0.10$), UNC0642 ($pK_i = 5.97 \pm 0.05$), and UNC0646 ($pK_i = 6.23 \pm 0.02$) (Fig. 1).

The present study aimed to develop new MS Binding Assays for the MB327 binding site of the nAChR utilizing one of these quinazoline derivatives as reporter ligand. Such Binding Assays were expected to be more robust and specific due to the distinctly increased affinity of the employed reporter ligand as compared to that of MB327 in the [$^2H_6$]MB327-based MS Binding Assays. Moreover, such Binding Assays should provide additional solid information on the interaction of the aforementioned quinazoline derivatives with the MB327 binding site of the nAChR, which so far had only been studied in competitive [$^2H_6$]MB327 MS binding experiments. For the new Binding Assays, the concept of MS Binding Assays was followed due to simple reasons: As often discussed in the literature, this type of Binding Assays benefits from not requiring radiolabeled substances, which makes them highly flexible with regard to the compounds used as reporter ligands. Besides, MS Binding Assays do not suffer from drawbacks that commonly arise when radioactivity is

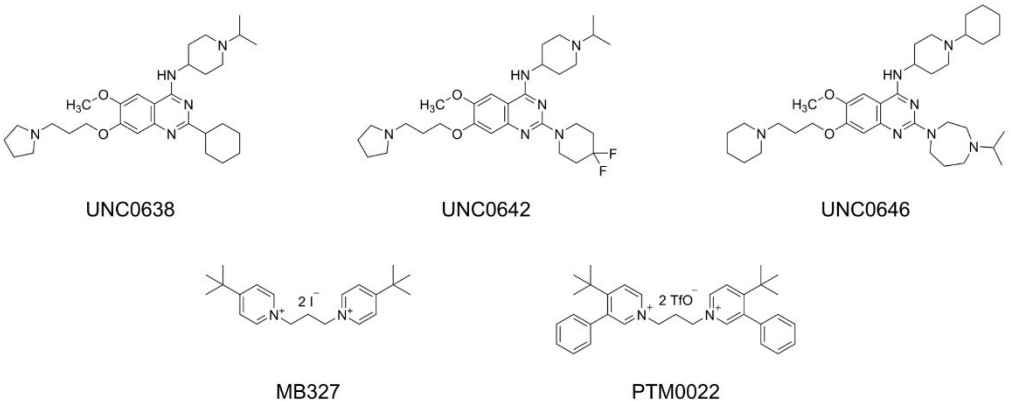

Fig. 1. Ligands of the MB327 binding site of the nAChR: MB327, PTM0022, UNC0638, UNC0642, and UNC0646.

involved in an experimental setting (Höfner and Wanner, 2015; Wanner et al., 2007).

To gain knowledge on the intrinsic activity of the newly identified quinazoline derivatives addressing the MB327 binding site, their capability to restore muscle force in *ex vivo* experiments with soman-poisoned diaphragm muscle tissues were studied, too. In addition, using docking approaches and molecular dynamics (MD) simulations, the binding mode and key interaction partners of the analog with the highest binding affinity, UNC0646, in MB327-PAM-1 were studied.

2. Materials and methods

2.1. Materials

UNC0638 and UNC0642 (purity for both ≥ 95%) were purchased from MedChemExpress (Sollentuna, Sweden). UNC0646 (purity ≥ 99%) was received from Axon Medchem (Groningen, Netherlands) and carbachol (carbamoylcholine chloride, purity ≥ 98%) from Sigma Aldrich. MB327 and PTM0022 were synthesized in-house by Rappenglück et al., purities ≥ 95% (Rappenglück et al., 2018b). Frozen tissue of *Torpedo californica* electroplaque was purchased from Aquatic Research Consultants (San Pedro, CA, USA). Water was obtained from a Sartorius arium pro ultrapure water system (Sartorius, Göttingen, Germany) for all purposes. Organic solvents for LC-MS were received from VWR Prolabo (Darmstadt, Germany) in LS-MS grade. Ammonium formate as additive for LC-MS (purity ≥ 99%) was purchased from Sigma Aldrich (Taufkirchen, Germany). All other chemicals were purchased in analytical grade. Polypropylene reaction tubes and 96-deep well plates as well as pipette tips were received from Sarstedt (Nümbrecht, Germany).

2.2. Preparation of nAChR-enriched membrane fragments

The nAChR-enriched membrane fragments were prepared from frozen electroplaque of *Torpedo californica* as described by Sichler et al. (2018).

2.3. UNC0642 centrifugation-based MS Binding Assays

In general, for MS binding experiments with UNC0642 at *Torpedo*-nAChR, the reporter ligand was incubated with aliquots of the membrane preparation from *Torpedo californica* electroplaque (approx. 75 µg protein per sample) in incubation buffer (120 mM NaCl, 5 mM KCl, 8.05 mM Na_2HPO_4 and 1.95 mM NaH_2PO_4, pH 7.4). With a total volume of 1.25 mL, each binding sample was generated in a 1.5 mL reaction tube. Incubation took place in a shaking water bath (2 h, 25 °C). After that, the reaction tubes were centrifuged for 5 min at 4 °C and 23000 rpm (approx. 49000 x *g*, Heraeus Biofuge Stratos, rotor 3331, Thermo Scientific, Waltham, USA). In the next step, the formed pellets were freed from the supernatant using a Pasteur pipette, which was connected to a vacuum pump via a vacuum filter flask. Thereafter, pellets were washed two times by the addition of 1.5 mL ice-cold incubation buffer and instant removal of the latter by a vacuum-coupled Pasteur pipette. To liberate the bound reporter ligand, 500 µL acetonitrile (containing 500 nM UNC0638 as internal standard) were given to the pellets. The mixtures were subsequently subjected to ultrasound in an ultrasonic bath (SONOREX RK100, Bandelin electronic, Berlin, Germany) for 1 h. Next, the samples were vortexed intensively before they were centrifuged again under the same conditions as described before. Of the resulting supernatants 10 µL were transferred into a 96-deep well plate and diluted by the addition of 490 µL acetonitrile to each well. The 96-deep well plate was sealed with aluminum foil before the samples were finally analyzed via LC-ESI-MS/MS. For saturation experiments, total binding was determined for fifteen reporter ligand concentrations, reaching from 200 nM to 100 µM. For the evaluation of non-specific binding, binding samples with the five lowest reporter ligand concentrations (200 nM - 1 µM) were, in addition, provided with an excess of competitor UNC0646 (100 µM). Regarding the amount of DMSO introduced by the stock solutions of the used compounds (10 mM in DMSO), all binding samples were adjusted to the same amount of 1% DMSO (*v*/*v*). Competition experiments were performed in analogy to saturation experiments, except that the reporter ligand concentration in the binding samples was set to a fixed concentration of 1 µM. Furthermore, binding samples contained test compounds in general in six but at least in five different concentrations (100 nM - 10 mM). Total binding in the absence of any test compound was determined by means of control samples with only 1 µM of the reporter ligand UNC0642 present in addition to the *Torpedo* membrane preparation. For the determination of non-specific binding of the reporter ligand, binding samples containing 1 µM UNC0642 and *Torpedo* membrane preparation were additionally provided with 100 µM of UNC0646 as a competitor.

2.4. Data analysis

The concentration of the reporter ligand, UNC0642, in each sample was calculated by the Analyst software v. 1.6.1 (AB Sciex, Darmstadt, Germany) based on an underlying calibration curve. To ensure a reliable quantification, calibration standards, and a corresponding calibration function were generated for each binding experiment (see "2.7 Validation of the LC-ESI-MS/MS method" for details). Further analysis (e.g., linear regression, non-linear regression, and normalization) of the data to evaluate the binding experiments was done with the Prism software v. 6.07 (GraphPad software, La Jolla, CA, USA). For saturation experiments, non-specific binding was determined only for the lowest five concentration levels (200 nM - 1 µM). By analyzing this data via linear regression forced through zero a linear regression function was established. This was subsequently used for the calculation of non-specific binding values for all reporter ligand concentrations applied in the assay. Subtracting non-specific binding from total binding yielded specific binding, which was further analyzed by the "One site binding (hyperbola)" regression tool to obtain the values for B_{max} and K_d. For competition experiments, the data received was firstly normalized with the total binding of the reporter ligand in the absence of a test compound being set to 100% and non-specific binding to 0%. The data was then analyzed with the "One site – fit Ki" regression tool, fixing top and bottom levels to 100% and 0% respectively, yielding competition curves. The derived IC_{50} values were automatically transformed into K_i values according to the Cheng-Prusoff equation by the additional input of the K_d value for the reporter ligand, UNC0642 (K_d = 6.7 µM), which was determined in saturation experiments as described above. If not stated otherwise, the results of binding experiments (B_{max}, K_d, K_i) are given as means from three experiments ± SEM.

2.5. LC-MS instrumentation

For preliminary experiments and method development, an API3200 triple quadrupole mass spectrometer with a TurboV-ESI source (Sciex, Darmstadt, Germany) was used in positive mode. After UNC0642 had been selected as a reporter ligand, all subsequent experiments were performed on an API5000. The two mass selectors, Q1 and Q3, were operated under unit resolution. For LC-ESI-MS/MS measurements the MS instrument was provided with an Agilent 1200 Series HPLC system (vacuum degasser G1379B, binary pump G1312B, oven G1316B, Agilent, Waldbronn, Germany). The stationary phase consisted of a YMC-Triart Diol-HILIC (50 mm × 2.0 mm, 3 µm; YMC Europe GmbH, Dinslaken, Germany) protected by two in-line filters (0.5 µm and 0.2 µm, IDEX, Wertheim-Mondfeld, Germany). The mobile phase consisted of a mixture of acetonitrile and an ammonium formate buffer (20 mM, pH 3.0) in a ratio of 80:20 (*v*/*v*). The flow rate amounted to 800 µL/min and the temperature of the column oven was set to 20 °C. For sample injection (injection volume: 10 µL), a HTS-PAL autosampler (CTC-Analytics, Zwingen, Switzerland) equipped with a 50 µL syringe was used.

For the direct infusion of compound solutions into the ESI source, the HPLC system of the LC-ESI-MS/MS unit was exchanged by a syringe pump (Harvard Apparatus, Holliston, MA, USA).

2.6. Establishing compound- and source-specific parameters

Mass transitions and compound-specific parameters for UNC0638, UNC0642, and UNC0646 were determined automatically by the "Compound optimization" tool of the Analyst software according to the manual of the respective mass spectrometer. For these experiments, the analytes were dissolved in a mixture of methanol and 0.1% aqueous formic acid [50:50 (*v/v*)]. This solution was then directly introduced into the ESI source using a syringe pump. The optimized compound-dependent parameters for the determined mass transitions that were used for the detection of the analytes via MS/MS are listed in Table 1. Source-specific parameters were optimized for the reporter ligand UNC0642 using the "Flow Injection Analysis" tool of the Analyst software, to which end a solution of acetonitrile containing 5 nM UNC0642 and 1:50 (*v/v*) matrix blank was repeatedly injected. The obtained parameters are as follows: collision gas (N_2) = 6 psi, curtain gas (N_2) = 20 psi, nebulizing gas (N_2) = 30 psi, auxiliary gas (N_2) = 50 psi, ionspray voltage = 1500 V and temperature = 600 °C.

2.7. Validation of the LC-ESI-MS/MS method

Matrix zero calibrator samples, which were necessary for the generation of calibration standards and quality control samples, were prepared in the same way as binding samples (see above: "2.3 UNC0642 centrifugation-based MS Binding Assays") with the exception that the incubation was carried out in the absence of any compounds. Instead, matrix zero calibrator samples were later spiked with a defined amount of the reporter ligand, UNC0642, in order to generate the corresponding calibration standards and quality control samples. Thus, the dilution step prior to LC-ESI-MS/MS measurement was adapted (compared to binding samples) and 10 µL supernatant (containing no UNC0642, but like binding samples 500 nM of the internal standard, UNC0638) were diluted with 440 µL acetonitrile and another 50 µL of acetonitrile, which then contained an according amount of the reporter ligand, UNC0642. Following this procedure, quality control samples investigated the subsequently given concentration levels for the reporter ligand, UNC0642, with each prepared in six replicates: 50 pM (LLOQ), 500 pM, 5 nM, 50 nM. Calibration standards were studied in eight different reporter ligand concentration levels, each generated in three replicates (50 pM, 150 pM, 400 pM, 1.2 nM, 3.5 nM, 10 nM, 30 nM, 75 nM). The data for calibration standards was plotted in a coordinate system with peak area ratios of analyte vs. internal standard on the y-axis and the concentration ratios of analyte vs. internal standard on the x-axis. Calibration curves were then obtained by linear regression with a weighting factor of $1/x^2$. Matrix blanks were prepared analogously to binding samples (see above: "2.3 UNC0642 centrifugation-based MS Binding Assays") except that there were no compounds present during the incubation and with the difference, that acetonitrile without internal standard was added to the pellet after the washing process of the samples.

Table 1
Compound-specific parameters and corresponding mass transitions used for the detection of UNC0638, UNC0642, and UNC0646. DP = declustering potential, EP = entrance potential, CE = collision energy, CXP = cell exit potential.

analyte	parent ion $[M+H]^+$ *m/z*	fragment ion *m/z*	DP [V]	EP [V]	CE [V]	CXP [V]
UNC0638	510.3	112.2	86	10	37	18
UNC0642	547.3	112.1	80	10	43	18
UNC0646	622.5	126.1	91	10	55	4

2.8. Docking of UNC0646

The structure of the *Torpedo*-nAChR [PDB-ID: 6UWZ (Rahman et al., 2020)] was used for docking. The α-neurotoxin and molecules from the crystallization buffer were removed, and the receptor was protonated using Protonate3D, as implemented in MOE v2020.09 (Chemical Computing Group, 2020) at pH 7. The termini were capped with *N*-methyl amide (NME) and acetyl (ACE) groups, respectively, using Maestro (Release 2022–3) (Schrödinger, 2021). The 3D conformation of the ligand was retrieved from the SMILES code and subsequently docked using MOE v2020.09 with default parameters for flexible docking (Chemical Computing Group, 2020).

2.9. Molecular dynamics simulations

The nAChR in complex with two UNC0646 ligands, both at the negative (i.e., between the β- and α-subunit and the γ- and α-subunit) site of the α-subunit, was embedded in a membrane consisting of 1-palmitoyl-2-oleoyl-*sn*-glycero-3-phosphocholine (POPC) lipids and solvated in a rectangular box of "optimal point charge" (OPC) water using Packmol-Memgen (Schott-Verdugo and Gohlke, 2019) from AmberTools22 (Case et al., 2023; Case et al., 2022). The edge of the box was set to be at least 12 Å away from the receptor atoms. KCl was added at a concentration of 150 mM and Cl^- ions were used to neutralize the system. The AMBER22 package of molecular simulations software (Case et al., 2005) was used to perform MD simulations in combination with the ff19SB force field (Tian et al., 2020) for the protein and the Lipid21 force field (Dickson et al., 2022) for lipids. Ligand charges were calculated according to the RESP procedure (Bayly et al., 1993) with default parameters as implemented in antechamber (Wang et al., 2006) using electrostatic potentials generated with Gaussian16 (M. J. Frisch et al., 2016) at the HF 6–31 G* level of theory; force field parameters for the ligand were taken from the gaff force field (Wang et al., 2004). Simulations were subsequently performed as described earlier (Kaiser et al., 2023). In short, first, a combination of steepest descent and conjugate gradient minimization was performed while lowering the positional harmonic restraints on receptor and ligand atoms from a force constant of 25 kcal mol^{-1} $Å^{-2}$ to one of zero. Then, the system was stepwise heated to 300 K and, subsequently, positional harmonic restraints were decreased from a force constant of 25 kcal mol^{-1} $Å^{-2}$ to one of zero.

Thereafter, 12 replicas of 500 ns length each of unbiased MD simulations were performed, using Langevin dynamics with a collision frequency of 2 ps^{-1} for temperature control and the Berendsen barostat with semi-isotropic pressure adaption. The trajectories were analyzed with CPPTRAJ (Roe and Cheatham, 2013). The per-residue effective binding energy was computed using the MM-PBSA method, as implemented in AMBER21 (Miller et al., 2012), in the presence of a heterogenous-dielectric implicit membrane model with spline fitting (Greene et al., 2019), an ionic strength of 0.15 M, and an internal dielectric constant of 4.

2.10. Binding mode of UNC0642

Based on the MD simulations with UNC0646 bound to nAChR, we clustered the binding of UNC0646 to obtain a representative binding mode using the *k-means* algorithm, as implemented in CPPTRAJ (Roe and Cheatham, 2013). Based on the biggest cluster (containing 37% of all frames), we replaced the substituents of the quinazoline ring of UNC0646 according to the substitution pattern of UNC0642 and subsequently minimized the ligand in the presence of the receptor with all receptor atoms constrained using MOE v.2022.02 (Chemical Computing Group, 2023).

2.11. Image generation

Images of nAChR were generated using PyMol v2.4.0 (Schrodinger,

2015).

2.12. Alignment of subunits

Sequences of subunits were retrieved from the UniProt database (accessed on the 30th of January, 2023) (The UniProt, 2023) and aligned using Jalview v2.11.2.6 (Waterhouse et al., 2009).

2.13. Rat diaphragm myography

All procedures using animals followed animal care regulations. Preparation of rat diaphragm hemispheres from male Wistar rats (300 ± 50 g) and experimental protocol of myography was performed as described before with slight modifications (Seeger et al., 2012; Seeger et al., 2007). The stimulation was shortened from 25 Hz to 20 Hz and the pulsewidth from 50 to 10 μs. In short, for all procedures (including wash-out steps, preparation of soman and test compound solutions) aerated Tyrode solution (125 mM NaCl, 24 mM $NaHCO_3$, 5.4 mM KCl, 1 mM $MgCl_2$, 1.8 mM $CaCl_2$, 10 mM glucose, 95% O_2, 5% CO_2; pH 7.4; 25 ± 0.5 °C) was used. After the recording of control muscle force one hour after preparation, the muscles were incubated in the Tyrode solution, containing 3 μM soman for 20 min. Following a 20 min wash-out period, the test compounds were added in ascending concentrations (0.1 μM to 100 μM). The incubation time was 20 min for each concentration. The electric field stimulation was performed with 10 μs pulse width and 2 A amplitudes. The tetanic stimulation of 20 Hz, 50 Hz, 100 Hz were applied for 1 s and in 10 min intervals. Muscle force was calculated as a time-force integral (area under the curve, AUC) and constrained to values obtained for maximal force generation (muscle force in the presence of Tyrode solution without any additives; 100%).

All results were expressed in means ± SD (n = 6 - 12). For all data analysis, Prism 5.0 (GraphPad Software, San Diego, CA, USA) was used.

3. Results and discussion

3.1. MS Binding Assays addressing the Torpedo-nAChR with quinazoline derivatives

3.1.1. LC-ESI-MS/MS method development

For performing the MS Binding Assays with one of the newly identified ligands of the MB327 binding site with a quinazoline scaffold, i.e., UNC0638, UNC0642, and UNC0646, first, a reliable LC-MS/MS method for quantification was needed. To this end, a triple quadrupole mass spectrometer in the multiple reaction monitoring (MRM) mode, in combination with a pneumatically assisted electrospray ionization source (ESI) and an HPLC system, should be used. This setup has repeatedly been demonstrated to achieve the selectivity and sensitivity required for marker quantification in MS Binding Assays and, thus, to be well suited for this purpose (Ackermann et al., 2021; Ackermann et al., 2019; Grimm et al., 2015; Hess et al., 2011; Neiens et al., 2018; Neiens et al., 2015). In the literature, for the three compounds UNC0638, UNC0642, and UNC0646, only MS studies reporting their parent ions but no mass fragmentations are known (Liu et al., 2011; Liu et al., 2013; Vedadi et al., 2011). Accordingly, first, the mass transitions of UNC0638, UNC0642, and UNC0646 were analyzed in direct infusion experiments. The most intense mass transitions found, all of which originated from the parent ion $[M+H]^+$, were (see Fig. S1 for product ion spectra): UNC0638 *m/z* 510.3/112.2, UNC0642 *m/z* 547.3/112.1, and UNC0646 *m/z* 622.5/126.1. Next, a suitable LC-ESI-MS/MS method for the quantification of these compounds had to be developed. To enable a reasonably high sample throughput of the MS Binding Assays, such a method should have a short run time while still separating the analyte from contents in the sample matrix interfering with the MS analysis, which, according to our experience, can commonly be reached when the retention factors of the analytes are > 1. In their recent work, Sichler et al. described LC-ESI-MS/MS quantification methods for MS Binding Assays that were all based on the same LC conditions, though the analytes, all polar ligands, varied (e.g., MB327 and phencyclidine) (Sichler et al., 2018). This method is based on a YMC-Triart Diol-HILIC column operated under classical HILIC conditions [mobile phase acetonitrile/ammonium formate buffer (20 mM, pH 3.0) = 80:20; flow rate 800 μL/min]. The quinazoline derivatives UNC0638, UNC0642, and UNC0646 are to be expected to be protonated and, consequently, to possess a high polarity under these chromatographic conditions. Hence, we reasoned that these conditions might also be suitable for their analysis. Indeed, the chromatograms for UNC0638 and UNC0642 obtained with these LC-parameters were satisfying, with the retention factor *k* amounting to 1.7 and 2.1 for UNC0642 and UNC0638, respectively, and the run time to < 3 min (for a chromatogram, see Fig. 2). Under the same chromatographic conditions, UNC0646, however, yielded a peak with a retention factor of > 10, which was far too high for the intended purpose and the peak shape was poor. This issue could be overcome by raising the amount of buffer in the mobile phase from 20% to 35%, whereas the flow rate had to be reduced from 800 to 600 μL/min to not exceed the limits for back pressure. This led to a retention factor $k = 1.2$ for UNC0646 (for a chromatogram, see Fig. S2), which was in the desired range. Finally, preliminary binding experiments should be performed to explore, which of the three compounds might be best suited as a reporter ligand for the planned MS Binding Assays.

3.1.2. Preliminary binding experiments and determination of final assay conditions

When developing a binding assay, irrespective of whether this is, e.g., a radioligand or MS Binding Assay, a decision regarding the technique has to be made that is used for the separation of the target protein with the bound reporter ligand from the rest of the incubation mixture containing the non-bound ligand. In general, filtration is preferred for separation, as it offers an efficient way of handling binding samples and a high sample throughput. Unfortunately, for a filtration-based binding assay, a ligand with a high binding affinity is required. According to the literature, the K_d value should be in the range of 10^{-7} to 10^{-8} M or lower (Hulme and Trevethick, 2010; McKinney and Raddatz, 2006), as otherwise the k_{off} rate (indirectly reflected by the K_d value) is too high and the loss of specifically bound reporter ligand during washing steps will exceed the 10% limit, which will affect the results to a non-tolerable extent. As an alternative to the separation process, centrifugation may be used for ligands with affinities that are too low for filtration. This approach suffers, however, from the fact that the separation step is laborious and the throughput rather low. From the pK_i values determined in the [$^2H_6$]MB327 MS Binding Assay for UNC0638 ($pK_i = 6.01 \pm 0.10$), UNC0642 ($pK_i = 5.97 \pm 0.05$), and UNC0646 ($pK_i = 6.23 \pm 0.02$), it is obvious that with these compounds as reporter ligands only centrifugation can be used for the separation step. As UNC0646 has the highest affinity for the MB327 binding site compared to UNC0638 and UNC0642, it was first chosen as a reporter ligand. When following the general assay procedure Sichler et al. had developed for the centrifugation-based MS Binding Assay with [$^2H_6$]MB327 as reporter ligand addressing *Torpedo*-nAChR, we were indeed able to observe specific binding for UNC0646 in preliminary binding experiments (Rappenglück et al., 2018b; Sichler et al., 2018). For the sake of completeness, also filtration was tested as a separation technique with UNC0646 as the reporter ligand. The experiments, however, led to results suggesting that most of the target-bound ligand had been lost during this assay based on the filtration approach. Hence, centrifugation should be used for the separation step for all further experiments. Much to our surprise, when attempting to finalize the conditions for the MS Binding Assay with UNC0646 as the reporter ligand, we encountered repeatedly difficulties regarding the reproducibility of the compound quantification. Hence, we decided to test UNC0642 as a reporter ligand in MS Binding Assays, although its binding affinity is lower than that of UNC0646. Again, for the MS Binding Assays with UNC0642 as a reporter ligand, we kept close to the conditions that Sichler et al. had established

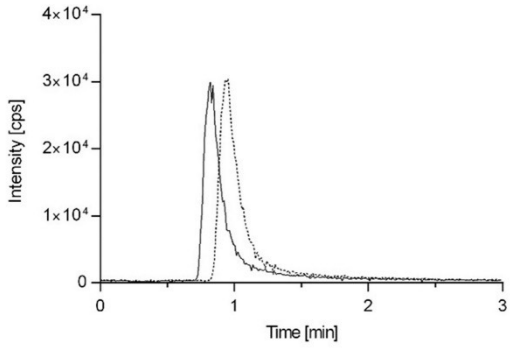

Fig. 2. LC-ESI-MS/MS-MRM chromatogram of a matrix standard containing the reporter ligand UNC0642 (solid line) at a concentration of 5 nM and the internal standard UNC0638 (dashed line) at 10 nM. For quantification, the mass transitions *m/z* 547.3/112.1 and *m/z* 510.3/112.2 for UNC0642 and UNC0638, respectively, were used. A YMC-Triart Diol-HILIC (50 mm × 2.0 mm, 3 μm) column was used as a stationary phase in combination with an 80:20 (*v/v*) mixture of acetonitrile and ammonium formate buffer (20 mM, pH 3.0) as mobile phase. The injection volume amounted to 10 μL and the flow rate to 800 μL/min.

for their centrifugation-based [$^2H_6$]MB327 MS Binding Assay addressing the *Torpedo*-nAChR (see Materials and methods for details). However, in the case of the new binding assay, non-specific binding was determined by the competitor approach, whereas Sichler et al. had applied the heat shock method, by which the target material is denatured to lose specific binding (Sichler et al., 2018). For the new Binding Assays, highly affine ligands of the MB327 binding site were available that appeared well suited for the determination of non-specific binding by the competitor approach with competitors not yet identified when Sichler et al. developed their [$^2H_6$]MB327 MS Binding Assay. Hence, we opted for this approach, as this is the most common one (Hulme and Trevethick, 2010; Motulsky and Neubig, 2002). As a competitor for the determination of non-specific binding, UNC0646 was selected as one of the two quinazoline derivatives with high affinities for the MB327 binding site, UNC0638 and UNC0646. This decision was made, as the reporter ligand should be quantified using an internal standard to improve the robustness of the quantification method. Hence, one of the two aforementioned quinazoline derivatives was needed to this end. As only UNC0638 exhibits a chromatographic behavior similar to that of the reporter ligand UNC0642 but not UNC0646 (see Section 3.1.1), which is essential for a compound to be used as an internal standard, UNC0638 could serve this function. Accordingly, for determining non-specific binding in the binding assay, quinazoline derivative UNC0646 had to be used.

3.1.3. LC-ESI-MS/MS method and method validation

With the conditions of the MS Binding Assays and, thus, also the matrix of the analytical samples being defined, the preconditions for the validation of the LC-ESI-MS/MS method for the quantification of the reporter ligand UNC0642 with UNC0638 as internal standard were given. As indicated above, the LC method was largely the same as the one developed by Sichler et al. (Sichler et al., 2018). In Fig. 2, a chromatogram of the ligand UNC0642 and the internal standard UNC0638 obtained applying these LC conditions is given with the most important parameters of the LC-ESI-MS/MS method being listed in the caption (for further details see Materials and methods). For the validation of the analytical method, the recommendations of the FDA guidance for bioanalytical method validation were followed regarding the criteria linearity, accuracy, precision, sensitivity, and selectivity (FDA, 2018). The results of the validation process are briefly discussed in the following. Detailed validation data of the corresponding three validation series can be found in the SI (see Fig. S3 and Table S1). For the validation experiments, matrix blank and matrix zero calibrator samples were prepared in analogy to the samples of the MS binding experiments. Matrix zero calibrator samples were used to create calibration standards and quality control samples (see Materials and methods for details). Calibration standards were prepared for eight different concentrations in the range from 50 pM (lower limit of quantification, LLOQ) to 75 nM and quality control samples for the four concentrations 50 pM (LLOQ), 500 pM, 5 nM, and 50 nM. In calibration standards and quality control samples, the internal standard UNC0638 was present at 10 nM. To evaluate the linearity of the quantification method in the investigated concentration range (50 pM to 75 nM), the calibration standards were analyzed via linear regression to obtain a calibration curve (see Materials and methods for details). The criteria of the FDA guideline for linearity demand calibration standard deviations from the nominal concentrations to be within a limit of ± 15% (± 20% at LLOQ). As we determined calibration standard deviations from the nominal concentrations in the range from 93% to 112%, the criteria of the FDA guideline for linearity were fulfilled. Deviations of the measured concentrations from nominal concentrations within ± 15% (± 20% at LLOQ) are required for accuracy by the FDA guidelines for quality control samples. For intra-run samples, accuracies from 91 - 103% and for inter-run samples accuracies from 94 - 101% were found, thus fulfilling the acceptance criteria of the FDA guideline for these criteria. The quality control samples were also examined regarding precision (expressed by the relative standard deviation), which amounted to 2.5 - 6.5% and 4.0 - 6.3% for intra-run and inter-run precisions, respectively, being in line with the acceptance criteria of ± 15% (± 20% at LLOQ) of the FDA guidelines. Also, the sensitivity of the LC-ESI-MS/MS method was guaranteed as the intensity of the peak corresponding to the LLOQ of 50 pM as compared to the noise signals was in line with the required signal-to-noise ratio of at least five. When a matrix blank sample was measured, no interference was found, demonstrating the selectivity of the established LC-ESI-MS/MS method. Overall, all studied validation criteria of the analytical method comply with the standards defined by the FDA guidelines.

3.1.4. UNC0642 MS Binding Assays

3.1.4.1. Saturation experiments. Next, with the validated quantification method for UNC0642 at hand, the binding of this compound to *Torpedo*-nAChR should be characterized in saturation experiments. For saturation experiments, the target is in general incubated with the reporter ligand in a concentration range from 0.1 K_d to 10 K_d for the determination of total binding. As the K_d of UNC0642 was expected to be in the very low micromolar range, we investigated fifteen different reporter ligand concentrations ranging from 200 nM to 100 μM for total binding. For the determination of non-specific binding, a further set of binding samples containing UNC0646 as competitor was prepared. Because of its low solubility, UNC0646 could only be used in an assay concentration of up to 100 μM. Since the affinity of UNC0646 ($pK_i = 6.23 \pm 0.02$) determined in [$^2H_6$]MB327 MS Binding Assays is similar to that of the reporter ligand UNC0642 ($pK_i = 5.97 \pm 0.05$), according to common rules, at least a hundredfold excess of the competitor UNC0646 over the reporter ligand UNC0642 had to be applied. Hence, because of the limited solubility of UNC0646, non-specific binding could only be measured for the five lowest reporter ligand concentrations (200 nM - 1 μM). Based on these data, a linear regression function, which was forced through zero, was established and finally used for the calculation of non-specific binding values for all reporter ligand concentrations employed in the assay (Davenport and Russell, 1996).

Specific binding as the difference between total and non-specific binding was finally analyzed by non-linear regression, generating saturation isotherms that revealed a binding affinity for UNC0642 of 6.7 ± 0.4 μM (K_d) and a maximum density of binding sites $B_{max} = 2980$

± 130 pmol/mg protein. The results of a representative saturation experiment are depicted in Fig. 3. The obtained K_d value of 6.7 ± 0.4 μM, corresponding to a pK_d of 5.17 ± 0.03, is in reasonable accordance with the pK_i value of 5.97 ± 0.05 previously determined by Sichler et al. (Sichler et al., 2024). The B_{max} value found in our experiments appears to be rather high, which may be explained by recent *in silico* experiments suggesting that there are multiple MB327 binding sites in the nAChR (Kaiser et al., 2023). Overall, the results of these saturation experiments indicate that UNC0642 binds to nAChR in a specific and saturable manner, which in combination with the data found by Sichler et al. in competition experiments with [$^2H_6$]MB327 as reporter ligand (Sichler et al., 2024), further supports the assumption that both address the same binding site, the MB327 binding pocket of *Torpedo*-nAChR.

3.1.4.2. Competition experiments. Finally, with the methodology for performing saturation experiments with UNC0642 as a reporter ligand at hand, competitive MS Binding Assays addressing the MB327 binding site of *Torpedo*-nAChR should be established. These should be used to characterize the binding affinities of a representative set of ligands of the MB327 binding pocket known from [$^2H_6$]MB327 MS Binding Assays. As the binding affinity of MB327 towards the MB327 binding site of *Torpedo*-nAChR is rather low, the results from MS Binding Assays based on [$^2H_6$]MB327 as a reporter ligand might deviate from the real value. Yet, these results should still be a reasonable basis for a comparison with the data obtained from the new MS Binding Assay with UNC0642 as a reporter ligand. The comparison might allow us to validate the results of the UNC0642 MS Binding Assay and, in addition, further support the assumption that UNC0642 and MB327 address the same binding pocket of *Torpedo*-nAChR. The set of competitors to be studied in the UNC0642 MS Binding Assays contains MB327, as the reporter ligand from the [$^2H_6$]MB327 MS Binding Assay and most prototypic representative of bispyridinium salts addressing nAChR, and PTM0022, as this compound shows the highest affinity so far found within the class of bispyridinium salts (Rappenglück et al., 2018b). Furthermore, the quinazoline derivative UNC0646 should be included in this set of test compounds, as it represents the compound with the highest affinity for the MB327 binding site so far known (Sichler et al., 2024). For control purposes, finally, also the effect of carbachol, which is a well-known ligand of the orthosteric binding site of nAChR, in the new competitive MS Binding Assays with UNC0642 as the reporter ligand should be studied. The competition experiments were performed in analogy to the saturation experiments with the following adaption. The concentration of the reporter ligand UNC0642 was kept constant at 1 μM. Binding samples were provided with increasing concentrations of the respective test compounds, usually covering a range of three orders of magnitude around the expected IC_{50}. After quantification of the reporter ligand via LC-ESI-MS/MS, the obtained data was normalized. For this, binding samples had been prepared, which contained no competitor (equivalent to 100% specific binding) or 100 μM UNC0646 as competitor (i.e., non-specific binding, 0% specific binding). Competition curves were created by non-linear regression yielding the respective IC_{50} values of the test compounds from which K_i values were calculated according to the Cheng-Prusoff equation (see Materials and methods for details). The competition curves that resulted when the above-mentioned test compounds were characterized in the new competitive MS Binding Assays with UNC0642 as reporter ligand – in three independent experiments in every case – are given in Figs. 4a and 4b.

Except for carbachol, for all other test compounds, the shape of the competition curves was well in line with theoretical models. The analysis of the curves revealed IC_{50} values from which pK_i values of 3.40 ± 0.04, 4.80 ± 0.03, and 5.83 ± 0.05 for MB327, PTM0022, and UNC0646, respectively, were calculated. Overall, pK_i values found in the new MS Binding Assay utilizing UNC0642 as reporter ligand were lower

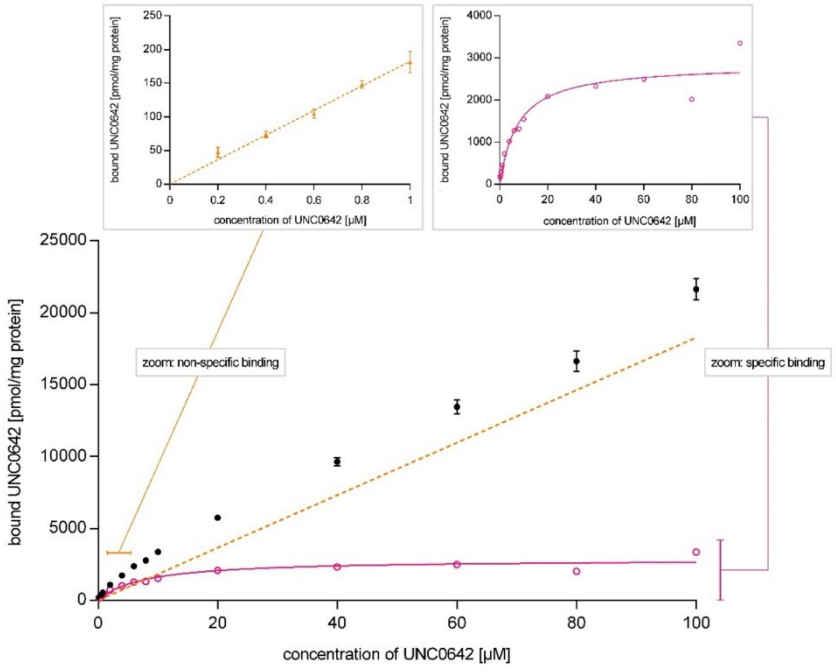

Fig. 3. Representative saturation experiment for UNC0642 binding to *Torpedo*-nAChR. Total binding (black circles) and non-specific binding (orange triangles). Linear regression of non-specific binding is shown as an orange dashed line. Total binding (black circles) was not further analyzed and only used to calculate specific binding. Accordingly, no black line is given in the figure. Specific binding (pink circles) was calculated as the difference between total binding and non-specific binding and analyzed by non-linear regression (solid pink line). Experimental values are means ± SD, n = 3.

than those determined in the [$^2H_6$]MB327 MS Binding Assay, but most importantly the rank order of affinities remained the same (MB327 < PTM0022 < UNC0646, see Table 2). Interestingly, also carbachol affected the binding of UNC0642. Up to a concentration of 1 μM carbachol, the UNC0642 binding remained largely unchanged, whereas it decreased for higher carbachol concentrations to reach a plateau of 75 - 80% at about 10 μM, which persists up to the highest concentration applied (1 mM). Notably, the change of UNC0642 binding occurs in the same range of carbachol concentration – 1 μM to 10 μM – that is known from functional studies to affect the transition of *Torpedo*-nAChR from its resting into its active state (Niessen et al., 2016). If the concentration of an orthosteric ligand present at the nAChR is far above the amount required for activation, the receptor switches into a desensitized state (Papke, 2014). This has to be taken into account for the analysis of the above-described data, as the transition of *Torpedo*-nAChR into the desensitized state likely occurs at a carbachol concentration covered in the experiments, i.e., ≥ 100 μM (Währa et al., 2023). Thus, the decrease of UNC0642 binding to the MB327 binding site upon increasing the carbachol concentration is likely the result of a conformational change due to the orthosteric ligand binding, which exerts an allosteric effect between the orthosteric and the MB327 binding site (Kaiser et al., 2023). However, for a better understanding of the interaction between the MB327 binding site and the orthosteric binding site, further studies are needed.

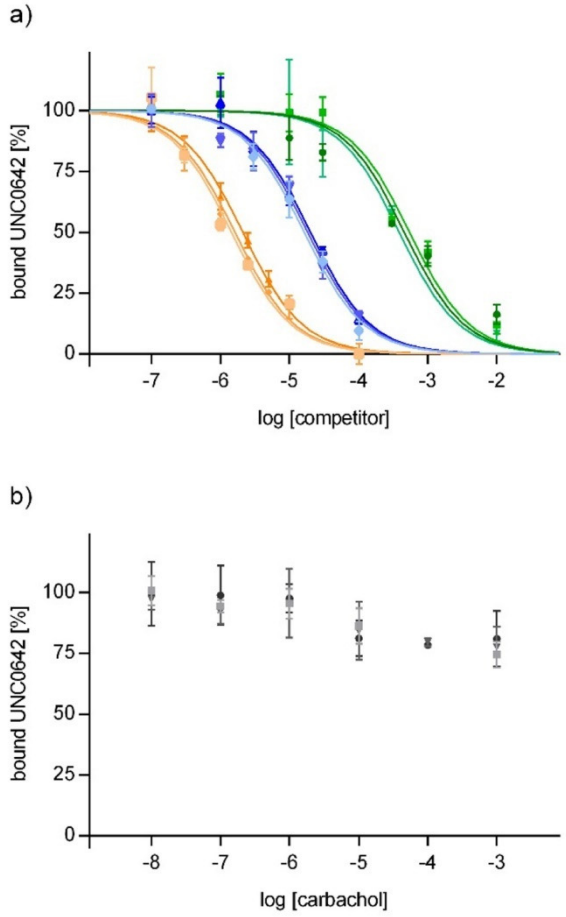

Fig. 4. a) Competition curves obtained for MB327 (green), PTM0022 (blue), and UNC0646 (orange). b) Influence of carbachol on UNC0642 binding. Data points (mean ± SD, $n = 3$) represent the specific binding of UNC0642.

Overall, according to the results of the UNC0642 MS Binding Assays, it is reasonable to conclude that UNC0642 alike MB327 addresses the MB327 binding site of the nAChR. In particular, the binding of UNC0642 can completely be inhibited by MB327, and both the MS Binding Assay based on UNC0642 and on [$^2H_6$]MB327 yield pK_i values that are in reasonable to good agreement and lead to the same rank order of potencies in competitive experiments for the set of ligands studied (see Table 2). Hence, the UNC0642 MS Binding Assays represent a valuable new tool for the characterization of the affinity of ligands of the MB327 binding site of the nAChR. With the binding affinity of UNC0642 being distinctly higher than that of [$^2H_6$]MB327, the reporter ligands of the UNC0642 and [$^2H_6$]MB327 MS Binding Assays, the former can be considered more robust with regard to its performance and results than the latter. In addition, the former MS Binding Assay has the advantage that its reporter ligand, UNC0642, is commercially available, which eases its setup.

3.2. *In silico investigation of the UNC0646 binding mode in MB327-PAM-1*

Recently, we proposed a novel binding site, MB327-PAM-1, in nAChR for binding of MB327 that can explain the allosteric modulation relevant for treating poisoning with OPC (Kaiser et al., 2023). MB327-PAM-1 is located in between two adjacent subunits at the transition of the extracellular to the transmembrane region and is different from two allosteric and one orthosteric binding pocket that had been proposed before for bispyridinium compounds using in silico methods (Epstein et al., 2021; Wein et al., 2018). To investigate the binding site of the ligand with the highest binding affinity in this study, UNC0646, first, we performed flexible docking experiments to place the ligand in MB327-PAM-1. To do so, we selected all residues within 9 Å of the centrally located E199α (respectively, Q209β, E210δ, E200γ in the other subunits) as a potential binding site. UNC0646 was placed similarly at the negative side of the two α subunits, whereas in the other three subunits, the ligand was either placed in the middle between two possible binding sites or more towards the pore, which would result in a high solvent exposure (SI Fig. S4). In between the γ- and α-subunit (binding site A), the best-scored conformation contains a twist conformation of the cyclohexane ring and a boat conformation of the piperidine ring of the side chain in the 4-position of the quinazoline ring (SI Fig. S5). As these ring conformations are energetically unfavorable, we chose the second best-scored conformation. The orientation of UNC0646 in the binding pocket is similar there but the rings have chair conformations. Overall, in both binding sites at the negative side of the α-subunits, the orientation of UNC0646 is comparable. However, while in between the β- and α-subunit (binding site B) the nitrogen of the piperidine ring in the 4-position of the quinazoline ring is interacting with E199α, the ligand is placed more deeply in the binding site A, which facilitates interaction between this nitrogen and E65γ (Fig. 5A, SI Fig. S6).

To further scrutinize interactions with surrounding amino acids, we performed 12 replicas of 500 ns long unbiased MD simulations starting from the docked conformations of UNC0646 in binding sites A and B

Table 2
pK_i values obtained from IC_{50} values determined in UNC0642 MS Binding Assays and [$^2H_6$]MB327 MS Binding Assays, respectively (Rappenglück et al., 2018b; Sichler et al., *Unpublished results*).

compound	UNC0642 MS Binding Assay pK_i	[$^2H_6$]MB327 MS Binding Assay
MB327	3.40 ± 0.04	4.73 ± 0.03
PTM0022	4.80 ± 0.03	5.16 ± 0.07
UNC0646	5.83 ± 0.05	6.23 ± 0.02

resulting in 6 μs (12 x 500 ns) of cumulative simulation time. During MD simulations, the receptor and membrane remained structurally virtually invariant (SI Fig. S7, S8). Throughout the MD simulations, UNC0646 showed smaller movements in binding site A (RMSD = 3.02 ± 0.30 Å) than binding site B (RMSD = 5.13 ± 0.58 Å, $p = 0.004$ according to a two-sided t-test). Furthermore, UNC0646 leaves the binding site B in six out of 12 replicas [distance to I65α < 5 Å in the last frame, as done previously (Kaiser et al., 2023)], whereas this does not occur in any of the 12 replicas in binding site A. Together, this suggests that the orientation of UNC0646 in binding site A is preferred.

Thus, we used this orientation to further predict important residues for interactions, in particular, salt bridge interactions of the three tertiary amines in the substituents of the quinazoline ring with the glutamates in the binding site; glutamates were ranked as the most important residues for ligand binding in per-residue decompositions of the effective binding energy computed with MMPBSA (SI Fig. S9). E65γ, previously described to be important for interactions with MB327 (Kaiser et al., 2023), shows the most conserved interactions with the piperidyl moiety in position 4 of the quinazoline ring (71.8 ± 7.4% of all frames, Fig. 5). Second, the positively charged nitrogen of the substituent in the 7-position interacts primarily with E69α (28.2 ± 10.5%). As this nitrogen is located in an area surrounded by four glutamates (E69α, E199α,

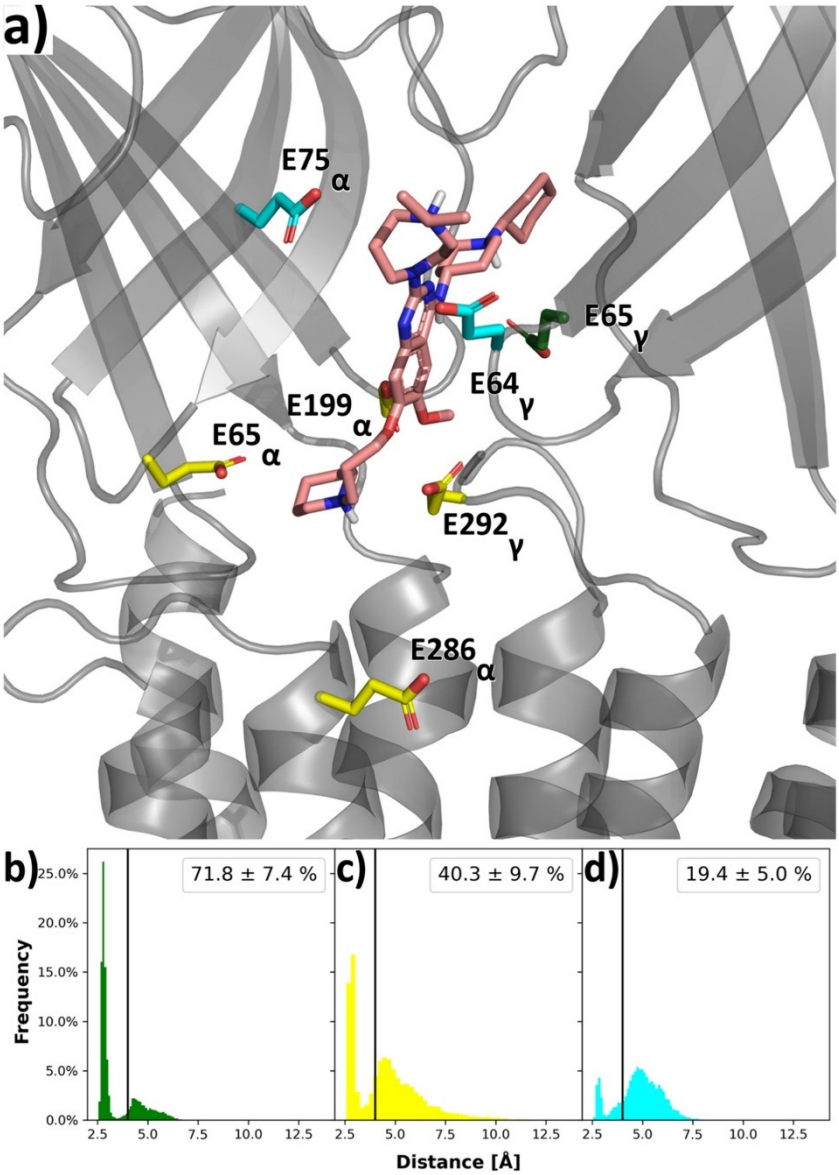

Fig. 5. UNC0646 and interacting residues in *Torpedo*-nAChR. a) Docked binding mode of UNC0646 as starting point for MD simulations. b) Minimal distance of the positively charged piperidyl nitrogen in the sidechain at position 4 to the carboxylate oxygens of E65γ. c) Minimal distance of the positively charged piperidyl nitrogen in the side chain at position 7 to the carboxylate oxygens of E65α, E199α, E286α, and E292γ. d) Minimal distance of the positively charged nitrogen in the diazepane ring to the carboxylate oxygens of E75α and E64γ. Amino acids in panel A are colored according to the plot colors in panels b) - d). The values in panels B-D indicate the mean ± SEM (taken over 12 replicas each) of the frequency of hydrogen bonds (distance of nitrogen to carboxylate oxygen < 4 Å).

Table 3
Sequence similarity of *Torpedo* and human adult muscle-type nAChR subunits. Amino acids shown in Fig. 5 are represented with green shadings. Amino acids at structurally homologous positions in other subunits are shown on a white background; amino acids with deviating physicochemical properties are shown in italics.

Human muscle-type nAChR				Torpedo nAChR			
α	β	δ	ε	α	β	δ	γ
E	E	E	E	E69	E	E	E
T	*S*	*T*	*T*	E75	*T*	*T*	*T*
E	*Q*	E	E	E199	*Q*	E	E
E	D	*K*	*Q*	E286	D	*Q*	*Q*
N	D	E	E	*N*	*I*	D	E64
Q	E	E	E	*Q*	E	E	E65
S	E	*A*	E	*S*	E	E	E292

E286α, and E292γ), additional salt bridge interactions can form. Considering all four glutamates, the nitrogen is interacting with carboxylate oxygens in 40.3 ± 9.7% of all frames. In contrast, the tertiary amine nitrogen in the diazepane ring at position 2 shows only minor interactions with the two surrounding glutamates (E75α, and E64γ; in 19.4 ± 5.0% of all frames). These results indicate that the side chain in the 4-position of the quinazoline ring is most important for forming salt bridge interactions whereas the diazepane ring is least important. These findings are in line with a structure-affinity relationship deduced from compounds UNC0646, UNC0642, and UNC0638, where removing the positive charge in the 2-position of the quinazoline ring has only minor effects on ligand affinity. Furthermore, the findings are supported by residue conservation analysis according to which E65γ, E69α, E199α, and E286α are highly conserved among different subunits of the *Torpedo* and human muscle-type nAChR such that acidic side chains at each position are available in at least three of the five subunits and hydrogen bond acceptors are available in all subunits but one (Table 3). By contrast, E292γ, E75α, and E64γ are less conserved (Table 3).

Based on a representative binding mode of UNC0646 during MD simulations in binding site A, we replaced the substituents of the quinazoline ring of UNC0646 to match those of UNC0642 using MOE and subsequently minimized the ligand in the binding site (SI Fig. S10). The substituents in 4- and 7-position of the quinazoline ring of UNC0642 interact similarly as those of UNC0646, whereas due to a lack of protonation sites interactions with the ring system in 2-position are missing.

3.3. Evaluation of the muscle force recovery of quinazoline-based compounds

To gain more knowledge on the intrinsic effects of UNC0638, UNC0642 and UNC0646 we performed myographic experiments with soman-poisoned and also un-poisoned rat diaphragms. The corresponding results of these experiments are summarized in Fig. 6. Interestingly, the compound with the highest known affinity to the MB327 binding site, UNC0646, was the only compound in this series of experiments that did not seem to have a beneficial effect on the restoration of muscle force after soman poisoning. UNC0638 and UNC0642 instead induced the regeneration of muscle force at a maximum of 30 μM and 10 μM, respectively. The highest extent of recovery was observed for a stimulation frequency of 20 Hz and amounted to 18.4 ± 16.1% for UNC0638 at 30 μM and 16.2 ± 12.8% for UNC0642 at 10 μM (mean ± SD, n = 5). The maximum amplitudes of UNC0638 and UNC0642 are thus lower than the maximum amplitude observed for MB327 [approximately 30% at 20 Hz (Niessen et al., 2018; Seeger et al., 2012)], but favorably the concentration needed to generate the described effect was distinctly lower for UNC0638 and UNC0642 than for MB327, which showed its maximum effect at a concentration of 300 μM. To obtain a recovery comparable to that exhibited by UNC0638 and UNC0642 at a concentration of 30 μM and 10 μM, respectively, MB327 had to be used at 100 μM (Niessen et al., 2018; Seeger et al., 2012). Noteworthy, the muscle force restoration effected by UNC0638 and UNC0642 declined at higher concentrations after the maximum had been reached at 30 μM and 10 μM, respectively. This phenomenon has been observed for MB327 and some MB327 analogs before (Niessen et al., 2018). It has been speculated, that counteracting effects, mediated by different binding sites may be responsible for the observed course of muscle force as a function of the compound concentration. In the present case, i.e. for UNC0638, UNC0642, and UNC0646, this theory is supported by results, that have been obtained in myographic experiments performed in analogy to those above except for using native, functionally active instead of soman-poisoned rat-diaphragms.

Here, the muscle force of the functionally active muscle decreased when UNC0638 and UNC0642 were applied at high concentrations (i.e. ≥ 10 μM). This effect was even more pronounced for UNC0646, as it started at distinctly lower concentrations and led to a nearly complete inhibition of the muscle force at 1 μM (see Fig. 6). Hence, the "bell-shape" of the curve of muscle-force recovery in soman-poisoned rat diaphragms upon treatment with UNC0638 and UNC0642 may be attributed to the above-described counteracting effect, which is, however, moderate, so that at lower concentration a positive effect still prevails. In contrast, in the case of UNC0646 no positive effect on muscle force recovery remains, as here the counteracting effect starts at distinctly lower concentrations and is more pronounced.

Finally, it should be mentioned, that the muscle force decreasing potential of the studied compounds appears to be reversible, as the muscle force partly recovers when the respective samples are subjected to a washing step (see Fig. 6).

Overall, the quinazoline derivatives UNC0638, UNC0642 and UNC0646 identified as binders of the MB327-PAM-1 binding site of the nAChR are in principle also able to restore muscle function of soman-poisoned muscle tissue. Though the maximum amplitudes for muscle force recovery of UNC0638 and UNC0642 are lower than those found for MB327, the maximum values are, remarkably, reached for the two quinazoline derivatives at distinctly lower concentrations than for MB327, which is likely to result from their higher binding affinities. Future studies will have to aim on a better understanding of the factors responsible for the counteracting effects regarding the recovery of muscle force in soman-poisoned rat diaphragms that might finally lead to more potent compounds.

4. Conclusion

The quinazoline-based compounds UNC0638, UNC0642, and UNC0646 had been identified as hits in a recent library screening campaign using competitive [$^2H_6$]MB327 MS Binding Assays in the search for new ligands addressing the MB327-PAM-1 binding site of the nAChR. In the present study, these compounds, which exhibit the

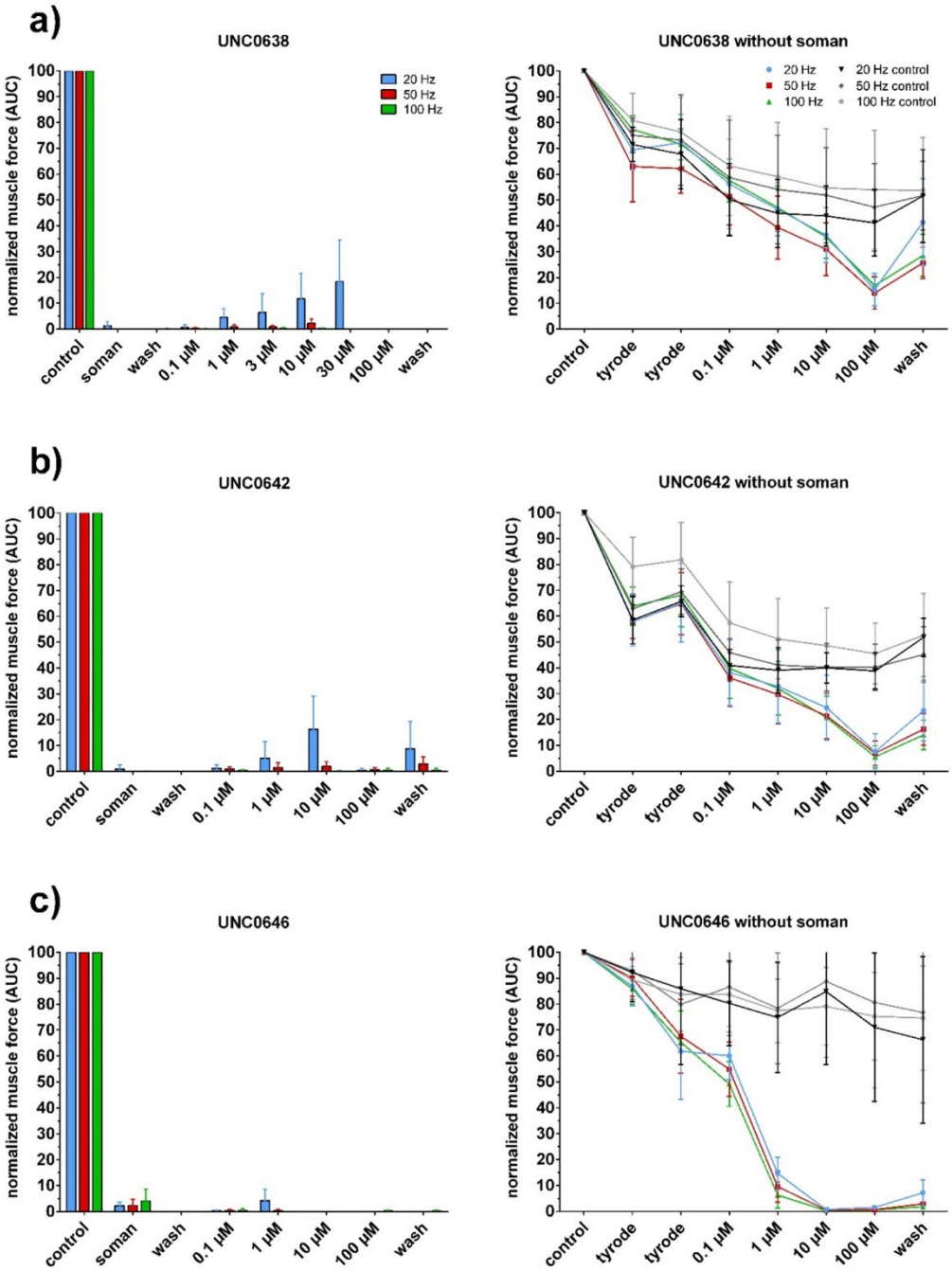

Fig. 6. Muscle force of soman-poisoned (left) and un-poisoned (right) rat diaphragms after treatment with a) UNC0638, b) UNC0642, and c) UNC0646. Left: Muscle force of diaphragm muscle was blocked by 3 µM soman. Right: Muscle force generation of un-poisoned muscle. Muscle force generation was measured as the area under the curve normalized to muscle force under control conditions at the start of the measurement (n = 6 - 12).

highest affinities known so far for the MB327-PAM-1 binding site, have been used for the development of new MS Binding Assays for the aforementioned binding site of the nAChR with UNC0642 serving as reporter ligand, UNC0638 as internal standard and UNC0646 as competitor for the determination of non-specific binding. The new UNC0642 MS Binding Assays comprised the characterization of the binding of UNC0642 to the MB327-PAM-1 binding site of *Torpedo*-nAChR in saturation experiments and the determination of the binding affinity of a set of ligands of the aforementioned binding site in competition experiments. The results were in good accord with those obtained from the [$^2H_6$]MB327 MS Binding Assays, that had been used so far for the determination of binding affinities for the MB327 binding

site. Carbachol used as a control had only a very small effect on reporter ligand binding in respective competition experiments. As this compound, carbachol, represents a ligand of the orthosteric binding site of the nAChR the observed effect on reporter ligand binding is likely to be attributed to an allosteric interaction between both binding sites. Based on the results obtained with the new UNC0642 MS Binding Assay it is reasonable to conclude, that this binding assay addresses the same binding site as the [$^2H_6$]MB327 MS Binding Assay, i.e. the MB327-PAM-1 binding site of the nAChR. Hence, the UNC0642 MS Binding Assays represent a valuable alternative to the [$^2H_6$]MB327 MS Binding Assays and profit from the high affinity of the reporter ligand, which will contribute to the robustness of the Binding Assays, and from the commercial availability of said compound.

By using docking approaches and molecular dynamics simulations, the binding mode and key interactions of UNC0646 in the recently proposed allosteric binding site of the nAChR, the MB327-PAM-1 binding site, could be successfully unveiled.

Ex vivo studies revealed a beneficial effect of UNC0638 and UNC0642 on muscle force recovery of soman-poisoned rat diaphragms. In experiments with un-poisoned muscle tissues, a muscle force-reducing effect was uncovered for all three test compounds, which in the case of UNC0646 is likely to be so strong that it overcompensates the positive effect, that might originate from this compound on soman-poisoned muscle tissue, as well. This may explain the observed lack of such an effect for this compound. Though the maximum effect in muscle force recovery mediated by UNC0638 and UNC0642 was lower than that observed for MB327 and some analogs, this effect was reached at distinctly lower concentrations for UNC0638 and UNC0642 than that needed in the case of MB327. This might reflect the distinctly higher binding affinities of UNC0638 and UNC0642 for the MB327-PAM-1 binding site as compared to MB327 and analogs.

Overall, UNC0638, UNC0642, and UNC0646 have been found to address the MB327-PAM-1 binding site of the nAChR with high affinity, which renders quinazoline derivatives a promising class of compounds for further studies aiming at the development of drugs for the treatment of the nAChR-mediated pathological effects of organophosphorus poisoning.

CRediT authorship contribution statement

Worek Franz: Writing – review & editing. **Gohlke Holger:** Writing – review & editing, Supervision, Software, Conceptualization. **Steinritz Dirk:** Writing – review & editing. **Kaiser Jesko:** Writing – original draft, Methodology, Investigation. **Gertzen Christoph G.W.:** Writing – review & editing, Supervision. **Seeger Thomas:** Writing – original draft, Methodology, Investigation. **Niessen Karin V.:** Writing – review & editing, Investigation. **Paintner Franz F.:** Writing – review & editing, Supervision, Funding acquisition, Conceptualization. **Wanner Klaus T.:** Writing – review & editing, Supervision, Funding acquisition, Data curation, Conceptualization. **Nitsche Valentin:** Writing – original draft, Methodology, Investigation. **Höfner Georg:** Writing – review & editing, Methodology.

Declaration of Competing Interest

Authors declare that they have no known competing financial interests or personal relationships that could have appeared to influence the work reported in this paper.

Data Availability

Data will be made available on request.

Acknowledgments

This work was supported by the German Ministry of Defence (E/U2AD/KA019/IF558). We are grateful for computational support and infrastructure provided by the "Zentrum für Informations- und Medientechnologie" (ZIM) at the Heinrich Heine University Düsseldorf and the computing time provided by the John von Neumann Institute for Computing (NIC) to HG on the supercomputer JUWELS at Jülich Supercomputing Center (JSC) (user IDs: HKF7, VSK33, nAChR).

Appendix A. Supporting information

Supplementary data associated with this article can be found in the online version at doi:10.1016/j.toxlet.2024.01.003.

References

Ackermann, T.M., Bhokare, K., Höfner, G., Wanner, K.T., 2019. MS Binding Assays for GlyT1 based on Org24598 as nonlabelled reporter ligand. Neuropharmacology 161, 107561.

Ackermann, T.M., Allmendinger, L., Höfner, G., Wanner, K.T., 2021. MS Binding Assays for glycine transporter 2 (GlyT2) employing Org25543 as reporter ligand. ChemMedChem 16, 199–215.

Bayly, C.I., Cieplak, P., Cornell, W., Kollman, P.A., 1993. A well-behaved electrostatic potential based method using charge restraints for deriving atomic charges: the RESP model. J. Phys. Chem. 97, 10269–10280.

Buckley, N.A., Roberts, D., Eddleston, M., 2004. Overcoming apathy in research on organophosphate poisoning. BMJ 329, 1231–1233.

Case, D.A., Cheatham 3rd, T.E., Darden, T., Gohlke, H., Luo, R., Merz Jr., K.M., Onufriev, A., Simmerling, C., Wang, B., Woods, R.J., 2005. The Amber biomolecular simulation programs. J. Comput. Chem. 26, 1668–1688.

Case, D.A., H.M, A., Belfon, K., Ben-Shalom, I.Y., Berryman, J.T., Brozell, S.R., Cerutti, D. S., Cheatham 3rd, T.E., Cisneros, G.A., Cruzeiro, V.W.D., Darden, T.A., Duke, R.E., Giambasu, G., Gilson, M.K., Gohlke, H., Goetz, A.W., Harris, R., Izadi, S., Izmailov, S. A., Kasavajhala, K., Kaymak, M.C., King, E., Kovalenko, A., Kurtzmann, T., Lee, T.S., Le Grand, S., Li, P., Lin, C., Liu, J., Luchko, T., Luo, R., Machado, M., Man, V., Manathunga, M., Merz, K.M., Miao, Y., Mikhailovskii, O., Monard, G., Nguyen, H., O'Hearn, K.A., Onufriev, A., Pan, F., Pantano, S., Qi, R., Rahnamoun, A., Roe, D.R., Roitberg, A., Sagui, E., Schott-Verdugo, S., Shajan, A., Shen, J., Simmerling, C.L., Skrynnikov, N.R., Smith, J., Swails, J., Walker, R.C., Wang, J., Wang, J., Wei, H., Wolf, R.M., Wu, X., Xiong, Y., Xue, Y., York, D.M., Zhao, S., Kollmann, P.A., 2022. Amber 2022. vol. Amber 2022. University of California, San Francisco.

Case, D.A., Aktulga, H.M., Belfon, K., Cerutti, D.S., Cisneros, G.A., Cruzeiro, V.W.D., Forouzesh, N., Giese, T.J., Gotz, A.W., Gohlke, H., Izadi, S., Kasavajhala, K., Kaymak, M.C., King, E., Kurtzman, T., Lee, T.S., Li, P., Liu, J., Luchko, T., Luo, R., Manathunga, M., Machado, M.R., Nguyen, H.M., O'Hearn, K.A., Onufriev, A.V., Pan, F., Pantano, S., Qi, R., Rahnamoun, A., Risheh, A., Schott-Verdugo, S., Shajan, A., Swails, J., Wang, J., Wei, H., Wu, X., Wu, Y., Zhang, S., Zhao, S., Zhu, Q., Cheatham 3rd, T.E., Roe, D.R., Roitberg, A., Simmerling, C., York, D.M., Nagan, M. C., Merz Jr., K.M., 2023. AmberTools. J. Chem. Inf. Model 63, 6183–6191.

Chemical Computing Group, U., 2020. Molecular Operating Environment (MOE). vol. 2020.09, 1010 Sehrbooke St. West, Suite #910, Montreal, QC, Canada, H3A, 2R7.

Chemical Computing Group, U., 2023. Molecular Operating Environment (MOE). vol. 2022.02, 1010 Sehrbooke St. West, Suite #910, Montreal, QC, Canada, H3A, 2R7.

Costanzi, S., Machado, J.H., Mitchell, M., 2018. Nerve agents: what they are, how they work, how to counter them. ACS Chem. Neurosci. 9, 873–885.

Davenport, A.P., Russell, F.D., 1996. Radioligand Binding Assays: theory and practice. In: Mather, S.J. (Ed.), Current Directions in Radiopharmaceutical Research and Development. Springer Netherlands, Dordrecht, pp. 169–179.

Dickson, C.J., Walker, R.C., Gould, I.R., 2022. Lipid21: complex lipid membrane simulations with AMBER. J. Chem. Theory Comput. 18, 1726–1736.

Eddleston, M., Phillips, M.R., 2004. Self poisoning with pesticides. BMJ 328, 42–44.

Epstein, M., Bali, K., Piggot, T.J., Green, A.C., Timperley, C.M., Bird, M., Tattersall, J.E. H., Bermudez, I., Biggin, P.C., 2021. Molecular determinants of binding of non-oxime bispyridinium nerve agent antidote compounds to the adult muscle nAChR. Toxicol. Lett. 340, 114–122.

FDA, 2018. FDA (United States Food and Drug Administration), 2018. Guidance for industry: Bioanalytical method validation, ⟨https://www.fda.gov/files/drugs/published/Bioanalytical-Method-Validation-Guidance-for-Industry.pdf⟩ from 04.04.2022.

Frisch, M.J., G.W.T, Schlegel, H.B., Scuseria, G.E., Robb, M.A., J.R.C, Scalmani, G., Barone, V., Petersson, G.A., H.N, Li, X., Caricato, M., Marenich, A.V., Bloino, J., B.G J, Gomperts, R., Mennucci, B., Hratchian, H.P., Ortiz, J.V., A.F.I, Sonnenberg, J.L., Williams-Young, D., Ding, F., F.L, Egidi, F., Goings, J., Peng, B., Petrone, A., Henderson, T., D.R, Zakrzewski, V.G., Gao, J., Rega, N., Zheng, G., W.I, Hada, M., Ehara, M., Toyota, K., Fukuda, R., Hasegawa, J., M.I, Nakajima, T., Honda, Y., Kitao, O., Nakai, H., Vreven, T., K.T, Montgomery Jr., J.A., Peralta, J.E., Ogliaro, F., M.J.B, Heyd, J.J., Brothers, E.N., Kudin, K.N., Staroverov, V.N., T.A.K, Kobayashi, R., Normand, J., Raghavachari, K., A.P.R, Burant, J.C., Iyengar, S.S., Tomasi, J., M.C, Millam, J.M., Klene, M., Adamo, C., Cammi, R., Ochterski, J.W., R.L.M, Morokuma, K., Farkas, O., Foresman, J.B., a.D.J.F, 2016. Gaussian16. vol. Revision A.03. Gaussian Inc., Wallingford CT.

Greene, D.A., Qi, R., Nguyen, R., Qiu, T., Luo, R., 2019. Heterogeneous dielectric implicit membrane model for the calculation of MMPBSA binding free energies. J. Chem. Inf. Model. 59, 3041–3056.

Grimm, S.H., Höfner, G., Wanner, K.T., 2015. MS Binding Assays for the three monoamine transporters using the triple reuptake inhibitor (1R,3S)-indatraline as native marker. ChemMedChem 10, 1027–1039.
Hess, M., Höfner, G., Wanner, K.T., 2011. (S)- and (R)-fluoxetine as native markers in mass spectrometry (MS) Binding Assays addressing the serotonin transporter. ChemMedChem 6, 1900–1908.
Höfner, G., Wanner, K.T., 2015. MS Binding Assays. Anal. Biomol. Interact. Mass Spectrom. 165–198.
Holmstedt, B., 1959. Pharmacology of organophosphorus cholinesterase inhibitors. Pharmacol. Rev. 11, 567.
Hulme, E.C., Trevethick, M.A., 2010. Ligand Binding Assays at equilibrium: validation and interpretation. Br. J. Pharm. 161, 1219–1237.
John, H., van der Schans, M.J., Koller, M., Spruit, H.E.T., Worek, F., Thiermann, H., Noort, D., 2018. Fatal sarin poisoning in Syria 2013: forensic verification within an international laboratory network. Forensic Toxicol. 36, 61–71.
Kaiser, J., Gertzen, C.G.W., Bernauer, T., Höfner, G., Niessen, K.V., Seeger, T., Paintner, F.F., Wanner, K.T., Worek, F., Thiermann, H., Gohlke, H., 2023. A novel binding site in the nicotinic acetylcholine receptor for MB327 can explain its allosteric modulation relevant for organophosphorus-poisoning treatment. Toxicol. Lett. 373, 160–171.
Kassa, J., Timperley, C.M., Bird, M., Green, A.C., Tattersall, J.E.H., 2022. Influence of experimental end point on the therapeutic efficacy of essential and additional antidotes in organophosphorus nerve agent-intoxicated mice. Toxics 10.
Liu, F., Barsyte-Lovejoy, D., Allali-Hassani, A., He, Y., Herold, J.M., Chen, X., Yates, C.M., Frye, S.V., Brown, P.J., Huang, J., Vedadi, M., Arrowsmith, C.H., Jin, J., 2011. Optimization of cellular activity of G9a inhibitors 7-aminoalkoxy-quinazolines. J. Med Chem. 54, 6139–6150.
Liu, F., Barsyte-Lovejoy, D., Li, F., Xiong, Y., Korboukh, V., Huang, X.P., Allali-Hassani, A., Janzen, W.P., Roth, B.L., Frye, S.V., Arrowsmith, C.H., Brown, P.J., Vedadi, M., Jin, J., 2013. Discovery of an in vivo chemical probe of the lysine methyltransferases G9a and GLP. J. Med Chem. 56, 8931–8942.
, 2006McKinney,M., Raddatz, R., 2006. Practical aspects of radioligand binding. Curr ProtocPharmacol Chapter 1, Unit1 3.
Miller 3rd, B.R., McGee Jr., T.D., Swails, J.M., Homeyer, N., Gohlke, H., Roitberg, A.E., 2012. MMPBSA.py: an efficient program for end-state free energy calculations. J. Chem. Theory Comput. 8, 3314–3321.
Motulsky, H., Neubig, R., 2002. Analyzing radioligand binding data. Curr Protoc Neurosci Chapter 7, Unit 7 5.
Neiens, P., Höfner, G., Wanner, K.T., 2015. MS Binding Assays for D1 and D5 dopamine receptors. ChemMedChem 10, 1924–1931.
Neiens, P., De Simone, A., Höfner, G., Wanner, K.T., 2018. Simultaneous multiple ms Binding Assays for the dopamine, norepinephrine, and serotonin transporters. ChemMedChem 13, 453–463.
Newmark, J., 2004. Therapy for nerve agent poisoning. Arch. Neurol. 61, 649–652.
Niessen, K.V., Muschik, S., Langguth, F., Rappenglück, S., Seeger, T., Thiermann, H., Worek, F., 2016. Functional analysis of Torpedo californica nicotinic acetylcholine receptors in multiple activation states by SSM-based electrophysiology. Toxicol. Lett. 247, 1–10.
Niessen, K.V., Seeger, T., Rappenglück, S., Wein, T., Höfner, G., Wanner, K.T., Thiermann, H., Worek, F., 2018. In vitro pharmacological characterization of the bispyridinium non-oxime compound MB327 and its 2- and 3-regioisomers. Toxicol. Lett. 293, 190–197.
Papke, R.L., 2014. Merging old and new perspectives on nicotinic acetylcholine receptors. Biochem Pharm. 89, 1–11.
Rahman, M.M., Teng, J., Worrell, B.T., Noviello, C.M., Lee, M., Karlin, A., Stowell, M.H. B., Hibbs, R.E., 2020. Structure of the native muscle-type nicotinic receptor and inhibition by snake venom toxins. Neuron 106, 952–962 e955.
Rappenglück, S., Sichler, S., Höfner, G., Wein, T., Niessen, K.V., Seeger, T., Paintner, F.F., Worek, F., Thiermann, H., Wanner, K.T., 2018a. Synthesis of a series of non-symmetric bispyridinium and related compounds and their affinity characterization at the nicotinic acetylcholine receptor. ChemMedChem 13, 2653–2663.
Rappenglück, S., Sichler, S., Höfner, G., Wein, T., Niessen, K.V., Seeger, T., Paintner, F.F., Worek, F., Thiermann, H., Wanner, K.T., 2018b. Synthesis of a series of structurally diverse MB327 derivatives and their affinity characterization at the nicotinic acetylcholine receptor. ChemMedChem 13, 1806–1816.
Roe, D.R., Cheatham 3rd, T.E., 2013. PTRAJ and CPPTRAJ: software for processing and analysis of molecular dynamics trajectory data. J. Chem. Theory Comput. 9, 3084–3095.
Schott-Verdugo, S., Gohlke, H., 2019. PACKMOL-memgen: a simple-to-use, generalized workflow for membrane-protein-lipid-bilayer system building. J. Chem. Inf. Model 59, 2522–2528.
Schrödinger, 2021. Maestro. vol. 2022–3. Schrödinger, LLC, New York, NY.
Schrodinger, L.L.C., 2015. The PyMOL Molecular Graphics System, Version 1.8.
Seeger, T., Worek, F., Szinicz, L., Thiermann, H., 2007. Reevaluation of indirect field stimulation technique to demonstrate oxime effectiveness in OP-poisoning in muscles in vitro. Toxicology 233, 209–213.
Seeger, T., Eichhorn, M., Lindner, M., Niessen, K.V., Tattersall, J.E., Timperley, C.M., Bird, M., Green, A.C., Thiermann, H., Worek, F., 2012. Restoration of soman-blocked neuromuscular transmission in human and rat muscle by the bispyridinium non-oxime MB327 in vitro. Toxicology 294, 80–84.
Sheridan, R.D., 2005. Nicotinic antagonists in the treatment of nerve agent intoxication. J. R. Soc. Med. 98, 114–115.
Shih, T.M., Rowland, T.C., McDonough, J.H., 2007. Anticonvulsants for nerve agent-induced seizures: The influence of the therapeutic dose of atropine. J. Pharm. Exp. Ther. 320, 154–161.
Sichler, S., Höfner, G., Rappenglück, S., Wein, T., Niessen, K.V., Seeger, T., Worek, F., Thiermann, H., Paintner, F.F., Wanner, K.T., 2018. Development of MS Binding Assays targeting the binding site of MB327 at the nicotinic acetylcholine receptor. Toxicol. Lett. 293, 172–183.
Sichler, S., Höfner, G., Nitsche, V., Niessen, K.V., Seeger, T., Worek, F., Paintner, F.F., Wanner, K.T., 2024. Screening for New nAChR-Ligands at the MB327-Binding Site by Means of MS Binding Assays. Toxicol. Lett., submitted.
The UniProt, C., 2023. UniProt: the Universal Protein Knowledgebase in 2023. Nucleic Acids Res. 51, D523–D531.
Thiermann, H., Worek, F., 2022. Pro: Oximes should be used routinely in organophosphate poisoning. Br. J. Clin. Pharm. 88, 5064–5069.
Thiermann, H., Aurbek, N., Worek, F., 2016. CHAPTER 1 Treatment of Nerve Agent Poisoning. Chemical Warfare Toxicology: Volume 2: Management of Poisoning, vol. 2. The Royal Society of Chemistry, pp. 1–42.
Tian, C., Kasavajhala, K., Belfon, K.A.A., Raguette, L., Huang, H., Migues, A.N., Bickel, J., Wang, Y., Pincay, J., Wu, Q., Simmerling, C., 2020. ff19SB: amino-acid-specific protein backbone parameters trained against quantum mechanics energy surfaces in solution. J. Chem. Theory Comput. 16, 528–552.
Timperley, C.M., Bird, M., Green, C., Price, M.E., Chad, J.E., Turner, S.R., Tattersall, J.E. H., 2012. 1,1′-(Propane-1,3-diyl)bis(4-tert-butylpyridinium) di(methanesulfonate) protects guinea pigs from soman poisoning when used as part of a combined therapy. Med Chem. Commun. 3, 352–356.
Turner, S.R., Chad, J.E., Price, M., Timperley, C.M., Bird, M., Green, A.C., Tattersall, J.E., 2011. Protection against nerve agent poisoning by a noncompetitive nicotinic antagonist. Toxicol. Lett. 206, 105–111.
Vedadi, M., Barsyte-Lovejoy, D., Liu, F., Rival-Gervier, S., Allali-Hassani, A., Labrie, V., Wigle, T.J., Dimaggio, P.A., Wasney, G.A., Siarheyeva, A., Dong, A., Tempel, W., Wang, S.C., Chen, X., Chau, I., Mangano, T.J., Huang, X.P., Simpson, C.D., Pattenden, S.G., Norris, J.L., Kireev, D.B., Tripathy, A., Edwards, A., Roth, B.L., Janzen, W.P., Garcia, B.A., Petronis, A., Ellis, J., Brown, P.J., Frye, S.V., Arrowsmith, C.H., Jin, J., 2011. A chemical probe selectively inhibits G9a and GLP methyltransferase activity in cells. Nat. Chem. Biol. 7, 566–574.
Währa, M., Allmendinger, L., Höfner, G., Wanner, K.T., 2023. Benocyclidine (BTCP) as non-labelled reporter ligand for ms Binding Assays for the PCP Ion channel binding site of the desensitized torpedo nicotinic acetylcholine receptor (nAChR). ChemMedChem, e202300048.
Wang, J., Wolf, R.M., Caldwell, J.W., Kollman, P.A., Case, D.A., 2004. Development and testing of a general amber force field. J. Comput. Chem. 25, 1157–1174.
Wang, J., Wang, W., Kollman, P.A., Case, D.A., 2006. Automatic atom type and bond type perception in molecular mechanical calculations. J. Mol. Graph. Model. 25, 247–260.
Wanner, K.T., Höfner, G., Mannhold, R., Kubinyi, H., Folkers, G., 2007. Mass Spectrometry in Medicinal Chemistry: Applications in Drug Discovery. Wiley.
Waterhouse, A.M., Procter, J.B., Martin, D.M.A., Clamp, M., Barton, G.J., 2009. Jalview Version 2—a multiple sequence alignment editor and analysis workbench. Bioinformatics 25, 1189–1191.
Wein, T., Hofner, G., Rappengluck, S., Sichler, S., Niessen, K.V., Seeger, T., Worek, F., Thiermann, H., Wanner, K.T., 2018. Searching for putative binding sites of the bispyridinium compound MB327 in the nicotinic acetylcholine receptor. Toxicol. Lett. 293, 184–189.
Worek, F., Szinicz, L., Eyer, P., Thiermann, H., 2005. Evaluation of oxime efficacy in nerve agent poisoning: development of a kinetic-based dynamic model. Toxicol. Appl. Pharm. 209, 193–202.

Supporting Information

Figure S1. Product ion spectra of UNC0638 (a), UNC0642 (b), and UNC0646 (c).

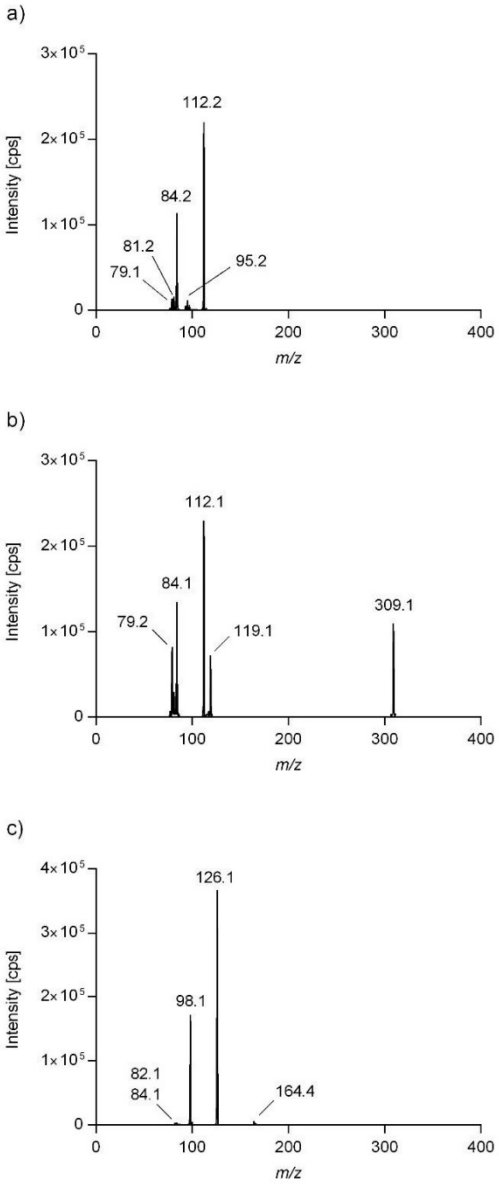

Figure S2. Representative LC-ESI-MS/MS-MRM chromatogram of UNC0646 (*m*/*z* 622.5/126.1, 10 nM in acetonitrile) recorded at an API3200, using the following chromatographic parameters. Stationary phase: YMC-Triart Diol-HILIC (50 mm x 2.0 mm, 3 µm). Mobile Phase: 65:35 (*v*/*v*) acetonitrile and ammonium formate buffer (20 mM, pH 3.0), 20 °C. Flow rate: 600 µL/min. Injection volume: 10 µL.

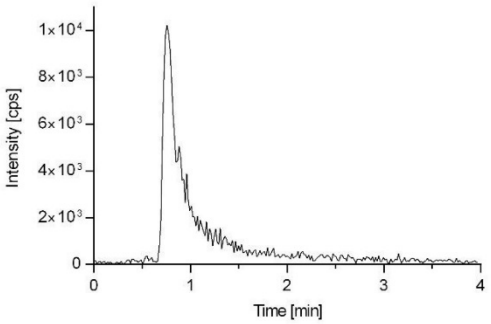

Table S1. Validation results of the LC-ESI-MS/MS method for the quantification of UNC0642

Sample (n)	Intra-Series									Inter-Series		
	Series 1			Series 2			Series 3					
	M	A	P	M	A	P	M	A	P	M	A	P
50 pM Cal (3)	0.0502	100	11.4	0.0514	103	11.1	0.0507	101	9.51	0.0508	102	9.31
150 pM Cal (3)	0.148	98.7	0.676	0.141	93.8	7.67	0.144	96.0	5.24	0.144	96.1	5.08
400 pM Cal (3)	0.399	99.7	4.40	0.375	93.8	3.53	0.386	96.4	4.31	0.386	96.6	4.45
1.2 nM Cal (3)	1.22	102	2.96	1.23	102	0.471	1.28	106	0.452	1.24	103	2.62
3.5 nM Cal (3)	3.41	97.3	4.78	3.54	101	5.67	3.33	95.2	1.25	3.43	97.9	4.65
10 nM Cal (3)	11.1	111	2.38	10.9	109	1.92	11.2	112	3.73	11.0	110	2.72
30 nM Cal (3)	27.9	92.9	2.10	28.5	95.1	1.42	27.8	92.6	1.62	28.1	93.5	1.98
75 nM Cal (3)	73.6	98.1	1.13	77.1	103	1.40	74.7	100	2.70	75.1	100	2.63
Equation of the calibration curve [a]	y = 1.57 * x + 0.00292 (r = 0.9973)			y = 1.74 * x + 0.00217 (r = 0.9971)			y = 1.86 * x + 0.00182 (r = 0.9914)			-		
50 pM QC (6)	0.0471	94.2	5.45	0.0467	93.5	6.51	0.0502	100	5.15	0.0480	96.0	6.31
500 pM QC (6)	0.484	96.8	3.84	0.467	93.5	5.80	0.460	91.1	4.89	0.470	94.1	5.09
5 nM QC (6)	4.93	98.6	2.60	5.16	103	5.28	5.03	101	2.46	5.04	101	4.01
50 nM QC (6)	47.5	95.0	2.69	49.1	98.0	5.68	46.0	92.1	2.66	47.6	95.1	4.66

M = mean concentration [nM], **A** = accuracy [%], **P** = precision [%], [a] weighting factor: $1/x^2$

Figure S3. Representative LC-ESI-MS/MS-MRM chromatograms of UNC0642 (*m*/*z* 547.3/112.1) recorded as part of the validation process of the applied LC-ESI-MS/MS quantification method. Chromatographic conditions: stationary phase, YMC-Triart Diol-HILIC (50 mm x 2.0 mm, 3 µm); mobile phase, 80:20 (*v*/*v*) acetonitrile and ammonium formate buffer (20 mM, pH 3.0), 20 °C; flow rate: 800 µL/min; injection volume: 10 µL. (a) LLOQ of 50 pM, (b) Matrix blank.

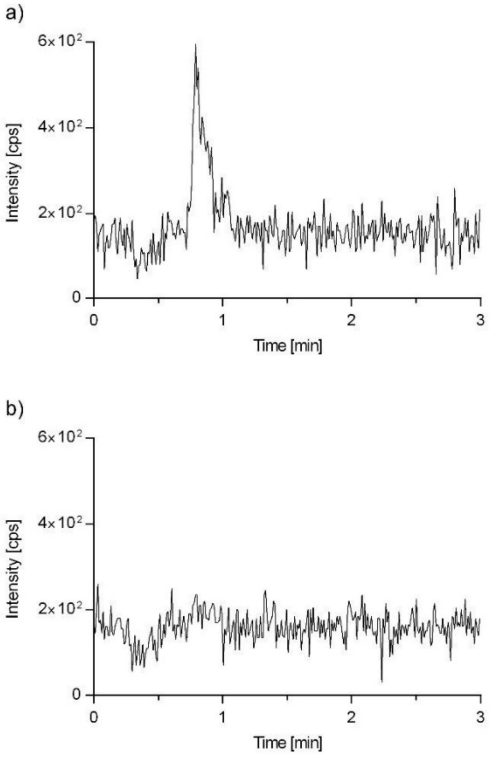

Figure S4. Conformations of UNC0646 in MB327-PAM-1 in each subunit after blind docking experiments. a) Extracellular view of the receptor. The two α-subunits are colored yellow and green, the δ-subunit pink, the β-subunit cyan, and the γ-subunit salmon. Binding mode of UNC0646 in between the b) γ- and α-subunit, c) α- and δ-subunit, d) δ- and β-subunit, e) β- and α-subunit, and f) α- and γ-subunit. The receptor is shown as ribbon, the surface as a grey contour, and the ligand as sticks.

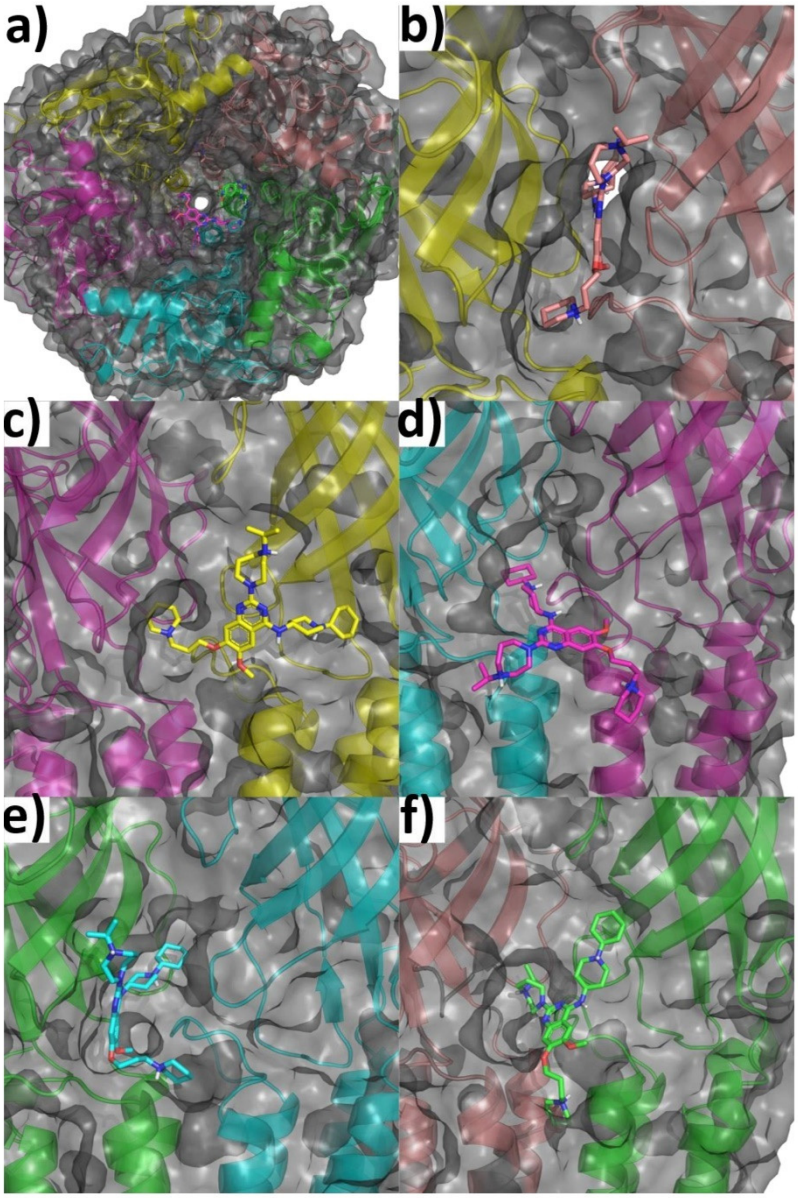

Figure S5. Docked orientation of UNC0646 between the γ- and α-(yellow) subunit. The γ-subunit has been omitted for clarity. The substituent in position 4 of the quinazoline ring is oriented in a) in a boat-twist conformation in the best-ranked pose and b) in a chair-chair conformation in the second-best-ranked conformation.

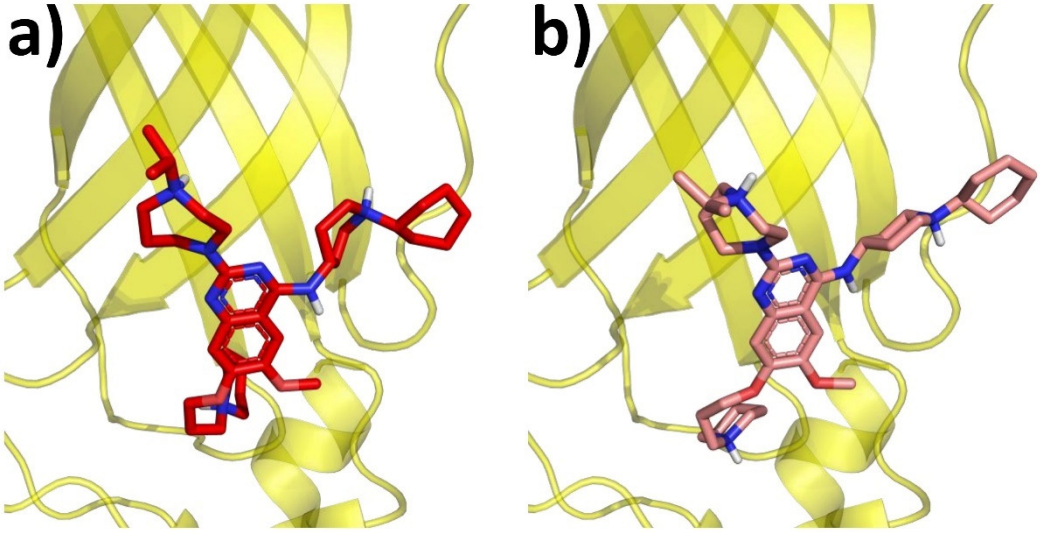

Figure S6. Docked binding mode of UNC0646 in between the β- and α-subunit. The ligand is shown in cyan and side chains similar to those in Figure 1 are shown in forest green.

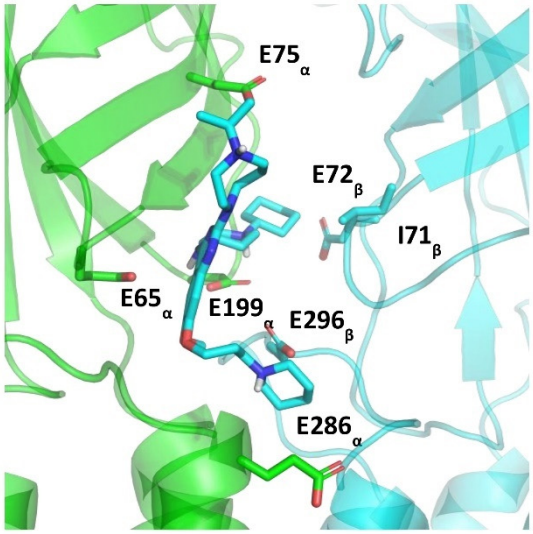

Figure S7. Backbone (C, CA, N) RMSD of nAChR during 12 replicas of 500 ns long MD simulations compared to the first frame of the production runs.

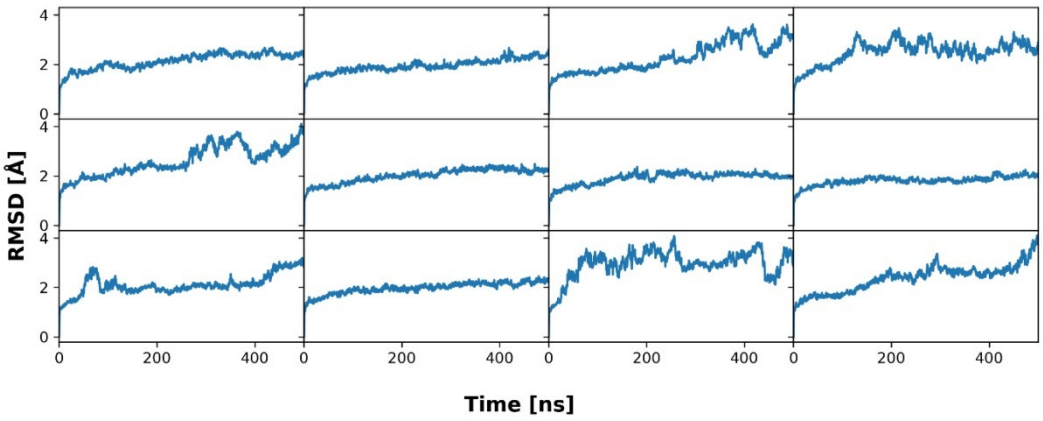

Figure S8. Electron density of water and membrane components over all 12 replicas of 500 ns long MD simulations. The electron density is plotted against the z-coordinate with the membrane centered at 0 Å for phosphatidylcholine (PC), oleic acid (OL), palmitoyl acid (PA), and water (WAT).

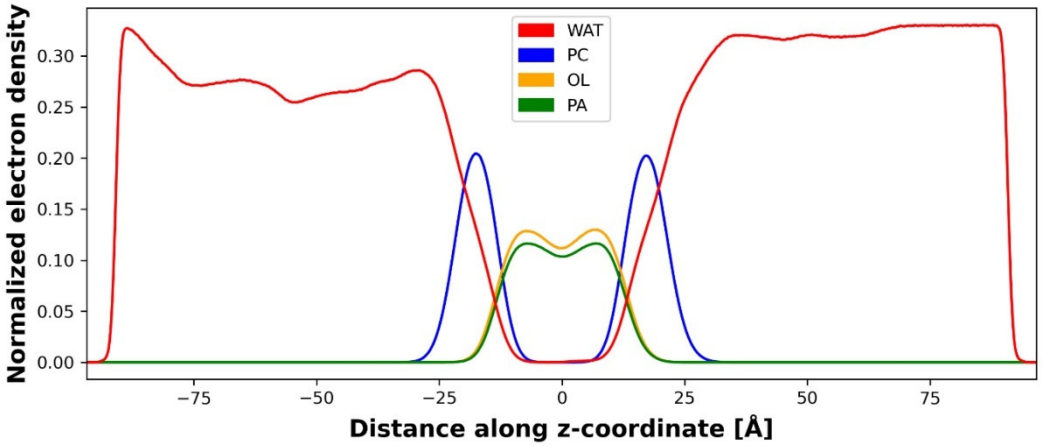

Figure S9. MMPBSA per-residue decomposition of the binding effective energy of UNC0646 in the subunits composing binding site A (γ- and α-subunit). Glutamates are shown in red.

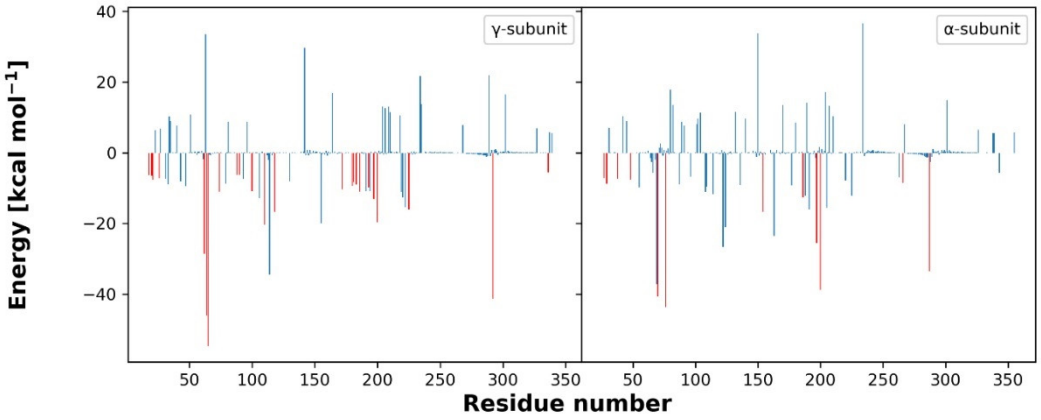

Figure S10. Binding mode of UNC0642 in MB327-PAM-1. The binding mode was obtained from a representative binding mode of UNC0646 in binding site A (between the γ- and α-subunit) and subsequent minimization of the ligand in the binding site.

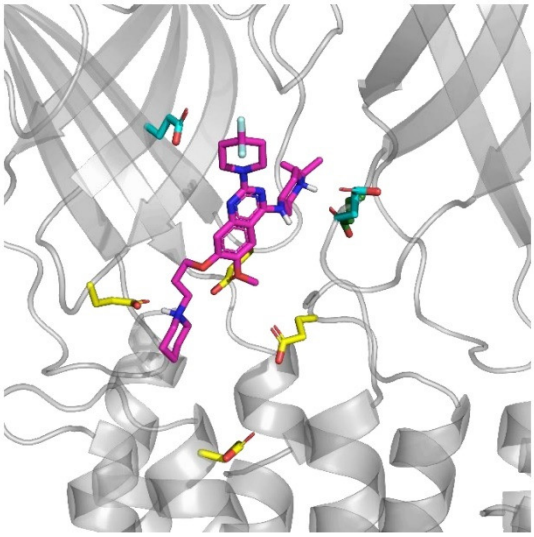

11.3. Publication III

Identification of ligands binding to MB327-PAM-1, a binding pocket relevant for resensitization of nAChRs

Jesko Kaiser, Christoph G.W. Gertzen, Tamara Bernauer, Valentin Nitsche, Georg Höfner, Karin V. Niessen, Thomas Seeger, Franz F. Paintner, Klaus T. Wanner, Dirk Steinritz, Franz Worek, Holger Gohlke

Toxicology Letters, 2024. *in press*. [§3]

[§3] See **REPRINT PERMISSION**

Journal Pre-proof

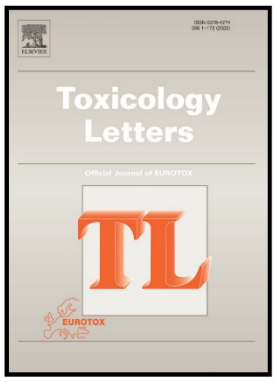

Identification of ligands binding to MB327-PAM-1, a binding pocket relevant for resensitization of nAChRsIdentification of ligands binding to MB327-PAM-1

Jesko Kaiser, Christoph G.W. Gertzen, Tamara Bernauer, Valentin Nitsche, Georg Höfner, Karin V. Niessen, Thomas Seeger, Franz F. Paintner, Klaus T. Wanner, Dirk Steinritz, Franz Worek, Holger Gohlke

PII: S0378-4274(24)00105-X

DOI: https://doi.org/10.1016/j.toxlet.2024.05.013

Reference: TOXLET11516

To appear in: *Toxicology Letters*

Received date: 21 December 2023
Revised date: 13 April 2024
Accepted date: 17 May 2024

Please cite this article as: Jesko Kaiser, Christoph G.W. Gertzen, Tamara Bernauer, Valentin Nitsche, Georg Höfner, Karin V. Niessen, Thomas Seeger, Franz F. Paintner, Klaus T. Wanner, Dirk Steinritz, Franz Worek and Holger Gohlke, Identification of ligands binding to MB327-PAM-1, a binding pocket relevant for resensitization of nAChRsIdentification of ligands binding to MB327-PAM-1, *Toxicology Letters,* (2024) doi:https://doi.org/10.1016/j.toxlet.2024.05.013

Identification of ligands binding to MB327-PAM-1, a binding pocket relevant for resensitization of nAChRs

Jesko Kaiser[1], Christoph G.W. Gertzen[1], Tamara Bernauer[2], Valentin Nitsche[2], Georg Höfner[2], Karin V. Niessen[3], Thomas Seeger[3], Franz F. Paintner[2], Klaus T. Wanner[2], Dirk Steinritz[3], Franz Worek[3], Holger Gohlke[1,4,*]

[1]Institute for Pharmaceutical and Medicinal Chemistry, Heinrich Heine University Düsseldorf, Düsseldorf, Germany

[2]Department of Pharmacy – Center for Drug Research, Ludwig-Maximilians-Universität München, München, Germany

[3]Bundeswehr Institute of Pharmacology and Toxicology, München, Germany

[4]Institute of Bio- and Geosciences (IBG-4: Bioinformatics), Forschungszentrum Jülich, Jülich, Germany

Running title: Identification of ligands binding to MB327-PAM-1

Keywords: nAChR; virtual screening; molecular dynamics simulations; MS Binding Assay

Author ORCID

Jesko Kaiser: 0000-0002-6429-0911

Christoph Gertzen: 0000-0002-9562-7708

Tamara Bernauer: 0000-0001-9570-1253

Valentin Nitsche: 0009-0000-3351-1227

Georg Höfner: 0000 0002 7957 4503

Karin V. Niessen: 0009-0008-6810-5294

Thomas Seeger: 0009-0007-5713-4367

Franz Paintner: 0000-0002-6795-586X

Klaus T. Wanner: 0000-0003-4399-1425

Dirk Steinritz: 0000-0002-2073-5683

Franz Worek: 0000-0003-3531-3616

Holger Gohlke: 0000-0001-8613-1447

*Corresponding Author:

Address: Universitätsstr. 1, 40225 Düsseldorf, Germany.

Phone: (+49) 211 81 13662

E-mail: gohlke@uni-duesseldorf.de

Abstract

Desensitization of nicotinic acetylcholine receptors (nAChRs) can be induced by overstimulation with acetylcholine (ACh) caused by an insufficient degradation of ACh after poisoning with organophosphorus compounds (OPCs). Currently, there is no generally applicable treatment for OPC poisoning that directly targets the desensitized nAChR. The bispyridinium compound MB327, an allosteric modulator of nAChR, has been shown to act as a resensitizer of nAChRs, indicating that drugs binding directly to nAChRs can have beneficial effects after OPC poisoning. However, MB327 also acts as an inhibitor of nAChRs at higher concentrations and can thus not be used for OPC poisoning treatment. Consequently, novel, more potent resensitizers are required. To successfully design novel ligands, the knowledge of the binding site is of utmost importance. Recently, we performed *in silico* studies to identify a new potential binding site of MB327, MB327-PAM-1, for which a more affine ligand, UNC0646, has been described. In this work, we performed ligand-based screening approaches to identify novel analogs of UNC0646 to help further understand the structure-affinity relationship of this compound class. Furthermore, we used structure-based screenings and identified compounds representing four new chemotypes binding to MB327-PAM-1. One of these compounds, cycloguanil, is the active metabolite of the antimalaria drug proguanil and shows a higher affinity towards MB327-PAM-1 than MB327. Furthermore, cycloguanil can reestablish the muscle force in soman-inhibited rat muscles. These results can act as a starting point to develop more potent resensitizers of nAChR and to close the gap in the treatment after OPC poisoning.

Introduction

Chemical warfare agents remain a serious threat to the military and civilian population. Organophosphorus compounds (OPCs) are one class of chemical warfare agents and block acetylcholinesterase (AChE) covalently [1]. This inhibits the decomposition of acetylcholine causing inflated acetylcholine (ACh) concentrations in the synaptic gap and, thereby, an overstimulation of muscarinic (mAChR) and nicotinic (nAChR) acetylcholine receptors. The overstimulation leads to structural rearrangements of nAChR, resulting in a non-functional, desensitized state [1-3].

While the overstimulation of mAChRs can be treated with atropine, only antidotes (oximes) with insufficient efficiency are available to treat the overstimulation of nAChRs indirectly by reactivating AChE. However, these oximes are ineffective against several OPCs, in particular, when aging leads to altered OPC-enzyme complexes that are less susceptible to reactivation [4, 5]. Thus, novel antidotes are required to treat OPC poisonings.

The compound MB327 can reestablish the muscle force of OPC-poisoned muscles by interacting directly with nAChRs from several species via an allosteric modulation [6-10]. Furthermore, administration of MB327 can prolong the survival rates of guinea pigs after tabun poisoning compared to the oxime HI-6, both in combination with physostigmine and hyoscine [11]. While these results are promising, MB327 cannot be used in the treatment of OPC poisoning so far because the therapeutic range is too narrow. Restoration of the muscle force in a rat diaphragm myography assay by MB327 increases up to concentrations of 300 µM but decreases at higher concentrations [9, 10]. Similarly, MB327 initially shows positive allosteric effects on nicotine binding, which decrease at micromolar concentrations. Likewise, MB327 increases the binding of the orthosteric ligand epibatidine up to micromolar concentrations but at higher concentrations decreases it [7, 9]. These results indicate that MB327 transmits inhibitory effects on nAChR via binding to the orthosteric binding site, which has recently been experimentally validated for related bispyridinium compounds [12]. Additionally, we

observed the binding of MB327 to the orthosteric binding site using free ligand diffusion molecular dynamics (MD) simulations [13]. Hence, novel compounds that are more affine and more selective to the allosteric binding site than MB327 need to be identified. A first step in this direction was recently done by us by identifying UNC0646 as an allosteric nAChR ligand with a higher affinity than MB327 [14].

One way to identify novel binders and improve the affinity of known ligands is by using computer-aided drug design methods [15]. In ligand-based screening, one can search for analogs based on two- (topological) or three- (structural) dimensional ligand representations. In two-dimensional similarity screening, the importance of the three-dimensional conformation in the binding site is not taken into account. This can lead to unsatisfactory results, especially for highly flexible ligands. Thus, three-dimensional ligand screening approaches can be more effective in identifying binders that can fit into the binding site and have been used for identifying novel binders successfully in the past [16-21]. However, ligand-based screening approaches neglect explicit knowledge of the receptor structure. Additionally, ligand-based screening may only identify hits with more similar chemical scaffolds compared to the query. Thus, structure-based screening is a popular approach to identifying novel ligands for biological targets and can help to identify novel chemical scaffolds [22-29]. Recently, we identified a novel allosteric binding site of MB327 (MB327-PAM-1) and described a potential binding mode of UNC0646 in MB327-PAM-1 [13, 30], providing necessary input for three-dimensional ligand-based screening and structure-based screening.

Here, we used this information to perform all three described screening approaches to increase the chance of success and validated hits by a mass spectrometry-based affinity determination (MS Binding Assay). We identified novel substituents (**1a-k, 2b-e, 2g**) at the UNC0646 quinazoline scaffold that lead to higher affinity and ligands with novel chemotypes [PTMD99-0001C (**3**), PTMD99-0016C (**4**), PTMD99-0026C (**5**), and cycloguanil (**6**)] binding to MB327-PAM-1.

Materials and Methods

Two-dimensional similarity search

The MolPort database was searched for compounds similar to UNC0646 using a two-dimensional search as implemented on the MolPort website (https://molport.com, accessed on October 21st, 2020). All compounds identified by the similarity search using default parameters were selected. From 22 compounds identified, twelve compounds were ordered for testing in this study.

Homology modeling of nAChR

The homology modeling of the human and *Torpedo* (recently reclassified as *Tetronarce*) nAChR was performed as previously described [13]. In short, homology models were generated using MODELLER version 9.19 [31] with the PDB structures 6PV8 [32], 5KXI [33], 2WN9 [34], and 6CNK [35] as templates. Water molecules and molecules from the crystallization buffer were removed. Amino acids not resolved in the templates were not included in the models; these amino acids are located within the intracellular loop, the *N*- and *C*-terminal region and, hence, not in the region that forms the MB327-PAM-1 pocket. The final models were selected based on the DOPE potential [36], TopScore [37], and visual inspection and subsequently protonated using PROPKA, v3.4.0 [38, 39] as implemented in Schrödinger Maestro, v2021-1 [40] at pH 7.4. The termini were capped with *N*-methyl amide (NME) and acetyl (ACE) groups, respectively.

Ligand-based screening with subsequent template-based docking

Based on our proposed binding mode of UNC0646 [30], we used the binding mode of PTMD01-0004 (**2a**) [Bernauer *et al.*, in preparation], a structurally reduced analog of UNC0646 that lacks the quinazoline substituent in 2-position, as input for ligand-based screening. We created a database from feasible organic reactions of building blocks of PTMD01-0004 (**2a**) with MolPort (https://molport.com) building blocks as implemented in the PINGUI webserver (https://scubidoo.pharmazie.uni-marburg.de/pingui/, accessed on May 19th, 2021) (SI Figure S1) [41], resulting in 69,223 in principle synthesizable compounds. We protonated the constituents of the database using OpenEye FixpKa, v2.1.1.0 [42] and filtered the database to only use compounds that are at least double positively charged as PTMD01-0004 (**2a**), resulting in 14,396 compounds and generated conformers using OpenEye OMEGA, v4.1.1.0 [43, 44] with default parameters except setting the *strictstereo* parameter to false. Initially, we used OpenEye vROCS, v3.4.1.0 [45, 46] (SI Figure S2) to filter the database by applying default parameters and the TanimotoCombo score. The best 1000 hits from the vROCS screening were further investigated using CCG MOE, v2020 [47] using a template-based docking with an upstream pharmacophore filter (SI Figure S3). The hits were analyzed based on visual inspection, and four compounds were selected for synthesizing.

Synthesis

All target compounds synthesized in the context of this study were cataloged with a PTMD number (Pharmacy and Toxicology Munich and Düsseldorf). All chemicals were used as purchased from commercial sources. Solvents used for purification were distilled before use. 5-Pyrrolidin-1-ylpentan-1-amine, which could only be purchased as the respective hydrochloride salt was converted into the free base before use [48]. Anhydrous reactions were carried out under an argon atmosphere in vacuum-dried glassware. For microwave reactions, a Discover SP microwave system by CEM GmbH was used. TLC-Analysis was performed on plates purchased from Merck (silica gel $60F_{254}$ on aluminum sheet). Flash chromatography was carried out using silica gel 60 (40-63 mm mesh size) as stationary phase, purchased from Merck. All synthesized compounds were dried under a high vacuum. ^{1}H and ^{13}C NMR spectra were recorded with a Bruker BioSpin Avance III HD 400 and 500 MHz at 25 °C. For data

processing, MestReNova (Version 14.1.0) from Mestrelab Research S.L. 2019, and for calibration, the solvent signal (CD_2Cl_2, CD_3OD or DMSO-d_6) was used. The purity of the test compounds was ≥ 95%, determined by means of quantitative NMR using TraceCERT® ethyl 4-(dimethylamino)benzoate from Merck as an internal calibrant [49, 50]. High-resolution mass spectra were recorded on a Finnigan MAT 95 (EI) or a Finnigan LTQ FT (ESI). Melting points were determined with a Büchi 510 melting point instrument and are uncorrected. For IR spectroscopy, an FT-IR Spectrometer 1600 from PerkinElmer was used. The analytical data of the synthesized compounds described below, obtained using the described methods, can be found in the Supporting Information.

Synthesis of 2,4-dichloro-6-methoxy-7-[3-(piperidin-1-yl)propoxy]quinazoline (**7**) recently reported by Vital *et al.* [51] and of *N*-(1-cyclohexylpiperidin-4-yl)-6-methoxy-7-[3-(piperidin-1-yl)propoxy]-quinazolin-4-amine (**2a**) was accomplished according to Bernauer *et al.* [Bernauer *et al.*, in preparation].

General Procedure: Synthesis of quinazolin-4-amines (GP): A solution of the respective 4-chloroquinazoline (**8**) or (**9**) (1.0 equiv), the corresponding amine (2.0 equiv - 10 equiv) and *N*,*N*-diisopropylethylamine (DIEA) (3.0 equiv) in *i*-PrOH (5 mL/mmol) was stirred at 160 °C for 15 to 60 min under microwave irradiation (200 W). The reaction mixture was concentrated in vacuo and the crude product was purified by flash chromatography [5% to 15% 3 M NH_3 (in MeOH) in CH_2Cl_2 or 10% MeOH in CH_2Cl_2 + 0.5% DMEA].

6-Methoxy-2-(piperidin-1-yl)-7-[3-(piperidin-1-yl)propoxy]-*N*-[5-(pyrrolidin-1-yl)pentyl]quinazolin-4-amine (1k): According to GP with **8** (126 mg, 0.300 mmol, 1.0 equiv), 5-(pyrrolidin-1-yl)pentan-1-amine (93.8 mg, 0.600 mmol, 2.0 equiv) and DIEA (160 µL, 119 mg, 0.900 mmol, 3.0 equiv) in *i*-PrOH (1.5 mL) for 15 min. **1k** (117 mg, 72% yield, 96% purity) was isolated by flash chromatography [7% to 15% 3 M NH_3 (in MeOH) in CH_2Cl_2] as a colorless solid.

***N*^{1}-Cyclohexyl-*N*^{2}-{6-methoxy-7-[3-(piperidin-1-yl)propoxy]quinazolin-4-yl}-*N*^{1}-methylethane-1,2-diamine (2b):** According to GP with **9** (101 mg, 0.300 mmol, 1.0 equiv), *N*^{1}-cyclohexyl-*N*^{1}-methylethane-1,2-diamine (104 µL, 93.8 mg, 0.600 mmol, 2.0 equiv) and DIEA (160 µL, 119 mg, 0.900 mmol, 3.0 equiv) in *i*-PrOH (1.5 mL) for 1 h. **2b** (127 mg, 93%) was isolated by flash chromatography [10% 3 M NH_3 (in MeOH) in CH_2Cl_2] as a yellow oil (96% purity).

6-Methoxy-*N*-[3-(4-methylpiperazin-1-yl)butyl]-7-[3-(piperidin-1-yl)propoxy]quinazolin-4-amine (2c): According to GP with **9** (101 mg, 0.300 mmol, 1.0 equiv), 3-(4-methylpiperazin-1-yl)butan-1-amine (114 µL, 108 mg, 0.600 mmol, 2.0 equiv) and DIEA (160 µL, 119 mg, 0.900 mmol, 3.0 equiv) in *i*-PrOH (1.5 mL) for 1 h. **2c** (110 mg, 78% yield, 97% purity) was isolated by flash chromatography [10% 3 M NH_3 (in MeOH) in CH_2Cl_2] as a pale yellow solid.

6-Methoxy-7-[3-(piperidin-1-yl)propoxy]-4-[4-(pyrrolidin-1-yl)piperidin-1-yl]quinazoline (2d): According to GP with **9** (101 mg, 0.300 mmol, 1.0 equiv), 4-(pyrrolidin-1-yl)piperidine (97.4 mg, 0.600 mmol, 2.0 equiv) and DIEA (160 µL, 119 mg, 0.900 mmol, 3.0 equiv) in *i*-PrOH (1.5 mL) for 1 h. **2d** (122 mg, 89%) was isolated by flash chromatography [10% 3 M NH_3 (in MeOH) in CH_2Cl_2] as a yellow oil (97% purity).

***N*-[1-(Azepan-1-yl)-2-methylpropan-2-yl]-6-methoxy-7-[3-(piperidin-1-yl)propoxy]quinazolin-4-amine (2e):** According to GP with **9** (134 mg, 0.400 mmol, 1.0 equiv), 1-(azepan-1-yl)-2-methylpropan-2-amine (717 mg, 4.00 mmol, 10 equiv) and DIEA (213 µL, 158 mg, 1.20 mmol, 3.0 equiv) in *i*-PrOH (2.0 mL) for 1 h. **2e** (46.4 mg, 25% yield, 97% purity) was isolated by flash chromatography [1. 10% 7 M NH_3 (in MeOH) in CH_2Cl_2, 2. 10% MeOH in CH_2Cl_2 + 0.5% DMEA] as a yellow oil. In addition, a further product fraction of lower purity was obtained (21% yield, 72% purity).

***N*-(1-Propan-2-ylpiperidin-4-yl)-6-methoxy-7-[3-(piperidin-1-yl)propoxy]quinazolin-4-amine (2f):** According to GP with **9** (33.6 mg, 0.100 mmol, 1.0 equiv), 1-propan-2-ylpiperidin-4-amine (31.6 µL, 28.4 mg, 0.200 mmol, 2.0 equiv) and DIEA (53.3 µL, 39.6 mg, 0.300 mmol, 3.0 equiv) in *i*-PrOH (0.5 mL) for 15 min. **2g** (41.2 mg, 93%) was isolated by flash chromatography [5% to 10% 3 M NH_3 (in MeOH) in CH_2Cl_2] as a colorless solid (96% purity).

***N*-(1-Propan-2-ylpiperidin-4-yl)-6-methoxy-7-[3-(piperidin-1-ylmethyl)pyrrolidin-1-yl]quinazolin-4-amine (2g):** A mixture of **10** (111 mg, 0.350 mmol, 1.0 equiv), 1-(pyrrolidin-3-ylmethyl)piperidine (310 mg, 1.75 mmol, 5.0 equiv) and potassium carbonate (53.2 mg, 0.385 mmol, 1.1 equiv) in *N*-methyl-2-pyrrolidone (NMP) (455 µL) was stirred at 135 °C for 20 h. The reaction mixture was concentrated and purified by flash chromatography [5% to 20% 3 M NH_3 (in MeOH) in CH_2Cl_2] to afford **2f** (147 mg, 90%) as a pale yellow solid (99% purity).

4-Chloro-6-methoxy-2-(piperidin-1-yl)-7-[3-(piperidin-1-yl)propoxy]quinazoline (8): A solution of **7** (370 mg, 1.00 mmol, 1.0 equiv) and 1-methylpiperidine (244 µL, 200 mg, 2.00 mmol, 2.0 equiv) in 1,4-dioxane (2.5 mL) was stirred at 150 °C for 1 h under microwave irradiation (300 W). **8** was isolated by flash chromatography (10% to 20% MeOH in CH_2Cl_2) as a yellow solid (327 mg, 78% yield, 95% purity).

4-Chloro-6-methoxy-7-[3-(piperidin-1-yl)propoxy]quinazoline (9) [52, 53]: To a slurry of **11** (22.2 mg, 0.100 mmol, 1.0 equiv), 3-piperidin-1-ylpropan-1-ol (19.9 µL, 18.8 mg, 0.125 mmol, 1.25 equiv), PPh_3 (34.4 mg, 0.130 mmol, 1.3 equiv) and dry THF (1.0 mL) was added di-*tert*-butyl azodicarboxylate (DBAD) (30.5 mg, 0.130 mmol, 1.3 equiv) in portions at 0 °C. The resulting solution was stirred overnight at rt and concentrated under reduced pressure. Purification by flash chromatography [5% 3 M NH_3 (in MeOH) in CH_2Cl_2] afforded **9** as a pale yellow solid (34.5 mg, > 99% yield, 96% purity).

7-Fluoro-*N*-(1-propan-2-ylpiperidin-4-yl)-6-methoxyquinazolin-4-amine (10): A mixture of **12** (20.2 mg, 0.100 mmol, 1.0 equiv), PyBOP (69.0 mg, 0.130 mmol, 1.5 equiv), diazabicycloundecene (DBU) (22.9 µL, 23.3 mg, 0.150 mmol, 1.5 equiv) and 1-propan-2-ylpiperidin-4-amine (23.7 µL, 21.3 mg, 0.150 mmol, 1.5 equiv) in acetonitrile (0.5 mL) was stirred at rt for 1 h. The mixture was concentrated in vacuo. **10** (29.3 mg, 92%) was isolated after flash chromatography [5% 3 M NH_3 (in MeOH) in CH_2Cl_2] as a colorless solid (97% purity).

Structure-based screening

The SMILES codes of in-stock compounds in the lead-like (3,434,621 compounds) and the double-protonated (129,606 compounds) subsets were downloaded from the ZINC20 database [54]. All compounds were protonated using OpenEye FixpKa, v2.1.1.0 , and conformers were generated using OpenEye OMEGA, v4.1.0.0 [43] with default parameters except setting the *strictstereo* parameter to false [43, 44]. The human and *Torpedo* homology models of nAChR were prepared for docking using OpenEye MakeReceptor, v4.0.0.0, and all compounds were docked using OpenEye FRED, v4.0.0.0 [55-57], writing out a maximum of one pose per compound. The best 1000 hits in each binding pocket were visually inspected, and 30 compounds were ordered for testing.

Commercially obtained compounds

The 42 commercially obtainable compounds were purchased from several suppliers with purities of at least 85%. A corresponding, detailed list can be found in the Supporting Information (SI Table S1). For affinity testing in MS Binding Assays, the compounds were applied as described in SI Table S1.

Molecular dynamics simulations of cycloguanil bound to nAChR

The receptor with the docked ligand was embedded in a membrane of 1-palmitoyl-2-oleoyl-*sn*-glycero-3-phosphocholine (POPC) lipids and solvated using Packmol-Memgen [58] in a rectangular box of TIP3P water [59]. KCl was added at a concentration of 150 mM and the system was neutralized using Cl^- ions. The edge of the box was set to be at least 12 Å away from receptor atoms. The AMBER22 package of molecular simulations software [60, 61] was used in combination with the *ff14SB* force field for the protein [62], the Lipid21 force field for the lipids [63], and the Joung and Cheatham parameters for monovalent ions [64]. Ligand charges were calculated according to the RESP procedure [65] with default parameters as implemented in antechamber [66] using electrostatic potentials generated by Gaussian16 [67] at the HF-6-31G* level of theory; ligand force field parameters were derived from the gaff2 force field. Since cycloguanil (**6**) should carry one positive charge (pK_a = 11.4 [68]) on the nitrogen atoms in the 1,6-dihydro-1,3,5-triazine-2,4-diamine ring system, *N*-3 was protonated.

Molecular dynamics (MD) simulations were performed as described earlier [13] using AMBER22. In short, a combination of steepest descent and conjugate gradient minimization was performed while lowering positional restraints with force constants from 25 kcal mol^{-1} $Å^{-2}$ to zero. Stepwise heating to 300 K and a subsequent reduction of harmonic restraints from 25 kcal mol^{-1} $Å^{-2}$ to zero followed.

Subsequently, 10 replicas of 1 µs length each of unbiased MD simulations were performed; for temperature control, the Langevin dynamics were applied with a collision frequency of 2 ps^{-1}, and the Berendsen barostat with semi-isotropic pressure adaption was used.

Based on the four replicas in which cycloguanil (**6**) remained within the binding site, we computed representative binding structures of cycloguanil (**6**) using the *k*-means clustering algorithm, as implemented in CPPTRAJ [69]. We then restarted simulations from the representative binding mode. Because the hydrogen bonds to $E62_\gamma$ and $E200_\gamma$ were highly conserved among all clusters except the largest one (containing 18.3% of all frames), we decided to restart simulations from the second largest cluster (containing 14.1% of all frames) (SI Figure S4). Therefore, we started directly with the production run with similar settings as for the docked structure. The first 10 ns of each replica were removed for further analysis.

All simulations were analyzed using CPPTRAJ [69].

Prediction of physicochemical and toxicological properties

Using OpenEye OMEGA, version 4.1.1.1 [44, 70], three-dimensional conformations of the compounds based on the SMILES code were generated using the default setting with the exception that only one conformation was generated for each compound. Pharmacokinetic properties and hERG inhibition were predicted using Schrödinger QikProp, version 2022-2 [71].

For PAINS filtering, the PAINS-remover webserver, v0.99 (https://www.cbligand.org/PAINS/) [72], was used. For the prediction of further toxicological properties, we used NEXUS Derek, v6.0.1 [73].

Image generation

Images of nAChR were created using UCSF Chimera [74].

Rat diaphragm myography

All procedures using animals followed animal care regulations and were approved by the responsible ethics committee. Preparation of rat diaphragm hemispheres and experimental protocol of myography were performed as described before [9]. In short, for all procedures (including wash-out steps,

preparation of soman and bispyridinium compound solutions) aerated Tyrode solution (125 mM NaCl, 24 mM $NaHCO_3$, 5.4 mM KCl, 1 mM $MgCl_2$, 1.8 mM $CaCl_2$, 10 mM glucose, 95 % O_2, 5% CO_2; pH 7.4; 25 ± 0.5 °C) was used. After the recording of control muscle force, the muscle preparations were incubated in the Tyrode solution, containing 3 µM soman. Following a 20 min wash-out period, the test compound cycloguanil (Merck KGaA) was added in ascending concentrations (1 µM, 10 µM, 30 µM, 70 µM, 100 µM, 150 µM, 200 µM, 300 µM, 500 µM, 1000 µM). In each preparation, four concentrations were measured to avoid the fatigue effects of muscle force generation. The incubation time was 20 min for each concentration. The electric field stimulation was performed with 10 µs pulse width and 0.2 A amplitudes. The titanic trains of 20 Hz, 50 Hz, 100 Hz were applied for 1 s and in 10 min intervals. Measurements on non-poisoned muscles were carried out according to the same scheme. Instead of soman, pure Tyrode was incubated. Muscle force was calculated as a time-force integral (area under the curve, AUC) and constrained to values obtained for maximal force generation (muscle force in the presence of Tyrode solution without any additives; 100 %).

UNC0642 MS Binding Assays

Competitive MS Binding Assays were performed as described previously [30]. In short, the reporter ligand (UNC0642, 1 µM) and the corresponding test compound (varying concentrations) were incubated with aliquots of a membrane preparation from *Torpedo californica* electroplaque (approx. 75 µg protein per sample) in incubation buffer (120 mM NaCl, 5 mM KCl, 8.05 mM Na_2HPO_4 and 1.95 mM NaH_2PO_4, pH 7.4). Samples were generated in triplicates. After separating the protein-bound from the non-bound reporter ligand in the incubation mixture by centrifugation, the protein-bound portion of UNC0642 was liberated and finally quantified via LC-ESI-MS/MS. Total binding of UNC0642 was normalized to 100% (i.e. reporter ligand binding in the absence of test compound) and 0% (i.e. non-specific reporter ligand binding, determined by the presence of 100 µM UNC0646 instead of test compound). Applying the non-linear regression function "One site – fit Ki" yielded competition curves, which then revealed IC_{50} and K_i values, respectively (Prism software v. 6.07, GraphPad software, La Jolla, CA, USA). Top and bottom levels were fixed at 100% and 0%, respectively, for that purpose. K_i values are given as mean pK_i values from three experiments ± SEM, if not stated otherwise. Next to the full-scale competition experiments, also competition experiments with only a single concentration of test compound (i.e. 10 µM) have been performed in this study. Compared to full-scale competition experiments, the obtained data was not analyzed via non-linear regression in this case and only normalized as described above to reveal the remaining reporter ligand binding as an indicator for the affinity of the respective test compound. If not stated otherwise, the remaining reporter ligand binding is given as the mean of triplicates ± SD.

Results and Discussion

Screening strategy

We used different strategies to identify novel binders of MB327-PAM-1. First, we performed ligand-based screening to identify analogs of UNC0646 using a two-dimensional similarity search as implemented on the MolPort website (https://molport.com) to identify compounds with high similarity to UNC0646 (Figure 1, blue scheme). Furthermore, we used PTMD01-0004 (**2a**), an analog with no substituent in the 2-position of the quinazoline ring, to perform ligand-based screening using its three-dimensional binding mode as a query using OpenEye vROCS [45, 46], followed by a pharmacophore-based docking of the best hits using CCG MOE [47] (Figure 1, yellow scheme). Second, to reveal new binders with novel chemical scaffolds, we performed structure-based virtual screenings (Figure 1, green scheme). There, we first docked a ZINC20 [54] lead-like library (3,434,621 compounds) into the human muscle-type nAChR using OpenEye FRED [55-57]. The lead-like library only includes compounds of a molecular weight between 250-350 g mol^{-1}. However, because a higher affinity of known ligands binding to MB327-PAM-1 generally correlates with a larger size of the ligands and most previously described binders feature at least two positive charges [14, 30, 75, 76], we performed an additional screening using a ZINC20 library [54] of in-stock compounds bearing at least two positive charges (129,606 compounds). To exploit that the amino acids interacting with MB327 and UNC0646 are highly conserved among the human muscle-type and *Torpedo* nAChR [13, 30] but that the conformations of the sidechains nevertheless vary, we now used the *Torpedo* nAChR for docking to increase the search space. Also, the *Torpedo* nAChR is used in our MS Binding Assays.

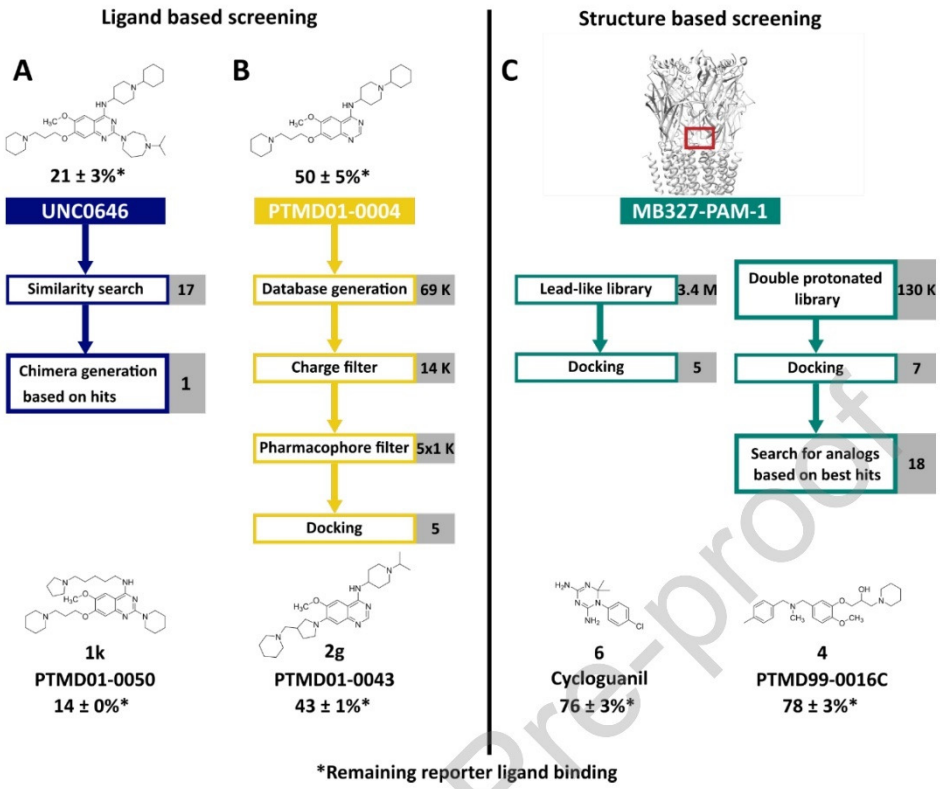

Figure 1: Screening strategies to identify novel binders of MB327-PAM-1. **A)** A two-dimensional similarity search using UNC0646 as a template was performed using MolPort (https://www.molport.com/). Based on the hits, one novel chimera compound was designed. **B)** Based on PTMD01-0004 (**2a**), a UNC0646-analog lacking the side chain in the 2-position, a database was generated based on feasible organic reactions (SI Figure S1). After applying a charge filter and a pharmacophore filter, docking experiments led to five novel analogs of UNC0646. **C)** Based on structure-based screening experiments in the human muscle type and *Torpedo* nAChR, 5 respectively 7 compounds with novel chemotypes were ordered for affinity characterization in MS Binding Assays. After the first experimental results, 18 additional compounds based on three chemical scaffolds were selected from the initial screening and ordered. This resulted in the identification of cycloguanil (**6**) and PTMD99-0016C (**4**). For each screening strategy, the best hits are shown. Percentage values indicate the remaining reporter ligand binding in the presence of test compounds (at 10 μM concentration) as compared to 100% reporter ligand binding in the absence of a competitor using the reporter ligand UNC0642 in MS Binding Assays (1 μM UNC0642) (mean ± SD, n = 3).

Two-dimensional similarity search yields affine UNC0646 analogs with small substituents in 4-position

Based on a two-dimensional screening of the MolPort library using UNC0646 as a template (Figure 1, blue scheme), 12 compounds were tested in our MS Binding Assay for MB327-PAM-1 [30]. Of these, 10 compounds displaced the reporter ligand UNC0642 from the binding site at 10 μM (**1a**-**1j**; remaining reporter ligand binding at most 90 ± 7%, n = 3; Table 1, SI Table S2). The best result was obtained for PTMD01-0019C (**1a)**. In contrast to previously described UNC0646 analogs [14, 30], this is the only compound that does not have a side chain in 7-position with an aliphatic amino group, although mainly acidic amino acid side chains are available for ligand binding in MB327-PAM-1 [13, 30]. However, a study with related 4-amino-2-(*N,N*-diethylamino)quinazoline derivatives revealed that the two amino substituents impact the pK_a values of quinazolines resulting in pK_a values of up to 8.31 [77] compared to 3.51 of the unsubstituted quinazoline [78]. Thus, PTMD01-0019C (**1a**) can still be protonated under experimental and physiological conditions, similar to all previously described binders in MB327-PAM-1 [13, 30, 75, 76]. Furthermore, 4-aminopyridine has a pK_a of 9.17, indicating that even the residue in the 2-position of PTMD01-0019C (**1a**) may be protonated [79]. These results are in line with

suggestions that a positive charge is crucial for binding in MB327-PAM-1 but also indicate that the location of the positive charge is less important, which can be explained by the many acidic amino acids in MB327-PAM-1 (SI Figure S6, SI Table S3) [13, 30]. To verify the results obtained from the competition experiments by applying a single concentration, we performed full-scale competition studies for the best-binding compound PTMD01-0019C (**1a**), resulting in a pK_i of 5.19 ± 0.05 (SI Figure S5).

The second strongest reduction of reporter ligand binding was observed for UNC0379 (**1b**), a ligand with a substituent with increased flexibility at the 4-position compared to UNC0646. Along these lines, the results for ZT-12-037-01 (**1c**), C-021 (**1d**), MS012 (**1e**), PTMD01-0020C (**1f**), PTMD01-0021C (**1g**), PTMD01-0024C (**1h**), and PTMD01-0025C (**1i**) indicate that for affinity towards MB327-PAM-1, the positively charged amino side chain can be present at either position 2 or position 4 of the quinazoline building block. Furthermore, bunazosin (**1j**) has no basic side chains at the quinazoline ring but only the two electron donating groups in 2- and 4-positions, further indicating that the positive charge of the ligand might also be located within the heteroaromatic ring. This confirms the above observation that the location of the positive charge is not crucial for the binding of UNC0646 analogs. Based on these results, we synthesized PTMD01-0050 (**1k**), a chimera inspired by UNC0646, UNC0642, and UNC0379. The synthesis consisting of two steps started from **7** [51, 80] (Scheme 1). In analogy to a procedure described in the literature [81], **7** was reacted with *N*-methylpiperidine (2.0 equiv) at 150 °C under microwave irradiation for 1 h affording the quinazoline **8** with a piperidine ring in 2-position after column chromatography in good yield (78%). For the subsequent substitution of chloride in 4-position, **8** was stirred with 5-(pyrrolidin-1-yl)pentan-1-amine (2.0 equiv) in the presence of DIEA (3.0 equiv) under microwave irradiation at 160 °C for 15 min. The desired product PTMD01-0050 (**1k**) could be isolated in good yield (72%). Notably, this compound shows a higher reporter ligand displacement than UNC0646 (Table 1).

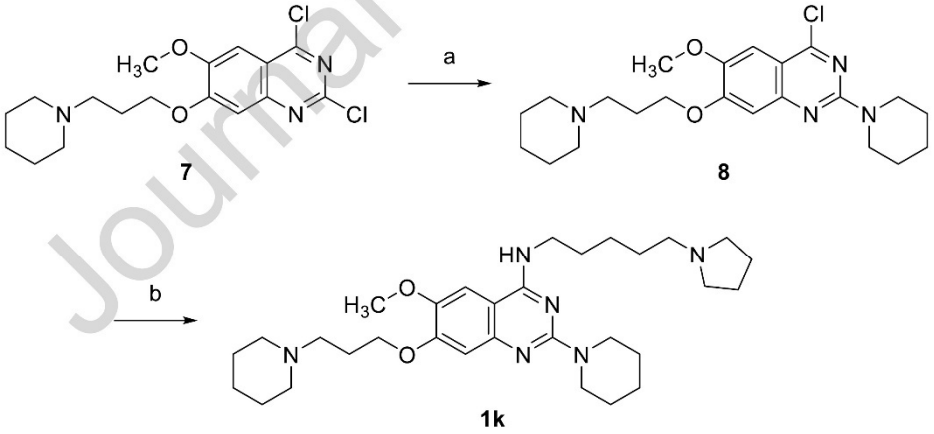

Scheme 1: Reagents and conditions: (a) 1-methylpiperidine (2.0 equiv), 1,4-dioxane, 150 °C (300 W), 1 h, 78%; (b) 5-(pyrrolidin-1-yl)pentan-1-amine (2.0 equiv), DIEA (3.0 equiv), *i*-PrOH, microwave: 200 W, 160 °C, 15 min, 72%.

Table 1: Selected analogs of UNC0646 identified by a two-dimensional similarity search and their affinities to MB327-PAM-1 in nAChR determined in MS Binding Assays.

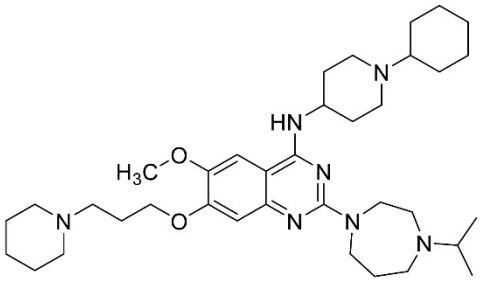

UNC0646

pK_i = 5.83 ± 0.05[a]

Remaining reporter ligand binding: 21 ± 3 %[b]

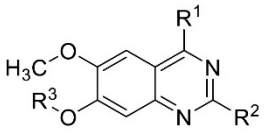

1a-k

Compound	Name / PTMD code	R^1	R^2	R^3	Remaining reporter ligand binding [%][b]
1a	PTMD01-0019C		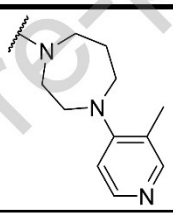		47 ± 3
1b	UNC0379	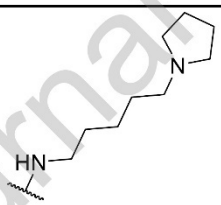	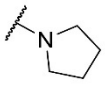		59 ± 4
1k	PTMD01-0050	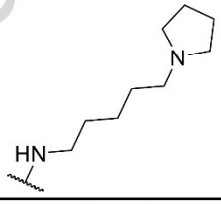	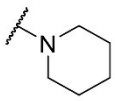	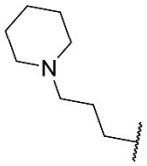	14 ± 0
1c	ZT-12-037-01	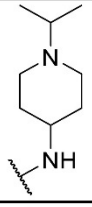	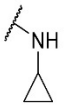		66 ± 5
1d	C-021	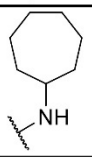	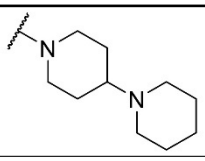		63 ± 2

1e	MS012	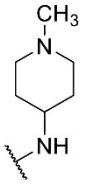	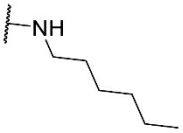		83 ± 6
1f	PTMD01-0020C		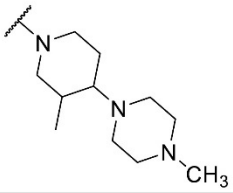		73 ± 7
1g	PTMD01-0021C		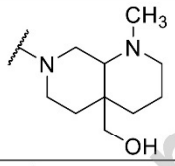		87 ± 2
1h	PTMD01-0024C		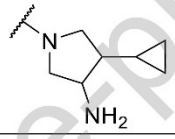		83 ± 4
1i	PTMD01-0025C		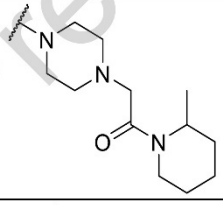		81 ± 5
1j	Bunazosin		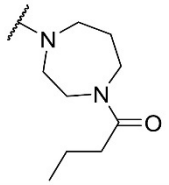		90 ± 7

[a] The pK_i value has been reported in ref. [30].

[b] Characterized by UNC0642 MS Binding Assays; Percentage of remaining reporter ligand binding in the presence of test compounds as compared to 100% reporter ligand binding in the absence of a competitor. Results are based on thirty measurements for UNC0646 and three measurements for all other compounds at a test compound concentration of 10 µM and a reporter ligand concentration of 1 µM. Mean and standard deviation are displayed.

Ligand-based screening using PTMD01-0004 (2a) as a template representing an analog of UNC0646 with a reduced molecular structure

While the two-dimensional similarity search based on UNC0646 yielded new, affine molecules binding to MB327-PAM-1, this approach did not consider the position and orientation of the ligand in MB327-PAM-1. Thus, we also performed a ligand-based screening in MB327-PAM-1 using PTMD01-0004 (**2a**) [80] as a template (Figure 1, yellow scheme). We started with this analog of UNC0646 because the substituent in the 2-position of UNC0646 shows minor interactions with the receptor in our proposed binding mode [30], and UNC0646 violates the molecular weight rule of Lipinski's "rule of five" [82], in

contrast to PTMD01-0004 (**2a**). Furthermore, the absence of an electron-donating group in the 2-position only has a minor impact on the affinity [14].

We performed a two-step screening (see Materials and Methods) using a database of synthesizable compounds based on the building blocks of PTMD01-0004 (**2a**) (SI Figure S1). We selected five compounds that we synthesized (see below) and tested for affinity towards MB327-PAM-1 (**2b**-**2e**, **2g**, Table 2). The substituents chosen for position 4 did not increase the affinity in any compound compared to PTMD01-0004 (**2a**). Still, slight modifications in this substituent can influence reporter ligand displacement significantly.

As to the UNC0646 building block, our two-dimensional similarity search revealed that substituting it with flexible linkers in the 4-position can lead to highly affine compounds as seen for PTMD01-0050 (**1k**). The compound with increased flexibility between the quinazoline ring and the basic side chain nitrogen located within the cyclohexyl ring, PTMD01-0032 (**2b**), has a higher affinity than PTMD01-0053 (**2c**). However, the piperazine ring of PTMD01-0053 (**2c**) might also result in an alternative distance between the positive charge of the side chain and the quinazoline moiety, depending on the protonation site. Still, the relation between linker flexibility and affinity is also observed in PTMD01-0027 (**2d**), PTMD01-0030 (**2e**), and PTMD01-0032 (**2b**), where the distance between the quinazoline ring to the positively charged nitrogen is 3-4 heavy atoms long. The increased flexibility potentially enables improved interactions with the side chains acting as hydrogen bond acceptors in the β1-β2 loop within MB327-PAM-1 ($E65_\gamma$ in SI Figure S6). However, this trend does not always apply. PTMD01-0053 (**2c**) with a more flexible side chain than PTMD01-0030 (**2e**) has a lower affinity. Thus, the additional polar atom and the additional methyl substituent of the piperazine ring as well as the different distance between the positive charge in the side chain and the quinazoline moiety of PTMD01-0053 (**2c**) may also lead to a decrease in affinity. Although experimentally observed structure-affinity relationships for UNC0646 analogs are based on measurements with the *Torpedo* nAChR, this knowledge is presumably transferable to the human muscle-type nAChR because of the high sequence identity within the binding site (SI Figure S6, SI Table S3). However, one limitation of these structure-affinity relationships is that MB327-PAM-1 can be present in five subunits of the heteropentamer. Thus, the relationships need to be considered as a representation over all five potential MB327-PAM-1 binding sites, and structure-affinity relationships between binding sites of one species might vary.

In the 7-position, we identified in PTMD01-0043 (**2g**), an alternative substituent that leads to a higher reporter ligand displacement than if the same substituent as in UNC0646 is used in the in 7-position [PTMD01-0005 (**2f**)]. PTMD01-0043 (**2g**) otherwise bears the same side chains as PTMD01-0005 (**2f**) except in the 7-position of the quinazoline ring. As for the assessment of the two-dimensional similarity search, we verified our results by characterizing the binding affinity of the most affine compound according to the single point determinations [PTMD01-0043 (**2g**); remaining reporter ligand binding 43 ± 1%] in a full-scale MS Binding Assay yielding a pK_i of 5.46 ± 0.04 (SI Figure S7).

Table 2: Selected analogs of PTMD01-0004 (**2a**) identified by a ligand-based screening followed by template-based docking and their affinities to MB327-PAM-1 in nAChR determined in MS Binding Assays.

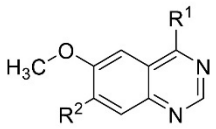

2a-g

Compound	PTMD code	R^1	R^2	Remaining reporter ligand binding [%][a]
2a	PTMD01-0004[b]	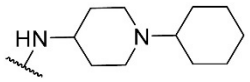	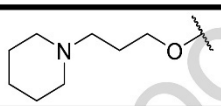	50 ± 5[c]
2b	PTMD01-0032	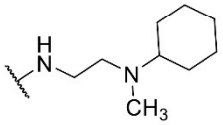	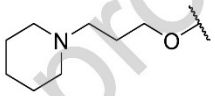	50 ± 7
2c	PTMD01-0053	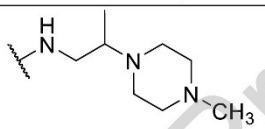	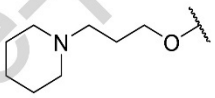	76 ± 7
2d	PTMD01-0027	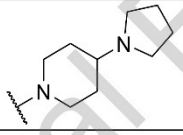	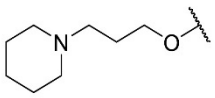	71 ± 3
2e	PTMD01-0030	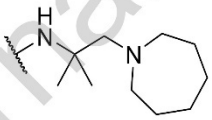	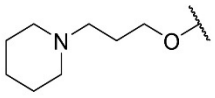	60 ± 3
2f	PTMD01-0005[b]	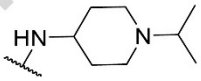	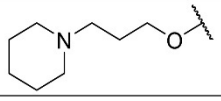	63 ± 4[d]
2g	PTMD01-0043	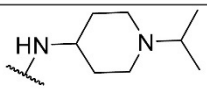	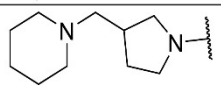	43 ± 1

[a] Characterized by UNC0642 MS Binding Assays; Percentage of remaining reporter ligand binding in the presence of test compounds as compared to 100% reporter ligand binding in the absence of a competitor. If not stated otherwise, results are based on three measurements at a test compound concentration of 10 µM and a reporter ligand concentration of 1 µM. Mean and standard deviation are displayed.

[b] PTMD01-0004 (**2a**) [80] and PTMD01-0005 (**2f**) were not identified in this study but are shown as reference structures to compare to PTMD01-0043 (**2g**).

[c,d] Results are based on twelve and six measurements, respectively, at a test compound concentration of 10 µM and a reporter ligand concentration of 1 µM. Mean and standard deviation are displayed.

Synthesis of compounds 2b-g:

Target compounds **2b**-**2f** were easily accessible by a two-step synthesis from commercially available building block **11** (Scheme 2). First, key intermediate **9** [52] was obtained in quantitative yield (> 99%) by reaction of quinazoline derivative **11** with 1.25 equiv 3-(piperidin-1-yl)propan-1-ol under *Mitsunobu* conditions (1.3 equiv PPh_3, 1.3 equiv DBAD, THF, rt, 20 h) following a literature procedure [83]. In the second step, the 4-amino substituents were introduced to afford the target compounds **2b**-**2f**. Nucleophilic displacement of the 4-chloro substituent was achieved according to a procedure reported in the literature [84] by heating **9** with the corresponding amines (2.0 equiv) in the presence of DIEA (3.0 equiv) to 160 °C under microwave irradiation. Thus, 4-aminoquinazolines **2b**-**2d** and **2f** were isolated in good to excellent yields (78-93%). However, the reaction with the sterically demanding amine 1-(azepan-1-yl)-2-methylpropan-2-amine to get **2e** was sluggish. Hence, a higher excess of the amine (10 equiv) was applied. This led to the target compound, which could be isolated in a yield of 25% only, which is partly due to the fact, that also a small amount of a side-product had formed being difficult to separate.

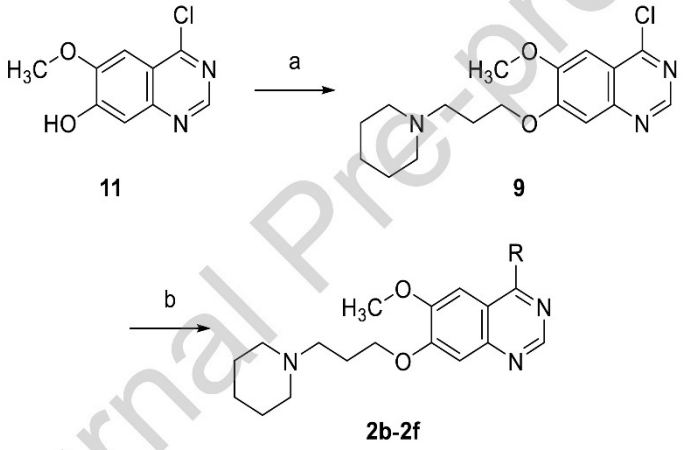

Scheme 2: Reagents and conditions: (a) 3-piperidin-1-ylpropan-1-ol (1.25 equiv), PPh_3 (1.3 equiv), DBAD (1.3 equiv), THF, rt, 20 h, > 99%; (b) amines (2.0-10 equiv), DIEA (3.0 equiv), *i*-PrOH, microwave: 200 W, 160 °C, 15 min-60 min, **2b**: 93%, **2c**: 78%, **2d**: 89%, **2e**: 25%, **2f**: 93%.

The 7-aminoquinazoline **2g** was synthesized in two steps starting from commercially available 7-fluoro substituted quinazoline-4(3*H*)-one **12** (Scheme 3). In the first step, the lactame **12** was converted to the 4-aminoquinazoline **10** by a phosphonium-mediated S_NAr reaction according to a procedure described in the literature [85]. Thus, **12** was reacted with 1.5 equiv of 1-propan-2-ylpiperidin-4-amine, PyBOP and DBU in acetonitrile at rt for 1 h, to obtain product **10** in excellent yield (92%). The subsequent substitution of the fluorine in 7-position of **10** to afford target compound **2g** was achieved by a reaction of **10** with a 5-fold excess of 1-(pyrrolidin-3-ylmethyl)piperidine in NMP at 135 °C in the presence of K_2CO_3 (1.1 equiv) according to a procedure reported in the literature [86]. In this way, the product **2g** could be isolated in 90% yield and high purity (99%).

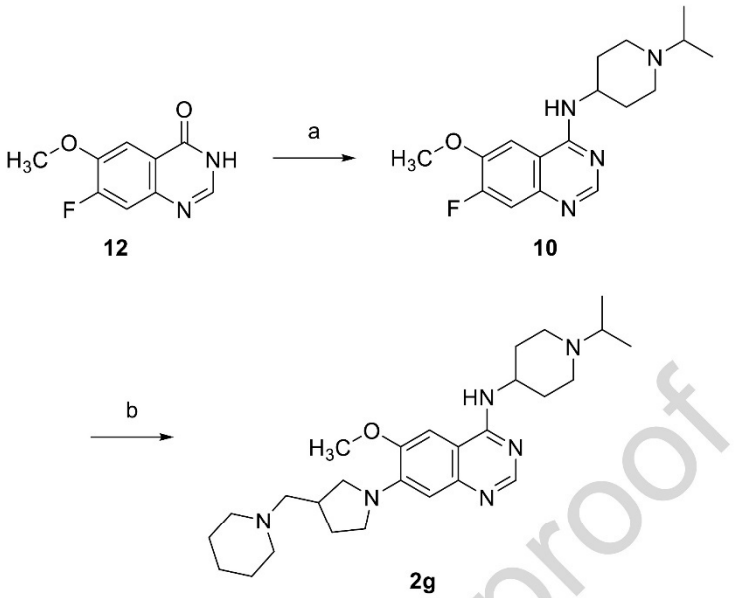

Scheme 3: Reagents and conditions: (a) 1-propan-2ylpiperidin-4-amine (1.5 equiv), PyBOP (1.5 equiv), DBU (1.5 equiv), acetonitrile, rt, 1 h, 92%; (b) 1-(pyrrolidin-3-ylmethyl)piperidine (5.0 equiv), K_2CO_3 (1.1 equiv), NMP, 135 °C, 20 h, 90%.

Structure-based screening reveals new chemotypes with a higher affinity than MB327

We first screened the lead-like library of ZINC20 [54] with 3,434,621 molecules using the homology model of the human muscle-type nAChR and OpenEye FRED [55-57] as docking engine with default parameters (Figure 1, green scheme). However, we know from previous work that larger molecules, such as UNC0646, usually bind to MB327-PAM-1 with a higher affinity than smaller ones, such as MB327. Furthermore, the two previously identified binders in MB327-PAM-1, UNC0646, and MB327, carry at least two positive charges. Thus, we decided to also screen a subset of the ZINC20 database [54] containing all doubly protonated in-stock compounds (129,606 compounds) by docking into the *Torpedo* nAChR (see also above).

We ordered 12 compounds based on visual inspection of the best 1000 hits in MB327-PAM-1 in each subunit in each of the screenings (2 x 5 x 1000 = 10,000 hits in total) (Figure 2, SI Table S4) (PTMD99-0001C – PTMD99-0015C). (In preliminary MS binding studies (the results of which had later on to be partly revised; for final results see SI Table S4), PTMD99-0006C (**13**), PTMD99-0010C (**14**), and PTMD99-0014C (**15**) showed the most promising results.) Thus, we decided to inspect the best 1000 hits in both screenings in each subunit again to find structurally similar chemotypes. We ordered three analogs of PTMD099-0006C (**13**), seven analogs of PTMD99-0010C (**14**), and eight analogs of PTMD99-0014C (**15**) (SI Table S5). In each group, at least one compound (at 10 µM concentration) displaced the reporter ligand UNC0642 (at 1 µM concentrations) from MB327-PAM-1 during single-concentration MS Binding Assay experiments indicating that these compounds show a higher affinity towards MB327-PAM-1 than MB327, which shows a remaining marker ligand binding of 102 ± 9% (n = 6) under identical conditions (1 µM reporter ligand, 10 µM test ligand) [80]. In total, four new chemotypes, all containing at least one positive charge, were identified that displace UNC0642 from MB327-PAM-1 at concentrations of 10 µM (reporter ligand concentration of 1 µM) to any appreciable extent. However, for two of these compounds the remaining reporter ligand binding values are slightly not significantly different from 100%, while the two other compounds differ significantly from 100% {$p < 0.05$ according

to a two-sided one-sample *t*-test; *p* [PTMD99-0001C (**3**)] = 0.064, *p* [PTMD99-0016C (**4**)] = 0.005, *p* [PTMD99-0026C (**5**)] = 0.079, *p* [cycloguanil (**6**)] = 0.006}.

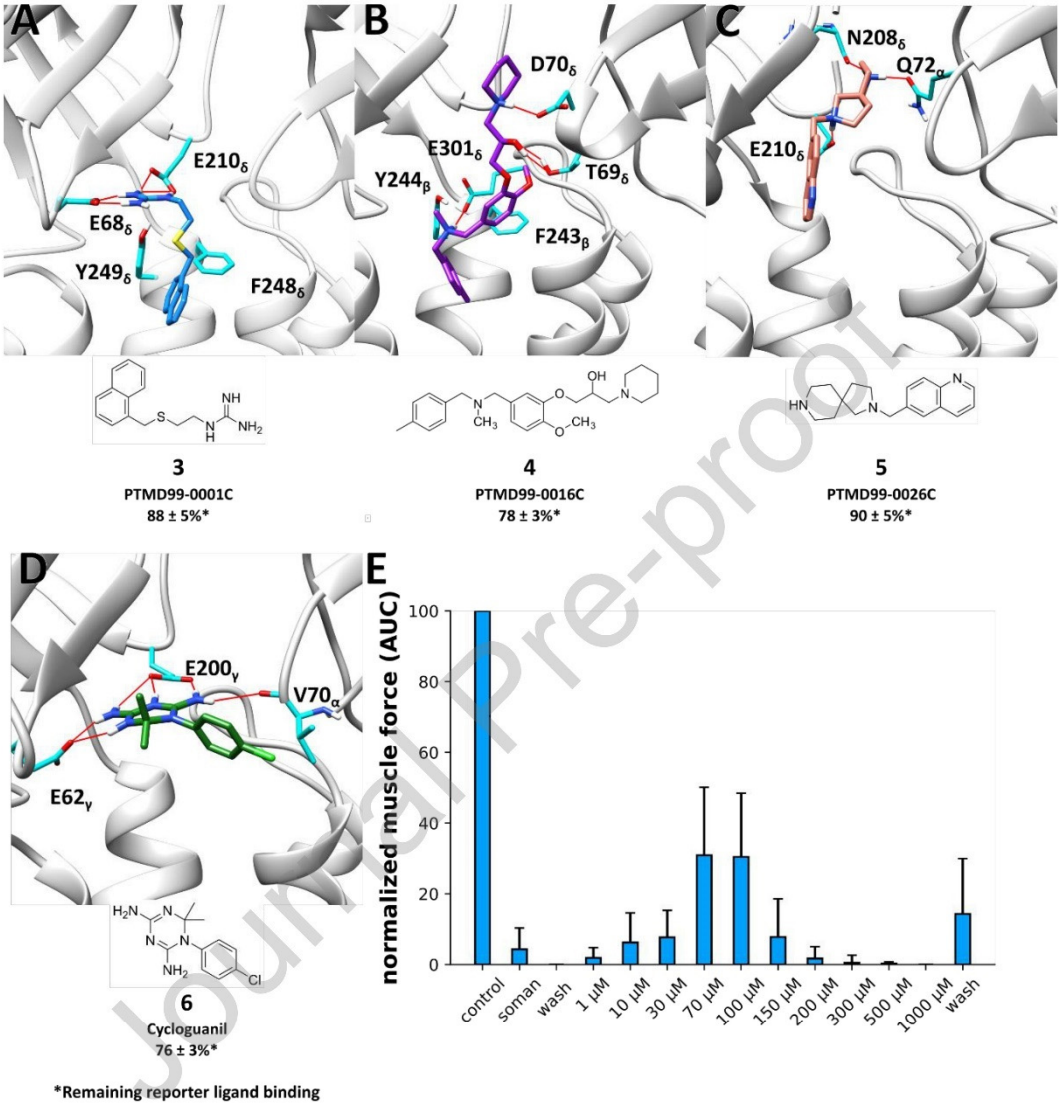

Figure 2: Docked binding mode and MS Binding Assay affinity data of selected hits from a structure-based screening in different subunits and species of nAChR. Docked binding mode of **(A)** PTMD99-0001C (**3**) in between the α- and δ-subunits of the human nAChR, **(B)** PTMD99-0016C (**4**) in between the δ- and β-subunits of the *Torpedo* nAChR, **(C)** PTMD99-0026C (**5**) in between the α- and δ-subunits of the *Torpedo* nAChR, and **(D)** cycloguanil (**6**) in between the α- and γ-subunits of *Torpedo* nAChR. Red lines indicate hydrogen bonds. Percentage values indicate the remaining reporter ligand binding in the presence of test compounds (at 10 µM concentration) as compared to 100% reporter ligand binding in the absence of a competitor using the reporter ligand UNC0642 in MS Binding Assays (1 µM UNC0642) (mean ± SD, *n* = 3). Compounds displaying chirality were tested as racemats. **(E)** Resoration of muscle force of soman-inhibited muscles after treatment with cycloguanil (**6**). Error bars indicate the standard deviation (*n* is between 5 and 27). Since the largest efficacies are observed at low stimulation frequencies [10], results are only shown for a stimulation frequency of 20 Hz (see SI Table S6 for all stimulation frequencies applied).

Of the analogs based on PTMD99-0006C (**13**), PTMD99-0016C (**4**) shows the highest affinity within this group and is the only compound able to displace UNC0642 to any appreciable extent during measurements with test compound concentrations of 10 µM and reporter ligand concentrations of 1 µM. Small changes in the 4-methylbenzyl group can have a high impact on affinity. For example,

PTMD99-0020C (**16**) (SI Table S5), bearing a (3-methylpyridin-4-yl)methyl substituent instead of the 4-methylbenzyl group, does not show a displacement of the reporter ligand to any appreciable extent anymore under identical experimental conditions. In fact, all compounds bearing a heteroaromatic ring instead of the 4-methylbenzyl group fail to displace UNC0642 to any appreciable extent under identical experimental conditions to a reasonable extent.

Based on the initial results for PTMD99-0010C (**14**), we identified PTMD99-0026C (**5**), able to displace the reporter ligand (concentration 1 µM) to any appreciable extent at 10 µM test compound concentration. However, compounds with an amide group in 3-position to the nitrogen at position 2 of the 2,8-diazaspiro[4.5]decane system do not displace the reporter ligand UNC0642 under similar experimental conditions to any appreciable extent (PTMD99-0010C (**14**), -0023C (**17**), -0024C (**18**), -0025C (**19**), -0028C (**20**) (SI Table S4, S5)). Furthermore, replacing the quinolinyl substituent by a 5-(*tert*-butyl)-pyrazol-3-yl substituent (PTMD99-0031C (**21**) (SI Table S5)) also abrogates the reporter ligand displacement indicating that hydrogen bond donors as substituents of the 2,8-diazaspiro[4.5]decane ring might be unfavorable.

Additionally, as the fourth novel chemotype binding to MB327-PAM-1, the 1,6-dihydro-1,3,5-triazine-2,4-diamine building block was identified. Most interesting, the compound showing the highest affinity, cycloguanil (**6**, 10 µM test compound concentration at 1 µM reporter ligand concentration, Figure 2D), is the active metabolite of the antimalarial drug proguanil. In competitive MS binding experiments, we observed a pK_i value for cycloguanil (**6**) of 3.64 ± 0.03 (SI Figure S8), significantly higher compared to MB327 [pK_i (MB327) = 3.40 ± 0.04 [30], $p < 0.01$, according to a two-sided *t*-test]. Cycloguanil (**6**) forms salt bridges both with $E62_\gamma$ and $E200_\gamma$ in the docked pose (Figure 2D). These two amino acids are highly conserved among different subunits of several species (Table 3), including the *Torpedo* nAChR, which is used in our MS Binding Assay, the rat muscle nAChR, which is used in our rat diaphragm assays, and in the human nAChR, in which the compounds need to exhibit an effect after OPC poisoning. Furthermore, these glutamates are crucial for the stabilization of the calcium ion in the α7 nAChR that can act as a positive allosteric modulator [87-89]. According to our screening results, we can, in general, see that larger substituents at both rings of cycloguanil (**6**) lead to a decrease in affinity (**22**-**28**, SI Table S5). Compounds based on the 1,3,5-triazin-2,4-diamin building block are overall much smaller than UNC0646 (M [UNC0646] = 621.93 g mol^{-1}; M [Cycloguanil (**6**)] = 251.72 g mol^{-1}), leading to compounds with an improved ligand efficiency.

Enough substance to conduct competition experiments with varying ligand concentrations and to perform rat diaphragm assays in order to investigate the restoration of muscle force after soman poisoning was only commercially available for cycloguanil (**6**). Treatment with cycloguanil (**6**) led to significant restoration of muscle force in rat diaphragm hemispheres after soman inhibition (Figure 2E, SI Table S6). The maximum restoration at stimulation frequencies of 20 Hz is comparable to the maximum restoration when using MB327 as a treatment option. However, while concentrations of 300 µM are necessary for the maximum effect of MB327 [26.29 ± 18.43% (mean ± SD; $n = 27$) restoration of muscle force, values taken from ref. [13]], cycloguanil (**6**) exerts a comparable effect at concentrations of 70 µM (30.87 ± 19.23%; $n = 5$). At a concentration of 100 µM, cycloguanil (**6**) leads to a significantly increased restoration of muscle force compared to MB327 [30.42 ± 18.04% vs. 17.77 ± 7.5%, values for MB327 taken from ref. [13], $p < 0.01$ according to a two-sided *t*-test ($n = 27$)]. Like MB327, cycloguanil (**6**) has a small therapeutic index, leading to muscle force inhibition at concentrations ≥ 300 µM (Figure 2E, SI Figure S9). To compare the therapeutic range of cycloguanil to that of MB327, we compared the muscle force reestablishing capabilities of both compounds. Therefore, we calculated at which concentrations cycloguanil significantly reestablishes the muscle force after soman poisoning compared to the first wash-out, as done previously for MB327 [9]. Starting at concentrations of 10 µM [6.2 ± 8.4% (n = 18; $p = 0.02$)] (100 µM for MB327 [25.7 ± 17.7%] [9]),

cycloguanil significantly and earlier than MB327 reestablishes the muscle force. The effect increases dose-dependently at concentrations of 30 and 70 µM to a maximum at 100 µM [30.4 ± 18.0% (n = 27)], whereas the maximum is reached at 300 µM [33.2 ± 27.7%] for MB327 [9]). At this concentration, the reestablishing capabilities of cycloguanil vanish, whereas this is observed for MB327 at 700 µM [9] (SI Table S6). Considering that experiments were performed at precise compound concentrations with missing data for intermediate concentrations, this implies that cycloguanil and MB327 have comparable concentration-dependent and maximal reestablishing capabilities as well as therapeutic ranges, although the effect of cycloguanil is shifted to lower concentrations. Thus, cycloguanil (**6**) currently cannot be considered as a treatment option but as a novel lead structure for treating OPC poisoning.

To further investigate the binding mode of cycloguanil (**6**), we performed MD simulations starting from the docked conformation. In 6 out of 10 replicas over 1 µs simulation time each, the ligand left the binding site (SI Figure S10). In the replicas where cycloguanil (**6**) remained in the binding site, the binding mode shifted. Whereas the interaction with the two glutamates persisted, the aromatic system of cycloguanil (**6**) moved towards the transmembrane region of nAChR in the direction of $Y239_{\gamma}$ (Figure 3A). This amino acid is located in a hydrophobic part of the binding site. Thus, we clustered the replica in which cycloguanil (**6**) remained in the binding site and performed additional 10 replicas of 1 µs long MD simulations starting from a representative structure. During the simulations, the membrane and receptor remained structurally virtually invariant (SI Figure S11, S12). Cycloguanil (**6**) continued to remain in the binding site in all replicas and showed highly conserved interactions with $E62_{\gamma}$ and $E200_{\gamma}$ (Figure 3B, C). Thus, we conclude that according to the MD-optimized binding mode, the interactions with the two glutamates persist and the hydrophobic interactions with amino acids close to $Y239_{\gamma}$ are important for ligand stabilization.

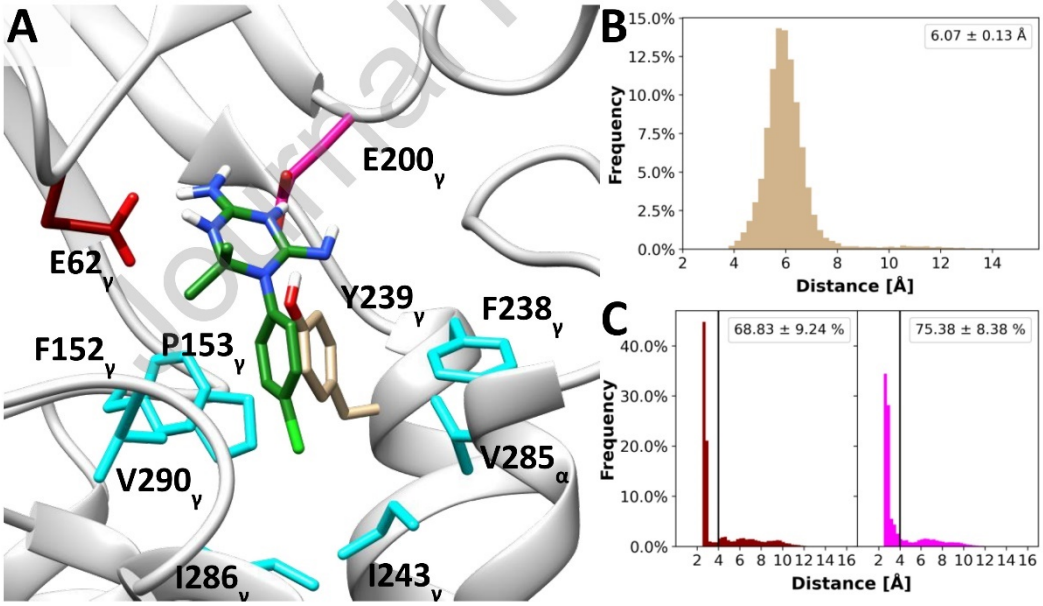

Figure 3: Binding mode of cycloguanil during MD simulations. **A)** Representative (according to a *k-means* clustering based on receptor and ligand atoms; the biggest cluster containing 48.2% of all frames is shown) binding mode of cycloguanil during 10 replicas of 1 µs long unbiased MD simulations starting from the docked conformation. **B)** Distance of the center of mass (COM) of the phenyl ring of cycloguanil to the phenyl ring of $Y239_{\gamma}$. The mean ± SEM distance is displayed as a legend. **C)** Distance of the nitrogens that can act as hydrogen bond donors of cycloguanil to the side chain oxygens of $E62_{\gamma}$ (dark red) and $E200_{\gamma}$ (pink). The frequency of contacts (distance < 4 Å; mean ± SEM) is displayed as a legend.

Table 3: Sequence conservation of $E62_\gamma$ and $E200_\gamma$ (green shadings) in the human muscle-type, *Torpedo*, and rat nAChR with respect to structurally homologous positions in the γ-subunit of the *Torpedo* nAChR.[a]

Human muscle type				*Torpedo*				Rat			
α	β	δ	ε	α	β	δ	γ	α	β	δ	ε
E	E	E	E	E	E	E	E62	E	E	E	E
E	*Q*	E	E	E	*Q*	E	E200	E	*Q*	E	E

[a] $E62_\gamma$ and $E200_\gamma$ are important for interactions with cycloguanil (**6**) in the docked binding mode and during MD simulations (Figure 3; see also text).

Prediction of pharmacokinetic and toxicological properties of best hits

UNC0646, the best hits of both ligand-based screenings [PTMD01-0050 (**1k**), PTMD01-0043 (**2g**)], and the best hit of each novel chemotype from the structure-based screening [PTMD99-0001C (**3**), PTMD99-0016C (**4**), PTMD99-0026C (**5**), and cycloguanil (**6**)] were initially probed in a pan interference compounds (PAINS) filter as implemented in the PAINS-remover webserver [72]; all compounds passed this filter, suggesting that they are less likely to react nonspecifically with biological targets. We further predicted the pharmacokinetic and toxicological properties using Schrödinger QikProp [71] and NEXUS Derek [73] (Table 4, Table 5). By far the most predictions for UNC0646 fall outside a 95% range for values of known drugs, questioning the drug-like properties of this compound. Along these lines, UNC0646 shows the worst Caco-2 cell permeability prediction as a model for gut-blood barrier permeation among all tested compounds and also violates two rules of Lipinski's rule of five and one rule of Jorgensen's rule of three, which are used as indicators for oral bioavailability. By contrast, all newly identified chemotypes show no violations of Lipinski's rule of five, and only PTMD99-0026C (**5**) violates one rule of Jorgensen's rule of three. Note, however, that the violated pharmacokinetic descriptors describe oral availability, whereas in the case of OPC poisoning drugs may be injected. On the other hand, improved oral bioavailability and reduced side effects might lead to the possibility to provide the antidote to a broader group of civilians and military members in the case of a high risk of OPC poisoning. Finally, the newly identified chemotypes [PTMD99-0001C (**3**), PTMD99-0016C (**4**), PTMD99-0026C (**5**), and cycloguanil (**6**)] show a reduced predicted affinity towards the HERG K^+ channel and a reduced toxicological alert count compared to UNC0646 and its analogs [PTMD01-0050 (**1k**), PTMD01-0043 (**2g**)]. Also, for the new chemotypes – except PTMD99-0026C (**5**) – no bacterial mutagenicity is predicted. To overcome the predicted mutagenicity of UNC0646 and its analogs, the substituted 4-anilinoquinazoline would need to be substituted, which is a common building block in all UNC0646 analogs tested in our binding assays so far [30]. In that respect, all novel compounds identified from the screenings show improved predicted pharmacokinetic properties compared to UNC0646 (Table 4) and, besides PTMD99-0026C (**5**), all novel chemotypes also display improved predicted toxicological properties (Table 5). Particularly, PTMD99-0001C (**3**) does not present any toxicologic alerts. PTM99-0016C (**4**) only shows toxicologic alerts regarding HERG channel inhibition (SI Table S7), however, the predicted IC_{50} is higher than for UNC0646. Because this parameter is problematic for nearly all compounds, it needs to be thoroughly investigated and experimentally validated during lead optimization. PTMD99-0026C (**5**) raises toxicological concerns regarding mammal mutagenicity and androgen receptor modulation – two parameters where no other compounds show toxicological alerts. Noteworthy, the reason for these toxicological alerts is the quinoline building block. Lastly, cycloguanil raises toxicological concerns regarding nephrotoxicity because of the halogenated benzene. However, proguanil, the prodrug of cycloguanil, is already used in malaria treatment and is considered well tolerated. Thus, in further approaches to optimize these new lead structures, the quinoline substructure of PTM99-0026C (**5**) and the halogenated benzene of cycloguanil (**6**) would need to be modified to avoid these toxicological alerts. Both building blocks are not involved

in any hydrogen bonds in the docked binding mode and, thus, might be replaced without compromising affinity towards MB327-PAM-1.

Table 4: Predicted pharmacokinetic properties of the best screening hits.

Compound	#stars[a]	QPlogPo/w[b]	QPPCaco[c]	RuleOfFive[d]	RuleOfThree[e]
UNC0646	7	6.014	125.427	2	1
PTMD01-0050 (**1k**)	1	5.609	428.531	2	0
PTMD01-0043 (**2g**)	0	4.541	297.484	0	0
PTMD99-0001C (**3**)	0	2.568	615.239	0	0
PTMD99-0016C (**4**)	0	3.718	277.071	0	1
PTMD99-0026C (**5**)	0	2.446	201.628	0	0
Cycloguanil (**6**)	1	1.592	446.492	0	0

[a] Number of properties falling outside the 95% range of similar values for known drugs.
[b] Octanol/water partition coefficient (recommended values: -2.0 – 6.5).
[c] Caco-2 cell permeability [nm/s] as a model for gut-blood barrier permeation (values < 25 poor, > 500 great).
[d] Number of violations of Lipinski's rule of five.
[e] Number of violations of Jorgensen's rule of three.

Table 5: Predicted toxicological properties of the best screening hits.

Compound	QPlogHERG[a]	Toxicological alert count[b]	Bacterial mutagenicity[d]
UNC0646	-8.224	4	EQUIVOCAL
PTMD01-0050 (**1k**)	-6.109	2	EQUIVOCAL
PTMD01-0043 (**2g**)	-7.460	4	EQUIVOCAL
PTMD99-0001C (**3**)	-4.980	0	INACTIVE
PTMD99-0016C (**4**)	-6.125	2	INACTIVE
PTMD99-0026C (**5**)	-6.528	4	PLAUSIBLE
Cycloguanil (**6**)	-3.989	1	INACTIVE

[a] IC_{50} value for blockage of HERG K^+ channels (recommended values: above -5).
[b] Number of alerts for toxicological predictions. For further information see SI Table S6.
[c] Bacterial mutagenicity *in vitro.*

Conclusion

To find new compounds representing novel chemotypes that bind to MB327-PAM-1 and to better understand structure-affinity relationships of the known binder UNC0646, we performed exhaustive virtual screening followed by an MS Binding Assay. As to the importance of the substituents of UNC0646 analogs, overall, beneficial substituents in position 4 are also more flexible, suggesting that conformational adaptability may be favorable compared to the loss of conformational entropy. Furthermore, while all compounds known to bind to MB327-PAM-1 carry at least one positive charge, our results indicate that the location of the positive charge plays a minor role. Based on our results, we developed PTMD01-0050 (**1k**), which leads to a higher reporter ligand displacement at test compound concentrations of 10 µM than UNC0646.

UNC0646 analogs in general show increased binding affinity with increased molecular weight and size. Due to concerns for oral bioavailability and because for some pharmacokinetic and toxicological predictions UNC0646 lies outside the recommended value range, together with the fact that despite an increased affinity UNC0646 and its analogs show no increased muscle force restoration compared to MB327 [30], we also aimed to find novel chemotypes binding to MB327-PAM-1. The identified compounds with four novel chemotypes can displace UNC0642 from MB327-PAM-1 (mean ± SD < 100%) at test compound concentrations of 10 µM and reporter ligand concentrations of 1 µM. While one compound (PTMD99-0016C (**4**)) already has a molecular weight > 400 Da, the other three hits have a molecular weight < 300 Da. These compounds can be used as a starting point for optimization in terms of affinity, pharmacokinetics, and resensitization capability of a desensitized nAChR. Because only for one of those compounds, cycloguanil (**6**), enough substance was available to perform rat diaphragm myography assays, it was tested for its resensitizing capabilities in soman-inhibited rat muscles and led to a significant muscle force restoration at a concentration of 1 µM. Furthermore, the muscle force restoration was significantly increased compared to MB327 at a concentration of 100 µM. Thus, the cycloguanil building block can be a promising starting point for further ligand optimization with a focus on annihilating the inhibitory effect at higher concentrations. All novel chemotypes display acceptable predicted pharmacokinetic properties. Cycloguanil already is described to be well-tolerated and shows the least risk for HERG inhibition based on the predictions of toxicological parameters, followed by PTMD99-0001C (**3**). PTMD99-0016C (**4**) and PTMD99-0026 (**5**) lie outside the recommended range. Additionally, PTM99-0026C (**5**) raises further toxicological concerns regarding mutagenicity and androgen receptor modulation. Taken together, cycloguanil and PTMD99-0001C (**3**) are the most promising lead structures, followed by PTMD99-0016C (**4**) because of its size and potential HERG inhibition. PTMD99-0026C (**5**) already raises several toxicological concerns, which might make lead optimization demanding. However, which novel chemotype is ultimately most promising and should be favored in further studies highly depends on rat diaphragm myography assays for the remaining three compounds.

The identification of more potent resensitizers of nAChR is of utmost importance to improve the currently insufficient treatment after OPC poisonings. Identifying novel chemotypes by structure-based screening and showing with our MS Binding Assay that these compounds can bind in the same binding site as MB327 suggests that the hits also bind to the allosteric binding site MB327-PAM-1.

Acknowledgments

This work was supported by the German Ministry of Defense (E/U2AD/KA019/IF558). We are grateful for computational support and infrastructure provided by the "Zentrum für Informations- und Medientechnologie" (ZIM) at the Heinrich Heine University Düsseldorf and the computing time provided by the John von Neumann Institute for Computing (NIC) to HG on the supercomputer JUWELS at Jülich Supercomputing Centre (JSC) (user IDs: VSK33, nAChR). HG is grateful to OpenEye Scientific Software for granting a Free Public Domain Research License.

Data availability

Data will be made available on request.

Declaration of competing interest

The authors declare that they have no known competing financial or personal interests.

Author contribution

J.K. performed modeling, screening, and MD simulation experiments. C.G. supported the computational experiments. T.B. synthesized analogs of UNC0646. V.N. performed MS Binding Assays, and T.S. performed rat diaphragm assays. H.G. conceived the study and supervised the project. G.H., K.N., F.P., K.W., D.S., and F.W. supervised respective study parts. All authors contributed to writing the manuscript.

References

1. Wiener, S.W. and R.S. Hoffman, *Nerve agents: a comprehensive review.* J. Intensive Care Med., 2004. **19**(1): p. 22-37.
2. Albuquerque, E.X., et al., *Mammalian nicotinic acetylcholine receptors: from structure to function.* Physiol. Rev., 2009. **89**(1): p. 73-120.
3. Unwin, N., *Nicotinic acetylcholine receptor and the structural basis of neuromuscular transmission: insights from Torpedo postsynaptic membranes.* Q. Rev. Biophys., 2013. **46**(4): p. 283-322.
4. Thiermann, H., F. Worek, and K. Kehe, *Limitations and challenges in treatment of acute chemical warfare agent poisoning.* Chem. Biol. Interact., 2013. **206**(3): p. 435-43.
5. Worek, F., et al., *Evaluation of oxime efficacy in nerve agent poisoning: Development of a kinetic-based dynamic model.* Toxicology and Applied Pharmacology, 2005. **209**(3): p. 193-202.
6. Sichler, S., et al., *Development of MS Binding Assays targeting the binding site of MB327 at the nicotinic acetylcholine receptor.* Toxicol. Lett., 2018. **293**: p. 172-183.
7. Scheffel, C., et al., *Electrophysiological investigation of the effect of structurally different bispyridinium non-oxime compounds on human alpha7-nicotinic acetylcholine receptor activity-An in vitro structure-activity analysis.* Toxicol. Lett., 2018. **293**: p. 157-166.
8. Niessen, K.V., et al., *Functional analysis of Torpedo californica nicotinic acetylcholine receptors in multiple activation states by SSM-based electrophysiology.* Toxicol. Lett., 2016. **247**: p. 1-10.
9. Niessen, K.V., et al., *In vitro pharmacological characterization of the bispyridinium non-oxime compound MB327 and its 2- and 3-regioisomers.* Toxicol. Lett., 2018. **293**: p. 190-197.
10. Seeger, T., et al., *Restoration of soman-blocked neuromuscular transmission in human and rat muscle by the bispyridinium non-oxime MB327 in vitro.* Toxicology, 2012. **294**(2-3): p. 80-4.
11. Turner, S.R., et al., *Protection against nerve agent poisoning by a noncompetitive nicotinic antagonist.* Toxicol. Lett., 2011. **206**(1): p. 105-11.
12. Epstein, M., et al., *Molecular determinants of binding of non-oxime bispyridinium nerve agent antidote compounds to the adult muscle nAChR.* Toxicol. Lett., 2021. **340**: p. 114-122.
13. Kaiser, J., et al., *A novel binding site in the nicotinic acetylcholine receptor for MB327 can explain its allosteric modulation relevant for organophosphorus-poisoning treatment.* Toxicol. Lett., 2023. **373**: p. 160-171.
14. Sichler, S., et al., *Screening for new ligands of the MB327-PAM-1 binding site of the nicotinic acetylcholine receptor.* Toxicol. Lett., 2024. **394**: p. 23-31.
15. Leelananda, S.P. and S. Lindert, *Computational methods in drug discovery.* Beilstein J. Org. Chem., 2016. **12**: p. 2694-2718.
16. Metz, A., et al., *From determinants of RUNX1/ETO tetramerization to small-molecule protein-protein interaction inhibitors targeting acute myeloid leukemia.* J. Chem. Inf. Model., 2013. **53**(9): p. 2197-202.
17. Dick, M., et al., *Pyrazolidine-3,5-dione-based inhibitors of phosphoenolpyruvate carboxylase as a new class of potential C4 plant herbicides.* FEBS Lett., 2017. **591**(20): p. 3369-3377.
18. Porta, N., et al., *Small-molecule inhibitors of nisin resistance protein NSR from the human pathogen Streptococcus agalactiae.* Biorg. Med. Chem., 2019. **27**(20): p. 115079.
19. Huo, D., et al., *Discovery of Novel Epidermal Growth Factor Receptor (EGFR) Inhibitors Using Computational Approaches.* J. Chem. Inf. Model., 2022. **62**(21): p. 5149-5164.
20. Ha, H., et al., *Discovery of Novel CXCR2 Inhibitors Using Ligand-Based Pharmacophore Models.* J. Chem. Inf. Model., 2015. **55**(8): p. 1720-1738.
21. Menendez-Gonzalez, J.B., et al., *Ligand-based discovery of a novel GATA2 inhibitor targeting acute myeloid leukemia cells.* Frontiers in Drug Discovery, 2022. **2**.
22. Gunera, J., et al., *Structure-Based Discovery of Novel Ligands for the Orexin 2 Receptor.* J. Med. Chem., 2020. **63**(19): p. 11045-11053.
23. Park, H., et al., *Structure-Based Virtual Screening and De Novo Design to Identify Submicromolar Inhibitors of G2019S Mutant of Leucine-Rich Repeat Kinase 2.* Int. J. Mol. Sci., 2022. **23**(21): p. 12825.

24. Fink, E.A., et al., *Structure-based discovery of nonopioid analgesics acting through the α_{2A}-adrenergic receptor.* Science, 2022. **377**(6614): p. eabn7065.
25. Park, H., et al., *Structure-Based Virtual Screening and De Novo Design of PIM1 Inhibitors with Anticancer Activity from Natural Products.* Pharmaceuticals, 2021. **14**(3): p. 275.
26. Benod, C., et al., *Structure-based Discovery of Antagonists of Nuclear Receptor LRH-1 *.* Journal of Biological Chemistry, 2013. **288**(27): p. 19830-19844.
27. Song, Y., et al., *Discovery of non-peptide inhibitors of Plasmepsin II by structure-based virtual screening.* Bioorg. Med. Chem. Lett., 2013. **23**(7): p. 2078-2082.
28. Diao, Y., et al., *Discovery of Diverse Human Dihydroorotate Dehydrogenase Inhibitors as Immunosuppressive Agents by Structure-Based Virtual Screening.* J. Med. Chem., 2012. **55**(19): p. 8341-8349.
29. Song, C.-H., et al., *Structure-based Virtual Screening and Identification of a Novel Androgen Receptor Antagonist *.* J. Biol. Chem., 2012. **287**(36): p. 30769-30780.
30. Nitsche, V., et al., *MS Binding Assays with UNC0642 as reporter ligand for the MB327 binding site of the nicotinic acetylcholine receptor.* Toxicol. Lett., 2024. **392**: p. 94-106.
31. Eswar, N., et al., *Comparative protein structure modeling using Modeller.* Curr Protoc Bioinformatics, 2006. **Chapter 5**: p. Unit-5 6.
32. Gharpure, A., et al., *Agonist Selectivity and Ion Permeation in the α3β4 Ganglionic Nicotinic Receptor.* Neuron, 2019. **104**(3): p. 501-511.e6.
33. Morales-Perez, C.L., C.M. Noviello, and R.E. Hibbs, *X-ray structure of the human α4β2 nicotinic receptor.* Nature, 2016. **538**(7625): p. 411-415.
34. Hibbs, R.E., et al., *Structural determinants for interaction of partial agonists with acetylcholine binding protein and neuronal α7 nicotinic acetylcholine receptor.* The EMBO Journal, 2009. **28**(19): p. 3040-3051.
35. Walsh, R.M., et al., *Structural principles of distinct assemblies of the human α4β2 nicotinic receptor.* Nature, 2018. **557**(7704): p. 261-265.
36. Shen, M.Y. and A. Sali, *Statistical potential for assessment and prediction of protein structures.* Protein Sci., 2006. **15**(11): p. 2507-24.
37. Mulnaes, D. and H. Gohlke, *TopScore: Using Deep Neural Networks and Large Diverse Data Sets for Accurate Protein Model Quality Assessment.* J. Chem. Theory Comput., 2018. **14**(11): p. 6117-6126.
38. Sondergaard, C.R., et al., *Improved Treatment of Ligands and Coupling Effects in Empirical Calculation and Rationalization of pKa Values.* J. Chem. Theory Comput., 2011. **7**(7): p. 2284-95.
39. Olsson, M.H., et al., *PROPKA3: Consistent Treatment of Internal and Surface Residues in Empirical pKa Predictions.* J. Chem. Theory Comput., 2011. **7**(2): p. 525-37.
40. Schrödinger, *Maestro*. 2020, Schrödinger, LLC.: New York, NY, USA.
41. Chevillard, F., et al., *Binding-Site Compatible Fragment Growing Applied to the Design of beta2-Adrenergic Receptor Ligands.* J. Med. Chem., 2018. **61**(3): p. 1118-1129.
42. *QUACPAC 2.1.1.0*. 2020, OpenEye Scientific Software: Santa Fe, NM.
43. *OMEGA 4.1.0.0*. 2020, Openeye Scientific Software: Santa Fe, NM, USA.
44. Hawkins, P.C.D., et al., *Conformer Generation with OMEGA: Algorithm and Validation Using High Quality Structures from the Protein Databank and Cambridge Structural Database.* J. Chem. Inf. Model., 2010. **50**(4): p. 572-584.
45. Hawkins, P.C., A.G. Skillman, and A. Nicholls, *Comparison of shape-matching and docking as virtual screening tools.* J. Med. Chem., 2007. **50**(1): p. 74-82.
46. *ROCS 3.4.1.0*. OpenEye Scientific Software: Santa Fe, NM.
47. Chemical Computing Group, U., *Molecular Operating Environment (MOE)*. 2021: 1010 Sehrbooke St. West, Suite #910, Montreal, QC, Canada, H3A, 2R7.
48. Mellsted, H., et al., *2-phenyl-3H-imidazo [4, 5-B] pyridine derivates useful as inhibitors of mammalian tyrosine kinase ROR1 activity (WO/2016/124553)*, W.I.P. Organization, Editor. 2016.

49. Pauli, G.F., et al., *Importance of Purity Evaluation and the Potential of Quantitative 1H NMR as a Purity Assay.* J. Med. Chem., 2014. **57**(22): p. 9220-9231.
50. Cushman, M., et al., *Absolute Quantitative 1H NMR Spectroscopy for Compound Purity Determination.* J. Med. Chem., 2014. **57**(22): p. 9219-9219.
51. Vital, T., et al., *MS0621, a novel small-molecule modulator of Ewing sarcoma chromatin accessibility, interacts with an RNA-associated macromolecular complex and influences RNA splicing.* Front. Oncol., 2023. **13**: p. 1099550.
52. Hennequin, L.F., et al., *Quinazoline Derivatives as Angiogenesis Inhibitors (WO-2000047212-A1)*, W.I.P. Organization, Editor. 2000.
53. Ravez, S., et al., *Inhibition of tumor cell growth and angiogenesis by 7-Aminoalkoxy-4-aryloxy-quinazoline ureas, a novel series of multi-tyrosine kinase inhibitors.* Eur. J. Med. Chem., 2014. **79**: p. 369-381.
54. Irwin, J.J., et al., *ZINC20-A Free Ultralarge-Scale Chemical Database for Ligand Discovery.* J. Chem. Inf. Model., 2020. **60**(12): p. 6065-6073.
55. *OEDOCKING 4.0.0.0*. 2020, OpenEye Scientific Software: Santa Fe, NM, USA.
56. McGann, M., *FRED and HYBRID docking performance on standardized datasets.* J. Comput. Aided Mol. Des., 2012. **26**(8): p. 897-906.
57. McGann, M., *FRED Pose Prediction and Virtual Screening Accuracy.* J. Chem. Inf. Model., 2011. **51**(3): p. 578-596.
58. Schott-Verdugo, S. and H. Gohlke, *PACKMOL-Memgen: A Simple-To-Use, Generalized Workflow for Membrane-Protein-Lipid-Bilayer System Building.* J. Chem. Inf. Model., 2019. **59**(6): p. 2522-2528.
59. Jorgensen, W.L., et al., *Comparison of simple potential functions for simulating liquid water.* The Journal of Chemical Physics, 1983. **79**(2): p. 926-935.
60. Case, D.A., et al., *The Amber biomolecular simulation programs.* J. Comput. Chem., 2005. **26**(16): p. 1668-88.
61. Case, D.A., et al., *Amber 2022*. 2022, University of California: San Francisco.
62. Maier, J.A., et al., *ff14SB: Improving the Accuracy of Protein Side Chain and Backbone Parameters from ff99SB.* J. Chem. Theory Comput., 2015. **11**(8): p. 3696-3713.
63. Dickson, C.J., R.C. Walker, and I.R. Gould, *Lipid21: Complex Lipid Membrane Simulations with AMBER.* J. Chem. Theory Comput., 2022. **18**(3): p. 1726-1736.
64. Joung, I.S. and T.E. Cheatham, III, *Determination of Alkali and Halide Monovalent Ion Parameters for Use in Explicitly Solvated Biomolecular Simulations.* The Journal of Physical Chemistry B, 2008. **112**(30): p. 9020-9041.
65. Bayly, C.I., et al., *A well-behaved electrostatic potential based method using charge restraints for deriving atomic charges: the RESP model.* The Journal of Physical Chemistry, 1993. **97**(40): p. 10269-10280.
66. Wang, J., et al., *Automatic atom type and bond type perception in molecular mechanical calculations.* Journal of Molecular Graphics and Modelling, 2006. **25**(2): p. 247-260.
67. M. J. Frisch, G.W.T., H. B. Schlegel, G. E. Scuseria,, et al., *Gaussian16*. 2016, Gaussian Inc.: Wallingford CT.
68. Charman, S.A., et al., *An in vitro toolbox to accelerate anti-malarial drug discovery and development.* Malaria Journal, 2020. **19**(1): p. 1.
69. Roe, D.R. and T.E. Cheatham, 3rd, *PTRAJ and CPPTRAJ: Software for Processing and Analysis of Molecular Dynamics Trajectory Data.* J. Chem. Theory Comput., 2013. **9**(7): p. 3084-95.
70. *OMEGA 4.1.1.1*. 2021, Openeye Scientific Software: Santa Fe, NM, USA.
71. *Schrödinger Release 2022-2: QikProp*. 2022, Schrödinger, LLC: New York, NY.
72. Baell, J.B. and G.A. Holloway, *New Substructure Filters for Removal of Pan Assay Interference Compounds (PAINS) from Screening Libraries and for Their Exclusion in Bioassays.* J. Med. Chem., 2010. **53**(7): p. 2719-2740.
73. Greene, N., et al., *Knowledge-based expert systems for toxicity and metabolism prediction: DEREK, StAR and METEOR.* SAR QSAR Environ Res, 1999. **10**(2-3): p. 299-314.

74. Pettersen, E.F., et al., *UCSF Chimera—A visualization system for exploratory research and analysis.* J. Comput. Chem., 2004. **25**(13): p. 1605-1612.
75. Rappengluck, S., et al., *Synthesis of a Series of Non-Symmetric Bispyridinium and Related Compounds and Their Affinity Characterization at the Nicotinic Acetylcholine Receptor.* ChemMedChem, 2018. **13**(24): p. 2653-2663.
76. Rappengluck, S., et al., *Synthesis of a Series of Structurally Diverse MB327 Derivatives and Their Affinity Characterization at the Nicotinic Acetylcholine Receptor.* ChemMedChem, 2018. **13**(17): p. 1806-1816.
77. Zieliński, W. and A. Kudelko, *A study concerning the synthesis, basicity and hydrolysis of 4-amino-2-(N,N-diethylamino)quinazoline derivatives.* J. Heterocycl. Chem., 2002. **39**(6): p. 1289-1292.
78. Armarego, W.L.F., *Quinazolines*, in *Adv. Heterocycl. Chem.*, A.R. Katritzky, Editor. 1963, Academic Press. p. 253-309.
79. Albert, A., R. Goldacre, and J. Phillips, *455. The strength of heterocyclic bases.* Journal of the Chemical Society (Resumed), 1948(0): p. 2240-2249.
80. Bernauer, T., et al., *Synthesis and Biological Evaluation of Novel MB327 Analogs as Resensitizers for Desensitized Nicotinic Acetylcholine Receptors after Intoxication with Nerve Agents.* bioRxiv, 2024: p. 2024.02.09.579646.
81. Yoshida, K. and M. Taguchi, *Reaction of N-substituted cyclic amines with 2,4-dichloroquinazoline, 2,4-dichloropyrimidine, and its 5-methyl derivative.* J. Chem. Soc., Perkin Trans. 1, 1992(7): p. 919-922.
82. Lipinski, C.A., et al., *Experimental and computational approaches to estimate solubility and permeability in drug discovery and development settings.* Adv. Drug Del. Rev., 1997. **23**(1): p. 3-25.
83. Tasler, S., et al., *Substituted 2-arylbenzothiazoles as kinase inhibitors: Hit-to-lead optimization.* Biorg. Med. Chem., 2009. **17**(18): p. 6728-6737.
84. Liu, F., et al., *Optimization of Cellular Activity of G9a Inhibitors 7-Aminoalkoxy-quinazolines.* J. Med. Chem., 2011. **54**(17): p. 6139-6150.
85. Wan, Z.-K., et al., *The Scope and Mechanism of Phosphonium-Mediated SNAr Reactions in Heterocyclic Amides and Ureas.* The Journal of Organic Chemistry, 2007. **72**(26): p. 10194-10210.
86. Harris, C.S., J.G. Kettle, and E.J. Williams, *Facile synthesis of 7-amino anilinoquinazolines via direct amination of the quinazoline core.* Tetrahedron Lett., 2005. **46**(43): p. 7381-7384.
87. Niessen, K.V., et al., *Affinities of bispyridinium non-oxime compounds to [(3)H]epibatidine binding sites of Torpedo californica nicotinic acetylcholine receptors depend on linker length.* Chem. Biol. Interact., 2013. **206**(3): p. 545-54.
88. Galzi, J.L., et al., *Identification of calcium binding sites that regulate potentiation of a neuronal nicotinic acetylcholine receptor.* EMBO J., 1996. **15**(21): p. 5824-32.
89. Noviello, C.M., et al., *Structure and gating mechanism of the alpha7 nicotinic acetylcholine receptor.* Cell, 2021. **184**(8): p. 2121-2134 e13.

Declaration of Competing Interest

The authors declare that they have no known competing financial interests or personal relationships that could have appeared to influence the work reported in this paper.

Graphical abstract

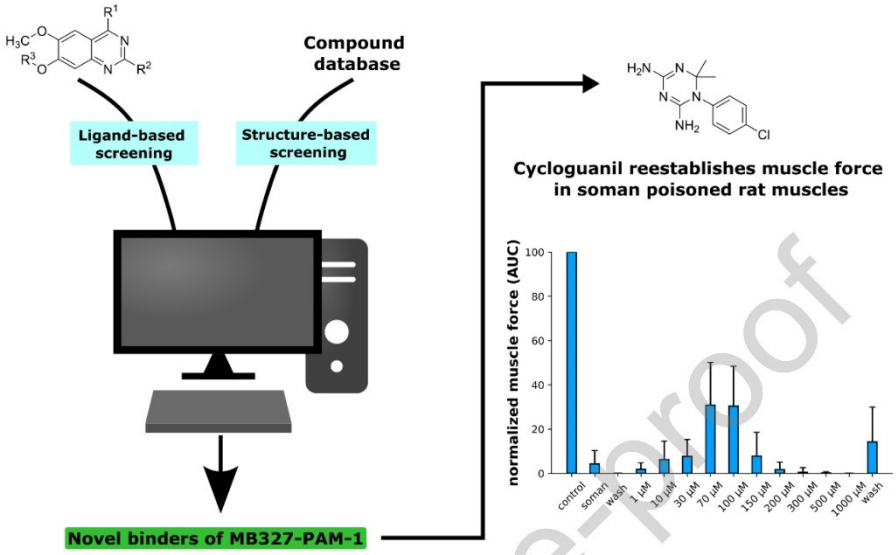

Highlights

- Identification of novel analogs of UNC0646 and new chemotypes binding to MB327-PAM-1.
- Cycloguanil can reestablish rat diaphragm muscle force after soman poisoning.
- Molecular dynamics simulations shed light on the binding mode of cycloguanil.

Supporting Information

Identification of ligands binding to MB327-PAM-1, a binding pocket relevant for resensitization of nAChRs

Jesko Kaiser[1], Christoph G.W. Gertzen[1], Tamara Bernauer[2], Valentin Nitsche[2], Georg Höfner[2], Karin V. Niessen[3], Thomas Seeger[3], Franz F. Paintner[2], Klaus T. Wanner[2], Dirk Steinritz[3], Franz Worek[3], Holger Gohlke[1,4,*]

[1]Institute for Pharmaceutical and Medicinal Chemistry, Heinrich Heine University Düsseldorf, Düsseldorf, Germany

[2]Department of Pharmacy – Center for Drug Research, Ludwig-Maximilians-Universität München, München, Germany

[3]Bundeswehr Institute of Pharmacology and Toxicology, München, Germany

[4]Institute of Bio- and Geosciences (IBG-4: Bioinformatics), Forschungszentrum Jülich, Jülich, Germany

Table of Content

Supplemental Figures

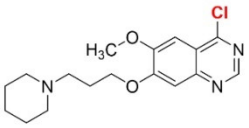

Buchwald-Hartwig
Heck
Negishi
Stille

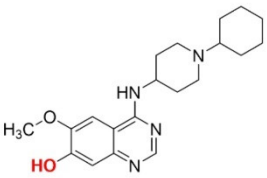

Mitsunobu

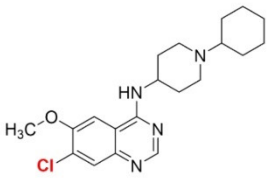

Buchwald-Hartwig
Heck
Negishi
Stille
Suzuki

Figure S1: Building blocks of PTMD01-0004 (**2a**) for the generation of a virtual database. For each building block, the stated virtual syntheses have been performed with building blocks available on MolPort (https://molport.com) using PINGUI [1]. Functional groups that participate in the respective reaction are shown in red.

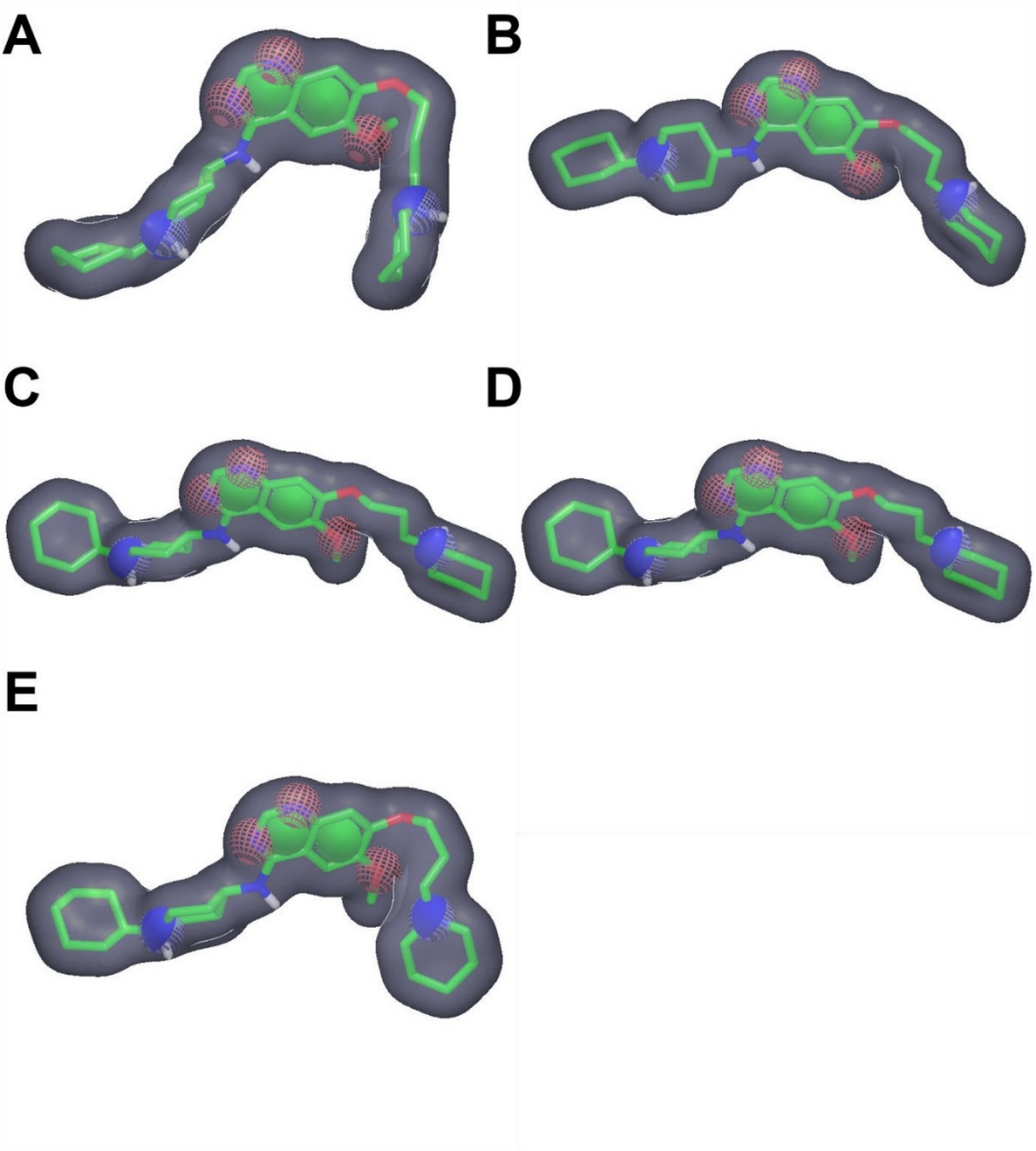

Figure S2: Pharmacophore models used for database filtering during template-based docking. Conformations of PTMD01-0004 (**2a**) (green) are shown as sticks between the **A)** α- and δ-, **B)** δ- and β-, **C)** β- and α-, **D)** α- and γ-, and **E)** γ- and α-subunits. Colored elements indicate pharmacophore filters: the grey surface indicates the ligand surface, green circles indicate aromatic systems, blue circles indicate hydrogen bond donor cations, and red circles indicate hydrogen bond acceptors. Figures were generated using OpenEye vROCS [2].

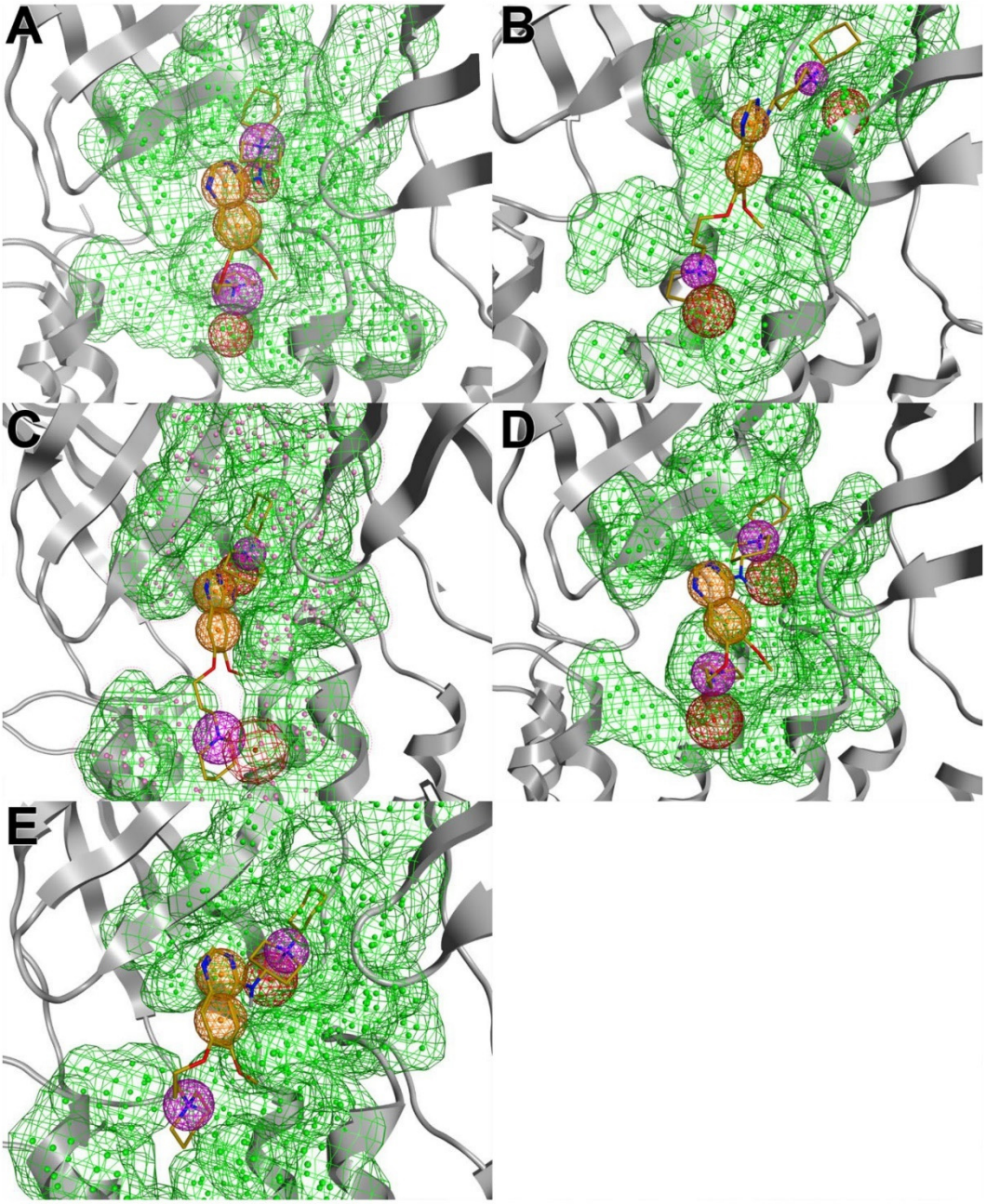

Figure S3: Binding mode of and pharmacophore model for template-based docking based on PTMD01-0004 (**2a**) (gold) shown between the **A)** α- and δ-, **B)** δ- and β-, **C)** β- and α-, **D)** α- and γ-, and **E)** γ- and α-subunits. Colored mesh areas indicate features of the pharmacophore filter: green area indicates the surface of the receptor where no atoms of the ligands are allowed to overlap, orange circles indicate the presence of an aromatic system, purple circles indicate the presence of a cation donor, and red circles indicate the direction of the hydrogen bond donor orientation. Figures were generated using Chemical Computing Group MOE [3].

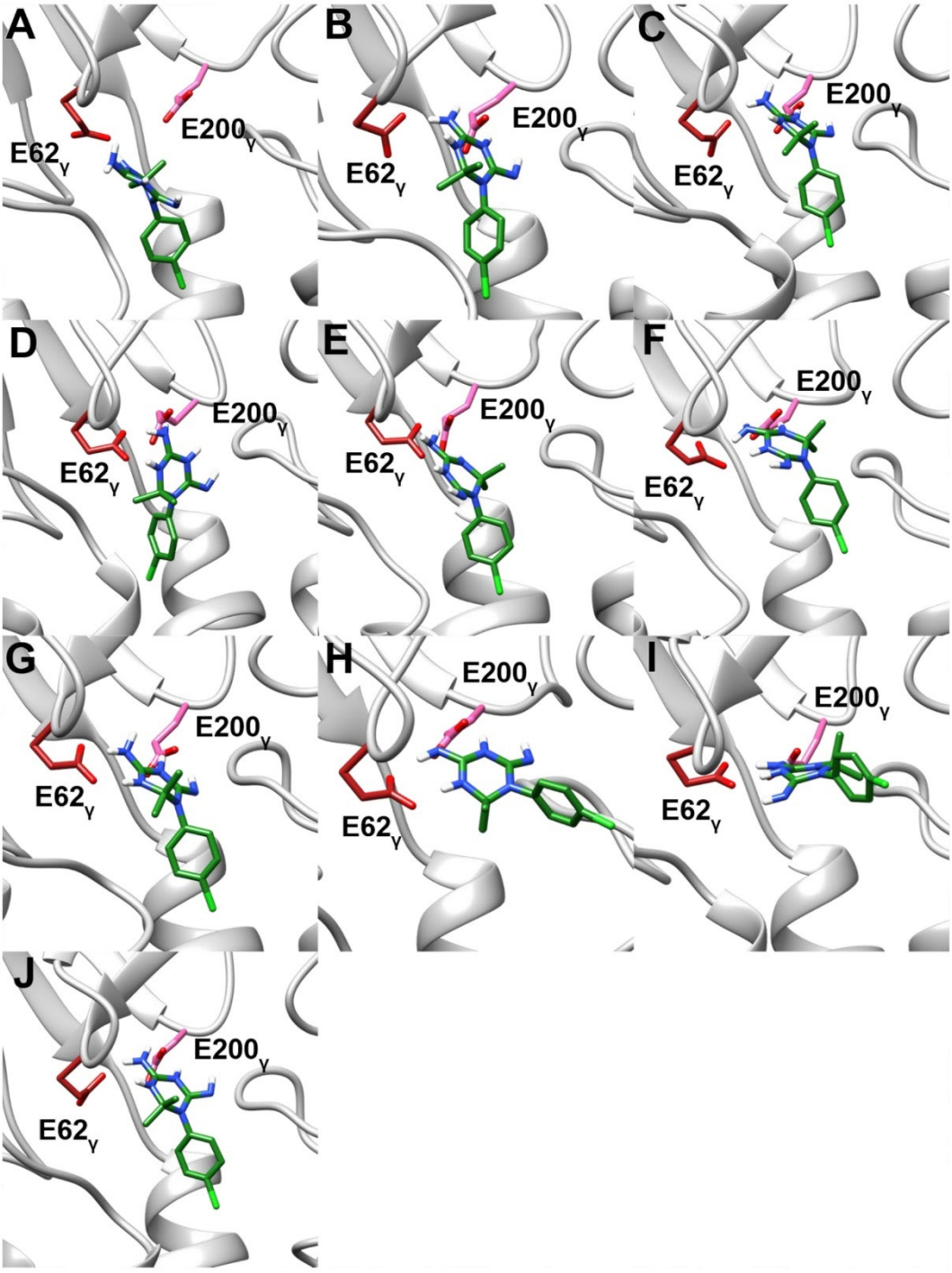

Figure S4: Representative binding modes of cycloguanil in MD simulations starting from the docked binding mode after clustering using the *k-means* algorithm as implemented in CPPTRAJ [4]. **A)** Only in the largest cluster (containing 18.3% of all frames) cycloguanil is not interacting with $E200_{\gamma}$. In the **B)** second (containing 14.1% of all frames), **C)** third (containing 12.4 % of all frames, **D)** fourth (containing 10.9% of all frames), **E)** fifth (containing 10.8% of all frames), **F)** sixth (containing 10.5% of all frames), **G)** seventh (containing 10.1% of all frames), **H)** eight (containing 6.7% of all frames), **I)** ninth (containing 3.6% of all frames), and **J)** tenth (containing 2.5% of all frames) largest cluster, cycloguanil is interacting with $E200_{\gamma}$ and $E62_{\gamma}$.

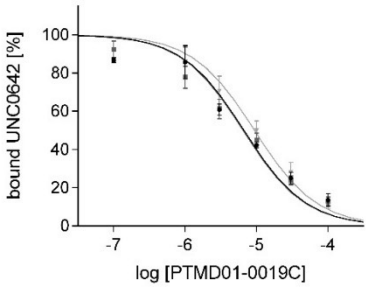

Figure S5: Competition curves obtained for PTMD01-0019C (**1a**) in UNC0642 MS Binding Assays. Data points (mean ± SD, *n* = 3) represent the specific binding of UNC0642.

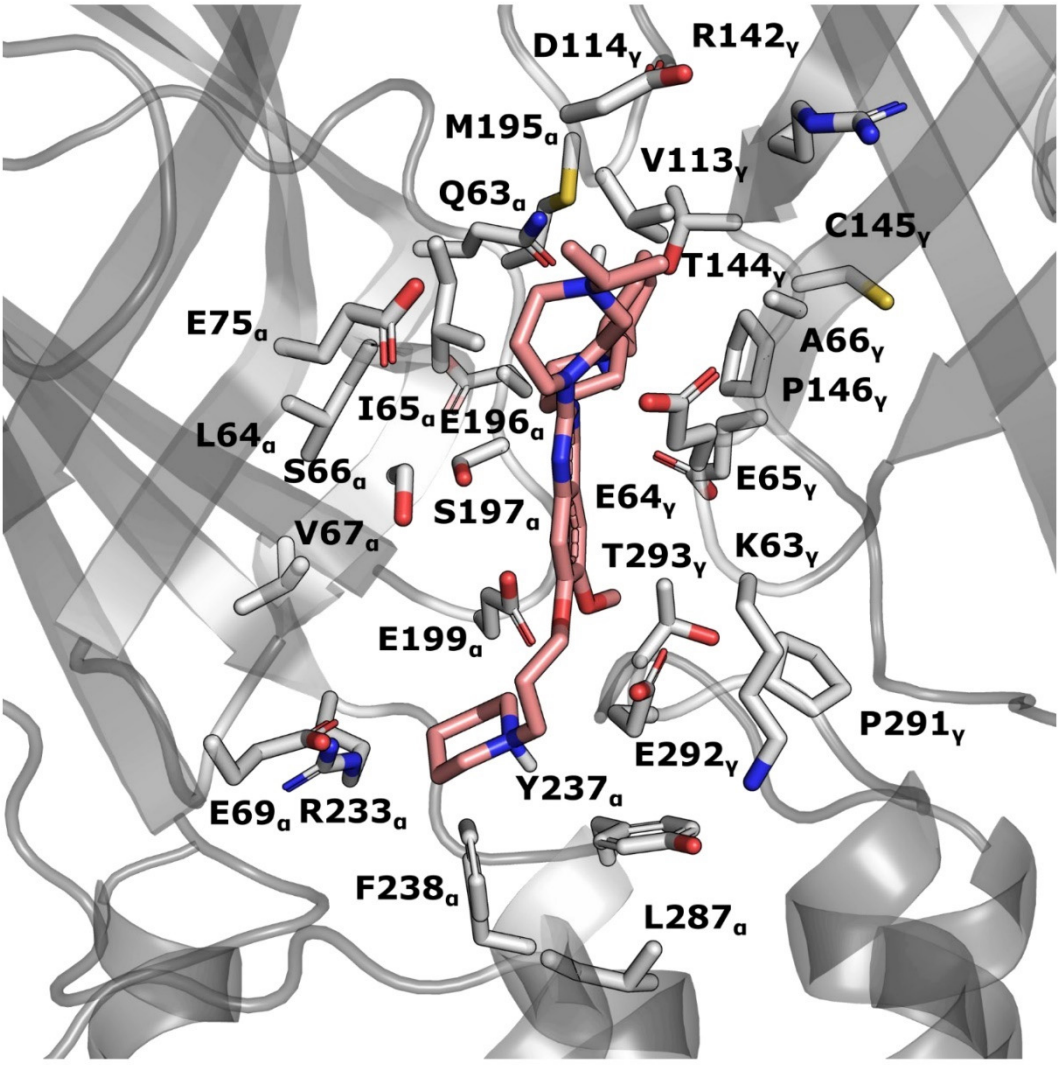

Figure S6: Amino acids within 5 Å of UNC0646 in the recently proposed binding mode of UNC0646 [5].

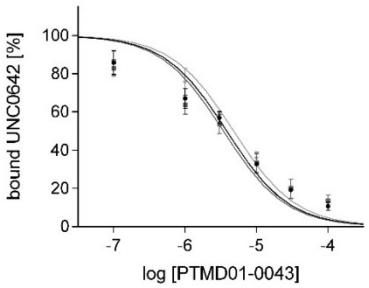

Figure S7: Competition curves obtained for PTMD01-0043 (**2g**) in UNC0642 MS Binding Assays. Data points (mean ± SD, *n* = 3) represent the specific binding of UNC0642.

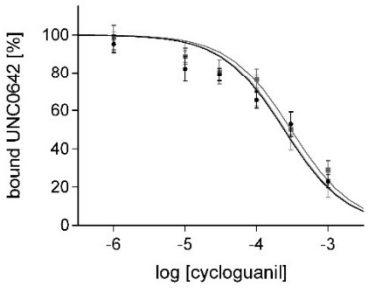

Figure S8: Competition curves obtained for cycloguanil (**6**) in UNC0642 MS Binding Assays. Data points (mean ± SD, *n* = 3) represent the specific binding of UNC0642.

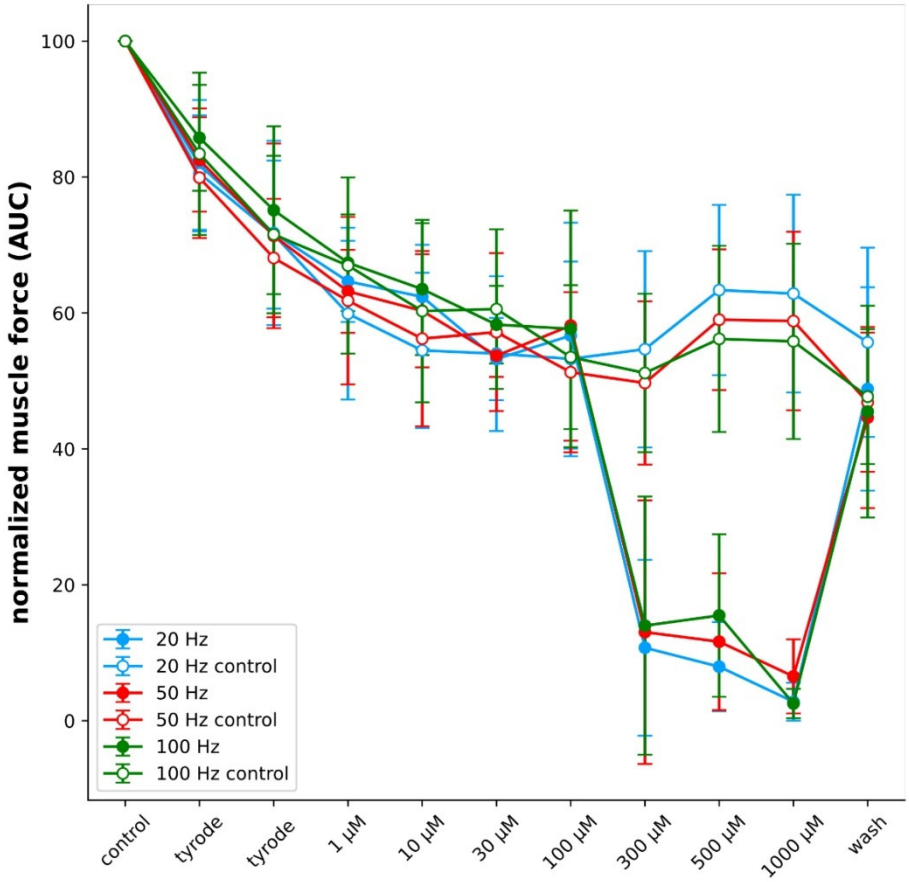

Figure S9: Normalized rat muscle force in the presence of increasing cycloguanil (**6**) concentrations and in the absence of cycloguanil (**6**) (control) during indirect electric field stimulations of 20, 50, and 100 Hz. Error bars indicate the standard deviation (*n* is between 3 and 13).

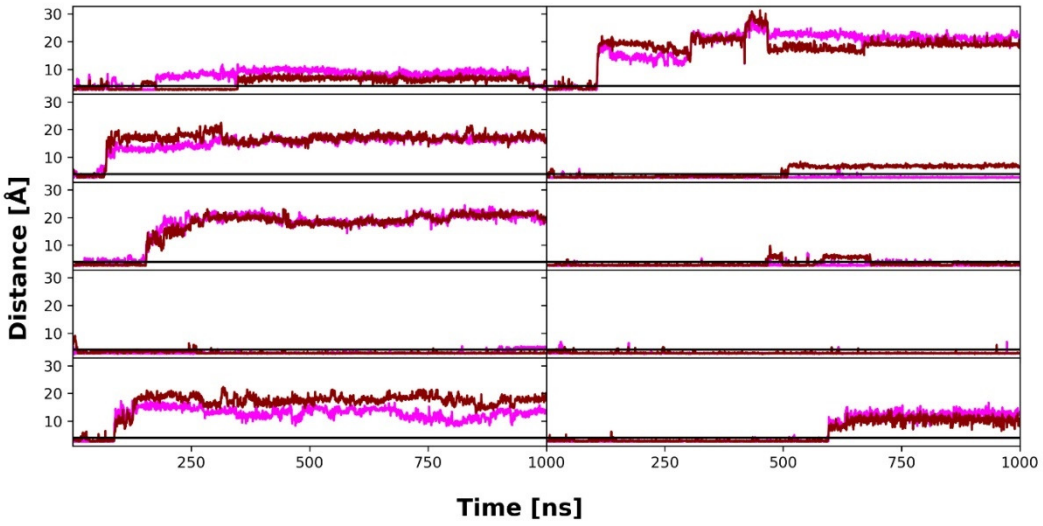

Figure S10: Distance of nitrogens that can act as hydrogen bond donors of cycloguanil to side chain oxygens of $E62_{\gamma}$ (pink) and $E200_{\gamma}$ (dark red) during 10 replicas of unbiased MD simulations.

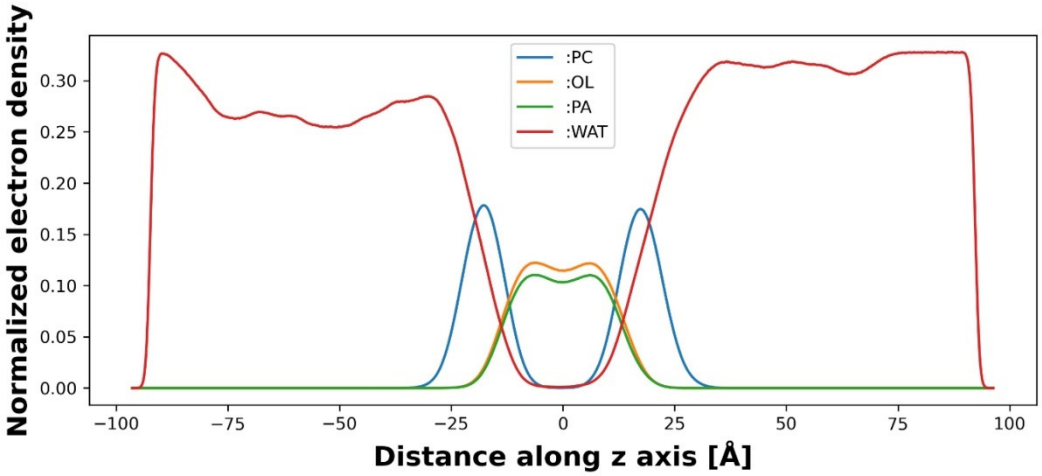

Figure S11: Normalized (number of electrons per volume [e^{-}/Å^3]) electron density of membrane components and water averaged over all 10 replicas of 1 µs long MD simulations. The electron density is plotted against the z-coordinate, which is parallel to the membrane normal. The membrane is centered at 0 Å for phosphatidylcholine (:PC), oleic acid (:OL), palmitoyl acid (:PA), and water (:WAT).

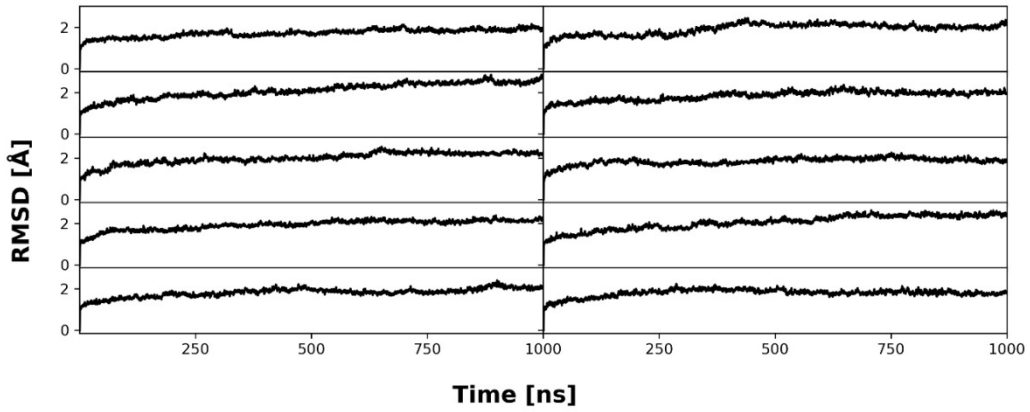

Figure S12: Backbone (C, CA, N) RMSD of nAChR during 10 replicas of 1 µs long MD simulations with respect to the first frame of the production run.

Supplemental Tables

Table S1: List of commercially obtained test compounds.

#	Compound	Salt	Purity	Supplier
1	Bunazosin	-	≥ 95%	Angene (Honk Kong, China)
2	C-021	-	≥ 97%	BIONET – KeyOrganics Ltd (Cornwall, United Kingdom)
3	Cycloguanil	HCl	≥ 95%	Otava Ltd (Kiew, Ukraine)
4	MS012	-	≥ 90%	TimTec, LLC (Newark, United States)
5	PTMD01-0019C	-	≥ 85%	ChemBridge Corporation (San Diego, United States)
6	PTMD01-0020C	-	≥ 90%	Enamine Ltd (Kiew, Ukraine)
7	PTMD01-0021C	-	≥ 85%	ChemBridge Corporation (San Diego, United States)
8	PTMD01-0022C	-	≥ 85%	ChemBridge Corporation (San Diego, United States)
9	PTMD01-0023C	-	≥ 90%	Enamine Ltd (Kiew, Ukraine)
10	PTMD01-0024C	-	≥ 85%	ChemBridge Corporation (San Diego, United States)
11	PTMD01-0025C	-	≥ 90%	Enamine Ltd (Kiew, Ukraine)
12	PTMD99-0001C	HI	≥ 90%	Enamine Ltd (Kiew, Ukraine)
13	PTMD99-0002C	-	≥ 90%	UkrOrgSynthesis Ltd. (Kiew, Ukraine)
14	PTMD99-0004C	2 HCl	≥ 85%	ChemBridge Corporation (San Diego, United States)
15	PTMD99-0005C	-	≥ 90%	ChemBridge Corporation (San Diego, United States)
16	PTMD99-0006C	-	≥ 85%	ChemBridge Corporation (San Diego, United States)
17	PTMD99-0008C	H_2SO_4	≥ 90%	Vitas-M Laboratory Ltd (Causeway Bay, Hong Kong)
18	PTMD99-0009C	HBr	≥ 90%	Enamine Ltd (Kiew, Ukraine)
19	PTMD99-0010C	2 HCl	≥ 85%	ChemBridge Corporation (San Diego, United States)
20	PTMD99-0011C	-	≥ 85%	ChemBridge Corporation (San Diego, United States)
21	PTMD99-0013C	HCl	≥ 90%	ChemBridge Corporation (San Diego, United States)
22	PTMD99-0014C	HCl	≥ 90%	Enamine Ltd (Kiew, Ukraine)
23	PTMD99-0015C	-	≥ 85%	ChemBridge Corporation (San Diego, United States)
24	PTMD99-0016C	-	≥ 85%	ChemBridge Corporation (San Diego, United States)
25	PTMD99-0020C	-	≥ 85%	ChemBridge Corporation (San Diego, United States)
26	PTMD99-0021C	-	≥ 85%	ChemBridge Corporation (San Diego, United States)
27	PTMD99-0023C	2 HCl	≥ 85%	ChemBridge Corporation (San Diego, United States)
28	PTMD99-0024C	2 HCl	≥ 85%	ChemBridge Corporation (San Diego, United States)
29	PTMD99-0025C	2 HCl	≥ 85%	ChemBridge Corporation (San Diego, United States)
30	PTMD99-0026C	2 HCl	≥ 85%	ChemBridge Corporation (San Diego, United States)
31	PTMD99-0028C	2 HCl	≥ 85%	ChemBridge Corporation (San Diego, United States)
32	PTMD99-0029C	2 HCl	≥ 85%	ChemBridge Corporation (San Diego, United States)
33	PTMD99-0031C	2 HCl	≥ 85%	ChemBridge Corporation (San Diego, United States)
34	PTMD99-0032C	HCl	≥ 90%	Maybridge Ltd (Cornwall, United Kingdom)
35	PTMD99-0035C	HCl	≥ 90%	Otava Ltd (Kiew, Ukraine)
36	PTMD99-0036C	HCl	≥ 90%	ChemBridge Corporation (San Diego, United States)
37	PTMD99-0038C	HCl	≥ 95%	Otava Ltd (Kiew, Ukraine)
38	PTMD99-0041C	HCl	≥ 85%	ChemBridge Corporation (San Diego, United States)
39	PTMD99-0044C	HCl	≥ 90%	Maybridge Ltd (Cornwall, United Kingdom)
40	PTMD99-0045C	HCl	≥ 90%	Maybridge Ltd (Cornwall, United Kingdom)
41	UNC0379	-	≥ 98%	TargetMol (Boston, United States)
42	ZT-12-037-01	-	≥ 98%	TargetMol (Boston, United States)

Table S2: All analogs of UNC0646 tested for affinity to MB327-PAM-1 in nAChR determined in MS Binding Assays based on a two-dimensional similarity search.

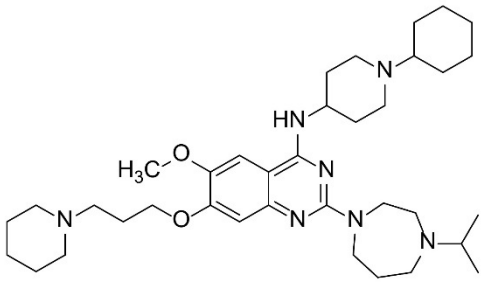

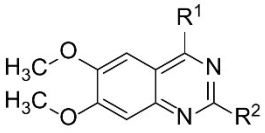

UNC0646
pK_i = 5.83 ± 0.05[a]

Remaining reporter ligand binding: 21 ± 3 %[b]

Compound	R^1	R^2	Remaining reporter ligand binding [%][b]
C-021	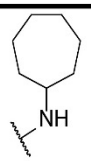	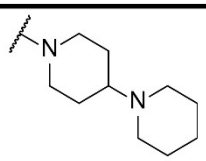	63 ± 2
ZT-12-037-01	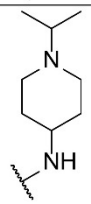	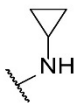	66 ± 5
MS012	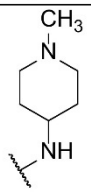	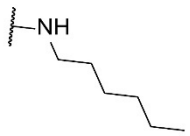	83 ± 6
UNC0379	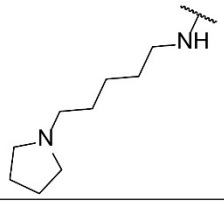		59 ± 4
Bunazosin		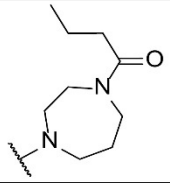	90 ± 7

PTMD01-0019C		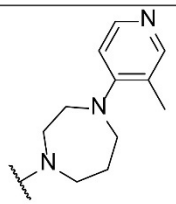	47 ± 3
PTMD01-0020C		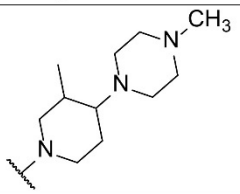	73 ± 7
PTMD01-0021C		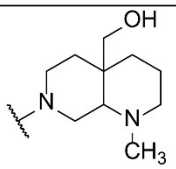	87 ± 2
PTMD01-0022C		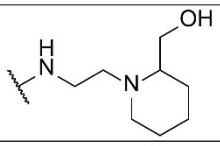	108 ± 10
PTMD01-0023C		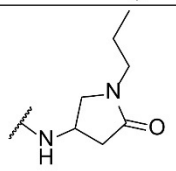	98 ± 3
PTMD01-0024C		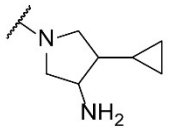	83 ± 4
PTMD01-0025C		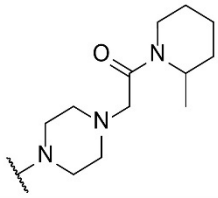	81 ± 5

[a] The pK_i value of UNC0646 has been reported in ref. [6].

[b] Characterized by UNC0642 MS Binding Assays; Percentage of remaining reporter ligand binding in the presence of test compounds as compared to 100% reporter ligand binding in the absence of a competitor. Results are based on thirty measurements for UNC0646 and three measurements for all other compounds at a test compound concentration of 10 µM and a reporter ligand concentration of 1 µM. Mean and standard deviation are displayed.

Table S3: Sequence similarity between the *Torpedo* and human muscle-type nAChR.[a]

α - subunit		β - subunit		δ - subunit		γ - subunit		ε - subunit
Torpedo	human	*Torpedo*	human	*Torpedo*	human	*Torpedo*	human	human
Q63	Q	N	Q	N	N	N	N	N
L64	L	L	L	L	L	L	L	L
I65	I	L	I	I	I	I	I	I
S66	N	I	S	S	S	S	S	S
V67	V	L	L	L	L	L	L	L
E69	E	E	E	E	E	E	E	E
E75	T	T	S	T	T	T	T	T
M195	M	T	I	T	T	T	T	T
E196	E	E	E	E	E	E	E	E
S197	S	N	N	N	N	N	N	N
E199	E	Q	Q	E	E	E	E	E
R233	R	R	R	R	R	R	R	R
Y237	Y	F	F	F	F	F	F	F
F238	F	Y	Y	Y	Y	Y	Y	Y
L287	L	K	K	R	R	K	K	K
V	V	K	K	T	V	K63	R	K
N	N	I	D	D	E	E64	E	E
Q	Q	E	E	E	E	E65	E	E
I	I	E	E	T	T	A66	A	T
A	A	N	N	N	N	V113	V	I
D	D	D	D	D	D	D114	D	D
K	K	R	R	R	R	R142	R	R
Y	Y	S	S	S	S	T144	A	V
C	C	C	C	C	C	C145	C	C
E	E	T	S	P	P	P146	S	A
P	P	P	P	P	P	P291	P	P
S	S	E	E	E	A	E292	E	E
T	T	T	T	T	T	T293	T	T

[a] Numbered amino acids are also shown in Figure 2. Amino acid differences between *Torpedo* and human muscle-type nAChR are colored blue for identical chemical properties and orange for deviating chemical properties.

Table S4: Results of affinity testing to MB327-PAM-1 in nAChR determined in MS Binding Assays of initial compounds ordered based on structure-based screening.

Name	Structure	Remaining reporter ligand binding [%][a]
PTMD99-0001C (**3**)	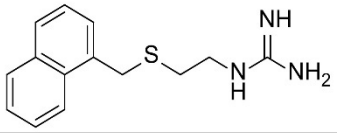	88 ± 5
PTMD99-0002C	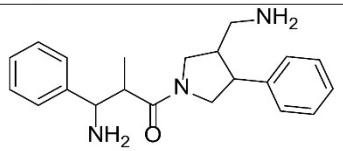	101 ± 9
PTMD99-0004C	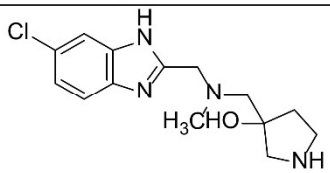	92 ±7
PTMD99-0005C	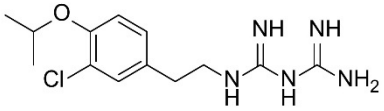	101 ± 3
PTMD99-0006C (**13**)	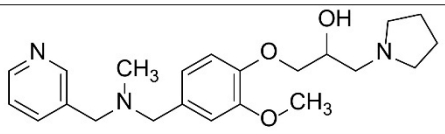	93 ± 7
PTMD99-0008C	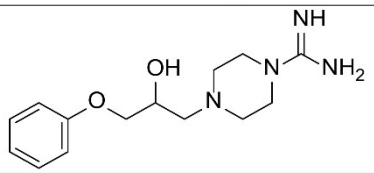	95 ± 4
PTMD99-0009C	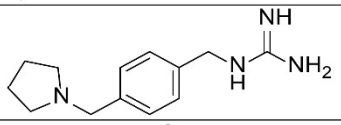	92 ± 9
PTMD99-0010C (**14**)	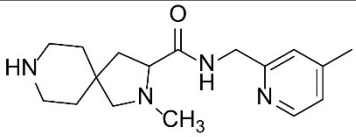	96 ± 5
PTMD99-0011C	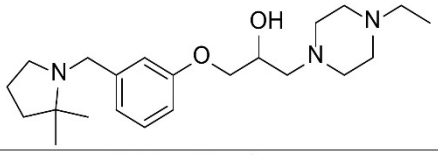	95 ± 7
PTMD99-0013C	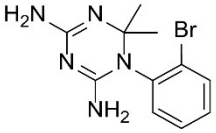	101 ± 6

PTMD99-0014C (**15**)	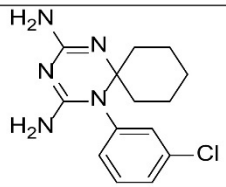	94 ± 6
PTMD99-0015C	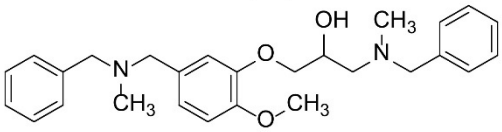	98 ± 8

[a] Characterized by UNC0642 MS Binding Assays; Percentage of remaining reporter ligand binding in the presence of test compounds as compared to 100% reporter ligand binding in the absence of a competitor. If not stated otherwise, results are based on three measurements at a test compound concentration of 10 µM and a reporter ligand concentration of 1 µM. Mean and standard deviation are displayed.

Table S5: Results of affinity testing of compounds analogous to the best hits from the initially ordered compounds based on structure-based screening.

Name	Structure	Remaining reporter ligand binding [%][a]
PTMD99-0016C (**4**)	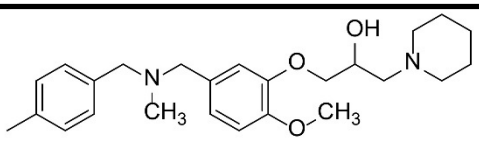	78 ± 3
PTMD99-0020C (**16**)	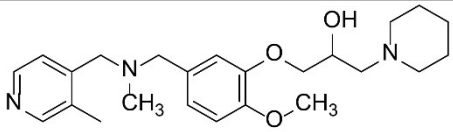	97 ± 4
PTMD99-0021C	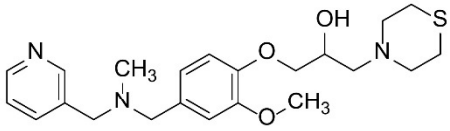	107 ± 11
PTMD99-0023C (**17**)	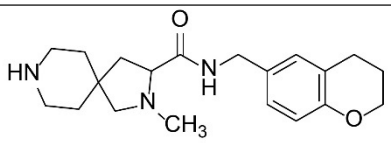	108 ± 4
PTMD99-0024C (**18**)	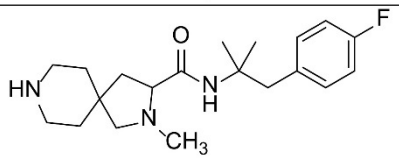	99 ± 6
PTMD99-0025C (**19**)	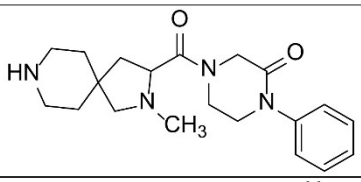	100 ± 6
PTMD99-0026C (**5**)	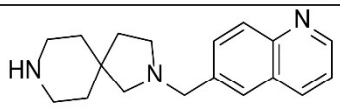	90 ± 5
PTMD99-0028C (**20**)	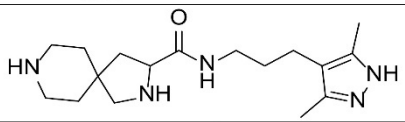	101 ± 7
PTMD99-0029C	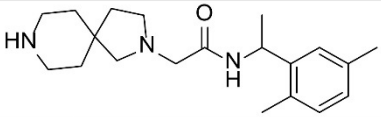	98 ± 4
PTMD99-0031C (**21**)	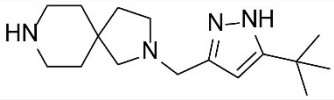	101 ± 8
PTMD99-0032C (**22**)	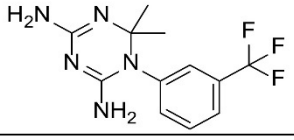	98 ± 6

PTMD99-0035C (**23**)	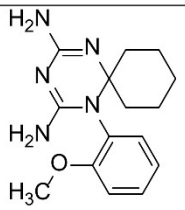	109 ± 8
PTMD99-0036C (**24**)	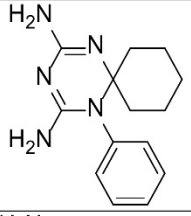	93 ± 4
PTMD99-0038C (**25**)	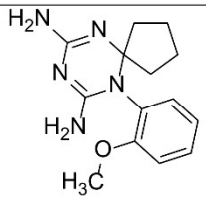	100 ± 4
Cycloguanil (**6**)	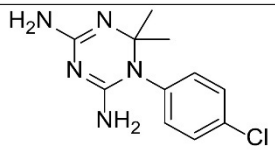	76 ± 3
PTMD99-0041C (**26**)	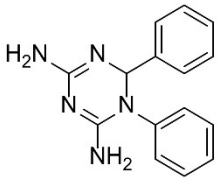	81 ± 3
PTMD99-0044C (**27**)	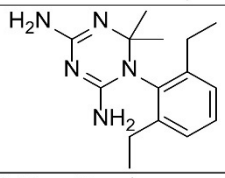	106 ± 6
PTMD99-0045C (**28**)	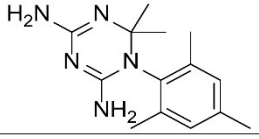	95 ± 8

[a] Characterized by UNC0642 MS Binding Assays; Percentage of remaining reporter ligand binding in the presence of test compounds as compared to 100% reporter ligand binding in the absence of a competitor. If not stated otherwise, results are based on three measurements at a test compound concentration of 10 µM and a reporter ligand concentration of 1 µM. Mean and standard deviation are displayed.

Table S6: Restoration of muscle force in soman-inhibited rat muscles after cyclouanil (**6**) treatment.[a]

	20 Hz			50 Hz			100 Hz		
	Mean [%]	SD [%]	n	Mean [%]	SD [%]	n	Mean [%]	SD [%]	n
control	100.00	0.00	27	100.00	0.00	27	100.00	0.00	27
soman	4.30	6.02	27	3.86	8.36	27	4.51	8.95	27
wash	0.00	0.00	27	0.00	0.00	27	0.00	0.00	27
1 µM	1.86	2.91	13	0.64	1.29	13	0.40	1.00	13
10 µM	6.20	8.40	18	0.82	1.28	18	0.25	0.56	18
30 µM	7.66	7.64	5	1.38	2.34	5	1.14	2.51	5
70 µM	30.87	19.23	5	2.76	3.51	5	0.68	1.32	5
100 µM	30.42	18.04	27	4.68	4.76	27	1.29	2.72	27
150 µM	7.78	10.79	9	0.85	1.33	9	0.28	0.57	9
200 µM	1.69	3.35	4	0.23	0.41	4	0.00	0.00	4
300 µM	0.51	2.09	17	0.51	1.69	17	0.71	2.44	17
500 µM	0.24	0.53	5	1.37	3.05	5	1.67	3.73	5
1000 µM	0.00	0.00	5	0.73	1.62	5	1.05	2.35	5
wash	14.30	15.66	27	2.43	3.89	27	0.39	1.44	27

[a] For the stimulation frequencies of 20, 50, and 100 Hz, the mean muscle force restoration, the standard deviation (SD), and the number of experiments (*n*) are displayed at each testing point.

Table S7: Breakdown of the toxicological alert count of the best screening hits.[a]

Compound	HERG channel inhibition *in vitro* mammal alert count	Mutagenicity *in vitro* bacterium alert count	Phospho-lipidosis mammal alert count	Androgen receptor modulation mammal alert count	Mutagenicity *in vivo* mammal alert count	Nephrotoxicity mammal alert count
UNC0646	2	1	1	0	0	0
PTMD01-0050 (**1k**)	1	1	0	0	0	0
PTMD01-0043 (**2g**)	2	1	1	0	0	0
PTMD99-0001C (**3**)	0	0	0	0	0	0
PTMD99-0016C (**4**)	2	0	0	0	0	0
PTMD99-0026C (**5**)	1	1	0	1	1	0
Cycloguanil (**6**)	0	0	0	0	0	1

[a] Predictions where no compound displays alert counts (Skin sensitization mammal alert count, Teratogenicity mammal alert count) are not shown as a column.

Analytical Data

6-Methoxy-2-(piperidin-1-yl)-7-[3-(piperidin-1-yl)propoxy]-*N*-[5-(pyrrolidin-1-yl)pentyl]quinazolin-4-amine (1k): mp.: 54 °C. R_f = 0.34 [10% 3 M NH_3 (in MeOH) in CH_2Cl_2]. IR (film): $\tilde{\nu}$ = 2935, 1581, 1493, 1244, 754 cm^{-1}. ^1H NMR (500 MHz, CD_2Cl_2): δ = 1.37-1.47 (m, 2 H, CH_2CH$_2$CH$_2$NCH$_2$CH$_2$CH$_2$O), 1.48-1.55 (m, 2 H, CH_2CH$_2$CH$_2$NH), 1.55-1.61 (m, 8 H, CH$_2$CH_2CH$_2$NC, CH$_2$CH_2CH$_2$NCH$_2$CH$_2$CH$_2$O), 1.62-1.70 (m, 4 H, CH_2CH$_2$CH$_2$NC, CH_2CH$_2$CH$_2$CH$_2$NH), 1.74 (p, J = 7.0 Hz, 2 H, CH_2CH$_2$NH), 1.80-1.89 [m, 4 H, CH_2CH$_2$N(CH$_2$)$_5$NH], 2.00 (p, J = 6.9 Hz, 2 H, CH_2CH$_2$O), 2.22-2.42 (m, 4 H, CH_2NCH$_2$CH$_2$CH$_2$O), 2.42-2.48 (m, 2 H, CH_2CH$_2$CH$_2$O), 2.57-2.66 [m, 2 H, CH_2(CH$_2$)$_4$NH], 2.66-2.84 [m, 4 H, CH_2N(CH$_2$)$_5$NH], 3.53-3.64 (m, 2 H, CH_2NH), 3.73-3.84 (m, 4 H, CH$_2$NC), 3.89 (s, 3 H, CH$_3$O), 4.11 (t, J = 6.7 Hz, 2 H, CH$_2$O), 5.77 (s, 1 H, NH), 6.84 (s, 1 H, C*H*COCH$_2$), 6.98 (s, 1 H, C*H*COCH$_3$). ^{13}C NMR (126 MHz, CD_2Cl_2): δ = 23.82 [*C*H$_2$CH$_2$N(CH$_2$)$_5$NH], 24.94 (*C*H$_2$CH$_2$CH$_2$NCH$_2$CH$_2$CH$_2$O), 25.17 (*C*H$_2$CH$_2$CH$_2$NH), 25.57 (*C*H$_2$CH$_2$CH$_2$NC), 26.41 (*C*H$_2$CH$_2$NCH$_2$CH$_2$CH$_2$O)*, 26.46 (*C*H$_2$CH$_2$NC)*, 27.05 (*C*H$_2$CH$_2$O), 28.02 [*C*H$_2$(CH$_2$)$_3$NH], 29.19 (*C*H$_2$CH$_2$NH), 41.36 (*C*H$_2$NH), 45.39 (*C*H$_2$NC), 54.41 [*C*H$_2$N(CH$_2$)$_5$NH], 55.00 (*C*H$_2$NCH$_2$CH$_2$CH$_2$O), 55.97 (*C*H$_2$CH$_2$CH$_2$O), 56.31 [*C*H$_2$(CH$_2$)$_4$NH], 56.96 (CH$_3$O), 67.57 (CH$_2$O), 102.41 (*C*HCOCH$_3$), 103.30 (*C*CNH), 106.82 (*C*HCOCH$_2$), 145.83 (*C*OCH$_3$), 149.62 (*C*CCNH), 154.35 (*C*OCH$_2$), 159.04 (*C*NCNH), 159.49 (CNH). HRMS-EI m/z $[M]^+$ calcd. for $C_{31}H_{50}N_6O_2$: 538.3995, found: 538.3989.

***N*^{1}-Cyclohexyl-*N*^{2}-{6-methoxy-7-[3-(piperidin-1-yl)propoxy]quinazolin-4-yl}-*N*^{1}-methylethane-1,2-diamine (2b):** R_f = 0.38 [10% 3 M NH_3 (in MeOH) in CH_2Cl_2]. IR (film): $\tilde{\nu}$ = 3020, 1641, 1215 cm^{-1}. ^1H NMR (500 MHz, CD_2Cl_2): δ = 1.03-1.16 (m, 1 H, CH_2CH$_2$CH$_2$CHN), 1.19-1.37 (m, 4 H, CH_2CH_2CHN), 1.37-1.47 (m, 2 H, CH_2CH$_2$CH$_2$NCH$_2$CH$_2$CH$_2$O), 1.47-1.59 (m, 4 H, CH_2CH$_2$NCH$_2$CH$_2$CH$_2$O), 1.59-1.66 (m, 1 H, CH_2CH$_2$CH$_2$CHN), 1.77-1.87 (m, 4 H, CH_2CH_2CHN), 2.02 (p, J = 6.8 Hz, 2 H, CH_2CH$_2$O), 2.32 (s, 3 H, CH$_3$N), 2.34-2.43 (m, 4 H, CH_2NCH$_2$CH$_2$CH$_2$O), 2.43-2.52 (m, 3 H, CH_2CH$_2$CH$_2$O, CH$_2$C*H*N), 2.68-2.88 (m, 2 H, CH_2CH$_2$NH), 3.53-3.67 (m, 2 H, CH_2NH), 3.94 (s, 3 H, CH$_3$O), 4.16 (t, J = 6.7 Hz, 2 H, CH$_2$O), 6.50 (d, J = 13.6 Hz, 1 H, NH), 6.95 (s, 1 H, C*H*COCH$_3$), 7.14 (s, 1 H, C*H*COCH$_2$), 8.43 (s, 1 H, C*H*NCNH). ^{13}C NMR (126 MHz, CD_2Cl_2): δ = 24.97 (*C*H$_2$CH$_2$CH$_2$NCH$_2$CH$_2$CH$_2$O), 26.35 (*C*H$_2$CH$_2$CHN), 26.52 (*C*H$_2$CH$_2$NCH$_2$CH$_2$CH$_2$O), 26.68 (*C*H$_2$CH$_2$O), 27.02 (*C*H$_2$CH$_2$CH$_2$CHN), 29.26 (*C*H$_2$CHN), 37.08 (CH$_3$N), 38.38 (CH$_2$NH), 52.08 (*C*H$_2$CH$_2$NH), 55.03 (*C*H$_2$NCH$_2$CH$_2$CH$_2$O), 55.91 (*C*H$_2$CH$_2$CH$_2$O), 56.39 (CH$_3$O), 63.59 (CH$_2$*C*HN), 67.87 (CH$_2$O), 100.42 (*C*HCOCH$_3$), 108.83 (*C*HCOCH$_2$), 109.02 (14), 146.84 (15), 149.46 (12), 154.21 (11), 154.49 (*C*HNCNH), 158.65 (19). HRMS-ESI m/z $[M+H]^+$ calcd. for $C_{26}H_{42}N_5O_2$: 456.3339, found: 456.3334.

6-Methoxy-*N*-[3-(4-methylpiperazin-1-yl)butyl]-7-[3-(piperidin-1-yl)propoxy]quinazolin-4-amine (2c): mp.: 85 °C. R_f = 0.22 [10% 3 M NH_3 (in MeOH) in CH_2Cl_2]. IR (film): $\tilde{\nu}$ = 2100, 1622, 1504, 1338, 1217 cm^{-1}. ^1H NMR (500 MHz, CD_2Cl_2): δ = 1.05 (d, J = 6.6 Hz, 3 H, CH_3CH), 1.37-1.49 (m, 2 H, CH_2CH$_2$CH$_2$NCH$_2$CH$_2$CH$_2$O), 1.51-1.61 (m, 4 H, CH_2CH$_2$NCH$_2$CH$_2$CH$_2$O), 1.65-1.97 (m, 2 H, CH_2CH$_2$NH), 1.98-2.08 (m, 2 H, CH_2CH$_2$O), 2.26 (s, 3 H, CH$_3$N), 2.28-2.62 (m, 12 H, CH_2CH$_2$NCH$_3$, CH$_2$NCH_2CH$_2$CH$_2$O), 2.64-2.77 (m, 2 H, CH_2CH$_2$NCH$_3$), 2.78-2.96 (m, 1 H, C*H*CH$_3$), 3.58-3.70 (m, 1 H, CH_2NH), 3.72-3.85 (m, 1 H, CH_2NH), 3.97 (s, 3 H, CH$_3$O), 4.17 (t, J = 6.6 Hz, 2 H, CH$_2$O), 6.71 (s, 1 H, NH), 7.05 (s, 1 H, C*H*COCH$_3$), 7.15 (s, 1 H, C*H*COCH$_2$), 8.43 (s, 1 H, C*H*NCNH). ^{13}C NMR (126 MHz, CD_2Cl_2): δ = 13.74 (*C*H$_3$CH), 24.92 (*C*H$_2$CH$_2$CH$_2$NCH$_2$CH$_2$CH$_2$O), 26.47 (*C*H$_2$CH$_2$NCH$_2$CH$_2$CH$_2$O), 26.98 (*C*H$_2$CH$_2$O), 32.20 (*C*H$_2$CH$_2$NH), 40.71 (CH$_2$NH), 46.07 (CH$_3$N), 48.75 (*C*H$_2$CH$_2$NCH$_3$), 55.01 (*C*H$_2$NCH$_2$CH$_2$CH$_2$O), 55.93 (*C*H$_2$NCH$_3$, *C*H$_2$CH$_2$CH$_2$O), 57.61 (CH$_3$O), 59.32 (*C*HCH$_3$), 67.81 (CH$_2$O), 102.33 (*C*HCOCH$_3$), 108.99 (*C*HCOCH$_2$), 109.06 (*C*CNH), 147.20 (*C*CCNH), 149.40 (*C*OCH$_3$), 154.51 (*C*HNCNH, *C*OCH$_2$), 158.94 (CNH). HRMS-ESI m/z $[M+H]^+$ calcd. for $C_{26}H_{43}N_6O_2$: 471.3447, found: 471.3443.

6-Methoxy-7-[3-(piperidin-1-yl)propoxy]-4-[4-(pyrrolidin-1-yl)piperidin-1-yl]quinazoline (2d): IR (film): $\tilde{\nu}$ = 2937, 1643, 1504, 1209 cm^{-1}. ^1H NMR (500 MHz, CD_2Cl_2): δ = 1.36-1.49 (m, 2 H, CH_2CH$_2$CH$_2$NCH$_2$CH$_2$CH$_2$O), 1.49-1.59 (m, 4 H, CH_2CH$_2$NCH$_2$CH$_2$CH$_2$O), 1.69-1.82 (m, 6 H, CH_2CHN, CH_2CH$_2$NCH), 1.98-2.10 (m, 4 H, CH_2CHN, CH_2CH$_2$O), 2.28 (tt, *J* = 10.2, 4.0 Hz, 1 H, C*H*NCH$_2$), 2.32-2.43 (m, 4 H, CH_2NCH$_2$CH$_2$CH$_2$O), 2.46 (t, *J* = 7.1 Hz, 2 H, CH_2CH$_2$CH$_2$O), 2.51-2.64 (m, 4 H, CH_2NCH), 3.04-3.15 (m, 2 H, CH$_2$NC), 3.94 (s, 3 H, CH$_3$O), 4.04-4.14 (m, 2 H, CH$_2$NC), 4.18 (t, *J* = 6.7 Hz, 2 H, CH$_2$O), 7.11 (s, 1 H, C*H*COCH$_3$), 7.19 (s, 1 H, C*H*COCH$_2$), 8.55 (s, 1 H, CHNCN). ^{13}C NMR (126 MHz, CD_2Cl_2): δ = 23.74 (*C*H$_2$CH$_2$NCH), 24.96 (*C*H$_2$CH$_2$CH$_2$NCH$_2$CH$_2$CH$_2$O), 26.52 (*C*H$_2$CH$_2$NCH$_2$CH$_2$CH$_2$O), 26.98 (*C*H$_2$CH$_2$O), 32.07 (*C*H$_2$CHN), 49.09 (*C*H$_2$CH$_2$CHN), 51.78 (*C*H$_2$NCH), 55.03 (*C*H$_2$NCH$_2$CH$_2$CH$_2$O), 55.89 (*C*H$_2$CH$_2$CH$_2$O), 56.31 (CH$_3$O), 62.21 (*C*HNCH$_2$), 67.92 (CH$_2$O), 103.89 (*C*HCOCH$_3$), 108.49 (*C*HCOCH$_2$), 111.84 (*C*CHCOCH$_3$), 149.03 (*C*OCH$_3$), 149.47 (*C*CCNCH$_2$), 153.34 (*C*HNCN), 154.41 (*C*OCH$_2$), 164.49 (*C*NCH$_2$). HRMS-ESI m/z $[M+H]^+$ calcd. for $C_{26}H_{40}N_5O_2$: 454.3182, found: 454.3177.

***N*-[1-(Azepan-1-yl)-2-methylpropan-2-yl]-6-methoxy-7-[3-(piperidin-1-yl)propoxy]quinazolin-4-amine (2e):** Hygroscopic. R_f = 0.30 [5% 7 M NH_3 (in MeOH) in CH_2Cl_2]. IR (film): $\tilde{\nu}$ = 2926, 1643, 1498 cm^{-1}. ^1H NMR (500 MHz, CD_2Cl_2): δ = 1.38-1.47 (m, 2 H, CH_2CH$_2$CH$_2$NCH$_2$CH$_2$CH$_2$O), 1.52-1.62 (m, 10 H, CH$_3$C, CH_2CH$_2$NCH$_2$CH$_2$CH$_2$O), 1.62-1.78 (m, 8 H, CH_2CH_2CH$_2$NCH$_2$CNH), 2.03 (p, *J* = 6.9 Hz, 2 H, CH_2CH$_2$O), 2.26-2.46 (m, 4 H, CH_2NCH$_2$CH$_2$CH$_2$O), 2.46-2.57 (m, 2 H, CH_2CH$_2$CH$_2$O), 2.75 (s, 2 H, CH_2CNH), 2.82-2.96 (m, 4 H, CH_2NCH$_2$CNH), 3.95 (s, 3 H, CH$_3$O), 4.16 (t, *J* = 6.6 Hz, 2 H, CH$_2$O), 6.84 (s, 1 H, NH), 6.93 (s, 1 H, C*H*COCH$_3$), 7.12 (s, 1 H, C*H*COCH$_2$), 8.40 (s, 1 H, C*H*NCNH). ^{13}C NMR (126 MHz, CD_2Cl_2): δ = 24.91 (*C*H$_2$CH$_2$CH$_2$NCH$_2$CH$_2$CH$_2$O), 25.77 (*C*H$_3$C), 26.45 (*C*H$_2$CH$_2$NCH$_2$CH$_2$CH$_2$O), 26.97 (*C*H$_2$CH$_2$O), 27.51 (*C*H$_2$CH$_2$CH$_2$NCH$_2$CNH), 29.59 (*C*H$_2$CH$_2$NCH$_2$CNH), 54.36 (CH$_3$*C*), 55.00 (*C*H$_2$NCH$_2$CH$_2$CH$_2$O), 55.91 (*C*H$_2$CH$_2$CH$_2$O), 56.38 (CH$_3$O), 58.82 (*C*H$_2$NCH$_2$CNH), 67.81 (CH$_2$O), 69.97 (*C*H$_2$CNH), 100.45 (*C*HCOCH$_3$), 109.02 (*C*HCOCH$_2$), 109.86 (*C*CNH), 146.93 (*C*CCNH), 149.32 (*C*OCH$_3$), 153.88 (*C*OCH$_2$), 154.04 (*C*HNCNH), 158.64 (NCNH). HRMS-ESI m/z $[M+H]^+$ calcd. for $C_{27}H_{44}N_5O_2$: 470.3495, found: 470.3492.

***N*-(1-Propan-2-ylpiperidin-4-yl)-6-methoxy-7-[3-(piperidin-1-yl)propoxy]quinazolin-4-amine (2f):** mp.: 166 °C. R_f = 0.18 [10% 4 M NH_3 (in MeOH) in CH_2Cl_2]. IR (film): $\tilde{\nu}$ = 2933, 1593, 1506, 1254 cm^{-1}. ^1H NMR (500 MHz, CD_3OD): δ = 1.14 (d, *J* = 6.6 Hz, 6 H, C*H*$_3$CH), 1.45-1.56 (m, 2 H, CH_2CH$_2$CH$_2$NCH$_2$CH$_2$CH$_2$O), 1.57-1.69 (m, 4 H, CH_2CH$_2$NCH$_2$CH$_2$CH$_2$O), 1.69-1.81 (m, 2 H, CH_2CHNH), 2.04-2.18 (m, 4 H, CH_2CH$_2$O, CH_2CHNH), 2.38-2.48 (m, 2 H, CH_2NCH), 2.48-2.60 (m, 4 H, CH_2NCH$_2$CH$_2$CH$_2$O), 2.60-2.69 (m, 2 H, CH_2CH$_2$CH$_2$O), 2.82 (hept, *J* = 6.5 Hz, 1 H, CH$_3$C*H*), 2.98-3.09 (m, 2 H, CH_2NCH), 3.97 (s, 3 H, CH$_3$O), 4.09-4.30 (m, 3 H, CH$_2$O, C*H*NH), 7.07 (s, 1 H, CHCN), 7.60 (s, 1 H, CHCCN), 8.30 (s, 1 H, CHNCNH). ^{13}C NMR (126 MHz, CD_3OD): δ = 18.47 (*C*H$_3$CH), 25.04 (*C*H$_2$CH$_2$CH$_2$NCH$_2$CH$_2$CH$_2$O), 26.38 (*C*H$_2$CH$_2$NCH$_2$CH$_2$CH$_2$O), 27.00 (*C*H$_2$CH$_2$O), 32.37 (*C*H$_2$CHNH), 48.83 (*C*H$_2$NCH), 49.84 (*C*HNH), 55.46 (*C*H$_2$NCH$_2$CH$_2$CH$_2$O), 56.06 (CH$_3$*C*H), 56.82 (CH$_3$O), 57.00 (*C*H$_2$CH$_2$CH$_2$O), 68.32 (CH$_2$O), 102.94 (*C*HCCN), 107.81 (*C*HCN), 110.17 (*C*CNH), 146.65 (*C*CCNH), 150.87 (CH$_3$O*C*), 154.28 (*C*HNCNH), 155.48 (CH$_2$O*C*), 159.65 (CNH). HRMS-ESI m/z $[M+H]^+$ calcd. for $C_{25}H_{40}N_5O_2$: 442.3182, found: 442.3175.

***N*-(1-Propan-2-ylpiperidin-4-yl)-6-methoxy-7-[3-(piperidin-1-ylmethyl)pyrrolidin-1-yl]quinazolin-4-amine (2g):** mp.: 244 °C. R_f = 0.35 [10% 3 M NH_3 (in MeOH) in CH_2Cl_2]. IR (film): $\tilde{\nu}$ = 2935, 1612, 1504, 1363 cm^{-1}. ^1H NMR (500 MHz, CD_2Cl_2): δ = 1.04 (d, *J* = 6.6 Hz, 6 H, C*H*$_3$CH), 1.33-1.47 (m, 2 H, CH_2CH$_2$CH$_2$N), 1.47-1.60 (m, 6 H, CH$_2$CH_2CH$_2$N, CH_2CHNH), 1.60-1.78 (m, 1 H, CH$_2$CH_2CHCH$_2$N), 2.02-2.09 (m, 1 H, CH$_2$CH_2CHCH$_2$N), 2.09-2.17 (m, 2 H, CH_2CHNH), 2.19-2.44 (m, 8 H, CH_2NCH_2CHCH$_2$N,

C*H*$_2$CH$_2$CHNH), 2.49 (hept, *J* = 7.0 Hz, 1 H, C*H*CH$_2$N), 2.76 (hept, *J* = 6.4 Hz, 1 H, CH$_3$C*H*), 2.83-2.93 (m, 2 H, C*H*$_2$CH$_2$CHNH), 3.26 (dd, *J* = 10.2, 7.2 Hz, 1 H, CHC*H*$_2$NC), 3.51-3.62 (m, 3 H, C*H*$_2$NC), 3.90 (s, 3 H, CH$_3$O), 4.10-4.26 (m, 1 H, C*H*NH), 5.01-5.18 (m, 1 H, NH), 6.76 (s, 1 H, C*H*COCH$_3$), 6.79 (s, 1 H, C*H*CNCH$_2$), 8.34 (s, 1 H, CHNC). ^{13}C NMR (126 MHz, CD_2Cl_2): δ = 18.46 (*C*H$_3$CH), 24.97 (*C*H$_2$CH$_2$CH$_2$N), 26.55 (CH$_2$*C*H$_2$CH$_2$N), 30.45 (*C*H$_2$CHCH$_2$N), 33.37 (*C*H$_2$CHNH), 36.58 (*C*HCH$_2$N), 48.05 (*C*H$_2$CH$_2$CHNH), 48.85 (CHNH), 50.56 (*C*H$_2$CH$_2$CHCH$_2$N), 54.85 (CH$_3$*C*H), 55.41 (CH$_2$CH$_2$*C*H$_2$N), 55.84 (CN*C*H$_2$CH), 56.33 (CH$_3$O), 63.20 (*C*H$_2$CHCH$_2$NC), 100.12 (*C*HCOCH$_3$), 106.53 (*C*CNH), 109.46 (*C*HCNCH$_2$), 145.49 (*C*NCH$_2$), 147.48 (*C*CCNH), 150.16 (*C*OCH$_3$), 154.18 (*C*HNCNH), 157.71 (CNH). HRMS-ESI m/z [M+H]$^+$ calcd. for $C_{27}H_{43}N_6O$: 467.3498; found: 467.3489.

4-Chloro-6-methoxy-2-(piperidin-1-yl)-7-[3-(piperidin-1-yl)propoxy]quinazoline (8): mp.: 138 °C. R_f = 0.35 (15% MeOH in CH_2Cl_2 IR (film): ṽ = 2931, 1626, 1585, 1495, 1238, 754 cm^{-1}. ^{1}H NMR (500 MHz, CD_3OD): δ = 1.59-1.70 (m, 6 H, C*H*$_2$CH$_2$CH$_2$NCH$_2$CH$_2$CH$_2$O, C*H*$_2$CH$_2$NC), 1.70-1.77 (m, 2 H, C*H*$_2$CH$_2$CH$_2$NC), 1.77-1.89 (m, 4 H, C*H*$_2$CH$_2$NCH$_2$CH$_2$CH$_2$O), 2.15-2.37 (m, 2 H, C*H*$_2$CH$_2$O), 2.87-3.17 (m, 6 H, C*H*$_2$NC*H*$_2$CH$_2$CH$_2$O), 3.81-3.88 (m, 4 H, CH$_2$NC), 3.95 (s, 3 H, CH$_3$O), 4.25 (t, *J* = 5.8 Hz, 2 H, CH$_2$O), 7.00 (s, 1 H, CHCOCH$_2$), 7.26 (s, 1 H, C*H*COCH$_3$). ^{13}C NMR (126 MHz, CD_3OD): δ = 23.72 (*C*H$_2$CH$_2$CH$_2$NCH$_2$CH$_2$CH$_2$O), 25.29 (*C*H$_2$CH$_2$NCH$_2$CH$_2$CH$_2$O), 25.74 (*C*H$_2$CH$_2$O)*, 25.92 (*C*H$_2$CH$_2$CH$_2$NC)*, 26.88 (*C*H$_2$CH$_2$NC), 46.31 (*C*H$_2$NC), 55.01 (*C*H$_2$NCH$_2$CH$_2$CH$_2$O), 56.54 (CH$_3$O), 56.73 (*C*H$_2$CH$_2$CH$_2$O), 68.09 (CH$_2$O), 104.82 (*C*HCOCH$_3$), 106.56 (*C*HCOCH$_2$), 113.18 (*C*CCl), 148.82 (*C*OCH$_3$), 152.67 (*C*CCCl), 157.42 (*C*OCH$_2$), 158.93 (*C*NCH$_2$), 160.90 (CCl). HRMS-ESI m/z [M+H]$^+$ calcd. for $C_{22}H_{32}ClN_4O_2$: 419.224, found: 419.2206.

4-Chloro-6-methoxy-7-[3-(piperidin-1-yl)propoxy]quinazoline (9) [7, 8]**:** mp.: 106 °C. R_f = 0.21 [5% 4 M NH_3 (in MeOH) in CH_2Cl_2]. IR (film): ṽ = 2933, 2358, 1500, 1232, 1020 cm^{-1}. ^{1}H NMR (500 MHz, DMSO-d_6) δ = 1.31-1.43 (m, 2 H, C*H*$_2$CH$_2$CH$_2$NCH$_2$CH$_2$CH$_2$O), 1.45-1.54 (m, 4 H, C*H*$_2$CH$_2$NCH$_2$CH$_2$CH$_2$O), 1.95 (p, *J* = 6.7 Hz, 2 H, C*H*$_2$CH$_2$O), 2.26-2.38 (m, 4 H, C*H*$_2$NCH$_2$CH$_2$CH$_2$O), 2.38-2.43 (m, 2 H, C*H*$_2$CH$_2$CH$_2$O), 4.00 (s, 3 H, CH$_3$O), 4.25 (t, *J* = 6.4 Hz, 2 H, CH$_2$O), 7.38 (s, 1 H, CHCN), 7.44 (s, 1 H, CHCCN), 8.86 (s, 1 H, CHN). ^{13}C NMR (126 MHz, DMSO-d_6) δ = 24.13 (*C*H$_2$CH$_2$CH$_2$NCH$_2$CH$_2$CH$_2$O), 25.60 (*C*H$_2$CH$_2$NCH$_2$CH$_2$CH$_2$O), 25.92 (*C*H$_2$CH$_2$O), 54.11 (*C*H$_2$NCH$_2$CH$_2$CH$_2$O), 54.93 (*C*H$_2$CH$_2$CH$_2$O), 56.21 (*C*H$_3$O), 67.65 (CH$_2$O), 102.30 (*C*HCCN), 107.32 (*C*HCN), 118.48 (*C*CCl), 148.60 (*C*CCCl), 151.49 (CH$_3$O*C*), 152.19 (CHN), 156.11 (CH$_2$O*C*), 157.84 (CCl). HRMS-ESI m/z [M+H]$^+$ calcd. for $C_{17}H_{23}ClN_3O_2$: 336.1479, found: 336.1476. The analytical data agree with those previously reported in the literature [7, 8].

7-Fluoro-*N*-(1-propan-2-ylpiperidin-4-yl)-6-methoxyquinazolin-4-amine (10): mp.: 233 °C (decomposition). R_f = 0.48 [10% 3 M NH_3 (in MeOH) in CH_2Cl_2]. IR (film): ṽ = 2968, 1593, 1537, 1045 cm^{-1}. ^{1}H NMR (500 MHz, CD_2Cl_2): δ = 1.04 (d, *J* = 6.6 Hz, 6 H, C*H*$_3$CH), 1.52-1.64 (m, 2 H, C*H*$_2$CHNH), 2.11-2.20 (m, 2 H, C*H*$_2$CHNH), 2.31-2.42 (m, 2 H, C*H*$_2$CH$_2$CHNH), 2.71-2.84 (m, 1 H, CH$_3$C*H*), 2.83-2.96 (m, 2 H, C*H*$_2$CH$_2$CHNH), 4.00 (s, 3 H, CH$_3$O), 4.15-4.31 (m, 1 H, C*H*NH), 5.43 (d, *J* = 7.6 Hz, 1 H, NH), 7.02 (d, *J* = 8.6 Hz, 1 H, C*H*COCH$_3$), 7.44 (d, *J* = 12.0 Hz, 1 H, CHCF), 8.48 (s, 1 H, C*H*NCNH). ^{13}C NMR (126 MHz, CD_2Cl_2): δ = 18.43 (*C*H$_3$CH), 33.01 (*C*H$_2$CHNH), 48.00 (*C*H$_2$CH$_2$CHNH), 49.23 (CHNH), 54.86 (CH$_3$*C*H), 56.96 (CH$_3$O), 102.29 (d, *J* = 3.5 Hz, *C*HCOCH$_3$), 111.90 (*C*CNH), 114.04 (d, *J* = 17.6 Hz, *C*HCF), 146.26 (d, *J* = 12.0 Hz, *C*CHCF), 147.82 (d, *J* = 13.0 Hz, *C*OCH$_3$), 154.79 (*C*HNCNH), 156.64 (d, *J* = 255.1 Hz, CF), 158.12 (CNH). HRMS-ESI m/z [M+H]$^+$ calcd. for $C_{17}H_{24}FN_4O$: 319.1934, found: 319.1929.

* Due to signal overlap in 2D-NMR, signals could not be unambiguously assigned.

Supplemental References

1. Chevillard, F., et al., *Binding-Site Compatible Fragment Growing Applied to the Design of beta2-Adrenergic Receptor Ligands.* J. Med. Chem., 2018. **61**(3): p. 1118-1129.
2. *ROCS 3.4.1.0*. OpenEye Scientific Software: Santa Fe, NM.
3. Chemical Computing Group, U., *Molecular Operating Environment (MOE)*. 2021: 1010 Sehrbooke St. West, Suite #910, Montreal, QC, Canada, H3A, 2R7.
4. Roe, D.R. and T.E. Cheatham, 3rd, *PTRAJ and CPPTRAJ: Software for Processing and Analysis of Molecular Dynamics Trajectory Data.* J. Chem. Theory Comput., 2013. **9**(7): p. 3084-95.
5. Nitsche, V., et al., *MS Binding Assays with UNC0642 as reporter ligand for the MB327 binding site of the nicotinic acetylcholine receptor.* Toxicol. Lett., 2024. **392**: p. 94-106.
6. Nitsche, V., et al., *MS Binding Assays with UNC0642 as reporter ligand for the MB327 binding site of the nicotinic acetylcholine receptor.* bioRxiv, 2023: p. 2023.11.15.567260.
7. Hennequin, L.F., et al., *Quinazoline Derivatives as Angiogenesis Inhibitors (WO-2000047212-A1)*, W.I.P. Organization, Editor. 2000.
8. Ravez, S., et al., *Inhibition of tumor cell growth and angiogenesis by 7-Aminoalkoxy-4-aryloxy-quinazoline ureas, a novel series of multi-tyrosine kinase inhibitors.* Eur. J. Med. Chem., 2014. **79**: p. 369-381.

11.4. Publication IV

Synthesis and Biological Evaluation of Novel MB327 Analogs as Resensitizers for Desensitized Nicotinic Acetylcholine Receptors after Intoxication with Nerve Agents

Tamara Bernauer, Valentin Nitsche, **Jesko Kaiser**, Christoph G.W. Gertzen, Georg Höfner, Karin V. Niessen, Thomas Seeger, Dirk Steinritz, Franz Worek, Holger Gohlke, Klaus T. Wanner, Franz F. Paintner,

Toxicology Letters., 2024. **397**: p. 151-162. [§4]

[§4] See **REPRINT PERMISSION**

Toxicology Letters 397 (2024) 151–162

Contents lists available at ScienceDirect

Toxicology Letters

journal homepage: www.journals.elsevier.com/toxicology-letters

Synthesis and biological evaluation of novel MB327 analogs as resensitizers for desensitized nicotinic acetylcholine receptors after intoxication with nerve agents

Tamara Bernauer[a,1], Valentin Nitsche[a,2], Jesko Kaiser[b,3], Christoph G.W. Gertzen[b,4], Georg Höfner[a,5], Karin V. Niessen[c,6], Thomas Seeger[c,7], Dirk Steinritz[c,8], Franz Worek[c,9], Holger Gohlke[b,d,10], Klaus T. Wanner[a,11], Franz F. Paintner[a,*,12]

[a] Department of Pharmacy - Center for Drug Research, Ludwig-Maximilians-Universität München, Munich, Germany
[b] Institute for Pharmaceutical and Medicinal Chemistry, Heinrich Heine University Düsseldorf, Düsseldorf, Germany
[c] Bundeswehr Institute of Pharmacology and Toxicology, Munich, Germany
[d] John von Neumann Institute for Computing (NIC), Jülich Supercomputing Centre (JSC), Institute of Biological Information Processing (IBI-7: Structural Biochemistry) & Institute of Bio- and Geosciences (IBG-4: Bioinformatics), Forschungszentrum Jülich, Jülich, Germany

ARTICLE INFO

Editor: Dr. Angela Mally

Keywords:
Neurological agents
Nicotinic acetylcholine receptor
MB327-PAM-1 binding site
Bispyridinium salts
Resensitizer
In silico studies
Myographic studies

ABSTRACT

Poisoning with organophosphorus compounds, which can lead to a cholinergic crisis due to the inhibition of acetylcholinesterase and the subsequent accumulation of acetylcholine (ACh) in the synaptic cleft, is a serious problem for which treatment options are currently insufficient. Our approach to broadening the therapeutic spectrum is to use agents that interact directly with desensitized nicotinic acetylcholine receptors (nAChRs) in order to induce functional recovery after ACh overstimulation. Although MB327, one of the most prominent compounds investigated in this context, has already shown positive properties in terms of muscle force recovery, this compound is not suitable for use as a therapeutic agent due to its insufficient potency. By means of *in silico* studies based on our recently presented allosteric binding pocket at the nAChR, i.e. the MB327-PAM-1 binding site, three promising MB327 analogs with a 4-aminopyridinium ion partial structure (PTM0056, PTM0062, and PTM0063) were identified. In this study, we present the synthesis and biological evaluation of a series of new analogs of the aforementioned compounds with a 4-aminopyridinium ion partial structure (PTM0064-PTM0072), as well as hydroxy-substituted analogs of MB327 (PTMD90–0012 and PTMD90–0015) designed to substitute entropically unfavorable water clusters identified during molecular dynamics simulations. The compounds were characterized in terms of their binding affinity towards the aforementioned binding site by applying the UNC0642 MS Binding Assays and in terms of their muscle force reactivation in rat diaphragm myography. More potent compounds were identified compared to MB327, as some of them showed a higher affinity towards MB327-PAM-1 and also a higher recovery of neuromuscular transmission at lower compound concentrations. To

* Correspondence to: Butenandtstr. 5-13, 81377 München, Germany.
E-mail address: Franz.Paintner@cup.uni-muenchen.de (F.F. Paintner).
[1] ORCID 0000–0001-9570–1253
[2] ORCID 0009–0000-3351–1227
[3] ORCID 0000–0002-6429–0911
[4] ORCID 0000–0002-9562–7708
[5] ORCID 0000 0002 7957 4503
[6] ORCID 0009–0008-6810–5294
[7] ORCID0009–0007-5713–4367
[8] ORCID 0000–0002-2073–5683
[9] ORCID 0000–0003-3531–3616
[10] ORCID 0000–0001-8613–1447
[11] ORCID 0000–0003-4399–1425
[12] ORCID 0000–0002-6795–586X

https://doi.org/10.1016/j.toxlet.2024.05.011
Received 12 February 2024; Received in revised form 6 May 2024; Accepted 14 May 2024
Available online 15 May 2024

improve the treatment of organophosphate poisoning, direct targeting of nAChRs with appropriate compounds is a key step, and this study is an important contribution to this research.

1. Introduction

The verified use of sarin in the Syrian war in 2013 (Dolgin, 2013; Pita and Domingo, 2014) and 2017 (OPCW, 2017), as well as the politically motivated Novichok attack on Russian opposition politician Alexei Navalny in 2020 (Steindl et al., 2021), provide clear evidence that highly toxic organophosphorus nerve agents still pose a major threat to military personnel and civilians, even after their international ban by the Chemical Weapons Convention in 1997 (Thakur and Haru, 2007). Intoxication with organophosphorus compounds (OPCs) leads to the irreversible inhibition of acetylcholinesterase (AChE), resulting in an uncontrolled accumulation of acetylcholine (ACh) in the synaptic cleft of cholinergic neurons. As a result, cholinergic signaling is disrupted by overstimulation of muscarinic and nicotinic acetylcholine receptors (mAChRs and nAChRs, respectively) (Koelle, 1981; Maselli, Leung, 1993; Massoulié et al., 1993). This condition, known as a "cholinergic crisis", can be life-threatening due to respiratory paralysis as a result of the disruption of nAChR-mediated neuromuscular transmission (Brown and Brix, 1998; Thiermann et al., 2010). Standard treatment for nerve agent poisoning currently includes a muscarinic acetylcholine receptor antagonist, e.g. atropine, to reduce mAChR overstimulation and an oxime-based AChE reactivator, e.g. obidoxime. According to Sheridan et al. (Sheridan et al., 2005) neuromuscular blockers (competitive nAChR antagonists) are not suitable for the treatment of nerve agent poisoning. Hence, reactivation of inhibited AChE appears to be crucial to counteract nicotinic overstimulation. However, despite decades of effort, there is still no universally applicable AChE reactivator that can efficiently cleave all OPC-AChE conjugates (Worek et al., 2020). Therefore, there is an urgent need to develop novel antidotes to counteract desensitization of muscle-type nAChRs as a result of overstimulation. One approach is to use agents that directly target the nAChR to restore its function after it has been desensitized by overstimulation (Sheridan et al., 2005; Turner et al., 2011).

Indeed, a number of bispyridinium salts, such as the prototypical compound MB327 (Fig. 1), are able to restore the function of desensitized nAChR of *Torpedo californica* (recently reclassified as *Tetronarce californica*) in *in vitro* experiments by interacting directly with the receptor most likely via an allosteric mechanism (Niessen et al., 2016; Niessen et al., 2018; Seeger et al., 2012; Sichler et al., 2018). Since the *Torpedo californica* nAChR has a high sequence identity to the rat and human muscle-type nAChRs, it is reasonable to assume that MB327 has similar effects on the desensitized nAChRs of the latter species as well. Indeed, in *ex vivo* experiments, MB327 shows a muscle force-restoring effect on both soman-poisoned rat diaphragms and soman-poisoned human intercostal muscles, which is thought to be due to the resensitization of desensitized nAChR (Niessen et al., 2018; Seeger et al., 2012). In addition, MB327 (or the corresponding methanesulfonate salt MB399, respectively) in combination with the mAChR antagonist hyoscine and the indirect parasympathomimetic physostigmine, was shown to increase the survival rates of guinea pigs poisoned with sarin or tabun in *in vivo* studies (Timperley et al., 2012; Turner et al., 2011). Despite these promising results, MB327 is not suitable for human use due to its narrow therapeutic window. Nevertheless, MB327 is a promising starting point for further investigation.

Recently, based on blind docking experiments and molecular dynamics simulations, we proposed a new allosteric binding site of MB327 at the muscle-type nAChR, termed MB327-PAM-1 (Kaiser et al., 2023). This binding site is located at the transition from the extracellular to the trans-membrane region and, according to a rigidity analysis, is expected to exert an allosteric effect on the orthosteric binding pocket upon binding of MB327. The amino acids interacting with MB327 in this binding site, predominantly glutamate residues, are highly conserved within the different nAChR subunits as well as in different species. Accordingly, comparable resensitizing effects of MB327 should be observable on desensitized nAChR of different species (e.g. *Torpedo californica*, rats and humans).

However, recently published results also show that bispyridinium compounds related to MB327 have inhibitory activity on the nAChR, most likely mediated via the orthosteric binding site (Epstein et al., 2021). Indeed, free ligand diffusion MD simulations performed by us indicated that MB327 also has affinity for the orthosteric binding site (Kaiser et al., 2023). The fact that the muscle force restoring activity of MB327 on soman-poisoned rat diaphragms is lost at higher concentrations after a peak at 300 μM may be explained by this inhibitory activity (Niessen et al., 2018).

The binding mode of MB327 in the MB327-PAM-1 binding pocket indicates that one of the two *tert*-butyl groups projects into a polar region of the binding pocket. This allowed us to predict structural modifications of MB327 that led to the more potent resensitizers PTM0062 (**1**) and PTM0063 (**2**), which have a more polar substituent, i.e., an amino and a methylamino group, respectively, instead of one of the two *tert*-butyl residues of MB327 (Fig. 1) (Kaiser et al., 2023). Interestingly, the recently described dimethylamino analog PTM0056 (**3**) (Fig. 1), which has a less polar substituent than PTM0062 (**1**) or PTM0063 (**2**), also shows a slightly higher affinity for the MB327-PAM-1 binding site than MB327 (Rappenglück et al., 2018) and a muscle force-restoring activity comparable to PTM0062 (**1**) and PTM0063 (**2**) in preliminary, unpublished *ex vivo* studies with soman-poisoned rat diaphragm hemispheres. Therefore, PTM0056 (**3**) appeared to be a promising starting point for the development of new, possibly even more potent, resensitizers for the desensitizied muscle type nAChR.

In this study, we report the development of a series of non-symmetric MB327 analogs derived from PTM0062 (**1**), PTM0063 (**2**) and PTM0056 (**3**), respectively, as resensitizers for desensitized muscle-type nAChRs. To obtain a structurally diverse set of analogs, the 4-amino substituents of compounds **1**-**3** were replaced by either acylamino groups, dialkylamino groups previously not considered or cyclic amino groups (e.g. pyrrolidino, piperidino, morpholino and piperazino groups).

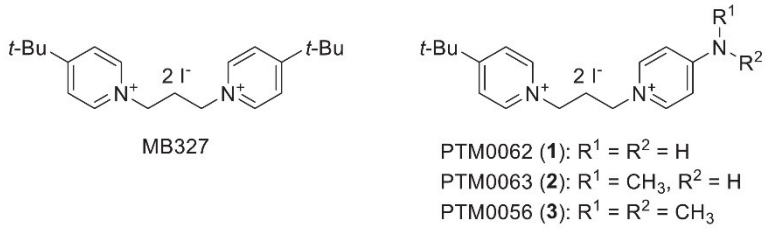

Fig. 1. Chemical structures: MB327, PTM0062 (**1**), PTM0063 (**2**) and PTM0056 (**3**).

Furthermore, based on identifying entropically unfavorable water clusters in MB327-PAM-1 using molecular dynamics (MD) simulations in combination with Grid Inhomogeneous Solvent Theory (GIST) computations (Lazaridis, 1998; Nguyen et al., 2011; Nguyen et al., 2012; Ramsey et al., 2016), we designed novel MB327 analogs potentially able to substitute these water clusters. To determine the affinities of the newly developed compounds at the MB327-PAM-1 binding site of *Torpedo*-nAChR, our recently developed UNC0642 MS Binding Assays were applied. To gain insight into the intrinsic activity of some selected representatives of the newly developed compounds, their ability to restore muscle force was also investigated in *ex vivo* experiments with soman-poisoned rat diaphragms. Some of the newly developed compounds showed a slightly higher affinity for the MB327-PAM-1 binding site of *Torpedo*-nAChR than the prototypical compound MB327 and a comparable or even higher muscle force-restoring effect on soman-poisoned rat diaphragms at lower concentrations than MB327.

2. Material and methods

2.1. Synthesis of novel MB327 analogs

Microwave reactions were carried out on a Discover SP microwave system by *CEM GmbH* in glass vials. All chemicals used in the syntheses were used as purchased from commercial sources. Solvents used for crystallization were distilled before use. Melting points were determined with a Büchi 510 melting point apparatus and are uncorrected. For IR spectroscopy, an FT-IR Spectrometer 1600 from *PerkinElmer* was used. High-resolution mass spectrometry was performed on a Finnigan MAT 95 (EI) or a Finnigan LTQ FT (ESI). ^{1}H and ^{13}C NMR spectra were recorded on a Bruker BioSpin Avance III HD 400 and 500 MHz at 25 °C. For data processing, MestReNova (Version 14.1.0) from Mestrelab Research S.L. 2019, and for calibration, the solvent signal (CD_3OD) was used. See Supporting Information (SI, Figures S1-S11) for the NMR spectra of the bispyridinium compounds. Unless otherwise noted, the purity of the test compounds was ≥ 98%, determined using quantitative ^{1}H NMR spectroscopy using TraceCERTS® ethyl 4-(dimethylamino) benzoate from *Sigma Aldrich* as internal calibrant (Cushman et al., 2014; Pauli et al., 2014).

All target compounds synthesized in the context of this study were cataloged with a certain PTM and PTMD number, respectively (Pharmacy and Toxicology Munich and Pharmacy and Toxicology Munich and Düsseldorf, respectively).

General Procedure (GP): Synthesis of non-symmetric MB327 analogs by *N*-alkylation with 4

A solution of 4-(*tert*-butyl)-1-(3-iodopropyl)pyridin-1-ium iodide (**4**) (Rappenglück et al., 2018) (1.0 equiv) and the corresponding 4-amino--substituted pyridine **5** (1.05–1.1 equiv) or 7-hydroxychinoline (**7**) in acetonitrile (2.0–2.7 mL/mmol) was stirred at 90 °C under microwave irradiation (150 W) for 1 h unless otherwise stated. The reaction mixture was concentrated in vacuo, and the residue was purified by recrystallization from different solvent mixtures.

Acetamido-1-{3-[4-(*tert*-butyl)pyridin-1-ium-1-yl] propyl}pyridin-1-ium diiodide (PTM0064, 6a)

According to the GP, with **4** (431 mg, 1.00 mmol, 1.0 equiv) and **5a** (150 mg, 1.10 mmol, 1.1 equiv) in MeCN (2.0 mL). Recrystallization from EtOAc/EtOH/MeOH (1:2:1) afforded **6a** (529 mg, 93%) as a yellow solid. m.p. 259 °C; ^{1}H NMR (400 MHz, CD_3OD): δ = 1.45 (s, 9 H), 2.27 (s, 3 H), 2.71–2.80 (m, 2 H), 4.66–4.72 (m, 2 H), 4.77–4.83 (m, 2 H), 8.12–8.16 (m, 2 H), 8.16–8.20 (m, 2 H), 8.79–8.86 (m, 2 H), 8.96–9.02 (m, 2 H); ^{13}C NMR (101 MHz, CD_3OD): δ = 24.61, 30.21, 33.27, 37.68, 57.42, 58.32, 116.48, 126.90, 145.43, 146.32, 154.33, 172.69, 173.27; IR (KBr): $\tilde{\nu}$ = 2964, 1645, 1518, 1207 cm^{-1}; HRMS (ESI): *m/z* calcd for $C_{19}H_{27}N_3OI_2$-Γ: 440.1199 [*M*-I]$^{+}$; found: 440.1185.

4-[(*tert*-Butoxycarbonyl)amino]-1-{3-[4-(*tert*-butyl)pyridin-1-ium-1-yl] propyl}-pyridin-1-ium diiodide (PTM0065, 6b)

According to the GP, a solution of **4** (323 mg, 0.750 mmol, 1.0 equiv) and **5b** (157 mg, 0.810 mmol, 1.08 equiv) in MeCN (2.0 mL) was stirred under microwave irradiation (150 W) at 60 °C for 15 h. Recrystallization from Et_2O/DMF (10:1) afforded **6b** (431 mg, 92%) as a yellow solid. Purity: 94%. m.p. 117 °C; ^{1}H NMR (400 MHz, CD_3OD): δ = 1.45 (s, 9 H), 1.56 (s, 9 H), 2.67–2.79 (m, 2 H), 4.59–4.67 (m, 2 H), 4.74–4.82 (m, 2 H), 7.87–8.02 (m, 2 H), 8.20–8.14 (m, 2 H), 8.68–8.76 (m, 2 H), 8.91–9.01 (m, 2 H); ^{13}C NMR (101 MHz, CD_3OD): δ = 28.25, 30.21, 33.19, 37.68, 57.16, 58.38, 84.27, 115.30, 126.90, 145.41, 145.85, 153.10, 155.64, 173.30; IR (KBr): $\tilde{\nu}$ = 2967, 1643, 1531, 1148 cm^{-1}; HRMS (ESI): *m/z* calcd for $C_{22}H_{33}N_3O_2I_2$-Γ: 498.1618 [*M*-I]$^{+}$; found: 498.1600.

4-[Benzyl(methyl)amino]-1-{3-[4-(*tert*-butyl)pyridin-1-ium-1-yl] propyl}pyridin-1-ium diiodide (PTM0066, 6c)

According to the GP, with **4** (323 mg, 0.750 mmol, 1.0 equiv) and **5c** (164 mg, 0.830 mmol, 1.1 equiv) in MeCN (2.0 mL). Recrystallization from EtOAc/EtOH/MeOH (10:5:1) afforded **6c** (354 mg, 75%) as a yellow solid. m.p. 185 °C; ^{1}H NMR (400 MHz, CD_3OD): δ = 1.45 (s, 9 H), 2.56–2.70 (m, 2 H), 3.34 (s, 3 H), 4.40 (t, *J* = 7.6 Hz, 1 H), 4.74 (t, *J* = 7.7 Hz, 2 H), 4.90 (s, 2 H), 7.03–7.19 (m, 2 H), 7.24–7.29 (m, 2 H), 7.29–7.41 (m, 3 H), 8.13–8.19 (m, 2 H), 8.20–8.40 (m, 2 H), 8.91–8.97 (m, 2 H); ^{13}C NMR (101 MHz, CD_3OD): δ = 30.20, 33.14, 37.67, 39.70, 55.41, 56.75, 58.52, 109.83, 126.86, 127.82, 129.11, 130.21, 136.21, 143.72, 145.38, 158.26, 173.24; IR (KBr): $\tilde{\nu}$ = 2967, 1645, 1556, 1193 cm^{-1}; HRMS (ESI): *m/z* calcd for $C_{25}H_{33}N_3I_2$-Γ: 502.1719 [*M*-I]$^{+}$; found: 502.1703.

4-(*tert*-Butyl)-1-{3-[4-(diethylamino)pyridin-1-ium-1-yl] propyl}pyridin-1-ium diiodide (PTM0067, 6d)

According to the GP, with **4** (431 mg, 1.00 mmol, 1.0 equiv) and **5d** (165 mg, 1.10 mmol, 1.1 equiv) in MeCN (2.0 mL). Recrystallization from EtOAc/EtOH (2.5:1) afforded **6d** (419 mg, 72%) as a yellow solid. m.p. 217 °C; ^{1}H NMR (400 MHz, CD_3OD): δ = 1.27 (t, *J* = 7.2 Hz, 6 H), 1.45 (s, 9 H), 2.60–2.71 (m, 2 H), 3.64 (q, *J* = 7.2 Hz, 4 H), 4.41 (t, *J* = 7.7 Hz, 2 H), 4.78 (t, *J* = 7.8 Hz, 2 H), 7.01–7.08 (m, 2 H), 8.13–8.21 (m, 2 H), 8.24–8.31 (m, 2 H), 8.97–9.02 (m, 2 H); ^{13}C NMR (101 MHz, CD_3OD): δ = 12.21, 30.23, 33.20, 37.66, 46.46, 55.15, 58.49, 109.23, 126.86, 143.44, 145.41, 156.42, 173.11; IR (KBr): $\tilde{\nu}$ = 2968, 1648, 1561, 1197 cm^{-1}; HRMS (ESI): *m/z* calcd for $C_{21}H_{33}N_3I_2$-Γ: 454.1719 [*M*-I]$^{+}$; found: 454.1704.

4-(*tert*-Butyl)-1-{3-[4-(pyrrolidin-1-yl)pyridin-1-ium-1-yl] propyl}pyridin-1-ium diiodide (PTM0068, 6e)

According to the GP, with **4** (431 mg, 1.00 mmol, 1.0 equiv) and **5e** (159 mg, 1.05 mmol, 1.05 equiv) in MeCN (2.0 mL). Recrystallization from EtOAc/*i*-PrOH (1.1:1) afforded **6e** (457 mg, 79%) as a yellow solid. m.p. 178 °C; ^{1}H NMR (400 MHz, CD_3OD): δ = 1.45 (s, 9 H), 2.10–2.15 (m, 4 H), 2.60–2.69 (m, 2 H), 3.55–3.60 (m, 4 H), 4.40 (t, *J* = 7.7 Hz, 2 H), 4.76 (t, *J* = 7.8 Hz, 2 H), 6.86–6.91 (m, 2 H), 8.15–8.18 (m, 2 H), 8.24–8.29 (m, 2 H), 8.96–9.00 (m, 2 H); ^{13}C NMR (101 MHz, CD_3OD): δ = 26.14, 30.21, 33.22, 37.66, 49.83, 55.26, 58.52, 109.87, 126.86, 143.01, 145.40, 155.23, 173.15; IR (KBr): $\tilde{\nu}$ = 2961, 1647, 1561, 1192 cm^{-1}; HRMS (ESI): *m/z* calcd for $C_{21}H_{31}N_3I_2$-Γ: 452.1563 [*M*-I]$^{+}$; found: 452.1545.

4-(*tert*-Butyl)-1-{3-[4-(piperidin-1-yl)pyridin-1-ium-1-yl] propyl}pyridin-1-ium diiodide (PTM0069, 6f)

According to the GP, with **4** (216 mg, 0.500 mmol, 1.0 equiv) and **5 f** (85.2 mg, 0.530 mmol, 1.05 equiv) in MeCN (1.0 mL). Recrystallization from EtOAc/*i*-PrOH (1:1.2) afforded **6 f** (245 mg, 83%) as a yellow solid. m.p. 240 °C; ^{1}H NMR (400 MHz, CD_3OD): δ = 1.45 (s, 9 H), 1.69–1.76 (m, 4 H), 1.76–1.85 (m, 2 H), 2.58–2.71 (m, 2 H), 3.69–3.76 (m, 4 H), 4.39 (t, *J* = 7.6 Hz, 2 H), 4.77 (t, *J* = 7.7 Hz, 2 H), 7.12–7.20 (m, 2 H), 8.13–8.20 (m, 2 H), 8.21–8.29 (m, 2 H), 8.95–9.02 (m, 2 H); ^{13}C NMR (101 MHz, CD_3OD): δ = 24.93, 26.73, 30.22, 33.14, 37.66, 49.17, 55.07, 58.51, 109.45, 126.86, 143.58, 145.41, 156.92, 173.13; IR (KBr): $\tilde{\nu}$ = 2956, 1648, 1547, 1194 cm^{-1}; HRMS (ESI): *m/z* calcd for $C_{22}H_{33}N_3I_2$-Γ: 466.1719 [*M*-I]$^{+}$; found: 466.1711.

4-(*tert*-Butyl)-1-[3-(4-morpholinopyridin-1-ium-1-yl)propyl] pyridin-1-ium diiodide (PTM0070, 6g)

According to the GP, with **4** (431 mg, 1.00 mmol, 1.00 equiv) and **5 g** (172 mg, 1.10 mmol, 1.05 equiv) in MeCN (2.0 mL). Recrystallization from EtOAc/EtOH (1:1.4) afforded **6 g** (518 mg, 87%) as a yellow solid. m.p. 222 °C; ^{1}H NMR (400 MHz, CD_3OD): δ = 1.45 (s, 9 H), 2.62–2.72 (m, 2 H), 3.69–3.76 (m, 4 H), 3.80–3.85 (m, 4 H), 4.45 (t, *J* = 7.7 Hz, 2 H), 4.78 (t, *J* = 7.8 Hz, 2 H), 7.13–7.27 (m, 2 H), 8.14–8.20 (m, 2 H), 8.33–8.40 (m, 2 H), 8.97–9.04 (m, 2 H); ^{13}C NMR (101 MHz, CD_3OD): δ = 30.23, 33.21, 37.66, 47.73, 55.33, 58.44, 67.15, 109.72, 126.86, 143.86, 145.41, 157.85, 173.11; IR (KBr): $\tilde{\nu}$ = 2964, 1650, 1545, 1193 cm^{-1}; HRMS (ESI): *m/z* calcd for $C_{21}H_{31}N_3OI_2$-I⁻: 468.1512 [*M*-I]$^+$; found: 468.1493.

4-[4-(*tert*-Butoxycarbonyl)piperazin-1-yl]-1-{3-[4-(*tert*-butyl) pyridin-1-ium-1-yl] propyl}pyridin-1-ium diiodide (PTM0071, 6h)

According to the GP, with **4** (216 mg, 0.500 mmol, 1.0 equiv) and **5 h** (145 mg, 0.550 mmol, 1.1 equiv) in MeCN (1.0 mL). Recrystallization from EtOAc/EtOH (2:1) afforded **6 h** (320 mg, 92%) as a yellow solid. m.p. 149 °C; ^{1}H NMR (500 MHz, CD_3OD): δ = 1.45 (s, 9 H), 1.49 (s, 9 H), 2.61–2.69 (m, 2 H), 3.62–3.68 (m, 4 H), 3.76–3.80 (m, 4 H), 4.42 (t, *J* = 7.6 Hz, 2 H), 4.75 (t, *J* = 7.7 Hz, 2 H), 7.19–7.23 (m, 2 H), 8.15–8.19 (m, 2 H), 8.31–8.36 (m, 2 H), 8.95–8.99 (m, 2 H); ^{13}C NMR (126 MHz, CD_3OD): δ = 28.59, 30.21, 33.17, 37.67, 43.60, 47.12, 55.38, 58.48, 81.95, 109.85, 126.86, 143.79, 145.40, 156.17, 157.71, 173.22; IR (KBr): $\tilde{\nu}$ = 2967, 1649, 1416, 1169 cm^{-1}; HRMS (ESI): *m/z* calcd for $C_{26}H_{40}N_4O_2I_2$-I⁻: 567.2196 [*M*-I]$^+$; found: 567.2180.

4-(1-{3-[4-(*tert*-Butyl)pyridin-1-ium-1-yl] propyl}pyridin-1-ium-4-yl)piperazin-1-ium triiodide (PTM0072, 6i)

A solution of **6 h** (69.4 mg, 0.100 mmol, 1.0 equiv) and iodo(trimethyl)silane (80.0 mg, 0.400 mmol, 4.0 equiv) in MeCN (2.0 mL) was stirred under argon at rt for 2 h. **6i** (71.3 mg, 99%) was afforded after filtration of the reaction mixture as a yellow solid. m.p. 109 °C; ^{1}H NMR (400 MHz, CD_3OD): δ = 1.45 (s, 9 H), 2.65–2.75 (m, 2 H), 3.47–3.55 (m, 4 H), 4.03–4.12 (m, 4 H), 4.52 (t, *J* = 7.5 Hz, 2 H), 4.77–4.83 (m, 2 H), 7.33–7.39 (m, 2 H), 8.14–8.20 (m, 2 H), 8.45–8.52 (m, 2 H), 9.01–9.06 (m, 2 H); ^{13}C NMR (101 MHz, CD_3OD): δ = 30.23, 33.27, 37.65, 44.04, 44.65, 55.66, 58.33, 110.83, 126.84, 144.37, 145.44, 158.02, 173.07; IR (KBr): $\tilde{\nu}$ = 2963, 1647, 1549, 1191 cm^{-1}; HRMS (ESI): *m/z* calcd for $C_{21}H_{33}N_4I_3$-H$^+$-2I⁻: 467.1671 [*M*-I-I-H]$^+$; found: 467.1663.

1-{3-[4-(*tert*-Butyl)pyridin-1-ium-1-yl] propyl}-7-hydroxyquinolin-1-ium diiodide (PTMD90-0012, 8)

According to the GP, a solution of **4** (431 mg, 1.00 mmol, 1.0 equiv) and **7** (163 mg, 1.10 mmol, 1.1 equiv) in MeCN (2.0 mL) was stirred under microwave irradiation (150 W) at 90 °C for 3 h. Recrystallization from EtOH/EtOAc (2:1.5) afforded **8** (167 mg, 29%) as a yellow solid. m.p. 263 °C; ^{1}H NMR (400 MHz, CD_3OD): δ = 1.45 (s, 9 H), 2.76–2.89 (m, 2 H), 4.89–4.96 (m, 2 H), 5.09–5.19 (m, 2 H), 7.56 (dd, *J* = 9.0, 2.1 Hz, 1 H), 7.68 (d, *J* = 2.2 Hz, 1 H), 7.81 (dd, *J* = 8.1, 6.1 Hz, 1 H), 8.11–8.22 (m, 2 H), 8.29 (d, *J* = 9.1 Hz, 1 H), 8.95–9.04 (m, 3 H), 9.31 (dd, *J* = 6.1, 1.4 Hz, 1 H); ^{13}C NMR (101 MHz, CD_3OD): δ = 30.20, 31.59, 37.68, 54.85, 58.50, 101.59, 119.39, 123.77, 126.81, 126.88, 134.57, 142.53, 145.41, 148.20, 148.99, 167.19, 173.30; IR (film): $\tilde{\nu}$ = 2968, 1628, 1209, 849 cm^{-1}; HRMS (ESI): *m/z* calcd for $C_{21}H_{26}N_2OI_2$-H$^+$-2I⁻: 321.1967 [*M*-I-I-H]$^+$; found: 321.1961.

1,1′-(2-Hydroxypropan-1,3-diyl)bis[4-(*tert*-butyl)pyridin-1-ium] dibromide (PTMD90-0015, 11)

A mixture of **9** (108 µL, 229 mg, 1.00 mmol, 1.0 equiv) and **10** (352 µL, 325 mg, 2.40 mmol, 2.4 equiv) was stirred at 145 °C for 2 h. The reaction mixture was concentrated in vacuo and the residue was purified by recrystallization from EtOAc/EtOH (1:2) to afford **11** (196 mg, 40%) as a colorless solid. m.p. 248 °C; ^{1}H NMR (400 MHz, CD_3OD): δ = 1.45 (s, 18 H), 4.43–4.69 (m, 3 H), 4.97–5.22 (m, 2 H), 8.11–8.24 (m, 4 H), 8.83–9.01 (m, 4 H); ^{13}C NMR (101 MHz, CD_3OD): δ = 30.19, 37.70, 63.74, 71.06, 126.42, 146.09, 173.58; IR (film): $\tilde{\nu}$ = 2972, 1643, 1468, 1117 cm^{-1}; HRMS (ESI): *m/z* calcd for $C_{21}H_{32}N_2OBr_2$-H$^+$-2Br⁻: 327.2436 [*M*-Br-Br-H]$^+$; found: 327.2430.

2.2. UNC0642 MS Binding Assays

Competitive MS Binding Assays were performed as previously described (Kaiser et al., 2024; Nitsche et al., 2024) apart from one minor difference: in order to obtain competition curves for compounds bearing a 4-aminopyridinium moiety, the non-linear regression function "log (inhibitor) vs. normalized response – Variable slope" (Prism Software v. 6.07, GraphPad Software, La Jolla, CA, USA) was used instead of the recently used function "One site – fit Ki". Statistically significant differences were verified by a two-sided *t*-test (alpha = 0.05).

2.3. Rat diaphragm myography

All experiments were conducted at the Bundeswehr Institute of Pharmacology and Toxicology (InstPharmToxBw) which is the only institute in Germany authorized to use chemical warfare agents (CWA) for research in the areas of pathomechanisms, prevention, detection, treatment, and epidemiology of CWA-induced health disorders.

All procedures using animals followed animal care regulations. Preparation of rat diaphragm hemispheres from male Wistar rats (300 ± 50 g) and experimental protocol of myography was performed as previously described (Nitsche et al., 2024; Seeger et al., 2012). In brief, for all procedures (including wash-out steps, preparation of soman and test compound solutions) aerated Tyrode solution (125 mM NaCl, 24 mM $NaHCO_3$, 5.4 mM KCl, 1 mM $MgCl_2$, 1.8 mM $CaCl_2$, 10 mM glucose, 95% O_2, 5% CO_2; pH 7.4; 25 ± 0.5 °C) was used. The organophosphorus compound (OPC) soman (pinacolylmethylphosphonofluoridate; >93% by GC-MS, ^{1}H NMR and ^{31}P NMR) was provided by the German Ministry of Defence (Bonn, Germany). Soman stock solutions (0.1% v/v) were prepared in acetonitrile, stored at 20 °C and appropriately diluted in Tyrode buffer just before the experiment, and were kept at room temperature until use. All experiments were carried out in a chemical safety hood. After the recording of control muscle force one hour after preparation, the muscles were incubated in the Tyrode solution, containing 3 µM soman for 20 min. Following a 20 min wash-out period, the test compounds were added in ascending concentrations (0.1 µM to 300 µM). The incubation time was 20 min for each concentration. The electric field stimulation was performed with 10 µs pulse width and 2 A amplitudes. The titanic stimulation of 20 Hz, 50 Hz, 100 Hz were applied for 1 s and in 10 min intervals. Measurements on non-toxic muscle were carried out according to the same scheme. Instead of soman, pure Tyrode was incubated. Muscle force was calculated as a time-force integral (area under the curve, AUC) and constrained to values obtained for maximum force generation at the start of the measurements (muscle force in the presence of Tyrode solution without any additives; 100%). All results were expressed in means ± SD (n = 6–12). Prism 5.0 (GraphPad Software, San Diego, CA, USA) was used for data analysis.

2.4. MD simulations

The model of the human muscle type nAChR was generated using Modeller with the PDB structure of the α7-nAChR as the template (PDB ID: 7KOX (Noviello et al., 2021). The orthosteric ligand nicotine and a sodium ion in the transmembrane pore were included by aligning the structure of the α3β4-nAChR (PDB ID: 6PV7 (Gharpure et al., 2019) to the homology model. Nicotine was subsequently minimized using SZYBKI (OpenEye Scientific Software, 2021). MB327 was docked in MB327-PAM-1 using MOE with an induced-fit refinement using default parameters (Chemical Computing Group, 2020). Ligand charges were calculated using Gaussian16 (M. J. Frisch et al., 2016) at the HF/6–31 G* level of theory; force field parameters for the ligand were taken from the gaff force field (Wang et al., 2004). Using Packmol-Memgen (Schott-Verdugo and Gohlke, 2019), the system was embedded in a membrane containing 1-palmitoyl-2-oleoyl-*sn*-glycero-3-phosphocholine (POPC) lipids, solvated using the Optimal Point

Charge water model (Izadi et al., 2014) with a minimum distance of 12 Å between receptor atoms and the edge of the box, KCl was added in a concentration of 150 mM, and the system was neutralized using Cl^- ions. To perform MD simulations, the AMBER22 package of molecular simulations software (Case et al., 2005; Case et al., 2022), the ff19SB force field (Tian et al., 2020) for the protein, the Lipid17 force field (Gould et al., unpublished) for lipids, the gaff force field for the ligand, and the Joung and Cheatham parameters for monovalent ions were used (Joung and Cheatham, 2008). MD simulations were performed as described previously (Kaiser et al., 2023). In short, a combination of steepest descent and conjugate gradient minimization was performed while gradually decreasing positional harmonic restraints. The system was then heated in a stepwise manner to 300 K, and harmonic restraints on receptor and ligand atoms were gradually removed subsequently. Then, 12 replicas of 1 μs long unbiased MD simulations were performed in the NPT ensemble using semi-isotropic pressure adaptation with the Berendsen barostat. The RMSD, electron density profiles and representative binding modes were computed using CPPTRAJ (Roe and Cheatham, 2013), as implemented in AmberTools (Case et al., 2023).

2.5. GIST computations

GIST (Lazaridis, 1998; Nguyen et al., 2011, 2012; Ramsey et al., 2016) computations, as implemented in CPPTRAJ (Roe and Cheatham, 2013), were performed in replicas where MB327 remained in the binding site (distance to I64δ (respectively, I61ε, I61α, I64β) < 5 Å, as done previously) (Kaiser et al., 2023) during MD simulations. The backbone of each frame during these MD simulations was aligned to the starting structure of the simulations using CPPTRAJ (Roe and Cheatham, 2013). The middle carbon atom of the C3-linker in MB327 was used as the center of the box for GIST grid generations with grid dimensions of 40 increments along each axis and a grid spacing of 0.5 Å. In GIST, the entropy term of water in each voxel consists of both an orientational and translational contribution. Furthermore, for the energetic contribution the solute-water and water-water interaction is computed based on Lennard-Jones and electrostatic interactions. The results were filtered based on the density of oxygen centers in each voxel compared to bulk density (cutoff: > 1.75) and the solvent free energy (cutoff: > −0.25 kcal mol^{-1}). Visualization of water clusters and manual modification of MB327 to PTMD90–0012 (**8**) and PTMD90–0015 (**11**) was performed using MOE (Chemical Computing Group, 2020).

2.6. Image generation

Images of nAChR in complex with MB327 and its analogs were created using UCSF Chimera (Pettersen et al., 2004).

3. Results and discussion

3.1. Synthesis of novel MB327 analogs

To identify novel non-symmetric MB327 analogs that should exhibit higher binding affinities to the MB327-PAM-1 binding site as well as higher intrinsic activities compared to MB327, a series of non-symmetric bispyridinium compounds **6a-6i** with a 4-aminopyridinium ion partial structure derived from compounds **1**-**3** was synthesized. In addition, based on modeling studies (see chapter 3.3), novel MB327 analogs **8** and **11** with an additional OH function were synthesized with the assumption that this modification should increase the binding affinity by displacing water molecules from the binding pocket.

3.1.1. Non-symmetric MB327 analogs PTM0064-PTM0072 (6a-6i) and PTMD90-0012 (8)

Non-symmetric MB327 analogs **6a**-**6 h** bearing a 4-aminopyridinium ion moiety were readily accessible in one step by *N*-alkylation of 4-aminopyridines **5** with *N*-(3-iodopropyl)pyridinium building block **4**, analogous to the method described by Rappenglück et al. (2018) (Scheme 1). To cover a wider variety of 4-amino substituents in the target compounds, the set of commercially available 4-aminopyridines **5a**, **5b,** and **5e**-**5 g** was extended with some building blocks (**5c**, **5d** and **5 h**), synthesized according to literature (Hay et al., 2015; Price et al., 2006; Wang et al., 2019). *N*-Alkylation of the pyridines **5a** and **5c**-**5 h** with building block **4** (Rappenglück et al., 2018) was accomplished by stirring the components in acetonitrile at 90 °C under microwave irradiation for 1 h. After removing the reaction solvent, the resulting residues were purified by crystallization to yield the target compounds **6a** and **6c**-**6 h** in good to excellent yields (72–93%) and high purities (≥ 98%). Reaction with *tert*-butyl pyridin-4-ylcarbamate (**5b**), however, required a lower reaction temperature to prevent cleavage of the Boc group as a reaction at 90 °C for 1 h had led to a mixture of product **6b** and 4-amino-analog **1** in a ratio of 3:1. By stirring **5b** with building block **4** at 60 °C for 15 h no side product **1** was observed and the product **6b** was afforded in excellent yield (92%) and sufficient purity (94%). To get the hydroiodide **6i**, the Boc protecting group of **6 h** was cleaved by stirring with trimethylsilyl iodide (TMSI) (4.0 equiv) in acetonitrile at room temperature for 1 h (Lott et al., 1979). Thus, compound **6i** was isolated in quantitative yield (99%) and with high purity (100%).

PTMD90–0012 (**8**) was synthesized from building block **4** (Rappenglück et al., 2018) and 7-hydroxyquinoline (**7**) under the reaction conditions described for bispyridinium compounds **6a**-**6 h**. However, the reaction time had to be increased to 3 h to compensate for the lower reactivity of the sterically more demanding quinoline **7** as compared to the 4-aminopyridines **5**. That way, PTMD90–0012 (**8**) was obtained in 29% yield after recrystallization (purity ≥ 98%) (Scheme 2).

3.1.2. MB327 analog PTMD90-0015 (11)

The symmetric bispyridinium compound PTMD90–0015 (**11**) with a 2-hydroxypropyl linker between the two pyridinium rings, was synthesized by heating 1,3-dibromopropan-2-ol (**9**) with an excess of 4-*tert*-butylpyridine (**10**) to 145 °C for 2 h. Bis-alkylation product PTMD90–0015 (**11**) was obtained in 40% yield and in high purity (100%) after recrystallization (Scheme 3). In contrast, reaction of **8** with epichlorohydrine or 1,3-dichloropropan-2-ol under the reaction conditions described above led only to the corresponding monosubstituted products.

3.2. Biological evaluation

3.2.1. Affinity to the MB327-PAM-1 binding site of Torpedo californica nAChR

All of the newly developed compounds presented in this study, i.e. PTM0064-PTM0072 (**6a-6i**), PTMD90–0012 (**8**) and PTMD90–0015 (**11**) as well as MB327 and its recently reported analogs PTM0062 (**1**) (Kaiser et al., 2023), PTM0063 (**2**) (Kaiser et al., 2023) and PTM0056 (**3**) (Rappenglück et al., 2018) were evaluated for their binding affinity towards the MB327-PAM-1 binding site of *Torpedo californica* nAChR by means of the recently introduced UNC0642 MS Binding Assays (Table 1) (Kaiser et al., 2024; Nitsche et al., 2024). First, for economic reasons, all test compounds were studied at a single concentration of 10 μM and a reporter ligand concentration of 1 μM. For a set of selected compounds also the binding affinity constants (pK_i values) were determined in full-scale MS competition experiments.

Remaining reporter ligand binding in the presence of 10 μM of the respective compounds listed in Table 1 range from 102% ± 9% for MB327 (Table 1, entry 1) to 64% ± 8% for the *N*-Boc-piperazino derivative PTM0071 (**6 h**, Table 1, entry 12). For clarity reasons it may be stated that increasing binding affinities of the test compounds are reflected by decreasing values of the remaining reporter ligand binding. Substitution of one of the two 4-*tert*-butyl residues of MB327 by an amino [PTM0062 (**1**), 93% ± 5%, Table 1, entry 2], an *N*-methylamino [PTM0063 (**2**), 92% ± 1%, Table 1, entry 3], or dimethylamino group

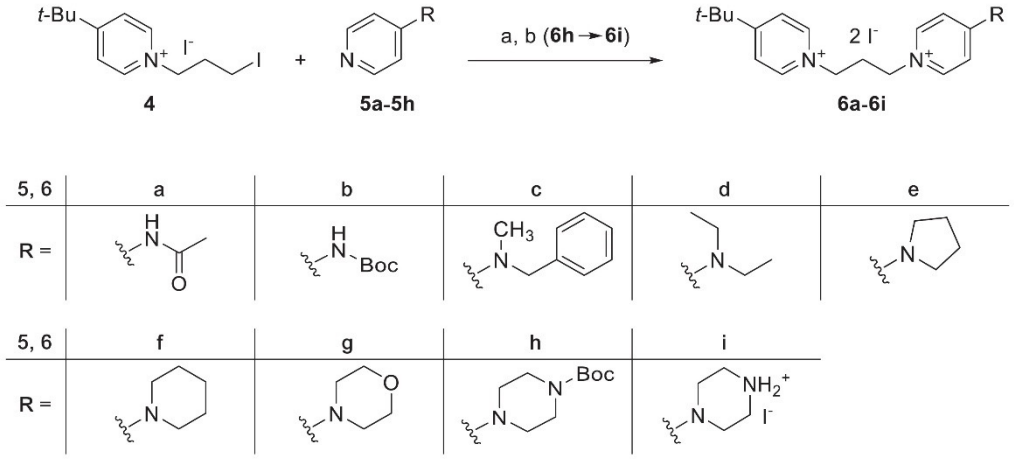

Scheme 1. Synthesis of **6a-6i**. Reagents and conditions: (a) 4-(*tert*-butyl)-1-(3-iodopropyl)pyridin-1-ium iodide (**4**) (1.0 equiv), pyridines **5a-5 h** (1.05–1.1 equiv), MeCN, microwave: 150 W, 60–90 °C, 1–15 h, 72–93%; (b) **6i**: **6 h** (1.0 equiv), TMSI (4.0 equiv), MeCN, rt, 1 h, 99%.

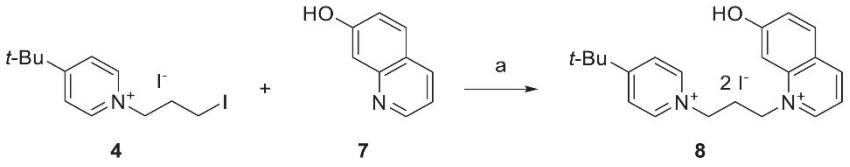

Scheme 2. Synthesis of PTMD90–0012 (**8**). Reagents and conditions: (a) 4-(*tert*-butyl)-1-(3-iodopropyl)pyridin-1-ium iodide (**4**) (1.0 equiv), 7-hydroxyquinoline (**7**) (1.1 equiv), MeCN, microwave: 150 W, 90 °C, 3 h, 29%.

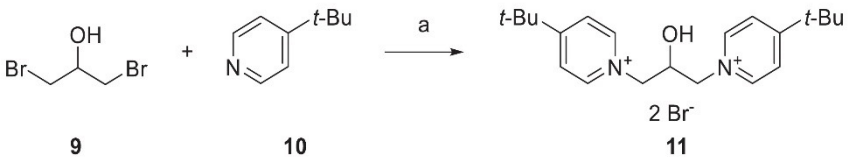

Scheme 3. Synthesis of PTMD90–0015 (**11**). Reagents and conditions: (a) 1,3-dibromopropan-2-ol (**9**) (1.0 equiv), 4-*tert*-butylpyridine (**10**) (2.4 equiv), 145 °C, 2 h, 40%.

[PTM0056 (**3**), 90% ± 5%, Table 1, entry 4] results in a nominal yet not statistically significant reduction of remaining reporter ligand binding as compared to MB327. This is also true for compounds PTM0064 (**6a**, 90% ± 6%, Table 1, entry 5) and PTM0065 (**6b**, 90% ± 4%, Table 1, entry 6) displaying an *N*-acetamido- and an *N*-*tert*-butoxycarbonylamino moiety, respectively effecting a reduction to 90% of remaining reporter ligand binding. According to the data obtained for **1**-**3** and **6a**-**6b** the capability of the nitrogen substituents, present in these compounds to participate in hydrogen bonding seems to have only little if any influence on the binding affinities, the remaining reporter ligand binding amounting in any case to about 90%. Likewise, when the dimethylamino group in PTM0056 (**3**, 90% ± 5%, Table 1, entry 4) is replaced by a sterically more demanding *N*,*N*-diethylamino moiety, the binding affinity of the resulting PTM0067 (**6d**) remains with 91% ± 11% virtually unaltered (remaining reporter ligand binding, Table 1, entry 8). Although **1**-**3** as well as **6a**, **6b** and **6d** effect remaining reporter ligand binding nominally below that of MB327 (Table 1, entry 1), for none of these compounds the observed differences are statistically significant. However, for the *N*-benzyl-*N*-methylamino derivative PTM0066 (**6c**) with an enlarged lipophilic domain, remaining reporter ligand binding reaches 85% ± 8% (Table 1, entry 7), which is statistically significantly lower than that of MB327 (102% ± 9%, Table 1, entry 1).

Notably, the pyrrolidino and the piperidino substituted derivatives PTM0068 (**6e**) and PTM0069 (**6 f**), of which the former can be considered as a cyclic analog of the diethylamino substituted **6d,** reduce remaining reporter ligand binding to 85% ± 0.5% (Table 1, entry 9) and 73% ± 6% (Table 1, entry 10), both values being also statistically significantly below than that of MB327 (102% ± 9%, Table 1, entry 1).

Upon transition from the piperidino-substituted bispyridinium salt **6 f** to the more polar morpholino-substituted analog PTM0070 (**6 g**), again a decline in binding affinity is observed with the remaining reporter ligand binding increasing to 90% ± 8% (Table 1, entry 11). However, for the nitrogen analog of the morpholino derivative **6 g**, the piperazino derivative PTM0072 (**6i**), the decline in binding affinity compared to **6 f** displaying a piperidino residue (73% ± 6%, Table 1, entry 10) was less pronounced, with the remaining reporter ligand binding amounting to 83% ± 5% (Table 1, entry 13). Obviously, the binding affinity-diminishing effect of the additional heteroatom seems to be less distinct for the piperazino derivative **6i** than for the morpholino derivative **6 g** (as compared to the piperidino analog **6 f**). This can possibly be attributed to the capability of the terminal amino function of the piperazino group of **6i** - present in free form or as a salt or both - to participate in a hydrogen bridge with the protein. Still, this ability to be part of a hydrogen bond appears to be of less overall

Table 1
Binding affinities of bispyridinium compounds for the MB327-PAM-1 binding site of *Torpedo californica* nAChR, determined in UNC0642 MS Binding Assays.

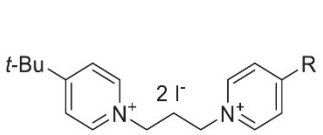

MB327, 1-3, 6a-6i

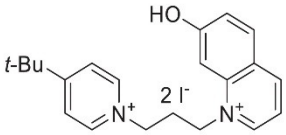

8

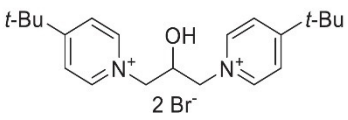

11

Entry	Compound	R	Remaining Reporter Ligand Binding [%] [a]	PTM code
1	**MB327**		102 ± 9 (pK_i = 3.40 ± 0.04[b])	-
2	**1**		93 ± 5	0062[c]
3	**2**	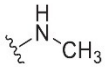	92 ± 1	0063[c]
4	**3**	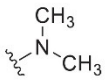	90 ± 5	0056[d]
5	**6a**	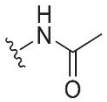	90 ± 6	0064
6	**6b**	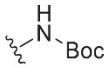	90 ± 4	0065
7	**6c**	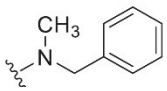	85 ± 8*	0066
8	**6d**	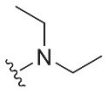	91 ± 11	0067
9	**6e**		85 ± 0.5*	0068
10	**6 f**	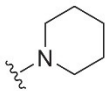	73 ± 6** (pK_i = 3.96 ± 0.08)	0069
11	**6 g**	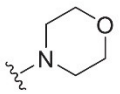	90 ± 8	0070
12	**6 h**	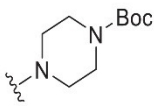	64 ± 8** (pK_i = 4.17 ± 0.02)	0071
13[e]	**6i**	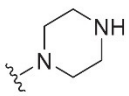	83 ± 5*	0072
14	**8**	-	93 ± 9 (pK_i = 3.69 ± 0.03)	D90–0012
15	**11**	-	98 ± 5 (pK_i = 3.29 ± 0.05)	D90–0015

Asterisks indicate statistically significantly lower values for the remaining reporter ligand binding of the respective compound compared to the MB327 value (* $p < 0.05$, ** $p < 0.01$, based on a two-sided *t*-test)

[a] The results of UNC0642 MS Binding Assays are given as percentages representing the remaining reporter ligand binding (UNC0642, 1 μM) in presence of 10 μM test compound as compared to 100% reporter ligand binding in the absence of a competitor. Values are given as means ± SD of triplicate experiments, except for MB327, which was determined in two experiments from a triplicate determination each. The pK_i values given in brackets represent means ± SEM of three independent experiments determined in UNC0642 MS Binding Assays in full scale competition experiments (mean Hill coefficient = 0.45–0.61).

[b] pK_i value of MB327 from (Nitsche et al., 2024).

[c] Compound from (Kaiser et al., 2023).

[d] Compound from (Rappenglück et al., 2018).

[e] Compound tested as hydroiodide.

importance, since although it is lost by the attachment of an *N*-Boc substituent to the piperazino moiety of **6i**, resulting in PTM0071 (**6 h**, Table 1, entry 12), the binding affinity is distinctly improved. Thus, a remaining reporter ligand binding of 64% ± 8% could be measured for this compound, which is statistically significantly lower than that of the piperazino-substituted compound **6i** (Table 1, entry 13). Hence, the piperidino-substituted compound **6 f** (Table 1, entry 10) and the *N*-Boc-piperazino derivative **6 h** (Table 1, entry 12) possess the highest binding affinities for the MB327-PAM-1 binding site of the nAChR of the compounds evaluated in this study.

Modeling studies (see chapter 3.3) indicated, that the presence of an OH function in ligands of the MB327-PAM-1 binding site might be favorable for the binding affinity by displacing water molecules present in the binding pocket. In particular, the MB327 analog **11** with an OH function in the spacer linking the two pyridinium subunits in the molecule as well as **8** with a 7-hydroxyquinolinium replacing one of the two pyridinium subunits in MB327 were expected to possess improved binding affinities. Hence, the binding affinities of PTMD90–0015 (**11**) and PTMD90–0012 (**8**) were studied. Both compounds, however, show no or only a negligible improvement of the binding affinity compared to MB327 (Table 1, entry 1), the remaining reporter ligand binding amounting to 98% ± 5% for **11** (Table 1, entry 15) and 93% ± 9% for **8** (Table 1, entry 14). Although no clear improvement of the binding affinity could be achieved with **11** and **8**, the results indicate that the presence of an additional polar OH function is tolerated in the binding pocket.

Finally, for a small set of compounds, the pK_i values as a more accurate measure of the binding affinity were determined in full-scale competitive MS Binding Assays. This set comprised the two compounds **6 f** and **6 h**, which had shown the highest binding affinities in the single point determinations described above (reduction of the remaining reporter ligand binding to < 75%) as well as the two OH function-containing derivatives **8** and **11**, which had emerged as candidate compounds for testing from modeling studies. Notably, the piperidino derivative **6 f** (Table 1, entry 10) exhibits a pK_i of 3.96 ± 0.08, which was approximately 0.5 log units and thus statistically significantly higher than the pK_i of MB327 previously determined to be 3.40 ± 0.04 (Table 1, entry 1) (Nitsche et al., 2024). The *N*-Boc-piperazino derivative **6 h** (Table 1, entry 12) showed an even higher pK_i of 4.17 ± 0.02, as to be expected from the preliminary binding data (remaining reporter ligand binding 64% ± 5%), exceeding that of MB327 by approximately 0.8 log units. For the MB327 analog **11** with an OH function as part of the propan-1,3-diyl spacer (Table 1, entry 15), the pK_i value (3.29 ± 0.05) matched that of MB327 within the limits of error. For the 7-hydroxyquinolinium derivative **8** (Table 1, entry 14), a pK_i value of 3.69 ± 0.03 was found, almost 0.3 log units higher than that of MB327, which is statistically significantly different, indicating the higher binding affinity of this compound compared to MB327.

3.2.2. Evaluation of muscle force recovery in soman-poisoned rat diaphragm hemispheres

In addition to the binding affinities, the intrinsic activities of a selection of the test compounds have been determined by means of an *ex vivo* assay based on rat diaphragm hemispheres. In this assay dissected rat diaphragm hemispheres are treated with a solution containing 3 μM soman. Whereas upon indirect electric field stimulation commonly carried out at frequencies of 20 Hz, 50 Hz and 100 Hz, unpoisoned rat diaphragms undergo muscle contractions, in case of poisoned samples no or only very faint contractions occur. This inhibition further does not vanish, when the poisoned samples are freed from the toxin by washing, typically performed as a control, as this has no effect on the irreversible inhibition of the AChE by the nerve agent. The positive intrinsic activity of the test compounds becomes apparent, when their addition to the poisoned muscle preparations, typically performed in increasing concentrations from 0.1 to 300 μM, affects a recovery of the muscle force of the soman-impaired rat diaphragm hemispheres. Muscle force inhibition reappears, when samples are subjected to a subsequent washout step, which is due to the irreversible inactivation of the AChE and indicative of the reversibility of the receptor-mediated resensitizing effect of the test compounds.

For the characterization of the muscle force restoring potency of soman-poisoned rat diaphragms in the aforementioned test system, the piperidino- and the *N*-Boc-piperazino derivatives **6 f** and **6 h** were selected as they had shown the highest binding affinities among the new test compounds presented in this study. In addition, the piperazino derivative **6i**, closely related to **6 h**, the *N*,*N*-dimethylamino-substituted compound **3** as parent compound, as well as the hydroxy-substituted compounds **8** and **11** as analogs of MB327 devoid of an amino-substituent were evaluated in this test system.

Since it is known, that the largest efficacy is observed at low stimulation frequencies (Seeger et al., 2012), only the results of experiments performed at 20 Hz will be presented (Fig. 2) and discussed in the following. The data of measurements carried out at higher frequencies (50 Hz, 100 Hz) can be found in the Supporting Information (SI, Figure S12).

As reference, the published data obtained for MB327 in the test system have been included in Fig. 2 (Niessen et al., 2018). As previously reported, MB327 addition (Fig. 2A) leads to a concentration-dependent reactivation of soman-impaired muscle. The recovery gradually increases with the MB327 concentration (Fig. 2A). At a MB327 concentration of 100 μM, the muscle force recovery amounts to 14.8% ± 9.2%, reaches 30.2% ± 9.5% at 300 μM (both values statistically significantly different from the value obtained for the soman-poisoned muscle), to finally decrease to 4.2% ± 4.2% at 1000 μM MB327 (not shown in Fig. 2A)(Niessen et al., 2018).

Similar to MB327, the analogs **3**, **6 f**, **6 h** and **6i** exhibiting a 4-amino group at one of the two pyridinium subunits instead of a *tert*-butyl moiety (present in MB327) lead to an increase of the regeneration of the muscle force of soman-poisoned rat diaphragms with increasing concentrations, whereas the onset and the size of this effect differ. The *N*,*N*-dimethylamino-substituted analog **3** shows its maximum recovery at a concentration of 100 μM (45.8% ± 17.4%), which statistically significantly exceeds that of MB327 ($p < 0.01$) at the same concentration (14.8% ± 9.2%). However, the reactivation decreases nominally at 300 μM to 37.0% ± 15.8%, approximating that of MB327 at the same concentration (30.2% ± 9.5%). At a compound concentration of 100 μM, the results for the piperidino- and the piperazino-substituted compounds **6 f** (47.5% ± 29.8%) and **6i** (47.3% ± 21.8%) are comparable to the value observed for the dimethylamino derivative **3**, which are also nominally the highest values of all three compounds. At

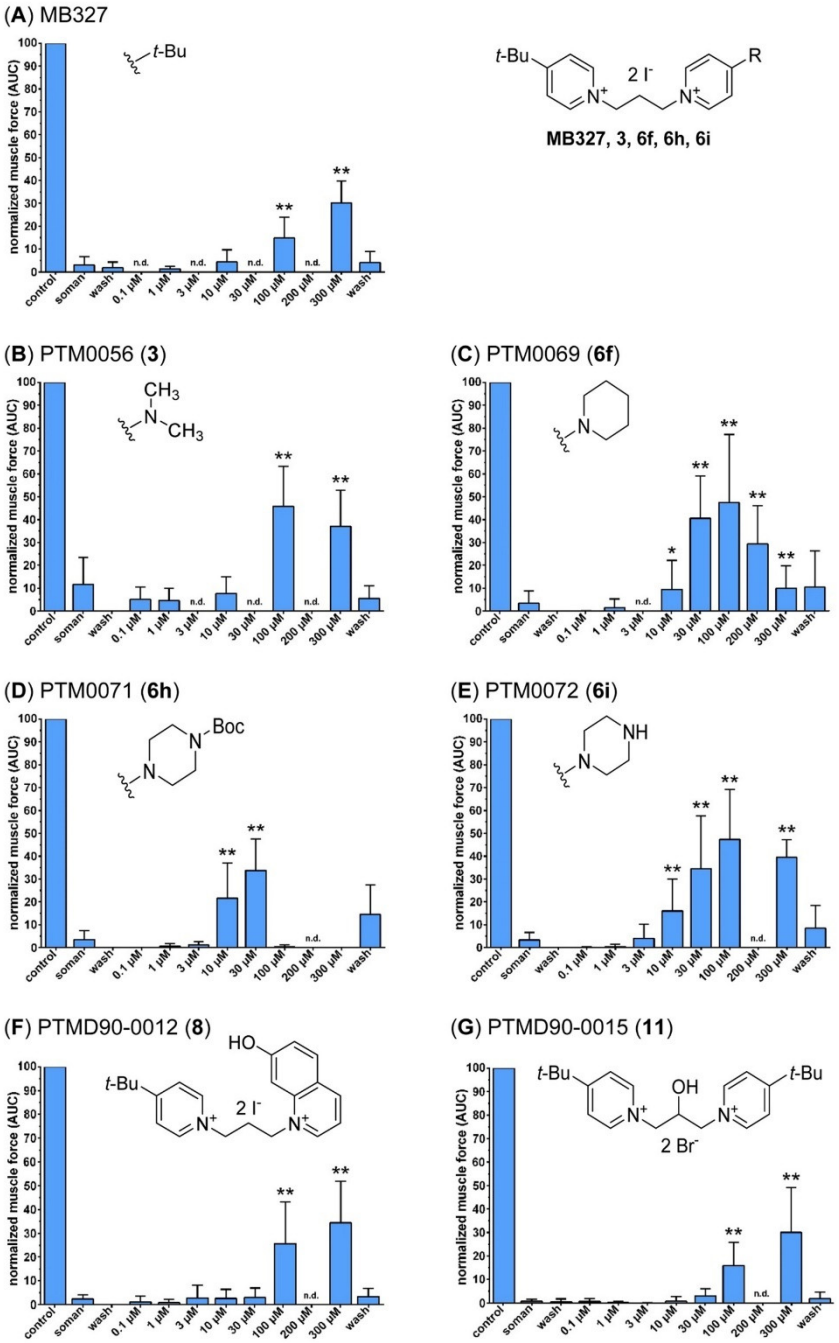

Fig. 2. Concentration-dependent restoration of muscle force of soman-poisoned rat diaphragms by (**A**) MB327 (Niessen et al., 2018), (**B**) PTM0056 (**3**), (**C**) PTM0069 (**6 f**), (**D**) PTM0071 (**6 h**), (**E**) PTM0072 (**6i**), (**F**) PTMD90–0012 (**8**) and (**G**) PTMD90–0015 (**11**). For indirect stimulation, a frequency of 20 Hz was applied. Data are shown as % of control and are given as mean ± SD (n = 4–25). Asterisks indicate statistically significantly higher values for the respective compound concentration compared to the soman value (* $p < 0.05$, ** $p < 0.01$, based on a two-sided *t*-test). n.d.: not determined.

concentrations above 100 µM, alike observed for the dimethylamino derivative **3**, the muscle force declines again for **6 f** as well as **6i**, which is in the case of **6i** with 39.5% ± 7.7% muscle force recovery at 300 µM compound concentration far less pronounced than for **6 f** with 10.0% ± 9.8% (statistically significant, $p < 0.01$; **6 f** at 200 µM 29.3% ± 16.8%).

The *N*-Boc-piperazino derivative **6 h** induces a rather strong muscle force recovery already at 10 µM with a value amounting to 21.7% ± 15.3%, which is nominally the highest for all tested compounds at this concentration, which further increases at 30 µM to 33.8% ± 13.8% followed by a sharp drop to almost 0% (0.3% ± 0.8%) at 100 µM (0.0%

± 0.0% at 300 μM). This strong muscle force recovery effect of **6 h** at a low concentration might be a result of its high binding affinity, which is the highest of all compounds studied.

Notably, all three MB327 analogs with cyclic amino residues exert already at a concentration of 10 μM a muscle force recovery that is statistically significantly higher than that of the soman-poisoned but untreated muscle, whereas this is neither the case for the dimethylamino derivative **3** nor for MB327. For the piperidino derivative **6 f,** the respective recovery of muscle force at 10 μM amounts to 9.5% ± 12.7%, for the *N*-Boc-piperazino analog **6 h** to 21.7% ± 15.3% and the piperazino derivative **6i** to 16.0% ± 14.1%. Statistical significance of muscle force recovery over the soman-poisoned but untreated muscle as reference value is reached for these three compounds also at a test compound concentration of 30 μM (**6 f**, 40.6% ± 18.5%; **6 h**, 33.8% ± 13.8%; **6i**, 34.5% ± 23.2%). Yet, it remains unclear, whether this is also the case for the dimethylamino derivative **3** and MB327, as data for these two compounds when applied at 30 μM are missing.

The two MB327 analogs featuring an additional hydroxy group either in the spacer, **11**, or as part of a quinolinium moiety, **8**, show very similar effects in terms of muscle force regeneration after soman-intoxication. Also, muscle force recovery effected by **11** and **8** at concentrations of 100 μM and 300 μM is statistically significant as compared to the soman value. Thereby, the values for muscle force recovery of soman-poisoned muscle amounted for **11** to 15.9% ± 9.9% at 100 μM and to 30.1% ± 19.1% at 300 μM, whereas those for **8** are higher with 25.6% ± 17.5% at 100 μM and 34.3% ± 17.5% at 300 μM. For both compounds, no decrease in muscle force could be observed up to the highest concentration of 300 μM studied.

Finally, the effects of test compounds that were still available in sufficient amounts, i.e., of MB327 and the dimethylamino **3**, the piperidino **6 f** as well as the quinolinium derivative **8,** on the muscle force of rat diaphragm hemispheres not been poisoned with soman were studied (SI, Figure S13). These experiments were carried out in analogy to those for the determination of muscle force recovery of soman-poisoned rat diaphragm hemispheres. Accordingly, the muscle force of rat diaphragm hemispheres not exposed to soman was measured as a function of increasing concentrations of the test compounds under indirect electric field stimulation at 20 Hz, 50 Hz and 100 Hz. Data from analogous experiments performed in parallel but without the application of test compounds served as reference by unveiling the loss of muscle force purely due to the washing steps. MB327 and dimethylamino derivative **3** showed no inhibitory effect up to the maximum concentration of 300 μM, as did the quinolinium derivative **8** up to 200 μM as the highest concentration still feasible due to a shortage of the compound. For the piperidino derivative **6 f**, however, although the muscle force remained unaffected up to a concentration of 100 μM, a distinct reduction occurred at a concentration of 300 μM. The latter might explain the bell-shaped curve observed for this compound, **6 f**, in the muscle force recovery experiments of soman-poisoned rat diaphragm hemispheres (Fig. 2C). The positive effect of **6 f** on soman-poisoned rat diaphragms mediated by binding to the MB327-PAM-1 binding site of the nAChR might be counteracted by a direct negative effect on muscle force, mediated by different binding sites, which seems to become dominating at concentrations above 100 μM of **6 f,** leading to the observed decline of muscle force recovery in soman-poisoned muscles (Fig. 2C) above this concentration.

3.3. Substituting entropically unfavorable water clusters using in silico methods

We performed unbiased MD simulations (12 replicas of 1 μs length each) of the human nAChR with MB327 bound to the recently identified allosteric binding site MB327-PAM-1 in all five subunits (Kaiser et al., 2023). During the simulations, the receptor and membrane stayed structurally invariant shortly after the simulations started (SI, Figure S14, S15). MB327 mostly or completely remained within the binding sites in between the α- and δ-subunits (ten out of twelve replicas) as well as in between the α- and ε-subunits (twelve out of twelve replicas) using the distance of heavy atoms of MB327 to heavy atoms of I64δ (respectively I61ε) to characterize unbinding as done previously (Kaiser et al., 2023). For these two binding sites, Grid Inhomogeneous Solvent Theory (GIST) computations (Lazaridis, 1998; Nguyen et al., 2011; Nguyen et al., 2012; Ramsey et al., 2016) were subsequently performed to identify potential entropically unfavorable water clusters (Fig. 3B, SI, Figure S16A). We then visualized the docked MB327 binding mode and representative MB327 structures from MD simulations in the presence of such water clusters and manually created new MB327 analogs with substituents replacing these water clusters. Initially, during the first few replicas (5 out of 12) of MD simulations and subsequent GIST computations, a network of entropically unfavorable water molecules near the linker of MB327 was identified between E65α, V66α, and Q68α (SI, Figure S17). Based on these preliminary results, PTMD90–0015 (**11**) was designed. However, after completion of the MD simulations, the hydroxyl group located at the C3-linker would not result in replacing entropically unfavorable water molecules as indicated by GIST. Hence, PTMD90–0012 (**8**) was designed based on the results after 1 μs long simulations (Fig. 3C, SI, Figure S16B), such that it should substitute entropically unfavorable water molecules in close proximity to I63ε, E65ε, and E204ε (respectively L66δ, E68δ, and E210δ). As only the analogs based on the docked structure [PTMD90–0012 (**8**)] and those based on the initial MD simulations results [PTMD90–0015 (**11**)] could be synthesized, they were subsequently tested for affinity and resensitizing potential.

4. Conclusion

The recently developed non-symmetric MB327 analogs PTM0062 (**1**), PTM0063 (**2**) and PTM0056 (**3**), which have an amino, methylamino or dimethylamino group in place of one of the two *tert*-butyl residues of MB327, respectively, show higher muscle force restoring activity on soman-poisoned rat diaphragms than MB327. They are therefore promising starting points for the development of new resensitizers for desensitized muscle-type nAChRs as antidots for OPC poisoning.

In the present study, a series of new non-symmetric MB327 analogs, PTM0064-PTM0072 (**6a-6i**), with a 4-amino-substituted pyridinium ion substructure derived from compounds **1**-**3**, were synthesized and evaluated for their binding affinity towards the MB327-PAM-1 binding site of *Torpedo californica* nAChR using the recently introduced UNC0642 MS Binding Assays. In addition, selected compounds were evaluated for their intrinsic activity on soman-poisoned rat diaphragms in myography assays.

Among the compounds evaluated in this study, the piperidino derivative PTM0069 (**6 f**) and the *N*-Boc-piperazino derivative PTM0071 (**6 h**) showed the highest affinities for the MB327-PAM-1 binding site of the nAChR. The pK_i values for **6 f** and **6 h** exceeded that of MB327 by approximately 0.5 and 0.8 log units, respectively. PTMD90–0015 (**11**), designed to substitute unfavorable water clusters in MB327- PAM-1 after preliminary MD simulations, showed reduced affinity towards MB327-PAM-1 and no beneficial resensitizing effects compared to MB327. These results are concordant with that the hydroxy group located at the C3-linker would not result in replacing entropically unfavored water molecules as indicated by GIST after 1 μs long MD simulations. By contrast, PTMD90–0012 (**8**), designed using extended MD data, showed a statistically significant increase of affinity compared to MB327. Likely, this may result from replacing entropically unfavored water molecules close to $I63_{\varepsilon}$, $E65_{\varepsilon}$, and $E204_{\varepsilon}$ (or $L66_{\delta}$, $E68_{\delta}$, and $E210_{\delta}$) with the 7-hydroxy quinazoline moiety.

Ex vivo studies in soman-poisoned rat diaphragms showed a clear muscle force restoring activity for all compounds tested [PTM0069 (**6 f**), PTM0071 (**6 h**), PTM0056 (**3**), PTM0072 (**6i**), PTMD90–0012 (**8**), and

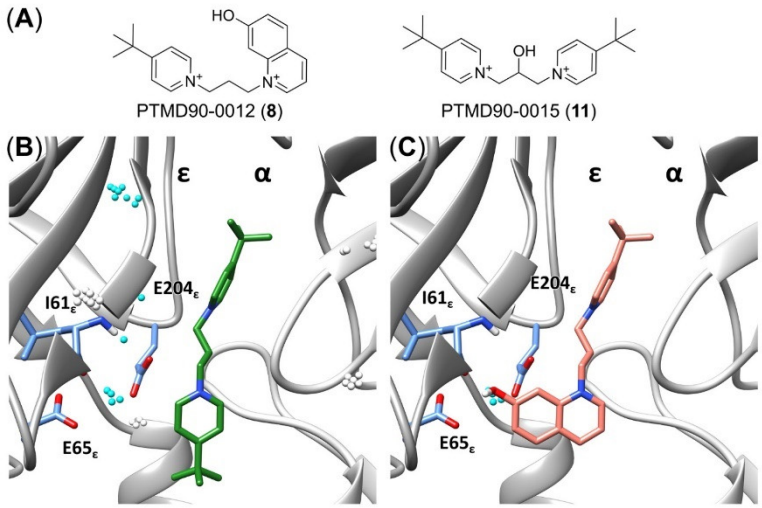

Fig. 3. Design of MB327 analogs based on substituting water clusters in MB327-PAM-1. **A)** Structure of the MB327 analogs PTMD90–0012 (**8**) and PTMD90–0015 (**11**). **B)** MB327 (green) binding in between the α- and ε-subunit. Water clusters identified during GIST computations are shown as spheres. Water clusters within 5 Å of MB327 are shown in cyan. **C)** Proposed binding mode of PTMD90–0012 (**8**) (salmon) in between the α- and ε-subunit. Modification of MB327 to PTMD90–0012 (**8**) (salmon) leads to a substitution of a water cluster located in proximity to $I63_{\varepsilon}$, $E65_{\varepsilon}$, and $E204_{\varepsilon}$; for $I61_{\varepsilon}$, the backbone atoms are shown in addition to the side chain.

PTMD90–0015 (**11**)]. In particular, compounds PTM0069 (**6 f**), PTM0071 (**6 h**) and PTM0072 (**6i**), which all have cyclic aliphatic amino substituents instead of one of the two *tert*-butyl residues of MB327, showed a statistically significantly higher activity at lower concentrations than MB327. Thus, to achieve muscle force recovery comparable to that of the aforementioned compounds, MB327 must be used at a tenfold higher concentration. This could be due to the fact that PTM0069 (**6 f**) and PTM0071 (**6 h**), in particular, but also PTM0072 (**6i**) have statistically significantly higher binding affinities for the MB327-PAM-1 binding site than MB327. It is noteworthy that the recovery of muscle force with PTM0069 (**6 f**) and PTM0071 (**6 h**) at higher concentrations decreased significantly immediately after reaching the maximum value, a phenomenon also observed for MB327. Experiments with PTM0069 (**6 f**) and rat diaphragms that had not been poisoned with soman showed that in the presence of higher concentrations of PTM0069 (**6 f**), a significant inhibition of muscle force occurs, which is reversible as it almost completely disappears after a subsequent washout step. Interestingly, this reversible inhibition occurs in the same concentration range in which the muscle force restoring effect of compound **6 f** decreases in the experiments with soman-poisoned rat diaphragms.

Taken together, this indicates that the positive resensitizing effect mediated by binding to the MB327-PAM-1 binding site is counteracted by a muscle force inhibitory effect becoming generally prominent at higher concentrations that appears to be due to reversible binding to a different binding site.

Therefore, future efforts must focus, on the one hand, on further increasing the affinity of new compounds for the MB327-PAM-1 binding site and, on the other hand, on reducing the direct muscle inhibitory effect.

CRediT authorship contribution statement

Franz F. Paintner: Writing – review & editing, Supervision, Funding acquisition, Data curation, Conceptualization. **Holger Gohlke:** Writing – review & editing, Supervision, Software, Methodology, Conceptualization. **Klaus T. Wanner:** Writing – review & editing, Supervision, Funding acquisition, Conceptualization. **Dirk Steinritz:** Writing – review & editing. **Franz Worek:** Writing – review & editing. **Karin V. Niessen:** Writing – review & editing. **Thomas Seeger:** Writing – original draft, Methodology, Investigation. **Christoph G.W. Gertzen:** Writing – review & editing, Supervision, Methodology. **Georg Höfner:** Writing – review & editing, Methodology. **Valentin Nitsche:** Writing – original draft, Methodology, Investigation. **Jesko Kaiser:** Writing – original draft, Methodology, Investigation. **Tamara Bernauer:** Writing – original draft, Methodology, Investigation.

Declaration of Competing Interest

The authors declare that they have no known competing financial interests or personal relationships that could have appeared to influence the work reported in this paper.

Data availability

Data will be made available on request.

Acknowledgments

This work was supported by the German Ministry of Defence (E/U2AD/KA019/IF558). We are grateful for computational support and infrastructure provided by the "Zentrum für Informations- und Medientechnologie" (ZIM) at the Heinrich Heine University Düsseldorf and the computing time provided by the John von Neumann Institute for Computing (NIC) to HG on the supercomputer JUWELS at Jülich Supercomputing Center (JSC) (user IDs: HKF7, VSK33, nAChR). HG is grateful to OpenEye Scientific Software for granting a Free Public Domain Research License.

Appendix A. Supporting information

Supplementary data associated with this article can be found in the online version at doi:10.1016/j.toxlet.2024.05.011.

References

Brown, M.A., Brix, K.A., 1998. Review of health consequences from high-, intermediate- and low-level exposure to organophosphorus nerve agents. J. Appl. Toxicol. 18, 393–408.

Case, D.A., Aktulga, H.M., Belfon, K., Cerutti, D.S., Cisneros, G.A., Cruzeiro, V.W.D., Forouzesh, N., Giese, T.J., Götz, A.W., Gohlke, H., Izadi, S., Kasavajhala, K., Kaymak, M.C., King, E., Kurtzman, T., Lee, T.-S., Li, P., Liu, J., Luchko, T., Luo, R., Manathunga, M., Machado, M.R., Nguyen, H.M., O'Hearn, K.A., Onufriev, A.V., Pan, F., Pantano, S., Qi, R., Rahnamoun, A., Risheh, A., Schott-Verdugo, S., Shajan, A., Swails, J., Wang, J., Wei, H., Wu, X., Wu, Y., Zhang, S., Zhao, S., Zhu, Q., Cheatham III, T.E., Roe, D.R., Roitberg, A., Simmerling, C., York, D.M., Nagan, M.C., Merz Jr., K.M., 2023. AmberTools. J. Chem. Inf. Model. 63, 6183–6191.

Case, D.A., Cheatham 3rd, T.E., Darden, T., Gohlke, H., Luo, R., Merz Jr., K.M., Onufriev, A., Simmerling, C., Wang, B., Woods, R.J., 2005. The Amber biomolecular simulation programs. J. Comput. Chem. 26, 1668–1688.

Case, D.A., H.M, A., Belfon, K., Ben-Shalom, I.Y., Berryman, J.T., Brozell, S.R., Cerutti, D. S., Cheatham, T.E., 3rd, Cisneros, G.A., Cruzeiro, V.W.D., Darden, T.A., Duke, R.E., Giambasu, G., Gilson, M.K., Gohlke, H., Goetz, A.W., Harris, R., Izadi, S., Izmailov, S. A., Kasavajhala, K., Kaymak, M.C., King, E., Kovalenko, A., Kurtzmann, T., Lee, T.S., Le Grand, S., Li, P., Lin, C., Liu, J., Luchko, T., Luo, R., Machado, M., Man, V., Manathunga, M., Merz, K.M., Miao, Y., Mikhailovskii, O., Monard, G., Nguyen, H., O'Hearn, K.A., Onufriev, A., Pan, F., Pantano, S., Qi, R., Rahnamoun, A., Roe, D.R., Roitberg, A., Sagui, E., Schott-Verdugo, S., Shajan, A., Shen, J., Simmerling, C.L., Skrynnikov, N.R., Smith, J., Swails, J., Walker, R.C., Wang, J., Wang, J., Wei, H., Wolf, R.M., Wu, X., Xiong, Y., Xue, Y., York, D.M., Zhao, S., Kollmann, P.A., 2022. Amber 2022. vol. Amber 2022. University of California, San Francisco.

Chemical Computing Group, U., 2020. Molecular Operating Environment (MOE). vol. 2019.01, 1010 Sehrbooke St. West, Suite #910, Montreal, QC, Canada, H3A, 2R7.

Cushman, M., Georg, G.I., Holzgrabe, U., Wang, S., 2014. Absolute Quantitative 1H NMR spectroscopy for compound purity determination. J. Med. Chem. 57, 9219-9219.

Dolgin, E., 2013. Syrian gas attack reinforces need for better anti-sarin drugs. Nat. Med. 19, 1194–1195.

Epstein, M., Bali, K., Piggot, T.J., Green, A.C., Timperley, C.M., Bird, M., Tattersall, J.E. H., Bermudez, I., Biggin, P.C., 2021. Molecular determinants of binding of non-oxime bispyridinium nerve agent antidote compounds to the adult muscle nAChR. Toxicol. Lett. 340, 114–122.

Gharpure, A., Teng, J., Zhuang, Y., Noviello, C.M., Walsh Jr., R.M., Cabuco, R., Howard, R.J., Zaveri, N.T., Lindahl, E., Hibbs, R.E., 2019. Agonist selectivity and ion permeation in the alpha3beta4 ganglionic nicotinic receptor. Neuron 104 (501-511), e506.

Hay, D.A., Rogers, C.M., Fedorov, O., Tallant, C., Martin, S., Monteiro, O.P., Müller, S., Knapp, S., Schofield, C.J., Brennan, P.E., 2015. Design and synthesis of potent and selective inhibitors of BRD7 and BRD9 bromodomains. MedChemComm 6, 1381–1386.

Izadi, S., Anandakrishnan, R., Onufriev, A.V., 2014. Building water models: a different approach. J. Phys. Chem. Lett. 5, 3863–3871.

Joung, I.S., Cheatham III, T.E., 2008. Determination of alkali and halide monovalent ion parameters for use in explicitly solvated biomolecular simulations. J. Phys. Chem. B 112, 9020–9041.

Kaiser, J., Gertzen, C.G.W., Bernauer, T., Höfner, G., Niessen, K.V., Seeger, T., Paintner, F.F., Wanner, K.T., Worek, F., Thiermann, H., Gohlke, H., 2023. A novel binding site in the nicotinic acetylcholine receptor for MB327 can explain its allosteric modulation relevant for organophosphorus-poisoning treatment. Toxicol. Lett. 373, 160–171.

Kaiser, J., Gertzen, C.G.W., Bernauer, T., Nitsche, V., Höfner, G., Niessen, K.V., Seeger, T., Paintner, F.F., Wanner, K.T., Steinritz, D., Worek, F., Gohlke, H., 2024. Identification of ligands binding to MB327-PAM-1, a binding pocket relevant for resensitization of nAChRs. bioRxiv. https://doi.org/10.1101/2023.12.21.572862.

Koelle, G.B., 1981. Organophosphate poisoning—an overview. Fundam. Appl. Toxicol. 1, 129–134.

Lazaridis, T., 1998. Inhomogeneous fluid approach to solvation thermodynamics. 1. theory. J. Phys. Chem. B 102, 3531–3541.

Lott, R.S., Chauhan, V.S., Stammer, C.H., 1979. Trimethylsilyl iodide as a peptide deblocking agent. J. Chem. Soc., Chem. Commun. 495–496.

M.J. Frisch, G.W.T, H.B. Schlegel, G.E. Scuseria,, M.A. Robb, J.R.C, G. Scalmani, V. Barone, G.A. Petersson, H.N, X. Li, M. Caricato, A.V. Marenich, J. Bloino, B.G.J, R. Gomperts, B. Mennucci, H.P. Hratchian, J.V. Ortiz, A.F.I, J.L. Sonnenberg, D. Williams-Young, F. Ding, F.L, F. Egidi, J. Goings, B. Peng, A. Petrone, T. Henderson, D.R, V.G. Zakrzewski, J. Gao, N. Rega, G. Zheng, W.L, M. Hada, M. Ehara, K. Toyota, R. Fukuda, J. Hasegawa, M.I, T. Nakajima, Y. Honda, O. Kitao, H. Nakai,, T. Vreven, K.T, J.A. Montgomery, Jr., J.E. Peralta, F. Ogliaro, M.J.B, J.J. Heyd, E.N. Brothers, K. N. Kudin,, V.N. Staroverov, T.A.K, R. Kobayashi, J. Normand, K. Raghavachari, A.P. R, J.C. Burant, S.S. Iyengar, J. Tomasi, M.C, J.M. Millam, M. Klene, C. Adamo, R. Cammi, J.W. Ochterski, R.L.M, K. Morokuma, O. Farkas, J.B. Foresman, a.D.J.F, 2016. Gaussian16. vol. Revision A.03. Gaussian Inc., Wallingford CT.

Maselli, R.A., Leung, C., 1993. Analysis of anticholinesterase-induced neuromuscular transmission failure. Muscle Nerve 16, 548–553.

Massoulié, J., Pezzementi, L., Bon, S., Krejci, E., Vallette, F.-M., 1993. Molecular and cellular biology of cholinesterases. Prog. Neurobiol. 41, 31–91.

Nguyen, C., Gilson, M.K., Young, T., 2011. Structure and thermodynamics of molecular hydration via grid inhomogeneous solvation theory. arXiv 1108, 4876.

Nguyen, C.N., Young, T.K., Gilson, M.K., 2012. Grid inhomogeneous solvation theory: hydration structure and thermodynamics of the miniature receptor cucurbit[7]uril. J. Chem. Phys. 137, 044101.

Niessen, K.V., Muschik, S., Langguth, F., Rappenglück, S., Seeger, T., Thiermann, H., Worek, F., 2016. Functional analysis of Torpedo californica nicotinic acetylcholine receptors in multiple activation states by SSM-based electrophysiology. Toxicol. Lett. 247, 1–10.

Niessen, K.V., Seeger, T., Rappenglück, S., Wein, T., Höfner, G., Wanner, K.T., Thiermann, H., Worek, F., 2018. In vitro pharmacological characterization of the bispyridinium non-oxime compound MB327 and its 2- and 3-regioisomers. Toxicol. Lett. 293, 190–197.

Nitsche, V., Höfner, G., Kaiser, J., Gertzen, C.G.W., Seeger, T., Niessen, K.V., Steinritz, D., Worek, F., Gohlke, H., Paintner, F.F., Wanner, K.T., 2024. MS Binding Assays with UNC0642 as reporter ligand for the MB327 binding site of the nicotinic acetylcholine receptor. Toxicol. Lett. 392, 94–106.

Noviello, C.M., Gharpure, A., Mukhtasimova, N., Cabuco, R., Baxter, L., Borek, D., Sine, S.M., Hibbs, R.E., 2021. Structure and gating mechanism of the α7 nicotinic acetylcholine receptor. Cell 184, 2121–2134 e2113.

OPCW, 2017. OPCW Director-General Shares Incontrovertible Laboratory Results Concluding Exposure to Sarin, 19.04.2017.

OpenEye Scientific Software, I., 2021. SZYBKI. OpenEye Scientific Software, Santa Fe, NM.

Pauli, G.F., Chen, S.-N., Simmler, C., Lankin, D.C., Gödecke, T., Jaki, B.U., Friesen, J.B., McAlpine, J.B., Napolitano, J.G., 2014. Importance of purity evaluation and the potential of quantitative 1H NMR as a purity assay. J. Med. Chem. 57, 9220–9231.

Pettersen, E.F., Goddard, T.D., Huang, C.C., Couch, G.S., Greenblatt, D.M., Meng, E.C., Ferrin, T.E., 2004. UCSF Chimera—a visualization system for exploratory research and analysis. J. Comput. Chem. 25, 1605–1612.

Pita, R., Domingo, J., 2014. The use of chemical weapons in the syrian conflict. Toxics 2, 391–402.

Price, K.E., Mason, B.P., Bogdan, A.R., Broadwater, S.J., Steinbacher, J.L., McQuade, D. T., 2006. Microencapsulated Linear Polymers: "Soluble" Heterogeneous Catalysts. J. Am. Chem. Soc. 128, 10376–10377.

Ramsey, S., Nguyen, C., Salomon-Ferrer, R., Walker, R.C., Gilson, M.K., Kurtzman, T., 2016. Solvation thermodynamic mapping of molecular surfaces in AmberTools: GIST. J. Comput. Chem. 37, 2029–2037.

Rappenglück, S., Sichler, S., Höfner, G., Wein, T., Niessen, K.V., Seeger, T., Paintner, F.F., Worek, F., Thiermann, H., Wanner, K.T., 2018. Synthesis of a series of non-symmetric bispyridinium and related compounds and their affinity characterization at the nicotinic acetylcholine receptor. ChemMedChem 13, 2653–2663.

Roe, D.R., Cheatham 3rd, T.E., 2013. PTRAJ and CPPTRAJ: software for processing and analysis of molecular dynamics trajectory data. J. Chem. Theory Comput. 9, 3084–3095.

Schott-Verdugo, S., Gohlke, H., 2019. PACKMOL-Memgen: a simple-to-use, generalized workflow for membrane-protein-lipid-bilayer system building. J. Chem. Inf. Model 59, 2522–2528.

Seeger, T., Eichhorn, M., Lindner, M., Niessen, K.V., Tattersall, J.E.H., Timperley, C.M., Bird, M., Green, A.C., Thiermann, H., Worek, F., 2012. Restoration of soman-blocked neuromuscular transmission in human and rat muscle by the bispyridinium non-oxime MB327 in vitro. Toxicology 294, 80–84.

Sheridan, R.D., Smith, A.P., Turner, S.R., Tattersall, J.E.H., 2005. Nicotinic antagonists in the treatment of nerve agent intoxication. J. R. Soc. Med. 98, 114–115.

Sichler, S., Höfner, G., Rappenglück, S., Wein, T., Niessen, K.V., Seeger, T., Worek, F., Thiermann, H., Paintner, F.F., Wanner, K.T., 2018. Development of MS Binding Assays targeting the binding site of MB327 at the nicotinic acetylcholine receptor. Toxicol. Lett. 293, 172–183.

Steindl, D., Boehmerle, W., Körner, R., Praeger, D., Haug, M., Nee, J., Schreiber, A., Scheibe, F., Demin, K., Jacoby, P., Tauber, R., Hartwig, S., Endres, M., Eckardt, K.-U., 2021. Novichok nerve agent poisoning. Lancet 397, 249–252.

Thakur, R., Haru, E., 2007. The Chemical Weapons Convention: Implementation, Challenges, Opportunities.

Thiermann, H., Seeger, T., Gonder, S., Herkert, N., Antkowiak, B., Zilker, T., Eyer, F., Worek, F., 2010. Assessment of neuromuscular dysfunction during poisoning by organophosphorus compounds. Chem. -Biol. Interact. 187, 265–269.

Tian, C., Kasavajhala, K., Belfon, K.A.A., Raguette, L., Huang, H., Migues, A.N., Bickel, J., Wang, Y., Pincay, J., Wu, Q., Simmerling, C., 2020. ff19SB: amino-acid-specific protein backbone parameters trained against quantum mechanics energy surfaces in solution. J. Chem. Theory Comput. 16, 528–552.

Timperley, C.M., Bird, M., Green, C., Price, M.E., Chad, J.E., Turner, S.R., Tattersall, J.E., 2012. 1, 1′-(Propane-1, 3-diyl) bis (4-tert-butylpyridinium) di (methanesulfonate) protects guinea pigs from soman poisoning when used as part of a combined therapy. MedChemComm (3), 352–356.

Turner, S.R., Chad, J.E., Price, M., Timperley, C.M., Bird, M., Green, A.C., Tattersall, J.E. H., 2011. Protection against nerve agent poisoning by a noncompetitive nicotinic antagonist. Toxicol. Lett. 206, 105–111.

Wang, J., Wolf, R.M., Caldwell, J.W., Kollman, P.A., Case, D.A., 2004. Development and testing of a general amber force field. J. Comput. Chem. 25, 1157–1174.

Wang, X., Long, C.-Y., Su, M.-H., Qu, Y.-X., Li, S.-H., Zhang, X.-J., Huang, S.-J., Wang, X.-Q., 2019. Rapid amination of methoxy pyridines with aliphatic amines. Org. Process Res. Dev. 23, 1587–1593.

Worek, F., Thiermann, H., Wille, T., 2020. Organophosphorus compounds and oximes: a critical review. Arch. Toxicol. 94, 2275–2292.

Supporting Information

Synthesis and Biological Evaluation of Novel MB327 Analogs as Resensitizers for Desensitized Nicotinic Acetylcholine Receptors after Intoxication with Nerve Agents

Tamara Bernauer,[a] Valentin Nitsche,[a] Jesko Kaiser,[b] Christoph G.W. Gertzen,[b] Georg Höfner,[a] Karin V. Niessen,[c] Thomas Seeger,[c] Dirk Steinritz,[c] Franz Worek,[c] Holger Gohlke,[b,d] Klaus T. Wanner,[a] and Franz F. Paintner*[a]

[a] T. Bernauer, V. Nitsche, Dr. G. Höfner, Prof. Dr. K. T. Wanner, Prof. Dr. F. F. Paintner
Department of Pharmacy, Center for Drug Research
Ludwig-Maximilians-Universität München
Butenandtstrasse 5-13, 81377 Munich (Germany)
E-mail: Franz.Paintner@cup.uni-muenchen.de

[b] J. Kaiser, Dr. C. G. W. Gertzen, Prof. Dr. H. Gohlke
Institute for Pharmaceutical and Medicinal Chemistry
Heinrich Heine Universität Düsseldorf
Universitätsstrasse 1, 40225 Düsseldorf (Germany)

[c] Dr. K. V. Niessen, Dr. T. Seeger, Prof. Dr. D. Steinritz, Prof. Dr. F. Worek
Bundeswehr Institute of Pharmacology and Toxicology
Neuherbergstrasse 11, 80937 Munich (Germany)

[d] Prof. Dr. H. Gohlke
John von Neumann Institute for Computing (NIC), Jülich Supercomputing Centre (JSC), Institute of Biological Information Processing (IBI-7: Structural Biochemistry) & Institute of Bio- and Geosciences (IBG-4: Bioinformatics)
Forschungszentrum Jülich
Wilhelm-Johnen-Strasse, 52428 Jülich (Germany)

Table of Content

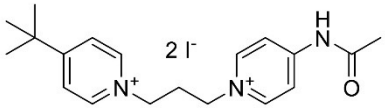

6a (PTM0064)

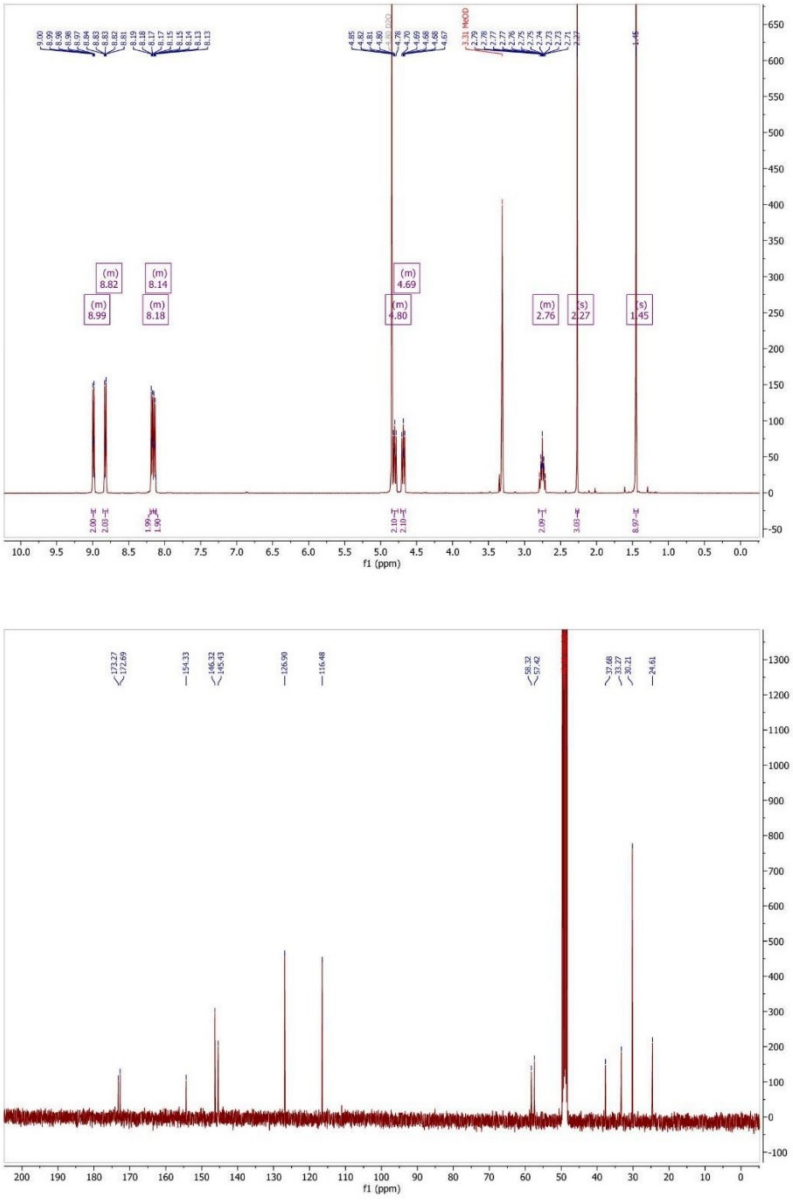

Figure S1: ^{1}H and ^{13}C NMR spectrum of **6a** (PTM0064).

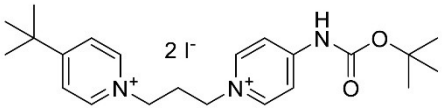

6b (PTM0065)

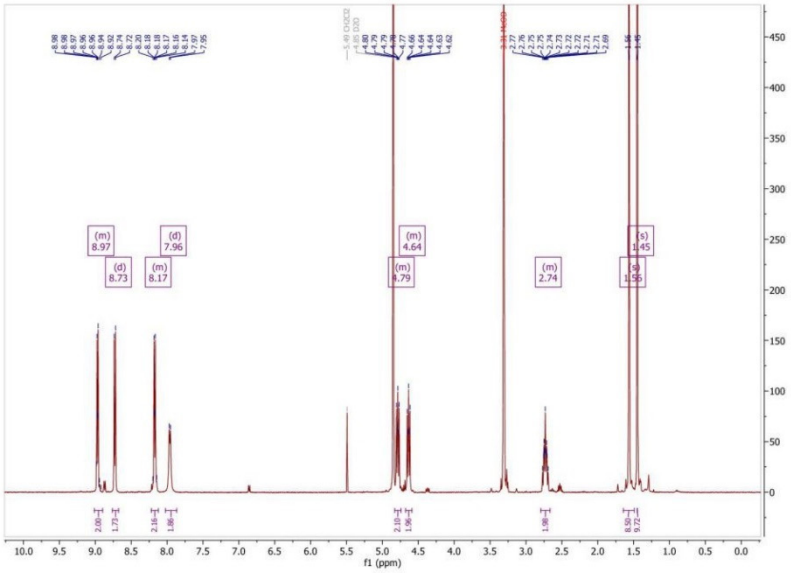

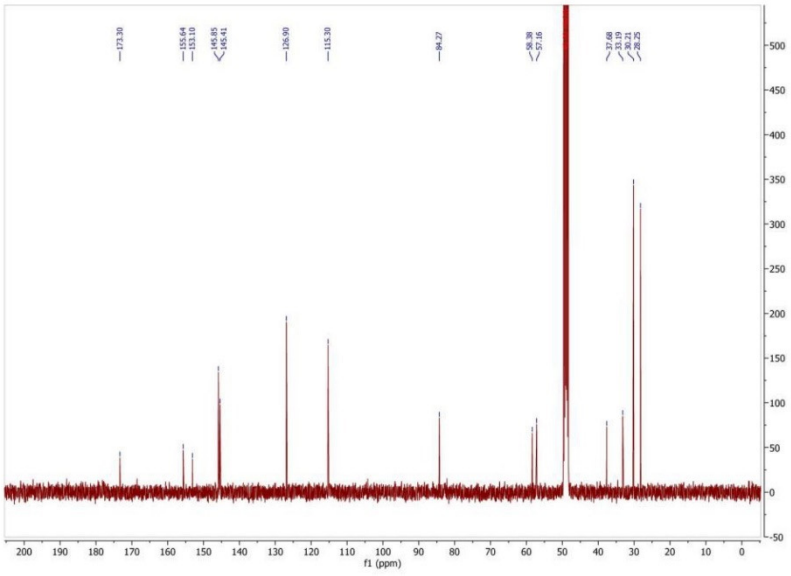

Figure S2: ^{1}H and ^{13}C NMR spectrum of **6b** (PTM0065).

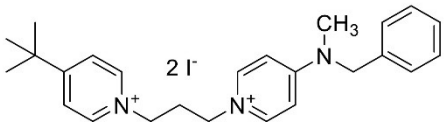

6c (PTM0066)

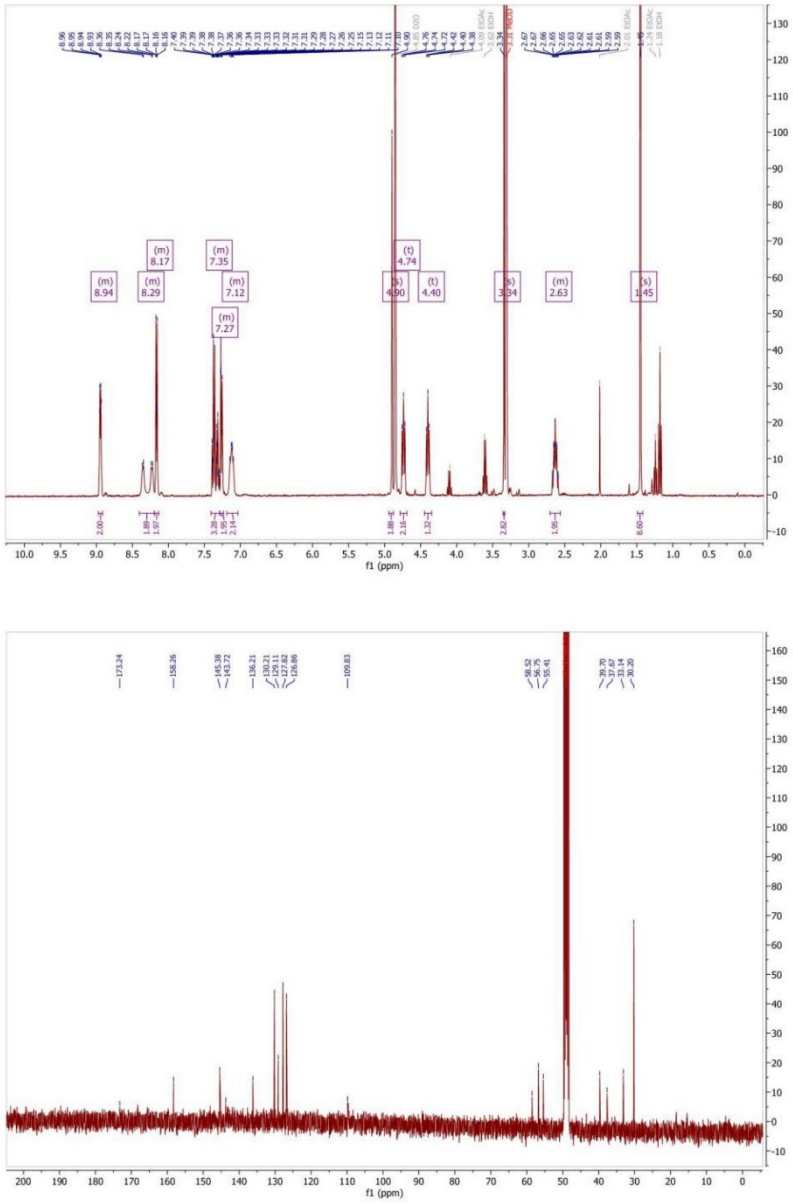

Figure S3: ^{1}H and ^{13}C NMR spectrum of **6c** (PTM0066).

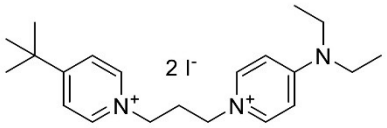

6d (PTM0067)

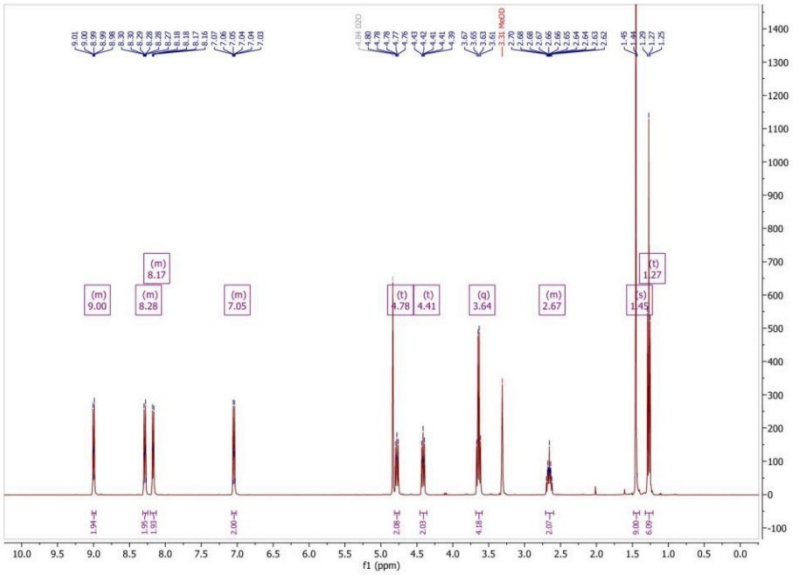

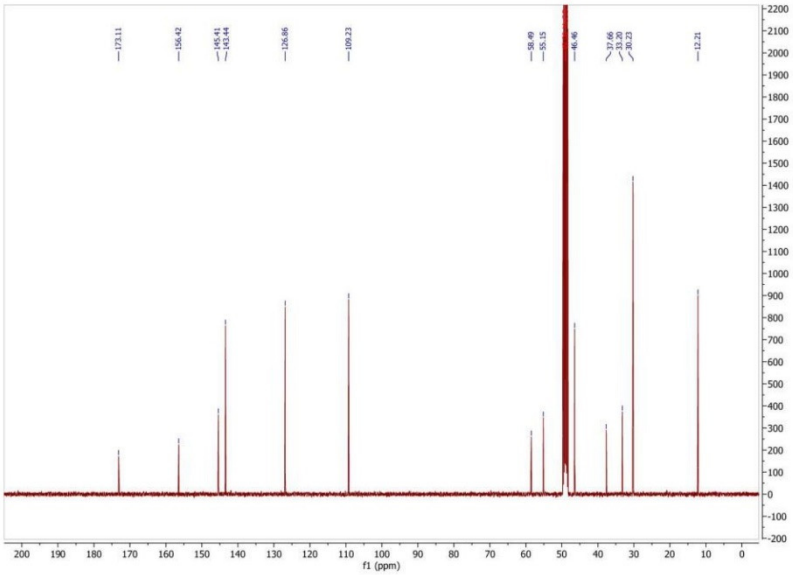

Figure S4: ^{1}H and ^{13}C NMR spectrum of **6d** (PTM0067).

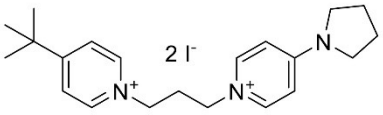

6e (PTM0068)

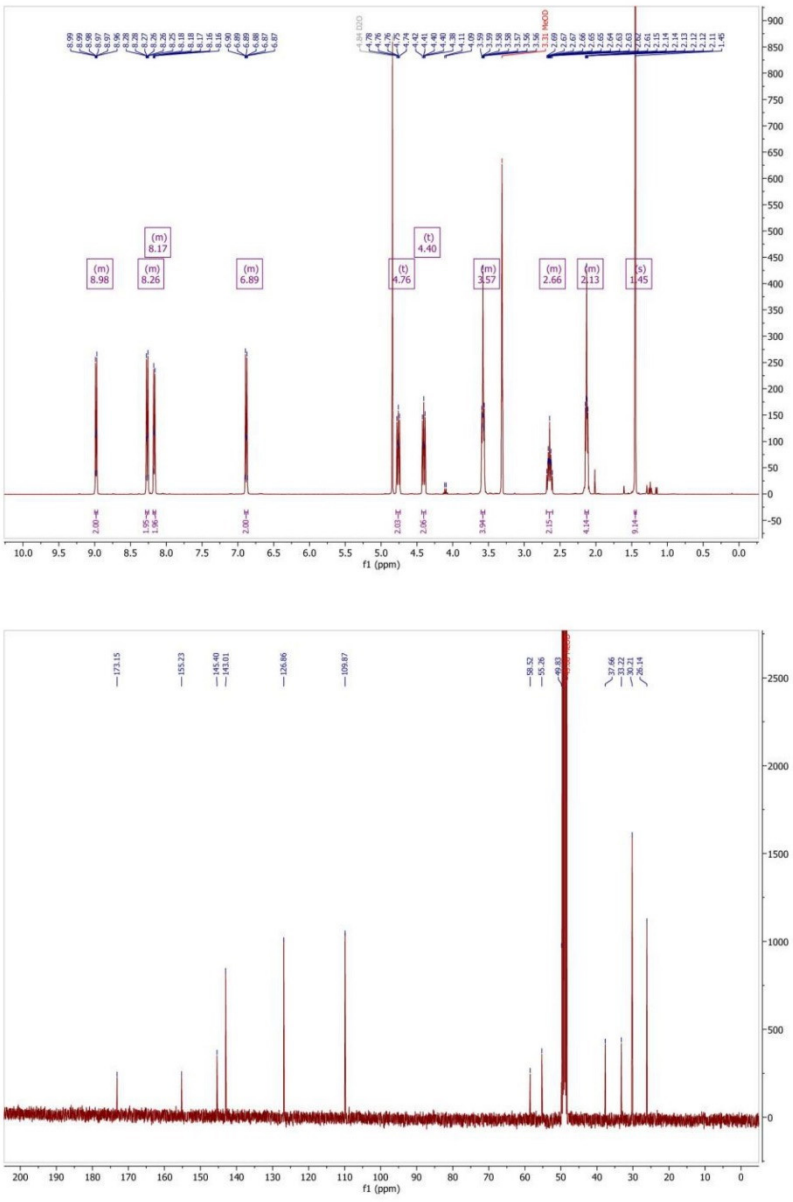

Figure S5: ^{1}H and ^{13}C NMR spectrum of **6e** (PTM0068).

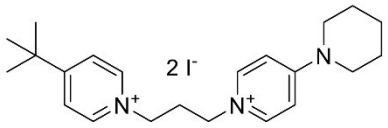

6f (PTM0069)

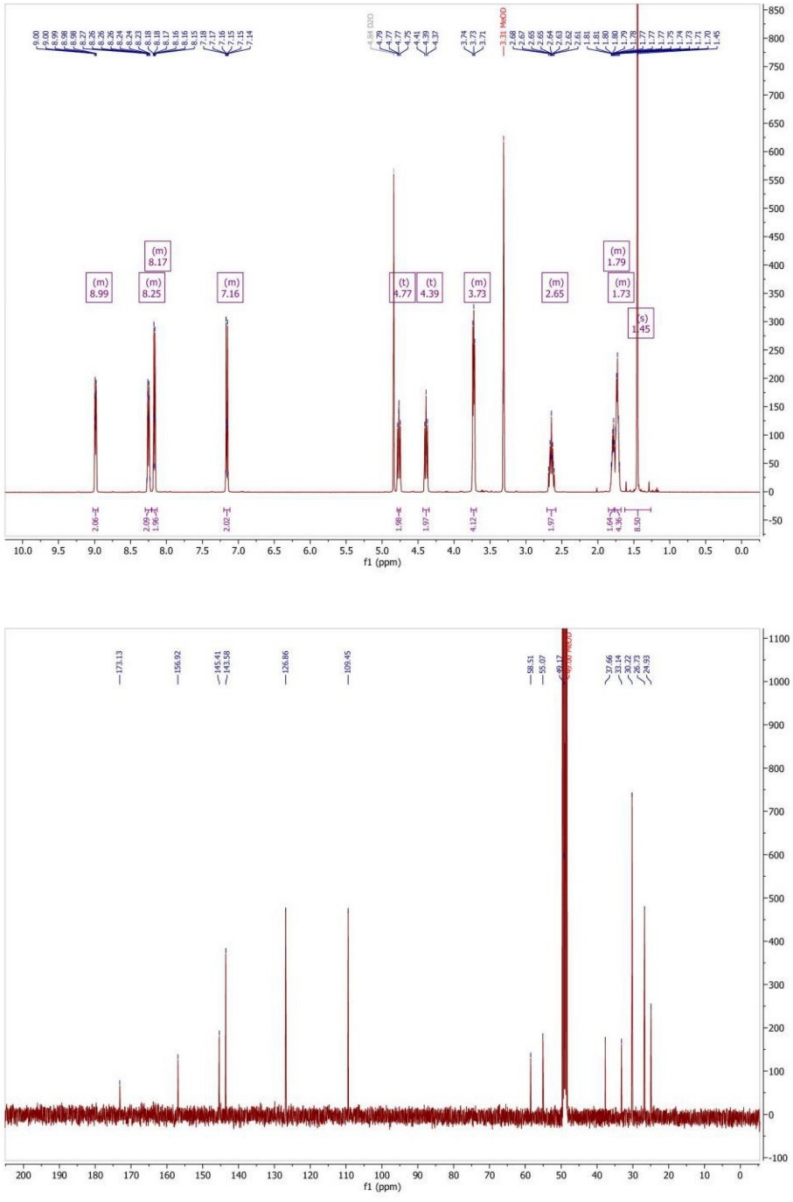

Figure S6: ^{1}H and ^{13}C NMR spectrum of **6f** (PTM0069).

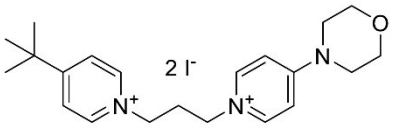

6g (PTM0070)

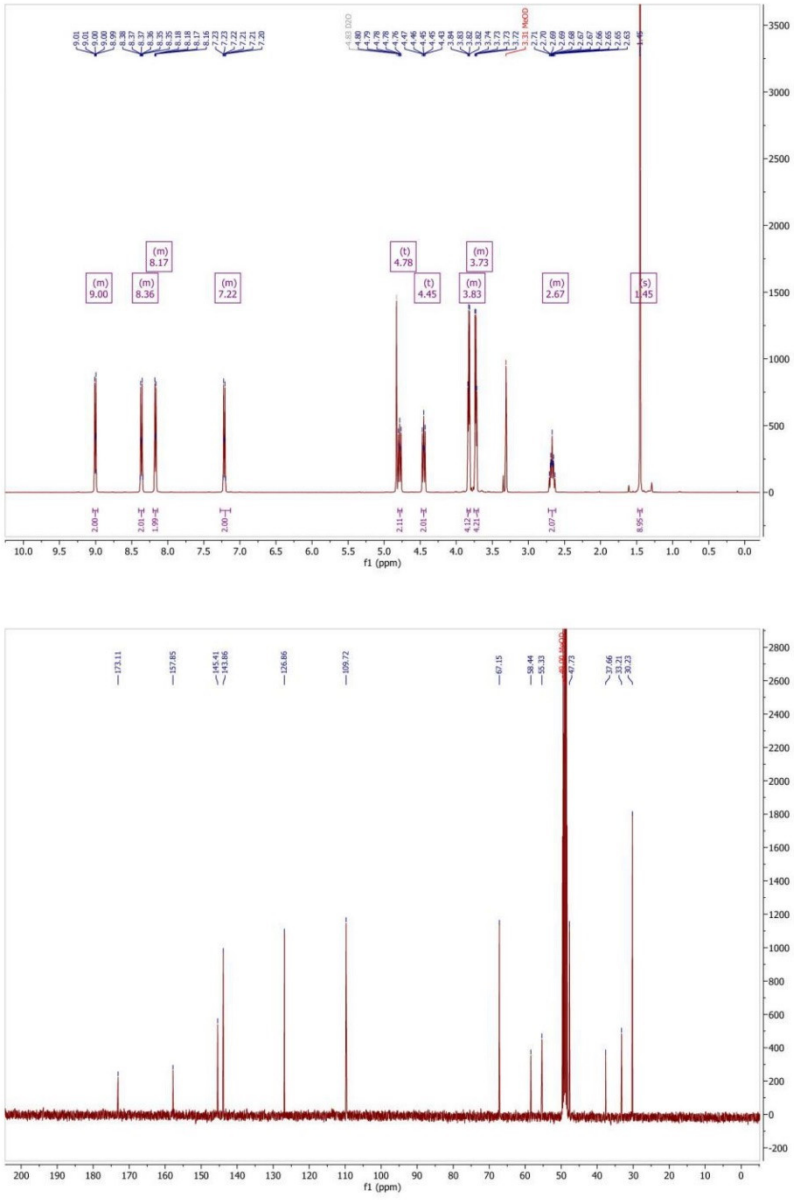

Figure S7: ^{1}H and ^{13}C NMR spectrum of **6g** (PTM0070).

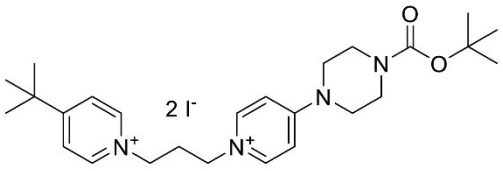

6h (PTM0071)

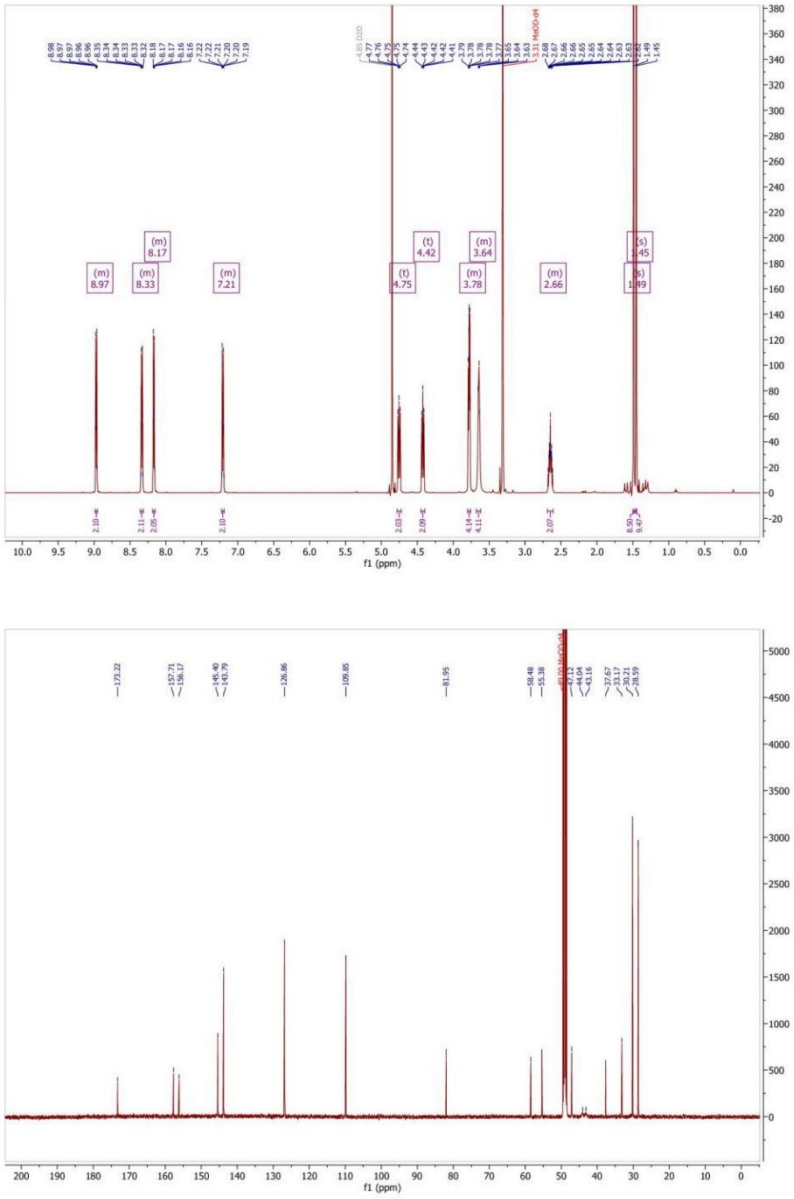

Figure S8: ^{1}H and ^{13}C NMR spectrum of **6h** (PTM0071).

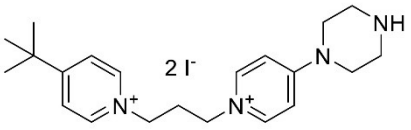

6i (PTM0072)

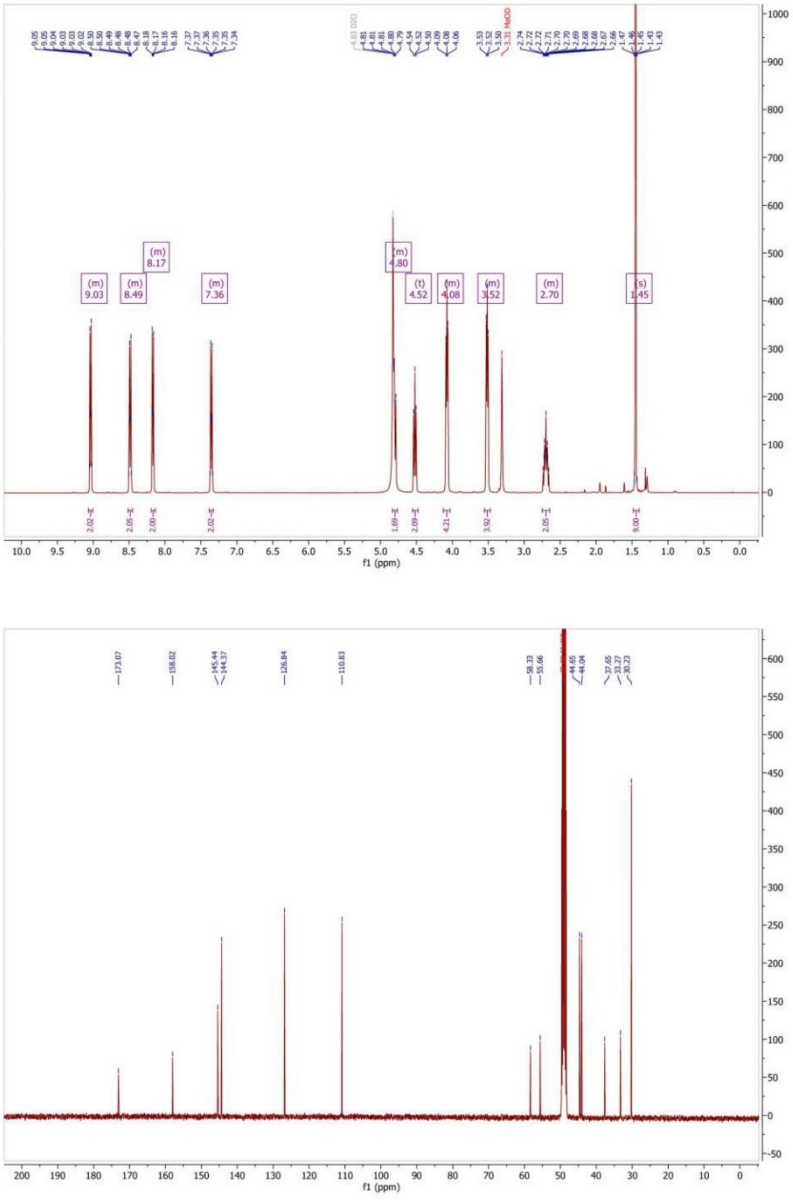

Figure S9: ^{1}H and ^{13}C NMR spectrum of **6i** (PTM0072).

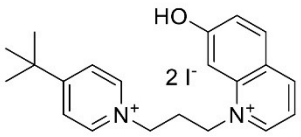

8 (PTMD90-0012)

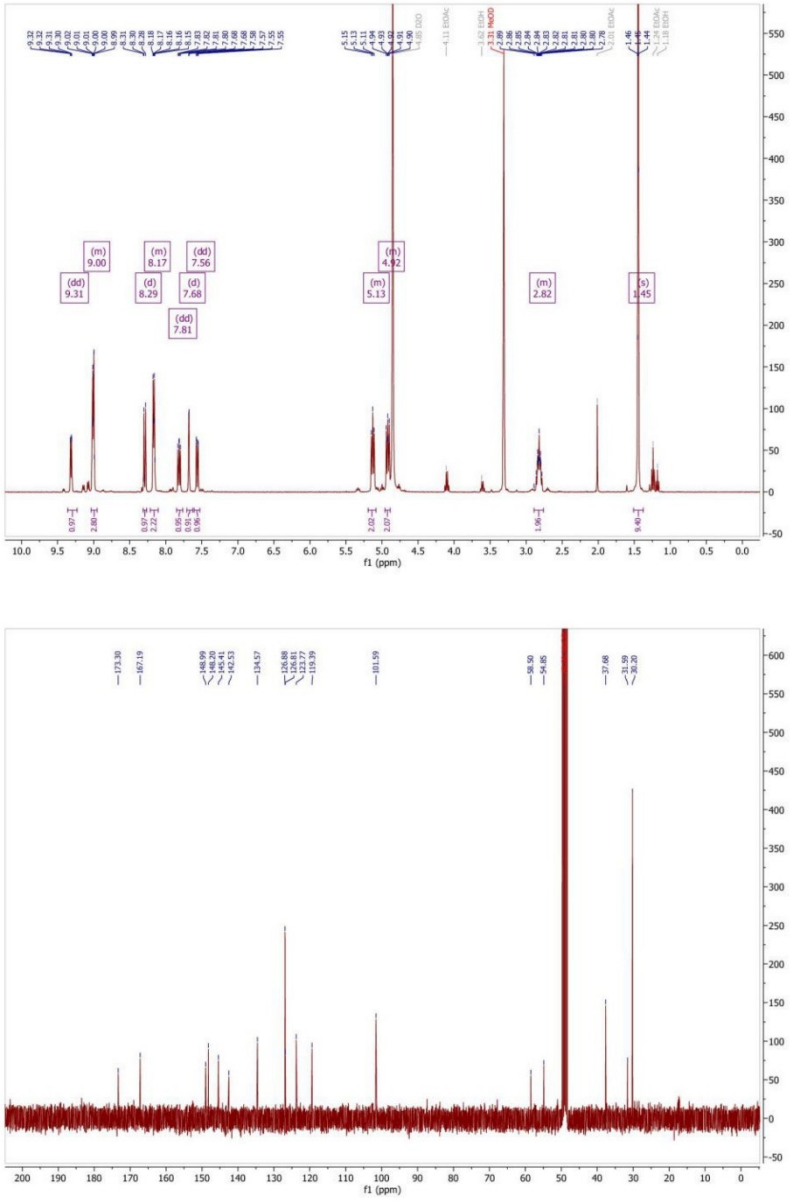

Figure S10: ^{1}H and ^{13}C NMR spectrum of **8** (PTMD90-0012).

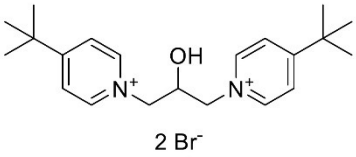

11 (PTMD90-0015)

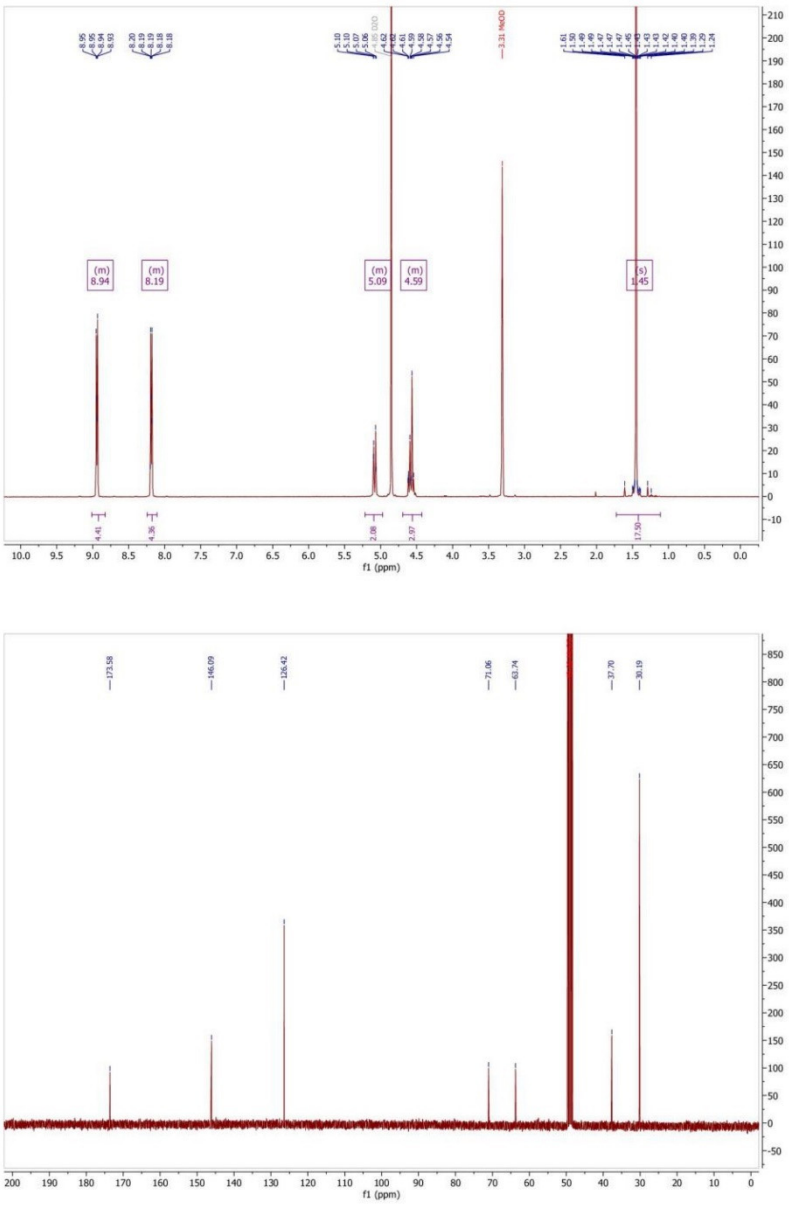

Figure S11: ^{1}H and ^{13}C NMR spectrum of **11** (PTMD90-0015).

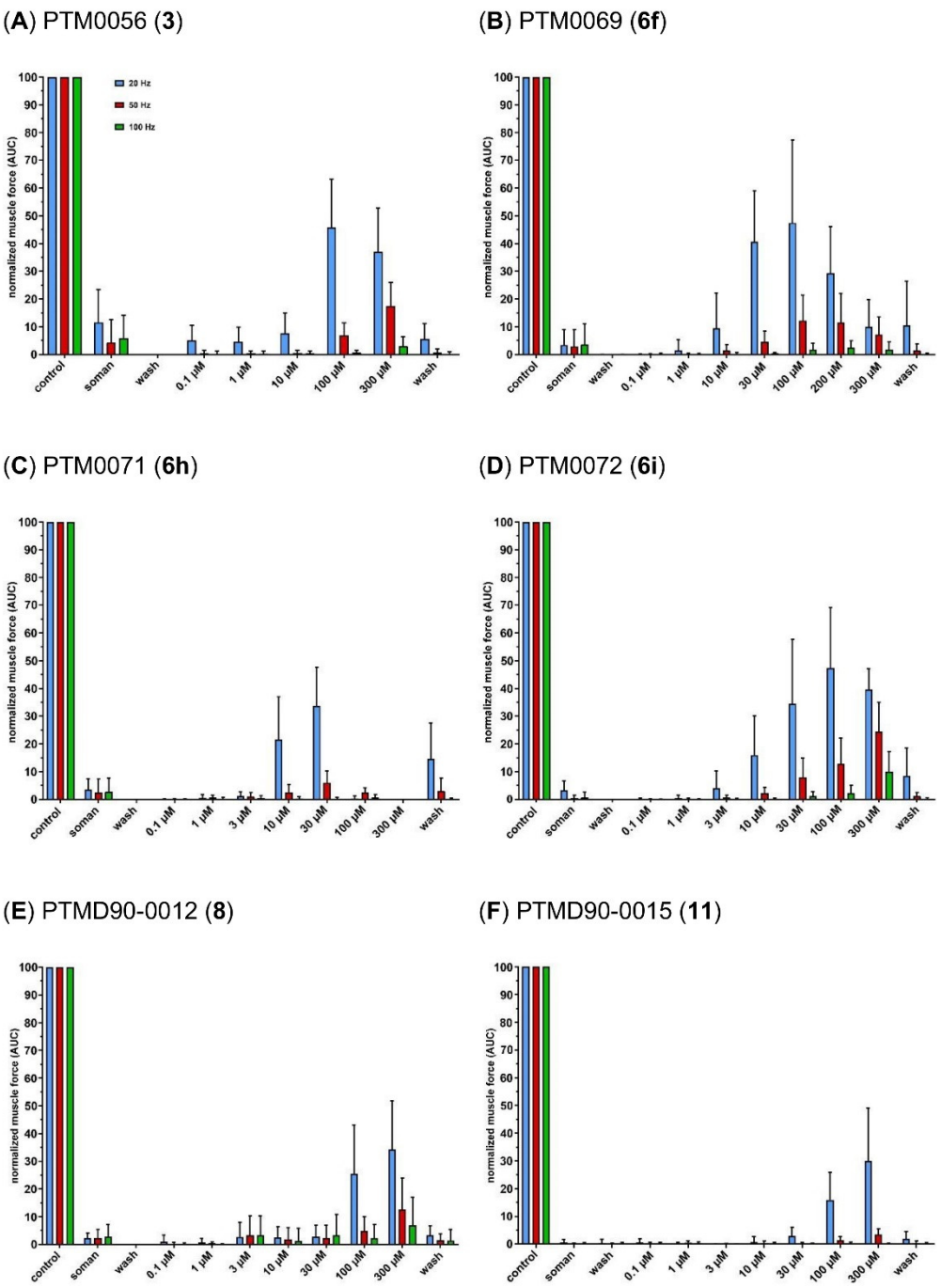

Figure S12: Concentration-dependent restoration of the muscle force by (**A**) PTM0056 (**3**), (**B**) PTM0069 (**6f**), (**C**) PTM0071 (**6h**), (**D**) PTM0072 (**6i**), (**E**) PTMD90-0012 (**8**), (**F**) PTMD90-0015 (**11**) of rat diaphragm preparations after poisoning with soman (3 µM). For indirect stimulation, a frequency of 20 Hz, 50 Hz and 100 Hz was applied. Data are shown as % of control and are given as mean ± SD (n = 4-25).

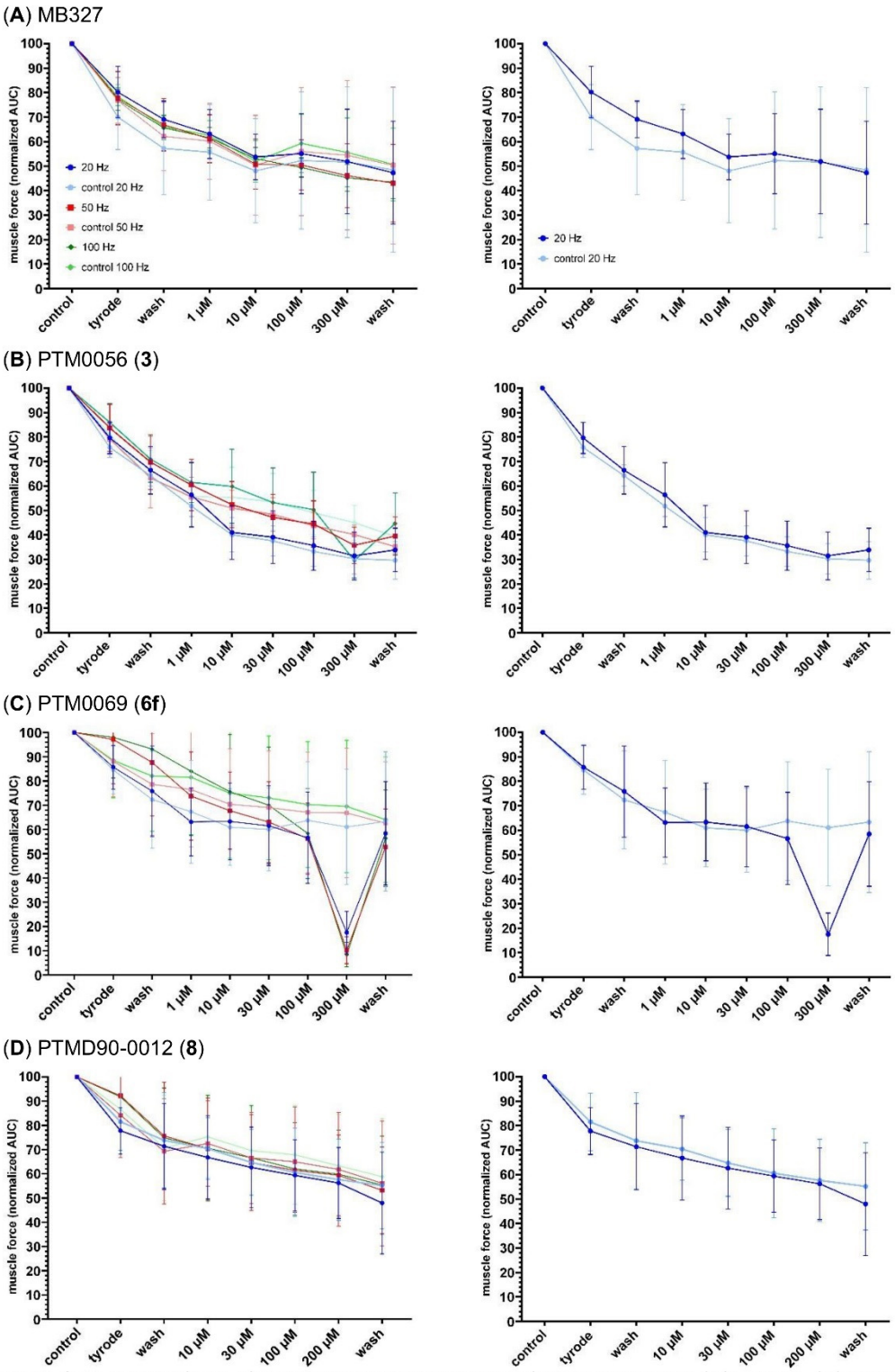

Figure S13: Muscle force of unpoisoned rat diaphragms after treatment with (**A**) MB327, (**B**) PTM0056 (**3**), (**C**) PTM0069 (**6f**) and (**D**) PTMD90-0012 (**8**). For indirect stimulation, a frequency of 20 Hz, 50 Hz and 100 Hz was applied. Muscle force generation was presented as the area under the curve normalized to muscle force under control conditions at the start of the measurement.

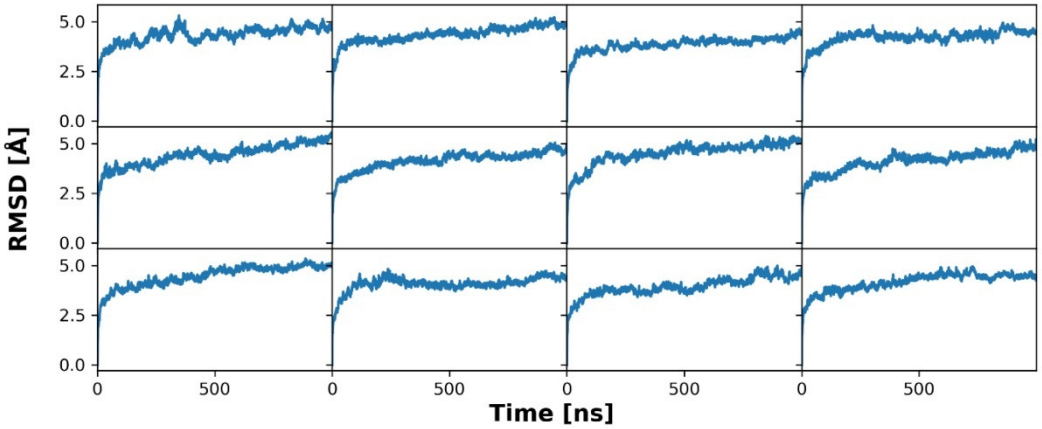

Figure S14: Backbone (C, CA, N) RMSD of 12 replicas of 1 µs long MD simulations of MB327 bound to the human nAChR compared to the first frame of each simulation.

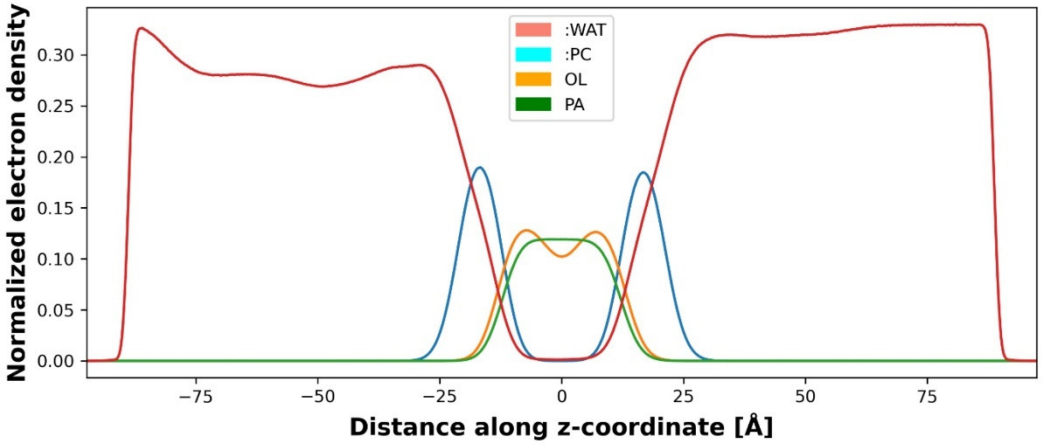

Figure S15: Normalized electron density of water and membrane components averaged over all replicas during MD simulations.

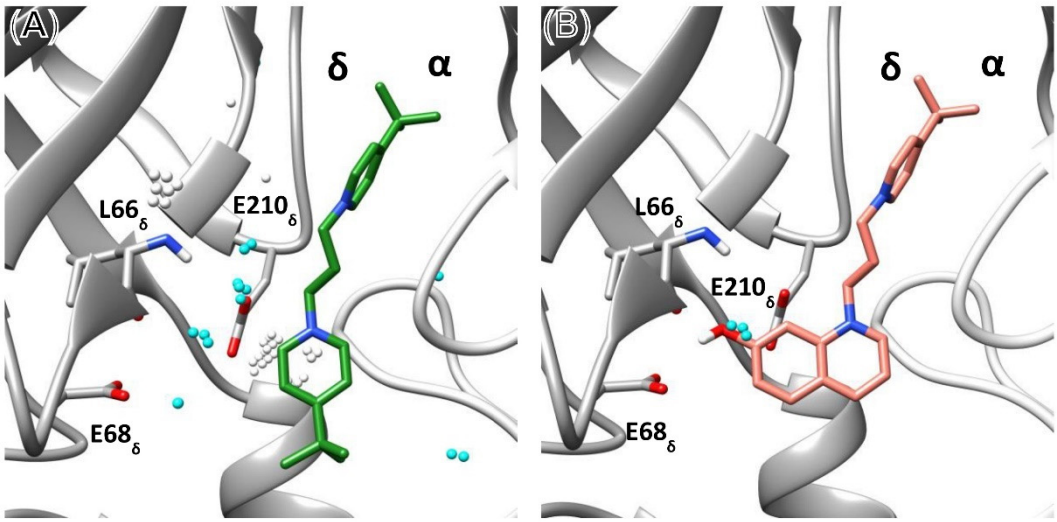

Figure S16: MB327 analog based on substituting water molecules in the allosteric MB327-PAM-1 binding pocket between the α- and δ-subunit. **A)** MB327 binding in between the α- and δ-subunit. Water clusters as identified by GIST are shown as spheres; clusters within 5 Å of MB327 are colored cyan. **B)** Proposed binding mode of PTMD90-0012 (salmon) in between the α- and δ-subunit. Modification of MB327 to PTMD90-0012 (salmon) leads to a substitution of a water cluster located in proximity to L66$_{\delta}$, E68$_{\delta}$, and E210$_{\delta}$. For L66 $_{\delta}$, the backbone atoms are shown in addition to the side chain.

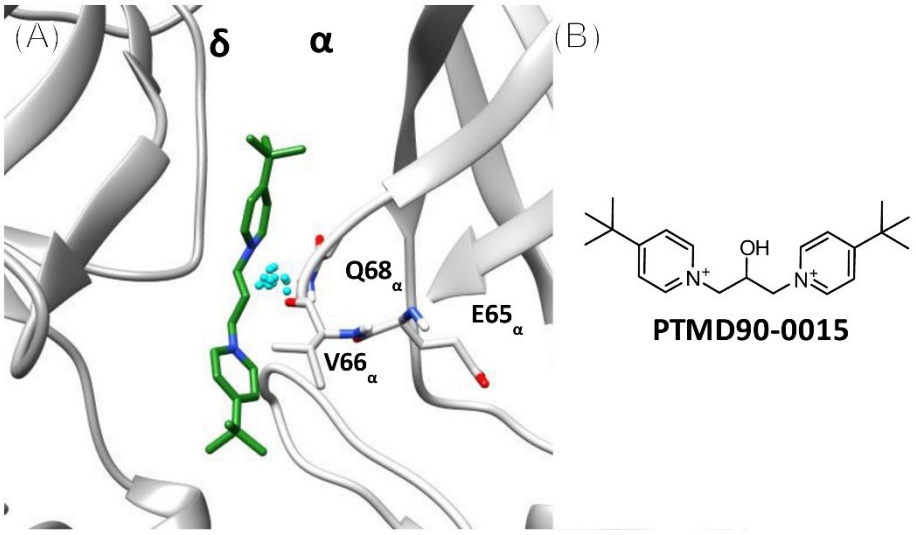

Figure S17: Initial water cluster leading to the design of PTMD90-0015. **A)** During the first few replicas (5 out of 12) of MD simulations of MB327 in MB327-PAM-1, an energetically unfavorable cluster of water molecules was identified in between the backbone atoms of E65$_{\alpha}$, V66$_{\alpha}$, and Q68$_{\alpha}$ close to the C3-linker of MB327 in a representative binding mode during MD simulations (*k*-means clustering based on MB327 atoms ligand between the α- and δ-subunit). Based on these preliminary results, **B)** PTMD90-0015 was designed. This water cluster was later only observed in between the δ- and α-subunit. However, there, no docked or representative structure from MD simulations was in the range to form interactions with the protein after modification of MB327 to PTMD90-0015.

12. CURRICULUM VITAE

Personal Information

Name:

Jesko Fabian Kaiser

Date of birth:

11th December 1994

Languages

German ●●●●●

English ●●●●●

Russian ●○○○○

Jesko Fabian Kaiser

Professional experience

Scientific employee **10/2020 – today**
Heinrich Heine University, Düsseldorf

- Utilizing bioinformatic techniques, particularly MD simulations, for computer-aided drug design and *in silico* structural biology.
- Data analysis and visualization using Python.
- Working in a Linux and HPC-cluster environment.
- Supervision and project design for master students.

Pharmacist **01/2022 – 06/2023**
Apotheke am Aachener Platz, Düsseldorf

Intern **05/2019 – 10/2019**
Second half of the pharmaceutical practical year
Einhorn-Apotheke, Hanau

Intern **11/2018 – 04/2019**
First half of the pharmaceutical practical year
Menarini Research & Business GmbH, Berlin
Department R&D - Stability assessment

Education

PhD in Computational Chemistry **2020 – today**
Heinrich Heine University, Düsseldorf
"Development of novel nAChR modulators"
Expected finish: 2024

Master of Chemistry **2016 – 2020**
Philipps University Marburg
Master thesis "*In silico* design of P2Y10 ligands" in the lab of Prof. Dr. Peter Kolb

Technical Skills

Amber Suite for MD simulations

●●●●●

Microsoft Office

●●●●○

Linux (Bash scripting)

●●●●○

Python

●●●○○

OpenEye Scientific Software

●●●○○

CCG MOE

●●●○○

Schroedinger Maestro

●○○○○

R

●○○○○

Pharmacy **2014 – 2019**
Philipps University Marburg

Bachelor of Material Sciences **2013 – 2014**
No degree
RWTH Aachen

High School degree (Abitur) **06 / 2013**
Karl-Rehbein-Schule Hanau

Awards

Wiley presentation award **02/2022**
Doktorandentagung DPhG

13. REFERENCES

1. Wiener, S.W. and Hoffman, R.S., *Nerve agents: a comprehensive review.* J Intensive Care Med, 2004. **19**(1): p. 22-37.
2. Human Rights Watch, *Death by Chemicals*. 01.05.2023, accessed 05 January 2024, <https://www.hrw.org/report/2017/05/01/death-chemicals/syrian-governments-widespread-and-systematic-use-chemical-weapons>.
3. Human Rights Watch, *Attacks on Ghouta: Analysis of Alleged Use of Chemical Weapons in Syria*. 10.09.2023, accessed 05 January 2024, <https://www.hrw.org/report/2013/09/10/attacks-ghouta/analysis-alleged-use-chemical-weapons-syria>.
4. Sugiyama, A., Matsuoka, T., Sakamune, K., Akita, T., Makita, R., Kimura, S., Kuroiwa, Y., Nagao, M. and Tanaka, J., *The Tokyo subway sarin attack has long-term effects on survivors: A 10-year study started 5 years after the terrorist incident.* PLoS One, 2020. **15**(6): p. e0234967.
5. Suzuki, T., Morita, H., Ono, K., Maekawa, K., Nagai, R., Yazaki, Y., Nozaki, H., Aikawa, N., Shinozawa, Y., Hori, S., Fujishima, S., Takuma, K. and Sagoh, M., *Sarin poisoning in Tokyo subway.* The Lancet, 1995. **345**(8955): p. 980-981.
6. Okumura, T., Takasu, N., Ishimatsu, S., Miyanoki, S., Mitsuhashi, A., Kumada, K., Tanaka, K. and Hinohara, S., *Report on 640 Victims of the Tokyo Subway Sarin Attack.* Ann Emerg Med, 1996. **28**(2): p. 129-135.
7. Sudakin, D.L. and Power, L.E., *Organophosphate exposures in the United States: a longitudinal analysis of incidents reported to poison centers.* J Toxicol Environ Health A, 2007. **70**(2): p. 141-7.
8. Choudhary, A., Ali, A.S. and Ali, S.A., *Adverse Health Effects of Organophosphate Pesticides among Occupationally Exposed Farm Sprayers: A Case Study of Bhopal Madhya Pradesh, India.* Asian J Biomed Pharm Sci, 2014. **4**(35): p. 30.
9. Muñoz-Quezada, M.T., Lucero, B., Iglesias, V., Levy, K., Muñoz, M.P., Achú, E., Cornejo, C., Concha, C., Brito, A.M. and Villalobos, M., *Exposure to organophosphate (OP) pesticides and health conditions in agricultural and non-agricultural workers from Maule, Chile.* Int J Environ Health Res, 2017. **27**(1): p. 82-93.
10. Perwitasari, D.A., Prasasti, D., Supadmi, W., Jaikishin, S.A.D. and Wiraagni, I.A., *Impact of organophosphate exposure on farmers' health in Kulon Progo, Yogyakarta: Perspectives of physical, emotional and social health.* SAGE Open Medicine, 2017. **5**: p. 2050312117719092.
11. Slavica, V., Dubravko, B. and Milan, J., *Acute organophosphate poisoning: 17 years of experience of the National Poison Control Center in Serbia.* Toxicology, 2018. **409**: p. 73-79.
12. Marnay, A. and Nachmansohn, D., *Choline esterase in voluntary muscle.* J Physiol, 1938. **92**(1): p. 37-47.
13. Nachmansohn, D., *Choline Esterase in the Central Nervous System.* Nature, 1937. **140**(3540): p. 427-427.
14. Stedman, E., Stedman, E. and Easson, L.H., *Choline-esterase. An enzyme present in the blood-serum of the horse.* Biochem J, 1932. **26**(6): p. 2056-66.
15. Matthes, K., *The action of blood on acetylcholine.* J Physiol, 1930. **70**(4): p. 338-48.
16. DALE, H.H., *THE ACTION OF CERTAIN ESTERS AND ETHERS OF CHOLINE, AND THEIR RELATION TO MUSCARINE.* J Pharmacol Exp Ther, 1914. **6**(2): p. 147-190.
17. Quinn, D.M., *Acetylcholinesterase: enzyme structure, reaction dynamics, and virtual transition states.* Chem Rev, 1987. **87**(5): p. 955-979.
18. Aldridge, W.N. and Davison, A.N., *The mechanism of inhibition of cholinesterases by organophosphorus compounds.* Biochem J, 1953. **55**(5): p. 763-6.
19. Aldridge, W.N., *[The inhibition of erythrocyte cholinesterase by tri-esters of phosphoric acid. III. The nature of the inhibitory process].* Biochem J, 1953. **54**(3): p. 442-8.
20. Schaffer, N.K., May, S.C. and Summerson, W.H., *SERINE PHOSPHORIC ACID FROM DIISOPROPYLPHOSPHORYL CHYMOTRYPSIN.* J Biol Chem, 1953. **202**(1): p. 67-76.

21. Jokanović, M. and Kosanović, M., *Neurotoxic effects in patients poisoned with organophosphorus pesticides.* Environ Toxicol Pharmacol, 2010. **29**(3): p. 195-201.
22. Moore, W., *Two Cases of Poisoning with Di-isopropylfluorophosphonate (DFP).* Br J Ind Med, 1956. **13**(3): p. 214.
23. Sidell, F.R., *Soman and sarin: clinical manifestations and treatment of accident of accidental poisoning by organophosphates.* Clin Toxicol, 1974. **7**(1): p. 1-17.
24. Fatt, P., *The electromotive action of acetylcholine at the motor end-plate.* J Physiol, 1950. **111**(3-4): p. 408-22.
25. Katz, B. and Thesleff, S., *A study of the desensitization produced by acetylcholine at the motor end-plate.* J Physiol, 1957. **138**(1): p. 63-80.
26. Lundy, P.M., Hansen, A.S., Hand, B.T. and Boulet, C.A., *Comparison of several oximes against poisining by soman, tabun and GF.* Toxicology, 1992. **72**(1): p. 99-105.
27. Sidell, F.R. and Groff, W.A., *The reactivatibility of cholinesterase inhibited by VX and sarin in man.* Toxicol Appl Pharmacol, 1974. **27**(2): p. 241-252.
28. Murtha, E.F., Fleisher, J.H., Torre, M.A. and Innerebner, T.A., *Reactivatability of soman-inhibited end plate cholinesterase and neuromuscular transmission.* Toxicol Appl Pharmacol, 1970. **16**(1): p. 214-226.
29. Wilson, I.B. and Ginsburg, S., *A powerful reactivator of alkylphosphate-inhibited acetylcholinesterase.* Biochim Biophys Acta, 1955. **18**: p. 168-170.
30. Childs, A.F., Davies, D.R., Green, A.L. and Rutland, J.P., *The reactivation by oximes and hydroxamic acids of cholinesterase inhibited by organo-phosphorus compounds.* Br J Pharmacol Chemother, 1955. **10**(4): p. 462-5.
31. Poziomek, E.J., Hackley jr, B.E. and Steinberg, G.M., *Pyridinium aldoximes1.* J Org Chem, 1958. **23**(5): p. 714-717.
32. Hobbiger, F., O'sullivan, D. and Sadler, P., *New potent reactivators of acetocholinesterase inhibited by tetraethyl pyrophosphate.* Nature, 1958. **182**: p. 1498-9.
33. Harris, L.W., Anderson, D.R., Lennox, W.J., Woodard, C.L., Pastelak, A.M. and Vanderpool, B.A., *Evaluation of several oximes as reactivators of unaged soman-inhibited whole blood acetylcholinesterase in rabbits.* Biochem Pharmacol, 1990. **40**(12): p. 2677-2682.
34. Dawson, R.M., *Review of oximes available for treatment of nerve agent poisoning.* J Appl Toxicol, 1994. **14**(5): p. 317-331.
35. Worek, F., Eyer, P., Aurbek, N., Szinicz, L. and Thiermann, H., *Recent advances in evaluation of oxime efficacy in nerve agent poisoning by in vitro analysis.* Toxicol Appl Pharmacol, 2007. **219**(2): p. 226-234.
36. Shih, T., Whalley, C.E. and Valdes, J.J., *A comparison of cholinergic effects of HI-6 and pralidoxime-2-chloride (2-PAM) in soman poisoning.* Toxicol Lett, 1991. **55**(2): p. 131-47.
37. Fleisher, J.H., Harris, L.W., Miller, G.R., Thomas, N.C. and Cliff, W.J., *Antagonism of sarin poisoning in rats and guinea pigs by atropine, oximes, and mecamylamine.* Toxicol Appl Pharmacol, 1970. **16**(1): p. 40-47.
38. Askew, B.M., *Oximes and atropine in sarin poisoning.* Br J Pharmacol Chemother, 1957. **12**(3): p. 340-3.
39. Michel, H.O., Hackley, B.E., Berkowitz, L., List, G., Hackley, E.B., Gillilan, W. and Pankau, M., *Ageing and dealkylation of soman (pinacolylmethylphosphonofluoridate)-inactivated eel cholinesterase.* Arch Biochem Biophys, 1967. **121**(1): p. 29-34.
40. Hobbiger, F., *Effect of nicotinhydroxamic acid methiodide on human plasma cholinesterase inhibited by organophosphates containing a dialkylphosphato group.* Br J Pharmacol Chemother, 1955. **10**(3): p. 356-62.
41. Wilson, I.B., *Promotion of acetylcholinesterase activity by the anionic site.* Discuss Faraday Soc, 1955. **20**: p. 119-125.
42. Worek, F., Thiermann, H. and Wille, T., *Organophosphorus compounds and oximes: a critical review.* Arch Toxicol, 2020. **94**(7): p. 2275-2292.
43. Quinn, D.M., Topczewski, J., Yasapala, N. and Lodge, A., *Why is Aged Acetylcholinesterase So Difficult to Reactivate?* Molecules, 2017. **22**(9): 1464.

44. Turner, S.R., Chad, J.E., Price, M., Timperley, C.M., Bird, M., Green, A.C. and Tattersall, J.E., *Protection against nerve agent poisoning by a noncompetitive nicotinic antagonist.* Toxicol Lett, 2011. **206**(1): p. 105-11.
45. Seeger, T., Eichhorn, M., Lindner, M., Niessen, K.V., Tattersall, J.E., Timperley, C.M., Bird, M., Green, A.C., Thiermann, H. and Worek, F., *Restoration of soman-blocked neuromuscular transmission in human and rat muscle by the bispyridinium non-oxime MB327 in vitro.* Toxicology, 2012. **294**(2-3): p. 80-4.
46. Niessen, K.V., Seeger, T., Rappengluck, S., Wein, T., Hofner, G., Wanner, K.T., Thiermann, H. and Worek, F., *In vitro pharmacological characterization of the bispyridinium non-oxime compound MB327 and its 2- and 3-regioisomers.* Toxicol Lett, 2018. **293**: p. 190-197.
47. Scheffel, C., Niessen, K.V., Rappengluck, S., Wanner, K.T., Thiermann, H., Worek, F. and Seeger, T., *Electrophysiological investigation of the effect of structurally different bispyridinium non-oxime compounds on human alpha7-nicotinic acetylcholine receptor activity-An in vitro structure-activity analysis.* Toxicol Lett, 2018. **293**: p. 157-166.
48. Rappenglück, S., Sichler, S., Höfner, G., Wein, T., Niessen, K.V., Seeger, T., Paintner, F.F., Worek, F., Thiermann, H. and Wanner, K.T., *Synthesis of a Series of Structurally Diverse MB327 Derivatives and Their Affinity Characterization at the Nicotinic Acetylcholine Receptor.* ChemMedChem, 2018. **13**(17): p. 1806-1816.
49. Rappenglück, S., Sichler, S., Höfner, G., Wein, T., Niessen, K.V., Seeger, T., Paintner, F.F., Worek, F., Thiermann, H. and Wanner, K.T., *Synthesis of a Series of Non-Symmetric Bispyridinium and Related Compounds and Their Affinity Characterization at the Nicotinic Acetylcholine Receptor.* ChemMedChem, 2018. **13**(24): p. 2653-2663.
50. Sichler, S., Höfner, G., Nitsche, V., Niessen, K.V., Seeger, T., Worek, F., Wanner, K.T. and Paintner, F.F., *Screening for new ligands of the MB327-PAM-1 binding site of the nicotinic acetylcholine receptor.* Toxicol Lett, 2024. **394**: p. 23-31.
51. Nitsche, V., Höfner, G., Kaiser, J., Gertzen, C.G.W., Seeger, T., Niessen, K.V., Steinritz, D., Worek, F., Gohlke, H., Paintner, F.F. and Wanner, K.T., *MS Binding Assays with UNC0642 as reporter ligand for the MB327 binding site of the nicotinic acetylcholine receptor.* Toxicol Lett, 2024. **392**: p. 94-106.
52. Niessen, K.V., Seeger, T., Tattersall, J.E., Timperley, C.M., Bird, M., Green, C., Thiermann, H. and Worek, F., *Affinities of bispyridinium non-oxime compounds to [(3)H]epibatidine binding sites of Torpedo californica nicotinic acetylcholine receptors depend on linker length.* Chem Biol Interact, 2013. **206**(3): p. 545-54.
53. Rohde, L.A.H., Ahring, P.K., Jensen, M.L., Nielsen, E.Ø., Peters, D., Helgstrand, C., Krintel, C., Harpsøe, K., Gajhede, M., Kastrup, J.S. and Balle, T., *Intersubunit bridge formation governs agonist efficacy at nicotinic acetylcholine α4β2 receptors: unique role of halogen bonding revealed.* J Biol Chem, 2012. **287**(6): p. 4248-4259.
54. Olsen, J.A., Balle, T., Gajhede, M., Ahring, P.K. and Kastrup, J.S. *Molecular recognition of the neurotransmitter acetylcholine by an acetylcholine binding protein reveals determinants of binding to nicotinic acetylcholine receptors*. PLoS One, 2014. **9**, e91232 DOI: 10.1371/journal.pone.0091232.
55. Ussing, C.A., Hansen, C.P., Petersen, J.G., Jensen, A.A., Rohde, L.A.H., Ahring, P.K., Nielsen, E.Ø., Kastrup, J.S., Gajhede, M., Frølund, B. and Balle, T., *Synthesis, pharmacology, and biostructural characterization of novel α4β2 nicotinic acetylcholine receptor agonists.* J Med Chem, 2013. **56**(3): p. 940-951.
56. Olsen, J.A., Ahring, P.K., Kastrup, J.S., Gajhede, M. and Balle, T., *Structural and functional studies of the modulator NS9283 reveal agonist-like mechanism of action at α4β2 nicotinic acetylcholine receptors.* J Biol Chem, 2014. **289**(36): p. 24911-24921.
57. Shahsavar, A., Ahring, P.K., Olsen, J.A., Krintel, C., Kastrup, J.S., Balle, T. and Gajhede, M., *Acetylcholine-Binding Protein Engineered to Mimic the α4-α4 Binding Pocket in α4β2 Nicotinic Acetylcholine Receptors Reveals Interface Specific Interactions Important for Binding and Activity.* Mol Pharmacol, 2015. **88**(4): p. 697-707.

58. Kaczanowska, K., Camacho Hernandez, G.A., Bendiks, L., Kohs, L., Cornejo-Bravo, J.M., Harel, M., Finn, M.G. and Taylor, P., *Substituted 2-Aminopyrimidines Selective for α7-Nicotinic Acetylcholine Receptor Activation and Association with Acetylcholine Binding Proteins.* J Am Chem Soc, 2017. **139**(10): p. 3676-3684.
59. Bueno, R.V., Davis, S., Dawson, A., Ondachi, P.W., Carroll, F.I. and Hunter, W.N., *Interactions between 2'-fluoro-(carbamoylpyridinyl)deschloroepibatidine analogues and acetylcholine-binding protein inform on potent antagonist activity against nicotinic receptors.* Acta Crystallogr D Struct Biol, 2022. **78**(3): p. 353-362.
60. Nemecz, Á. and Taylor, P., *Creating an α7 nicotinic acetylcholine recognition domain from the acetylcholine-binding protein: crystallographic and ligand selectivity analyses.* J Biol Chem, 2011. **286**(49): p. 42555-42565.
61. Spurny, R., Debaveye, S., Farinha, A., Veys, K., Vos, A.M., Gossas, T., Atack, J., Bertrand, S., Bertrand, D., Danielson, U.H., Tresadern, G. and Ulens, C., *Molecular blueprint of allosteric binding sites in a homologue of the agonist-binding domain of the α7 nicotinic acetylcholine receptor.* Proc Natl Acad Sci USA, 2015. **112**(19): p. E2543-52.
62. Delbart, F., Brams, M., Gruss, F., Noppen, S., Peigneur, S., Boland, S., Chaltin, P., Brandao-Neto, J., von Delft, F., Touw, W.G., Joosten, R.P., Liekens, S., Tytgat, J. and Ulens, C., *An allosteric binding site of the α7 nicotinic acetylcholine receptor revealed in a humanized acetylcholine-binding protein.* J Biol Chem, 2018. **293**(7): p. 2534-2545.
63. Parker, H.P., Dawson, A., Jones, M.J., Yan, R., Ouyang, J., Hong, R. and Hunter, W.N., *Delineating the activity of the potent nicotinic acetylcholine receptor agonists (+)-anatoxin-a and (-)-hosieine-A.* Acta Crystallogr F Struct Biol Commun, 2022. **78**(9): p. 313-323.
64. Zhao, Y., Liu, S., Zhou, Y., Zhang, M., Chen, H., Eric Xu, H., Sun, D., Liu, L. and Tian, C., *Structural basis of human α7 nicotinic acetylcholine receptor activation.* Cell Res, 2021. **31**(6): p. 713-716.
65. Noviello, C.M., Gharpure, A., Mukhtasimova, N., Cabuco, R., Baxter, L., Borek, D., Sine, S.M. and Hibbs, R.E., *Structure and gating mechanism of the α7 nicotinic acetylcholine receptor.* Cell, 2021. **184**(8): p. 2121-2134.e13.
66. Bondarenko, V., Chen, Q., Singewald, K., Haloi, N., Tillman, T.S., Howard, R.J., Lindahl, E., Xu, Y. and Tang, P., *Structural Elucidation of Ivermectin Binding to α7nAChR and the Induced Channel Desensitization.* ACS Chem Neurosci, 2023. **14**(6): p. 1156-1165.
67. Rahman, M.M., Basta, T., Teng, J., Lee, M., Worrell, B.T., Stowell, M.H.B. and Hibbs, R.E., *Structural mechanism of muscle nicotinic receptor desensitization and block by curare.* Nat Struct Mol Biol, 2022. **29**(4): p. 386-394.
68. Goswami, U., Rahman, M.M., Teng, J. and Hibbs, R.E. *Structural interplay of anesthetics and paralytics on muscle nicotinic receptors*. Nat Commun, 2023. **14**, 3169 DOI: 10.1038/s41467-023-38827-5.
69. Galzi, J.L., Bertrand, S., Corringer, P.J., Changeux, J.P. and Bertrand, D., *Identification of calcium binding sites that regulate potentiation of a neuronal nicotinic acetylcholine receptor.* EMBO J, 1996. **15**(21): p. 5824-32.
70. Epstein, M., Bali, K., Piggot, T.J., Green, A.C., Timperley, C.M., Bird, M., Tattersall, J.E.H., Bermudez, I. and Biggin, P.C., *Molecular determinants of binding of non-oxime bispyridinium nerve agent antidote compounds to the adult muscle nAChR.* Toxicol Lett, 2021. **340**: p. 114-122.
71. Carrington, H.C., Crowther, A.F., Davey, D.G., Levi, A.A. and Rose, F.L., *A Metabolite of 'Paludrine' with High Antimalarial Activity.* Nature, 1951. **168**(4286): p. 1080-1080.
72. Crowther, A.F. and Levi, A.A., *Proguanil, the isolation of a metabolite with high antimalarial activity.* Br J Pharmacol Chemother, 1953. **8**(1): p. 93-7.
73. Atri, A., Sherman, S., Norman, K.A., Kirchhoff, B.A., Nicolas, M.M., Greicius, M.D., Cramer, S.C., Breiter, H.C., Hasselmo, M.E. and Stern, C.E., *Blockade of Central Cholinergic Receptors Impairs New Learning and Increases Proactive Interference in a Word Paired-Associate Memory Task.* Behav Neurosci, 2004. **118**(1): p. 223-236.

74. De Rosa, E. and Hasselmo, M.E., *Muscarinic cholinergic neuromodulation reduces proactive interference between stored odor memories during associative learning in rats.* Behav Neurosci, 2000. **114**(1): p. 32-41.
75. Hasselmo, M.E. and Bower, J.M., *Acetylcholine and memory.* Trends Neurosci, 1993. **16**(6): p. 218-222.
76. Beatty, W.W., Butters, N. and Janowsky, D.S., *Patterns of memory failure after scopolamine treatment: implications for cholinergic hypotheses of dementia.* Behav Neural Biol, 1986. **45**(2): p. 196-211.
77. Sherman, S.J., Atri, A., Hasselmo, M.E., Stern, C.E. and Howard, M.W., *Scopolamine impairs human recognition memory: data and modeling.* Behav Neurosci, 2003. **117**(3): p. 526-39.
78. Dikshit, B.B., *Action of acetylcholine on the brain and its occurrence therein.* J Physiol, 1934. **80**(4): p. 409-21.
79. Stief, C., Benard, F., Bosch, R., Aboseif, S., Nunes, L., Lue, T.F. and Tanagho, E.A., *Acetylcholine as a possible neurotransmitter in penile erection.* J Urol, 1989. **141**(6): p. 1444-8.
80. Masland, R.H., Mills, J.W., Cassidy, C. and Boycott, B.B., *The functions of acetylcholine in the rabbit retina.* Proc R Soc Lond B Biol Sci, 1984. **223**(1230): p. 121-139.
81. Blumenthal, M.R., Wang, H., Markee, S. and Wang, S., *Effects of acetylcholine on the heart.* Am J Physiol, 1968. **214**(6): p. 1280-1287.
82. Fatt, P. and Katz, B., *An analysis of the end-plate potential recorded with an intracellular electrode.* J Physiol, 1951. **115**(3): p. 320-70.
83. Dale, H.H., Feldberg, W. and Vogt, M., *Release of acetylcholine at voluntary motor nerve endings.* J Physiol, 1936. **86**(4): p. 353-80.
84. Feldberg, W. and Vartiainen, A., *Further observations on the physiology and pharmacology of a sympathetic ganglion.* J Physiol, 1934. **83**(1): p. 103-28.
85. Pickford, M., *The inhibitory effect of acetylcholine on water diuresis in the dog, and its pituitary transmission.* J Physiol, 1939. **95**(1): p. 226-38.
86. Feldberg, W. and Gaddum, J.H., *The chemical transmitter at synapses in a sympathetic ganglion.* J Physiol, 1934. **81**(3): p. 305-19.
87. Nachmansohn, D. and Machado, A.L., *THE FORMATION OF ACETYLCHOLINE. A NEW ENZYME: "CHOLINE ACETYLASE".* J Neurophysiol, 1943. **6**(5): p. 397-403.
88. Nachmansohn, D. and Berman, M., *STUDIES ON CHOLINE ACETYLASE: III. ON THE PREPARATION OF THE COENZYME AND ITS EFFECT ON THE ENZYME.* J Biol Chem, 1946. **165**(2): p. 551-563.
89. Lipmann, F. and Kaplan, N.O., *A COMMON FACTOR IN THE ENZYMATIC ACETYLATION OF SULFANILAMIDE AND OF CHOLINE.* J Biol Chem, 1946. **162**(3): p. 743-744.
90. Robertis, E.d., Arnaiz, G.R.d.L., Iraldi, L.S.A.P.d. and Zieher, L.M., *ISOLATION OF SYNAPTIC VESICLES AND STRUCTURAL ORGANIZATION OF THE ACETYLCHOLINE SYSTEM WITHIN BRAIN NERVE ENDINGS*.* J Neurochem, 1963. **10**(4): p. 225-235.
91. Whittaker, V.P., Essman, W.B. and Dowe, G.H., *The isolation of pure cholinergic synaptic vesicles from the electric organs of elasmobranch fish of the family Torpedinidae.* Biochem J, 1972. **128**(4): p. 833-45.
92. Whittaker, V.P. and Sheridan, M.N., *THE MORPHOLOGY AND ACETYLCHOLINE CONTENT OF ISOLATED CEREBRAL CORTICAL SYNAPTIC VESICLES.* J Neurochem, 1965. **12**(5): p. 363-372.
93. Wilson, W.S., Schulz, R.A. and Cooper, J.R., *THE ISOLATION OF CHOLINERGIC SYNAPTIC VESICLES FROM BOVINE SUPERIOR CERVICAL GANGLION AND ESTIMATION OF THEIR ACETYLCHOLINE CONTENT.* J Neurochem, 1973. **20**(3): p. 659-667.
94. De Robertis, E., Fiszer, S., Pasquini, J.M. and Soto, E.F., *Isolation and chemical nature of the receptor for d-tubocurarine in nerve-ending membranes of the cerebral cortex.* J Neurobiol, 1969. **1**(1): p. 41-52.
95. La Torre, J.L., Lunt, G.S. and De Robertis, E., *Isolation of a cholinergic proteolipid receptor from electric tissue.* Proc Natl Acad Sci USA, 1970. **65**(3): p. 716-720.

96. Trendelenburg, U., *TRANSMISSION OF PREGANGLIONIC IMPULSES THROUGH THE MUSCARINIC RECEPTORS OF THE SUPERIOR CERVICAL GANGLION OF THE CAT.* J Pharmacol Exp Ther, 1966. **154**(3): p. 426-440.
97. Curtis, D.R. and Ryall, R.W., *The synaptic excitation of Renshaw cells.* Exp Brain Res, 1966. **2**(1): p. 81-96.
98. Eccles, J.C., Fatt, P. and Koketsu, K., *Cholinergic and inhibitory synapses in a pathway from motor-axon collaterals to motoneurones.* J Physiol, 1954. **126**(3): p. 524-62.
99. Takeshige, C. and Volle, R.L., *BIMODAL RESPONSE OF SYMPATHETIC GANGLIA TO ACETYLCHOLINE FOLLOWING ESERINE OR REPETITIVE PREGANGLIONIC STIMULATION.* J Pharmacol Exp Ther, 1962. **138**(1): p. 66-73.
100. Takeshige, C. and Volle, R.L., *ASYNCHRONOUS POSTGANGLIONIC FIRING FROM THE CAT SUPERIOR CERVICAL SYMPATHETIC GANGLION TREATED WITH NEOSTIGMINE.* Br J Pharmacol Chemother, 1963. **20**(1): p. 214-220.
101. Takeshige, C., Pappano, A.J., DeGroat, W.C. and Volle, R.L., *GANGLIONIC BLOCKADE PRODUCED IN SYMPATHETIC GANGLIA BY CHOLINOMIMETIC DRUGS.* J Pharmacol Exp Ther, 1963. **141**(3): p. 333-342.
102. Jones, A., *GANGLIONIC ACTIONS OF MUSCARINIC SUBSTANCES.* J Pharmacol Exp Ther, 1963. **141**(2): p. 195-205.
103. Gyermek, L., Sigg, E.B. and Bindler, E., *Ganglionic stimulant action of muscarine.* Am J Physiol, 1963. **204**(1): p. 68-70.
104. Nathanson, N.M., Klein, W.L. and Nirenberg, M., *Regulation of adenylate cyclase activity mediated by muscarinic acetylcholine receptors.* Proc Natl Acad Sci USA, 1978. **75**(4): p. 1788-1791.
105. Traber, J., Fischer, K., Buchen, C. and Hamprecht, B., *Muscarinic response to acetylcholine in neuroblastoma × glioma hybrid cells.* Nature, 1975. **255**(5509): p. 558-560.
106. Hulme, E.C., Berrie, C.P., Birdsall, N.J.M., Jameson, M. and Stockton, J.M., *Regulation of muscarinic agonist binding by cations and guanine nucleotides.* Eur J Pharmacol, 1983. **94**(1): p. 59-72.
107. Berrie, C.P., Birdsall, N.J.M., Hulme, E.C., Keen, M. and Stockton, J.M., *Solubilization and characterization of guanine nucleotide-sensitive muscarinic agonist binding sites from rat myocardium.* Br J Pharmacol, 1984. **82**(4): p. 853-861.
108. Lazareno, S., Kendall, D.A. and Nahorski, S.R., *Pirenzepine indicates heterogeneity of muscarinic receptors linked to cerebral inositol phospholipid metabolism.* Neuropharmacology, 1985. **24**(6): p. 593-595.
109. Berrie, C.P., Birdsall, N.J.M., Burgen, A.S.V. and Hulme, E.C., *Guanine nucleotides modulate muscarinic receptor binding in the heart.* Biochem Biophys Res Commun, 1979. **87**(4): p. 1000-1005.
110. Brown, J.H., *Cholinergic inhibition of catecholamine-stimulable cyclic AMP accumulation in murine atria.* J Cyclic Nucleotide Res, 1979. **5**(6): p. 423-433.
111. Watanabe, A.M., McConnaughey, M.M., Strawbridge, R.A., Fleming, J.W., Jones, L.R. and Besch, H., *Muscarinic cholinergic receptor modulation of beta-adrenergic receptor affinity for catecholamines.* J Biol Chem, 1978. **253**(14): p. 4833-4836.
112. Biegon, R.L. and Pappano, A.J., *Dual mechanism for inhibition of calcium-dependent action potentials by acetylcholine in avian ventricular muscle. Relationship to cyclic AMP.* Circul Res, 1980. **46**(3): p. 353-362.
113. Quist, E.E., *Evidence for a carbachol stimulated phosphatidylinositol effect in heart.* Biochem Pharmacol, 1982. **31**(19): p. 3130-3133.
114. Gil, D.W. and Wolfe, B.B., *Pirenzepine distinguishes between muscarinic receptor-mediated phosphoinositide breakdown and inhibition of adenylate cyclase.* J Pharmacol Exp Ther, 1985. **232**(3): p. 608-616.
115. Kasai, M. and Changeux, J.P., *In Vitro excitation of purified membrane fragments by cholinergic agonists : I. Pharmalogical properties of the excitable membrane fragments.* J Membr Biol, 1971. **6**(1): p. 1-23.

116. Katz, B. and Miledi, R., *The statistical nature of the acetycholine potential and its molecular components.* J Physiol, 1972. **224**(3): p. 665-99.
117. Hucho, F., *Molecular weight and quaternary structure of the cholinergic receptor protein extracted by detergents from Electrophorus electricus electric tissue.* FEBS Lett, 1973. **38**(1): p. 11-15.
118. Weill, C.L., McNamee, M.G. and Karlin, A., *Affinity-labeling of purified acetylcholine receptor from Torpedo californica.* Biochem Biophys Res Commun, 1974. **61**(3): p. 997-1003.
119. Lindstrom, J., Walter, B. and Einarson, B., *Immunochemical similarities between subunits of acetylcholine receptors from Torpedo, Electrophorus, and mammalian muscle.* Biochemistry, 1979. **18**(21): p. 4470-4480.
120. Castillo, J.D. and Katz, B., *Interaction at end-plate receptors between different choline derivatives.* Proc R Soc Lond B Biol Sci, 1957. **146**(924): p. 369-381.
121. Fambrough, D.M., Drachman, D.B. and Satyamurti, S., *Neuromuscular junction in myasthenia gravis: decreased acetylcholine receptors.* Science, 1973. **182**(4109): p. 293-5.
122. Simpson, J.A., *Myasthenia Gravis: A New Hypothesis.* Scott Med J, 1960. **5**(10): p. 419-436.
123. Patrick, J. and Lindstrom, J., *Autoimmune response to acetylcholine receptor.* Science, 1973. **180**(4088): p. 871-2.
124. Lennon, V.A., Lindstrom, J.M. and Seybold, M.E., *Experimental autoimmune myasthenia: A model of myasthenia gravis in rats and guinea pigs.* J Exp Med, 1975. **141**(6): p. 1365-75.
125. Lindstrom, J.M., Lennon, V.A., Seybold, M.E. and Whittingham, S., *EXPERIMENTAL AUTOIMMUNE MYASTHENIA GRAVIS AND MYASTHENIA GRAVIS: BIOCHEMICAL AND IMMUNOCHEMICAL ASPECTS*.* Ann NY Acad Sci, 1976. **274**(1): p. 254-274.
126. Appel, S.H., Almon, R.R. and Levy, N., *Acetylcholine Receptor Antibodies in Myasthenia Gravis.* New Engl J Med, 1975. **293**(15): p. 760-761.
127. Shimohama, S., Taniguchi, T., Fujiwara, M. and Kameyama, M., *Changes in Nicotinic and Muscarinic Cholinergic Receptors in Alzheimer-Type Dementia.* J Neurochem, 1986. **46**(1): p. 288-293.
128. Whitehouse, P.J., Martino, A.M., Antuono, P.G., Lowenstein, P.R., Coyle, J.T., Price, D.L. and Kellar, K.J., *Nicotinic acetylcholine binding sites in Alzheimer's disease.* Brain Res, 1986. **371**(1): p. 146-51.
129. Perry, E.K., Morris, C.M., Court, J.A., Cheng, A., Fairbairn, A.F., McKeith, I.G., Irving, D., Brown, A. and Perry, R.H., *Alteration in nicotine binding sites in Parkinson's disease, Lewy body dementia and Alzheimer's disease: possible index of early neuropathology.* Neuroscience, 1995. **64**(2): p. 385-95.
130. Nordberg, A., *Nicotinic receptor abnormalities of Alzheimer's disease: therapeutic implications.* Biol Psychiatry, 2001. **49**(3): p. 200-210.
131. Bird, T.D., Stranahan, S., Sumi, S.M. and Raskind, M., *Alzheimer's disease: choline acetyltransferase activity in brain tissue from clinical and pathological subgroups.* Ann Neurol, 1983. **14**(3): p. 284-93.
132. Davies, P. and Maloney, A.J.F., *SELECTIVE LOSS OF CENTRAL CHOLINERGIC NEURONS IN ALZHEIMER'S DISEASE.* The Lancet, 1976. **308**(8000): p. 1403.
133. Perry, E.K., Gibson, P.H., Blessed, G., Perry, R.H. and Tomlinson, B.E., *Neurotransmitter enzyme abnormalities in senile dementia: Choline acetyltransferase and glutamic acid decarboxylase activities in necropsy brain tissue.* J Neurol Sci, 1977. **34**(2): p. 247-265.
134. Rösler, M., Anand, R., Cicin-Sain, A., Gauthier, S., Agid, Y., Dal-Bianco, P., Stähelin, H.B., Hartman, R. and Gharabawi, M., *Efficacy and safety of rivastigmine in patients with Alzheimer's disease: international randomised controlled trial.* BMJ, 1999. **318**(7184): p. 633-8.
135. Rogers, S.L., Farlow, M.R., Doody, R.S., Mohs, R., Friedhoff, L.T. and Group*, D.S., *A 24-week, double-blind, placebo-controlled trial of donepezil in patients with Alzheimer's disease.* Neurology, 1998. **50**(1): p. 136-145.
136. Rogers, S.L. and Friedhoff, L.T., *The Efficacy and Safety of Donepezil in Patients with Alzheimer's Disease: Results of a US Multicentre, Randomized, Double-Blind, Placebo-Controlled Trial.* Dementia 1996. **7**(6): p. 293-303.

137. Knapp, M.J., Knopman, D.S., Solomon, P.R., Pendlebury, W.W., Davis, C.S. and Gracon, S.I., *A 30-week randomized controlled trial of high-dose tacrine in patients with Alzheimer's disease. The Tacrine Study Group.* JAMA, 1994. **271**(13): p. 985-91.
138. Maitra, S.K. and Sarkar, R., *Influence of methyl parathion on gametogenic and acetylcholinesterase activity in the testis of whitethroated munia (Lonchura malabarica).* Arch Environ Contam Toxicol, 1996. **30**(3): p. 384-389.
139. Nachmansohn, D., Rothenberg, M.A. and Feld, E.A., *STUDIES ON CHOLINESTERASE: V. KINETIC OF THE ENZYME INHIBITION.* J Biol Chem, 1948. **174**(1): p. 247-256.
140. Aldridge, W., *Some properties of specific cholinesterase with particular reference to the mechanism of inhibition by diethyl p-nitrophenyl thiophosphate (E 605) and analogues.* Biochem J, 1950. **46**(4): p. 451.
141. Grundfest, H., Nachmansohn, D. and Rothenberg, M., *Effect of di-isopropyl fluorphosphate (DFP) on action potential and cholinesterase of nerve. III.* J Neurophysiol, 1947. **10**(2): p. 155-164.
142. Minton, N.A. and Murray, V.S., *A review of organophosphate poisoning.* Med Toxicol Adverse Drug Exp, 1988. **3**: p. 350-375.
143. DuBois, K.P., Doull, J., Salerno, P.R. and Coon, J.M., *STUDIES ON THE TOXICITY AND MECHANISM OF ACTION OF p-NITROPHENYL DIETHYL THIONOPHOSPHATE (PARATHION).* J Pharmacol Exp Ther, 1949. **95**(1): p. 79-91.
144. Costa, L.G., *Organophosphorus Compounds at 80: Some Old and New Issues.* Toxicol Sci, 2017. **162**(1): p. 24-35.
145. Thiermann, H., Kehe, K., Riehm, J. and Zöller, L., *Chemical and Biological Weapons and Their Regulation.* Regulatory Toxicology, 2020: p. 1-15.
146. Corradi, J. and Bouzat, C., *Understanding the Bases of Function and Modulation of α7 Nicotinic Receptors: Implications for Drug Discovery.* Mol Pharmacol, 2016. **90**(3): p. 288-99.
147. Howes, L., *Novichok compound poisoned Navalny.* Chem. Eng. News, 2020. **98**(5).
148. Steindl, D., Boehmerle, W., Körner, R., Praeger, D., Haug, M., Nee, J., Schreiber, A., Scheibe, F., Demin, K., Jacoby, P., Tauber, R., Hartwig, S., Endres, M. and Eckardt, K.-U., *Novichok nerve agent poisoning.* The Lancet, 2021. **397**(10270): p. 249-252.
149. Vale, J.A., Marrs, T.C. and Maynard, R.L., *Novichok: a murderous nerve agent attack in the UK.* Clin Toxicol, 2018. **56**(11): p. 1093-1097.
150. Shafferman, A., Kronman, C., Flashner, Y., Leitner, M., Grosfeld, H., Ordentlich, A., Gozes, Y., Cohen, S., Ariel, N., Barak, D. and et al., *Mutagenesis of human acetylcholinesterase. Identification of residues involved in catalytic activity and in polypeptide folding.* J Biol Chem, 1992. **267**(25): p. 17640-8.
151. Morales-Perez, C.L., Noviello, C.M. and Hibbs, R.E., *X-ray structure of the human α4β2 nicotinic receptor.* Nature, 2016. **538**(7625): p. 411-415.
152. HUNT, C.C. and WALTER F. RIKER, J., *THE EFFECT OF CHRONIC POISONING WITH DI-ISOPROPYL FLUOROPHOSPHATE ON NEUROMUSCULAR FUNCTION IN THE CAT.* J Pharmacol Exp Ther, 1947. **91**(3): p. 298-305.
153. Sanson, B., Nachon, F., Colletier, J.-P., Froment, M.-T., Toker, L., Greenblatt, H.M., Sussman, J.L., Ashani, Y., Masson, P., Silman, I. and Weik, M., *Crystallographic Snapshots of Nonaged and Aged Conjugates of Soman with Acetylcholinesterase, and of a Ternary Complex of the Aged Conjugate with Pralidoxime.* J Med Chem, 2009. **52**(23): p. 7593-7603.
154. Ekström, F., Pang, Y.-P., Boman, M., Artursson, E., Akfur, C. and Börjegren, S., *Crystal structures of acetylcholinesterase in complex with HI-6, Ortho-7 and obidoxime: Structural basis for differences in the ability to reactivate tabun conjugates.* Biochem Pharmacol, 2006. **72**(5): p. 597-607.
155. Bird, S.B., Gaspari, R.J. and Dickson, E.W., *Early death due to severe organophosphate poisoning is a centrally mediated process.* Acad Emerg Med, 2003. **10**(4): p. 295-8.
156. Bosković, B., Kovacević, V. and Jovanović, D., *PAM-2 Cl, HI-6, and HGG-12 in soman and tabun poisoning.* Fundam Appl Toxicol, 1984. **4**(2 Pt 2): p. S106-15.

157. Cohen, S. and Ashani, Y., *Nucleophilicity of some reactivators of phosphorylated acetylcholinesterase. 5.* J Med Chem, 1971. **14**(7): p. 621-626.
158. Wong, L., Radić, Z., Brüggemann, R.J.M., Hosea, N., Berman, H.A. and Taylor, P., *Mechanism of Oxime Reactivation of Acetylcholinesterase Analyzed by Chirality and Mutagenesis.* Biochemistry, 2000. **39**(19): p. 5750-5757.
159. Peter, J.V., Moran, J.L. and Graham, P., *Oxime therapy and outcomes in human organophosphate poisoning: an evaluation using meta-analytic techniques.* Crit Care Med, 2006. **34**(2): p. 502-10.
160. Rahimi, R., Nikfar, S. and Abdollahi, M., *Increased morbidity and mortality in acute human organophosphate-poisoned patients treated by oximes: a meta-analysis of clinical trials.* Hum Exp Toxicol, 2006. **25**(3): p. 157-162.
161. Sichler, S., Hofner, G., Rappengluck, S., Wein, T., Niessen, K.V., Seeger, T., Worek, F., Thiermann, H., Paintner, F.F. and Wanner, K.T., *Development of MS Binding Assays targeting the binding site of MB327 at the nicotinic acetylcholine receptor.* Toxicol Lett, 2018. **293**: p. 172-183.
162. Haufe, Y., Loser, D., Danker, T. and Nicke, A., *Symmetrical Bispyridinium Compounds Act as Open Channel Blockers of Cation-Selective Ion Channels.* ACS Pharmacol Transl Sci, 2024. **7**(3): p. 771-786.
163. White, D.S., Chowdhury, S., Idikuda, V., Zhang, R., Retterer, S.T., Goldsmith, R.H. and Chanda, B., *cAMP binding to closed pacemaker ion channels is non-cooperative.* Nature, 2021. **595**(7868): p. 606-610.
164. Kuschke, S., Thon, S., Sattler, C., Schwabe, T., Benndorf, K. and Schmauder, R., *cAMP binding to closed pacemaker ion channels is cooperative.* Proc Natl Acad Sci USA, 2024. **121**(9): p. e2315132121.
165. Baenziger, J.E., Hénault, C.M., Therien, J.P.D. and Sun, J., *Nicotinic acetylcholine receptor–lipid interactions: Mechanistic insight and biological function.* Biochim Biophys Acta, 2015. **1848**(9): p. 1806-1817.
166. Amend, N., Timperley, C.M., Bird, M., Green, A.C., Worek, F. and Seeger, T., *Restoration of nerve agent impaired neuromuscular transmission in rat diaphragm by bispyridinium non-oximes – Structure-activity relationships.* Toxicology, 2024. **503**: p. 153741.
167. Amend, N., Timperley, C.M., Bird, M., Green, A.C., Worek, F. and Seeger, T., *The use of bispyridinium non-oxime analogues for the restoration of nerve agent impaired neuromuscular transmission in rat hemidiaphragms – Structure optimization.* Toxicol Lett, 2024. **397**: p. 42-47.
168. Lipinski, C.A., Lombardo, F., Dominy, B.W. and Feeney, P.J., *Experimental and computational approaches to estimate solubility and permeability in drug discovery and development settings1PII of original article: S0169-409X(96)00423-1. The article was originally published in Advanced Drug Delivery Reviews 23 (1997) 3–25.1.* Adv Drug Del Rev, 2001. **46**(1): p. 3-26.
169. De Gieter, S., Gallagher, C.I., Wijckmans, E., Pasini, D., Ulens, C. and Efremov, R.G. *Sterol derivative binding to the orthosteric site causes conformational changes in an invertebrate Cys-loop receptor*. eLife, 2023. **12**, e86029 DOI: 10.7554/elife.86029.
170. Bondarenko, V., Wells, M.M., Chen, Q., Tillman, T.S., Singewald, K., Lawless, M.J., Caporoso, J., Brandon, N., Coleman, J.A., Saxena, S., Lindahl, E., Xu, Y. and Tang, P. *Structures of highly flexible intracellular domain of human α7 nicotinic acetylcholine receptor*. Nat Commun, 2022. **13**, 793 DOI: 10.1038/s41467-022-28400-x.
171. Nys, M., Zarkadas, E., Brams, M., Mehregan, A., Kambara, K., Kool, J., Casewell, N.R., Bertrand, D., Baenziger, J.E., Nury, H. and Ulens, C. *The molecular mechanism of snake short-chain α-neurotoxin binding to muscle-type nicotinic acetylcholine receptors*. Nat Commun, 2022. **13**, 4543 DOI: 10.1038/s41467-022-32174-7.
172. Zarkadas, E., Pebay-Peyroula, E., Thompson, M.J., Schoehn, G., Uchański, T., Steyaert, J., Chipot, C., Dehez, F., Baenziger, J.E. and Nury, H., *Conformational transitions and ligand-binding to a muscle-type nicotinic acetylcholine receptor.* Neuron, 2022. **110**(8): p. 1358-1370.e5.

173. Mukherjee, S., Erramilli, S.K., Ammirati, M., Alvarez, F.J.D., Fennell, K.F., Purdy, M.D., Skrobek, B.M., Radziwon, K., Coukos, J., Kang, Y., Dutka, P., Gao, X., Qiu, X., Yeager, M., Eric Xu, H., Han, S. and Kossiakoff, A.A. *Synthetic antibodies against BRIL as universal fiducial marks for single-particle cryoEM structure determination of membrane proteins*. Nat Commun, 2020. **11**, 1598 DOI: 10.1038/s41467-020-15363-0.
174. Rahman, M.M., Teng, J., Worrell, B.T., Noviello, C.M., Lee, M., Karlin, A., Stowell, M.H.B. and Hibbs, R.E., *Structure of the Native Muscle-type Nicotinic Receptor and Inhibition by Snake Venom Toxins.* Neuron, 2020. **106**(6): p. 952-962.e5.
175. Gharpure, A., Teng, J., Zhuang, Y., Noviello, C.M., Walsh, R.M., Cabuco, R., Howard, R.J., Zaveri, N.T., Lindahl, E. and Hibbs, R.E., *Agonist Selectivity and Ion Permeation in the α3β4 Ganglionic Nicotinic Receptor.* Neuron, 2019. **104**(3): p. 501-511.e6.
176. Walsh, R.M., Roh, S.-H., Gharpure, A., Morales-Perez, C.L., Teng, J. and Hibbs, R.E., *Structural principles of distinct assemblies of the human α4β2 nicotinic receptor.* Nature, 2018. **557**(7704): p. 261-265.
177. Claudio, T., Ballivet, M., Patrick, J. and Heinemann, S., *Nucleotide and deduced amino acid sequences of Torpedo californica acetylcholine receptor gamma subunit.* Proc Natl Acad Sci U S A, 1983. **80**(4): p. 1111-5.
178. Noda, M., Takahashi, H., Tanabe, T., Toyosato, M., Kikyotani, S., Furutani, Y., Hirose, T., Takashima, H., Inayama, S., Miyata, T. and Numa, S., *Structural homology of Torpedo californica acetylcholine receptor subunits.* Nature, 1983. **302**(5908): p. 528-532.
179. Devillers-Thiery, A., Giraudat, J., Bentaboulet, M. and Changeux, J.P., *Complete mRNA coding sequence of the acetylcholine binding alpha-subunit of Torpedo marmorata acetylcholine receptor: a model for the transmembrane organization of the polypeptide chain.* Proc Natl Acad Sci U S A, 1983. **80**(7): p. 2067-71.
180. Boulter, J., Evans, K., Goldman, D., Martin, G., Treco, D., Heinemann, S. and Patrick, J., *Isolation of a cDNA clone coding for a possible neural nicotinic acetylcholine receptor α-subunit.* Nature, 1986. **319**(6052): p. 368-374.
181. Whiting, P.J. and Lindstrom, J.M., *Purification and characterization of a nicotinic acetylcholine receptor from chick brain.* Biochemistry, 1986. **25**(8): p. 2082-2093.
182. Whiting, P.J., Schoepfer, R., Conroy, W.G., Gore, M.J., Keyser, K.T., Shimasaki, S., Esch, F. and Lindstrom, J.M., *Expression of nicotinic acetylcholine receptor subtypes in brain and retina.* Mol Brain Res, 1991. **10**(1): p. 61-70.
183. Boulter, J., O'Shea-Greenfield, A., Duvoisin, R.M., Connolly, J.G., Wada, E., Jensen, A., Gardner, P.D., Ballivet, M., Deneris, E.S., McKinnon, D. and et al., *Alpha 3, alpha 5, and beta 4: three members of the rat neuronal nicotinic acetylcholine receptor-related gene family form a gene cluster.* J Biol Chem, 1990. **265**(8): p. 4472-82.
184. Goldman, D., Deneris, E., Luyten, W., Kochhar, A., Patrick, J. and Heinemann, S., *Members of a nicotinic acetylcholine receptor gene family are expressed in different regions of the mammalian central nervous system.* Cell, 1987. **48**(6): p. 965-73.
185. Nef, P., Oneyser, C., Alliod, C., Couturier, S. and Ballivet, M., *Genes expressed in the brain define three distinct neuronal nicotinic acetylcholine receptors.* EMBO J, 1988. **7**(3): p. 595-601.
186. Wada, K., Ballivet, M., Boulter, J., Connolly, J., Wada, E., Deneris, E.S., Swanson, L.W., Heinemann, S. and Patrick, J., *Functional Expression of a New Pharmacological Subtype of Brain Nicotinic Acetylcholine Receptor.* Science, 1988. **240**(4850): p. 330-334.
187. Deneris, E.S., Boulter, J., Swanson, L.W., Patrick, J. and Heinemann, S., *Beta 3: a new member of nicotinic acetylcholine receptor gene family is expressed in brain.* J Biol Chem, 1989. **264**(11): p. 6268-72.
188. Deneris, E.S., Connolly, J., Boulter, J., Wada, E., Wada, K., Swanson, L.W., Patrick, J. and Heinemann, S., *Primary structure and expression of β2: a novel subunit of neuronal nicotinic acetylcholine receptors.* Neuron, 1988. **1**(1): p. 45-54.
189. Duvoisin, R.M., Deneris, E.S., Patrick, J. and Heinemann, S., *The functional diversity of the neuronal nicotinic acetylcholine receptors is increased by a novel subunit: beta 4.* Neuron, 1989. **3**(4): p. 487-96.

190. Schoepfer, R., Whiting, P., Esch, F., Blacher, R., Shimasaki, S. and Lindstrom, J., *cDNA clones coding for the structural subunit of a chicken brain nicotinic acetylcholine receptor.* Neuron, 1988. **1**(3): p. 241-8.
191. Mishina, M., Takai, T., Imoto, K., Noda, M., Takahashi, T., Numa, S., Methfessel, C. and Sakmann, B., *Molecular distinction between fetal and adult forms of muscle acetylcholine receptor.* Nature, 1986. **321**(6068): p. 406-411.
192. Bourne, Y., Talley, T.T., Hansen, S.B., Taylor, P. and Marchot, P., *Crystal structure of a Cbtx–AChBP complex reveals essential interactions between snake α-neurotoxins and nicotinic receptors.* EMBO J, 2005. **24**(8): p. 1512-1522.
193. Brejc, K.a., van Dijk, W.J., Klaassen, R.V., Schuurmans, M., van der Oost, J., Smit, A.B. and Sixma, T.K., *Crystal structure of an ACh-binding protein reveals the ligand-binding domain of nicotinic receptors.* Nature, 2001. **411**(6835): p. 269-276.
194. Celie, P.H.N., van Rossum-Fikkert, S.E., van Dijk, W.J., Brejc, K., Smit, A.B. and Sixma, T.K., *Nicotine and Carbamylcholine Binding to Nicotinic Acetylcholine Receptors as Studied in AChBP Crystal Structures.* Neuron, 2004. **41**(6): p. 907-914.
195. Celie, P.H.N., Klaassen, R.V., van Rossum-Fikkert, S.E., van Elk, R., van Nierop, P., Smit, A.B. and Sixma, T.K., *Crystal structure of acetylcholine-binding protein from Bulinus truncatus reveals the conserved structural scaffold and sites of variation in nicotinic acetylcholine receptors.* J Biol Chem, 2005. **280**(28): p. 26457-26466.
196. Celie, P.H.N., Kasheverov, I.E., Mordvintsev, D.Y., Hogg, R.C., van Nierop, P., van Elk, R., van Rossum-Fikkert, S.E., Zhmak, M.N., Bertrand, D., Tsetlin, V., Sixma, T.K. and Smit, A.B., *Crystal structure of nicotinic acetylcholine receptor homolog AChBP in complex with an alpha-conotoxin PnIA variant.* Nat Struct Mol Biol, 2005. **12**(7): p. 582-588.
197. Hansen, S.B., Sulzenbacher, G., Huxford, T., Marchot, P., Taylor, P. and Bourne, Y., *Structures of Aplysia AChBP complexes with nicotinic agonists and antagonists reveal distinctive binding interfaces and conformations.* EMBO J, 2005. **24**(20): p. 3635-3646.
198. Ulens, C., Hogg, R.C., Celie, P.H., Bertrand, D., Tsetlin, V., Smit, A.B. and Sixma, T.K., *Structural determinants of selective alpha-conotoxin binding to a nicotinic acetylcholine receptor homolog AChBP.* Proc Natl Acad Sci USA, 2006. **103**(10): p. 3615-3620.
199. Hansen, S.B. and Taylor, P., *Galanthamine and non-competitive inhibitor binding to ACh-binding protein: evidence for a binding site on non-alpha-subunit interfaces of heteromeric neuronal nicotinic receptors.* J Mol Biol, 2007. **369**(4): p. 895-901.
200. Ulens, C., Akdemir, A., Jongejan, A., van Elk, R., Bertrand, S., Perrakis, A., Leurs, R., Smit, A.B., Sixma, T.K., Bertrand, D. and de Esch, I.J.P., *Use of acetylcholine binding protein in the search for novel alpha7 nicotinic receptor ligands. In silico docking, pharmacological screening, and X-ray analysis.* J Med Chem, 2009. **52**(8): p. 2372-2383.
201. Hibbs, R.E., Sulzenbacher, G., Shi, J., Talley, T.T., Conrod, S., Kem, W.R., Taylor, P., Marchot, P. and Bourne, Y., *Structural determinants for interaction of partial agonists with acetylcholine binding protein and neuronal alpha7 nicotinic acetylcholine receptor.* EMBO J, 2009. **28**(19): p. 3040-3051.
202. Bourne, Y., Radic, Z., Aráoz, R., Talley, T.T., Benoit, E., Servent, D., Taylor, P., Molgó, J. and Marchot, P., *Structural determinants in phycotoxins and AChBP conferring high affinity binding and nicotinic AChR antagonism.* Proc Natl Acad Sci USA, 2010. **107**(13): p. 6076-6081.
203. Akdemir, A., Rucktooa, P., Jongejan, A., Elk, R.v., Bertrand, S., Sixma, T.K., Bertrand, D., Smit, A.B., Leurs, R., de Graaf, C. and de Esch, I.J.P., *Acetylcholine binding protein (AChBP) as template for hierarchical in silico screening procedures to identify structurally novel ligands for the nicotinic receptors.* Biorg Med Chem, 2011. **19**(20): p. 6107-6119.
204. Li, S.-X., Huang, S., Bren, N., Noridomi, K., Dellisanti, C.D., Sine, S.M. and Chen, L. *Ligand-binding domain of an α7-nicotinic receptor chimera and its complex with agonist*. Nat Neurosci, 2011. **14**, 1253-1259 DOI: 10.1038/nn.2908.
205. Grimster, N.P., Stump, B., Fotsing, J.R., Weide, T., Talley, T.T., Yamauchi, J.G., Nemecz, Á., Kim, C., Ho, K.-Y., Sharpless, K.B., Taylor, P. and Fokin, V.V., *Generation of candidate ligands for*

nicotinic acetylcholine receptors via in situ click chemistry with a soluble acetylcholine binding protein template. J Am Chem Soc, 2012. **134**(15): p. 6732-6740.

206. Rucktooa, P., Haseler, C.A., van Elk, R., Smit, A.B., Gallagher, T. and Sixma, T.K., *Structural characterization of binding mode of smoking cessation drugs to nicotinic acetylcholine receptors through study of ligand complexes with acetylcholine-binding protein.* J Biol Chem, 2012. **287**(28): p. 23283-23293.
207. Billen, B., Spurny, R., Brams, M., van Elk, R., Valera-Kummer, S., Yakel, J.L., Voets, T., Bertrand, D., Smit, A.B. and Ulens, C., *Molecular actions of smoking cessation drugs at α4β2 nicotinic receptors defined in crystal structures of a homologous binding protein.* Proc Natl Acad Sci USA, 2012. **109**(23): p. 9173-9178.
208. Zhang, H.-K., Eaton, J.B., Yu, L.-F., Nys, M., Mazzolari, A., van Elk, R., Smit, A.B., Alexandrov, V., Hanania, T., Sabath, E., Fedolak, A., Brunner, D., Lukas, R.J., Vistoli, G., Ulens, C. and Kozikowski, A.P., *Insights into the structural determinants required for high-affinity binding of chiral cyclopropane-containing ligands to α4β2-nicotinic acetylcholine receptors: an integrated approach to behaviorally active nicotinic ligands.* J Med Chem, 2012. **55**(18): p. 8028-8037.
209. Luo, J., Taylor, P., Losen, M., de Baets, M.H., Shelton, G.D. and Lindstrom, J., *Main immunogenic region structure promotes binding of conformation-dependent myasthenia gravis autoantibodies, nicotinic acetylcholine receptor conformation maturation, and agonist sensitivity.* J Neurosci, 2009. **29**(44): p. 13898-13908.
210. Bourne, Y., Sulzenbacher, G., Radić, Z., Aráoz, R., Reynaud, M., Benoit, E., Zakarian, A., Servent, D., Molgó, J., Taylor, P. and Marchot, P., *Marine Macrocyclic Imines, Pinnatoxins A and G: Structural Determinants and Functional Properties to Distinguish Neuronal α7 from Muscle α1(2)βγδ nAChRs.* Structure, 2015. **23**(6): p. 1106-1115.
211. Abraham, N., Healy, M., Ragnarsson, L., Brust, A., Alewood, P.F. and Lewis, R.J. *Structural mechanisms for α-conotoxin activity at the human α3β4 nicotinic acetylcholine receptor*. Sci Rep, 2017. **7**, 45466.
212. Xu, M., Zhu, X., Yu, J., Yu, J., Luo, S. and Wang, X., *The crystal structure of Ac-AChBP in complex with α-conotoxin LvIA reveals the mechanism of its selectivity towards different nAChR subtypes.* Protein Cell, 2017. **8**(9): p. 675-685.
213. Ho, T.N.T., Abraham, N. and Lewis, R.J., *Rigidity of loop 1 contributes to equipotency of globular and ribbon isomers of α-conotoxin AusIA.* Sci Rep, 2021. **11**(1): p. 21928.
214. Koizumi, W., Otsubo, S., Furutani, S., Niki, K., Takayama, K., Fujimura, S., Maekawa, T., Koyari, R., Ihara, M., Kai, K., Hayashi, H., Ali, M.S., Kage-Nakadai, E., Sattelle, D.B. and Matsuda, K., *Determinants of Subtype-Selectivity of the Anthelmintic Paraherquamide A on Caenorhabditis elegans Nicotinic Acetylcholine Receptors.* Mol Pharmacol, 2023. **103**(6): p. 299-310.
215. Ho, T.N.T., Abraham, N. and Lewis, R.J. *Unique Pharmacological Properties of α-Conotoxin OmIA at α7 nAChRs*. Front Pharmacol, 2021. **12**, 803397 DOI: 10.3389/fphar.2021.803397.
216. Montgomery, M., Rendine, S., Zimmer, C.T., Elias, J., Schaetzer, J., Pitterna, T., Benfatti, F., Skaljac, M. and Bigot, A., *Structural Biology-Guided Design, Synthesis, and Biological Evaluation of Novel Insect Nicotinic Acetylcholine Receptor Orthosteric Modulators.* J Med Chem, 2022. **65**(3): p. 2297-2312.
217. Unwin, N., *Refined Structure of the Nicotinic Acetylcholine Receptor at 4Å Resolution.* J Mol Biol, 2005. **346**(4): p. 967-989.
218. Mnatsakanyan, N. and Jansen, M., *Experimental determination of the vertical alignment between the second and third transmembrane segments of muscle nicotinic acetylcholine receptors.* J Neurochem, 2013. **125**(6): p. 843-854.
219. Unwin, N. and Fujiyoshi, Y., *Gating Movement of Acetylcholine Receptor Caught by Plunge-Freezing.* J Mol Biol, 2012. **422**(5): p. 617-634.
220. Zuber, B. and Unwin, N., *Structure and superorganization of acetylcholine receptor-rapsyn complexes.* Proc Natl Acad Sci USA, 2013. **110**(26): p. 10622-10627.
221. Kaiser, J., Gertzen, C.G.W., Bernauer, T., Höfner, G., Niessen, K.V., Seeger, T., Paintner, F.F., Wanner, K.T., Worek, F., Thiermann, H. and Gohlke, H., *A novel binding site in the nicotinic*

acetylcholine receptor for MB327 can explain its allosteric modulation relevant for organophosphorus-poisoning treatment. Toxicol Lett, 2023. **373**: p. 160-171.

222. Pavelka, A., Sebestova, E., Kozlikova, B., Brezovsky, J., Sochor, J. and Damborsky, J., *CAVER: Algorithms for Analyzing Dynamics of Tunnels in Macromolecules.* IEEE/ACM Trans Comput Biol Bioinform, 2016. **13**(3): p. 505-17.
223. Pan, J., Chen, Q., Willenbring, D., Mowrey, D., Kong, X.P., Cohen, A., Divito, C.B., Xu, Y. and Tang, P., *Structure of the pentameric ligand-gated ion channel GLIC bound with anesthetic ketamine.* Structure, 2012. **20**(9): p. 1463-9.
224. Coates, K.M. and Flood, P., *Ketamine and its preservative, benzethonium chloride, both inhibit human recombinant alpha7 and alpha4beta2 neuronal nicotinic acetylcholine receptors in Xenopus oocytes.* Br J Pharmacol, 2001. **134**(4): p. 871-9.
225. Spurny, R., Billen, B., Howard, R.J., Brams, M., Debaveye, S., Price, K.L., Weston, D.A., Strelkov, S.V., Tytgat, J., Bertrand, S., Bertrand, D., Lummis, S.C.R. and Ulens, C., *Multisite binding of a general anesthetic to the prokaryotic pentameric Erwinia chrysanthemi ligand-gated ion channel (ELIC).* J Biol Chem, 2013. **288**(12): p. 8355-8364.
226. Hurst, R.S., Hajós, M., Raggenbass, M., Wall, T.M., Higdon, N.R., Lawson, J.A., Rutherford-Root, K.L., Berkenpas, M.B., Hoffmann, W.E., Piotrowski, D.W., Groppi, V.E., Allaman, G., Ogier, R., Bertrand, S., Bertrand, D. and Arneric, S.P., *A Novel Positive Allosteric Modulator of the α7 Neuronal Nicotinic Acetylcholine Receptor: In Vitro and In Vivo Characterization.* The Journal of Neuroscience, 2005. **25**(17): p. 4396-4405.
227. Kim, J.J., Gharpure, A., Teng, J., Zhuang, Y., Howard, R.J., Zhu, S., Noviello, C.M., Walsh, R.M., Lindahl, E. and Hibbs, R.E., *Shared structural mechanisms of general anaesthetics and benzodiazepines.* Nature, 2020. **585**(7824): p. 303-308.
228. Masiulis, S., Desai, R., Uchański, T., Serna Martin, I., Laverty, D., Karia, D., Malinauskas, T., Zivanov, J., Pardon, E., Kotecha, A., Steyaert, J., Miller, K.W. and Aricescu, A.R., *GABAA receptor signalling mechanisms revealed by structural pharmacology.* Nature, 2019. **565**(7740): p. 454-459.
229. Belelli, D., Callachan, H., Hill-Venning, C., Peters, J.A. and Lambert, J.J., *Interaction of positive allosteric modulators with human and Drosophila recombinant GABA receptors expressed in Xenopus laevis oocytes.* Br J Pharmacol, 1996. **118**(3): p. 563-76.
230. Krause, R.M., Buisson, B., Bertrand, S., Corringer, P.-J., Galzi, J.-L., Changeux, J.-P. and Bertrand, D., *Ivermectin: A Positive Allosteric Effector of the α7 Neuronal Nicotinic Acetylcholine Receptor.* Mol Pharmacol, 1998. **53**(2): p. 283-294.
231. Jenkinson, D.H., *The antagonism between tubocurarine and substances which depolarize the motor end-plate.* J Physiol, 1960. **152**(2): p. 309-324.
232. Wein, T., Hofner, G., Rappengluck, S., Sichler, S., Niessen, K.V., Seeger, T., Worek, F., Thiermann, H. and Wanner, K.T., *Searching for putative binding sites of the bispyridinium compound MB327 in the nicotinic acetylcholine receptor.* Toxicol Lett, 2018. **293**: p. 184-189.
233. Cushman, D.W., Cheung, H.S., Sabo, E.F. and Ondetti, M.A., *Design of potent competitive inhibitors of angiotensin-converting enzyme. Carboxyalkanoyl and mercaptoalkanoyl amino acids.* Biochemistry, 1977. **16**(25): p. 5484-5491.
234. Ondetti, M.A., Rubin, B. and Cushman, D.W., *Design of Specific Inhibitors of Angiotensin-Converting Enzyme: New Class of Orally Active Antihypertensive Agents.* Science, 1977. **196**(4288): p. 441-444.
235. Lew, W., Chen, X. and Kim, U.C., *Discovery and Development of GS 4104 (oseltamivir) An Orally Active Influenza Neuraminidase Inhibitor.* Curr Med Chem, 2000. **7**(6): p. 663-672.
236. Ghosh, A.K., Dawson, Z.L. and Mitsuya, H., *Darunavir, a conceptually new HIV-1 protease inhibitor for the treatment of drug-resistant HIV.* Biorg Med Chem, 2007. **15**(24): p. 7576-7580.
237. Ghosh, A.K., Ramu Sridhar, P., Kumaragurubaran, N., Koh, Y., Weber, I.T. and Mitsuya, H., *Bis-Tetrahydrofuran: a Privileged Ligand for Darunavir and a New Generation of HIV Protease Inhibitors That Combat Drug Resistance.* ChemMedChem, 2006. **1**(9): p. 939-950.

238. Claude Cohen, N., *Medicine pipeline: Structure-Based Drug Design and the Discovery of Aliskiren (Tekturna®): Perseverance and Creativity to Overcome a R&D Pipeline Challenge‡.* Chem Biol Drug Des, 2007. **70**(6): p. 557-565.
239. Njoroge, F.G., Chen, K.X., Shih, N.-Y. and Piwinski, J.J., *Challenges in Modern Drug Discovery: A Case Study of Boceprevir, an HCV Protease Inhibitor for the Treatment of Hepatitis C Virus Infection.* Acc Chem Res, 2008. **41**(1): p. 50-59.
240. Cui, J.J., Tran-Dubé, M., Shen, H., Nambu, M., Kung, P.-P., Pairish, M., Jia, L., Meng, J., Funk, L., Botrous, I., McTigue, M., Grodsky, N., Ryan, K., Padrique, E., Alton, G., Timofeevski, S., Yamazaki, S., Li, Q., Zou, H., Christensen, J., Mroczkowski, B., Bender, S., Kania, R.S. and Edwards, M.P., *Structure Based Drug Design of Crizotinib (PF-02341066), a Potent and Selective Dual Inhibitor of Mesenchymal–Epithelial Transition Factor (c-MET) Kinase and Anaplastic Lymphoma Kinase (ALK).* J Med Chem, 2011. **54**(18): p. 6342-6363.
241. Harper, S., McCauley, J.A., Rudd, M.T., Ferrara, M., DiFilippo, M., Crescenzi, B., Koch, U., Petrocchi, A., Holloway, M.K., Butcher, J.W., Romano, J.J., Bush, K.J., Gilbert, K.F., McIntyre, C.J., Nguyen, K.T., Nizi, E., Carroll, S.S., Ludmerer, S.W., Burlein, C., DiMuzio, J.M., Graham, D.J., McHale, C.M., Stahlhut, M.W., Olsen, D.B., Monteagudo, E., Cianetti, S., Giuliano, C., Pucci, V., Trainor, N., Fandozzi, C.M., Rowley, M., Coleman, P.J., Vacca, J.P., Summa, V. and Liverton, N.J., *Discovery of MK-5172, a Macrocyclic Hepatitis C Virus NS3/4a Protease Inhibitor.* ACS Med Chem Lett, 2012. **3**(4): p. 332-336.
242. Hecker, S.J., Reddy, K.R., Totrov, M., Hirst, G.C., Lomovskaya, O., Griffith, D.C., King, P., Tsivkovski, R., Sun, D., Sabet, M., Tarazi, Z., Clifton, M.C., Atkins, K., Raymond, A., Potts, K.T., Abendroth, J., Boyer, S.H., Loutit, J.S., Morgan, E.E., Durso, S. and Dudley, M.N., *Discovery of a Cyclic Boronic Acid β-Lactamase Inhibitor (RPX7009) with Utility vs Class A Serine Carbapenemases.* J Med Chem, 2015. **58**(9): p. 3682-3692.
243. Murray, C.W., Newell, D.R. and Angibaud, P., *A successful collaboration between academia, biotech and pharma led to discovery of erdafitinib, a selective FGFR inhibitor recently approved by the FDA.* MedChemComm, 2019. **10**(9): p. 1509-1511.
244. Jumper, J., Evans, R., Pritzel, A., Green, T., Figurnov, M., Ronneberger, O., Tunyasuvunakool, K., Bates, R., Žídek, A., Potapenko, A., Bridgland, A., Meyer, C., Kohl, S.A.A., Ballard, A.J., Cowie, A., Romera-Paredes, B., Nikolov, S., Jain, R., Adler, J., Back, T., Petersen, S., Reiman, D., Clancy, E., Zielinski, M., Steinegger, M., Pacholska, M., Berghammer, T., Bodenstein, S., Silver, D., Vinyals, O., Senior, A.W., Kavukcuoglu, K., Kohli, P. and Hassabis, D., *Highly accurate protein structure prediction with AlphaFold.* Nature, 2021. **596**(7873): p. 583-589.
245. Varadi, M., Anyango, S., Deshpande, M., Nair, S., Natassia, C., Yordanova, G., Yuan, D., Stroe, O., Wood, G., Laydon, A., Žídek, A., Green, T., Tunyasuvunakool, K., Petersen, S., Jumper, J., Clancy, E., Green, R., Vora, A., Lutfi, M., Figurnov, M., Cowie, A., Hobbs, N., Kohli, P., Kleywegt, G., Birney, E., Hassabis, D. and Velankar, S., *AlphaFold Protein Structure Database: massively expanding the structural coverage of protein-sequence space with high-accuracy models.* Nucleic Acids Res, 2021. **50**(D1): p. D439-D444.
246. Li, Z.-l. and Buck, M., *Beyond history and "on a roll": The list of the most well-studied human protein structures and overall trends in the protein data bank.* Protein Sci, 2021. **30**(4): p. 745-760.
247. Hillisch, A., Pineda, L.F. and Hilgenfeld, R., *Utility of homology models in the drug discovery process.* Drug Discovery Today, 2004. **9**(15): p. 659-669.
248. Cavasotto, C.N. and Phatak, S.S., *Homology modeling in drug discovery: current trends and applications.* Drug Discovery Today, 2009. **14**(13): p. 676-683.
249. Rost, B., *Twilight zone of protein sequence alignments.* Protein Eng Des Sel, 1999. **12**(2): p. 85-94.
250. Altschul, S.F., Gish, W., Miller, W., Myers, E.W. and Lipman, D.J., *Basic local alignment search tool.* J Mol Biol, 1990. **215**(3): p. 403-10.
251. Altschul, S.F., Madden, T.L., Schäffer, A.A., Zhang, J., Zhang, Z., Miller, W. and Lipman, D.J., *Gapped BLAST and PSI-BLAST: a new generation of protein database search programs.* Nucleic Acids Res, 1997. **25**(17): p. 3389-402.

252. Lipman, D.J. and Pearson, W.R., *Rapid and Sensitive Protein Similarity Searches.* Science, 1985. **227**(4693): p. 1435-1441.
253. Steinegger, M., Meier, M., Mirdita, M., Vöhringer, H., Haunsberger, S.J. and Söding, J., *HH-suite3 for fast remote homology detection and deep protein annotation.* BMC Bioinformatics, 2019. **20**(1): p. 473.
254. Šali, A. and Blundell, T.L., *Comparative Protein Modelling by Satisfaction of Spatial Restraints.* J Mol Biol, 1993. **234**(3): p. 779-815.
255. *Molecular Operating Environment (MOE)*. 2023, Chemical Computing Group ULC: 910-1010 Sherbrooke St. W., Montreal, QC H3A 2R7, Canada.
256. Mulnaes, D., Porta, N., Clemens, R., Apanasenko, I., Reiners, J., Gremer, L., Neudecker, P., Smits, S.H.J. and Gohlke, H., *TopModel: Template-Based Protein Structure Prediction at Low Sequence Identity Using Top-Down Consensus and Deep Neural Networks.* J Chem Theory Comput, 2020. **16**(3): p. 1953-1967.
257. Pei, J., Kim, B.-H. and Grishin, N.V., *PROMALS3D: a tool for multiple protein sequence and structure alignments.* Nucleic Acids Res, 2008. **36**(7): p. 2295-2300.
258. Schwede, T., Kopp, J., Guex, N. and Peitsch, M.C., *SWISS-MODEL: An automated protein homology-modeling server.* Nucleic Acids Res, 2003. **31**(13): p. 3381-5.
259. Jacobson, M.P., Friesner, R.A., Xiang, Z. and Honig, B., *On the Role of the Crystal Environment in Determining Protein Side-chain Conformations.* J Mol Biol, 2002. **320**(3): p. 597-608.
260. Jacobson, M.P., Pincus, D.L., Rapp, C.S., Day, T.J.F., Honig, B., Shaw, D.E. and Friesner, R.A., *A hierarchical approach to all-atom protein loop prediction.* Proteins: Struct Funct Bioinform, 2004. **55**(2): p. 351-367.
261. Sutcliffe, M.J., Haneef, I., Carney, D. and Blundell, T.L., *Knowledge based modelling of homologous proteins, Part I: Three-dimensional frameworks derived from the simultaneous superposition of multiple structures.* Protein Eng, 1987. **1**(5): p. 377-84.
262. Bates, P.A., Kelley, L.A., MacCallum, R.M. and Sternberg, M.J.E., *Enhancement of protein modeling by human intervention in applying the automatic programs 3D-JIGSAW and 3D-PSSM.* Proteins: Struct Funct Bioinform, 2001. **45**(S5): p. 39-46.
263. Song, Y., DiMaio, F., Wang, R.Y., Kim, D., Miles, C., Brunette, T., Thompson, J. and Baker, D., *High-resolution comparative modeling with RosettaCM.* Structure, 2013. **21**(10): p. 1735-42.
264. Levitt, M., *Accurate modeling of protein conformation by automatic segment matching.* J Mol Biol, 1992. **226**(2): p. 507-33.
265. Webb, B. and Sali, A., *Comparative Protein Structure Modeling Using MODELLER.* Curr Protoc Bioinformatics, 2016. **54**: p. 5.6.1-5.6.37.
266. Fiser, A., Do, R.K. and Sali, A., *Modeling of loops in protein structures.* Protein Sci, 2000. **9**(9): p. 1753-73.
267. Fiser, A., Feig, M., Brooks, C.L., 3rd and Sali, A., *Evolution and physics in comparative protein structure modeling.* Acc Chem Res, 2002. **35**(6): p. 413-21.
268. Sali, A. and Overington, J.P., *Derivation of rules for comparative protein modeling from a database of protein structure alignments.* Protein Sci, 1994. **3**(9): p. 1582-96.
269. Mezei, M., *Chameleon sequences in the PDB.* Protein Eng Des Sel, 1998. **11**(6): p. 411-414.
270. Kabsch, W. and Sander, C., *On the use of sequence homologies to predict protein structure: identical pentapeptides can have completely different conformations.* Proc Natl Acad Sci U S A, 1984. **81**(4): p. 1075-8.
271. Shapovalov, Maxim V. and Dunbrack, Roland L., *A Smoothed Backbone-Dependent Rotamer Library for Proteins Derived from Adaptive Kernel Density Estimates and Regressions.* Structure, 2011. **19**(6): p. 844-858.
272. Scouras, A.D. and Daggett, V., *The dynameomics rotamer library: Amino acid side chain conformations and dynamics from comprehensive molecular dynamics simulations in water.* Protein Sci, 2011. **20**(2): p. 341-352.
273. Mirdita, M., Schütze, K., Moriwaki, Y., Heo, L., Ovchinnikov, S. and Steinegger, M., *ColabFold: making protein folding accessible to all.* Nat Methods, 2022. **19**(6): p. 679-682.

274. Evans, R., O'Neill, M., Pritzel, A., Antropova, N., Senior, A., Green, T., Žídek, A., Bates, R., Blackwell, S., Yim, J., Ronneberger, O., Bodenstein, S., Zielinski, M., Bridgland, A., Potapenko, A., Cowie, A., Tunyasuvunakool, K., Jain, R., Clancy, E., Kohli, P., Jumper, J. and Hassabis, D., *Protein complex prediction with AlphaFold-Multimer. 2022,* bioRxiv: https://doi.org/10.1101/2021.10.04.463034.
275. Abramson, J., Adler, J., Dunger, J., Evans, R., Green, T., Pritzel, A., Ronneberger, O., Willmore, L., Ballard, A.J., Bambrick, J., Bodenstein, S.W., Evans, D.A., Hung, C.-C., O'Neill, M., Reiman, D., Tunyasuvunakool, K., Wu, Z., Žemgulytė, A., Arvaniti, E., Beattie, C., Bertolli, O., Bridgland, A., Cherepanov, A., Congreve, M., Cowen-Rivers, A.I., Cowie, A., Figurnov, M., Fuchs, F.B., Gladman, H., Jain, R., Khan, Y.A., Low, C.M.R., Perlin, K., Potapenko, A., Savy, P., Singh, S., Stecula, A., Thillaisundaram, A., Tong, C., Yakneen, S., Zhong, E.D., Zielinski, M., Žídek, A., Bapst, V., Kohli, P., Jaderberg, M., Hassabis, D. and Jumper, J.M., *Accurate structure prediction of biomolecular interactions with AlphaFold 3.* Nature, 2024.
276. Halgren, T., *New Method for Fast and Accurate Binding-site Identification and Analysis.* Chem Biol Drug Des, 2007. **69**(2): p. 146-148.
277. Halgren, T.A., *Identifying and Characterizing Binding Sites and Assessing Druggability.* J Chem Inf Model, 2009. **49**(2): p. 377-389.
278. *Maestro*. Schrödinger, LLC: New York, NY.
279. *SiteMap*. Schrödinger, LLC: New York, NY.
280. Volkamer, A., Griewel, A., Grombacher, T. and Rarey, M., *Analyzing the Topology of Active Sites: On the Prediction of Pockets and Subpockets.* J Chem Inf Model, 2010. **50**(11): p. 2041-2052.
281. Volkamer, A., Kuhn, D., Grombacher, T., Rippmann, F. and Rarey, M., *Combining Global and Local Measures for Structure-Based Druggability Predictions.* J Chem Inf Model, 2012. **52**(2): p. 360-372.
282. Schöning-Stierand, K., Diedrich, K., Ehrt, C., Flachsenberg, F., Graef, J., Sieg, J., Penner, P., Poppinga, M., Ungethüm, A. and Rarey, M., *ProteinsPlus: a comprehensive collection of web-based molecular modeling tools.* Nucleic Acids Res, 2022. **50**(W1): p. W611-W615.
283. Hedderich, J.B., Persechino, M., Becker, K., Heydenreich, F.M., Gutermuth, T., Bouvier, M., Bünemann, M. and Kolb, P., *The pocketome of G-protein-coupled receptors reveals previously untargeted allosteric sites.* Nat Commun, 2022. **13**(1): p. 2567.
284. Gertzen, C.G., Spomer, L., Smits, S.H., Häussinger, D., Keitel, V. and Gohlke, H., *Mutational mapping of the transmembrane binding site of the G-protein coupled receptor TGR5 and binding mode prediction of TGR5 agonists.* Eur J Med Chem, 2015. **104**: p. 57-72.
285. Wang, J., Morin, P., Wang, W. and Kollman, P.A., *Use of MM-PBSA in Reproducing the Binding Free Energies to HIV-1 RT of TIBO Derivatives and Predicting the Binding Mode to HIV-1 RT of Efavirenz by Docking and MM-PBSA.* J Am Chem Soc, 2001. **123**(22): p. 5221-5230.
286. Moro, S., Guo, D., Camaioni, E., Boyer, J.L., Harden, T.K. and Jacobson, K.A., *Human P2Y1 Receptor: Molecular Modeling and Site-Directed Mutagenesis as Tools To Identify Agonist and Antagonist Recognition Sites.* J Med Chem, 1998. **41**(9): p. 1456-1466.
287. de Graaf, C., Pospisil, P., Pos, W., Folkers, G. and Vermeulen, N.P., *Binding mode prediction of cytochrome p450 and thymidine kinase protein-ligand complexes by consideration of water and rescoring in automated docking.* J Med Chem, 2005. **48**(7): p. 2308-18.
288. Ragno, R., Simeoni, S., Castellano, S., Vicidomini, C., Mai, A., Caroli, A., Tramontano, A., Bonaccini, C., Trojer, P., Bauer, I., Brosch, G. and Sbardella, G., *Small Molecule Inhibitors of Histone Arginine Methyltransferases: Homology Modeling, Molecular Docking, Binding Mode Analysis, and Biological Evaluations.* J Med Chem, 2007. **50**(6): p. 1241-1253.
289. Porta, N., Zaschke-Kriesche, J., Frieg, B., Gopalswamy, M., Zivkovic, A., Etzkorn, M., Stark, H., Smits, S.H.J. and Gohlke, H., *Small-molecule inhibitors of nisin resistance protein NSR from the human pathogen Streptococcus agalactiae.* Bioorg Med Chem, 2019. **27**(20): p. 115079.

290. Lim, V.J.Y., Proudman, R.G.W., Monteleone, S., Kolb, P. and Baker, J.G., *The Isoleucine at Position 118 in Transmembrane 2 Is Responsible for the Selectivity of Xamoterol, Nebivolol, and ICI89406 for the Human β1-Adrenoceptor.* Mol Pharmacol, 2023. **103**(2): p. 89-99.
291. Ishikawa, Y. and Fujii, S., *Binding mode prediction and inhibitor design of anti-influenza virus diketo acids targeting metalloenzyme RNA polymerase by molecular docking.* Bioinformation, 2011. **6**(6): p. 221-5.
292. Westermaier, Y., Ruiz-Carmona, S., Theret, I., Perron-Sierra, F., Poissonnet, G., Dacquet, C., Boutin, J.A., Ducrot, P. and Barril, X., *Binding mode prediction and MD/MMPBSA-based free energy ranking for agonists of REV-ERBα/NCoR.* J Comput-Aided Mol Des, 2017. **31**(8): p. 755-775.
293. Rinne, A., Mobarec, J.C., Mahaut-Smith, M., Kolb, P. and Bünemann, M., *The mode of agonist binding to a G protein–coupled receptor switches the effect that voltage changes have on signaling.* Sci Signal, 2015. **8**(401): p. ra110-ra110.
294. Coleman, R.G., Carchia, M., Sterling, T., Irwin, J.J. and Shoichet, B.K., *Ligand pose and orientational sampling in molecular docking.* PLoS One, 2013. **8**(10): p. e75992.
295. Morris, G.M., Goodsell, D.S., Halliday, R.S., Huey, R., Hart, W.E., Belew, R.K. and Olson, A.J., *Automated docking using a Lamarckian genetic algorithm and an empirical binding free energy function.* J Comput Chem, 1998. **19**(14): p. 1639-1662.
296. Trott, O. and Olson, A.J., *AutoDock Vina: Improving the speed and accuracy of docking with a new scoring function, efficient optimization, and multithreading.* J Comput Chem, 2010. **31**(2): p. 455-461.
297. Rarey, M., Kramer, B., Lengauer, T. and Klebe, G., *A Fast Flexible Docking Method using an Incremental Construction Algorithm.* J Mol Biol, 1996. **261**(3): p. 470-489.
298. Halgren, T.A., Murphy, R.B., Friesner, R.A., Beard, H.S., Frye, L.L., Pollard, W.T. and Banks, J.L., *Glide: A New Approach for Rapid, Accurate Docking and Scoring. 2. Enrichment Factors in Database Screening.* J Med Chem, 2004. **47**(7): p. 1750-1759.
299. Goodsell, D.S. and Olson, A.J., *Automated docking of substrates to proteins by simulated annealing.* Proteins: Struct Funct Bioinform, 1990. **8**(3): p. 195-202.
300. McGann, M., *FRED Pose Prediction and Virtual Screening Accuracy.* J Chem Inf Model, 2011. **51**(3): p. 578-596.
301. Jones, G., Willett, P., Glen, R.C., Leach, A.R. and Taylor, R., *Development and validation of a genetic algorithm for flexible docking11Edited by F. E. Cohen.* J Mol Biol, 1997. **267**(3): p. 727-748.
302. McGann, M., *FRED and HYBRID docking performance on standardized datasets.* J Comput-Aided Mol Des, 2012. **26**(8): p. 897-906.
303. Morris, G.M., Huey, R., Lindstrom, W., Sanner, M.F., Belew, R.K., Goodsell, D.S. and Olson, A.J., *AutoDock4 and AutoDockTools4: Automated docking with selective receptor flexibility.* J Comput Chem, 2009. **30**(16): p. 2785-91.
304. Meng, E.C., Shoichet, B.K. and Kuntz, I.D., *Automated docking with grid-based energy evaluation.* J Comput Chem, 1992. **13**(4): p. 505-524.
305. Jain, A.N., *Scoring noncovalent protein-ligand interactions: A continuous differentiable function tuned to compute binding affinities.* J Comput-Aided Mol Des, 1996. **10**(5): p. 427-440.
306. Krammer, A., Kirchhoff, P.D., Jiang, X., Venkatachalam, C.M. and Waldman, M., *LigScore: a novel scoring function for predicting binding affinities.* J Mol Graph Model, 2005. **23**(5): p. 395-407.
307. Böhm, H.-J., *The development of a simple empirical scoring function to estimate the binding constant for a protein-ligand complex of known three-dimensional structure.* J Comput-Aided Mol Des, 1994. **8**(3): p. 243-256.
308. Eldridge, M.D., Murray, C.W., Auton, T.R., Paolini, G.V. and Mee, R.P., *Empirical scoring functions: I. The development of a fast empirical scoring function to estimate the binding affinity of ligands in receptor complexes.* J Comput-Aided Mol Des, 1997. **11**(5): p. 425-445.

309. Baxter, C.A., Murray, C.W., Clark, D.E., Westhead, D.R. and Eldridge, M.D., *Flexible docking using tabu search and an empirical estimate of binding affinity.* Proteins: Struct Funct Bioinform, 1998. **33**(3): p. 367-382.
310. Korb, O., Stützle, T. and Exner, T.E., *Empirical Scoring Functions for Advanced Protein−Ligand Docking with PLANTS.* J Chem Inf Model, 2009. **49**(1): p. 84-96.
311. Wang, R., Lai, L. and Wang, S., *Further development and validation of empirical scoring functions for structure-based binding affinity prediction.* J Comput-Aided Mol Des, 2002. **16**(1): p. 11-26.
312. Muegge, I., *PMF Scoring Revisited.* J Med Chem, 2006. **49**(20): p. 5895-5902.
313. Muegge, I. and Martin, Y.C., *A General and Fast Scoring Function for Protein−Ligand Interactions: A Simplified Potential Approach.* J Med Chem, 1999. **42**(5): p. 791-804.
314. Gohlke, H., Hendlich, M. and Klebe, G., *Predicting binding modes, binding affinities andhot spots' for protein-ligand complexes using a knowledge-based scoring function.* Perspect Drug Discov Des, 2000. **20**: p. 115-144.
315. Gohlke, H., Hendlich, M. and Klebe, G., *Knowledge-based scoring function to predict protein-ligand interactions.* J Mol Biol, 2000. **295**(2): p. 337-356.
316. Dittrich, J., Schmidt, D., Pfleger, C. and Gohlke, H., *Converging a knowledge-based scoring function: DrugScore2018.* J Chem Inf Model, 2018. **59**(1): p. 509-521.
317. Cross, J.B., Thompson, D.C., Rai, B.K., Baber, J.C., Fan, K.Y., Hu, Y. and Humblet, C., *Comparison of Several Molecular Docking Programs: Pose Prediction and Virtual Screening Accuracy.* J Chem Inf Model, 2009. **49**(6): p. 1455-1474.
318. Li, Y., Han, L., Liu, Z. and Wang, R., *Comparative Assessment of Scoring Functions on an Updated Benchmark: 2. Evaluation Methods and General Results.* J Chem Inf Model, 2014. **54**(6): p. 1717-1736.
319. Ferrara, P., Gohlke, H., Price, D.J., Klebe, G. and Brooks, C.L., 3rd, *Assessing scoring functions for protein-ligand interactions.* J Med Chem, 2004. **47**(12): p. 3032-47.
320. Wang, Z., Sun, H., Yao, X., Li, D., Xu, L., Li, Y., Tian, S. and Hou, T., *Comprehensive evaluation of ten docking programs on a diverse set of protein-ligand complexes: the prediction accuracy of sampling power and scoring power.* Phys Chem Chem Phys, 2016. **18**(18): p. 12964-75.
321. Su, M., Yang, Q., Du, Y., Feng, G., Liu, Z., Li, Y. and Wang, R., *Comparative Assessment of Scoring Functions: The CASF-2016 Update.* J Chem Inf Model, 2019. **59**(2): p. 895-913.
322. Bissantz, C., Folkers, G. and Rognan, D., *Protein-Based Virtual Screening of Chemical Databases. 1. Evaluation of Different Docking/Scoring Combinations.* J Med Chem, 2000. **43**(25): p. 4759-4767.
323. Stahl, M. and Rarey, M., *Detailed Analysis of Scoring Functions for Virtual Screening.* J Med Chem, 2001. **44**(7): p. 1035-1042.
324. Kontoyianni, M., McClellan, L.M. and Sokol, G.S., *Evaluation of Docking Performance: Comparative Data on Docking Algorithms.* J Med Chem, 2004. **47**(3): p. 558-565.
325. Cummings, M.D., DesJarlais, R.L., Gibbs, A.C., Mohan, V. and Jaeger, E.P., *Comparison of Automated Docking Programs as Virtual Screening Tools.* J Med Chem, 2005. **48**(4): p. 962-976.
326. Warren, G.L., Andrews, C.W., Capelli, A.-M., Clarke, B., LaLonde, J., Lambert, M.H., Lindvall, M., Nevins, N., Semus, S.F., Senger, S., Tedesco, G., Wall, I.D., Woolven, J.M., Peishoff, C.E. and Head, M.S., *A Critical Assessment of Docking Programs and Scoring Functions.* J Med Chem, 2006. **49**(20): p. 5912-5931.
327. Plewczynski, D., Łaźniewski, M., Augustyniak, R. and Ginalski, K., *Can we trust docking results? Evaluation of seven commonly used programs on PDBbind database.* J Comput Chem, 2011. **32**(4): p. 742-755.
328. Iorga, B., Herlem, D., Barré, E. and Guillou, C., *Acetylcholine nicotinic receptors: finding the putative binding site of allosteric modulators using the "blind docking" approach.* J Mol Model, 2006. **12**(3): p. 366-372.
329. Hetényi, C. and van der Spoel, D., *Blind docking of drug-sized compounds to proteins with up to a thousand residues.* FEBS Lett, 2006. **580**(5): p. 1447-1450.

330. Hetényi, C. and van der Spoel, D., *Efficient docking of peptides to proteins without prior knowledge of the binding site.* Protein Sci, 2002. **11**(7): p. 1729-1737.
331. Grosdidier, A., Zoete, V. and Michielin, O., *Blind docking of 260 protein–ligand complexes with EADock 2.0.* J Comput Chem, 2009. **30**(13): p. 2021-2030.
332. Sierra-Campos, E., Valdez-Solana, M., Avitia-Domínguez, C., Campos-Almazán, M., Flores-Molina, I., García-Arenas, G. and Téllez-Valencia, A., *Effects of Moringa oleifera Leaf Extract on Diabetes-Induced Alterations in Paraoxonase 1 and Catalase in Rats Analyzed through Progress Kinetic and Blind Docking.* Antioxidants, 2020. **9**(9): p. 840.
333. Liang, J., Karagiannis, C., Pitsillou, E., Darmawan, K.K., Ng, K., Hung, A. and Karagiannis, T.C., *Site mapping and small molecule blind docking reveal a possible target site on the SARS-CoV-2 main protease dimer interface.* Comput Biol Chem, 2020. **89**: p. 107372.
334. Österberg, F. and Åqvist, J., *Exploring blocker binding to a homology model of the open hERG K+ channel using docking and molecular dynamics methods.* FEBS Lett, 2005. **579**(13): p. 2939-2944.
335. Zhou, M., Luo, H., Li, R. and Ding, Z., *Exploring the binding mode of HIV-1 Vif inhibitors by blind docking, molecular dynamics and MM/GBSA.* RSC Adv, 2013. **3**(44): p. 22532-22543.
336. Pineda, O., Farràs, J., Maccari, L., Manetti, F., Botta, M. and Vilarrasa, J., *Computational comparison of microtubule-stabilising agents laulimalide and peloruside with taxol and colchicine.* Bioorg Med Chem Lett, 2004. **14**(19): p. 4825-4829.
337. Czech, L., Gertzen, C., Smits, S.H.J. and Bremer, E., *Guilty by association: Importers, exporters and MscS-type mechanosensitive channels encoded in biosynthetic gene clusters for the stress-protectant ectoine.* Environ Microbiol, 2022. **24**(11): p. 5306-5331.
338. Luttmann, E., Ludwig, J., Höffle-Maas, A., Samochocki, M., Maelicke, A. and Fels, G., *Structural Model for the Binding Sites of Allosterically Potentiating Ligands on Nicotinic Acetylcholine Receptors.* ChemMedChem, 2009. **4**(11): p. 1874-1882.
339. Pavlovicz, R.E., Henderson, B.J., Bonnell, A.B., Boyd, R.T., McKay, D.B. and Li, C., *Identification of a Negative Allosteric Site on Human α4β2 and α3β4 Neuronal Nicotinic Acetylcholine Receptors.* PLoS One, 2011. **6**(9): p. e24949.
340. Liu, Y., Grimm, M., Dai, W.-t., Hou, M.-c., Xiao, Z.-X. and Cao, Y., *CB-Dock: a web server for cavity detection-guided protein–ligand blind docking.* Acta Pharmacol Sin, 2020. **41**(1): p. 138-144.
341. Liu, Y., Yang, X., Gan, J., Chen, S., Xiao, Z.-X. and Cao, Y., *CB-Dock2: improved protein–ligand blind docking by integrating cavity detection, docking and homologous template fitting.* Nucleic Acids Res, 2022. **50**(W1): p. W159-W164.
342. Jofily, P., Pascutti, P.G. and Torres, P.H.M., *Improving Blind Docking in DOCK6 through an Automated Preliminary Fragment Probing Strategy.* Molecules, 2021. **26**(5): p. 1224.
343. Grasso, G., Di Gregorio, A., Mavkov, B., Piga, D., Labate, G.F.D.U., Danani, A. and Deriu, M.A., *Fragmented blind docking: a novel protein–ligand binding prediction protocol.* J Biomol Struct Dyn, 2022. **40**(24): p. 13472-13481.
344. Ghersi, D. and Sanchez, R., *Improving accuracy and efficiency of blind protein-ligand docking by focusing on predicted binding sites.* Proteins: Struct Funct Bioinform, 2009. **74**(2): p. 417-424.
345. Hassan, N.M., Alhossary, A.A., Mu, Y. and Kwoh, C.-K., *Protein-Ligand Blind Docking Using QuickVina-W With Inter-Process Spatio-Temporal Integration.* Sci Rep, 2017. **7**(1): p. 15451.
346. Saadi, H., Nouali Taboudjemat, N., Rahmoun, A., imbernón, B., Pérez-Sánchez, H. and Cecilia, J.M., *Efficient GPU-based parallelization of solvation calculation for the blind docking problem.* J Supercomput, 2020. **76**(3): p. 1980-1998.
347. Che, X., Chai, S., Zhang, Z. and Zhang, L., *Prediction of ligand binding sites using improved blind docking method with a Machine Learning-Based scoring function.* Chem Eng Sci, 2022. **261**: p. 117962.
348. Wu, Q., Peng, Z., Zhang, Y. and Yang, J., *COACH-D: improved protein–ligand binding sites prediction with refined ligand-binding poses through molecular docking.* Nucleic Acids Res, 2018. **46**(W1): p. W438-W442.

349. Gohlke, H., Hergert, U., Meyer, T., Mulnaes, D., Grieshaber, M.K., Smits, S.H.J. and Schmitt, L., *Binding Region of Alanopine Dehydrogenase Predicted by Unbiased Molecular Dynamics Simulations of Ligand Diffusion.* J Chem Inf Model, 2013. **53**(10): p. 2493-2498.
350. Dror, R.O., Pan, A.C., Arlow, D.H., Borhani, D.W., Maragakis, P., Shan, Y., Xu, H. and Shaw, D.E., *Pathway and mechanism of drug binding to G-protein-coupled receptors.* Proc Natl Acad Sci USA, 2011. **108**(32): p. 13118-13123.
351. Giorgino, T., Buch, I. and De Fabritiis, G., *Visualizing the Induced Binding of SH2-Phosphopeptide.* J Chem Theory Comput, 2012. **8**(4): p. 1171-1175.
352. Buch, I., Giorgino, T. and De Fabritiis, G., *Complete reconstruction of an enzyme-inhibitor binding process by molecular dynamics simulations.* Proc Natl Acad Sci USA, 2011. **108**(25): p. 10184-10189.
353. Kruse, A.C., Hu, J., Pan, A.C., Arlow, D.H., Rosenbaum, D.M., Rosemond, E., Green, H.F., Liu, T., Chae, P.S., Dror, R.O., Shaw, D.E., Weis, W.I., Wess, J. and Kobilka, B.K., *Structure and dynamics of the M3 muscarinic acetylcholine receptor.* Nature, 2012. **482**(7386): p. 552-556.
354. Shan, Y., Kim, E.T., Eastwood, M.P., Dror, R.O., Seeliger, M.A. and Shaw, D.E., *How Does a Drug Molecule Find Its Target Binding Site?* J Am Chem Soc, 2011. **133**(24): p. 9181-9183.
355. Bhatia, S., Diedrich, D., Frieg, B., Ahlert, H., Stein, S., Bopp, B., Lang, F., Zang, T., Kröger, T., Ernst, T., Kögler, G., Krieg, A., Lüdeke, S., Kunkel, H., Rodrigues Moita, A.J., Kassack, M.U., Marquardt, V., Opitz, F.V., Oldenburg, M., Remke, M., Babor, F., Grez, M., Hochhaus, A., Borkhardt, A., Groth, G., Nagel-Steger, L., Jose, J., Kurz, T., Gohlke, H., Hansen, F.K. and Hauer, J., *Targeting HSP90 dimerization via the C terminus is effective in imatinib-resistant CML and lacks the heat shock response.* Blood, 2018. **132**(3): p. 307-320.
356. Schott-Verdugo, S., Müller, L., Classen, E., Gohlke, H. and Groth, G., *Structural Model of the ETR1 Ethylene Receptor Transmembrane Sensor Domain.* Sci Rep, 2019. **9**(1): p. 8869.
357. Frieg, B., Gremer, L., Heise, H., Willbold, D. and Gohlke, H., *Binding modes of thioflavin T and Congo red to the fibril structure of amyloid-β(1–42).* Chem Commun, 2020. **56**(55): p. 7589-7592.
358. Gopalswamy, M., Kroeger, T., Bickel, D., Frieg, B., Akter, S., Schott-Verdugo, S., Viegas, A., Pauly, T., Mayer, M., Przibilla, J., Reiners, J., Nagel-Steger, L., Smits, S.H.J., Groth, G., Etzkorn, M. and Gohlke, H., *Biophysical and pharmacokinetic characterization of a small-molecule inhibitor of RUNX1/ETO tetramerization with anti-leukemic effects.* Sci Rep, 2022. **12**(1): p. 14158.
359. Bhatia, S., Spanier, L., Bickel, D., Dienstbier, N., Woloschin, V., Vogt, M., Pols, H., Lungerich, B., Reiners, J., Aghaallaei, N., Diedrich, D., Frieg, B., Schliehe-Diecks, J., Bopp, B., Lang, F., Gopalswamy, M., Loschwitz, J., Bajohgli, B., Skokowa, J., Borkhardt, A., Hauer, J., Hansen, F.K., Smits, S.H.J., Jose, J., Gohlke, H. and Kurz, T., *Development of a First-in-Class Small-Molecule Inhibitor of the C-Terminal Hsp90 Dimerization.* ACS Cent Sci, 2022. **8**(5): p. 636-655.
360. Bello, M. and Rodríguez-Fonseca, R.A., *Complexation of methotrexate via ligand diffusion molecular dynamic simulations under neutral, basic, and acidic conditions.* J Mol Graph Model, 2019. **93**: p. 107443.
361. Hopkins, C.W., Le Grand, S., Walker, R.C. and Roitberg, A.E., *Long-Time-Step Molecular Dynamics through Hydrogen Mass Repartitioning.* J Chem Theory Comput, 2015. **11**(4): p. 1864-74.
362. Alberty, R.A. and Hammes, G.G., *Application of the Theory of Diffusion-controlled Reactions to Enzyme Kinetics.* J Phys Chem, 1958. **62**(2): p. 154-159.
363. Daviter, T., Johnson, C.M., McLaughlin, S., H. and Williams, M.A., *Protein-Ligand Interactions - Methods and Applications*. 3 ed. Methods Mol Biol. 2021, New York, NY: Humana. 492.
364. Georgi, V., Schiele, F., Berger, B.-T., Steffen, A., Marin Zapata, P.A., Briem, H., Menz, S., Preusse, C., Vasta, J.D., Robers, M.B., Brands, M., Knapp, S. and Fernández-Montalván, A., *Binding Kinetics Survey of the Drugged Kinome.* J Am Chem Soc, 2018. **140**(46): p. 15774-15782.
365. Talibov, V.O., Linkuvienė, V., Matulis, D. and Danielson, U.H., *Kinetically Selective Inhibitors of Human Carbonic Anhydrase Isozymes I, II, VII, IX, XII, and XIII.* J Med Chem, 2016. **59**(5): p. 2083-2093.

366. Yu, Z., van Veldhoven, J.P.D., Louvel, J., 't Hart, I.M.E., Rook, M.B., van der Heyden, M.A.G., Heitman, L.H. and Ijzerman, A.P., *Structure–Affinity Relationships (SARs) and Structure–Kinetics Relationships (SKRs) of Kv11.1 Blockers.* J Med Chem, 2015. **58**(15): p. 5916-5929.
367. Willemsen-Seegers, N., Uitdehaag, J.C.M., Prinsen, M.B.W., de Vetter, J.R.F., de Man, J., Sawa, M., Kawase, Y., Buijsman, R.C. and Zaman, G.J.R., *Compound Selectivity and Target Residence Time of Kinase Inhibitors Studied with Surface Plasmon Resonance.* J Mol Biol, 2017. **429**(4): p. 574-586.
368. Cramer, J., Krimmer, S.G., Fridh, V., Wulsdorf, T., Karlsson, R., Heine, A. and Klebe, G., *Elucidating the Origin of Long Residence Time Binding for Inhibitors of the Metalloprotease Thermolysin.* ACS Chem Biol, 2017. **12**(1): p. 225-233.
369. Heroven, C., Georgi, V., Ganotra, G.K., Brennan, P., Wolfreys, F., Wade, R.C., Fernández-Montalván, A.E., Chaikuad, A. and Knapp, S., *Halogen–Aromatic π Interactions Modulate Inhibitor Residence Times.* Angew Chem Int Ed, 2018. **57**(24): p. 7220-7224.
370. Regan, J., Pargellis, C.A., Cirillo, P.F., Gilmore, T., Hickey, E.R., Peet, G.W., Proto, A., Swinamer, A. and Moss, N., *The kinetics of binding to p38MAP kinase by analogues of BIRB 796.* Bioorg Med Chem Lett, 2003. **13**(18): p. 3101-3104.
371. Yoshikawa, M., Saitoh, M., Katoh, T., Seki, T., Bigi, S.V., Shimizu, Y., Ishii, T., Okai, T., Kuno, M., Hattori, H., Watanabe, E., Saikatendu, K.S., Zou, H., Nakakariya, M., Tatamiya, T., Nakada, Y. and Yogo, T., *Discovery of 7-Oxo-2,4,5,7-tetrahydro-6H-pyrazolo[3,4-c]pyridine Derivatives as Potent, Orally Available, and Brain-Penetrating Receptor Interacting Protein 1 (RIP1) Kinase Inhibitors: Analysis of Structure–Kinetic Relationships.* J Med Chem, 2018. **61**(6): p. 2384-2409.
372. Gaspari, R., Rechlin, C., Heine, A., Bottegoni, G., Rocchia, W., Schwarz, D., Bomke, J., Gerber, H.-D., Klebe, G. and Cavalli, A., *Kinetic and Structural Insights into the Mechanism of Binding of Sulfonamides to Human Carbonic Anhydrase by Computational and Experimental Studies.* J Med Chem, 2016. **59**(9): p. 4245-4256.
373. Schuetz, D.A., Richter, L., Amaral, M., Grandits, M., Grädler, U., Musil, D., Buchstaller, H.-P., Eggenweiler, H.-M., Frech, M. and Ecker, G.F., *Ligand Desolvation Steers On-Rate and Impacts Drug Residence Time of Heat Shock Protein 90 (Hsp90) Inhibitors.* J Med Chem, 2018. **61**(10): p. 4397-4411.
374. Sykes, D.A. and Charlton, S.J., *Slow receptor dissociation is not a key factor in the duration of action of inhaled long-acting β2-adrenoceptor agonists.* Br J Pharmacol, 2012. **165**(8): p. 2672-83.
375. Sykes, D.A., Moore, H., Stott, L., Holliday, N., Javitch, J.A., Lane, J.R. and Charlton, S.J., *Extrapyramidal side effects of antipsychotics are linked to their association kinetics at dopamine D2 receptors.* Nat Commun, 2017. **8**(1): p. 763.
376. Doornbos, M.L.J., Cid, J.M., Haubrich, J., Nunes, A., van de Sande, J.W., Vermond, S.C., Mulder-Krieger, T., Trabanco, A.A., Ahnaou, A., Drinkenburg, W.H., Lavreysen, H., Heitman, L.H., Ijzerman, A.P. and Tresadern, G., *Discovery and Kinetic Profiling of 7-Aryl-1,2,4-triazolo[4,3-a]pyridines: Positive Allosteric Modulators of the Metabotropic Glutamate Receptor 2.* J Med Chem, 2017. **60**(15): p. 6704-6720.
377. Bosma, R., Witt, G., Vaas, L.A.I., Josimovic, I., Gribbon, P., Vischer, H.F., Gul, S. and Leurs, R., *The Target Residence Time of Antihistamines Determines Their Antagonism of the G Protein-Coupled Histamine H1 Receptor.* Front Pharmacol, 2017, **8**: p. 667.
378. Gillard, M., Perren, C.V.D., Moguilevsky, N., Massingham, R. and Chatelain, P., *Binding Characteristics of Cetirizine and Levocetirizine to Human H(1) Histamine Receptors: Contribution of Lys(191)and Thr(194).* Mol Pharmacol, 2002. **61**(2): p. 391-399.
379. Tautermann, C.S., Kiechle, T., Seeliger, D., Diehl, S., Wex, E., Banholzer, R., Gantner, F., Pieper, M.P. and Casarosa, P., *Molecular Basis for the Long Duration of Action and Kinetic Selectivity of Tiotropium for the Muscarinic M3 Receptor.* J Med Chem, 2013. **56**(21): p. 8746-8756.
380. Wittmann, H.-J., Seifert, R. and Strasser, A., *Influence of the N-terminus and the E2-loop onto the binding kinetics of the antagonist mepyramine and the partial agonist phenoprodifen to H1R.* Biochem Pharmacol, 2011. **82**(12): p. 1910-1918.

381. Fleck, B.A., Hoare, S.R.J., Pick, R.R., Bradbury, M.J. and Grigoriadis, D.E., *Binding Kinetics Redefine the Antagonist Pharmacology of the Corticotropin-Releasing Factor Type 1 Receptor.* J Pharmacol Exp Ther, 2012. **341**(2): p. 518-531.
382. Winquist, J., Geschwindner, S., Xue, Y., Gustavsson, L., Musil, D., Deinum, J. and Danielson, U.H., *Identification of Structural–Kinetic and Structural–Thermodynamic Relationships for Thrombin Inhibitors.* Biochemistry, 2013. **52**(4): p. 613-626.
383. Benkherouf, A.Y., Taina, K.-R., Meera, P., Aalto, A.J., Li, X.-G., Soini, S.L., Wallner, M. and Uusi-Oukari, M., *Extrasynaptic δ-GABAA receptors are high-affinity muscimol receptors.* J Neurochem, 2019. **149**(1): p. 41-53.
384. Wenningmann, I. and Dilger, J.P., *The Kinetics of Inhibition of Nicotinic Acetylcholine Receptors by (+)-Tubocurarine and Pancuronium.* Mol Pharmacol, 2001. **60**(4): p. 790-796.
385. Schreiter, C., Gjoni, M., Hovius, R., Martinez, K.L., Segura, J.-M. and Vogel, H., *Reversible Sequential-Binding Probe Receptor–Ligand Interactions in Single Cells.* ChemBioChem, 2005. **6**(12): p. 2187-2194.
386. Tzitzoglaki, C., McGuire, K., Lagarias, P., Konstantinidi, A., Hoffmann, A., Fokina, N.A., Ma, C., Papanastasiou, I.P., Schreiner, P.R., Vázquez, S., Schmidtke, M., Wang, J., Busath, D.D. and Kolocouris, A., *Chemical Probes for Blocking of Influenza A M2 Wild-type and S31N Channels.* ACS Chem Biol, 2020. **15**(9): p. 2331-2337.
387. Knapp, B., Ospina, L. and Deane, C.M., *Avoiding False Positive Conclusions in Molecular Simulation: The Importance of Replicas.* J Chem Theory Comput, 2018. **14**(12): p. 6127-6138.
388. Pfleger, C., Rathi, P.C., Klein, D.L., Radestock, S. and Gohlke, H., *Constraint Network Analysis (CNA): a Python software package for efficiently linking biomacromolecular structure, flexibility, (thermo-)stability, and function.* J Chem Inf Model, 2013. **53**(4): p. 1007-15.
389. Pfleger, C., Radestock, S., Schmidt, E. and Gohlke, H., *Global and local indices for characterizing biomolecular flexibility and rigidity.* J Comput Chem, 2013. **34**(3): p. 220-233.
390. Pfleger, C., Minges, A., Boehm, M., McClendon, C.L., Torella, R. and Gohlke, H., *Ensemble- and Rigidity Theory-Based Perturbation Approach To Analyze Dynamic Allostery.* J Chem Theory Comput, 2017. **13**(12): p. 6343-6357.
391. Hansson, T., Marelius, J. and Åqvist, J., *Ligand binding affinity prediction by linear interaction energy methods.* J Comput-Aided Mol Des, 1998. **12**(1): p. 27-35.
392. Kearsley, S.K. and Smith, G.M., *An alternative method for the alignment of molecular structures: Maximizing electrostatic and steric overlap.* Tetrahedron Comput Methodol, 1990. **3**(6, Part C): p. 615-633.
393. Nussinov, R. and Wolfson, H.J., *Efficient detection of three-dimensional structural motifs in biological macromolecules by computer vision techniques.* Proc Natl Acad Sci USA, 1991. **88**(23): p. 10495-10499.
394. Carbó, R., Leyda, L. and Arnau, M., *How similar is a molecule to another? An electron density measure of similarity between two molecular structures.* Int J Quantum Chem, 1980. **17**(6): p. 1185-1189.
395. Redington, P.K., *MOLFIT: A computer program for molecular superposition.* Comput Chem, 1992. **16**(3): p. 217-222.
396. Rarey, M. and Stahl, M., *Similarity searching in large combinatorial chemistry spaces.* J Comput-Aided Mol Des, 2001. **15**(6): p. 497-520.
397. Patterson, D.E., Cramer, R.D., Ferguson, A.M., Clark, R.D. and Weinberger, L.E., *Neighborhood Behavior: A Useful Concept for Validation of "Molecular Diversity" Descriptors.* J Med Chem, 1996. **39**(16): p. 3049-3059.
398. Rogers, D. and Hahn, M., *Extended-Connectivity Fingerprints.* J Chem Inf Model, 2010. **50**(5): p. 742-754.
399. Makara, G.M., *Measuring Molecular Similarity and Diversity: Total Pharmacophore Diversity.* J Med Chem, 2001. **44**(22): p. 3563-3571.
400. McGregor, M.J. and Muskal, S.M., *Pharmacophore Fingerprinting. 1. Application to QSAR and Focused Library Design.* J Chem Inf Comput Sci, 1999. **39**(3): p. 569-574.

401. Durant, J.L., Leland, B.A., Henry, D.R. and Nourse, J.G., *Reoptimization of MDL keys for use in drug discovery.* J Chem Inf Comput Sci, 2002. **42**(6): p. 1273-80.
402. Stiefl, N., Watson, I.A., Baumann, K. and Zaliani, A., *ErG: 2D pharmacophore descriptions for scaffold hopping.* J Chem Inf Model, 2006. **46**(1): p. 208-20.
403. Daylight Chemical Information Systems, Inc, *Daylight theory manual,* accessed 24 June 2024, <https://www.daylight.com/dayhtml/doc/theory/theory.finger.html>.
404. Petrone, P.M., Simms, B., Nigsch, F., Lounkine, E., Kutchukian, P., Cornett, A., Deng, Z., Davies, J.W., Jenkins, J.L. and Glick, M., *Rethinking Molecular Similarity: Comparing Compounds on the Basis of Biological Activity.* ACS Chem Biol, 2012. **7**(8): p. 1399-1409.
405. Tversky, A., *Features of similarity.* Psychol Rev, 1977. **84**(4): p. 327-352.
406. Tanimoto, T.T., *IBM internal report*, 17th November 1957.
407. Hawkins, P.C.D., Skillman, A.G. and Nicholls, A., *Comparison of Shape-Matching and Docking as Virtual Screening Tools.* J Med Chem, 2007. **50**(1): p. 74-82.
408. Rush, T.S., Grant, J.A., Mosyak, L. and Nicholls, A., *A Shape-Based 3-D Scaffold Hopping Method and Its Application to a Bacterial Protein−Protein Interaction.* J Med Chem, 2005. **48**(5): p. 1489-1495.
409. Briem, H. and Kuntz, I.D., *Molecular Similarity Based on DOCK-Generated Fingerprints.* J Med Chem, 1996. **39**(17): p. 3401-3408.
410. LaLonde, J.M., Elban, M.A., Courter, J.R., Sugawara, A., Soeta, T., Madani, N., Princiotto, A.M., Kwon, Y.D., Kwong, P.D., Schön, A., Freire, E., Sodroski, J. and Smith, A.B., *Design, synthesis and biological evaluation of small molecule inhibitors of CD4-gp120 binding based on virtual screening.* Biorg Med Chem, 2011. **19**(1): p. 91-101.
411. Metz, A., Schanda, J., Grez, M., Wichmann, C. and Gohlke, H., *From Determinants of RUNX1/ETO Tetramerization to Small-Molecule Protein–Protein Interaction Inhibitors Targeting Acute Myeloid Leukemia.* J Chem Inf Model, 2013. **53**(9): p. 2197-2202.
412. David, B., Schneider, P., Schäfer, P., Pietruszka, J. and Gohlke, H., *Discovery of new acetylcholinesterase inhibitors for Alzheimer's disease: virtual screening and in vitro characterisation.* J Enzyme Inhib Med Chem, 2021. **36**(1): p. 491-496.
413. Canela, M.-D., Pérez-Pérez, M.-J., Noppen, S., Sáez-Calvo, G., Díaz, J.F., Camarasa, M.-J., Liekens, S. and Priego, E.-M., *Novel Colchicine-Site Binders with a Cyclohexanedione Scaffold Identified through a Ligand-Based Virtual Screening Approach.* J Med Chem, 2014. **57**(10): p. 3924-3938.
414. Chen, W.-L., Wang, Z.-H., Feng, T.-T., Li, D.-D., Wang, C.-H., Xu, X.-L., Zhang, X.-J., You, Q.-D. and Guo, X.-K., *Discovery, design and synthesis of 6H-anthra[1,9-cd]isoxazol-6-one scaffold as G9a inhibitor through a combination of shape-based virtual screening and structure-based molecular modification.* Biorg Med Chem, 2016. **24**(22): p. 6102-6108.
415. Li, Q., Yang, H., Mo, J., Chen, Y., Wu, Y., Kang, C., Sun, Y. and Sun, H., *Identification by shape-based virtual screening and evaluation of new tyrosinase inhibitors.* PeerJ, 2018. **6**: p. e4206.
416. Imran, M., Waqar, S., Ogata, K., Ahmed, M., Noreen, Z., Javed, S., Bibi, N., Bokhari, H., Amjad, A. and Muddassar, M., *Identification of novel bacterial urease inhibitors through molecular shape and structure based virtual screening approaches.* RSC Adv, 2020. **10**(27): p. 16061-16070.
417. Sun, H., Coussens, N.P., Danchik, C., Wachsmuth, L.M., Henderson, M.J., Patnaik, S., Hall, M.D., Molinaro, A.L., Daines, D.A. and Shen, M., *Discovery of Small-Molecule VapC1 Nuclease Inhibitors by Virtual Screening and Scaffold Hopping from an Atomic Structure Revealing Protein–Protein Interactions with a Native VapB1 Inhibitor.* J Chem Inf Model, 2022. **62**(5): p. 1249-1258.
418. Matter, H., Zoller, G., Herling, A.W., Sanchez-Arias, J.-A., Philippo, C., Namane, C., Kohlmann, M., Pfenninger, A. and Voss, M.D., *Benzimidazole-carboxamides as potent and bioavailable stearoyl-CoA desaturase (SCD1) inhibitors from ligand-based virtual screening and chemical optimization.* Bioorg Med Chem Lett, 2013. **23**(6): p. 1817-1822.

419. Fan, Y., Lai, M.H., Sullivan, K., Popiolek, M., Andree, T.H., Dollings, P. and Pausch, M.H., *The identification of neurotensin NTS1 receptor partial agonists through a ligand-based virtual screening approach.* Bioorg Med Chem Lett, 2008. **18**(21): p. 5789-5791.
420. Chen, Y., Lin, H., Yang, H., Tan, R., Bian, Y., Fu, T., Li, W., Wu, L., Pei, Y. and Sun, H., *Discovery of new acetylcholinesterase and butyrylcholinesterase inhibitors through structure-based virtual screening.* RSC Adv, 2017. **7**(6): p. 3429-3438.
421. Hamza, A., Zhao, X., Tong, M., Tai, H.-H. and Zhan, C.-G., *Novel human mPGES-1 inhibitors identified through structure-based virtual screening.* Biorg Med Chem, 2011. **19**(20): p. 6077-6086.
422. Smelt, C.L.C., Sanders, V.R., Newcombe, J., Burt, R.P., Sheppard, T.D., Topf, M. and Millar, N.S., *Identification by virtual screening and functional characterisation of novel positive and negative allosteric modulators of the α7 nicotinic acetylcholine receptor.* Neuropharmacology, 2018. **139**: p. 194-204.
423. Capelli, A.M., Castelletti, L., Salvagno, C., Oliosi, B., Di Lenarda, E., Virginio, C., Lightfoot, A., Kew, J.N.C. and Teague, S., *Identification of novel α7 nAChR positive allosteric modulators with the use of pharmacophore in silico screening methods.* Bioorg Med Chem Lett, 2010. **20**(15): p. 4561-4565.
424. Mahasenan, K.V., Pavlovicz, R.E., Henderson, B.J., González-Cestari, T.F., Yi, B., McKay, D.B. and Li, C., *Discovery of Novel α4β2 Neuronal Nicotinic Receptor Modulators through Structure-Based Virtual Screening.* ACS Med Chem Lett, 2011. **2**(11): p. 855-860.
425. Wester, M.R., Johnson, E.F., Marques-Soares, C., Dijols, S., Dansette, P.M., Mansuy, D. and Stout, C.D., *Structure of mammalian cytochrome P450 2C5 complexed with diclofenac at 2.1 Å resolution: evidence for an induced fit model of substrate binding.* Biochemistry, 2003. **42**(31): p. 9335-9345.
426. Canan Koch, S.S., Thoresen, L.H., Tikhe, J.G., Maegley, K.A., Almassy, R.J., Li, J., Yu, X.-H., Zook, S.E., Kumpf, R.A. and Zhang, C., *Novel tricyclic poly (ADP-ribose) polymerase-1 inhibitors with potent anticancer chemopotentiating activity: design, synthesis, and X-ray cocrystal structure.* J Med Chem, 2002. **45**(23): p. 4961-4974.
427. Baldwin, E.T., Bhat, T.N., Gulnik, S., Liu, B., Topol, I.A., Kiso, Y., Mimoto, T., Mitsuya, H. and Erickson, J.W., *Structure of HIV-1 protease with KNI-272, a tight-binding transition-state analog containing allophenylnorstatine.* Structure, 1995. **3**(6): p. 581-90.
428. Xu, G., Liu, Z., Wang, X., Lu, T., DesJarlais, R.L., Thieu, T., Zhang, J., Devine, Z.H., Du, F., Li, Q., Milligan, C.M., Shaffer, P., Cedervall, P.E., Spurlino, J.C., Stratton, C.F., Pietrak, B., Szewczuk, L.M., Wong, V., Steele, R.A., Bruinzeel, W., Chintala, M., Silva, J., Gaul, M.D., Macielag, M.J. and Nargund, R., *Discovery of Potent and Orally Bioavailable Pyridine N-Oxide-Based Factor XIa Inhibitors through Exploiting Nonclassical Interactions.* J Med Chem, 2022. **65**(15): p. 10419-10440.
429. Lebon, G., Warne, T., Edwards, P.C., Bennett, K., Langmead, C.J., Leslie, A.G.W. and Tate, C.G., *Agonist-bound adenosine A2A receptor structures reveal common features of GPCR activation.* Nature, 2011. **474**(7352): p. 521-525.
430. Istvan, E.S. and Deisenhofer, J., *Structural Mechanism for Statin Inhibition of HMG-CoA Reductase.* Science, 2001. **292**(5519): p. 1160-1164.
431. Akif, M., Georgiadis, D., Mahajan, A., Dive, V., Sturrock, E.D., Isaac, R.E. and Acharya, K.R., *High-Resolution Crystal Structures of Drosophila melanogaster Angiotensin-Converting Enzyme in Complex with Novel Inhibitors and Antihypertensive Drugs.* J Mol Biol, 2010. **400**(3): p. 502-517.
432. Bar-On, P., Millard, C.B., Harel, M., Dvir, H., Enz, A., Sussman, J.L. and Silman, I., *Kinetic and Structural Studies on the Interaction of Cholinesterases with the Anti-Alzheimer Drug Rivastigmine.* Biochemistry, 2002. **41**(11): p. 3555-3564.
433. Pinto, D.J.P., Orwat, M.J., Koch, S., Rossi, K.A., Alexander, R.S., Smallwood, A., Wong, P.C., Rendina, A.R., Luettgen, J.M., Knabb, R.M., He, K., Xin, B., Wexler, R.R. and Lam, P.Y.S., *Discovery of 1-(4-Methoxyphenyl)-7-oxo-6-(4-(2-oxopiperidin-1-yl)phenyl)-4,5,6,7-tetrahydro-1H-pyrazolo[3,4-c]pyridine-3-carboxamide (Apixaban, BMS-562247), a Highly Potent,*

Selective, Efficacious, and Orally Bioavailable Inhibitor of Blood Coagulation Factor Xa. J Med Chem, 2007. **50**(22): p. 5339-5356.

434. Hartmann, M.D., Boichenko, I., Coles, M., Zanini, F., Lupas, A.N. and Hernandez Alvarez, B., *Thalidomide mimics uridine binding to an aromatic cage in cereblon.* J Struct Biol, 2014. **188**(3): p. 225-232.
435. Sun, Y., Meyers, B.A., Czako, B., Leonard, P., Mseeh, F., Harris, A.L., Wu, Q., Johnson, S., Parker, C.A., Cross, J.B., Di Francesco, M.E., Bivona, B.J., Bristow, C.A., Burke, J.P., Carrillo, C.C., Carroll, C.L., Chang, Q., Feng, N., Gao, G., Gera, S., Giuliani, V., Huang, J.K., Jiang, Y., Kang, Z., Kovacs, J.J., Liu, C.-Y., Lopez, A.M., Ma, X., Mandal, P.K., McAfoos, T., Miller, M.A., Mullinax, R.A., Peoples, M., Ramamoorthy, V., Seth, S., Spencer, N.D., Suzuki, E., Williams, C.C., Yu, S.S., Zuniga, A.M., Draetta, G.F., Marszalek, J.R., Heffernan, T.P., Kohl, N.E. and Jones, P., *Allosteric SHP2 Inhibitor, IACS-13909, Overcomes EGFR-Dependent and EGFR-Independent Resistance Mechanisms toward Osimertinib.* Cancer Res, 2020. **80**(21): p. 4840-4853.
436. Chen, S., Chandra Tjin, C., Gao, X., Xue, Y., Jiao, H., Zhang, R., Wu, M., He, Z., Ellman, J. and Ha, Y., *Pharmacological inhibition of PI5P4Kα/β disrupts cell energy metabolism and selectively kills p53-null tumor cells.* Proc Natl Acad Sci USA, 2021. **118**(21): p. e2002486118.
437. Kawanami, T., Karki, R.G., Cody, E., Liu, Q., Liang, G., Ksander, G.M., Rigel, D.F., Schiering, N., Gong, Y., Coppola, G.M., Iwaki, Y., Sun, R., Neubert, A., Fan, L., Ingles, S., D'Arcy, A., Villard, F., Ramage, P., Jeng, A.Y., Leung-Chu, J., Liu, J., Beil, M., Fu, F., Chen, W., Cumin, F., Wiesmann, C. and Mogi, M., *Structure-Guided Design of Substituted Biphenyl Butanoic Acid Derivatives as Neprilysin Inhibitors.* ACS Med Chem Lett, 2020. **11**(2): p. 188-194.
438. Ryan, K., Bolaňos, B., Smith, M., Palde, P.B., Cuenca, P.D., VanArsdale, T.L., Niessen, S., Zhang, L., Behenna, D., Ornelas, M.A., Tran, K.T., Kaiser, S., Lum, L., Stewart, A. and Gajiwala, K.S., *Dissecting the molecular determinants of clinical PARP1 inhibitor selectivity for tankyrase1.* J Biol Chem, 2021. **296**.
439. Isabelle, P.-T., Nathalie, T., Jérôme, F., Michel, F., André, U., Erin, G. and Marie-Edith, R.-O., *Met909 Plays a Key Role in the Activation of the Progesterone Receptor and Also in the High Potency of 13-Ethyl Progestins.* Mol Pharmacol, 2009. **75**(6): p. 1317.
440. Slavish, P.J., Cuypers, M.G., Rimmer, M.A., Abdolvahabi, A., Jeevan, T., Kumar, G., Jarusiewicz, J.A., Vaithiyalingam, S., Jones, J.C., Bowling, J.J., Price, J.E., DuBois, R.M., Min, J., Webby, R.J., Rankovic, Z. and White, S.W., *Chemical scaffold recycling: Structure-guided conversion of an HIV integrase inhibitor into a potent influenza virus RNA-dependent RNA polymerase inhibitor designed to minimize resistance potential.* Eur J Med Chem, 2023. **247**: p. 115035.
441. Jadhav, P.K., Ala, P., Woerner, F.J., Chang, C.-H., Garber, S.S., Anton, E.D. and Bacheler, L.T., *Cyclic Urea Amides: HIV-1 Protease Inhibitors with Low Nanomolar Potency against both Wild Type and Protease Inhibitor Resistant Mutants of HIV.* J Med Chem, 1997. **40**(2): p. 181-191.
442. Horbert, R., Pinchuk, B., Johannes, E., Schlosser, J., Schmidt, D., Cappel, D., Totzke, F., Schächtele, C. and Peifer, C., *Optimization of Potent DFG-in Inhibitors of Platelet Derived Growth Factor Receptorβ (PDGF-Rβ) Guided by Water Thermodynamics.* J Med Chem, 2015. **58**(1): p. 170-182.
443. Harriman, G., Greenwood, J., Bhat, S., Huang, X., Wang, R., Paul, D., Tong, L., Saha, A.K., Westlin, W.F., Kapeller, R. and Harwood, H.J., Jr., *Acetyl-CoA carboxylase inhibition by ND-630 reduces hepatic steatosis, improves insulin sensitivity, and modulates dyslipidemia in rats.* Proc Natl Acad Sci U S A, 2016. **113**(13): p. E1796-805.
444. Michaelides, I.N., Collie, G.W., Börjesson, U., Vasalou, C., Alkhatib, O., Barlind, L., Cheung, T., Dale, I.L., Embrey, K.J., Hennessy, E.J., Khurana, P., Koh, C.M., Lamb, M.L., Liu, J., Moss, T.A., O'Neill, D.J., Phillips, C., Shaw, J., Snijder, A., Storer, R.I., Stubbs, C.J., Han, F., Li, C., Qiao, J., Sun, D.-Q., Wang, J., Wang, P. and Yang, W., *Discovery and Optimization of the First ATP Competitive Type-III c-MET Inhibitor.* J Med Chem, 2023. **66**(13): p. 8782-8807.
445. Otake, K., Ubukata, M., Nagahashi, N., Ogawa, N., Hantani, Y., Hantani, R., Adachi, T., Nomura, A., Yamaguchi, K., Maekawa, M., Mamada, H., Motomura, T., Sato, M. and Harada, K., *Methyl and Fluorine Effects in Novel Orally Bioavailable Keap1–Nrf2 PPI Inhibitor.* ACS Med Chem Lett, 2023. **14**(5): p. 658-665.

446. De Fusco, C., Schimpl, M., Börjesson, U., Cheung, T., Collie, I., Evans, L., Narasimhan, P., Stubbs, C., Vazquez-Chantada, M., Wagner, D.J., Grondine, M., Sanders, M.G., Tentarelli, S., Underwood, E., Argyrou, A., Smith, J.M., Lynch, J.T., Chiarparin, E., Robb, G., Bagal, S.K. and Scott, J.S., *Fragment-Based Design of a Potent MAT2a Inhibitor and in Vivo Evaluation in an MTAP Null Xenograft Model.* J Med Chem, 2021. **64**(10): p. 6814-6826.
447. Hillisch, A., Gericke, K.M., Allerheiligen, S., Roehrig, S., Schaefer, M., Tersteegen, A., Schulz, S., Lienau, P., Gnoth, M., Puetter, V., Hillig, R.C. and Heitmeier, S., *Design, Synthesis, and Pharmacological Characterization of a Neutral, Non-Prodrug Thrombin Inhibitor with Good Oral Pharmacokinetics.* J Med Chem, 2020. **63**(21): p. 12574-12594.
448. Tesch, R., Rak, M., Raab, M., Berger, L.M., Kronenberger, T., Joerger, A.C., Berger, B.-T., Abdi, I., Hanke, T., Poso, A., Strebhardt, K., Sanhaji, M. and Knapp, S., *Structure-Based Design of Selective Salt-Inducible Kinase Inhibitors.* J Med Chem, 2021. **64**(12): p. 8142-8160.
449. Ramsey, S., Nguyen, C., Salomon-Ferrer, R., Walker, R.C., Gilson, M.K. and Kurtzman, T., *Solvation thermodynamic mapping of molecular surfaces in AmberTools: GIST.* J Comput Chem, 2016. **37**(21): p. 2029-37.
450. Abel, R., Young, T., Farid, R., Berne, B.J. and Friesner, R.A., *Role of the Active-Site Solvent in the Thermodynamics of Factor Xa Ligand Binding.* J Am Chem Soc, 2008. **130**(9): p. 2817-2831.
451. Young, T., Abel, R., Kim, B., Berne, B.J. and Friesner, R.A., *Motifs for molecular recognition exploiting hydrophobic enclosure in protein-ligand binding.* Proc Natl Acad Sci U S A, 2007. **104**(3): p. 808-13.
452. Dittrich, J., Schmidt, D., Pfleger, C. and Gohlke, H., *Converging a Knowledge-Based Scoring Function: DrugScore(2018).* J Chem Inf Model, 2019. **59**(1): p. 509-521.
453. Kaiser, J., Gertzen, C.G.W., Bernauer, T., Nitsche, V., Höfner, G., Niessen, K.V., Seeger, T., Paintner, F.F., Wanner, K.T., Steinritz, D., Worek, F. and Gohlke, H., *Identification of ligands binding to MB327-PAM-1, a binding pocket relevant for resensitization of nAChRs.* Toxicol Lett, 2024. *in press*.
454. Bernauer, T., Nitsche, V., Kaiser, J., Gertzen, C.G.W., Hoefner, G., Niessen, K.V., Seeger, T., Steinritz, D., Worek, F., Gohlke, H., Wanner, K.T. and Paintner, F.F., *Synthesis and biological evaluation of novel MB327 analogs as resensitizers for desensitized nicotinic acetylcholine receptors after intoxication with nerve agents.* Toxicol Lett, 2024. **397**: p. 151-162.
455. Dixon, S.L., Duan, J., Smith, E., Bargen, C.D.V., Sherman, W. and Repasky, M.P., *AutoQSAR: an automated machine learning tool for best-practice quantitative structure–activity relationship modeling.* Future Med Chem, 2016. **8**(15): p. 1825-1839.
456. *Schrödinger Maestro*. 2023, Schrödinger, LLC: New York, NY.
457. Todeschini, R. and Consonni, V., *Handbook of Molecular Descriptors*. Methods and Principles in Medicinal Chemistry. 2000, Weinheim, Germany: Wiley-VCH Verlag GmbH.
458. Ghose, A.K., Viswanadhan, V.N. and Wendoloski, J.J., *Prediction of Hydrophobic (Lipophilic) Properties of Small Organic Molecules Using Fragmental Methods: An Analysis of ALOGP and CLOGP Methods.* J Phys Chem A, 1998. **102**(21): p. 3762-3772.
459. Gasteiger, J. and Marsili, M., *Iterative partial equalization of orbital electronegativity—a rapid access to atomic charges.* Tetrahedron, 1980. **36**(22): p. 3219-3228.